Studies on Nucleophilic Enzymes Involved in the Cell Wall Biosynthesis of *Mycobacterium tuberculosis*



A thesis presented to the Board of the Faculty of Mathematical, Physical and Life Sciences in partial fulfillment of the requirements for the degree of Doctor of Philosophy at the University of Oxford

Mariska de Munnik

Hertford College

Hilary Term 2024

Abstract

The extraordinarily thick and complex cell wall of *Mycobacterium tuberculosis* (*Mtb*), the causative agent of tuberculosis (TB), may be considered as an Achilles' heel of the bacillus; however, the most important class of antibiotics targeting the bacterial cell wall (the β-lactams) has not been proven to be effective as TB treatment, likely in part due to resistance mechanisms, such as hydrolysis catalysed by the β-lactamase BlaC. β-Lactams are inhibitors of a class of transpeptidases of the peptidoglycan layer of the bacterial cell wall, i.e., the penicillin binding proteins (PBPs). *Mtb* additionally applies a second class transpeptidases, the L,D-transpeptidases (Ldts), which employ a nucleophilic cysteine in catalysis, and which are reported to be resistant to inactivation by most β-lactams.

In **Chapter 1**, an introduction to TB and TB drug development is described. **Chapter 2** describes a literature review of the function and inhibition of the Ldts, PBPs, and BlaC of *Mtb*. **Chapter 3** describes the identification of novel inhibitors for Ldt_{Mt2}, an essential Ldt of *Mtb*, via high-throughput screening (HTS), and detailed studies of their mechanism of inhibition. Several potent classes of inhibitors were identified, both from established inhibitor classes (e.g., β-lactams), and unexplored covalently reacting electrophilic groups (e.g., cyanamides). **Chapter 4** describes the mechanism of the αβ,α′β′-diepoxyketones as another class of unexplored mechanism-based inhibitors of nucleophilic cysteine enzymes identified in the HTS. **Chapter 5** describes studies on the mechanism of the transpeptidase activity of Ldt_{Mt2}. A crystal structure of Ldt_{Mt2} in complex with the covalent intermediate of the transpeptidase reaction informs on key interactions of Ldt_{Mt2} with its substrate, and provides strategies for the design of improved inhibitors. **Chapter 6** describes the cellular inhibition of a selection of β-lactams and Ldt_{Mt2} inhibitors identified in the HTS with the model organism *Mycobacterium smegmatis*. The results of a fluorescent assay evaluating the inhibition of Ldt and PBP transpeptidase activity in live cells suggests multifaceted correlation of transpeptidase inhibition with inhibition of growth and suggests that inhibition of PBP transpeptidase activity alone is insufficient to inhibit growth, which was often accompanied with partial Ldt inhibition. **Chapter 7** describes inhibition studies of BlaC. A cephalosporin identified in the HTS manifested notable stability of the acyl-enzyme complex with BlaC, leading to inhibition similarly to that of the commonly used β-lactamase inhibitor clavulanic acid.

Overall, the work provides novel insights into the function and inhibition of Ldt_{Mt2}. Novel potent inhibitors of Ldt_{Mt2} were identified, new insights into the protein-substrate interactions have been obtained, and understanding of the cellular role of Ldt inhibition has been advanced. The results provide guidance for the development of novel anti-TB drugs targeting the transpeptidases of *Mtb*.

Declaration

I, Mariska de Munnik, declare that the thesis I am submitting is entirely my own work except where indicated in the text, caption, footnote, or bibliography. This thesis has not been submitted in whole or in part for any other academic degree or professional qualification.



23/01/2024

Signature *Date*

Acknowledgements

I would like to thank my supervisor Prof. Christopher J. Schofield at the department of Chemistry, University of Oxford, for his continuous support and guidance, and for giving me the opportunity to continue working on this project. I would like to thank my supervisor Dr Beatriz Rodríguez Miquel at GlaxoSmithKline, Tres Cantos, for all her support in our continued collaboration, and for her advice. I would like to thank the Interdisciplinary Bioscience DTP, the Department of Chemistry, and the Tres Cantos Open Lab Foundation for funding this work.

I am very grateful to Dr Pauline Lang, for introducing me to so many lab techniques, from crystallography to protein preps to mass spectrometry and so much more, for countless patient hours, and for her enthusiasm and interest in the project. I would like to extend my sincere thanks to Dr Jürgen Brem for sharing his knowledge and expertise, for all the helpful discussions, and for all his input in the project.

I am also thankful to Dr Karina Calvopiña Tapia for introducing me to the world of microbiology, for all her input and all the questions answered. Many thanks to Dr Patrick Rabe for always being prepared to teach me new lab techniques and for all the help wherever it is needed. I would like to thank Jasper Lithgow and Siddhant Dhingra, for their efforts in synthetic organic chemistry relating to this project, as well as becoming familiar with the biochemistry side, and Dr Lennart Brewitz for his supervision of the synthetic organic chemistry side of the project and for extending our work to M^{pro} and PL^{pro}.

I would like to express my gratitude for receiving support from so many other colleagues that I have had the pleasure to work with. In particular, Dr Alistair Farley for his advice and collaboration, Dr Helen Smith for her work and advice relating to PBPs, Dr Anthony Tumber for his support with the RapidFire, Dr Ian Clifton for his support on crystallography, Dr Adam Hardy for ensuring the lab runs smoothly and for being a great problem solver, and Zahn, Gwen, and Jenny, for running the administrative side. My thanks also go to the support I have received from our collaborators at GlaxoSmithKline, in particular Dr Robert Bates, Dr Raquel Gabarro-Carrion, Dr Eugenia Meiler, Dr Mónica Cacho and Dr Paco de Dios Antón.

I am deeply grateful for the support I have had from my friends and family throughout my DPhil. I want to thank Patrick, Karina, Pauline, Jos, Liam, Tharindi, Helen, and Matt for all the chats, coffee, tea, and lunch breaks, as well as the great times outside of the lab. A special thanks goes to my parents, for their love and support. I would like to pay special thanks to my husband, Brian De Anda, for his love, support, and patience, and for always believing in me and encouraging me.

List of publications

These manuscripts have contributed towards this integrated thesis:

Mariska de Munnik, Pauline A. Lang, Francisco De Dios Anton, Mónica Cacho, Robert H. Bates, Jürgen Brem, Beatriz Rodríguez Miquel, and Christopher J. Schofield. High-throughput screen with the L,D-transpeptidase Ldt_{Mt2} of *Mycobacterium tuberculosis* reveals novel classes of covalently reacting inhibitors. *Chem. Sci.* **14**, 7262-7278 (2023).

Mariska de Munnik, Jasper Lithgow, Lennart Brewitz, Kirsten E. Christensen, Robert H. Bates, Beatriz Rodriguez Miquel, and Christopher J. Schofield. αβ,α'β'-Diepoxyketones are mechanism-based inhibitors of nucleophilic cysteine enzymes. *Chem. Commun.* **59**, 12859-12862 (2023).

Mariska de Munnik, Pauline A. Lang, Karina Calvopiña Tapia, Patrick Rabe, Jürgen Brem, and Christopher J. Schofield. Biochemical and crystallographic studies of Ldt_{Mt2} from *Mycobacterium tuberculosis* with its natural monomer substrate. *Submitted manuscript*.

Mariska de Munnik, Karina Calvopiña Tapia, Patrick Rabe, and Christopher J. Schofield. How inhibition of L,D-transpeptidases and D,D-transpeptidases leads to inhibition of mycobacteria. *Manuscript in preparation*.

These manuscripts were published prior to the work discussed in this thesis:

Mariska de Munnik, Christopher T. Lohans, Gareth W. Langley, Corentin Bon, Jürgen Brem, and Christopher J. Schofield. A Fluorescence-Based Assay for Screening β-Lactams Targeting the *Mycobacterium tuberculosis* Transpeptidase Ldt_{Mt2}. *ChemBioChem* **21**, 368-372 (2020).

Mariska de Munnik, Christopher T. Lohans, Pauline A. Lang, Gareth W. Langley, Tika R. Malla, Anthony Tumber, Christopher J. Schofield, and Jürgen Brem. Targeting the *Mycobacterium tuberculosis* transpeptidase Ldt_{Mt2} with cysteine-reactive inhibitors including ebselen. *Chem. Commun.* **55**, 10214-10217 (2019).

Christopher T. Lohans, H. T. Henry Chan, Tika R. Malla, Kiran Kumar, Jos J. A. G. Kamps, Darius J. B. McArdle, Emma van Groesen, **Mariska de Munnik**, Catherine L. Tooke, James Spencer, Robert S. Paton, Jürgen Brem, and Christopher J. Schofield. Non-Hydrolytic β-Lactam Antibiotic Fragmentation by L,D-transpeptidases and Serine β-Lactamase Cysteine Variants. *Angew. Chem. Int. Ed.* **58**, 1990-1994 (2019).

Giulia Rainoldi, Fabio Begnini, **Mariska de Munnik**, Leonardo Lo Presti, Christophe M. L. Vande Velde, Romano Orru, Giordano Lesma, Eelco Ruijter, and Alessandra Silvani. Sequential Multicomponent Strategy for the Diastereoselective Synthesis of Densely Functionalized Spirooxindole-Fused Thiazolidines. *ACS Comb. Sci.* **20**, 98–105 (2018).

List of abbreviations

2HREZ/4HR	Treatment regimen of two months of isoniazid, rifampicin, ethambutol and pyrazinamide, followed by four months of isoniazid and rifampicin
2xYT	2x yeast extract tryptone media
ADC	Albumin-dextrose-catalase
AG	Arabinogalactan
AR	Amplex Red
ASU	Asymmetric unit
ATP	Adenosine triphosphate
AVI	Avibactam
BLI	BLI-489
B. subtilis	*Bacillus subtilis*
CDAP	1-cyano-4-dimethylaminopyridinium tetrafluoroborate
CDTP	5-cyano-5H-dibenzo[b,d]thiophen-5-ium
C. jeikeium	*Corynebacterium jeikeium*
CLAV	Clavulanic acid
CLSI	Clinical & Laboratory Standards Institute
DAAO	D-Amino acid oxidase
DCM	Dichloromethane
DEK	αβ,α′β′-Diepoxyketone
DIC	N,N′-diisopropylcarbodiimide
DIPEA	N,N-diisopropylethylamine
DMF	Dimethylformamide
DMSO	Dimethyl sulfoxide
DOTS	Directly observed therapy, short-course
DSF	Differential scanning fluorimetry
E. coli	*Escherichia coli*
ESI	Electrospray ionisation
EUCAST	European Committee on Antimicrobial Susceptibility Testing
FAD	Flavin adenine dinucleotide
FAR	Faropenem
FBS	Fetal bovine serum
FDA	U.S. Food and Drug Administration
Fmoc	Fluorenylmethyloxycarbonyl protecting group
Fru-6-P	Fructose-6-phosphate

GlcNAc	*N*-acetylglucosamine
GSH	Glutathione
HEPES	4-(2-hydroxyethyl)-1-piperazineethanesulfonic acid
HIV	Human immunodeficiency virus
HPLC	High-performance liquid chromatography
HRP	Horse-radish peroxidase
HTS	High-throughput screen
IgD	Immunoglobulin-like domain
iGlu_{NH2}	*Iso*-glutamine
IPTG	Isopropyl β-D-1-thiogalactopyranoside
k_{cat}	Reaction rate constant
k_{chem}	Intrinsic thiol reactivity rate constant
$K_{i,app}$	Apparent inhibition constant
k_{inact}/K_I	Second order rate constant for the efficiency of irreversible reaction
K_m	Michaelis constant
k_{obs}	Observed kinetic rate constant
k_{off}	Off rate constant
LC	Liquid chromatography
Ldt	L,D-transpeptidase
MA	Mycolic acid
MAPc	Mycolic acid, arabinogalactan, and peptidoglycan complex
MBL	Metallo-β-lactamase
m-DAP	Meso-diaminopimelic acid
m-DAP_{NH2}	Amidated meso-diaminopimelic acid
MDR	Multidrug resistant
MEM	Minimal essential medium
MER	Meropenem
MIC	Minimum inhibitory concentration
M^{pro}	Main protease of SARS-CoV-2
MS	Mass spectrometry
Msm	*Mycobacterium smegmatis*
Mtb	*Mycobacterium tuberculosis*
MurNAc	*N*-acetylmuramic acid
MurNGlyc	*N*-glycolylmuramic acid
NEAA	Non-essential amino acids

NMR	Nuclear magnetic resonance
NSAID	Non-steroidal anti-inflammatory drug
NTCB	2-nitro-5-thiocyanobenzoic acid
NTM	Nontuberculous mycobacteria
OADC	Oleic acid-albumin-dextrose-catalase
Oxyma	Ethyl cyanohydroxyiminoacetate
PBP	Penicillin binding protein
PCR	Polymerase chain reaction
PDB	Protein data bank
PG	Peptidoglycan
Q-TOF	Quadrupole Time-of-Flight
RMSD	Root-mean-square deviation
SARS-CoV	Severe acute respiratory syndrome coronavirus
SBL	Serine β-lactamase
SDS-PAGE	Sodium dodecyl-sulfate polyacrylamide gel electrophoresis
SPE	Solid phase extraction
SUL	Sulbactam
$t_{1/2}$	Half-life
TAN	Taniborbactam
TAZ	Tazobactam
TB	Tuberculosis
TFA	Trifluoroacetic acid
T_m	Melting temperature
Tris	2-Amino-2-(hydroxymethyl)propane-1,3-diol
WHO	World health organisation
XDR	Extensively drug resistant
XER	Xeruborbactam

Standard amino acid abbreviations, SI unit abbreviations, and chemical symbols are used throughout this thesis.

Table of Contents

Abstract i
Declaration ii
Acknowledgements iii
List of publications iv
List of abbreviations v
Table of Contents viii
Chapter 1. Introduction. 1
1.1 Global burden of tuberculosis 3
1.2 Pathogenesis of tuberculosis 4
1.3 Treatment of tuberculosis 6
1.4 Tuberculosis drug research and development 10
1.5 The mycobacterial cell wall 14
1.6 Research objectives 19
1.7 References 20
Chapter 2. β-Lactam antibiotics targeting *Mycobacterium tuberculosis*. 30
2.1 Introduction 32
2.2 *In vitro* and *in vivo* activity of β-lactams in *Mycobacterium tuberculosis* 35
2.3 Targets of β-lactams in *Mycobacterium tuberculosis* 36
2.4 Inhibition of penicillin binding proteins and L,D-transpeptidases 45
2.5 Optimisation of β-lactams for *Mycobacterium tuberculosis* 50
2.6 Summary and conclusions 55
2.7 References 57
Chapter 3. High-throughput screen with the L,D-transpeptidase Ldt_{Mt2} of *Mycobacterium tuberculosis* reveals novel classes of covalently reacting inhibitors. 68
3.1 Abstract 70
3.2 Introduction 71
3.3 Results 73
3.4 Discussion 88
3.5 Conclusion 90
3.6 Methods 90
3.7 Data availability 97
3.8 References 97
3.9 Statement of authorship 101

Chapter 4. αβ,α′β′-Diepoxyketones are mechanism-based inhibitors of nucleophilic cysteine enzymes. 102

4.1 Abstract 104

4.2 Main text 105

4.3 Data availability 111

4.4 References 111

4.5 Statement of authorship 115

Chapter 5. Biochemical and crystallographic studies of Ldt_{Mt2} from *Mycobacterium tuberculosis* with its natural monomer substrate 116

5.1 Abstract 118

5.1 Introduction 119

5.3 Results 122

5.4 Discussion 129

5.5 Conclusion 132

5.6 Methods 132

5.7 Data availability 136

5.8 References 136

5.9 Statement of authorship 142

Chapter 6. How inhibition of L,D-transpeptidases and D,D-transpeptidases leads to inhibition of mycobacteria 143

6.1 Abstract 145

6.2 Introduction 146

6.3 Results 148

6.4 Discussion 154

6.5 Conclusion 157

6.6 Methods 157

6.7 Data availability 161

6.8 References 161

6.9 Statement of authorship 165

Chapter 7. Studies on inhibition of the β-lactamase BlaC from *Mycobacterium tuberculosis*. 166

7.1 Introduction 168

7.2 Production, purification, and characterisation of BlaC 170

7.3 Steady-state kinetics 172

7.4. Covalent interactions of BlaC with cephalosporins 175

7.5 Discussion 178

7.6 Summary and conclusions 179

7.7 Methods 180
7.8 References 182
Chapter 8. Discussion and conclusion. 186
8.1 L,D-Transpeptidases are promising drug targets for tuberculosis 188
8.2 Novel inhibitors for Ldt_{Mt2} have been identified 189
8.3 Insights into the mechanism of Ldt_{Mt2} 191
8.4 Cellular inhibition of L,D-transpeptidases and penicillin binding proteins 192
8.5 Inhibition of BlaC 193
8.6 Future perspectives 194
8.7 Conclusions 196
8.8 References 197
Appendix 201
Appendix I. Supplementary information for Chapter 3. 203
Appendix II. Supplementary information for Chapter 4. 263
Appendix III. Supplementary information for Chapter 5. 305
Appendix IV. Supplementary information for Chapter 6. 338
Appendix V. Protein purification 368
Appendix VI. Sequences of protein constructs 371

Chapter 1

Introduction

Contents

1.1 Global burden of tuberculosis 3
1.2 Pathogenesis of tuberculosis 4
1.2.1 The bacillus 4
1.2.2 Circumvention of the host immune response 4
1.2.3 Latent tuberculosis 5
1.2.4 Active tuberculosis 6
1.3 Treatment of tuberculosis 6
1.3.1 First-line treatment of tuberculosis 6
1.3.2 Treatment of drug-resistant tuberculosis 7
1.3.3 Challenges concerning tuberculosis treatment 8
1.3.4 Treatment of latent tuberculosis 9
1.3.5 Persister bacteria 10
1.4 Tuberculosis drug research and development 10
1.4.1 Challenges in tuberculosis drug development 10
1.4.2 Recent advances in tuberculosis treatment 11
1.4.3 Tuberculosis drugs in the pipeline 12
1.4.4 Repurposing of old drugs against tuberculosis 13
1.5 The mycobacterial cell wall 14
1.5.1 Peptidoglycan structure of *Mycobacterium tuberculosis* 15
1.5.2 Biosynthesis of peptidoglycan precursors 16
1.5.3 Transpeptidases of *Mycobacterium tuberculosis* 17
1.5.4 Inhibition of L,D-transpeptidases 18
1.6 Research objectives 19
1.7 References 20

1.1 Global burden of tuberculosis

Tuberculosis (TB) is an infectious disease that imposes a major burden on global health. With an estimated annual mortality rate of 1.6 million in 2021, TB was the leading cause of death from a single infectious agent prior to the coronavirus (COVID-19) pandemic.[1] While in a substantial part of the world the disease burden of TB has been reduced to less than 1 annual death per 100 000,[1] over two-thirds of the global TB burden is carried by Africa and Asia, in the latter case in particular affecting India, Indonesia and China.[2] It is widely accepted that research breakthroughs will be required in order to reduce the worldwide burden of TB.[3]

TB is caused by infection with *Mycobacterium tuberculosis* (*Mtb*). Infection occurs when bacilli are dispersed in the air from a patient with active TB (e.g., by coughing, sneezing, or speaking), and reach the alveoli of the newfound host. Infection may also occur via alternative pathways, e.g., when an *Mtb* infected surface is touched by skin with lesions or an open wound. Approximately a quarter to one third of the global population is estimated to be infected with *Mtb*.[1,4,5] However, most of those infected with *Mtb* will not develop active TB, but instead develop latent TB, during which bacilli remain dormant in the body, in most cases for lifetime.[4] Those that develop active TB typically display pulmonary TB, although other sites may be affected.

If untreated, the death rate from TB is approximately 50%.[6] Current recommended treatment regimens consist of a combination treatment of four anti-TB drugs, which are taken for the duration of 4-6 months, and cure ~80% of patients,[7] though an increasing incidence of resistance to available anti-TB drugs reduces the treatment success rate.[8]

Following the *Millennium Declaration* set by the United Nations in September 2000, which among other goals aimed to address the global epidemic of TB,[9] great progress has been made towards reducing the disease burden of TB: an estimated 43 million lives have been saved between 2000 and 2015.[10] However, the ambitious post-2015 global TB strategy, now known as the End TB Strategy,[11] is seeing the incidence of TB falling too slowly to be likely to meet its goals of reducing incidence of TB by 80%, and TB deaths by 90% by 2030.[3] Importantly, a clear relationship has been observed between TB incidence rates per capita and indicators of development, e.g., average income, and undernourishment.[12-14] For many TB patients, access to healthcare is affected by economic and financial barriers, with over half of TB patients facing catastrophic total costs due to TB; defined as exceeding 20% of the annual pre-TB household income.[15]

The End TB Strategy stands on three fundamental pillars: integrated prevention and care, bold policies and supportive systems, and intensified research and innovation.[16] The first pillar

underlines the needs for patient-centred care, in which early diagnosis is available, all patients receive treatment (including drug-resistant cases), preventive treatment is available for the most vulnerable groups in a population, and management of comorbidity, with particular attention devoted to comorbidity with the human immunodeficiency virus (HIV), is in place. The second pillar calls for a strong political commitment, additional engagement from communities, and greater financing. At the core of this lies the need for poverty alleviation and the implementation of universal health coverage, making access to healthcare available to all. The third pillar focusses on the importance of the development of safer, easier, and shorter treatments, better diagnostics, and effective vaccinations, all of which are deemed critical to accelerate the decline of TB incidence.

1.2 Pathogenesis of tuberculosis

1.2.1 The bacillus

Mtb is a rod-shaped aerobic bacterium of the *Mycobacterium* genus, first described by Robert Koch in 1882.[17] *Mtb* is remarkedly slow growing, with a doubling time of 12-24 hours.[18] A particularly notable feature of the bacterium is its extraordinarily thick, waxy, cell wall structure (Section 1.5).[19] Mycobacteria contain an outer membrane that is functionally similar to that of gram-negative bacteria, consisting of a lipid bilayer entailing mycolic acids and glycolipids, while the presence of a peptidoglycan layer generally classifies them as gram-positive, acid-fast bacteria.[18] However, genomically *Mtb* is more related to gram-negative bacteria than to gram-positive bacteria.[20]

The mycobacterial species include several pathogenic species (e.g., *Mtb*, *Mycobacterium leprae*, *Mycobacterium abscessus*, and *Mycobacterium avium*) and non-pathogenic species (e.g., *Mycobacterium smegmatis*), likely originating from various genetic deletions and insertions, that aid survival under diverse environmental conditions.[21] Person-to-person transmission of nontuberculous mycobacteria (NTM) is rare, though has been observed with *M. abcessus* in patients with cystic fibrosis.[22] The pathophysiology of *Mtb* and NTM appear to share fundamental similarities, though diversity in virulence mechanisms between mycobacterial species introduce distinctions in the host survival of the bacteria.[23,24]

1.2.2 Circumvention of the host immune response

Upon inhalation, *Mtb* cells may reach the pulmonary alveoli of a host, where they are rapidly phagocytised by alveolar macrophages (Figure 1.1). In most cases, this response will kill infecting bacteria.[25] However, *Mtb* is infamous for its ability to survive this first line of host

defence. It replicates in the macrophage, so promoting pathogenicity. The survival of *Mtb* in macrophages has been attributed to its complex cell wall, which protects *Mtb* from the macrophage defence mechanisms.[26] Further, interaction between *Mtb* and the macrophage leads to suppression of macrophage maturation and acidification of lysozymes, as well as inhibition of oxidative stress, apoptosis and autophagy.[27]

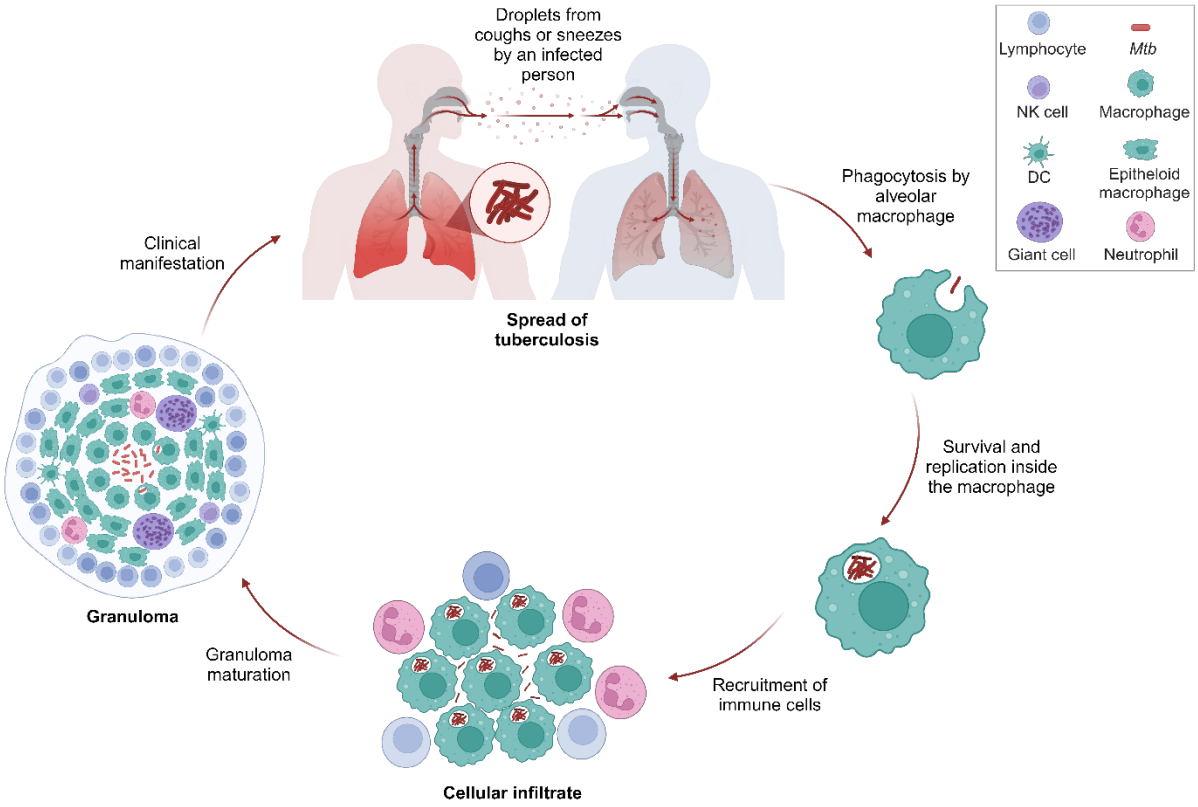

Figure 1.1 Pathogenesis of pulmonary tuberculosis. 'NK' represents natural killer, 'DC' represents dendritic cell. The figure was created using BioRender.com.

In addition to evasion of the innate immune response, the adaptive immune response to *Mtb* has been observed to be markedly delayed in comparison to many other infections or immunisations. Normally T-cell responses are initiated 3-5 days post infection, while in TB it is initiated 9-11 days post infection.[25,28] This allows for rapid increase of the *Mtb* population during the initial phase of infection.[25]

1.2.3 Latent tuberculosis

Once the adaptive immune response is initiated, various immune cells are migrated to the primary site of infection, including neutrophils and lymphocytes, accompanied with the recruitment of further macrophages, to form a cellular infiltrate, also known as the early stages of the granuloma (Figure 1.1).[29] The granuloma matures through further inclusion of macrophages, epithelioid cells, and multinucleated giant cells, and become surrounded by

fibrous cells, which calcify and ensure *Mtb* remains encapsulated within (Figure 1.1).[30,31] Typical for TB is the formation of caseous granulomas, characterised by necrosis at the centre of the granuloma, leading to a “cheese-like” consistency.[32] Granuloma formation is one of the main characteristics of the immune response to *Mtb*, creating a microenvironment in which the infection can be encapsulated and controlled.[33] However, the granuloma equally aids *Mtb*, as the bacteria enter a state of dormancy, and may survive in this state indefinitely.[34] In most instances, this creates little health problems, and it is proposed that an equilibrium between *Mtb* and the immune response is reached, a state which is referred to as latent TB.[35]

1.2.4 Active tuberculosis

It has been established that during latent TB, the majority of bacteria persist in a dormant state, though a small quantity of *Mtb* remains in active replicating state. These bacilli are named “scouts”, and are continuously killed by the host immune system during latent TB.[36] However, if the immune system fails to respond accordingly to these scouts, active disease develops.[37] The reason behind the conversion from latent to active TB, which occurs in 5-15% of those infected with *Mtb*,[38] is not fully elucidated, but likely involves various bacterial, environmental, and host factors.[4] Particularly immunocompromised individuals are at increased risk; established examples of this are coinfection with HIV,[39] use of immunosuppressants,[40-42] or cancer.[43] Active TB most commonly affects the lungs, causing patients to experience chest pain and a prolonged cough, in addition to constitutional symptoms such as fever, weight loss, and night sweats, though *Mtb* can cause disease in any organ, accompanied with site-specific disease presentation.[44]

1.3 Treatment of tuberculosis

1.3.1 First-line treatment of tuberculosis

Before the development of effective treatment options, TB was among the major causes of death both in Western and various non-Western countries.[45,46] The identification of streptomycin and *p*-aminosalicyclic acid, followed by the cell wall synthesis inhibitor isoniazid in 1952, opened the modern era to anti-TB chemotherapy, and represents major breakthroughs in the treatment of TB (Figure 1.2).[47] Following this, the fatty acid synthesis inhibitor pyrazinamide, the cell wall synthesis inhibitor ethambutol, and the DNA-dependent RNA polymerase inhibitor rifampicin were implemented in combinatorial treatments with isoniazid between the 1960s to 1970s.[48] To this day, isoniazid, pyrazinamide, ethambutol, and rifampicin (Figure 1.2) are the recommended first-line treatment for new patients with drug-

susceptible, uncomplicated TB. They are typically taken in combination for 2 months, followed by an additional four months of treatment with isoniazid and rifampicin (referred to as 2HREZ/4HR).[7] This treatment regimen yields a treatment success rate of ~80% in adults with drug-sensitive TB worldwide.[49]

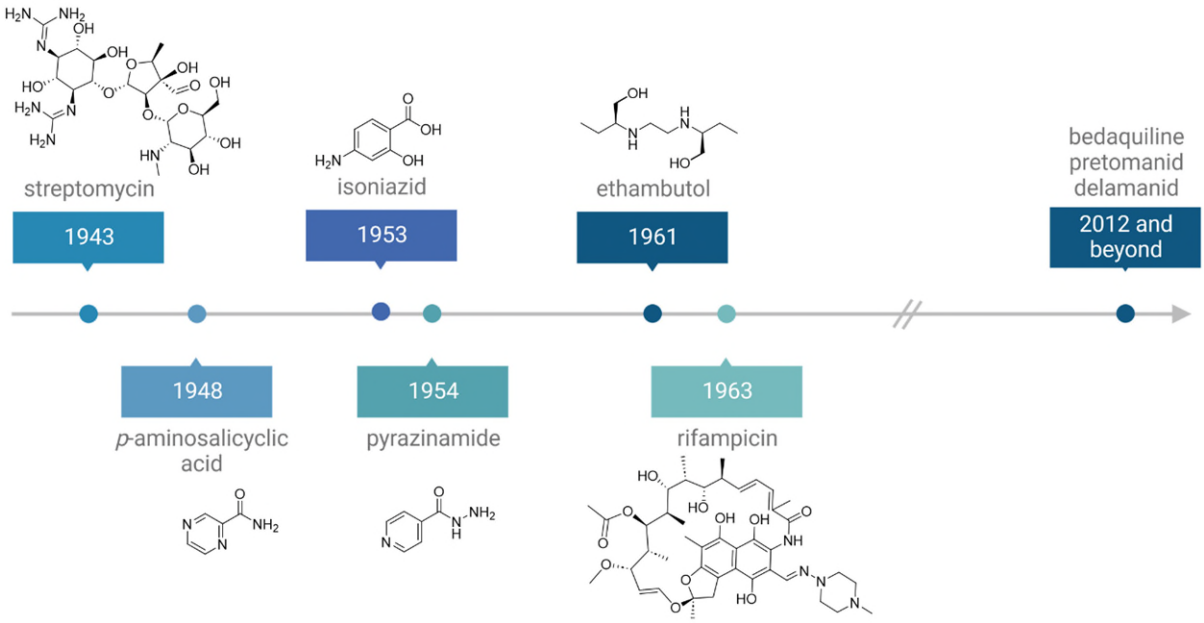

Figure 1.2. Discovery of breakthrough anti-TB drugs, including the currently recommended first-line drugs for the treatment of tuberculosis: isoniazid, pyrazinamide, ethambutol, and rifampicin. Note that anti-TB drugs have both chemically complex structures (e.g., streptomycin and rifampicin) and simple structures (e.g., isoniazid and pyrazinamide). The structures of bedaquiline, pretomanid, and delamanid are given in Figure 1.3. This figure shows drugs specifically developed for the treatment of TB. Drugs developed for other bacterial infections are also used in TB treatment (Section 1.4.4). The figure was created using BioRender.com.

1.3.2 Treatment of drug-resistant tuberculosis

The increasing emergence of drug resistance poses a significant threat to positive treatment outcomes. Besides drug-specific resistance, such as isoniazid-resistant TB, or rifampicin resistant TB, there is an increased incidence of multidrug resistant (MDR)-TB, defined as resistance to at least rifampicin and isoniazid, and extensively drug resistant (XDR)-TB, defined by additional resistance to any fluoroquinolone and at least three second-line injectable drugs (capreomycin, kanamycin, and amikacin), reduce the chance of a positive treatment outcome to 58% and 27%, respectively.[49]

Upon failure of first-line treatment, relapse, or infection with drug-resistant strains, several second-line therapeutics may be considered for use in TB treatment (Table 1.1), most of which were developed for other bacterial infections and repurposed for use in TB (e.g., levofloxacin,

moxifloxacin, and linezolid; Section 1.4.4), while some were developed specifically for TB treatment (e.g., bedaquiline, and delamanid; Section 1.4.2).[50] These drugs have been classified in three groups (A-C), based on drug class, level of certainty in the evidence of effectiveness, and safety; the increased treatment regimens required in the treatment of MDR-TB and XDR-TB are often associated with high rates of drug-related toxic events.[51] Group A drugs are recommended to all be included in the treatment of MDR-TB, and include the fluoroquinolones levofloxacin *or* moxifloxacin, bedaquiline, and linezolid.[50] Group B drugs consist of clofazimine and cycloserine *or* terizidone, and one or both are recommended to be used in addition to group A drugs. Group C drugs carry a lower priority, due to inferior evidence for effectivity, higher toxicity, and/or parenteral administration, and are recommended to only be considered if group A and B drugs cannot be used or are not efficacious in patients.[50] Considerations that contribute to the treatment regimen in MDR- and XRD-TB may include the results of drug-susceptibility testing, the clinical condition of the patient, history of previously used treatments, known contraindications, or prevalence of drug resistance in the region.[50] Generally, treatment of MDR-TB should be increased to last at least 18 months, though may be extended to 24 months.[50]

Table 1.1. Recommendations on the treatment of multidrug resistant tuberculosis.

Group	Recommendation	Medicine	Target
A	Include all three	Levofloxacin *or* moxifloxacin	DNA synthesis
		Bedaquiline	ATP synthesis
		Linezolid	Protein synthesis
B	Include one or both	Clofazimine	DNA synthesis
		Cycloserine *or* terizidone	Cell wall synthesis
C	Add to complete the regimen, and when group A and B medicines cannot be used	Ethambutol	Cell wall synthesis
		Delamanid	Cell wall synthesis
		Pyrazinamide	Fatty acid synthesis
		Imipenem-cilastatin *or* meropenem	Cell wall synthesis
		Amikacin *or* streptomycin	Protein synthesis
		Ethionamide *or* prothionamide	Cell wall synthesis
		P-aminosalicyclic acid	Folate synthesis

1.3.3 Challenges concerning tuberculosis treatment

As stated, an average worldwide success rate of drug-susceptible TB lies at ~80%, though this greatly varies on location, e.g., successful treatment outcome in Oceania was determined to be 83.9%, while only 75.9% was obtained in America.[49] However, clinical trials have

suggested that in optimal treatment regimens, efficacy of up to 95% may be obtained.[52] Patient nonadherence has been identified as one of the causes of low effectiveness, which may consist of premature discontinuing of taking some or all medications, or irregular medication use.[53] Treatment nonadherence has been observed to be related to a variety of factors such as lack of social support, lack of transportation, poor communication, feeling better, and lack of knowledge.[54]

Mtb has been known to be prone to the development of resistance since the emergence of the first anti-TB drugs, and this has been prevented by using combination chemotherapy. In 1993, standardised combinatorial chemotherapy with the directly observed therapy, short-course (DOTS) strategy was introduced, ensuring adherence to standardised 2HREZ/4HR treatment regimens by direct supervision of a health care worker.[8] However, a combination of treatment nonadherence and chaotic treatment regimens before the 1990s contribute to the emergence of MDR-TB strains.[8] In addition, the DOTS strategy was observed exacerbate the emergence of MDR-TB once resistance to one or more drugs was established.[55] Following the emergence of MDR-TB, community transmission and facility-based transmission have significantly increased incidence.[56] Currently, it has been observed that in the majority of cases, patients with MDR-TB have been infected with an MDR-TB strain, rather than acquiring resistance caused by inadequate treatment.[57]

1.3.4 Treatment of latent tuberculosis

Though individuals with latent TB infections do not have symptoms, nor are they infectious to others, they are at risk of developing active disease, and they represent a reservoir for active TB cases. Therefore, it is recommended they should be treated from the perspective of prevention.[58] Detection and treatment of latent TB is an essential element of the End TB Strategy.[11] Since an estimated 25-30% of the world's population currently have latent TB, prioritisation of screening and identification of populations at risk is essential, e.g., those who have been in contact with active TB cases, and immunocompromised individuals.[58] Treatment options include isoniazid monotherapy for 6-9 months, rifampicin monotherapy for 4 months, or combination therapy of isoniazid with rifampicin *or* rifapentine for 3-4 months.[4] Though it has been shown that treatment of latent TB is not associated with an increased risk of developing drug resistant TB, treatment adherence and completion rates are low due to the prolonged treatment regimens and side effects associated with treatments; shorter regimens are associated with improved completion rates and lower risk of drug related toxicity.[59,60]

1.3.5 Persister bacteria

The prolonged TB chemotherapy regimens required for eradicating disease can in part be attributed to the existence of a subpopulation of *Mtb* that exhibit transient resistance to lethal doses of antibiotics, referred to as bacterial persisters.[61] *Mtb* establishes persistence when residing in macrophages or granulomas, where the microenvironment involving hypoxia, oxidative stress, low pH, and nutrient starvation, affects the metabolic state of the bacteria, forming a heterogeneous bacterial population, including a subset of nonreplicating bacteria.[62] The nonreplicating subset of *Mtb* comprises the persister population, and their altered metabolic state contributes to resistance to antibiotics, latent infections and relapse.[61-64] The treatment of isoniazid alone is sufficient for reducing the bacterial load in the sputum of TB patients by over 90% in the first two days of treatment, whereas the remainder of the TB chemotherapy regimen is required to eradicate the relatively few persister bacteria.[65]

1.4 Tuberculosis drug research and development

1.4.1 Challenges in tuberculosis drug development

Though the development of the currently used TB chemotherapy has enabled the treatment of TB, shifting TB from a typically fatal disease to a treatable disease, the challenges concerning poor treatment adherence, insufficient treatment availability, and increasing incidence of MDR- and XDR-TB, demonstrate that the current regimens for TB chemotherapy are far from ideal. There is a clear need for the development of novel anti-TB therapeutics, though it is telling that all front-line therapeutics have been developed over 50 years ago. Though the *Millenium Declaration* and the End TB Strategy have ushered in a reawakening of TB drug research and development,[66] it has proven to be challenging to develop novel TB therapeutics that are improvements on current TB treatments.

Improvement on current TB treatments should ideally cover four primary goals: providing a shortened and simplified treatment of active, drug-sensitive TB, activity against drug-resistant TB, shortening the treatment of latent TB, and being able to be co-administered with HIV medications.[66,67] In order to achieve a shortened and simplified treatment regimen, both for active and latent TB, the development of drugs that are active against persister bacteria, i.e., non-replicating *Mtb*, will be essential, while a fundamental feature of developing drugs against drug-resistant TB will be the identification of new mechanisms of action.[66,67]

Research into the mechanism of host immunity evasion, metabolism of persisting bacteria, and identification of genes essential for *Mtb* growth have yielded novel insights into potential targets for the development drugs with novel mechanisms of action, both against replicating

and non-replicative TB.[68-70] Though, a complicating factor in the development of TB therapeutics is that drug candidates often exhibit poor penetration to persisting bacteria, which often reside within granulomas and macrophages, presenting complex pharmacokinetic and pharmacodynamic requirements.[71,72]

Besides challenges of the development of drug candidates regarding drug target identification, potency, and pharmacokinetic properties, the clinical trial phases of the drug development process are further complicated by a variety of factors.[66] The slow doubling time of *Mtb* requires extended growth of sputum cultures to assess bacterial load, and limited biomarkers of drug efficacy are available.[66] In addition, the lengthy treatment regimen of the current first-line TB treatment must be considered, necessitating a minimum of six-months of treatment in any phase 3 clinical trial, as well as lengthy follow-up times, in order to measure relapse rate.[66] Further, the normally high efficacy of current TB chemotherapies under controlled clinical trial conditions makes the demonstration of noninferiority of a new regimen particularly challenging, and requires a large number of patients, leading to lengthy enrolment periods.[66] Lastly, as monotherapy is known to be at risk towards the development of resistance, the testing of single drugs in clinical trials is unethical, and may not be performed beyond studies of early bactericidal activity of maximum 14 days.[73,74]

1.4.2 Recent advances in tuberculosis treatment

Despite the challenges described in Section 1.4.1, drug discovery and development projects from various industrial, academic, and non-profit organisations, have generated advances in the TB treatment strategies, and the first three new anti-TB drugs in over 50 years have now been approved (Figure 1.3). Among these is bedaquiline, an inhibitor of ATP synthesis via targeting of the membrane bound F_1F_o synthase complex with notable bactericidal activity.[75] It was approved in 2012 by the U.S. Food and Drug Administration (FDA) for use in MDR-TB and XDR-TB, and is currently recommended by the WHO as a class A drug in the treatment of MDR-TB.[50,76] Another novel anti-TB drug, pretomanid, was approved by the FDA in 2019, and currently has a place in the recommended treatment of MDR- and XDR-TB.[77] It exhibits potent activity against both replicating and non-replicating *Mtb* via two distinct mechanisms of action; under aerobic conditions it acts as inhibitor of protein and lipid synthesis of cell wall components, and under anaerobic conditions it generates des-nitro metabolites and nitric oxide is released.[78-80] A third novel anti-TB drug, delamanid, belong to the same chemical class as pretomanid (the nitroimidazoles), and has a similar mechanism of action.[81] Delamanid was approved by the European Medicines Agency in 2014, and is recommended to be considered in the treatment of MDR-TB as a class C drug.[81]

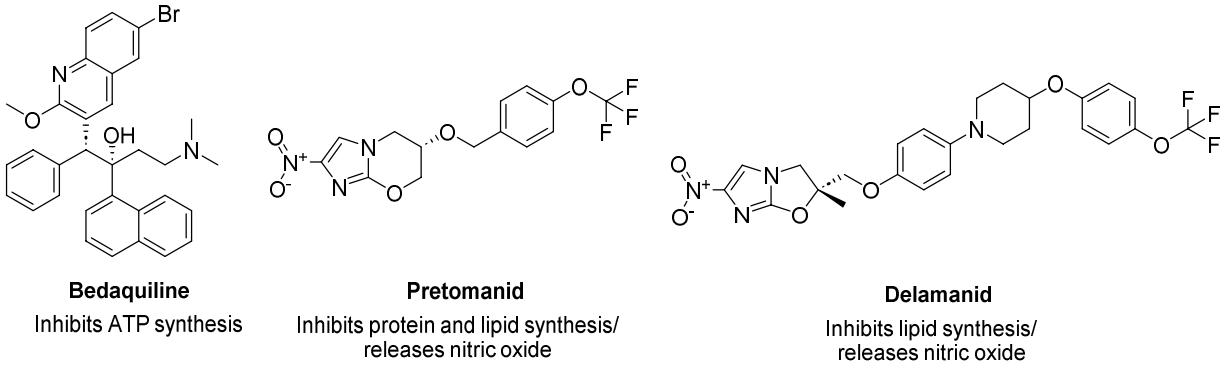

Figure 1.3. Recent approved drugs for the treatment of tuberculosis and their mechanism of action.

In addition to the approval of three novel drugs that are functional against drug resistant TB, assessment of drug combinations and treatment lengths are advancing towards simpler and shorter treatment regimens. The use of rifapentine and moxifloxacin in a 4-month regimen was found to be non-inferior to the standard 2HREZ/4HR regimen in drug-susceptible TB.[82] The approval of the novel TB drugs allowed for the development of the first 6-month regimen for MDR- and XDR-TB consisting of only three drugs: bedaquiline, pretomanid, and linezolid.[83] However, though representing progress, patients still require even shorter, safer, and more effective treatments.[67]

1.4.3 Tuberculosis drugs in the pipeline

The current pipeline of TB drug development exhibits an apparently diverse collection of 9 novel antibacterial classes, and 7 novel targets, with a total of 16 compounds being in clinical development, as of 2023 (Figure 1.4).[84,85] In addition, there are 12 new molecular entities in preclinical development, and numerous projects at the lead optimisation stage.[84] Genetic-based approaches appear to have significantly expanded the target-space of TB, and many of the compounds in development employ novel mechanisms of actions.[86] In addition, there are various compounds targeting known and clinically validated mechanisms, such as the oxazolidinones, targeting 23S rRNA binding similarly to linezolid,[87] the diarylquinolines, that inhibit ATP synthase analogously to bedaquiline,[88] and one β-lactam, targeting the peptidoglycan biosynthesis.[89]

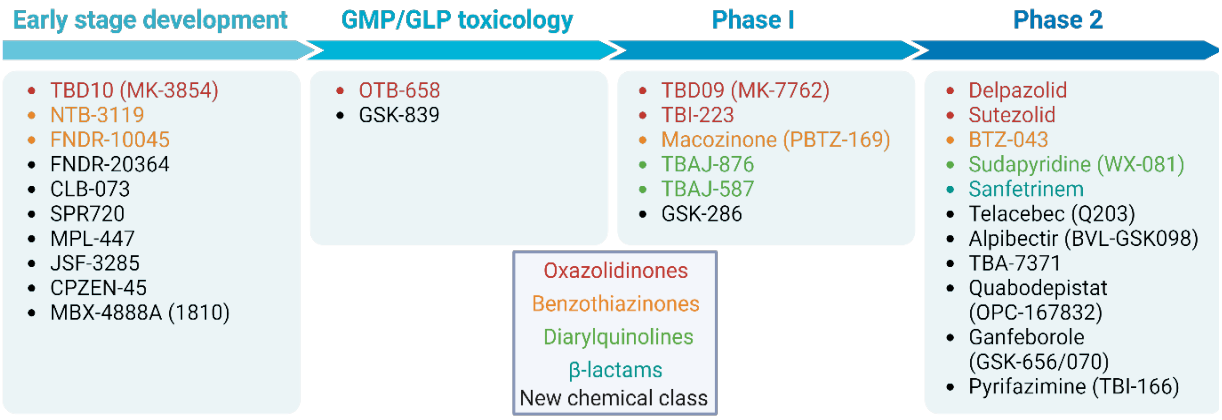

Figure 1.4. The current pipeline of TB drug development. As determined by the Working Group on new TB drugs, updated in November 2023.[84] Note that currently there are no reported phase 3 trials. Coloured compounds belong to known chemical classes, as indicated.

1.4.4 Repurposing of old drugs against tuberculosis

Repurposing of established drugs for novel targets is often considered to be relatively low in risk compared to the development of novel chemicals, as pharmacokinetics and pharmacodynamics, safety and toxicity profiles are already determined and optimised for such compounds, and this strategy may advance the investment of both time and funds. Drug repurposing has therefore been applied in various studies of anti-TB drug development, several leading to inclusion into second-line treatment recommendations for MDR- and XDR-TB,[90] and many more currently being considered in *in vitro* and *in vivo* studies, and in clinical trials.

Particularly anti-infectives have been considered in the repurposing towards anti-TB drugs. For example, fluoroquinolones (Figure 1.5) are broad-spectrum antibiotics that act as inhibitors of topoisomerase II and IV, disrupting DNA replication.[91] Studies with the newer generation fluoroquinolones moxifloxacin and gatifloxacin have exhibited potent inhibition against *Mtb in vitro* and *in vivo*, and led to the inclusion in the second-line treatment, and consideration for first-line treatment.[50,82,92] Another example are the oxazolidinones, e.g., linezolid, which is currently recommended to be used as a second-line TB therapeutic,[50,93] was originally used against gram-positive bacteria, acting by inhibition of protein synthesis through inhibition of the 50S ribosomal subunit.[94]

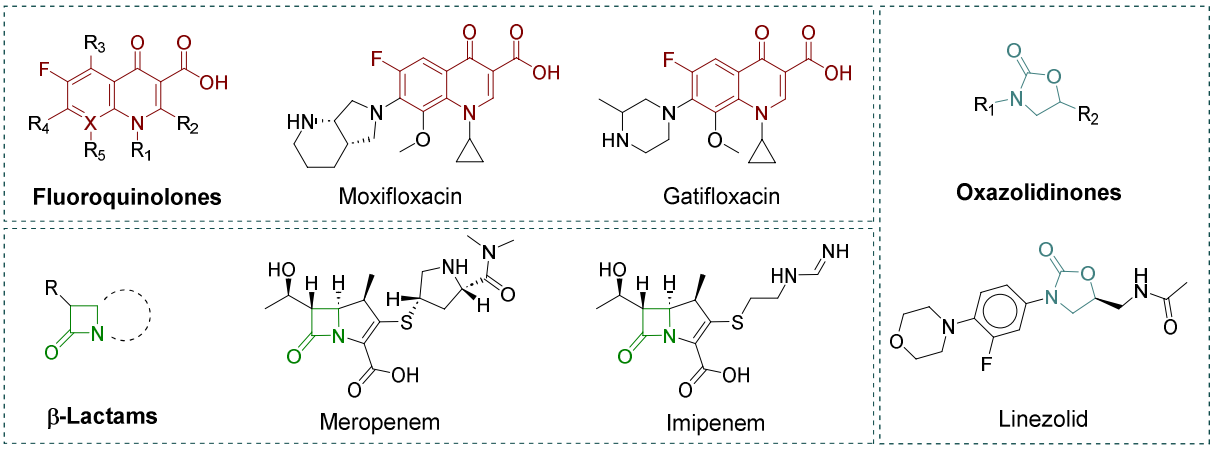

Figure 1.5. Examples of repurposed drugs for tuberculosis. The general structures of compounds classes are represented in red (fluoroquinolones), blue (oxazolidinones), or green (β-lactams).

β-Lactam antibiotics are among the most prescribed drugs in the clinic,[89] but have traditionally not been found to be effective against *Mtb*.[95] However, revisiting of this paradigm has identified various β-lactams with potent activity against *Mtb*.[96-98] Though clinical trials have failed to provide a conclusive place for β-lactams in the treatment of TB, imipenem and meropenem have been recommended to be considered as class C second-line treatment of MDR- and XDR-TB.[50,99-101] More details on the β-lactams targeting *Mtb* are described in Chapter 2.

Non-anti-infective agents have additionally been considered for the treatment of TB, and though this has not yet led to inclusion in the WHO recommended treatments, anti-TB properties have been reported.[102] Additionally, several non-steroidal anti-inflammatory drugs (NSAIDs, e.g., aspirin and ibuprofen) have been assessed as adjuvants, intended to keep inflammation at bay during treatment of TB while not having anti-mycobacterial effects.[103-105] Further, various anti-cancer, anti-psychotic, anti-diabetic, and cardiovascular drugs have shown promising activity against *Mtb in vitro* and *in vivo*.[90,102]

1.5 The mycobacterial cell wall

The unique cell wall of *Mtb*, and more generally mycobacteria, is a main feature of its innate resistance to many antimicrobial drugs, as well as its pathogenicity, with its low permeability and large number efflux pumps.[18] However, due to its importance it has been viewed as an Achilles' heel of the bacterium, and many front-line and second-line drugs (e.g., isoniazid, and ethambutol) target the cell wall biosynthesis.[106]

The main components of the mycobacterial cell wall are the peptidoglycan (PG) layer, the mycolic acid (MA) layer, and the arabinogalactan (AG) layer (Figure 1.6).[107] The PG layer is attached to the cell membrane of *Mtb*, which is in turn covalently attached to AG, while MA is

anchored to AG. This complex is considered as the cell wall core, or the MA-AG-PG complex (MAPc).[108] Besides the MAPc, the cell wall is made up of free lipids, phosphatidyl inositol mannosides, lipomannans, and lipoarabinomannans.[107] The PG layer in particular has been found to be playing a key role in cell growth, cell-cell communication, initiation of the host immune response, and has been found to be highly dynamic based on the cell's environment and metabolic state, and is therefore of particular interest.[106]

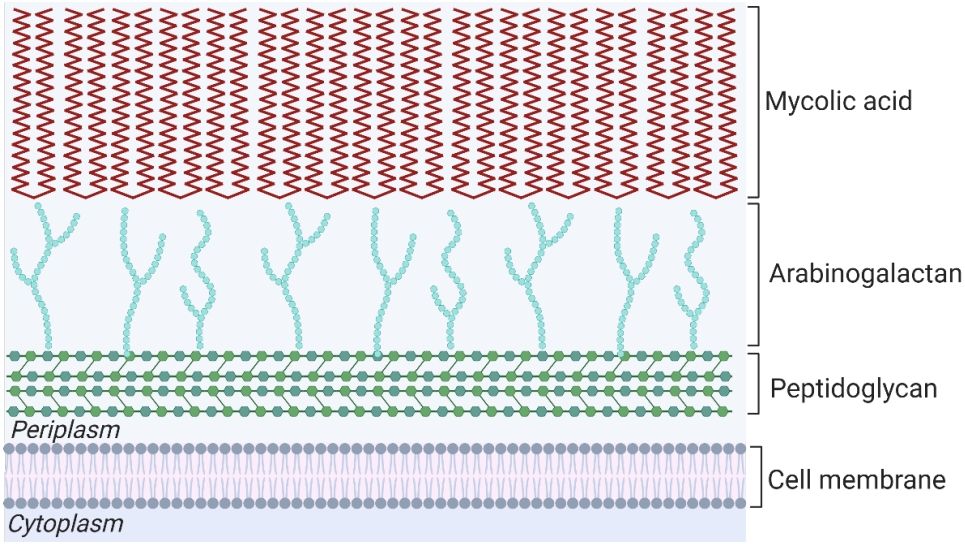

Figure 1.6. Main cell wall components of *Mycobacterium tuberculosis*. The figure was created using BioRender.com.

1.5.1 Peptidoglycan structure of *Mycobacterium tuberculosis*

The *Mtb* PG is made up of glycan strands with alternating *N*-acetylglucosamine (GlcNAc) and *N*-acetylmuramic acid (MurNAc) residues, connected via β(1→4) linkages,[109] where in some cases the *N*-acyl group of MurNAc has been oxidised to an *N*-glycolyl group (MurNGlyc).[110,111] The D-lactoyl residue of each MurNAc residue is linked to a penta- tetra- or tri-peptide stem with the sequence L-Ala^{1}-D-iGlu$_{NH2}$^{2}-*m*-DAP$_{NH2}$^{3}-D-Ala^{4}-D-Ala^{5}, and adjacent peptide stems may be cross-linked between the D-Ala^{4} and *m*-DAP$_{NH2}$^{3} (4→3 cross-links), or between *m*-DAP$_{NH2}$^{3} and *m*-DAP$_{NH2}$^{3} (3→3 cross-links).[112,113] Characteristic to mycobacteria is the high level of 3→3 cross-links during the stationary phase of growth, reaching up to 80%, while in most organisms the 4→3 cross-links are dominant.[114]

Virtually all bacteria contain a peptidoglycan layer, which is relatively thick in gram-positive bacteria (20-100 nm), and thinner in gram-negative bacteria (5-10 nm), while the width of the peptidoglycan layer of *Mtb* lies in between (10-20 nm).[115,116] Structurally, peptidoglycan is relatively conserved between bacteria, though small differences may be present, such as *N*-deacetylation or *O*-acetylation of GlcNAc and MurNAc, respectively, *N*-glycolylation of

MurNAc, and variations in peptide stem sequence, which in gram-negative bacteria typically consists of L-Ala[1]-γ-D-Glu[2]-*m*-DAP[3]-D-Ala[4]-D-Ala[5], while gram-positive bacteria typically contain an L-Lys residue in lieu of *m*-DAP. The *Mtb* PG peptide stems undergo amidation of D-iGlu (D-iGlu$_{NH2}$) and *m*-DAP (*m*-DAP$_{NH2}$).[117] D-iGlu amidation is thought to be of particular importance for the function of PG transpeptidases,[118,119] while *m*-DAP amidation is hypothesised to be involved in modulation of PG hydrolysis,[120,121] and evasion of the host immune response,[122-124] but may also modulate the function of PG transpeptidases.[125]

1.5.2 Biosynthesis of peptidoglycan precursors

The PG biosynthesis pathway (Figure 1.7) is relatively well characterised in several species, such as *Escherichia coli*. The PG biosynthesis pathway remains largely uncharacterised in *Mtb*, but it is generally assumed to be analogous to that of *E. coli*.[106,107]

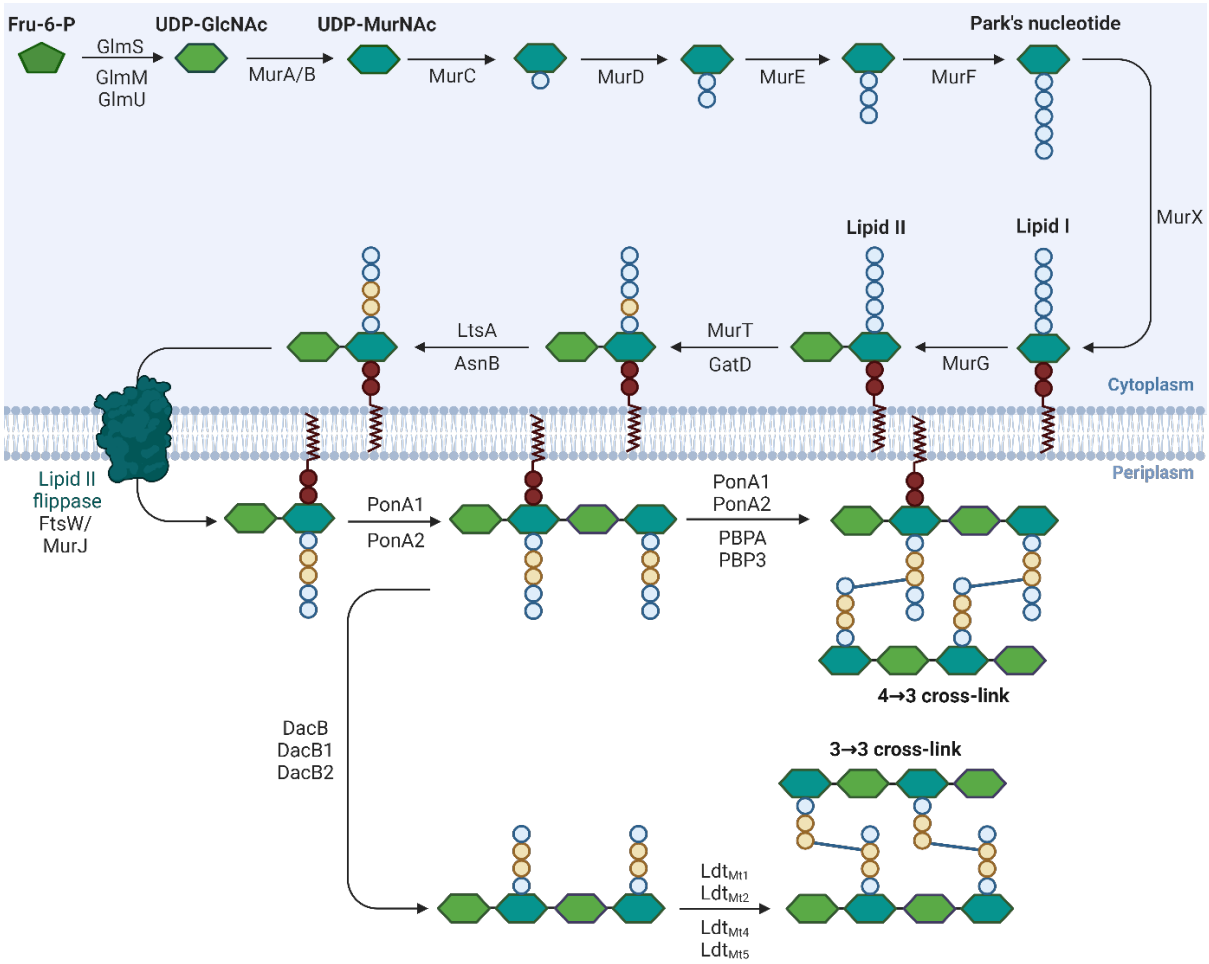

Figure 1.7. Proposed peptidoglycan biosynthesis pathway of *Mycobacterium tuberculosis*. Unmodified amino acids are in blue, and amidated amino acids are in yellow. The figure was created using BioRender.com.

PG biosynthesis is initiated in the cytoplasm with the conversion of fructose-6-phosphate (Fru-6-P), catalysed by GlmS, GlmM, and GlmU.[126] UDP-MurNAc is formed from UDP-GlcNAc, catalysed by MurA and MurB.[127] This is followed by the successive addition of L-Ala (by MurC), D-iGlu (by MurD), *m*-DAP (by MurE), and D-Ala-D-Ala (by MurF).[128] UDP-MurNAc-pentapeptide (also known as Park's nucleotide) is then transferred onto a decaprenyl phosphate lipid by MurX, to form lipid I. UDP-GlcNAc is then attached to lipid I by the glycosyltransferase MurG, thus forming lipid II.[129,130] Amidation of D-iGlu of both lipid I and lipid II is catalysed by MurT and GatD,[118,131] and amidation of *m*-DAP likely occurs on lipid II by LtsA and AsnB.[120,132] Following these modifications, lipid II is transported to the outer face of the cytoplasmic membrane, into the periplasmic space.

The identity of the lipid II flippase has not fully been elucidated, though likely involves either FtsW or MurJ. Assays with fluorescently labelled lipid II suggested FtsW, and not MurJ, is able to transport lipid II across bacterial membrane,[133] though genetic analysis suggests FtsW may instead act as glycosyltransferase.[134,135] Alternatively, deletion of *murJ* in *E. coli* leads to accumulation of precursors in the cytoplasm.[136,137] Further, non-denaturing mass spectrometry studies have established binding of lipid II with MurJ, and a colicin M-based assay suggests flippase activity across the membrane.[138,139]

1.5.3 Transpeptidases of *Mycobacterium tuberculosis*

Once across the cytoplasmic membrane, the class A penicillin-binding proteins (PBPs) PonA1 and PonA2, carry out both transpeptidase and glycosyltransferase activity using lipid II as a substrate, forming both β(1→4) linkages between GlcNAc and MurNAc, and 4→3 cross-links.[140,141] PonA1 and PonA2 have both been observed to be important in determining cell shape and viability, and PonA1 has particular importance in regulation of PG hydrolysis,[142] while PonA2 plays a role in the adaption into dormancy.[143] Two class B PBPs, PBPA and PBP3, also catalyse the formation of 4→3 cross-links, and are both involved in cell division and maintenance of cell shape, with particularly PBP3 being essential for cell division.[144-147] The class C PBPs DacB, DacB1, DacB2, catalyse the formation of tetrapeptide chains through the cleavage of the terminal D-Ala of pentapeptide chains.[148,149]

The 3→3 cross-links are formed between tetrapeptide chains, catalysed by the L,D-transpeptidases (Ldts). While the 3→3 cross-links have been identified in 1974,[150] their importance was not fully appreciated until the observation that 3→3 cross-links are dominant over 4→3 cross-links in the stationary phase of growth of *Mtb*.[114] *Mtb* contains five Ldts, Ldt_{Mt1-5}, and of these Ldt_{Mt2} has been identified as the main Ldt; loss of the ldt_{Mt2} gene led to loss of virulence, altered colony morphology, and increased susceptibility to β-lactams.[151] The precise

function of Ldts and their interplay with PBPs is not fully elucidated, though they are thought to be of particular importance for maintaining cell shape in the aging cell, and to be of importance for the physiology of persister *Mtb*.[152] Ldts, and particularly Ldt_{Mt2}, are thus considered as targets for the development of novel anti-TB therapeutics.

Ldt catalysis (Figure 1.8) revolves around a nucleophilic cysteine residue, which reacts with the L-chiral centre of the third residue of the donor tetrapeptide to form an acyl-enzyme complex, which then reacts with the D-chiral centre of the third residue of the acceptor tetrapeptide.[153,154] The reactivity of the catalytic cysteine residue is increased via the presence of a histidine residue, acting as base, and the backbone carbonyl of a serine residue, acting as acid, forming a catalytic triad often observed in enzymes employing nucleophilic cysteine in catalysis.[155] The tetrahedral intermediate of the initial step in catalysis is hypothesised to be stabilised by the oxyanion hole consisting of the backbone nitrogen atoms of the nucleophilic cysteine residue, and neighbouring glycine and histidine residues, in the Ldt-conserved $Hxx_{14\text{-}17}$(S/T)HGChN motif, in which h represents a hydrophobic residue.[155]

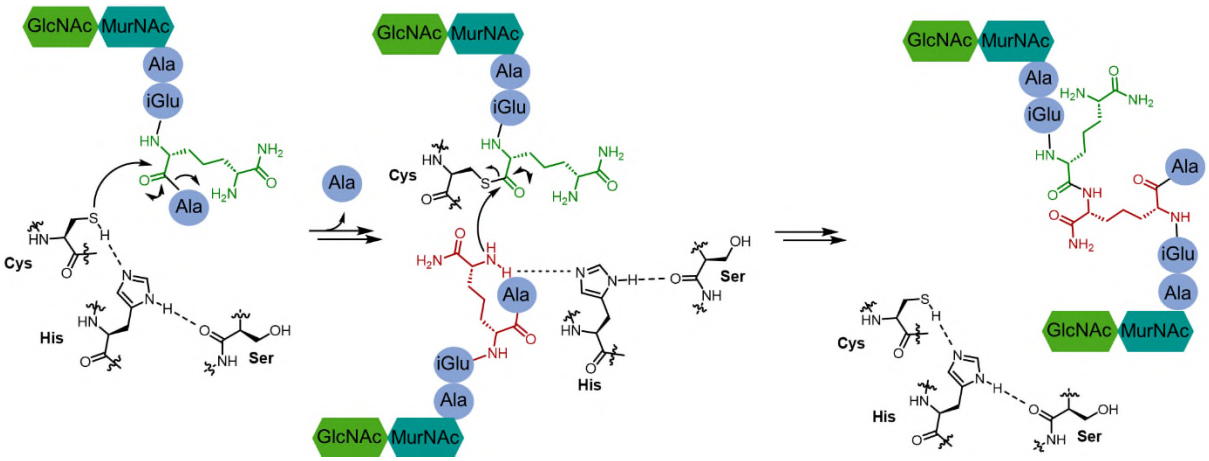

Figure 1.8. Outline of the proposed catalysis of the L,D-transpeptidases of *Mycobacterium tuberculosis*.

1.5.4 Inhibition of L,D-transpeptidases

Though several anti-TB drugs (e.g., isoniazid, ethambutol, pretomanid, and delamanid) act via inhibition of the cell wall biosynthesis, the most important class of antibiotics, the β-lactams – which inhibit cell wall biosynthesis through covalent inactivation of PBPs – have historically been considered as being ineffective against *Mtb*.[95] This is likely due to various resistance mechanisms, particularly the presence of the Ambler class A serine β-lactamase (SBL) BlaC, which has a broad spectrum of β-lactam substrates, hydrolysing all classes of β-lactams with particular penicillinase and cephalosporinase activity.[156,157] Additionally, the importance of the Ldts in *Mtb* has been assigned as contributing to β-lactam resistance, as most β-lactams are

unable to efficiently inhibit Ldts.[158] An exception to this are the carbapenem β-lactams, which are able to interact with all five Ldt paralogs of *Mtb* through covalent interaction with the active site cysteine residue.[159-163] Indeed, carbapenems in combination with a β-lactamase inhibitor have exhibited activity against *Mtb* both *in vitro* and *in vivo*,[96-98] and the only two β-lactams currently considered for the treatment of MDR- and XDR-TB are the carbapenems meropenem and imipenem, though they are currently only considered for use if other treatment options are not sufficient, or contra-indicated.[50] It is likely that optimisation of β-lactams for use against Ldts, or in particular *Mtb* Ldts, will be required to obtain clinically relevant activity, in particular for targeting *Mtb* in macrophages. Though several optimisation studies of carbapenems have been initiated,[160,164-167] the search for potent inhibitors of Ldts, and specifically Ldt_{Mt2}, is still ongoing.

1.6 Research objectives

Inhibition of the bacterial transpeptidases a validated mechanism of action for antibacterials, with β-lactams likely being the most successful class of antibacterials. Though not traditionally applied in the treatment of *Mtb*, inhibition of transpeptidases by β-lactams shows promise, though optimisation is likely required. However, the optimisation is complicated by the large variety of interaction partners, consisting of transpeptidases (Ldts and PBPs) and resistance mechanisms including the β-lactamase BlaC. Particularly the apparent redundancy of the *Mtb* transpeptidases imposes a complication regarding the target-based optimisation of inhibitors. **Chapter 2** comprises a literature review of the function and inhibition of the targets of β-lactams in *Mtb*, i.e., PBPs, Ldts, and BlaC, as well as summarising the reported optimisation studies of β-lactams against *Mtb*.

Inhibition studies of Ldt_{Mt2}, the essential Ldt of *Mtb*, have focussed primarily on β-lactams, though inhibition by cysteine-reactive reactive compounds, e.g., ebselen, has also been observed.[168] **Chapter 3 (Manuscript I)**, describes the identification of novel inhibitors of Ldt_{Mt2} obtained via high-throughput screening using a targeted library of electrophilic compounds, and studies of the mechanism of inhibition. **Chapter 4 (Manuscript II)** describes the mechanism of inhibition of a new class of mechanism-based inhibitors of nucleophilic cysteine enzymes (including Ldt_{Mt2}), the αβ,α′β′-diepoxyketones (DEKs).

The mechanism of the transpeptidase reaction catalysed by Ldt_{Mt2} is relatively unexplored. **Chapter 5 (Manuscript III)** describes studies on the mechanism of the transpeptidase reaction catalysed by Ldt_{Mt2}, using various biochemical and biophysical techniques, including X-ray crystallography.

Studies of the cellular inhibition the Ldt_{Mt2} inhibitors identified in Chapter 3 and 4 as well as a selection of β-lactam antibiotics against *M. smegmatis*, a validated model organism of *Mtb*,[169] are described in **Chapter 6 (Manuscript IV).**

Chapter 7 describes inhibition studies of BlaC, in particular with a cephalosporin identified in the high-throughput screen described in Chapter 3.

Chapter 8 summarises the results and puts them in perspective with regards to other reports on the inhibition of the transpeptidases of *Mtb*.

The studies described in this thesis aim to obtain insights into the mechanism and inhibition of Ldt_{Mt2}, and to increase understanding of the place of Ldt inhibition as a drug target of *Mtb*. Overall, these studies are intended to guide the development of novel therapeutics of *Mtb* with regards to the inhibition of Ldt_{Mt2} and related enzymes.

1.7 References

1 Global tuberculosis report 2022. . Report No. Licence: CC BY-NC-SA 3.0 IGO, (Geneva: World Health Organization, 2022).

2 Chakaya, J., Khan, M., Ntoumi, F., Aklillu, E., Fatima, R., Mwaba, P., Kapata, N., Mfinanga, S., Hasnain, S. E., Katoto, P. D. M. C., Bulabula, A. N. H., Sam-Agudu, N. A., Nachega, J. B., Tiberi, S., McHugh, T. D., Abubakar, I. & Zumla, A. Global Tuberculosis Report 2020 – Reflections on the Global TB burden, treatment and prevention efforts. *Int J Infect Dis.* **113**, S7-S12 (2021).

3 Floyd, K., Glaziou, P., Houben, R. M. G. J., Sumner, T., White, R. G. & Raviglione, M. Global tuberculosis targets and milestones set for 2016–2035: definition and rationale. *Int. J. Tuberc. Lung Dis.* **22**, 723-730 (2018).

4 Getahun, H., Matteelli, A., Chaisson, R. E. & Raviglione, M. Latent Mycobacterium tuberculosis Infection. *N. Engl. J. Med.* **372**, 2127-2135 (2015).

5 Houben, R. M. G. J. & Dodd, P. J. The Global Burden of Latent Tuberculosis Infection: A Re-estimation Using Mathematical Modelling. *PLoS Med.* **13**, e1002152 (2016).

6 Tiemersma, E. W., Van Der Werf, M. J., Borgdorff, M. W., Williams, B. G. & Nagelkerke, N. J. D. Natural History of Tuberculosis: Duration and Fatality of Untreated Pulmonary Tuberculosis in HIV Negative Patients: A Systematic Review. *PLoS One* **6**, e17601 (2011).

7 *Treatment of tuberculosis: guidelines*. (World Health Organization, 2010).

8 Seung, K. J., Keshavjee, S. & Rich, M. L. Multidrug-Resistant Tuberculosis and Extensively Drug-Resistant Tuberculosis. *Cold Spring Harb. Perspect. Med.* **5**, a017863 (2015).

9 Lomazzi, M., Borisch, B. & Laaser, U. The Millennium Development Goals: experiences, achievements and what's next. *Glob. Health Action* **7**, 23695 (2014).

10 Global tuberculosis report 2015, 20th ed., (Geneva: World Health Organization, 2015).

11 Uplekar, M., Weil, D., Lonnroth, K., Jaramillo, E., Lienhardt, C., Dias, H. M., Falzon, D., Floyd, K., Gargioni, G. & Getahun, H. WHO's new end TB strategy. *Lancet* **385**, 1799-1801 (2015).

12 Harling, G. & Castro, M. C. A spatial analysis of social and economic determinants of tuberculosis in Brazil. *Health Place.* **25**, 56-67 (2014).

13 Oxlade, O. & Murray, M. Tuberculosis and poverty: why are the poor at greater risk in India? *PloS One* **7**, e47533 (2012).

14 Hargreaves, J. R., Boccia, D., Evans, C. A., Adato, M., Petticrew, M. & Porter, J. D. The social determinants of tuberculosis: from evidence to action. *Am. J. Public Health.* **101**, 654-662 (2011).

15 Ghazy, R. M., El Saeh, H. M., Abdulaziz, S., Hammouda, E. A., Elzorkany, A. M., Khidr, H., Zarif, N., Elrewany, E. & Abd Elhafeez, S. A systematic review and meta-analysis of the catastrophic costs incurred by tuberculosis patients. *Sci. Rep.* **12**, 558 (2022).

16 Raviglione, M. & Sulis, G. Tuberculosis 2015: Burden, Challenges and Strategy for Control and Elimination. *Infect. Dis. Rep.* **8**, 6570 (2016).

17 Koch, R. Die Ätiologie der Tuberkulose. *Berliner Klinische Wochenschrift* **15**, 221-230 (1882).

18 Gordon, S. V. & Parish, T. Microbe Profile: *Mycobacterium tuberculosis*: Humanity's deadly microbial foe. *Microbiology (Reading, Engl.)* **164**, 437-439 (2018).

19 Cook, G. M., Berney, M., Gebhard, S., Heinemann, M., Cox, R. A., Danilchanka, O. & Niederweis, M. Physiology of mycobacteria. *Adv. Microb. Physiol.* **55**, 81-182, 318-189 (2009).

20 Fu, L. M. & Fu-Liu, C. S. Is *Mycobacterium tuberculosis* a closer relative to Gram-positive or Gram-negative bacterial pathogens? *Tuberculosis (Edinb.)* **82**, 85-90 (2002).

21 Brosch, R., Gordon, S. V., Marmiesse, M., Brodin, P., Buchrieser, C., Eiglmeier, K., Garnier, T., Gutierrez, C., Hewinson, G., Kremer, K., Parsons, L. M., Pym, A. S., Samper, S., van Soolingen, D. & Cole, S. T. A new evolutionary scenario for the *Mycobacterium tuberculosis* complex. *Proc. Natl. Acad. Sci. U.S.A.* **99**, 3684-3689 (2002).

22 Degiacomi, G., Sammartino, J. C., Chiarelli, L. R., Riabova, O., Makarov, V. & Pasca, M. R. *Mycobacterium abscessus*, an Emerging and Worrisome Pathogen among Cystic Fibrosis Patients. *Int. J. Mol. Sci.* **20** (2019).

23 Gopalaswamy, R., Shanmugam, S., Mondal, R. & Subbian, S. Of tuberculosis and non-tuberculous mycobacterial infections – a comparative analysis of epidemiology, diagnosis and treatment. *J. Biomed. Sci.* **27**, 74 (2020).

24 Ly, A. & Liu, J. Mycobacterial Virulence Factors: Surface-Exposed Lipids and Secreted Proteins. *Int. J. Mol. Sci.* **21** (2020).

25 Urdahl, K. B., Shafiani, S. & Ernst, J. D. Initiation and regulation of T-cell responses in tuberculosis. *Mucosal Immunol.* **4**, 288-293 (2011).

26 Rohini, K. & Srikumar, P. S. Insights from the docking and molecular dynamics simulation of the Phosphopantetheinyl transferase (PptT) structural model from *Mycobacterium tuberculosis*. *Bioinformation* **9**, 685-689 (2013).

27 Zhai, W., Wu, F., Zhang, Y., Fu, Y. & Liu, Z. The Immune Escape Mechanisms of *Mycobacterium Tuberculosis*. *Int. J. Mol. Sci.* **20** (2019).

28 Wolf, A. J., Desvignes, L., Linas, B., Banaiee, N., Tamura, T., Takatsu, K. & Ernst, J. D. Initiation of the adaptive immune response to *Mycobacterium tuberculosis* depends on antigen production in the local lymph node, not the lungs. *J. Exp. Med.* **205**, 105-115 (2008).

29 Ottenhoff, T. H. & Kaufmann, S. H. Vaccines against tuberculosis: where are we and where do we need to go? *PLoS Pathog.* **8**, e1002607 (2012).

30 Gonzalez-Juarrero, M., Turner, O. C., Turner, J., Marietta, P., Brooks, J. V. & Orme, I. M. Temporal and spatial arrangement of lymphocytes within lung granulomas induced by aerosol infection with *Mycobacterium tuberculosis*. *Infect. Immun.* **69**, 1722-1728 (2001).

31 Puissegur, M. P., Botanch, C., Duteyrat, J. L., Delsol, G., Caratero, C. & Altare, F. An in vitro dual model of mycobacterial granulomas to investigate the molecular interactions between mycobacteria and human host cells. *Cell Microbiol.* **6**, 423-433 (2004).

32 Silva Miranda, M., Breiman, A., Allain, S., Deknuydt, F. & Altare, F. The tuberculous granuloma: an unsuccessful host defence mechanism providing a safety shelter for the bacteria? *Clin. Dev. Immunol.* **2012**, 139127 (2012).

33 Adams, D. O. The granulomatous inflammatory response. A review. *Am. J. Pathol.* **84**, 164-192 (1976).

34 Delogu, G., Sali, M. & Fadda, G. The biology of *Mycobacterium tuberculosi*s infection. *Mediterr. J. Hematol. Infect. Dis.* **5**, e2013070 (2013).

35 Blaser, M. J. & Kirschner, D. The equilibria that allow bacterial persistence in human hosts. *Nature* **449**, 843-849 (2007).

36 Chao, M. C. & Rubin, E. J. Letting sleeping dos lie: does dormancy play a role in tuberculosis? *Annu. Rev. Microbiol.* **64**, 293-311 (2010).

37 Gengenbacher, M. & Kaufmann, S. H. *Mycobacterium tuberculosis*: success through dormancy. *FEMS Microbiol. Rev.* **36**, 514-532 (2012).

38 Comstock, G. W., Livesay, V. T. & Woolpert, S. F. The prognosis of a positive tuberculin reaction in childhood and adolescence. *Am. J. Epidemiol.* **99**, 131-138 (1974).

39 Pawlowski, A., Jansson, M., Sköld, M., Rottenberg, M. E. & Källenius, G. Tuberculosis and HIV co-infection. *PLoS Pathog.* **8**, e1002464 (2012).

40 Jick, S. S., Lieberman, E. S., Rahman, M. U. & Choi, H. K. Glucocorticoid use, other associated factors, and the risk of tuberculosis. *Arthritis Rheum.* **55**, 19-26 (2006).

41 Keane, J. & Bresnihan, B. Tuberculosis reactivation during immunosuppressive therapy in rheumatic diseases: diagnostic and therapeutic strategies. *Curr. Opin. Rheumatol.* **20** (2008).

42 Sidhu, A., Verma, G., Humar, A. & Kumar, D. Outcome of Latent Tuberculosis Infection in Solid Organ Transplant Recipients Over a 10-Year Period. *Transplantation* **98** (2014).

43 Cordonnier, C., Martino, R., Trabasso, P., Held, T. K., Akan, H., Ward, M. S., Fabian, K., Ullmann, A. J., Wulffraat, N., Ljungman, P., Alessandrino, E. P., Pretnar, J., Gmür, J., Varela, R., Vitek, A., Sica, S. & Rovira, M. Mycobacterial infection: a difficult and late diagnosis in stem cell transplant recipients. *Clin. Infect. Dis.* **38**, 1229-1236 (2004).

44 Lawn, S. D. & Zumla, A. I. Tuberculosis. *Lancet* **378**, 57-72 (2011).

45 Dubos, R. J. & Dubos, J. *The white plague: tuberculosis, man, and society*. (Rutgers University Press, 1987).

46 Johnston, W. *The modern epidemic: A history of tuberculosis in Japan*. (Harvard Univ Asia Center, 1995).

47 Robitzek, E. H. & Selikoff, I. J. Hydrazine derivatives of isonicotinic acid (rimifon marsilid) in the treatment of active progressive caseous-pneumonic tuberculosis; a preliminary report. *Am. Rev. Tuberc.* **65**, 402-428 (1952).

48 Murray, J. F., Schraufnagel, D. E. & Hopewell, P. C. Treatment of Tuberculosis. A Historical Perspective. *Ann. Am. Thorac. Soc.* **12**, 1749-1759 (2015).

49 Chaves Torres, N. M., Quijano Rodríguez, J. J., Porras Andrade, P. S., Arriaga, M. B. & Netto, E. M. Factors predictive of the success of tuberculosis treatment: A systematic review with meta-analysis. *PLoS One* **14**, e0226507 (2019).

50 WHO consolidated guidelines on tuberculosis. Report No. ISBN-13: 978-92-4-006312-9, (Geneva: World Health Organization, 2022).

51 Lan, Z., Ahmad, N., Baghaei, P., Barkane, L., Benedetti, A., Brode, S. K., Brust, J. C. M., Campbell, J. R., Chang, V. W. L., Falzon, D., Guglielmetti, L., Isaakidis, P., Kempker, R. R., Kipiani, M., Kuksa, L., Lange, C., Laniado-Laborín, R., Nahid, P., Rodrigues, D., Singla, R., Udwadia, Z. F. & Menzies, D. Drug-associated adverse events in the treatment of multidrug-resistant tuberculosis: an individual patient data meta-analysis. *Lancet Respir. Med.* **8**, 383-394 (2020).

52 Verbeeck, R. K., Günther, G., Kibuule, D., Hunter, C. & Rennie, T. W. Optimizing treatment outcome of first-line anti-tuberculosis drugs: the role of therapeutic drug monitoring. *Eur. J. Clin. Pharmacol.* **72**, 905-916 (2016).

53 Rabahi, M. F., Silva Júnior, J., Ferreira, A. C. G., Tannus-Silva, D. G. S. & Conde, M. B. Tuberculosis treatment. *J. Bras. Pneumol.* **43**, 472-486 (2017).

54 Tola, H. H., Tol, A., Shojaeizadeh, D. & Garmaroudi, G. Tuberculosis Treatment Non-Adherence and Lost to Follow Up among TB Patients with or without HIV in Developing Countries: A Systematic Review. *Iran J. Public Health* **44**, 1-11 (2015).

55 Keshavjee, S. & Farmer, P. E. Tuberculosis, Drug Resistance, and the History of Modern Medicine. *N. Engl. J. Med.* **367**, 931-936 (2012).

56 Cegielski, J. P. Extensively drug-resistant tuberculosis: "there must be some kind of way out of here". *Clin. Infect. Dis.* **50 Suppl 3**, S195-200 (2010).

57 Lin, H., Shin, S., Blaya, J. A., Zhang, Z., Cegielski, P., Contreras, C., Asencios, L., Bonilla, C., Bayona, J., Paciorek, C. J. & Cohen, T. Assessing spatiotemporal patterns of multidrug-resistant and drug-sensitive tuberculosis in a South American setting. *Epidemiol. Infect.* **139**, 1784-1793 (2011).

58 in *Latent tuberculosis infection: updated and consolidated guidelines for programmatic management* (World Health Organization, 2018).

59 Balcells, M. E., Thomas, S. L., Godfrey-Faussett, P. & Grant, A. D. Isoniazid preventive therapy and risk for resistant tuberculosis. *Emerg. Infect. Dis.* **12**, 744-751 (2006).

60 den Boon, S., Matteelli, A. & Getahun, H. Rifampicin resistance after treatment for latent tuberculous infection: a systematic review and meta-analysis. *Int. J. Tuberc. Lung Dis.* **20**, 1065-1071 (2016).

61 Gomez, J. E. & McKinney, J. D. *M. tuberculosis* persistence, latency, and drug tolerance. *Tuberculosis (Edinb.)* **84**, 29-44 (2004).

62 Zhang, Y., Yew, W. W. & Barer, M. R. Targeting persisters for tuberculosis control. *Antimicrob. Agents Chemother.* **56**, 2223-2230 (2012).

63 Zhang, Y. Persisters, persistent infections and the Yin-Yang model. *Emerg. Microbes Infect.* **3**, e3 (2014).

64 Monack, D. M., Mueller, A. & Falkow, S. Persistent bacterial infections: the interface of the pathogen and the host immune system. *Nat. Rev. Microbiol.* **2**, 747-765 (2004).

65 Donald, P. R., Sirgel, F. A., Botha, F. J., Seifart, H. I., Parkin, D. P., Vandenplas, M. L., Van de Wal, B. W., Maritz, J. S. & Mitchison, D. A. The early bactericidal activity of isoniazid related to its dose size in pulmonary tuberculosis. *Am. J. Respir. Crit. Care Med.* **156**, 895-900 (1997).

66 Ginsberg, A. M. & Spigelman, M. Challenges in tuberculosis drug research and development. *Nature Med.* **13**, 290-294 (2007).

67 Dartois, V. A. & Rubin, E. J. Anti-tuberculosis treatment strategies and drug development: challenges and priorities. *Nature Rev. Microbiol.* **20**, 685-701 (2022).

68 Cole, S. T., Brosch, R., Parkhill, J., Garnier, T., Churcher, C., Harris, D., Gordon, S. V., Eiglmeier, K., Gas, S., Barry, C. E., Tekaia, F., Badcock, K., Basham, D., Brown, D., Chillingworth, T., Connor, R., Davies, R., Devlin, K., Feltwell, T., Gentles, S., Hamlin, N., Holroyd, S., Hornsby, T., Jagels, K., Krogh, A., McLean, J., Moule, S., Murphy, L., Oliver, K., Osborne, J., Quail, M. A., Rajandream, M. A., Rogers, J., Rutter, S., Seeger, K., Skelton, J., Squares, R., Squares, S., Sulston, J. E., Taylor, K., Whitehead, S. & Barrell, B. G. Deciphering the biology of *Mycobacterium tuberculosis* from the complete genome sequence. *Nature* **393**, 537-544 (1998).

69 Sassetti, C. M. & Rubin, E. J. Genetic requirements for mycobacterial survival during infection. *Proc. Natl. Acad. Sci. U.S.A.* **100**, 12989-12994 (2003).

70 Sassetti, C. M., Boyd, D. H. & Rubin, E. J. Genes required for mycobacterial growth defined by high density mutagenesis. *Mol. Microbiol.* **48**, 77-84 (2003).

71 Dhar, N., McKinney, J. & Manina, G. Phenotypic Heterogeneity in *Mycobacterium tuberculosis*. *Microbiol. Spectr.* **4** (2016).

72 Mashabela, G. T., de Wet, T. J. & Warner, D. F. *Mycobacterium tuberculosis* Metabolism. *Microbiol. Spectr.* **7** (2019).

73 Daniels, M. & Hill, A. B. Chemotherapy of Pulmonary Tuberculosis in Young Adults. *Br. Med. J.* **1**, 1162-1168 (1952).

74 Selkon, J. B., Devadatta, S., Kulkarni, K. G., Mitchison, D. A., Narayana, A. S., Nair, C. N. & Ramachandran, K. The emergence of isoniazid-resistant cultures in patients with pulmonary tuberculosis during treatment with isoniazid alone plus PAS. *Bull World Health Organ.* **31**, 273-294 (1964).

75 Palomino, J. C. & Martin, A. TMC207 becomes bedaquiline, a new anti-TB drug. *Future microbiol.* **8**, 1071-1080 (2013).

76 Mahajan, R. Bedaquiline: First FDA-approved tuberculosis drug in 40 years. *Int. J. Appl. Basic. Med. Res.* **3**, 1-2 (2013).

77 Occhineri, S., Matucci, T., Rindi, L., Tiseo, G., Falcone, M., Riccardi, N. & Besozzi, G. Pretomanid for tuberculosis treatment: an update for clinical purposes. *Curr. Res. Pharmacol. Drug Discov.* **3**, 100128 (2022).

78 Pstragowski, M., Zbrzezna, M. & Bujalska-Zadrozny, M. Advances in pharmacotherapy of tuberculosis. *Acta. Pol. Pharm.* **74**, 3-11 (2017).

79 Singh, R., Manjunatha, U., Boshoff, H. I., Ha, Y. H., Niyomrattanakit, P., Ledwidge, R., Dowd, C. S., Lee, I. Y., Kim, P., Zhang, L., Kang, S., Keller, T. H., Jiricek, J. & Barry, C. E., 3rd. PA-824 kills nonreplicating *Mycobacterium tuberculosis* by intracellular NO release. *Science* **322**, 1392-1395 (2008).

80 Malo, A., Kellermann, T., Ignatius, E. H., Dooley, K. E., Dawson, R., Joubert, A., Norman, J., Castel, S. & Wiesner, L. A validated liquid chromatography tandem mass spectrometry assay for the analysis of pretomanid in plasma samples from pulmonary tuberculosis patients. *J. Pharm. Biomed. Anal.* **195**, 113885 (2021).

81 Xavier, A. S. & Lakshmanan, M. Delamanid: A new armor in combating drug-resistant tuberculosis. *J. Pharmacol. Pharmacother.* **5**, 222-224 (2014).

82 Dorman, S. E., Nahid, P., Kurbatova, E. V., Phillips, P. P. J., Bryant, K., Dooley, K. E., Engle, M., Goldberg, S. V., Phan, H. T. T., Hakim, J., Johnson, J. L., Lourens, M., Martinson, N. A., Muzanyi, G., Narunsky, K., Nerette, S., Nguyen, N. V., Pham, T. H., Pierre, S., Purfield, A. E., Samaneka, W., Savic, R. M., Sanne, I., Scott, N. A., Shenje, J., Sizemore, E., Vernon, A., Waja, Z., Weiner, M., Swindells, S. & Chaisson, R. E. Four-Month Rifapentine Regimens with or without Moxifloxacin for Tuberculosis. *N. Engl. J. Med.* **384**, 1705-1718 (2021).

83 Conradie, F., Diacon, A. H., Ngubane, N., Howell, P., Everitt, D., Crook, A. M., Mendel, C. M., Egizi, E., Moreira, J., Timm, J., McHugh, T. D., Wills, G. H., Bateson, A., Hunt, R., Van Niekerk, C., Li, M., Olugbosi, M. & Spigelman, M. Treatment of Highly Drug-Resistant Pulmonary Tuberculosis. *N. Engl. J. Med.* **382**, 893-902 (2020).

84 *Working group on New TB Drugs*, https://www.newtbdrugs.org/pipeline/clinical (2023).

85 Black, T. A. & Buchwald, U. K. The pipeline of new molecules and regimens against drug-resistant tuberculosis. *J. Clin. Tuberc. Other Mycobact. Dis.* **25**, 100285 (2021).

86 Rock, J. Tuberculosis drug discovery in the CRISPR era. *PLoS Pathog.* **15**, e1007975 (2019).

87 Leach, K. L., Brickner, S. J., Noe, M. C. & Miller, P. F. Linezolid, the first oxazolidinone antibacterial agent. *Ann. N. Y. Acad. Sci.* **1222**, 49-54 (2011).

88 Koul, A., Dendouga, N., Vergauwen, K., Molenberghs, B., Vranckx, L., Willebrords, R., Ristic, Z., Lill, H., Dorange, I., Guillemont, J., Bald, D. & Andries, K. Diarylquinolines target subunit c of mycobacterial ATP synthase. *Nat. Chem. Biol.* **3**, 323-324 (2007).

89 Bush, K. & Bradford, P. A. β-Lactams and β-Lactamase Inhibitors: An Overview. *Cold Spring Harb. Perspect. Med.* **6** (2016).

90 Maitra, A., Bates, S., Kolvekar, T., Devarajan, P. V., Guzman, J. D. & Bhakta, S. Repurposing—a ray of hope in tackling extensively drug resistance in tuberculosis. *Int. J. Infect. Dis.* **32**, 50-55 (2015).

91 Drlica, K. & Zhao, X. DNA gyrase, topoisomerase IV, and the 4-quinolones. *Microbiol. Mol. Biol. Rev.* **61**, 377-392 (1997).

92 Moadebi, S., Harder, C. K., Fitzgerald, M. J., Elwood, K. R. & Marra, F. Fluoroquinolones for the treatment of pulmonary tuberculosis. *Drugs* **67**, 2077-2099 (2007).

93 Fortún, J., Martín-Dávila, P., Navas, E., Pérez-Elías, M. J., Cobo, J., Tato, M., De la Pedrosa, E. G. G., Gómez-Mampaso, E. & Moreno, S. Linezolid for the treatment of multidrug-resistant tuberculosis. *J. Antimicrob. Chemother.* **56**, 180-185 (2005).

94 Hashemian, S. M. R., Farhadi, T. & Ganjparvar, M. Linezolid: a review of its properties, function, and use in critical care. *Drug Des. Devel. Ther.* **12**, 1759-1767 (2018).

95 Wivagg, C. N., Bhattacharyya, R. P. & Hung, D. T. Mechanisms of β-lactam killing and resistance in the context of *Mycobacterium tuberculosis*. *J. Antibiot.* **67**, 645-654 (2014).
96 Gun, M. A., Bozdogan, B. & Coban, A. Y. Tuberculosis and beta-lactam antibiotics. *Future Microbiol.* **15**, 937-944 (2020).
97 Jaganath, D., Lamichhane, G. & Shah, M. Carbapenems against *Mycobacterium tuberculosis*: a review of the evidence. *Int. J. Tuberc. Lung Dis.* **20**, 1436-1447 (2016).
98 Story-Roller, E. & Lamichhane, G. Have we realized the full potential of β-lactams for treating drug-resistant TB? *IUBMB Life* **70**, 881-888 (2018).
99 Diacon, A. H., van der Merwe, L., Barnard, M., von Groote-Bidlingmaier, F., Lange, C., García-Basteiro, A. L., Sevene, E., Ballell, L. & Barros-Aguirre, D. β-Lactams against Tuberculosis — New Trick for an Old Dog? *N. Engl. J. Med.* **375**, 393-394 (2016).
100 Sotgiu, G., D'Ambrosio, L., Centis, R., Tiberi, S., Esposito, S., Dore, S., Spanevello, A. & Migliori, G. B. Carbapenems to Treat Multidrug and Extensively Drug-Resistant Tuberculosis: A Systematic Review. *Int. J. Mol. Sci.* **17**, 373 (2016).
101 Tiberi, S., Sotgiu, G., D'Ambrosio, L., Centis, R., Abdo Arbex, M., Alarcon Arrascue, E., Alffenaar, J. W., Caminero, J. A., Gaga, M., Gualano, G., Skrahina, A., Solovic, I., Sulis, G., Tadolini, M., Alarcon Guizado, V., De Lorenzo, S., Roby Arias, A. J., Scardigli, A., Akkerman, O. W., Aleksa, A., Artsukevich, J., Auchynka, V., Bonini, E. H., Chong Marín, F. A., Collahuazo López, L., de Vries, G., Dore, S., Kunst, H., Matteelli, A., Moschos, C., Palmieri, F., Papavasileiou, A., Payen, M. C., Piana, A., Spanevello, A., Vargas Vasquez, D., Viggiani, P., White, V., Zumla, A. & Migliori, G. B. Comparison of effectiveness and safety of imipenem/clavulanate- versus meropenem/clavulanate-containing regimens in the treatment of MDR- and XDR-TB. *Eur. Respir. J.* **47**, 1758-1766 (2016).
102 Sharma, K., Ahmed, F., Sharma, T., Grover, A., Agarwal, M. & Grover, S. Potential Repurposed Drug Candidates for Tuberculosis Treatment: Progress and Update of Drugs Identified in Over a Decade. *ACS Omega* **8**, 17362-17380 (2023).
103 Kroesen, V. M., Rodríguez-Martínez, P., García, E., Rosales, Y., Díaz, J., Martín-Céspedes, M., Tapia, G., Sarrias, M. R., Cardona, P.-J. & Vilaplana, C. A beneficial effect of low-dose aspirin in a murine model of active tuberculosis. *Front. immunol.* **9**, 798 (2018).
104 Guzman, J. D., Evangelopoulos, D., Gupta, A., Birchall, K., Mwaigwisya, S., Saxty, B., McHugh, T. D., Gibbons, S., Malkinson, J. & Bhakta, S. Antitubercular specific activity of ibuprofen and the other 2-arylpropanoic acids using the HT-SPOTi whole-cell phenotypic assay. *BMJ open* **3**, e002672 (2013).
105 Padiadpu, J., Baloni, P., Anand, K., Munshi, M., Thakur, C., Mohan, A., Singh, A. & Chandra, N. Identifying and Tackling Emergent Vulnerability in Drug-Resistant Mycobacteria. *ACS Infect. Dis.* **2**, 592-607 (2016).
106 Maitra, A., Munshi, T., Healy, J., Martin, L. T., Vollmer, W., Keep, N. H. & Bhakta, S. Cell wall peptidoglycan in *Mycobacterium tuberculosis*: An Achilles' heel for the TB-causing pathogen. *FEMS Microbiol. Rev.* **43**, 548-575 (2019).
107 Alderwick, L. J., Harrison, J., Lloyd, G. S. & Birch, H. L. The Mycobacterial Cell Wall--Peptidoglycan and Arabinogalactan. *Cold Spring Harb. Perspect. Med.* **5**, a021113 (2015).
108 Brennan, P. J. Structure, function, and biogenesis of the cell wall of *Mycobacterium tuberculosis*. *Tuberculosis (Edinb.)* **83**, 91-97 (2003).
109 Lederer, E., Adam, A., Ciorbaru, R., Petit, J. F. & Wietzerbin, J. Cell walls of Mycobacteria and related organisms; chemistry and immunostimulant properties. *Mol. Cell Biochem.* **7**, 87-104 (1975).
110 Mahapatra, S., Crick, D. C. & Brennan, P. J. Comparison of the UDP-N-acetylmuramate: L-alanine ligase enzymes from *Mycobacterium tuberculosis* and *Mycobacterium leprae*. *J. Bacteriol.* **182**, 6827-6830 (2000).

111 Raymond, J. B., Mahapatra, S., Crick, D. C. & Pavelka, M. S., Jr. Identification of the namH gene, encoding the hydroxylase responsible for the N-glycolylation of the mycobacterial peptidoglycan. *J. Biol. Chem.* **280**, 326-333 (2005).

112 Ghuysen, J. M. Use of bacteriolytic enzymes in determination of wall structure and their role in cell metabolism. *Bacteriol. Rev.* **32**, 425-464 (1968).

113 Wietzerbin-Falszpan, J., Das, B. C., Azuma, I., Adam, A., Petit, J. F. & Lederer, E. Isolation and mass spectrometric identification of the peptide subunits of mycobacterial cell walls. *Biochem. Biophys. Res. Commun.* **40**, 57-63 (1970).

114 Lavollay, M., Arthur, M., Fourgeaud, M., Dubost, L., Marie, A., Veziris, N., Blanot, D., Gutmann, L. & Mainardi, J. L. The Peptidoglycan of Stationary-Phase *Mycobacterium tuberculosis* Predominantly Contains Cross-Links Generated by L,D-Transpeptidation. *J. Bacteriol.* **190**, 4360-4366 (2008).

115 Silhavy, T. J., Kahne, D. & Walker, S. The bacterial cell envelope. *Cold Spring Harb. Perspect. Biol.* **2**, a000414 (2010).

116 Schoonmaker, M. K., Bishai, W. R. & Lamichhane, G. Nonclassical Transpeptidases of *Mycobacterium tuberculosis* Alter Cell Size, Morphology, the Cytosolic Matrix, Protein Localization, Virulence, and Resistance to β-Lactams. *J. Bacteriol.* **196**, 1394-1402 (2014).

117 Vollmer, W., Blanot, D. & De Pedro, M. A. Peptidoglycan structure and architecture. *FEMS Microbiol. Rev.* **32**, 149-167 (2008).

118 Figueiredo, T. A., Sobral, R. G., Ludovice, A. M., de Almeida, J. M. F., Bui, N. K., Vollmer, W., de Lencastre, H. & Tomasz, A. Identification of genetic determinants and enzymes involved with the amidation of glutamic acid residues in the peptidoglycan of *Staphylococcus aureus*. *PLoS pathog.* **8**, e1002508 (2012).

119 Zapun, A., Philippe, J., Abrahams, K. A., Signor, L., Roper, D. I., Breukink, E. & Vernet, T. In vitro reconstitution of peptidoglycan assembly from the Gram-positive pathogen *Streptococcus pneumoniae*. *ACS Chem. Biol.* **8**, 2688-2696 (2013).

120 Dajkovic, A., Tesson, B., Chauhan, S., Courtin, P., Keary, R., Flores, P., Marliere, C., Filipe, S. R., Chapot-Chartier, M. P. & Carballido-Lopez, R. Hydrolysis of peptidoglycan is modulated by amidation of meso-diaminopimelic acid and Mg2+ in *Bacillus subtilis*. *Mol. Microbiol.* **104**, 972-988 (2017).

121 Ghuysen, J. M., Nakel, M. & Kandler, O. Wall peptidoglycan in *Aerococcus viridans* strains 201 Evans and ATCC 11563 and in *Gaffkya homari* strain ATCC 10400. *Biochemistry* **10**, 2170-2175 (1971).

122 Roychowdhury, A., Wolfert, M. A. & Boons, G. J. Synthesis and proinflammatory properties of muramyl tripeptides containing lysine and diaminopimelic acid moieties. *ChemBioChem* **6**, 2088-2097 (2005).

123 Wolfert, M. A., Roychowdhury, A. & Boons, G.-J. Modification of the structure of peptidoglycan is a strategy to avoid detection by nucleotide-binding oligomerization domain protein 1. *Infect. Immun.* **75**, 706-713 (2007).

124 Wang, Q., Matsuo, Y., Pradipta, A. R., Inohara, N., Fujimoto, Y. & Fukase, K. Synthesis of characteristic Mycobacterium peptidoglycan (PGN) fragments utilizing with chemoenzymatic preparation of meso-diaminopimelic acid (DAP), and their modulation of innate immune responses. *Org. Biomol. Chem.* **14**, 1013-1023 (2016).

125 Ngadjeua, F., Braud, E., Saidjalolov, S., Iannazzo, L., Schnappinger, D., Ehrt, S., Hugonnet, J.-E., Mengin-Lecreulx, D., Patin, D., Ethève-Quelquejeu, M., Fonvielle, M. & Arthur, M. Critical Impact of Peptidoglycan Precursor Amidation on the Activity of L,D-Transpeptidases from *Enterococcus faecium* and *Mycobacterium tuberculosis*. *Chem. Eur. J.* **24**, 5743-5747 (2018).

126 Heijenoort, J. v. Formation of the glycan chains in the synthesis of bacterial peptidoglycan. *Glycobiology* **11**, 25R-36R (2001).

127 Essers, L. & Schoop, H. J. Evidence for the incorporation of molecular oxygen, a pathway in biosynthesis of N-glycolylmuramic acid in *Mycobacterium phlei*. *Biochim. Biophys. Acta* **544**, 180-184 (1978).

128 Barreteau, H., Kovac, A., Boniface, A., Sova, M., Gobec, S. & Blanot, D. Cytoplasmic steps of peptidoglycan biosynthesis. *FEMS Microbiol. Rev.* **32**, 168-207 (2008).

129 Jha, R. K., Katagihallimath, N., Hota, S. K., Das, K. S. & de Sousa, S. M. An assay for exogenous sources of purified MurG, enabled by the complementation of *Escherichia coli* murG(Ts) by the *Mycobacterium tuberculosis* homologue. *FEMS Microbiol. Lett.* **326**, 161-167 (2012).

130 Trunkfield, A. E., Gurcha, S. S., Besra, G. S. & Bugg, T. D. Inhibition of *Escherichia coli* glycosyltransferase MurG and *Mycobacterium tuberculosis* Gal transferase by uridine-linked transition state mimics. *Bioorg. Med. Chem.* **18**, 2651-2663 (2010).

131 Münch, D., Roemer, T., Lee, S. H., Engeser, M., Sahl, H. G. & Schneider, T. Identification and in vitro analysis of the GatD/MurT enzyme-complex catalyzing lipid II amidation in *Staphylococcus aureus*. *PLoS pathog.* **8**, e1002509 (2012).

132 Levefaudes, M., Patin, D., de Sousa-d'Auria, C., Chami, M., Blanot, D., Hervé, M., Arthur, M., Houssin, C. & Mengin-Lecreulx, D. Diaminopimelic acid amidation in Corynebacteriales: new insights into the role of LtsA in peptidoglycan modification. *J. Biol. Chem.* **290**, 13079-13094 (2015).

133 Mohammadi, T., Van Dam, V., Sijbrandi, R., Vernet, T., Zapun, A., Bouhss, A., Diepeveen-de Bruin, M., Nguyen-Distèche, M., De Kruijff, B. & Breukink, E. Identification of FtsW as a transporter of lipid-linked cell wall precursors across the membrane. *EMBO J.* **30**, 1425-1432 (2011).

134 Meeske, A. J., Riley, E. P., Robins, W. P., Uehara, T., Mekalanos, J. J., Kahne, D., Walker, S., Kruse, A. C., Bernhardt, T. G. & Rudner, D. Z. SEDS proteins are a widespread family of bacterial cell wall polymerases. *Nature* **537**, 634-638 (2016).

135 Emami, K., Guyet, A., Kawai, Y., Devi, J., Wu, L. J., Allenby, N., Daniel, R. A. & Errington, J. RodA as the missing glycosyltransferase in Bacillus subtilis and antibiotic discovery for the peptidoglycan polymerase pathway. *Nature Microbiol.* **2**, 1-9 (2017).

136 Inoue, A., Murata, Y., Takahashi, H., Tsuji, N., Fujisaki, S. & Kato, J.-i. Involvement of an essential gene, mviN, in murein synthesis in *Escherichia coli*. *J. Bacteriol.* **190**, 7298-7301 (2008).

137 Ruiz, N. Bioinformatics identification of MurJ (MviN) as the peptidoglycan lipid II flippase in *Escherichia coli*. *Proc. Natl. Acad. Sci.* **105**, 15553-15557 (2008).

138 Bolla, J. R., Sauer, J. B., Wu, D., Mehmood, S., Allison, T. M. & Robinson, C. V. Direct observation of the influence of cardiolipin and antibiotics on lipid II binding to MurJ. *Nat. Chem.* **10**, 363-371 (2018).

139 Sham, L.-T., Butler, E. K., Lebar, M. D., Kahne, D., Bernhardt, T. G. & Ruiz, N. MurJ is the flippase of lipid-linked precursors for peptidoglycan biogenesis. *Science* **345**, 220-222 (2014).

140 Crick, D. C. & Brennan, P. J. Biosynthesis of the Arabinogalactan-Peptidoglycan Complex of *Mycobacterium Tuberculosis*. *The mycobacterial cell envelope*, 25-40 (2008).

141 Sauvage, E., Kerff, F., Terrak, M., Ayala, J. A. & Charlier, P. The penicillin-binding proteins: structure and role in peptidoglycan biosynthesis. *FEMS Microbiol. Rev.* **32**, 234-258 (2008).

142 Hett, E. C., Chao, M. C. & Rubin, E. J. Interaction and modulation of two antagonistic cell wall enzymes of mycobacteria. *PLoS Pathog.* **6**, e1001020 (2010).

143 Patru, M. M. & Pavelka, M. S., Jr. A role for the class A penicillin-binding protein PonA2 in the survival of *Mycobacterium smegmatis* under conditions of nonreplication. *J. Bacteriol.* **192**, 3043-3054 (2010).

144 Dasgupta, A., Datta, P., Kundu, M. & Basu, J. The serine/threonine kinase PknB of Mycobacterium tuberculosis phosphorylates PBPA, a penicillin-binding protein required for cell division. *Microbiology (Reading)* **152**, 493-504 (2006).

145 Botta, G. A. & Park, J. T. Evidence for involvement of penicillin-binding protein 3 in murein synthesis during septation but not during cell elongation. *J. bacteriol.* **145**, 333-340 (1981).

146 Plocinska, R., Martinez, L., Gorla, P., Pandeeti, E., Sarva, K., Blaszczyk, E., Dziadek, J., Madiraju, M. V. & Rajagopalan, M. *Mycobacterium tuberculosis* MtrB Sensor Kinase Interactions with FtsI and Wag31 Proteins Reveal a Role for MtrB Distinct from That Regulating MtrA Activities. *J. Bacteriol.* **196**, 4120-4129 (2014).

147 Datta, P., Dasgupta, A., Singh, A. K., Mukherjee, P., Kundu, M. & Basu, J. Interaction between FtsW and penicillin-binding protein 3 (PBP3) directs PBP3 to mid-cell, controls cell septation and mediates the formation of a trimeric complex involving FtsZ, FtsW and PBP3 in mycobacteria. *Mol. Microbiol.* **62**, 1655-1673 (2006).

148 DeJesus, M. A., Gerrick, E. R., Xu, W., Park, S. W., Long, J. E., Boutte, C. C., Rubin, E. J., Schnappinger, D., Ehrt, S., Fortune, S. M., Sassetti, C. M. & Ioerger, T. R. Comprehensive Essentiality Analysis of the *Mycobacterium tuberculosis* Genome via Saturating Transposon Mutagenesis. *mBio* **8**, 10.1128/mbio.02133-02116 (2017).

149 Prigozhin, D. M., Krieger, I. V., Huizar, J. P., Mavrici, D., Waldo, G. S., Hung, L. W., Sacchettini, J. C., Terwilliger, T. C. & Alber, T. Subfamily-specific adaptations in the structures of two penicillin-binding proteins from *Mycobacterium tuberculosis*. *PLoS One* **9**, e116249 (2014).

150 Wietzerbin, J., Das, B. C., Petit, J. F., Lederer, E., Leyh-Bouille, M. & Ghuysen, J. M. Occurrence of D-alanyl-(D)-meso-diaminopimelic acid and meso-diaminopimelyl-meso-diaminopimelic acid interpeptide linkages in the peptidoglycan of Mycobacteria. *Biochemistry* **13**, 3471-3476 (1974).

151 Gupta, R., Lavollay, M., Mainardi, J.-L., Arthur, M., Bishai, W. R. & Lamichhane, G. The *Mycobacterium tuberculosis* protein Ldt_{Mt2} is a nonclassical transpeptidase required for virulence and resistance to amoxicillin. *Nat. Med.* **16**, 466-469 (2010).

152 Baranowski, C., Welsh, M. A., Sham, L. T., Eskandarian, H. A., Lim, H. C., Kieser, K. J., Wagner, J. C., McKinney, J. D., Fantner, G. E., Ioerger, T. R., Walker, S., Bernhardt, T. G., Rubin, E. J. & Rego, E. H. Maturing *Mycobacterium smegmatis* peptidoglycan requires non-canonical crosslinks to maintain shape. *Elife* **7** (2018).

153 Li, W. J., Li, D. F., Hu, Y. L., Zhang, X. E., Bi, L. J. & Wang, D. C. Crystal structure of L,D-transpeptidase Ldt_{Mt2} in complex with meropenem reveals the mechanism of carbapenem against *Mycobacterium tuberculosis*. *Cell Res.* **23**, 728-731 (2013).

154 Erdemli, S. B., Gupta, R., Bishai, W. R., Lamichhane, G., Amzel, L. M. & Bianchet, M. A. Targeting the cell wall of *Mycobacterium tuberculosis*: structure and mechanism of L,D-transpeptidase 2. *Structure* **20**, 2103-2115 (2012).

155 Biarrotte-Sorin, S., Hugonnet, J.-E., Delfosse, V., Mainardi, J.-L., Gutmann, L., Arthur, M. & Mayer, C. Crystal structure of a novel β-lactam-insensitive peptidoglycan transpeptidase. *J. Mol. Biol.* **359**, 533-538 (2006).

156 Chambers, H. F., Moreau, D., Yajko, D., Miick, C., Wagner, C., Hackbarth, C., Kocagöz, S., Rosenberg, E., Hadley, W. K. & Nikaido, H. Can penicillins and other beta-lactam antibiotics be used to treat tuberculosis? *Antimicrob. Agents Chemother.* **39**, 2620-2624 (1995).

157 Flores, A. R., Parsons, L. M. & Pavelka, M. S. Genetic analysis of the beta-lactamases of *Mycobacterium tuberculosis* and *Mycobacterium smegmatis* and susceptibility to beta-lactam antibiotics. *Microbiology (Reading, Engl.)* **151**, 521-532 (2005).

158 Lun, S., Miranda, D., Kubler, A., Guo, H., Maiga, M. C., Winglee, K., Pelly, S. & Bishai, W. R. Synthetic Lethality Reveals Mechanisms of *Mycobacterium tuberculosis* Resistance to Beta-Lactams. *mBio* **5**, 10.1128/mbio.01767-01714 (2014).

159 Mainardi, J. L., Hugonnet, J. E., Rusconi, F., Fourgeaud, M., Dubost, L., Moumi, A. N., Delfosse, V., Mayer, C., Gutmann, L., Rice, L. B. & Arthur, M. Unexpected Inhibition of Peptidoglycan LD-Transpeptidase from *Enterococcus faecium* by the β-Lactam Imipenem. *J. Biol. Chem.* **282**, 30414-30422 (2007).

160 Kumar, P., Kaushik, A., Lloyd, E. P., Li, S.-G., Mattoo, R., Ammerman, N. C., Bell, D. T., Perryman, A. L., Zandi, T. A., Ekins, S., Ginell, S. L., Townsend, C. A., Freundlich, J. S. & Lamichhane, G. Non-classical transpeptidases yield insight into new antibacterials. *Nat. Chem. Biol.* **13**, 54-61 (2017).

161 Steiner, E. M., Schneider, G. & Schnell, R. Binding and processing of β-lactam antibiotics by the transpeptidase Ldt_{Mt2} from *Mycobacterium tuberculosis*. *FEBS J.* **284**, 725-741 (2017).
162 Cordillot, M., Dubée, V., Triboulet, S., Dubost, L., Marie, A., Hugonnet, J.-E., Arthur, M. & Mainardi, J.-L. In vitro cross-linking of *Mycobacterium tuberculosis* peptidoglycan by L,D-transpeptidases and inactivation of these enzymes by carbapenems. *Antimicrob. Agents Chemother.* **57**, 5940-5945 (2013).
163 Brammer Basta, L. A., Ghosh, A., Pan, Y., Jakoncic, J., Lloyd, E. P., Townsend, C. A., Lamichhane, G. & Bianchet, M. A. Loss of a Functionally and Structurally Distinct L,D-Transpeptidase, Ldt_{Mt5}, Compromises Cell Wall Integrity in *Mycobacterium tuberculosis*. *J. Biol. Chem.* **290**, 25670-25685 (2015).
164 Iannazzo, L., Soroka, D., Triboulet, S., Fonvielle, M., Compain, F., Dubée, V., Mainardi, J.-L., Hugonnet, J.-E., Braud, E., Arthur, M. & Etheve-Quelquejeu, M. Routes of Synthesis of Carbapenems for Optimizing Both the Inactivation of L,D-Transpeptidase Ldt_{Mt1} of *Mycobacterium tuberculosis* and the Stability toward Hydrolysis by β-Lactamase BlaC. *J. Med. Chem.* **59**, 3427-3438 (2016).
165 Gupta, R., Al-Kharji, N. M. S. A., Alqurafi, M. A., Nguyen, T. Q., Chai, W., Quan, P., Malhotra, R., Simcox, B. S., Mortimer, P., Brammer Basta, L. A., Rohde, K. H. & Buynak, J. D. Atypically Modified Carbapenem Antibiotics Display Improved Antimycobacterial Activity in the Absence of β-Lactamase Inhibitors. *ACS Infect. Dis.* **7**, 2425-2436 (2021).
166 Batchelder, H. R., Story-Roller, E., Lloyd, E. P., Kaushik, A., Bigelow, K. M., Maggioncalda, E. C., Nuermberger, E. L., Lamichhane, G. & Townsend, C. A. Development of a penem antibiotic against *Mycobacteroides abscessus*. *Commun. Biol.* **3**, 741 (2020).
167 Batchelder, H. R., Zandi, T. A., Kaushik, A., Naik, A., Story-Roller, E., Maggioncalda, E. C., Lamichhane, G., Nuermberger, E. L. & Townsend, C. A. Structure–Activity Relationship of Penem Antibiotic Side Chains Used against Mycobacteria Reveals Highly Active Compounds. *ACS Infect. Dis.* **8**, 1627-1636 (2022).
168 de Munnik, M., Lohans, C. T., Lang, P. A., Langley, G. W., Malla, T. R., Tumber, A., Schofield, C. J. & Brem, J. Targeting the *Mycobacterium tuberculosis* transpeptidase Ldt_{Mt2} with cysteine-reactive inhibitors including ebselen. *Chem. Commun.* **55**, 10214-10217 (2019).
169 Lelovic, N., Mitachi, K., Yang, J., Lemieux, M. R., Ji, Y. & Kurosu, M. Application of Mycobacterium smegmatis as a surrogate to evaluate drug leads against Mycobacterium tuberculosis. *J. Antibiot.* **73**, 780-789 (2020).

Chapter 2

β-Lactam antibiotics targeting *Mycobacterium tuberculosis*

Contents

2.1 Introduction 32
2.2 *In vitro* and *in vivo* activity of β-lactams in *Mycobacterium tuberculosis* 35
2.3 Targets of β-lactams in *Mycobacterium tuberculosis* 36
2.3.1 Penicillin binding proteins of *Mycobacterium tuberculosis* and their function 36
2.3.1.1 PonA1 38
2.3.1.2 PonA2 39
2.3.1.3 PBPA 39
2.3.1.4 PBP3 39
2.3.1.5 DacB 39
2.3.1.6 DacB1 40
2.3.1.7 DacB2 40
2.3.2 L,D-Transpeptidases of *Mycobacterium tuberculosis* and their function 40
2.3.2.1 Role of L,D-transpeptidases in mycobacteria 40
2.3.2.2 Ldt_{Mt1} 42
2.3.2.3 Ldt_{Mt2} 42
2.3.2.4 Ldt_{Mt3} 43
2.3.2.5 Ldt_{Mt4} 43
2.3.2.6 Ldt_{Mt5} 43
2.3.3 β-lactamases of *Mycobacterium tuberculosis* 43
2.3.3.1 BlaC 43
2.3.3.2 Inhibitors of BlaC 44
2.3.3.3 Resistance to β-lactamase inhibitors 45
2.4 Inhibition of penicillin binding proteins and L,D-transpeptidases 45
2.4.1 Studies on the targets of β-lactams in *Mycobacterium tuberculosis* 45
2.4.2 Biochemical studies of the inhibition of the penicillin binding proteins with β-lactams 47
2.4.2.1 Penicillins 47
2.4.2.2 Carbapenems 47
2.4.2.3 Cephalosporins 47
2.4.2.4 Penems 48
2.4.2.5 Monobactams 48
2.4.3 Biochemical studies of the inhibition of the L,D-transpeptidases 48
2.4.3.1 Carbapenems are inhibitors of L,D-transpeptidases 48
2.4.3.2 Faropenem is the most potent reported inhibitor of Ldt_{Mt1-4} 49
2.5 Optimisation of β-lactams for *Mycobacterium tuberculosis* 50
2.5.1 Reported recommendations on β-lactam optimisation 50
2.5.2 Development of β-lactams for *Mycobacterium tuberculosis* 51
2.5.2.1 Optimisation of carbapenems 51
2.5.2.2 Optimisation of penems 53
2.5.2.3 Optimisation of cephalosporins 53
2.5.2.4 Optimisation of monocyclic β-lactams 55
2.6 Summary and conclusions 55
2.7 References 57

2.1 Introduction

The discovery of β-lactams as antimicrobials in the 1920s represented a revolution in the treatment of bacterial infections,[1] and the β-lactams remain among the most prescribed drugs in the clinic.[2] Their structure consists of a relatively reactive four-membered β-lactam ring, which is generally fused with another heterocycle, giving rise to several classes of β-lactam antimicrobials; including penicillins, cephalosporins, carbapenems, penems, and (monocyclic) monobactams (Figure 2.1A).[2] β-Lactams have been optimised for the treatment of infections caused by a wide range of bacterial strains, including those showing resistance.[2] However, they have traditionally not been deemed useful for the treatment of TB.[3] While early studies suggested that β-lactams manifest activity against *Mycobacterium tuberculosis* (*Mtb*),[4] clinical effectiveness has not been established, likely due to various resistance mechanisms.[5]

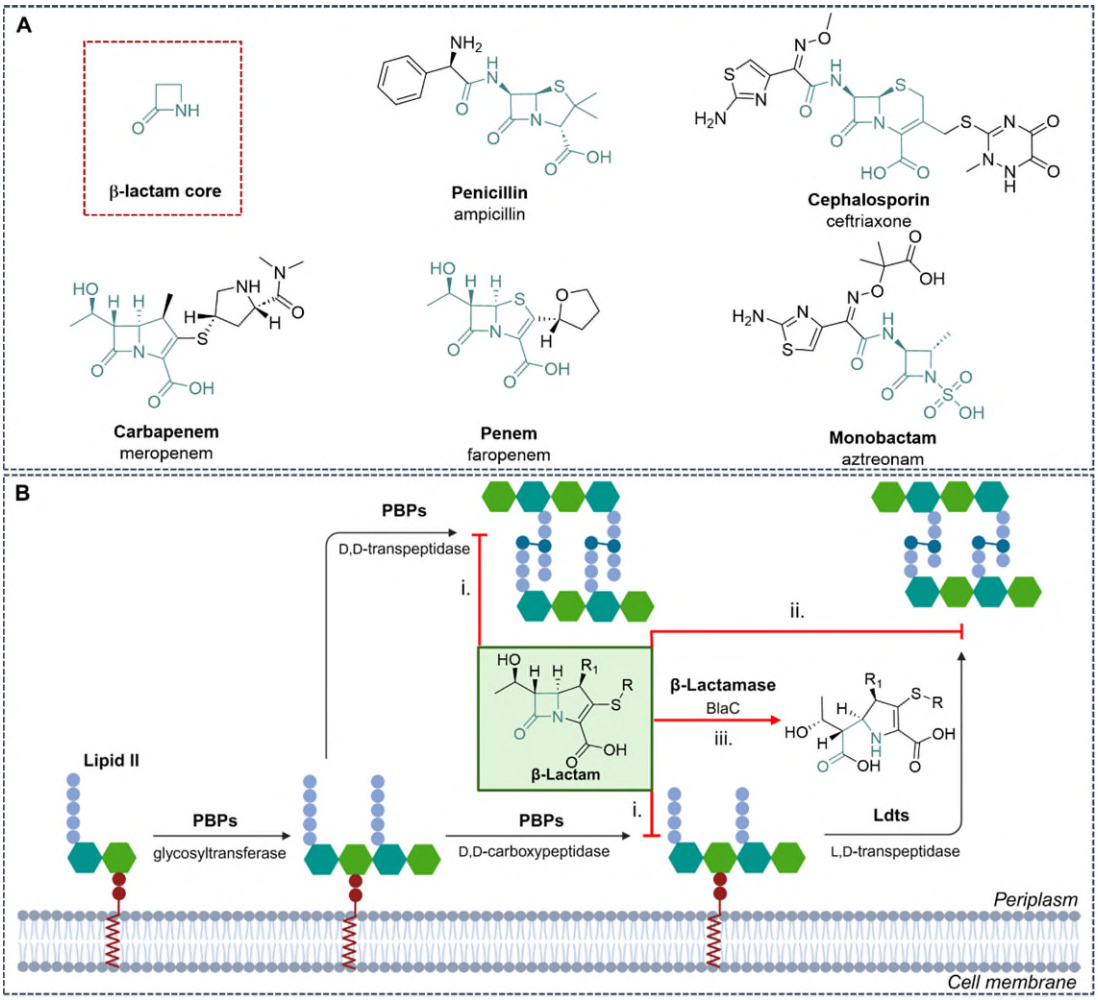

Figure 2.1. β-Lactams and their potential targets in *Mycobacterium tuberculosis*. A. Representative members of the classes of β-lactams (common core motifs are shown in teal). **B.** In *Mtb*, β-lactams potentially act as antibiotics through inhibition of various transpeptidase and carboxypeptidases in the peptidoglycan layer. Their antimicrobial activity is limited in *Mtb* due to hydrolysis by the β-lactamase BlaC.

β-Lactam antibiotics act as inhibitors of penicillin binding proteins (PBPs).[6,7] PBPs play various essential roles in the biosynthesis of the peptidoglycan (PG) layer of virtually all bacteria, and their inhibition commonly leads to an effective antibacterial effect.[8,9] The roles of PBPs in the PG biosynthesis comprise D,D-transpeptidase activity, catalysing the formation of 4→3 cross-links between pentapeptide chains, and D,D-carboxypeptidase activity, cleaving pentapeptide chains to form tetrapeptide chains (Figure 2.1B).[10] Selected D,D-transpeptidases additionally possess glycosyltransferase activity.[10] The interaction of β-lactams with PBPs is well studied in model organisms such as *Staphylococcus aureus*, *Bacillus subtilis*, and *Escherichia coli*; it is likely that the findings with these bacteria are broadly applicable to a wide range of bacteria.[11-14]

By contrast, the interaction of β-lactams with *Mtb* appears to follow an atypical mechanism. Unlike most bacteria, *Mtb* relies on a larger variety of enzymes to modify PG, employing the L,D-transpeptidases (Ldts) as well as PBPs.[15,16] Ldts catalyse the formation of 3→3 cross-links between tetrapeptide chains in the PG (Figure 2.1B).[17,18] While in most bacteria the 3→3 cross-links are apparently non-essential, occurring in negligible levels compared to 4→3 cross-links, during the stationary phase cross-linked PG if mycobacteria contain up to ~80% 3→3 cross-links.[19]

Resistance of mycobacteria towards β-lactam antibiotics is commonly accredited to the presence of β-lactamases (Figure 2.1B).[20] In particular in *Mtb*, the chromosomally encoded Ambler class A β-lactamase BlaC is known to hydrolyse all classes of β-lactams, but manifests decreased hydrolysis of carbapenems.[20,21] Further, the Ldts may enable resistance as they are not commonly inhibited by most β-lactams,[22] although it has been reported that carbapenems and penems can inhibit Ldts.[23-25] It should be noted that the Ldts not only have the potential to enable resistance to β-lactams in mycobacteria, but also in other bacteria, such as *Enterococcus faecium* and *E. coli*, in which 3→3 cross-links are apparently able to at least partially substitute for 4→3 cross-links that are disrupted upon β-lactam mediated inhibition of PBPs.[26-28]

The PBPs and Ambler class A β-lactamases both employ nucleophilic serine residues; they share structural and sequence similarities, and are likely to originate from the same evolutionary group.[29] However, while PBPs generally form a stable acyl-enzyme complex upon interaction with β-lactam inhibitors,[30] the β-lactamases are designed to readily hydrolyse the acyl-enzyme complex, making use of a strategically positioned water molecule (Figure 2.2A).[31] PBPs share a common overall fold and contain the highly conserved SxxK, SxN, and KTG(S/T) active site motifs (Figure 2.2B).[32,33] Similarly, Ambler class A β-lactamases share the conserved S^{70}xxK, S^{130}DN/G, and K^{234}TG motifs, as well as a conserved Glu^{166} residue

(Figure 2.2C).[34] By contract, the Ldts do not share structural similarities with PBPs or serine β-lactamases; instead, the Ldts likely originate from a different evolutionary group.[35] The Ldts share a common YkuD fold (named after the first identified member of this class), distinguished by two mixed β-sheets and one α-helix, and a set of four loops.[35-37] The Ldts employ a catalytic triad involving the sidechains of a nucleophilic cysteine and a histidine residue, and the backbone carbonyl of a third residue in a characteristic Hxx$_{14–17}$(S/T)HGCZN motif, in which Z represents a hydrophobic residue (Figure 2.2D).[35]

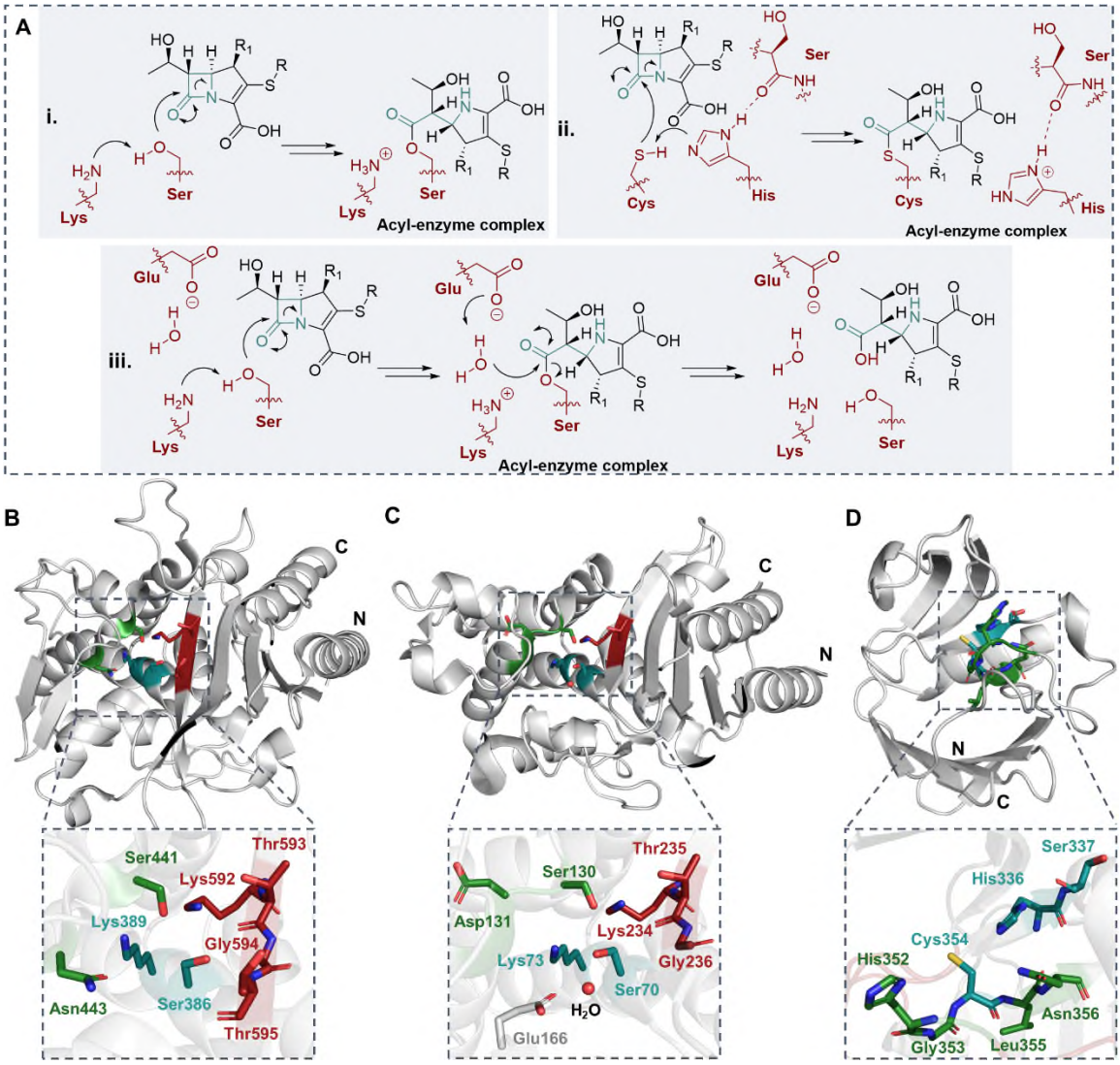

Figure 2.2. Conserved structural motifs of penicillin binding proteins, Ambler class A β-lactamases, and L,D-transpeptidases, and their interaction with β-lactams. A. The mechanism of β-lactam inhibition of PBPs (i) and Ldts (ii), and hydrolysis by serine β-lactamases (iii). **B.** The PBPs share a common fold of the catalytic domain, shown exemplary with the representative PBP3 of *Mtb* (PDB 6KGH).[38] The SxxK motif is in teal, the SxN motif is in green, and the KTGT motif is in red. **C**. The structure and conserved active site residues of Ambler class A β-lactamases, such as BlaC (PDB 2GDN).[39] The SxxK motif is in teal, the SDG motif is in green, the KTG motif is in red, Glu166 is in grey. **D**. The structure of Ldts, as exemplified by Ldt$_{Mt2}$ of *Mtb* (PDB 6RLG).[40] The Hxx$_{14–17}$(S/T)HGCZN motif is in green, with the catalytic triad residues in teal.

Reports that the β-lactam-β-lactamase inhibitor combination meropenem-clavulanic acid shows a substantial bactericidal effect on *Mtb* have reignited interest in β-lactams as anti-TB drugs,[41,42] but optimisation will likely be required to achieve sufficient effectivity in the clinic.[43] However, the intricate network of interaction partners of β-lactams in *Mtb*, including PBPs, Ldts and BlaC, complicates the optimisation of β-lactams. Knowledge of the function and inhibition of the individual targets is crucial for the optimisation of both β-lactam and non-β-lactam antibiotics for the treatment of infections caused by *Mtb*. Here, the *in vitro* and *in vivo* activity of β-lactams against *Mtb* will be briefly summarised, followed by an account of the known functions and inhibition of the *Mtb* PBPs, Ldts, and β-lactamases, as well as studies into the optimisation of β-lactams for TB.

2.2 *In vitro* and *in vivo* activity of β-lactams in *Mycobacterium tuberculosis*

The *in vitro* activity of β-lactams against *Mtb* has been widely characterised, the results of which have been summarised in various reviews.[43-45] Penicillins generally do not display potent antimicrobial activity against *Mtb*, likely due β-lactamase conferred resistance, as bactericidal activity is observed when penicillins are used in combination with a β-lactamase inhibitor.[46] Particularly potent combinations consists of the β-lactamase inhibitor clavulanic acid and the penicillins amoxicillin (Augmentin) or ampicillin, which confer clinically useful antibacterial efficacy.[46-49] Some cephalosporins have shown promising *in vitro* activity against *Mtb*, as well as exhibiting synergistic action together with cornerstone anti-TB drugs such as rifampicin and ethambutol.[50,51]

Carbapenems have been of particular interest for the development of treatments of infections conferred by *Mtb*, as they are inhibitors of both PBPs and Ldts,[43] and are slow substrates of BlaC.[52] They potently inhibit *Mtb in vitro,* even in the absence of a β-lactamase inhibitor, though potency is further increased through the addition of a β-lactamase inhibitor.[43] Carbapenems show activity against most drug susceptible strains as well as multidrug resistant (MDR) and extensively drug resistant (XDR) stains of *Mtb*.[41,53-55] The newer carbapenems doripenem and tebipenem are particularly potent.[53,56] Initial evidence suggests enhanced potency of meropenem compared to imipenem and ertapenem, particularly in MDR and XDR strains.[41,53] However, the limited hydrolytic stability of carbapenems in aqueous solution, in combination with the slow growth rate of *Mtb*, complicates the assessment of antimicrobial activity,[57] as MIC determination requires extended incubation (≥ 10 days).[58] The penem faropenem benefits from increased hydrolytic stability compared to carbapenems,[59] as well as increased activity against *Mtb* compared to meropenem.[60]

Despite promising *in vitro* activity against *Mtb*, clinical trials with β-lactams have yielded inconclusive results thus far. Initial anecdotal clinical evidence of amoxicillin/clavulanate (Augmentin) in patients with MDR-TB showed mixed results,[61,62] with subsequent clinical trials suggesting the use should be limited to last resort treatment of TB.[63,64] Anecdotal clinical evidence for the use of carbapenems to treat TB has been promising,[65] and clinical trials have suggested imipenem and meropenem in combination with clavulanic acid may be clinically useful in the treatment of MDR-TB, with treatment successes in over half of the patients.[42,66,67] However, these clinical trials have been limited to small, often retrospective studies that lack randomisation, and suffer from variable treatment regimens and high comorbidities, as carbapenems have only been used in patients with MDR-TB and XDR-TB with severe disease that have often failed standard second-line treatment.[43] The WHO currently recommends that imipenem or meropenem in combination with clavulanic acid may be considered for the treatment of MDR-TB or XDR-TB, with the caveat that there is low certainty of efficacy.[68]

2.3 Targets of β-lactams in *Mycobacterium tuberculosis*

2.3.1 Penicillin binding proteins of *Mycobacterium tuberculosis* and their function

There is no consensus regarding how many PBPs *Mtb* contains, but analysis of the *Mtb* genome identified at least 12 putative PBPs.[69] Of these, seven have confirmed PBP functionality: the D,D-transpeptidases and glycosyltransferases PonA1, PonA2, the D,D-transpeptidases PBPA, PBP3, and the D,D-carboxypeptidases DacB, DacB1, and DacB2 (Figure 2.3A). Putative PBPs of *Mtb*, based on homology with known PBPs, include PBP-lipo (Rv2864c), Rv0907, Rv1367, Rv1730, and Rv1922.[69] The D,D-transpeptidases and D,D-carboxypeptidases share a common penicillin binding domain, made up of two subdomains consisting of (i) five stranded β-sheets and three α-helices, and (ii) an all-helical domain (Figure 2.3B), and PonA1 and PonA2 contain an additional glycosyltransferase domain.[10]

The peptidase activity of PBPs involves a three-step mechanism (Figure 2.3C), initiated with the formation of a noncovalent interaction between the PBP active site and the peptidoglycan stem pentapeptide donor strand, which is followed by the formation of an acyl-enzyme complex with the active site serine and the terminal D-Ala-D-Ala peptide bond. This is followed by either cross-link formation via reaction with a second peptidoglycan stem peptide acceptor strand (in the case of D,D-transpeptidases) or hydrolysis (in the case of D,D-carboxypeptidases).

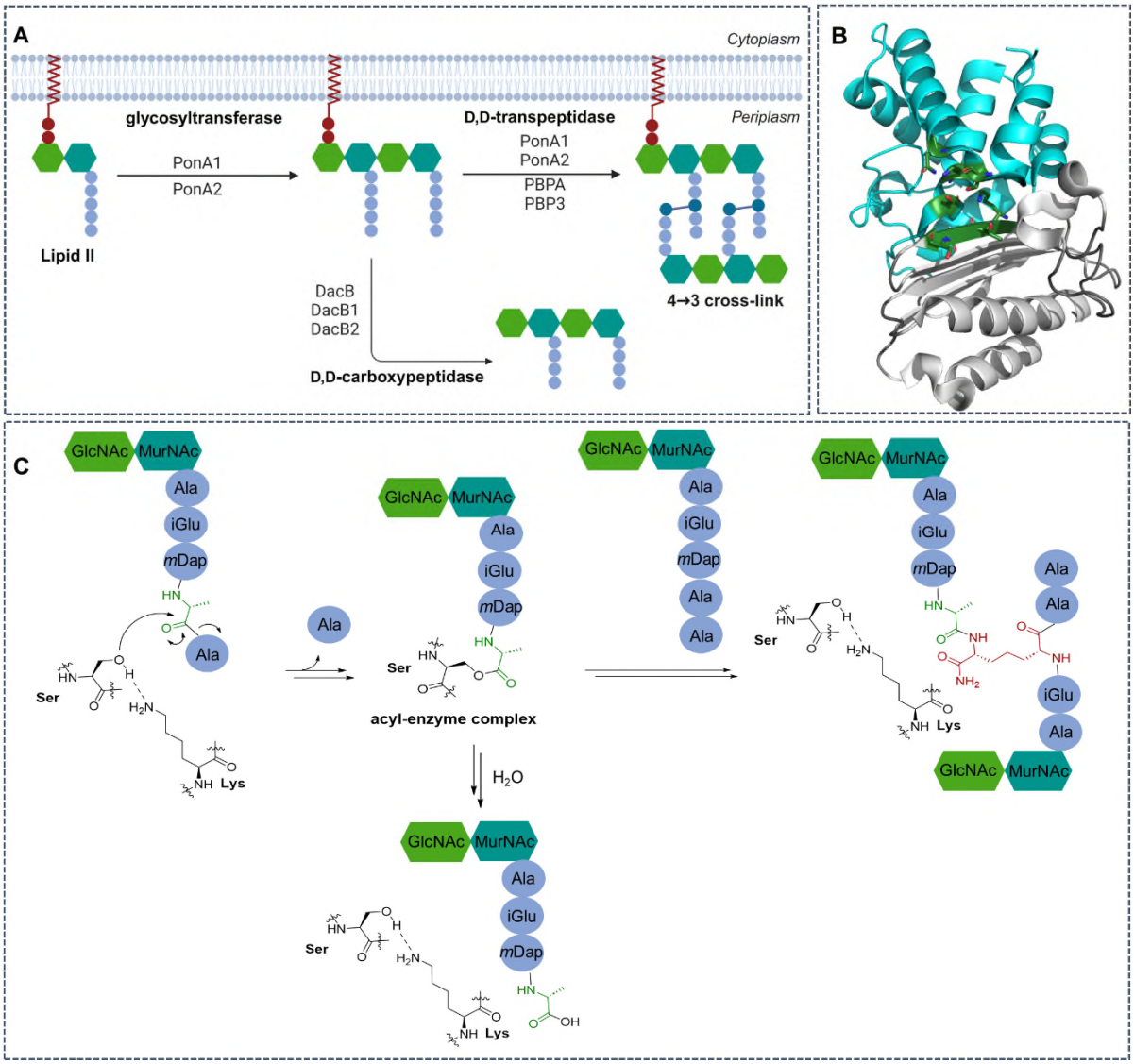

Figure 2.3. Penicillin binding proteins of *Mycobacterium tuberculosis*. A. The functions of the seven known PBPs of *Mtb*. **B.** The common penicillin-binding domain of PBPs, exemplified by PBP3 (PDB 6KGH).[38] The penicillin-binding domain is made up of two subdomains, consisting of a five stranded β-sheets and three α-helices (grey), and an all-helical domain (cyan), with the active site positioned in-between (green). **C.** Outline of the mechanism of the D,D-transpeptidase and D,D-carboxypeptidase activity of PBPs of *Mtb*, both moving through the same acyl-enzyme intermediate.

The roles of known PBPs in the PG biosynthesis in diverse metabolic states, and their susceptibility to β-lactam antibiotics, has yet to be fully elucidated, and likely involve an intricate network of different PB synthesis pathways and interaction complexes. As yet, biochemical and genetic studies of the PBPs of *Mtb* have clarified the roles of the individual PBPs, as summarised below, and in Table 2.1.

Table 2.1. Enzymes relevant to β-lactam activity in *Mycobacterium tuberculosis*, and their assigned functions.

Class	Enzyme	Rv #	Enzyme type	Role in *Mtb*
Class A PBP	PonA1	Rv0050	Glycosyltransferase and D,D-transpeptidase	Essential in *ΔponA2* strain;[70] Essential *Mtb* fitness during infection;[71] Polar elongation and division.[72,73]
	PonA2	Rv3682	Glycosyltransferase and D,D-transpeptidase	Essential in *ΔponA1* strain;[70] Essential *Mtb* fitness during infection;[74] Regulation of cell shape.[70]
Class B PBP	PBPA	Rv0016c	D,D-transpeptidase	Essential for survival in host;[75] Regulation of cell length.[76]
	PBP3	Rv2163c	D,D-transpeptidase	Essential for growth and cell division.[77]
Class C PBP	DacB	Rv3627c	D,D-carboxypeptidase	Putatively essential for growth and cell division.[78,79]
	DacB1	Rv3330	D,D-carboxypeptidase	Non-essential for growth;[79] Septal PG synthesis.[80]
	DacB2	Rv2911	D,D-carboxypeptidase	Putatively essential under specific stress conditions.[81,82]
Ldt	Ldt_{Mt1}	Rv0116c	L,D-transpeptidase	Non-essential for growth or morphology;[83] Increased importance in *Δldt_{Mt2}* strain.[83]
	Ldt_{Mt2}	Rv2518c	L,D-transpeptidase	Important for growth and morphology;[19] Essential for virulence;[19] Essential in *ΔponA1* strain.[70]
	Ldt_{Mt3}	Rv1433	unknown	Non-essential for growth or morphology.[19]
	Ldt_{Mt4}	Rv0192	L,D-transpeptidase	Non-essential for growth or morphology.[19]
	Ldt_{Mt5}	Rv0483	L,D-transpeptidase	Non-essential for growth or morphology;[19] Important for cell wall integrity.[84]
Class A SBL	BlaC	Rv2068c	Broad spectrum β-Lactamase	Hydrolysis of all classes of β-lactams;[52] Relative resistance to carbapenem hydrolysis.[52]

2.3.1.1 PonA1

PonA1 is a class A, high-molecular-weight, bifunctional PBP, with both D,D-transpeptidase and glycosyltransferase activities.[69] PonA1 has been identified to be a key element in PG synthesis during polar elongation and division, and is located in the cell pole and septum.[72,73] Deletion of *ponA1* does not affect growth of *Mtb*, but alters cell morphology, leading to an increase in cell length.[70] Interestingly, while PonA1 is not required for growth under standard laboratory culture conditions, growth is disrupted *in vivo* in mouse infection models, suggesting PonA1 to be of particular importance for *Mtb* fitness during infection.[71] Additionally, in the absence of

PonA2, PonA1 becomes essential for growth of *Mtb* under standard laboratory culture conditions.[70]

2.3.1.2 PonA2

PonA2 is another class A, high-molecular-weight, bifunctional PBP of *Mtb*.[69] Similarly to PonA1, loss of PonA2 does not alter cell growth under standard laboratory culture conditions, but does become essential in the absence of PonA1.[70] Further, infection models suggest PonA2, similarly to PonA1, to be important for *Mtb* fitness during infection.[74] However, despite observations that PonA1 and PonA2 catalyse similar reactions, and only one paralog is required for growth of *Mtb*, they are not functionally redundant.[70,85] Upon deletion of *ponA2*, *Mtb* cells increase in width rather than length.[70] Reports suggest that PonA2 is involved in the survival of mycobacteria in the stationary phase.[85] Inactivation of *ponA2* leads to increased susceptibility to β-lactams of the penicillin and carbapenem classes,[70,86] but leads to resistance to cephalosporins.[87]

2.3.1.3 PBPA

PBPA is a class B, high-molecular-weight D,D-transpeptidase, observed in distinct focal points to the poles, quarter cell, and mid-cell sites.[76] Deletion of PBPA does not affect growth of *Mtb*, but PBPA is required for the regulation of cell length, and attenuated growth is observed under nutrient-limiting conditions. Importantly, in a guinea pig infection model, PBPA was found to be required for bacterial survival as well as the formation of granulomas, suggesting PBPA plays a critical role in the survival of *Mtb* and its pathogenesis in the host.[75] Additionally, absence of *pbpA* leads to increased susceptibility to β-lactams.[75]

2.3.1.4 PBP3

PBP3, also known as FtsI or PBPB, is another class B, high-molecular-weight D,D-transpeptidase of *Mtb*. It is the only PBP of *Mtb* that has been confirmed to be essential for growth and plays a critical role in cell-division.[77] PBP3 is localized in the septum as a ternary complex with other cell-division proteins.[88,89] Inhibition of PBP3 by the β-lactams cefalexin and piperacillin resulted in filamentous cells with concentric rings and budding and branching, indicative of septa that are unable to complete cell-division,[90] and is therefore considered as a significant target for the development of anti-TB therapeutics.

2.3.1.5 DacB

DacB, also known as PBP4, is a class C, low-molecular-weight D,D-carboxypeptidase. The carboxypeptidase activity of DacB has been confirmed by Zhang *et al*. in 2019.[78] Detailed studies of its role in *Mtb* have not been reported to date, though transposon sequencing has suggested an essential role of DacB during cell growth.[79] Studies with the surrogate model

Mycobacterium smegmatis, which contains an equivalent protein to DacB with high homology (74% similarity), have suggested DacB to play an essential role in cell morphology and cell division.[78]

2.3.1.6 DacB1

DacB1, like DacB, is a class C, low-molecular-weight D,D-carboxypeptidase, though unlike DacB, it appears to be non-essential for growth.[79] Biochemically, the carboxypeptidase activity of DacB1 has been confirmed,[91] but detailed studies on its role in *Mtb* have not been reported to date. However, studies in *Mycobacterium abscessus* show DacB1 is localised in the septum, where it likely coordinates with PBP3 and PBP-lipo, and plays a role in septal PG synthesis in this complex.[80]

2.3.1.7 DacB2

Together with DacB and DacB1, DacB2 completes the confirmed class C, low-molecular-weight D,D-carboxypeptidases in *Mtb*. Deletion of *dacB2* does not alter growth under standard laboratory culture conditions, colony morphology, or antibiotic sensitivity.[81] However, reduced growth was observed in limited nutrient, acidic, and hypoxic conditions, suggesting DacB2 may only be required under specific stress conditions.[81,82] Notably, *in vitro* infection studies with a Δ*dacB2* strain in the human macrophage cell line THP-1 showed increased survival, suggesting the protein may be an interacting partner of a regulator protein, or part of a signalling cascade.[81,82]

2.3.2 L,D-Transpeptidases of *Mycobacterium tuberculosis* and their function

2.3.2.1 Role of L,D-transpeptidases in mycobacteria

Mtb contains five paralogs of L,D-transpeptidases (Ldts), referred to as Ldt_{Mt1-5}. Their role in the catalysis of 3→3 cross-links has been established (Figure 2.4), although their exact roles in the physiology of PG biosynthesis are poorly understood, perhaps more so than the relatively well studied PBPs.[92] It is unclear why bacteria produce both 4→3 and 3→3 cross-links, or why the role of the latter is apparently more pronounced in mycobacteria. The high conservation of Ldts suggests an evolutionary advantage, though most Ldts are apparently redundant, posing a poorly understood paradox.

In *E. coli*, reports suggest that the Ldts play a role under specific stress conditions on the bacterial cell wall, and are therefore part of the versatile mechanisms that maintain cell wall integrity under a variety of growth and stress conditions.[93-95] Some understanding on the role of Ldts in mycobacteria has been obtained from a strain of *M. smegmatis* lacking all Ldt paralogs, which suggested that 3→3 cross-links are formed in maturing PG, and are required

for rod shape and cell wall integrity in aging PG.[96,97] In the absence of 3→3 cross-links, cells were observed to increasingly rely on 4→3 cross-links.[96] Biochemical and genetic studies of the individual Ldt paralogs from *Mtb* have provided insight into their roles, as described in the following, and summarised in Table 2.1.

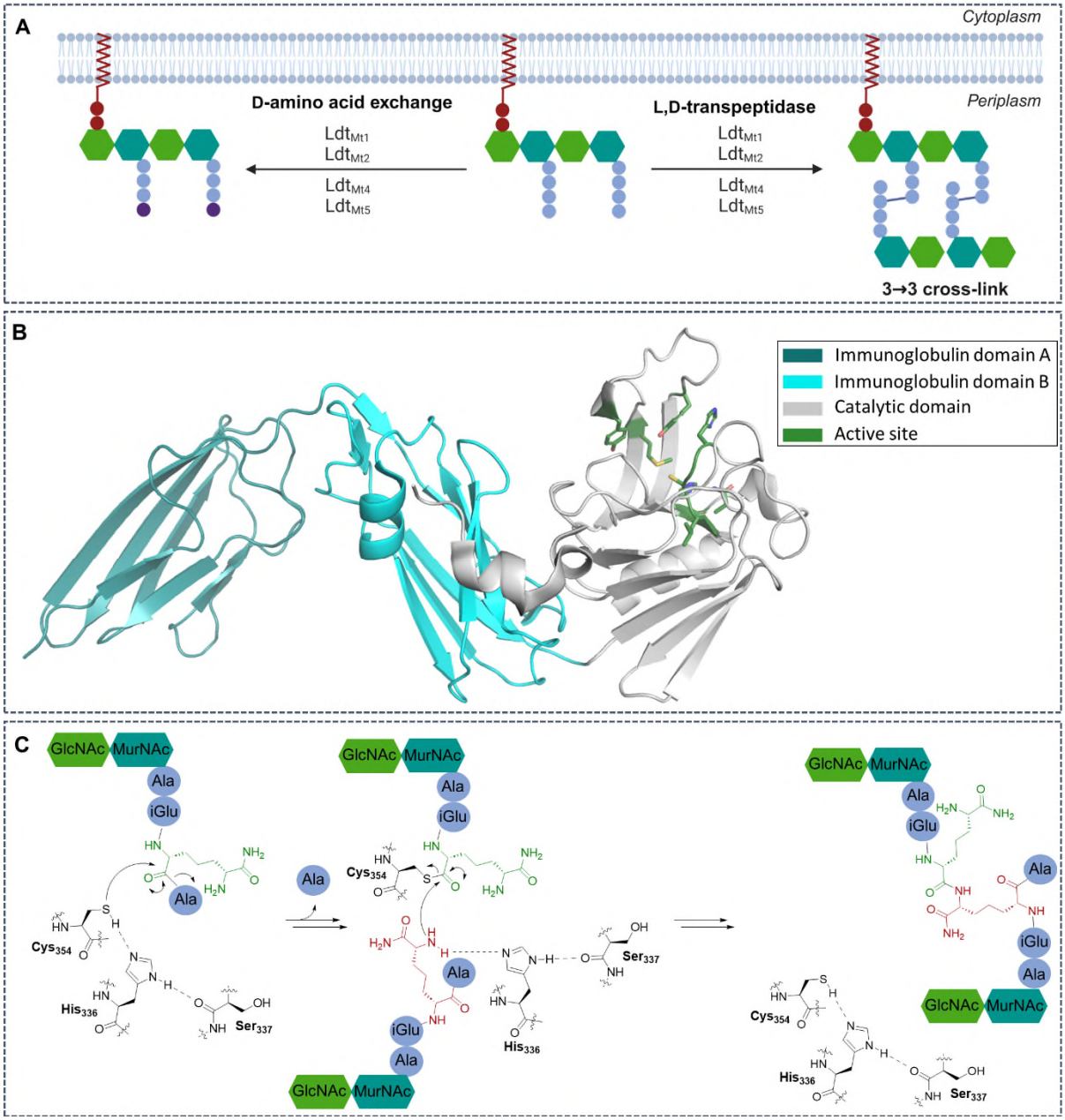

Figure 2.4. L,D-Transpeptidases of *Mycobacterium tuberculosis*. A. The Ldts of *Mtb* exhibit L,D-transpeptidase activity, and can exchange the terminal D-Ala to another D-amino acid (in purple). **B.** The common structure of Ldts, exemplified by Ldt$_{Mt2}$ (PDB: 6RLG) consisting of two immunoglobulin-like domains and the catalytic domain with the YkuD fold. **C.** Outline of the proposed mechanism for the L,D-transpeptidase reaction.

2.3.2.2 Ldt_{Mt1}

Ldt_{Mt1}, also known as LdtA, was the first Ldt identified in *Mtb*, and is a homologue of the *Enterococcus faecium* Ldt_{fm}.[98] The catalysis of 3→3 cross-link formation by recombinant Ldt_{Mt1} was first observed with isolated disaccharide tetrapeptide PG monomer.[98] Ldt_{Mt1} has also been found to catalyse an exchange reaction of the terminal D-alanine for D-methionine.[99] The gene for Ldt_{Mt1}, Rv0116c or *ldt_{Mt1}*, was shown to be upregulated 17-fold under nutrient starvation,[100] suggesting it to be involved in the adaptive response to the stationary phase. Loss of Ldt_{Mt1}, however, did not alter *in vitro* growth of *Mtb*, nor did it alter cell morphology.[83]

2.3.2.3 Ldt_{Mt2}

Ldt_{Mt2}, also known as LdtB, has been shown to catalyse the formation of 3→3 cross-links of the isolated disaccharide tetrapeptide PG monomer, as well as an exchange reaction of the terminal D-alanine for D-methionine.[19,99] Expression of the gene for Ldt_{Mt2}, Rv2518c or *ldt_{Mt2}*, was found to be at least 10-fold higher than that for *ldt_{Mt1}* during all stages of growth.[19] Loss of Ldt_{Mt2} leads to attenuated growth, and an altered, shorter, cell morphology.[19,83] Colonies with Δ*ldt_{Mt2}* *Mtb* exhibited altered morphology, manifesting punctuated aerial growth of reduced size, with a smooth surface.[19] In mouse infection models, Δ*ldt_{Mt2}* strains exhibited normal growth during the first two weeks of infection, but did not undergo further proliferation, along with lacking signs of morbidity and mortality.[19] Absence of *ldt_{Mt2}* increased susceptibility to amoxicillin-clavulanic acid, both *in vitro* and in mice.[19] These combined findings suggests that inhibition of Ldt_{Mt2} alone may be sufficient to target 3→3 cross-linking in *Mtb*, despite the presence of other Ldt paralogs.

Interestingly, the altered morphology and attenuated growth and virulence observed in the Δ*ldt_{Mt2}* strain was more pronounced in a double mutant lacking both *ldt_{Mt1}* and *ldt_{Mt2}*.[83] Cells of this double mutant were significantly shorter and contained deep surface depressions and bulges, which was exacerbated at the late exponential phase, where cells completely lost their rod shape.[83] The strain lacking both *ldt_{Mt1}* and *ldt_{Mt2}* manifested aggravated attenuation of growth compared to the strain lacking only *ldt_{Mt2}*.[83] Increased susceptibility to amoxicillin-clavulanate, imipenem, and ertapenem was observed in comparison to the strain lacking only *ldt_{Mt2}*.[83] Thus, while inhibition of only Ldt_{Mt2} may be sufficient to target the essential 3→3 cross-linking in *Mtb*, dual inhibition of Ldt_{Mt1} and Ldt_{Mt2} likely has enhanced impact.

Ldt_{Mt2} has been shown to become essential for growth in the absence of PonA1, suggesting 3→3 cross-linking to be sufficient to compensate for functions of 4→3 cross-linking in their absence.[70] A genetic interaction network with PonA1 and PonA2 has been identified, indicating *ldt_{Mt2}* interacts with both *ponA1* and *ponA2*.[70] Further evidence for interactions between Ldts

and PBPs was found in *E. coli*, when the Ldt YcbB was found to interact with PBP1b, a homolog to the *Mtb* PBP PonA2, at a K_d of 250 ± 30 nM.[28]

2.3.2.4 Ldt_{Mt3}

Ldt_{Mt3}, also known as Rv1433, is the only Ldt in *Mtb* that has not been shown to biochemically catalyse the formation of 3→3 cross-links, nor was it observed to catalyse an exchange reaction of the terminal D-alanine for D-methionine.[99] Ldt_{Mt3} may therefore be involved in yet unidentified cross-linking reactions in *Mtb*. Note that in *E. coli*, three of five Ldt paralogs are not involved in the formation of 3→3 cross-links in the PG layer, but rather anchor the Braun lipoprotein to PG.[101,102] A strain of *Mtb* lacking *ldt_{Mt3}* did not exhibit inhibited growth or morphological changes compared to its parental strain.[19]

2.3.2.5 Ldt_{Mt4}

Ldt_{Mt4}, also known as Rv0192, has been shown to biochemically catalyse the formation of 3→3 cross-links between isolated disaccharide tetrapeptide PG monomers, as well as catalysing an exchange reaction of the terminal D-alanine for D-methionine.[99] However, a strain lacking *ldt_{Mt4}* was not distinguishable from its parental strain, exhibiting similar growth and morphologies.[19] Ldt_{Mt4} is as yet both structurally and functionally poorly understood.

2.3.2.6 Ldt_{Mt5}

The final Ldt paralog of *Mtb*, Ldt_{Mt5} (Rv0483), has also been shown to biochemically catalyse the formation of 3→3 cross-links, as well as catalysing an exchange reaction of the terminal D-alanine for D-methionine.[99] Loss of Ldt_{Mt5} did not alter growth or cell morphology, but a *Mtb* strain lacking *ldt_{Mt5}* was found to have increased susceptibility to crystal violet and osmotic shock, indicating that Ldt_{Mt5} may be involved in cell wall integrity.[84] Additionally, increased susceptibility to doripenem and faropenem was observed in the Δ*ldt_{Mt5}* strain.[84]

2.3.3 β-lactamases of *Mycobacterium tuberculosis*

2.3.3.1 BlaC

Several PBPs have been observed to exhibit β-lactamase-type activity due to efficient hydrolysis of the β-lactam derived acyl-enzyme complex, in particular in the case of PonA1 and PonA2.[103] In addition, *Mtb* contains four enzymes with confirmed β-lactamase activity: BlaC,[39,104] Rv2068c, Rv0406c and Rv3677c,[105] as well as many putative β-lactamases.[106] Of these, BlaC is widely regarded as the enzyme responsible for β-lactam resistance in *Mtb*.[3,21] Indeed, a Δ*blaC* strain of *Mtb* showed increased susceptibility to β-lactam antibiotic classes

of penicillins, cephalosporins, and carbapenems, and exhibited no detectable residual β-lactamase activity.[21]

BlaC is an Ambler class A serine β-lactamase, exhibiting a broad substrate profile, hydrolysing all classes of β-lactams,[52] but exhibiting particularly penicillinase and cephalosporinase activity.[39] However, overall catalytic activity of isolated BlaC is not as high as observed in other class A β-lactamases, such as SHV and TEM-1.[107,108] Carbapenems are relatively more resistant to BlaC hydrolysis, though measurable carbapenemase activity has been observed.[52]

2.3.3.2 Inhibitors of BlaC

BlaC can be inhibited by clavulanic acid (typically used as its potassium salt),[20,39] a mechanism based inhibitor containing the β-lactam motif, that is generally a potent inhibitor of SBLs from Ambler class A (Figure 2.3).[31,109] However, while clavulanic acid generally inhibits class A β-lactamases with high potency of typically K_i < 0.1 μM, BlaC is relatively poorly inhibited, with a K_i of 2.4 μM.[39] Wang *et al.* hypothesise that several distinct active site features of BlaC contribute to the broad substrate profile as well as relative low inhibitory potency of clavulanic acid, including an active site significantly larger than most class A β-lactamases, as a result of amino acid substitutions of key residues and rearrangement of conserved active site chains.[39] Nonetheless, *in vitro* addition of clavulanic acid significantly increases β-lactam activity in *Mtb*.[20,46,110,111]

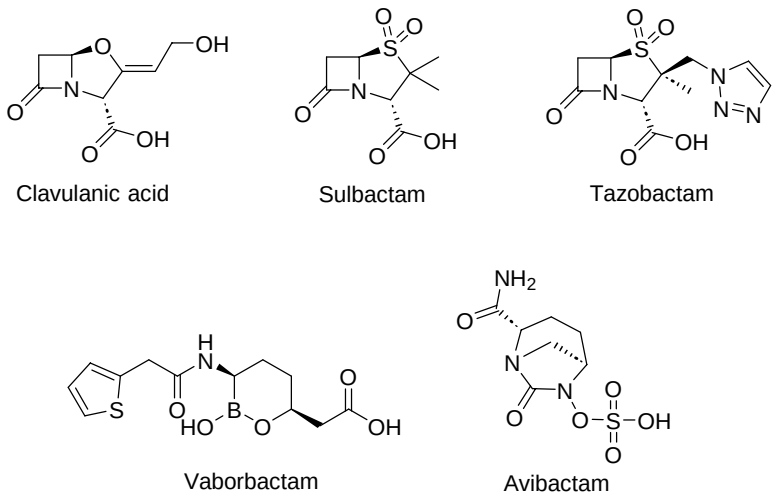

Figure 2.5. Chemical structure of clinically used β-lactamase inhibitors that inhibit BlaC.

Other β-lactamase inhibitors currently used in the clinic include the penam sulfones sulbactam and tazobactam,[112,113] the boronic acid vaborbactam,[114] and the diazabicyclooctane avibactam,[115] all of which are generally potent inhibitors of class A β-lactamases (Figure 2.5). Sulbactam and tazobactam have been found to inhibit BlaC,[116] though the generated covalent

adducts have been observed to be rapidly hydrolysed, with recovery of enzymatic activity within 30 and 45 minutes, respectively.[52] By contrast, recovery of BlaC activity following inhibition by clavulanic acid was found to occur more slowly, with ~50% recovery after 14 hours, though this was highly dependent on the presence of phosphate ions.[117] Avibactam was 100-fold less potent than clavulanic acid, though inhibition remained stable for at least 48 hours.[118] As with clavulanic acid, the *in vitro* application of sulbactam, tazobactam, and avibactam lead to an increase in potency of β-lactam antibiotics in *Mtb*.[54] Meropenem-vaborbactam was less active against *Mtb in vitro* compared to meropenem-clavulanic acid, though vaborbactam was able to reduce the MIC of meropenem two-fold.[119] Despite reported *in vivo* studies having focussed on β-lactam-β-lactamase inhibitor combinations with clavulanic acid,[45] *in vitro* studies have suggested that sulbactam serves as a more effective β-lactamase inhibitor in MDR-TB isolates.[53,54]

2.3.3.3 Resistance to β-lactamase inhibitors

Inhibition of BlaC has been shown to open prospects for the use of β-lactams to treat TB.[3,20,44] However, there is significant concern that drug resistance to a clinically applied β-lactamase inhibitor will develop. BlaC evolution experiments have shown that BlaC is able to develop resistance to clavulanic acid, sulbactam, and avibactam through single amino acid mutations.[120-122] The effect of these amino acid mutations, in particular K234R, was shown to translate to higher infection levels in a zebrafish-*Mycobacterium marinum* model of TB when treated with ampicillin-avibactam, compared to wildtype.[123] These results emphasise a potential risk for resistance development in the use of specific β-lactam-BlaC inhibitors to treat TB.

2.4 Inhibition of penicillin binding proteins and L,D-transpeptidases

2.4.1 Studies on the targets of β-lactams in *Mycobacterium tuberculosis*

As summarised above, *Mtb* contains many targets that are relevant to β-lactam inactivation, including seven PBPs, five Ldts, and a β-lactamase, many of which are essential for growth, virulence, and/or susceptibility to β-lactam antibiotics. Evaluating the roles of these targets in the inactivation of *Mtb* by β-lactams has therefore proven to be challenging, though the use of fluorescent probes has yielded various insights, consisting of both fluorescent reporters linked to inhibitors and substrate analogues.[124-126]

Fluorescent analogues of different classes of β-lactams have been assessed for interactions with cell lysates of *Mtb* including the monobactam aztreonam-Cy5, the cephalosporin cephalexin-Cy5, the carbapenem meropenem-Cy5 and the penicillin Bocillin-FL.[106] In their

study, Levine and Beatty included lysates from replicating *Mtb*, as well as dormant *Mtb*, induced by hypoxic conditions. They found that meropenem-Cy5 (Figure 2.6) inhibits the widest variety of PBP, Ldt and β-lactamase targets, including the PBPs PonA1, PonA2, PBPA, DacB, DacB1 and DacB2, the Ldts Ldt_{Mt2}, Ldt_{Mt3} and Ldt_{Mt5}, and the β-lactamase BlaC.[106] In dormancy, PonA1, PonA2, PBPA, Ldt_{Mt2}, Ldt_{Mt3} and Ldt_{Mt5} were found to remain active,[106] suggesting that these enzymes are important targets of meropenem in the latent phase of infection. In particular meropenem and faropenem exhibited inhibition of all labelled targets.[106] A study of *M. smegmatis* using fluorescent analogues of the pentapeptide substrate for PBPs and the tetrapeptide substrate for Ldts to asses PBP and Ldt activity in live cells (Figure 2.6), showed that D,D-transpeptidases could potently and dose-dependently be inhibited by meropenem, where Ldts were only inhibited by higher concentrations of the carbapenem.[127]

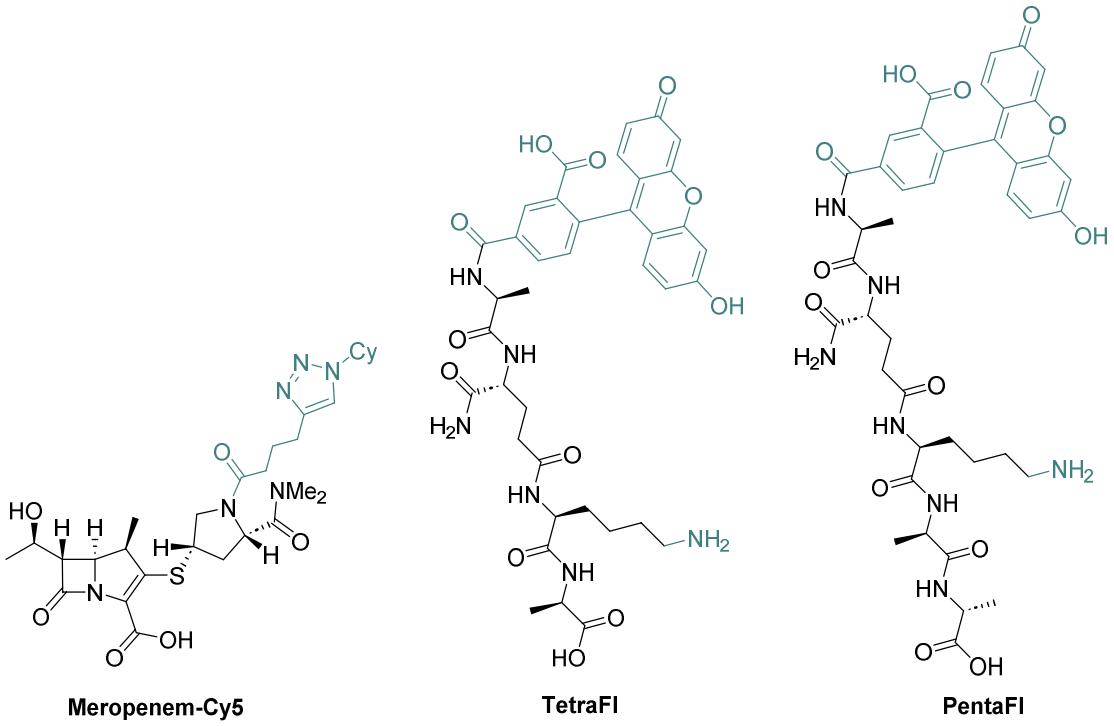

Figure 2.6. Fluorescent probes reported for inhibition studies of mycobacteria in cell lysate, or live cells. Meropenem-Cy5 was based on the inhibitor meropenem, with a linker and the fluorescent unit cyanine 5 (Cy5, represented as Cy). TetraFl and PentaFl represent fluorescent analogues of the substrates of Ldts and PBPs, respectively. Structural differences from native substrates or inhibitors are in teal.

The cephalosporin ceftriaxone, and in lesser degree cephalexin, effectively inhibited the PBPs, but not the Ldts or BlaC.[106] Interestingly, this observation contrasts with an earlier report by Lopez Quezada *et al.* (2020), who found that two non-commercial cephalosporin analogues active against non-replicating *Mtb* were unable to bind to PBPs, nor Ldts, and were therefore hypothesised to function through alternative targets.[128] Aztreonam did not appear to inhibit the

PBPs, Ldts, or BlaC, while the penicillins penicillin G, ampicillin, and carbenicillin exhibited inhibition of PBPA.[106] Interestingly, in *M. smegmatis*, ampicillin was found to inhibit PBP activity only at high concentrations, but not to affect Ldt activity.[127] Clavulanic acid only manifested binding to BlaC.[106]

2.4.2 Biochemical studies of the inhibition of the penicillin binding proteins with β-lactams

Chambers *et al.* (1995) initiated biochemical studies of the PBPs of *Mtb* by identifying four major PBPs using [^{3}H]penicillin-radiolabelling from the bacterial membrane.[20] The four PBPs identified has masses of ~94 kDa, ~82 kDa (tentatively assigned as PonA1 and PBP3, respectively),[129] ~52 kDa (tentatively assigned as PBPA),[129] and ~37 kDa (may corresponding to DacB, DacB1 or DacB2, based on molecular weight) were found all to be inhibited at therapeutically achievable concentrations of ampicillin, amoxicillin and imipenem.[20]

2.4.2.1 Penicillins

Kumar *et al.* (2022) have studied the interactions of a comprehensive panel of β-lactam antibiotics (penicillin, ampicillin, methicillin, cefdinir, cefotaxime, cefoxitin, imipenem, meropenem, biapenem, and faropenem) with all seven *Mtb* PBPs (PonA1, PonA2, PBPA, PBP3, DacB, DacB1 and DacB2).[103] They observed PBP3 to be consistently the most susceptible PBP to β-lactam inhibition.[103] The penicillins were observed to particularly target PBP3,[38,103] though penicillin and ampicillin additionally inhibited DacB2, and PBPA was susceptible to methicillin. In a different report, PBPA was found to be acylated by penicillin G,[130] though less efficiently than observed in other PBPs of different organisms.[131-133] Additionally, a crystal structure of PonA1 in complex with penicillin V has been reported.[134]

2.4.2.2 Carbapenems

Carbapenems have been observed to be efficient inhibitors of all PBPs.[103] The acylation efficiency of PBPA by the carbapenem imipenem was higher than penicillin and ceftriaxone.[130] There is evidence that meropenem does not inhibit PonA1 or DacB1,[103] though in the case of PonA1 this has been disputed.[134] Biapenem was apparently less efficient in inhibiting PonA1.[103] A crystal structure of DacB2 in complex with meropenem has been described.[135]

2.4.2.3 Cephalosporins

The cephalosporin cefoxitin manifested inhibition across a broad inhibition spectrum of PBPs, but cefotaxime did not inhibit DacB and DacB1.[103] PonA1 was found to bind cefotaxime with high affinity.[136] A study of the acylation rate of PBPA showed ceftriaxone to be a less efficient

acylating agent than imipenem, despite extensive interactions with particularly the R1 group in a crystal structure.[130]

2.4.2.4 Penems

Interestingly, Kumar *et al.* (2022) observed that faropenem, which is able to efficiently kill *Mtb*,[60] only inhibited PonA1 and DacB2.[103] However, this notion was disputed by the observation that PBP3 is covalently acylated by faropenem by Lu *et al.* (2020), who were additionally reported a crystal structure of this complex.[38]

2.4.2.5 Monobactams

Aztreonam known for its unique selectivity for PBP3 in gram-negative bacteria, but not gram-positive bacteria,[137,138] and was found to interact with PBP3 via extensive active site interactions in crystallographic studies.[38] However, no *in vitro* activity of aztreonam against *Mtb* has been observed,[139] despite PBP3 being an essential target.

2.4.3 Biochemical studies of the inhibition of the L,D-transpeptidases

2.4.3.1 Carbapenems are inhibitors of L,D-transpeptidases

The Ldts are generally not efficiently inhibited by most classes of β-lactam antibiotics; β-lactams are proposed to be mimics of a high energy confirmation of the D-ala-D-ala of the pentapeptide substrate of PBPs (Figure 2.5). Ldt_{Mt1} has not been observed to interact with the penicillin ampicillin in mass spectrometry (MS) studies,[98] though some inhibitory activity of penicillins for Ldt_{Mt2} has been reported.[25,140] Cephalosporins have been found to be poor inhibitors of Ldts, though covalent reaction and inhibition have been observed with Ldt_{Mt1}, particularly by ceftriaxone (k_{inact}/K_{app} 9.2 x 10^3 μM^{-1} min^{-1}).[141] Additionally, evidence for the inhibition of Ldt_{Mt2} by cephalothin has been reported in MS studies and nitrocefin hydrolysis studies.[24] The (carba)penem β-lactams are regarded as mimics of the L,D-chirality in the tetrapeptide substrate of Ldts, translating to more potent inhibition of Ldts (Figure 2.7).[24,99,142] Ldt_{Mt1-4} have been observed to covalently react with carbapenems, while modification of Ldt_{Mt5} was not demonstrated.[99] However, a crystal structure of Ldt_{Mt5} in complex with meropenem evidences the ability of Ldt_{Mt5} to react with carbapenems.[84]

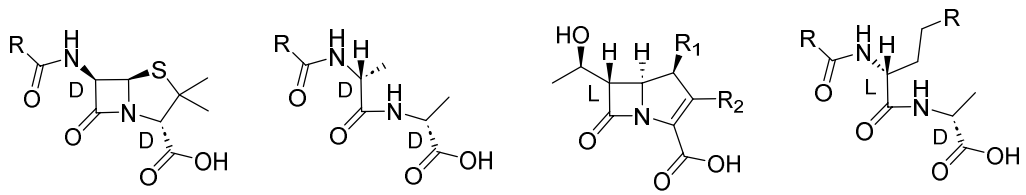

Figure 2.7. The chirality of most β-lactams, such as penicillins, mimic the D-Ala-D-Ala chirality of PBP substrates, while (carba)penems mimic the chirality of *m*-DAP-D-Ala, the substrate of Ldts.

The interaction of Ldt_{Mt2} with β-lactams has been particularly well characterised, likely due to its role as the dominant Ldt in *Mtb*. Steiner *et al.* (2017) systematically studied the inhibition of Ldt_{Mt2} by 16 β-lactam antibiotics using Ellman's reagent to assay the availability of the active site cysteine, and found that faropenem displayed the highest rate of covalent reaction, followed by the carbapenems tebipenem, meropenem, ertapenem, doripenem, and biapenem.[25] Similarly, Kumar *et al.* (2017) observed efficient interaction of Ldt_{Mt2} by the carbapenems doripenem and biapenem, while little to no inhibition was observed by penicillins and cephalosporins, with exception of cefalothin.[24] Efficient inhibition by meropenem was further shown by Zandi and Townsend (2021) with an inactivation rate of 0.04 μM^{-1} min^{-1}, though the inhibition was shown to be reversible.[143] Ldt_{Mt2} apparently is able to regain function through reformation of the β-lactam ring, hydrolysis of the thioester adduct, and through formation of the β-lactone product.[143]

2.4.3.2 Faropenem is the most potent reported inhibitor of Ldt_{Mt1-4}

Interestingly, as observed with Ldt_{Mt2}, faropenem has been identified as the superior inhibitor over the tested carbapenems for inhibition in Ldt_{Mt1}, Ldt_{Mt3} and Ldt_{Mt4}.[60] Acylation by faropenem compared to meropenem was 14-fold and 22-fold faster with Ldt_{Mt1} and Ldt_{Mt2}, respectively (590 and 11 μM^{-1} min^{-1} [10^3]), as determined by steady-state kinetics. With both Ldts meropenem was also hydrolysed 4-fold quicker (1.0 and 0.7 min^{-1} [10^3], respectively) compared to faropenem.[60] Ldt_{Mt3} and Ldt_{Mt4} were acylated 6-fold and 9-fold faster, (10.9 and 4.8 μM^{-1} min^{-1} [10^3], respectively), while Ldt_{Mt5} was apparently not modified by either meropenem or faropenem.[60] Upon interaction of faropenem with Ldt_{Mt1} or Ldt_{Mt2}, the resulting adduct is observed to fragment to a yield β-OH-butyryl adduct by MS studies.[24,25,144] A similar degradation product is observed in a crystal structure of Ldt_{Mt3} in complex with faropenem.[145]

2.5 Optimisation of β-lactams for *Mycobacterium tuberculosis*

2.5.1 Reported recommendations on β-lactam optimisation

As outlined above, there is increasing evidence that β-lactams have the potential to be used for the treatment of TB, and while there is benefit in repurposing known drugs, studies have shown optimisation for TB targets may be required to achieve potent inhibition of PBPs and Ldts, while being resistant to BlaC inactivation. Based on these requirements, β-lactam optimisation studies have focussed on the carbapenems subclass, due to their relative resistance to hydrolysis by BlaC, and their ability to inhibit Ldt_{Mt1-4} and all PBPs. The diverse sidechains of carbapenems were demonstrated to affect the acylation kinetics of Ldts paralogs differently, evidencing that sidechain modification could be used to optimise antibacterial activity.[99] Further, the combination of various inhibitors that inhibit different targets may be pursued, as evidenced by synergy between the two β-lactams meropenem and amoxicillin in combination with the β-lactamase inhibitor clavulanic acid across 28 clinical MDR-TB strains.[146]

Various structural studies of carbapenems reacted with PBPs and Ldts of *Mtb* have provided the basis for SAR based optimisation of carbapenems for their respective targets (Figure 2.8). Structures of Ldt_{Mt2} in complex with meropenem and imipenem have provided insights into the cause of the increased potency of imipenem for this enzyme, as tighter binding in the oxyanion hole was observed, in combination with more hydrogen bond interactions.[147] Gokulan *et al.* (2018) deducted that more flexible sidechains lead to improved inhibition, and that optimisation of the C2 chain of imipenem to interact with residues such as Tyr330, Ser331, Gly332 and Glu327 would lead to improved activity.[147] Alternatively, crystal structures of PBP3 with meropenem suggest that the C2 sidechain, which is largely exposed to the solvent, may be used to minimise BlaC hydrolysis, as well as optimising permeability and efflux properties.[38] By contrast, in DacB2 the distal end the meropenem C2 sidechain was observed to interact with a surface area that is varied between different PBPs, and may therefore lead to increased potency with this enzyme.[91] Carbapenems with pyrrolidine derivatives, such as meropenem, are generally observed to exhibit broader antimicrobial activities,[57,148,149] suggesting incorporation of this moiety in optimisation studies may be of interest.

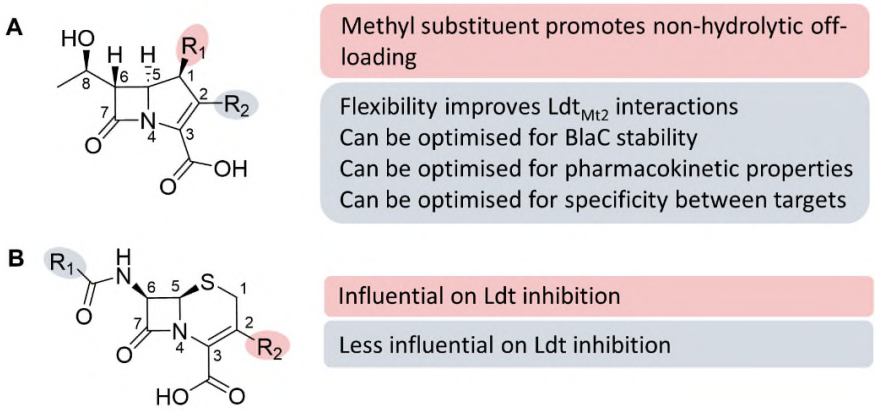

Figure 2.8. Recommendations on the optimisation of carbapenems (A) and cephalosporins (B) based on studies with PBPs and Ldts with commercial β-lactams.

Besides the optimisation of binding interactions of carbapenems, optimisation of the stability of the acyl-enzyme complex should be aimed for. Both PBPs and Ldts have been shown to hydrolyse carbapenems, indicating that even upon successful inhibition of BlaC, the effective drug concentration will still be reduced due to hydrolytic and nonhydrolytic (e.g., lactone formation, and β-lactam ring reformation, as observed with Ldt$_{Mt2}$ and meropenem) off-loading reactions from Ldts and PBPs.[103,143] From this perspective it is notable that a C1 1β-methyl substituent, present on the carbapenems meropenem, biapenem and doripenem, but not imipenem and panipenem, appears to be essential for lactone formation in β-lactamases.[150]

As described, cephalosporins are generally not efficient inhibitors of Ldts, but are inhibitors of PBPs.[24,25,103] However, Ldt$_{Mt1}$ has been shown to be inhibited by cephalosporins, in particular ceftriaxone.[141] Upon examination of the sidechains, the C2 chain has been identified to particularly influence inhibitory potency, suggesting optimisations of the C2 sidechain may lead to improved inhibitory activity of cephalosporins in Ldts.[141]

2.5.2 Development of β-lactams for *Mycobacterium tuberculosis*

2.5.2.1 Optimisation of carbapenems

The novel tricyclic prodrug carbapenem sanfetrinem cilexetil is currently in phase II clinical trials for the treatment of TB (Figure 2.9).[151] Sanfetrinem was initially developed in the 1990s for upper respiratory infections, but its development was halted due to commercial considerations.[152] In a screen of approximately 2000 β-lactams against *Mtb* it was identified as most the potent derivative, with an MIC of 0.5 µg/mL when residing in macrophages, and 1.5 µg/mL in media.[152]

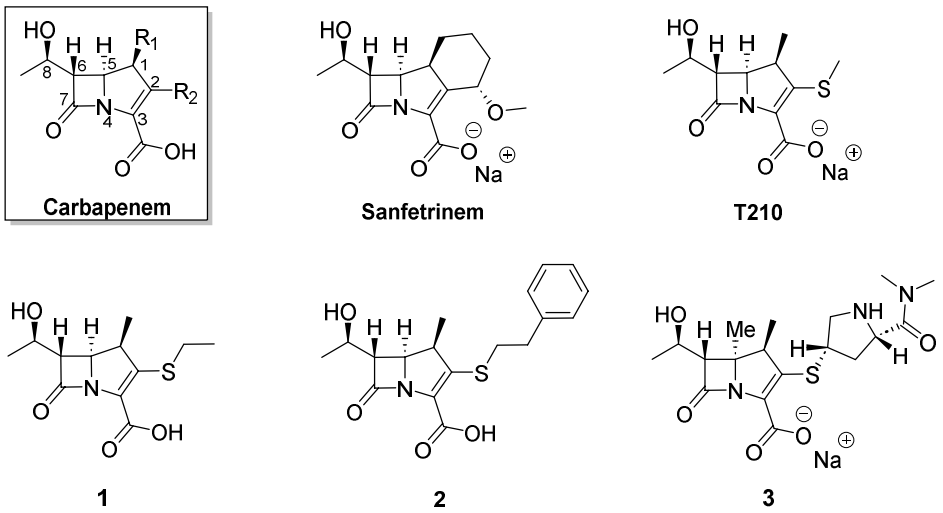

Figure 2.9. Optimised carbapenems against *Mycobacterium tuberculosis*.

Kumar *et al.* (2016) studied the effect of C2 substituents of carbapenems for Ldt_{Mt2} inhibition, based on the notion that the C2 substituents were mainly exposed to the solvent, and could therefore be used to modify physicochemical properties.[24] Naive Bayesian machine-leaning was applied to identify frequent sulphur substituents in known *Mtb* inhibitors, resulting in twelve carbapenems with *in vitro* activity against *Mtb*, as well as inhibition of Ldt_{Mt1} and Ldt_{Mt2} that was at least as efficient as known carbapenems.[24] Interestingly, the most potent *Mtb* inhibition was observed with T210 (Figure 2.9), a relatively simple carbapenem with a thiomethyl C2 sidechain, with Ldt_{Mt2} acylation kinetics of 0.07 μM^{-1} min^{-1}, and MIC of 0.25-0.5 µg/mL.[24]

Iannazzo *et al.* (2016) synthesised a set of carbapenems with various C2 sidechains, as well as C8 hydroxyl ester derivatives, which were subsequently tested for inhibition of Ldt_{Mt1} and hydrolysis by BlaC.[153] Eleven carbapenems with increased acylation efficiency over meropenem, and seven with increased acylation efficiency over ertapenem were identified, though overall the C2 sidechain had only limited impact on acylation efficiency.[153] Again, a relatively simple carbapenem with a thioethyl C2 sidechain (**1**; Figure 2.9) was identified as a potent inhibitor of Ldt_{Mt1} (k_2/K_{app} 10.8 x 10^3 M^{-1} s^{-1}).[153] Interestingly, the C2 sidechain was found to have a substantial effect on resistance to BlaC hydrolysis, without reducing inhibitory potency for Ldt_{Mt1}.[153] The most potent increase in Ldt_{Mt1} inhibition and decrease in BlaC hydrolysis was observed in a carbapenem with a thioethylphenol C2 sidechain (**2**; Figure 2.9), with an Ldt_{Mt1} k_2/K_{app} of 39.0 x 10^3 M^{-1} s^{-1} and a BlaC k_{cat}/K_m of 360 M^{-1} s^{-1}.[153]

Gupta *et al.* (2021) assessed the effect of C5α-modification of the carbapenem scaffold, and found that derivatisation of the C5α with a methyl-group in combination with a the meropenem pyrrolidine C2 side chain (**3**; Figure 2.9) improved the activity over meropenem in combination with clavulanic acid (MIC of 0.1 µg/mL and 0.5 µg/mL, respectively).[154] The compound was

shown to interact with Ldt_{Mt2} in MS studies, and avoid BlaC hydrolysis, factors which the authors hypothesise to contribute to the increased potency observed.

2.5.2.2 Optimisation of penems

Based on faropenem being the most potent reported inhibitor of Ldts in several mycobacteria, Batchelder *et al.* (2020) set out to further assess the penem subclass to target mycobacteria.[155] The penem T405 (Figure 2.10) was identified from a screen of a library of penems with varying C2 sidechains, with similarly potent inhibition of *Mtb* as meropenem (MIC of 0.5-1 µg/mL). In addition, T405 manifested particularly increased potency against *Mycobacterium abscessus* (MIC 2 µg/mL) over faropenem (MIC 512 µg/mL).[155] T405 was found to have a favourable pharmacokinetic and toxicologic profile.[155] Additionally, T405 was found to have a broader inhibition profile for all seven PBPs of *Mtb*, exhibiting increased potency compared to faropenem (e.g., IC_{50} of 6.6 µM and 126 µM, respectively, in the inhibition of PBP3).[103]

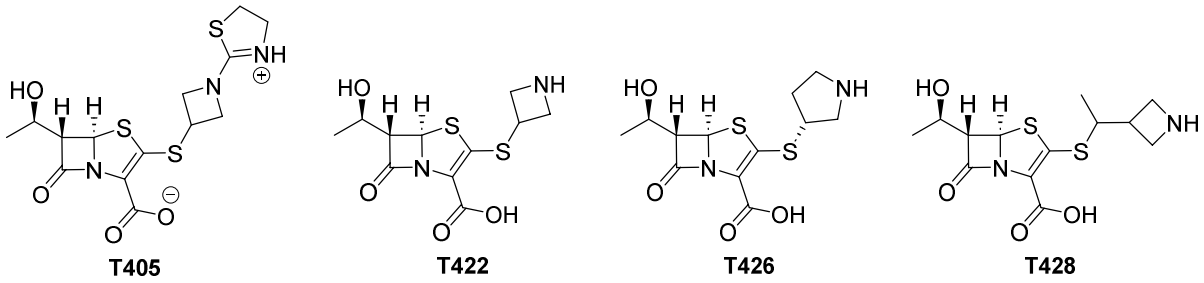

Figure 2.10. Optimised penems against *Mycobacterium tuberculosis*.

Encouraged by the promising results obtained with T405, a structure-activity relationship study based on this penem was performed, focusing on modification of the two rings on the T405 sidechain.[156] The resulting penems were tested against *Mtb* and resulted in a set of equally potent, or 2x increased potent inhibitors of *Mtb* (MIC 0.25-0.5 µg/mL), when tested in the presence of clavulanic acid.[156] The most potent penems, T422, T426, and T428 (Figure 2.10), were additionally tested for covalent inhibition of Ldt_{Mt2} and DacB2 in MS studies. All the penems reacted with Ldt_{Mt2}, giving the same fragmentation product observed with faropenem.[156] The penems additionally reacted with DacB2, though T405 and T428 were apparently prone to hydrolysis, making T422 and T426 more promising candidates.[156]

2.5.2.3 Optimisation of cephalosporins

A high-throughput screen against replicating and nonreplicating *Mtb* identified three cephalosporin esters that were selectively potent inhibitors of nonreplicating *Mtb* (MIC 0.5-2.7 µg/mL).[157] SAR studies based on the hit compounds yielded potent cephalosporins active against nonreplicating *Mtb* (e.g., **4** with MIC 0.88 µg/mL for nonreplicating *Mtb* but >100 µg/mL

for replicating *Mtb*; Figure 2.11), that exhibit a favourable pharmacokinetic profile as well as being non-toxic, and active in macrophages.[157]

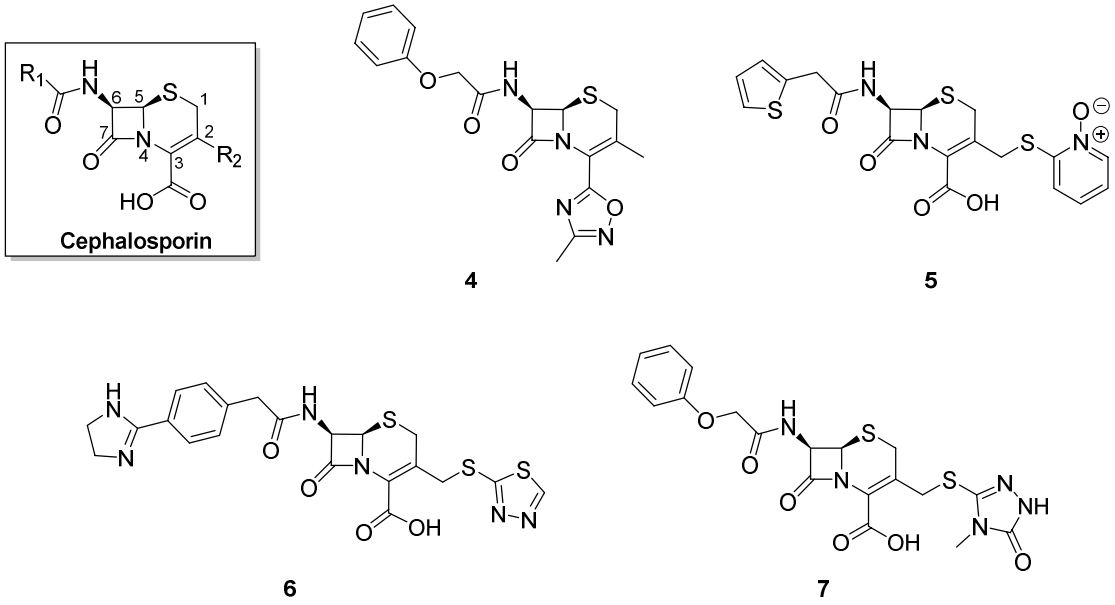

Figure 2.11. Optimised cephalosporins against *Mycobacterium tuberculosis.*

A targeted screen on a library of β-lactams against *Mtb* yielded the identification of cephalosporins active against *Mtb* both in replicating and nonreplicating conditions, referred to as dual-active inhibitors.[158] Interestingly, a set of four potent dual-active cephalosporins contained a pyrithione moiety at the C3 sidechain (e.g., **5** with MIC 1.56 μg/mL for both replicating and nonreplicating *Mtb*; Figure 2.11), which was observed to be released upon hydrolysis.[158] Interestingly, studies of the mode of action revealed that during the replicating state the release of this pyrithione moiety was not required, while it was required in order to inhibit *Mtb* in the nonreplicating state, suggesting these cephalosporins to act differently in the two different metabolic states.[158] BlaC was found to catalyse the release of the pyrithione moiety, though activity of the cephalosporins was independent of BlaC activity.[158] Interestingly, the cephalosporins were not observed to inhibit any transpeptidases of *Mtb*, suggesting the identified β-lactams to function via targeting of a diverse set of proteins.[128]

A large collaborative effort between pharmaceutical companies and academic institutions collectively tested ~8900 β-lactams, predominantly consisting of cephalosporins, for activity against *Mtb*.[159] Unexpectedly, a ≥90% inhibition hit rate of 18% was observed, with many of the β-lactams showing activity even in the absence of a β-lactamase inhibitor,[159] demonstrating the potential of β-lactams, and particularly cephalosporins, to be optimised for use in *Mtb*. One of the hit compounds, cephalosporin **6** (MIC 0.5 μM; Figure 2.11), was observed to be active in mice infected with *Mtb*.[159]

A high-throughput screen for Ldt_{Mt2} using a targeted library of various electrophilic compounds (as described in Chapter 3), including β-lactams, identified cephalosporins (e.g., **7**, IC_{50} 2.4 μM; Figure 2.11) with inhibitory profiles of Ldt_{Mt2} similar to carbapenems.[160] Though this did not translate to potent inhibition of *Mtb*, findings evidence that cephalosporins may be optimised for inhibition of Ldt_{Mt2}.[160]

2.5.2.4 Optimisation of monocyclic β-lactams

Monocyclic β-lactams have been observed to be active against a variety of pathogenic bacteria, including, in moderate levels, against *Mtb* (MIC 25-200 μg/mL).[161-163] Structure-activity relationship studies have shown that derivatisation of the sidechains (e.g., **8**; Figure 2.12) can improve the activity against *Mtb*.[164] Martelli *et al*. (2021) designed a series of low molecular weight monocyclic N-thiolated β-lactams, inspired by the fragmentation reactions leading to Ldt inhibition by faropenem.[165] Several of the resulting monocyclic β-lactams (e.g., **9**, rate of adduct formation of 0.018 s^{-1}; Figure 2.12) inhibit Ldt_{Mt2} as efficiently or more potently than meropenem, doripenem and ertapenem (rate of adduct formation of 0.011-0.018 s^{-1}), resulting in moderate activity against *Mtb* (MIC 10 μg/mL).[165]

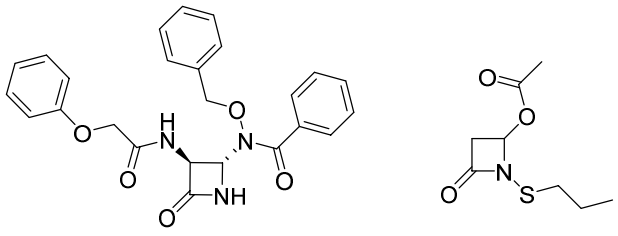

8 **9**

Figure 2.12. Optimised monocyclic β-lactams against *Mycobacterium tuberculosis*.

2.6 Summary and conclusions

Mtb has not classically been considered for treatment with β-lactam antibiotics, due to various resistance mechanisms, such as expression of the β-lactamase BlaC.[3,5] However, several *in vitro* studies employing β-lactam-β-lactamase inhibitor combinations have shown that upon inactivation of BlaC, β-lactams are active against *Mtb*.[43-45] However, there is increasing evidence that known β-lactams are insufficiently potent to achieve clinically relevant *in vivo* efficacy.[43]

A complication in the development of β-lactams for *Mtb* lies in the notion that the PG biosynthesis of mycobacteria employs not only the well-studied PBPs, but also Ldts.[15,16] Ldts catalyse 3→3 cross-linking between tetrapeptide strands and employ a nucleophilic cysteine residue, while PBPs catalyse 4→3 cross-linking between pentapeptide strands and employ a

catalytic serine residue.[17,18] Inhibitors targeting PG biosynthesis will likely require inhibition of both enzymatic classes.

The genome of *Mtb* encodes for at least seven PBPs and five Ldts.[69] Of these, only PBP3 is confirmed to be essential for *Mtb* growth,[77] with some evidence indicating an essential role also for DacB.[79] However, under certain circumstances, various additional PBPs and Ldts are essential. PonA1 and PonA2 are essential in each other's absence, as well as during infection.[70,71,74] PBPA was as well found to be essential for survival and granuloma formation during infection.[75] DacB was found to be required for efficient growth,[79] while DacB2 is required under specific stress conditions.[81,82] Ldt_{Mt2} acts apparently as the main Ldt of *Mtb*, as loss of the corresponding gene leads to the most pronounced alterations in growth, morphology, and virulence.[19] Ldt_{Mt2} is therefore considered to be a stand-alone target for drug development efforts. However, evidence suggests that dual inhibition of Ldt_{Mt2} and Ldt_{Mt1} would lead to an enhanced response in growth inhibition, morphology, and virulence.[83] While the functions of Ldt_{Mt3} and Ldt_{Mt4} are poorly understood, and the enzymes are apparently redundant,[19] deletion studies suggest that Ldt_{Mt5} is involved in cell wall integrity.[84] Both with Ldts and PBPs, several paralogs appear to have redundant roles, though their functionality does not overlap completely.

Carbapenems are a particularly promising class of β-lactams for the development of treatments against *Mtb*.[43] The carbapenems are inhibitors of both PBPs and Ldts and are slow substrates of the β-lactamase BlaC.[43,52] However, downsides of carbapenems are their low hydrolytic stability in aqueous solutions, and their poor oral bioavailability.[43] Conversely, there is evidence that cephalosporins, which exhibit increased hydrolytic stability and bioavailability over carbapenems, can be tailored not only towards inhibition of both PBPs and Ldts, but potentially also towards increased stability against BlaC catalysed hydrolysis.[141,159,160]

A limited set of optimisation studies of β-lactams tailored towards activity against *Mtb* has been reported. Efforts on optimisation have been focussed primarily on the optimisation of penems and carbapenems, and have demonstrated the potential for increased potency and BlaC stability through sidechain modification.[24,153-156] However, high-throughput studies of libraries containing β-lactams have identified various cephalosporins with potent activity against *Mtb*, and in the case of **6** (Figure 2.11) with activity against TB in mice.[158-160] Target-based optimisation of cephalosporins has not been reported.

Overall, the penems, carbapenems and cephalosporins manifest promise as templates for the optimisation of β-lactams for *Mtb*, holding potential for inhibition of essential targets of the PG layer synthesis, including both PBPs and Ldts. Studies of PBPs and Ldts have elucidated several essential targets, such as PBP3 and Ldt_{Mt2}, though the precise roles of many β-lactam

targets have yet to be determined. Both target-based discovery and whole-cell studies have yielded β-lactams with potent activity against *Mtb*, though further *in vitro* and *in vivo* studies will be essential in determining the future for β-lactams targeting *Mtb*.

2.7 References

1 Fleming, A. On the antibacterial action of a *Penicillium*, with special reference to their use in the isolation of *B. influenzae*. *Brit. J. Exp. Pathol.* **10**, 226-236 (1929).

2 Bush, K. & Bradford, P. A. β-Lactams and β-Lactamase Inhibitors: An Overview. *Cold Spring Harb. Perspect. Med.* **6** (2016).

3 Kurz, S. G. & Bonomo, R. A. Reappraising the use of β-lactams to treat tuberculosis. *Expert Rev. Anti Infect. Ther.* **10**, 999-1006 (2012).

4 Solotorovsky, M., Bugie, E. J. & Frost, B. M. The Effect of Penicillin on the Growth of *Mycobacterium tuberculosis* in Dubos' Medium. *J. Bacteriol.* **55**, 555-559 (1948).

5 Wivagg, C. N., Bhattacharyya, R. P. & Hung, D. T. Mechanisms of β-lactam killing and resistance in the context of *Mycobacterium tuberculosis*. *J. Antibiot.* **67**, 645-654 (2014).

6 Tipper, D. J. & Strominger, J. L. Mechanism of action of penicillins: a proposal based on their structural similarity to acyl-D-alanyl-D-alanine. *Proc. Natl. Acad. Sci. U.S.A.* **54**, 1133-1141 (1965).

7 Georgopapadakou, N., Hammarström, S. & Strominger, J. L. Isolation of the penicillin-binding peptide from D-alanine carboxypeptidase of *Bacillus subtilis*. *Proc. Natl. Acad. Sci. U.S.A.* **74**, 1009-1012 (1977).

8 Spratt, B. G. Properties of the penicillin-binding proteins of *Escherichia coli* K12. *Eur. J. Biochem.* **72**, 341-352 (1977).

9 Spratt, B. G. Penicillin-binding proteins and the future of beta-lactam antibiotics. The Seventh Fleming Lecture. *J. Gen. Microbiol.* **129**, 1247-1260 (1983).

10 Sauvage, E., Kerff, F., Terrak, M., Ayala, J. A. & Charlier, P. The penicillin-binding proteins: structure and role in peptidoglycan biosynthesis. *FEMS Microbiol. Rev.* **32**, 234-258 (2008).

11 Strominger, J. L., Blumberg, P. M., Suginaka, H., Umbreit, J. & Wickus, G. G. How penicillin kills bacteria: progress and problems. *Proc. R. Soc. Lond. B. Biol. Sci.* **179**, 369-383 (1971).

12 Hartmann, R., Höltje, J. V. & Schwarz, U. Targets of penicillin action in *Escherichia coli*. *Nature* **235**, 426-429 (1972).

13 Blumberg, P. M. & Strominger, J. L. Interaction of penicillin with the bacterial cell: penicillin-binding proteins and penicillin-sensitive enzymes. *Bacteriol. Rev.* **38**, 291-335 (1974).

14 Walsh, C. & Wencewicz, T. *Antibiotics: challenges, mechanisms, opportunities*. (John Wiley & Sons, 2020).

15 Seiler, P., Ulrichs, T., Bandermann, S., Pradl, L., Jörg, S., Krenn, V., Morawietz, L., Kaufmann, S. H. & Aichele, P. Cell-wall alterations as an attribute of *Mycobacterium tuberculosis* in latent infection. *J. Infect. Dis.* **188**, 1326-1331 (2003).

16 Bacon, J., Alderwick, L. J., Allnutt, J. A., Gabasova, E., Watson, R., Hatch, K. A., Clark, S. O., Jeeves, R. E., Marriott, A., Rayner, E., Tolley, H., Pearson, G., Hall, G., Besra, G. S., Wernisch, L., Williams, A. & Marsh, P. D. Non-replicating *Mycobacterium tuberculosis* elicits a reduced infectivity profile with corresponding modifications to the cell wall and extracellular matrix. *PLoS One* **9**, e87329 (2014).

17 Pisabarro, A. G., de Pedro, M. A. & Vazquez, D. Structural modifications in the peptidoglycan of *Escherichia coli* associated with changes in the state of growth of the culture. *J. Bacteriol.* **161**, 238-242 (1985).

18 Glauner, B., Höltje, J. & Schwarz, U. The composition of the murein of *Escherichia coli*. *J. Biol. Chem.* **263**, 10088-10095 (1988).

19 Gupta, R., Lavollay, M., Mainardi, J.-L., Arthur, M., Bishai, W. R. & Lamichhane, G. The *Mycobacterium tuberculosis* protein Ldt_{Mt2} is a nonclassical transpeptidase required for virulence and resistance to amoxicillin. *Nat. Med.* **16**, 466-469 (2010).

20 Chambers, H. F., Moreau, D., Yajko, D., Miick, C., Wagner, C., Hackbarth, C., Kocagöz, S., Rosenberg, E., Hadley, W. K. & Nikaido, H. Can penicillins and other beta-lactam antibiotics be used to treat tuberculosis? *Antimicrob. Agents Chemother.* **39**, 2620-2624 (1995).

21 Flores, A. R., Parsons, L. M. & Pavelka, M. S. Genetic analysis of the beta-lactamases of *Mycobacterium tuberculosis* and *Mycobacterium smegmatis* and susceptibility to beta-lactam antibiotics. *Microbiology (Reading, Engl.)* **151**, 521-532 (2005).

22 Lun, S., Miranda, D., Kubler, A., Guo, H., Maiga, M. C., Winglee, K., Pelly, S. & Bishai, W. R. Synthetic Lethality Reveals Mechanisms of *Mycobacterium tuberculosis* Resistance to Beta-Lactams. *mBio* **5**, 10.1128/mbio.01767-01714 (2014).

23 Mainardi, J. L., Hugonnet, J. E., Rusconi, F., Fourgeaud, M., Dubost, L., Moumi, A. N., Delfosse, V., Mayer, C., Gutmann, L., Rice, L. B. & Arthur, M. Unexpected Inhibition of Peptidoglycan LD-Transpeptidase from *Enterococcus faecium* by the β-Lactam Imipenem. *J. Biol. Chem.* **282**, 30414-30422 (2007).

24 Kumar, P., Kaushik, A., Lloyd, E. P., Li, S.-G., Mattoo, R., Ammerman, N. C., Bell, D. T., Perryman, A. L., Zandi, T. A., Ekins, S., Ginell, S. L., Townsend, C. A., Freundlich, J. S. & Lamichhane, G. Non-classical transpeptidases yield insight into new antibacterials. *Nat. Chem. Biol.* **13**, 54-61 (2017).

25 Steiner, E. M., Schneider, G. & Schnell, R. Binding and processing of β-lactam antibiotics by the transpeptidase Ldt_{Mt2} from *Mycobacterium tuberculosis*. *FEBS J.* **284**, 725-741 (2017).

26 Mainardi, J. L., Fourgeaud, M., Hugonnet, J. E., Dubost, L., Brouard, J. P., Ouazzani, J., Rice, L. B., Gutmann, L. & Arthur, M. A novel peptidoglycan cross-linking enzyme for a beta-lactam-resistant transpeptidation pathway. *J. Biol. Chem.* **280**, 38146-38152 (2005).

27 Hugonnet, J.-E., Mengin-Lecreulx, D., Monton, A., den Blaauwen, T., Carbonnelle, E., Veckerlé, C., Brun, Y. V., van Nieuwenhze, M., Bouchier, C., Tu, K., Rice, L. B. & Arthur, M. Factors essential for L,D-transpeptidase-mediated peptidoglycan cross-linking and β-lactam resistance in *Escherichia coli*. *eLife* **5**, e19469 (2016).

28 Caveney, N. A., Caballero, G., Voedts, H., Niciforovic, A., Worrall, L. J., Vuckovic, M., Fonvielle, M., Hugonnet, J.-E., Arthur, M. & Strynadka, N. C. J. Structural insight into YcbB-mediated beta-lactam resistance in *Escherichia coli*. *Nat. Commun.* **10**, 1849 (2019).

29 Massova, I. & Mobashery, S. Kinship and diversification of bacterial penicillin-binding proteins and beta-lactamases. *Antimicrob. Agents Chemother.* **42**, 1-17 (1998).

30 Frère, J. M. & Joris, B. Penicillin-sensitive enzymes in peptidoglycan biosynthesis. *Crit. Rev. Microbiol.* **11**, 299-396 (1985).

31 Drawz, S. M. & Bonomo, R. A. Three decades of beta-lactamase inhibitors. *Clin. Microbiol. Rev.* **23**, 160-201 (2010).

32 Andreeva, A., Howorth, D., Brenner, S. E., Hubbard, T. J., Chothia, C. & Murzin, A. G. SCOP database in 2004: refinements integrate structure and sequence family data. *Nucleic acids res.* **32**, D226-D229 (2004).

33 Goffin, C. & Ghuysen, J.-M. Multimodular penicillin-binding proteins: an enigmatic family of orthologs and paralogs. *Microbiol. Mol. Biol. Rev.* **62**, 1079-1093 (1998).

34 Philippon, A., Jacquier, H., Ruppé, E. & Labia, R. Structure-based classification of class A beta-lactamases, an update. *Curr. Res. Transl. Med.* **67**, 115-122 (2019).

35 Biarrotte-Sorin, S., Hugonnet, J.-E., Delfosse, V., Mainardi, J.-L., Gutmann, L., Arthur, M. & Mayer, C. Crystal structure of a novel β-lactam-insensitive peptidoglycan transpeptidase. *J. Mol. Biol.* **359**, 533-538 (2006).

36 Böth, D., Steiner, E. M., Stadler, D., Lindqvist, Y., Schnell, R. & Schneider, G. Structure of Ldt_{Mt2}, an L,D-transpeptidase from *Mycobacterium tuberculosis*. *Acta Crystallogr. D* **69**, 432-441 (2013).

37 Bielnicki, J., Devedjiev, Y., Derewenda, U., Dauter, Z., Joachimiak, A. & Derewenda, Z. S. *B. subtilis* ykuD protein at 2.0 Å resolution: insights into the structure and function of a novel, ubiquitous family of bacterial enzymes. *Proteins* **62**, 144-151 (2006).

38 Lu, Z., Wang, H., Zhang, A., Liu, X., Zhou, W., Yang, C., Guddat, L., Yang, H., Schofield, C. J. & Rao, Z. Structures of *Mycobacterium tuberculosis* Penicillin-Binding Protein 3 in Complex with Five β-Lactam Antibiotics Reveal Mechanism of Inactivation. *Mol. Pharmacol.* **97**, 287-294 (2020).

39 Wang, F., Cassidy, C. & Sacchettini, J. C. Crystal structure and activity studies of the *Mycobacterium tuberculosis* beta-lactamase reveal its critical role in resistance to beta-lactam antibiotics. *Antimicrob. Agents Chemother.* **50**, 2762-2771 (2006).

40 de Munnik, M., Lohans, C. T., Lang, P. A., Langley, G. W., Malla, T. R., Tumber, A., Schofield, C. J. & Brem, J. Targeting the *Mycobacterium tuberculosis* transpeptidase Ldt_{Mt2} with cysteine-reactive inhibitors including ebselen. *Chem. Commun.* **55**, 10214-10217 (2019).

41 Hugonnet, J.-E., Tremblay, L. W., Boshoff, H. I., Barry, C. E. & Blanchard, J. S. Meropenem-Clavulanate Is Effective Against Extensively Drug-Resistant *Mycobacterium tuberculosis*. *Science* **323**, 1215-1218 (2009).

42 Diacon, A. H., van der Merwe, L., Barnard, M., von Groote-Bidlingmaier, F., Lange, C., García-Basteiro, A. L., Sevene, E., Ballell, L. & Barros-Aguirre, D. β-Lactams against Tuberculosis — New Trick for an Old Dog? *N. Engl. J. Med.* **375**, 393-394 (2016).

43 Jaganath, D., Lamichhane, G. & Shah, M. Carbapenems against *Mycobacterium tuberculosis*: a review of the evidence. *Int. J. Tuberc. Lung Dis.* **20**, 1436-1447 (2016).

44 Gun, M. A., Bozdogan, B. & Coban, A. Y. Tuberculosis and beta-lactam antibiotics. *Future Microbiol.* **15**, 937-944 (2020).

45 Story-Roller, E. & Lamichhane, G. Have we realized the full potential of β-lactams for treating drug-resistant TB? *IUBMB Life* **70**, 881-888 (2018).

46 Cynamon, M. H. & Palmer, G. S. In vitro activity of amoxicillin in combination with clavulanic acid against *Mycobacterium tuberculosis*. *Antimicrob. Agents Chemother.* **24**, 429-431 (1983).

47 Sorg, T. B. & Cynamon, M. H. Comparison of four beta-lactamase inhibitors in combination with ampicillin against *Mycobacterium tuberculosis*. *J. Antimicrob. Chemother.* **19**, 59-64 (1987).

48 Solapure, S., Dinesh, N., Shandil, R., Ramachandran, V., Sharma, S., Bhattacharjee, D., Ganguly, S., Reddy, J., Ahuja, V., Panduga, V., Parab, M., Vishwas, K. G., Kumar, N., Balganesh, M. & Balasubramanian, V. In vitro and in vivo efficacy of β-lactams against replicating and slowly growing/nonreplicating *Mycobacterium tuberculosis*. *Antimicrob. Agents Chemother.* **57**, 2506-2510 (2013).

49 Wong, C. S., Palmer, G. S. & Cynamon, M. H. In-vitro susceptibility of *Mycobacterium tuberculosis*, *Mycobacterium bovis* and *Mycobacterium kansasii* to amoxycillin and ticarcillin in combination with clavulanic acid. *J. Antimicrob. Chemother.* **22**, 863-866 (1988).

50 Misiek, M., Moses, A. J., Pursiano, T. A., Leitner, F. & Price, K. E. In vitro activity of cephalosporins against *Mycobacterium tuberculosis* H37Rv: structure-activity relationships. *J. Antibiot. (Tokyo)* **26**, 737-744 (1973).

51 Ramón-García, S., González Del Río, R., Villarejo, A. S., Sweet, G. D., Cunningham, F., Barros, D., Ballell, L., Mendoza-Losana, A., Ferrer-Bazaga, S. & Thompson, C. J. Repurposing clinically approved cephalosporins for tuberculosis therapy. *Sci. Rep.* **6**, 34293 (2016).

52 Hugonnet, J.-E. & Blanchard, J. S. Irreversible Inhibition of the *Mycobacterium tuberculosis* β-Lactamase by Clavulanate. *Biochemistry* **46**, 11998-12004 (2007).

53 Horita, Y., Maeda, S., Kazumi, Y. & Doi, N. In vitro susceptibility of *Mycobacterium tuberculosis* isolates to an oral carbapenem alone or in combination with β-lactamase inhibitors. *Antimicrob. Agents Chemother.* **58**, 7010-7014 (2014).

54 Zhang, D., Wang, Y., Lu, J. & Pang, Y. *In Vitro* Activity of β-Lactams in Combination with β-Lactamase Inhibitors against Multidrug-Resistant *Mycobacterium tuberculosis* Isolates. *Antimicrob. Agents Chemother.* **60**, 393-399 (2016).

55 Forsman, L., Giske, C. G., Bruchfeld, J., Schön, T., Juréen, P. & Ängeby, K. Meropenem-clavulanate has high in vitro activity against multidrug-resistant *Mycobacterium tuberculosis*. *Int. J. Mycobacteriol.* **4 Suppl 1**, 80-81 (2015).

56 Kaushik, A., Makkar, N., Pandey, P., Parrish, N., Singh, U. & Lamichhane, G. Carbapenems and Rifampin Exhibit Synergy against *Mycobacterium tuberculosis* and *Mycobacterium abscessus*. *Antimicrob. Agents Chemother.* **59**, 6561-6567 (2015).

57 Papp-Wallace, K. M., Endimiani, A., Taracila, M. A. & Bonomo, R. A. Carbapenems: past, present, and future. *Antimicrob. Agents Chemother.* **55**, 4943-4960 (2011).

58 Woods, G. L., Brown-Elliott, B. A., Conville, P. S., Desmond, E. P., Hall, G. S., Lin, G., Pfyffer, G. E., Ridderhof, J. C., Siddiqi, S. H., Wallace, R. J., Jr., Warren, N. G. & Witebsky, F. G. in *Susceptibility Testing of Mycobacteria, Nocardiae, and Other Aerobic Actinomycetes* (Clinical and Laboratory Standards Institute, 2011).

59 Schurek, K. N., Wiebe, R., Karlowsky, J. A., Rubinstein, E., Hoban, D. J. & Zhanel, G. G. Faropenem: review of a new oral penem. *Expert Rev. Anti Infect. Ther.* **5**, 185-198 (2007).

60 Dhar, N., Dubée, V., Ballell, L., Cuinet, G., Hugonnet, J. E., Signorino-Gelo, F., Barros, D., Arthur, M. & McKinney, J. D. Rapid cytolysis of *Mycobacterium tuberculosis* by faropenem, an orally bioavailable β-lactam antibiotic. *Antimicrob. Agents Chemother.* **59**, 1308-1319 (2015).

61 Nadler, J. P., Berger, J., Nord, J. A., Cofsky, R. & Saxena, M. Amoxicillin-clavulanic acid for treating drug-resistant *Mycobacterium tuberculosis*. *Chest.* **99**, 1025-1026 (1991).

62 Yew, W. W., Wong, C. F., Lee, J., Wong, P. C. & Chau, C. H. Do beta-lactam-beta-lactamase inhibitor combinations have a place in the treatment of multidrug-resistant pulmonary tuberculosis? *Tuber. Lung Dis.* **76**, 90-92 (1995).

63 Chambers, H. F., Kocagöz, T., Sipit, T., Turner, J. & Hopewell, P. C. Activity of amoxicillin/clavulanate in patients with tuberculosis. *Clin. Infect. Dis.* **26**, 874-877 (1998).

64 Donald, P. R., Sirgel, F. A., Venter, A., Parkin, D. P., Van De Wal, W. B., Barendse, A., Smit, E., Carman, D., Talent, J. & Maritz, J. Early Bactericidal Activity of Amoxicillin in Combination with Clavulanic Acid in Patients with Sputum Smear-positive Pulmonary Tuberculosis. *Scand. J. Infect. Dis.* **33**, 466-469 (2001).

65 Keener, A. B. Oldie but goodie: Repurposing penicillin for tuberculosis. *Nat. Med.* **20**, 976-978 (2014).

66 Sotgiu, G., D'Ambrosio, L., Centis, R., Tiberi, S., Esposito, S., Dore, S., Spanevello, A. & Migliori, G. B. Carbapenems to Treat Multidrug and Extensively Drug-Resistant Tuberculosis: A Systematic Review. *Int. J. Mol. Sci.* **17**, 373 (2016).

67 Tiberi, S., Sotgiu, G., D'Ambrosio, L., Centis, R., Abdo Arbex, M., Alarcon Arrascue, E., Alffenaar, J. W., Caminero, J. A., Gaga, M., Gualano, G., Skrahina, A., Solovic, I., Sulis, G., Tadolini, M., Alarcon Guizado, V., De Lorenzo, S., Roby Arias, A. J., Scardigli, A., Akkerman, O. W., Aleksa, A., Artsukevich, J., Auchynka, V., Bonini, E. H., Chong Marín, F. A., Collahuazo López, L., de Vries, G., Dore, S., Kunst, H., Matteelli, A., Moschos, C., Palmieri, F., Papavasileiou, A., Payen, M. C., Piana, A., Spanevello, A., Vargas Vasquez, D., Viggiani, P., White, V., Zumla, A. & Migliori, G. B. Comparison of effectiveness and safety of imipenem/clavulanate- versus meropenem/clavulanate-containing regimens in the treatment of MDR- and XDR-TB. *Eur. Respir. J.* **47**, 1758-1766 (2016).

68 WHO consolidated guidelines on tuberculosis. Report No. ISBN-13: 978-92-4-006312-9, (Geneva: World Health Organization, 2022).

69 Cole, S. T., Brosch, R., Parkhill, J., Garnier, T., Churcher, C., Harris, D., Gordon, S. V., Eiglmeier, K., Gas, S., Barry, C. E., Tekaia, F., Badcock, K., Basham, D., Brown, D., Chillingworth, T., Connor, R., Davies, R., Devlin, K., Feltwell, T., Gentles, S., Hamlin, N., Holroyd, S., Hornsby, T., Jagels, K., Krogh, A., McLean, J., Moule, S., Murphy, L., Oliver, K., Osborne, J., Quail, M. A., Rajandream, M. A., Rogers, J., Rutter, S., Seeger, K., Skelton, J., Squares, R., Squares, S., Sulston, J. E., Taylor, K., Whitehead, S. & Barrell, B. G. Deciphering the biology of *Mycobacterium tuberculosis* from the complete genome sequence. *Nature* **393**, 537-544 (1998).

70 Kieser, K. J., Baranowski, C., Chao, M. C., Long, J. E., Sassetti, C. M., Waldor, M. K., Sacchettini, J. C., Ioerger, T. R. & Rubin, E. J. Peptidoglycan synthesis in *Mycobacterium tuberculosis* is organized into networks with varying drug susceptibility. *Proc. Natl. Acad. Sci. U.S.A.* **112**, 13087-13092 (2015).

71 Kieser, K. J., Boutte, C. C., Kester, J. C., Baer, C. E., Barczak, A. K., Meniche, X., Chao, M. C., Rego, E. H., Sassetti, C. M., Fortune, S. M. & Rubin, E. J. Phosphorylation of the Peptidoglycan Synthase PonA1 Governs the Rate of Polar Elongation in Mycobacteria. *PLoS Pathog* **11**, e1005010 (2015).

72 Hett, E. C., Chao, M. C. & Rubin, E. J. Interaction and modulation of two antagonistic cell wall enzymes of mycobacteria. *PLoS Pathog.* **6**, e1001020 (2010).

73 Chao, M. C., Kieser, K. J., Minami, S., Mavrici, D., Aldridge, B. B., Fortune, S. M., Alber, T. & Rubin, E. J. Protein complexes and proteolytic activation of the cell wall hydrolase RipA regulate septal resolution in mycobacteria. *PLoS Pathog.* **9**, e1003197 (2013).

74 Vandal, O. H., Roberts, J. A., Odaira, T., Schnappinger, D., Nathan, C. F. & Ehrt, S. Acid-susceptible mutants of *Mycobacterium tuberculosis* share hypersusceptibility to cell wall and oxidative stress and to the host environment. *J. Bacteriol.* **191**, 625-631 (2009).

75 Arora, D., Chawla, Y., Malakar, B., Singh, A. & Nandicoori, V. K. The transpeptidase PbpA and noncanonical transglycosylase RodA of *Mycobacterium tuberculosis* play important roles in regulating bacterial cell lengths. *J. Biol. Chem.* **293**, 6497-6516 (2018).

76 Plocinski, P., Ziolkiewicz, M., Kiran, M., Vadrevu, S. I., Nguyen, H. B., Hugonnet, J., Veckerle, C., Arthur, M., Dziadek, J., Cross, T. A., Madiraju, M. & Rajagopalan, M. Characterization of CrgA, a New Partner of the *Mycobacterium tuberculosis* Peptidoglycan Polymerization Complexes. *J. Bacteriol.* **193**, 3246-3256 (2011).

77 Botta, G. A. & Park, J. T. Evidence for involvement of penicillin-binding protein 3 in murein synthesis during septation but not during cell elongation. *J. bacteriol.* **145**, 333-340 (1981).

78 Zhang, W., Li, S., Ma, L., Ding, W. & Xu, Y. Identification of a novel carboxypeptidase encoded by Rv3627c that plays a potential role in mycobacteria morphology and cell division. *Enzyme Microb. Technol.* **126**, 32-40 (2019).

79 DeJesus, M. A., Gerrick, E. R., Xu, W., Park, S. W., Long, J. E., Boutte, C. C., Rubin, E. J., Schnappinger, D., Ehrt, S., Fortune, S. M., Sassetti, C. M. & Ioerger, T. R. Comprehensive Essentiality Analysis of the *Mycobacterium tuberculosis* Genome via Saturating Transposon Mutagenesis. *mBio* **8**, 10.1128/mbio.02133-02116 (2017).

80 Akusobi, C., Benghomari, B. S., Zhu, J., Wolf, I. D., Singhvi, S., Dulberger, C. L., Ioerger, T. R. & Rubin, E. J. Transposon mutagenesis in *Mycobacterium abscessus* identifies an essential penicillin-binding protein involved in septal peptidoglycan synthesis and antibiotic sensitivity. *Elife* **11** (2022).

81 Bourai, N., Jacobs, W. R. & Narayanan, S. Deletion and overexpression studies on DacB2, a putative low molecular mass penicillin binding protein from *Mycobacterium tuberculosis* H37Rv. *Microb. Pathog.* **52**, 109-116 (2012).

82 Kandasamy, S., Palaniyandi, K., Gupta, U. D. & Narayanan, S. Double deletion of PknI/DacB2 leads to attenuation of *Mycobacterium tuberculosis* for growth and virulence. *Tuberculosis* **123**, 101957 (2020).

83 Schoonmaker, M. K., Bishai, W. R. & Lamichhane, G. Nonclassical Transpeptidases of *Mycobacterium tuberculosis* Alter Cell Size, Morphology, the Cytosolic Matrix,

Protein Localization, Virulence, and Resistance to β-Lactams. *J. Bacteriol.* **196**, 1394-1402 (2014).

84 Brammer Basta, L. A., Ghosh, A., Pan, Y., Jakoncic, J., Lloyd, E. P., Townsend, C. A., Lamichhane, G. & Bianchet, M. A. Loss of a Functionally and Structurally Distinct L,D-Transpeptidase, Ldt_{Mt5}, Compromises Cell Wall Integrity in *Mycobacterium tuberculosis*. *J. Biol. Chem.* **290**, 25670-25685 (2015).

85 Patru, M. M. & Pavelka, M. S., Jr. A role for the class A penicillin-binding protein PonA2 in the survival of *Mycobacterium smegmatis* under conditions of nonreplication. *J. Bacteriol.* **192**, 3043-3054 (2010).

86 Flores, A. R., Parsons, L. M. & Pavelka, M. S., Jr. Characterization of novel *Mycobacterium tuberculosis* and *Mycobacterium smegmatis* mutants hypersusceptible to beta-lactam antibiotics. *J. Bacteriol.* **187**, 1892-1900 (2005).

87 Wivagg, C. N., Wellington, S., Gomez, J. E. & Hung, D. T. Loss of a Class A Penicillin-Binding Protein Alters β-Lactam Susceptibilities in *Mycobacterium tuberculosis*. *ACS Infect. Dis.* **2**, 104-110 (2016).

88 Plocinska, R., Martinez, L., Gorla, P., Pandeeti, E., Sarva, K., Blaszczyk, E., Dziadek, J., Madiraju, M. V. & Rajagopalan, M. *Mycobacterium tuberculosis* MtrB Sensor Kinase Interactions with FtsI and Wag31 Proteins Reveal a Role for MtrB Distinct from That Regulating MtrA Activities. *J. Bacteriol.* **196**, 4120-4129 (2014).

89 Datta, P., Dasgupta, A., Singh, A. K., Mukherjee, P., Kundu, M. & Basu, J. Interaction between FtsW and penicillin-binding protein 3 (PBP3) directs PBP3 to mid-cell, controls cell septation and mediates the formation of a trimeric complex involving FtsZ, FtsW and PBP3 in mycobacteria. *Mol. Microbiol.* **62**, 1655-1673 (2006).

90 Slayden, R. A. & Belisle, J. T. Morphological features and signature gene response elicited by inactivation of FtsI in *Mycobacterium tuberculosis*. *J. Antimicrob. Chemother.* **63**, 451-457 (2009).

91 Prigozhin, D. M., Krieger, I. V., Huizar, J. P., Mavrici, D., Waldo, G. S., Hung, L. W., Sacchettini, J. C., Terwilliger, T. C. & Alber, T. Subfamily-specific adaptations in the structures of two penicillin-binding proteins from *Mycobacterium tuberculosis*. *PLoS One* **9**, e116249 (2014).

92 Aliashkevich, A. & Cava, F. LD-transpeptidases: the great unknown among the peptidoglycan cross-linkers. *FEBS J.* **289**, 4718-4730 (2022).

93 Bernal-Cabas, M., Ayala, J. A. & Raivio, T. L. The Cpx envelope stress response modifies peptidoglycan cross-linking via the L,D-transpeptidase LdtD and the novel protein YgaU. *J. Bacteriol.* **197**, 603-614 (2015).

94 Delhaye, A., Collet, J. F. & Laloux, G. Fine-Tuning of the Cpx Envelope Stress Response Is Required for Cell Wall Homeostasis in *Escherichia coli*. *mBio* **7**, e00047-00016 (2016).

95 Morè, N., Martorana, A. M., Biboy, J., Otten, C., Winkle, M., Serrano, C. K. G., Montón Silva, A., Atkinson, L., Yau, H., Breukink, E., den Blaauwen, T., Vollmer, W. & Polissi, A. Peptidoglycan Remodeling Enables *Escherichia coli* To Survive Severe Outer Membrane Assembly Defect. *mBio* **10** (2019).

96 Baranowski, C., Welsh, M. A., Sham, L. T., Eskandarian, H. A., Lim, H. C., Kieser, K. J., Wagner, J. C., McKinney, J. D., Fantner, G. E., Ioerger, T. R., Walker, S., Bernhardt, T. G., Rubin, E. J. & Rego, E. H. Maturing *Mycobacterium smegmatis* peptidoglycan requires non-canonical crosslinks to maintain shape. *Elife* **7** (2018).

97 García-Heredia, A., Pohane, A. A., Melzer, E. S., Carr, C. R., Fiolek, T. J., Rundell, S. R., Lim, H. C., Wagner, J. C., Morita, Y. S., Swarts, B. M. & Siegrist, M. S. Peptidoglycan precursor synthesis along the sidewall of pole-growing mycobacteria. *Elife* **7** (2018).

98 Lavollay, M., Arthur, M., Fourgeaud, M., Dubost, L., Marie, A., Veziris, N., Blanot, D., Gutmann, L. & Mainardi, J. L. The Peptidoglycan of Stationary-Phase *Mycobacterium tuberculosis* Predominantly Contains Cross-Links Generated by L,D-Transpeptidation. *J. Bacteriol.* **190**, 4360-4366 (2008).

99 Cordillot, M., Dubée, V., Triboulet, S., Dubost, L., Marie, A., Hugonnet, J.-E., Arthur, M. & Mainardi, J.-L. In vitro cross-linking of *Mycobacterium tuberculosis* peptidoglycan by L,D-transpeptidases and inactivation of these enzymes by carbapenems. *Antimicrob. Agents Chemother.* **57**, 5940-5945 (2013).

100 Betts, J. C., Lukey, P. T., Robb, L. C., McAdam, R. A. & Duncan, K. Evaluation of a nutrient starvation model of *Mycobacterium tuberculosis* persistence by gene and protein expression profiling. *Mol. Microbiol.* **43**, 717-731 (2002).

101 Magnet, S., Bellais, S., Dubost, L., Fourgeaud, M., Mainardi, J. L., Petit-Frère, S., Marie, A., Mengin-Lecreulx, D., Arthur, M. & Gutmann, L. Identification of the L,D-transpeptidases responsible for attachment of the Braun lipoprotein to *Escherichia coli* peptidoglycan. *J. Bacteriol.* **189**, 3927-3931 (2007).

102 Magnet, S., Dubost, L., Marie, A., Arthur, M. & Gutmann, L. Identification of the L,D-transpeptidases for peptidoglycan cross-linking in *Escherichia coli*. *J. Bacteriol.* **190**, 4782-4785 (2008).

103 Kumar, G., Galanis, C., Batchelder, H. R., Townsend, C. A. & Lamichhane, G. Penicillin Binding Proteins and β-Lactamases of *Mycobacterium tuberculosis*: Reexamination of the Historical Paradigm. *mSphere* **7**, e0003922 (2022).

104 Iland, C. N. The effect of penicillin on the tubercle bacillus. *J. Pathol. Bacteriol.* **58**, 495-500 (1946).

105 Nampoothiri, K. M., Rubex, R., Patel, A. K., Narayanan, S. S., Krishna, S., Das, S. M. & Pandey, A. Molecular cloning, overexpression and biochemical characterization of hypothetical beta-lactamases of *Mycobacterium tuberculosis* H37Rv. *J. Appl. Microbiol.* **105**, 59-67 (2008).

106 Levine, S. R. & Beatty, K. E. Investigating β-Lactam Drug Targets in *Mycobacterium tuberculosis* Using Chemical Probes. *ACS Infect. Dis.* **7**, 461-470 (2021).

107 Helfand, M. S., Bethel, C. R., Hujer, A. M., Hujer, K. M., Anderson, V. E. & Bonomo, R. A. Understanding resistance to beta-lactams and beta-lactamase inhibitors in the SHV beta-lactamase: lessons from the mutagenesis of SER-130. *J. Biol. Chem.* **278**, 52724-52729 (2003).

108 Thomas, V. L., Golemi-Kotra, D., Kim, C., Vakulenko, S. B., Mobashery, S. & Shoichet, B. K. Structural consequences of the inhibitor-resistant Ser130Gly substitution in TEM beta-lactamase. *Biochemistry* **44**, 9330-9338 (2005).

109 Reading, C. & Cole, M. Clavulanic acid: a beta-lactamase-inhiting beta-lactam from *Streptomyces clavuligerus*. *Antimicrob. Agents Chemother.* **11**, 852-857 (1977).

110 Casal, M., Rodriguez, F., Benavente, M. & Luna, M. In vitro susceptibility of *Mycobacterium tuberculosis*, *Mycobacterium fortuitum* and *Mycobacterium chelonei* to augmentin. *Eur. J. Clin. Microbiol.* **5**, 453-454 (1986).

111 Tremblay, L. W., Hugonnet, J. E. & Blanchard, J. S. Structure of the covalent adduct formed between *Mycobacterium tuberculosis* beta-lactamase and clavulanate. *Biochemistry* **47**, 5312-5316 (2008).

112 English, A. R., Retsema, J. A., Girard, A. E., Lynch, J. E. & Barth, W. E. CP-45,899, a beta-lactamase inhibitor that extends the antibacterial spectrum of beta-lactams: initial bacteriological characterization. *Antimicrob. Agents Chemother.* **14**, 414-419 (1978).

113 Aronoff, S. C., Jacobs, M. R., Johenning, S. & Yamabe, S. Comparative activities of the beta-lactamase inhibitors YTR 830, sodium clavulanate, and sulbactam combined with amoxicillin or ampicillin. *Antimicrob. Agents Chemother.* **26**, 580-582 (1984).

114 Patel, T. S., Pogue, J. M., Mills, J. P. & Kaye, K. S. Meropenem-vaborbactam: a new weapon in the war against infections due to resistant Gram-negative bacteria. *Future Microbiol.* **13**, 971-983 (2018).

115 Coleman, K. Diazabicyclooctanes (DBOs): a potent new class of non-β-lactam β-lactamase inhibitors. *Curr. Opin. Microbiol.* **14**, 550-555 (2011).

116 Tassoni, R., Blok, A., Pannu, N. S. & Ubbink, M. New Conformations of Acylation Adducts of Inhibitors of β-Lactamase from *Mycobacterium tuberculosis*. *Biochemistry* **58**, 997-1009 (2019).

117 Elings, W., Tassoni, R., van der Schoot, S. A., Luu, W., Kynast, J. P., Dai, L., Blok, A. J., Timmer, M., Florea, B. I., Pannu, N. S. & Ubbink, M. Phosphate Promotes the Recovery of *Mycobacterium tuberculosis* β-Lactamase from Clavulanic Acid Inhibition. *Biochemistry* **56**, 6257-6267 (2017).
118 Xu, H., Hazra, S. & Blanchard, J. S. NXL104 Irreversibly Inhibits the β-Lactamase from *Mycobacterium tuberculosis*. *Biochemistry* **51**, 4551-4557 (2012).
119 Economou Lundeberg, E., Andersson, V., Wijkander, M., Groenheit, R., Mansjö, M., Werngren, J., Cortes, T., Barilar, I., Niemann, S., Merker, M., Köser, C. U. & Davies Forsman, L. In vitro activity of new combinations of β-lactam and β-lactamase inhibitors against the *Mycobacterium tuberculosis* complex. *Microbiol. Spectr.* **11**, e0178123 (2023).
120 van Alen, I., Chikunova, A., Safeer, A. A., Ahmad, M. U. D., Perrakis, A. & Ubbink, M. The G132S Mutation Enhances the Resistance of *Mycobacterium tuberculosis* β-Lactamase against Sulbactam. *Biochemistry* **60**, 2236-2245 (2021).
121 Kurz, S. G., Wolff, K. A., Hazra, S., Bethel, C. R., Hujer, A. M., Smith, K. M., Xu, Y., Tremblay, L. W., Blanchard, J. S., Nguyen, L. & Bonomo, R. A. Can Inhibitor-Resistant Substitutions in the *Mycobacterium tuberculosis* Beta-Lactamase BlaC Lead to Clavulanate Resistance?: a Biochemical Rationale for the Use of Beta-Lactam-Beta-Lactamase Inhibitor Combinations. *Antimicrob. Agents Chemother.* **57**, 6085-6096 (2013).
122 Egesborg, P., Carlettini, H., Volpato, J. P. & Doucet, N. Combinatorial active-site variants confer sustained clavulanate resistance in BlaC β-lactamase from *Mycobacterium tuberculosis*. *Protein Sci.* **24**, 534-544 (2015).
123 van Alen, I., Aguirre García, M. A., Maaskant, J. J., Kuijl, C. P., Bitter, W., Meijer, A. H. & Ubbink, M. *Mycobacterium tuberculosis* β-lactamase variant reduces sensitivity to ampicillin/avibactam in a zebrafish-*Mycobacterium marinum* model of tuberculosis. *Sci. Rep.* **13**, 15406 (2023).
124 Puri, A. W. & Bogyo, M. Using Small Molecules To Dissect Mechanisms of Microbial Pathogenesis. *ACS Chem. Biol.* **4**, 603-616 (2009).
125 Kocaoglu, O. & Carlson, E. E. Progress and prospects for small-molecule probes of bacterial imaging. *Nat. Chem. Biol.* **12**, 472-478 (2016).
126 Beatty, K. E. Fluorescent probes for investigating peptidoglycan biosynthesis in mycobacteria. *Curr. Opin. Chem. Biol.* **57**, 50-57 (2020).
127 Pidgeon, S. E., Apostolos, A. J., Nelson, J. M., Shaku, M., Rimal, B., Islam, M. N., Crick, D. C., Kim, S. J., Pavelka, M. S., Kana, B. D. & Pires, M. M. L,D-Transpeptidase Specific Probe Reveals Spatial Activity of Peptidoglycan Cross-Linking. *ACS Chem. Biol.* **14**, 2185–2196 (2019).
128 Lopez Quezada, L., Smith, R., Lupoli, T. J., Edoo, Z., Li, X., Gold, B., Roberts, J., Ling, Y., Park, S. W., Nguyen, Q., Schoenen, F. J., Li, K., Hugonnet, J. E., Arthur, M., Sacchettini, J. C., Nathan, C. & Aubé, J. Activity-Based Protein Profiling Reveals That Cephalosporins Selectively Active on Non-replicating *Mycobacterium tuberculosis* Bind Multiple Protein Families and Spare Peptidoglycan Transpeptidases. *Front. Microbiol.* **11**, 1248 (2020).
129 Goffin, C. & Ghuysen, J.-M. Biochemistry and Comparative Genomics of SxxK Superfamily Acyltransferases Offer a Clue to the Mycobacterial Paradox: Presence of Penicillin-Susceptible Target Proteins versus Lack of Efficiency of Penicillin as Therapeutic Agent. *Microbiol. Mol. Biol. Rev.* **66**, 702-738 (2002).
130 Fedarovich, A., Nicholas, R. A. & Davies, C. The Role of the β5–α11 Loop in the Active-Site Dynamics of Acylated Penicillin-Binding Protein A from *Mycobacterium tuberculosis*. *J. Mol. Biol.* **418**, 316-330 (2012).
131 Jamin, M., Hakenbeck, R. & Frere, J.-M. Penicillin binding protein 2x as a major contributor to intrinsic β-lactam resistance of *Streptococcus pneumoniae*. *FEBS lett.* **331**, 101-104 (1993).
132 Tomberg, J., Unemo, M., Davies, C. & Nicholas, R. A. Molecular and Structural Analysis of Mosaic Variants of Penicillin-Binding Protein 2 Conferring Decreased

Susceptibility to Expanded-Spectrum Cephalosporins in *Neisseria gonorrhoeae*: Role of Epistatic Mutations. *Biochemistry* **49**, 8062-8070 (2010).

133 Beadle, B. M., Nicholas, R. A. & Shoichet, B. K. Interaction energies between β-lactam antibiotics and *E. coli* penicillin-binding protein 5 by reversible thermal denaturation. *Protein Sci.* **10**, 1254-1259 (2001).

134 Filippova, E. V., Kieser, K. J., Luan, C. H., Wawrzak, Z., Kiryukhina, O., Rubin, E. J. & Anderson, W. F. Crystal structures of the transpeptidase domain of the *Mycobacterium tuberculosis* penicillin-binding protein PonA1 reveal potential mechanisms of antibiotic resistance. *Febs J.* **283**, 2206-2218 (2016).

135 Kumar, P., Arora, K., Lloyd, J. R., Lee, I. Y., Nair, V., Fischer, E., Boshoff, H. I. & Barry, C. E., 3rd. Meropenem inhibits D,D-carboxypeptidase activity in *Mycobacterium tuberculosis*. *Mol. Microbiol.* **86**, 367-381 (2012).

136 Bhakta, S. & Basu, J. Overexpression, purification and biochemical characterization of a class A high-molecular-mass penicillin-binding protein (PBP), PBP1∗ and its soluble derivative from *Mycobacterium tuberculosis*. *Biochem. J.* **361**, 635-639 (2002).

137 Davies, T. A., Page, M. G., Shang, W., Andrew, T., Kania, M. & Bush, K. Binding of ceftobiprole and comparators to the penicillin-binding proteins of Escherichia coli, Pseudomonas aeruginosa, Staphylococcus aureus, and Streptococcus pneumoniae. *Antimicrob. Agents Chemother.* **51**, 2621-2624 (2007).

138 Georgopapadakou, N. H., Smith, S. A. & Sykes, R. B. Mode of action of azthreonam. *Antimicrob. Agents Chemother.* **21**, 950-956 (1982).

139 Segura, C., Salvadó, M., Collado, I., Chaves, J. & Coira, A. Contribution of beta-lactamases to beta-lactam susceptibilities of susceptible and multidrug-resistant *Mycobacterium tuberculosis* clinical isolates. *Antimicrob. Agents Chemother.* **42**, 1524-1526 (1998).

140 de Munnik, M., Lohans, C. T., Langley, G. W., Bon, C., Brem, J. & Schofield, C. J. A Fluorescence-Based Assay for Screening β-Lactams Targeting the *Mycobacterium tuberculosis* Transpeptidase Ldt_{Mt2}. *ChemBioChem* **21**, 368-372 (2020).

141 Dubée, V., Triboulet, S., Mainardi, J. L., Ethève-Quelquejeu, M., Gutmann, L., Marie, A., Dubost, L., Hugonnet, J. E. & Arthur, M. Inactivation of *Mycobacterium tuberculosis* L,D-transpeptidase $LdtMt_1$ by carbapenems and cephalosporins. *Antimicrob. Agents Chemother.* **56**, 4189-4195 (2012).

142 Triboulet, S., Arthur, M., Mainardi, J. L., Veckerlé, C., Dubée, V., Nguekam Moumi, A., Gutmann, L., Rice, L. B. & Hugonnet, J. E. Inactivation Kinetics of a New Target of β-Lactam Antibiotics. *J. Biol. Chem.* **286**, 22777-22784 (2011).

143 Zandi, T. A. & Townsend, C. A. Competing off-loading mechanisms of meropenem from an L,D-transpeptidase reduce antibiotic effectiveness. *Proc. Natl. Acad. Sci. U.S.A.* **118** (2021).

144 Lohans, C. T., Chan, H. T. H., Malla, T. R., Kumar, K., Kamps, J. J. A. G., McArdle, D. J. B., Van Groesen, E., de Munnik, M., Tooke, C. L., Spencer, J., Paton, R. S., Brem, J. & Schofield, C. J. Non-Hydrolytic β-Lactam Antibiotic Fragmentation by L,D-Transpeptidases and Serine β-Lactamase Cysteine Variants. *Angew. Chem. Int. Ed.* **58**, 1990-1994 (2019).

145 Libreros-Zúñiga, G. A., Dos Santos Silva, C., Salgado Ferreira, R. & Dias, M. V. B. Structural Basis for the Interaction and Processing of β-Lactam Antibiotics by L,D-Transpeptidase 3 (Ldt_{Mt3}) from *Mycobacterium tuberculosis*. *ACS Infect. Dis.* **5**, 260-271 (2019).

146 Gonzalo, X. & Drobniewski, F. Is there a place for β-lactams in the treatment of multidrug-resistant/extensively drug-resistant tuberculosis? Synergy between meropenem and amoxicillin/clavulanate. *J. Antimicrob. Chemother.* **68**, 366-369 (2013).

147 Gokulan, K., Khare, S., Cerniglia, C. E., Foley, S. L. & Varughese, K. I. Structure and inhibitor specificity of L, D-transpeptidase (Ldt_{Mt2}) from *Mycobacterium tuberculosis* and antibiotic resistance: calcium binding promotes dimer formation. *AAPS J.* **20**, 1-14 (2018).

148 Moellering Jr, R. C., Eliopoulos, G. M. & Sentochnik, D. E. The carbapenems: new broad spectrum β-lactam antibiotics. *J. Antimicrob. Chemother.* **24**, 1-7 (1989).
149 Sunagawa, M., Matsumura, H., Inoue, T., Fukasawa, M. & Kato, M. A novel carbapenem antibiotic, SM-7338 structure-activity relationships. *J. Antibiot. (Tokyo)* **43**, 519-532 (1990).
150 Lohans, C. T., van Groesen, E., Kumar, K., Tooke, C. L., Spencer, J., Paton, R. S., Brem, J. & Schofield, C. J. A New Mechanism for β-Lactamases: Class D Enzymes Degrade 1β-Methyl Carbapenems through Lactone Formation. *Angew. Chem. Int. Ed. Engl.* **57**, 1282-1285 (2018).
151 *Working group on New TB Drugs*, https://www.newtbdrugs.org/pipeline/clinical (2023).
152 Ramón-García, S., Bates, R. H., González Del Río, R., Gamallo, P., Mendoza, A., Ferrer, S., Thompson, C. J. & Barros, D. *Sanfetrinem, repurposing an oral beta-lactam with intracellular activity for the treatment of tuberculosis*. Vol. 23 S591 (The International Journal of Tuberculosis and Lung Disease., 2020).
153 Iannazzo, L., Soroka, D., Triboulet, S., Fonvielle, M., Compain, F., Dubée, V., Mainardi, J.-L., Hugonnet, J.-E., Braud, E., Arthur, M. & Etheve-Quelquejeu, M. Routes of Synthesis of Carbapenems for Optimizing Both the Inactivation of L,D-Transpeptidase Ldt_{Mt1} of *Mycobacterium tuberculosis* and the Stability toward Hydrolysis by β-Lactamase BlaC. *J. Med. Chem.* **59**, 3427-3438 (2016).
154 Gupta, R., Al-Kharji, N. M. S. A., Alqurafi, M. A., Nguyen, T. Q., Chai, W., Quan, P., Malhotra, R., Simcox, B. S., Mortimer, P., Brammer Basta, L. A., Rohde, K. H. & Buynak, J. D. Atypically Modified Carbapenem Antibiotics Display Improved Antimycobacterial Activity in the Absence of β-Lactamase Inhibitors. *ACS Infect. Dis.* **7**, 2425-2436 (2021).
155 Batchelder, H. R., Story-Roller, E., Lloyd, E. P., Kaushik, A., Bigelow, K. M., Maggioncalda, E. C., Nuermberger, E. L., Lamichhane, G. & Townsend, C. A. Development of a penem antibiotic against *Mycobacteroides abscessus*. *Commun. Biol.* **3**, 741 (2020).
156 Batchelder, H. R., Zandi, T. A., Kaushik, A., Naik, A., Story-Roller, E., Maggioncalda, E. C., Lamichhane, G., Nuermberger, E. L. & Townsend, C. A. Structure–Activity Relationship of Penem Antibiotic Side Chains Used against Mycobacteria Reveals Highly Active Compounds. *ACS Infect. Dis.* **8**, 1627-1636 (2022).
157 Gold, B., Smith, R., Nguyen, Q., Roberts, J., Ling, Y., Lopez Quezada, L., Somersan, S., Warrier, T., Little, D. & Pingle, M. Novel cephalosporins selectively active on nonreplicating *Mycobacterium tuberculosis*. *J. Med. Chem.* **59**, 6027-6044 (2016).
158 Lopez Quezada, L., Li, K., McDonald, S. L., Nguyen, Q., Perkowski, A. J., Pharr, C. W., Gold, B., Roberts, J., McAulay, K., Saito, K., Somersan Karakaya, S., Javidnia, P. E., Porras De Francisco, E., Amieva, M. M., DíAz, S. P., Mendoza Losana, A., Zimmerman, M., Liang, H.-P. H., Zhang, J., Dartois, V., Sans, S., Lagrange, S., Goullieux, L., Roubert, C., Nathan, C. & Aubé, J. Dual-Pharmacophore Pyrithione-Containing Cephalosporins Kill Both Replicating and Nonreplicating *Mycobacterium tuberculosis*. *ACS Infectious Diseases* **5**, 1433-1445 (2019).
159 Gold, B., Zhang, J., Quezada, L. L., Roberts, J., Ling, Y., Wood, M., Shinwari, W., Goullieux, L., Roubert, C., Fraisse, L., Bacqué, E., Lagrange, S., Filoche-Rommé, B., Vieth, M., Hipskind, P. A., Jungheim, L. N., Aubé, J., Scarry, S. M., McDonald, S. L., Li, K., Perkowski, A., Nguyen, Q., Dartois, V., Zimmerman, M., Olsen, D. B., Young, K., Bonnett, S., Joerss, D., Parish, T., Boshoff, H. I., Arora, K., Barry, C. E., III, Guijarro, L., Anca, S., Rullas, J., Rodríguez-Salguero, B., Martínez-Martínez, M. S., Porras-De Francisco, E., Cacho, M., Barros-Aguirre, D., Smith, P., Berthel, S. J., Nathan, C. & Bates, R. H. Identification of β-Lactams Active against *Mycobacterium tuberculosis* by a Consortium of Pharmaceutical Companies and Academic Institutions. *ACS Infect. Dis.* **8**, 557-573 (2022).
160 de Munnik, M., Lang, P. A., De Dios Antos, F., Cacho, M., Bates, R. H., Brem, J., Rodríguez-Miquel, B. & Schofield, C. J. High-Throughput Screen with the L,D-

transpeptidase Ldt_{Mt2} of *Mycobacterium tuberculosis* Reveals Novel Classes of Covalently Reacting Inhibitors *Chem. Sci.* **14**, 7262-7278 (2023).

161 Bhattacharya, B. & Turos, E. Synthesis and biology of N-thiolated β-lactams. *Tetrahedron* **68**, 10665-10685 (2012).

162 Kostova, M. B., Myers, C. J., Beck, T. N., Plotkin, B. J., Green, J. M., Boshoff, H. I. M., Barry, C. E., Deschamps, J. R. & Konaklieva, M. I. C4-Alkylthiols with activity against *Moraxella catarrhalis* and *Mycobacterium tuberculosis*. *Bioorg. Med.Chem.* **19**, 6842-6852 (2011).

163 Turos, E., Konaklieva, M. I., Ren, R. X. F., Shi, H., Gonzalez, J., Dickey, S. & Lim, D. N-Thiolated Bicyclic and Monocyclic β-Lactams. *Tetrahedron* **56**, 5571-5578 (2000).

164 Majewski, M. W., Watson, K. D., Cho, S., Miller, P. A., Franzblau, S. G. & Miller, M. J. Syntheses and Biological Evaluations of Highly Functionalized Hydroxamate Containing and N-Methylthio Monobactams as Anti-Tuberculosis and β-Lactamase Inhibitory Agents. *Med. Chem. Comm.* **7**, 141-147 (2016).

165 Martelli, G., Pessatti, T. B., Steiner, E. M., Cirillo, M., Caso, C., Bisognin, F., Landreh, M., Monte, P. D., Giacomini, D. & Schnell, R. N-Thio-β-lactams targeting L,D-transpeptidase-2, with activity against drug-resistant strains of *Mycobacterium tuberculosis*. *Cell Chem. Biol.* **28**, 1321-1332.e1325 (2021).

Chapter 3

High-throughput screen with the L,D-transpeptidase Ldt_{Mt2} of *Mycobacterium tuberculosis* reveals novel classes of covalently reacting inhibitors

Manuscript I

Reproduced from

Mariska de Munnik, Pauline A. Lang, Francisco De Dios Anton, Mónica Cacho, Robert H. Bates, Jürgen Brem, Beatriz Rodríguez Miquel, and Christopher J. Schofield. High-throughput screen with the L,D-transpeptidase Ldt_{Mt2} of *Mycobacterium tuberculosis* reveals novel classes of covalently reacting inhibitors. *Chem. Sci.* **14**, 7262-7278 (2023).

with permission from the Royal Society of Chemistry.

Contents

3.1 Abstract 70
3.2 Introduction 71
3.3 Results 73
3.3.1 Optimisation and validation of the high-throughput screen for inhibition of Ldt_{Mt2} and BlaC 73
3.3.2 Robustness validations throughout the high-throughput screen 74
3.3.3 High-throughput screen of a targeted library has been performed 74
3.3.4 Hit compounds can be grouped into eight compound classes 75
3.3.5 Protein observed SPE-MS reveals covalent modification of Ldt_{Mt2} 77
3.3.6 Most hits react selectively with Cys354 78
3.3.7 Isatins 16-18 are reversibly binding Ldt_{Mt2} inhibitors 79
3.3.8 Nitriles 22-36 are electrophilic cyanating agents 79
3.3.9 Most hits are more reactive towards Ldt_{Mt2} compared to the intrinsic thiol reactivity 81
3.3.10 X-ray crystallographic studies 82
3.3.11 Selected hit compounds are active in *M. tuberculosis* residing in macrophages 88
3.4 Discussion 88
3.5 Conclusion 90
3.6 Methods 90
3.6.1 Materials 90
3.6.2 Ldt_{Mt2} fluorogenic assays 90
3.6.3 BlaC fluorogenic assays 91
3.6.4 HTS interference assay 91
3.6.5 Protein observed solid phase extraction mass spectrometry 92
3.6.6 Rate constant of covalent target inactivation (k_{inact}/K_I) 92
3.6.7 Intrinsic thiol reactivity 93
3.6.8 Differential scanning fluorimetry (DSF) thermal shift assays 94
3.6.9 Jump dilution assays 94
3.6.10 Nondenaturing MS assays 94
3.6.11 X-ray crystallography 95
3.6.12 Bacterial strain 95
3.6.13 Intracellular assays 95
3.6.14 Extracellular assays 96
3.6.15 HepG2 cytotoxicity assays 96
3.7 Data availability 97
3.8 References 97
3.9 Statement of authorship 101

3.1 Abstract

Disruption of bacterial cell wall biosynthesis in *Mycobacterium tuberculosis* (*Mtb*) is a promising target for treating tuberculosis. The L,D-transpeptidase Ldt_{Mt2}, which is responsible for the formation of 3→3 cross-links in the cell wall peptidoglycan, has been identified as essential for *Mtb* virulence. We optimised a high-throughput assay for Ldt_{Mt2}, and screened a targeted library of ~10 000 electrophilic compounds. Potent inhibitor classes were identified, including established (e.g., β-lactams) and unexplored covalently reacting electrophilic groups (e.g., cyanamides). Protein-observed mass spectrometric studies reveal most classes to react covalently and irreversibly with the Ldt_{Mt2} catalytic cysteine (Cys354). Crystallographic analyses of seven representative inhibitors reveal induced fit involving a loop enclosing the Ldt_{Mt2} active site. Several of the identified compounds have a bactericidal effect on *Mtb* within macrophages, one with an MIC_{50} value of ~1 μM. The results provide leads for the development of new covalently reaction inhibitors of Ldt_{Mt2} and other nucleophilic cysteine enzymes.

Key words: L,D-transpeptidase, *Mycobacterium tuberculosis,* high-throughput screen, HTS, nucleophilic cysteine enzyme, covalent inhibitors, antimicrobial resistance, AMR.

3.2 Introduction

Tuberculosis (TB), caused by *Mycobacterium tuberculosis* (*Mtb*), is estimated to account for 1.4 million deaths per year, imposing a major impact on global health.[1] Current TB treatments typically comprise a combination of three antibiotics taken for 3–6 months, and are effective in ~85% of cases.[2] However, in resistant strains, which are endemic in eastern Europe and central Asia, therapeutic effectiveness is reduced to <60%.[3] There is thus a clear need for improved treatments targeting *Mtb*.

β-Lactams are the most widely used antibacterials, though historically they have not been deemed to be generally useful for TB treatment, in part due to resistance mediated by the chromosomally encoded *Mtb* serine β-lactamase BlaC.[4,5] β-Lactams are covalently reacting inhibitors of the transpeptidases (penicillin binding proteins, PBPs) that catalyse the essential *m*-Dap-D-Ala (4→3) cross-linking transpeptidation step in peptidoglycan biosynthesis.[6] A mechanistically related class of enzymes, the L,D-transpeptidases (Ldts), also catalyses the formation of cross-links, but rather than 4→3 cross-links the Ldts produce *meso*-Dap-*meso*-Dap (3→3) cross-links.[7] By contrast with PBPs, which employ a nucleophilic serine-residue in catalysis, the Ldts employ a nucleophilic cysteine-residue.[7,8] While only low levels of 3→3 cross-linking are evident in the exponential growth phase of *Mtb*, they comprise ~80% of all cross-links in the stationary phase.[9] Ldt_{Mt2} in particular has been identified as being essential for *Mtb* virulence, making it an attractive target for TB treatment.[10]

The extramembrane section of Ldt_{Mt2} consists of three domains, two of which have an immunoglobulin-related fold, and the catalytic domain which has an ErfK/YbiS/YhnG fold (Figure 3.1A).[11] The Ldt_{Mt2} active site within the catalytic domain is bordered by a flexible loop (residues 300–323), sometimes referred to as the active site “lid”, which creates two entrances to the active site: the inner and outer cavities.[11] The Ldt mechanism is proposed to be analogous to that proposed for the PBPs, although employing a catalytic triad analogous to that observed in some cysteine-proteases, involving Cys354, His336 and Ser337, for the formation of the cross-link between the donor and acceptor stem substrates (Figure 3.1A and B).[12] The formation of a negatively charged tetrahedral enzyme-substrate intermediate is proposed to be stabilised by an oxyanion hole, consisting of the backbone NH groups of His352, Gly353 and Cys354 (Figure 3.1A).[13]

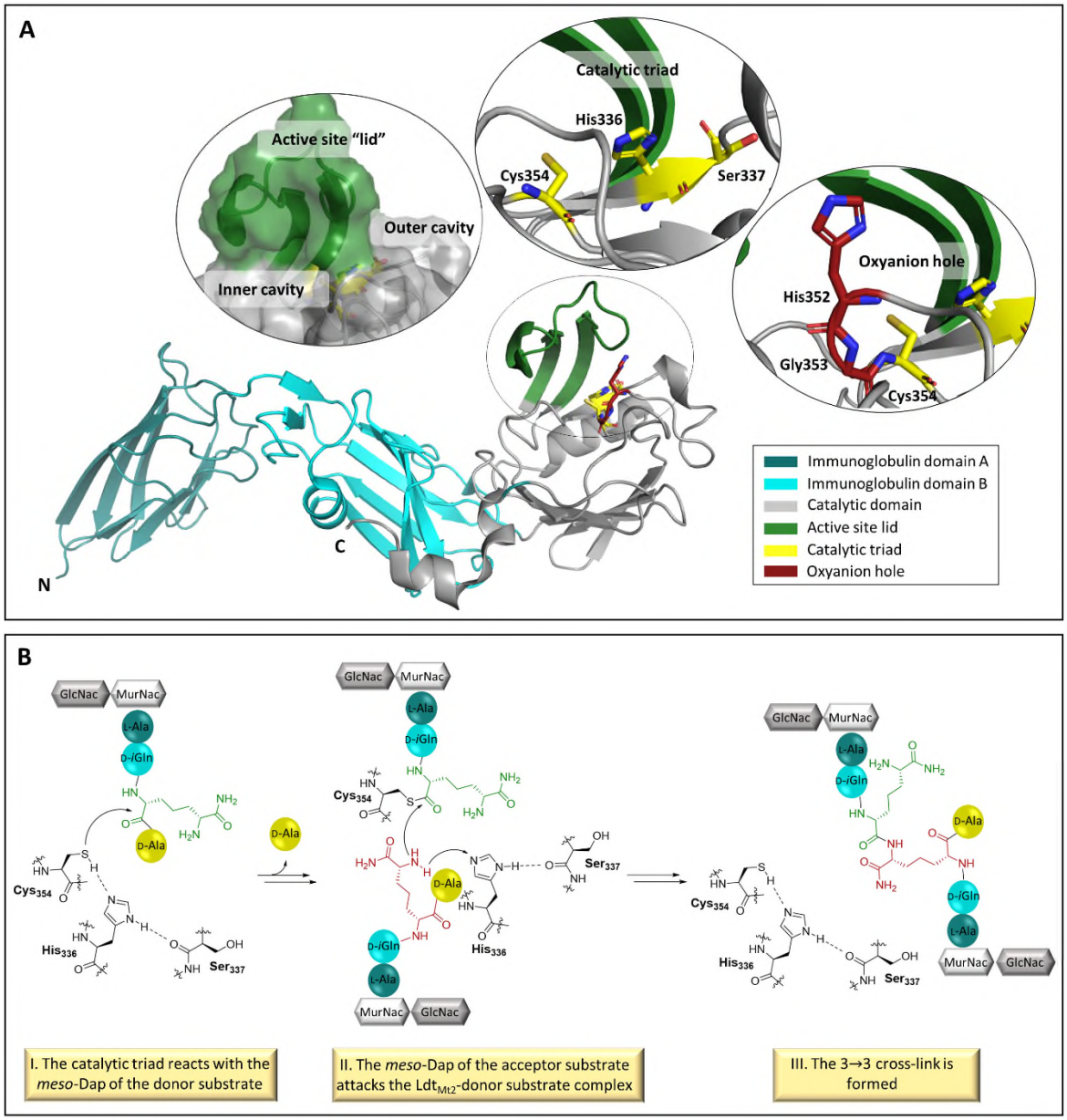

Figure 3.1. The structure and function of Ldt$_{Mt2}$. A. Views from a crystal structure of Ldt$_{Mt2}$ (PDB 6RLG),[14] showing entrances to the active site, the catalytic triad (consisting of residues Cys354, His336 and Ser337) and the oxyanion hole (consisting of the backbone NHs of His352, Gly353 and Cys354). The two Ldt$_{Mt2}$ immunoglobulin-like domains are in teal and cyan, the catalytic domain is in grey, the active site "lid" is in green, the catalytic triad is in yellow, and the oxyanion hole is in red. **B.** Outline mechanism for reaction of Ldt$_{Mt2}$ and the disaccharide tetrapeptide monomer of the *Mtb* peptidoglycan. The Ldt$_{Mt2}$ catalytic triad residues are in black, the *meso*-Dap residue of the donor substrate in green, and the *m*-Dap residue of the acceptor substrate in red.

In general, the Ldts are not reported to be efficiently inhibited by β-lactams, however, their nucleophilic cysteine reacts with the β-lactam rings of penems and carbapenems to form acyl-enzyme complexes.[15-17] Efforts have been made to identify β-lactams which more efficiently inhibit Ldt$_{Mt2}$, though to date with limited success.[18,19] In an alternative strategy for

Ldt_{Mt2} inhibition, we have reported on the inhibition of Ldt_{Mt2} by cysteine-reactive reagents such as ebselen.[14] The covalent modification of nucleophilic cysteine residues is a validated method for clinically useful inhibition of various cysteine proteases, including the main protease (M^{pro}) of SARS-CoV-2, highlighting a need for new functional groups targeting nucleophilic cysteine residues.[20-22]

Here we report on the development of a fluorescence based high-throughput screen (HTS) for Ldt_{Mt2} inhibition and its application to screen a library of potential nucleophilic cysteine reacting compounds. The results reveal the discovery of new mechanism-based nucleophilic cysteine enzyme targeting inhibitors.

3.3 Results

3.3.1 Optimisation and validation of the high-throughput screen for inhibition of Ldt_{Mt2} and BlaC

We optimised our fluorogenic assay for Ldt_{Mt2} that employs the cysteine-reactive probe **1** (Figure S1.1) for application in HTS.[23] Cross titrations identified the optimal protein and probe concentrations to be 300 nM and 15 µM, respectively (Figure S1.2A and B), giving a *Z′* value[24] of 0.87. Reaction volumes could be reduced to 10 µL without significant reduction in the *Z′* value (Figure S1.2C). Addition of the detergent Tween-20 to the previously identified preferred buffer conditions (50 mM sodium phosphate, pH 7.5)[23] improved assay robustness (Table S1.1). The combined optimisation efforts (Figure S1.2) led to an assay with a *Z′* of 0.87, well above the accepted cut-off value of 0.4.[25]

The assay manifested good tolerance for DMSO concentrations of ≤3% (*v*/*v*) (Figure S1.2F). Stock solutions of Ldt_{Mt2} and probe **1** in assay buffer were apparently stable over 7 hours when the reagents were kept on ice (Table S1.2). No evidence for nonspecific plate patterns was observed during the first hour after reaction initiation under the optimised conditions (Figure S1.3). The assay was validated in dose–response analyses of independent repeats in quadruplicate using a set of 24 tool compounds with known inhibitory activity for Ldt_{Mt2} (Table S1.3); the results showed high reproducibility and good correlation with reported values.[14,23]

A previously optimised and validated β-lactamase assay[26] was optimised for our assay set-up with BlaC, which we envisioned as a secondary assay for the HTS output. Cross titrations showed the optimal BlaC concentration to be 2.5 nM and the optimal probe concentration to be 2.5 µM in an assay volume of 10 µL (Figure S1.4), leading to a robust *Z′* of 0.84. A dose-response assay with the set of 24 tool compounds was performed in quadruplicate independent repeats to validate the assay, showing high reproducibility (Table S1.3).

3.3.2 Robustness validations throughout the high-throughput screen

To investigate the robustness and quality of the assay throughout the HTS for Ldt_{Mt2} and BlaC, *Z′* was calculated for each analysed plate; only plates with *Z′* ≥ 0.4 were accepted for analysis. Average *Z′* values of 0.64 and 0.76 were obtained for the HTS with Ldt_{Mt2} and BlaC, respectively (Figure S1.5). Throughout the HTS, high reproducibility for the obtained pIC_{50} values of the tool compounds was obtained (Figure S1.6, Table S1.4). Further, good correlation between the results of independent, blind repeats was observed (Figure S1.7).

3.3.3 High-throughput screen of a targeted library has been performed

A targeted library of ~10 000 electrophilic compounds was constructed from the GlaxoSmithKline high-throughput screening (GSK HTS) collection, including compounds with a β-lactam core, cysteine protease inhibitors, serine protease inhibitors, and compounds containing known nucleophilic cysteine warheads (Figure 3.2). These compounds were assessed for inhibition of Ldt_{Mt2} with two independent repeats at a single concentration of 100 μM. The results identified 733 potentially active compounds manifesting >78% apparent inhibition (an overall hit rate of 7.7%). The identified compounds were then subjected to dose-response analyses with Ldt_{Mt2} and BlaC (two independent repeats at concentrations 1.7 nM to 100 μM). In an effort to reduce false positives, an interference assay was performed, wherein the inhibitors were added after the completion of the reaction between Ldt_{Mt2} and probe **1** (5 hours at room temperature). Compounds with a pIC_{50} value >4.0 in the interference assay were excluded from further analyses. Compounds were then prioritised and selected for further studies based on their observed inhibitory potency for Ldt_{Mt2} and structural diversity, employing protein observed MS. The results for 39 selected compounds (**1**-**39**) are summarised in Table S1.5.

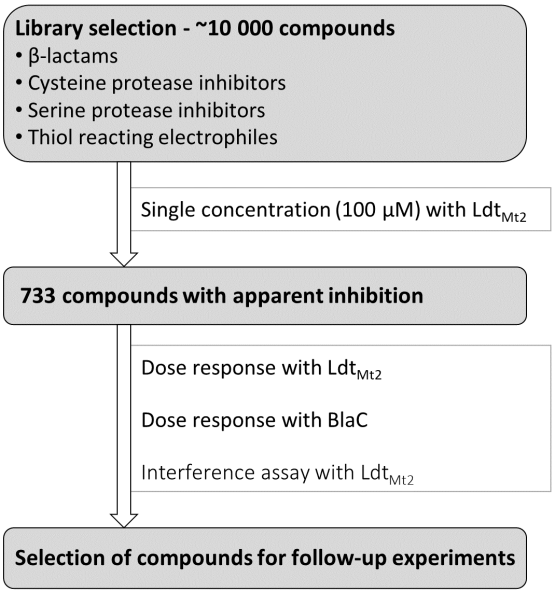

Figure 3.2. Approach for a high-throughput screen to identify Ldt$_{Mt2}$ inhibitors. A targeted library of approximately 10 000 electrophilic compounds was selected, consisting of compounds with a β-lactam core, cysteine protease inhibitors, serine protease inhibitors and compounds containing known/potential thiol reacting electrophiles. Compounds were initially screened for inhibitory activity against Ldt$_{Mt2}$ at a single concentration (100 µM), after which apparently active compounds (robust percent cut-off of ≥78.0% and ≥79.3% for respective independent repeats) were further analysed in a dose-response assay with Ldt$_{Mt2}$ and in a secondary screen for dose-response with the β-lactamase BlaC. Identified active compounds were subjected to an interference assay for the Ldt$_{Mt2}$ assay. Based on the combined results, compounds were selected for follow-up experiments.

3.3.4 Hit compounds can be grouped into eight compound classes

The 39 selected hit compounds (Table S1.5) cluster into eight distinct groups based on their proposed cysteine reactive functional groups: α-chloro ketones, maleimides, acrylamides, fumaryl amides, an ebsulfur analogue, isatins, nitriles, and β-lactams (Figure 3.3). Overall, pIC$_{50}$ values of 5.55-7.99 were observed for the inhibition of Ldt$_{Mt2}$ by the selected compounds (Figure 3.4A, Table S1.5, Figure S1.8), with ebsulfur analogue **15** being most potent inhibitor (pIC$_{50}$ 7.99). The majority of the hit compounds have molecular masses of 200 to 350 Da, and have a good ligand efficiency (0.28-0.86, Figure 3.4B), leaving scope for further development.

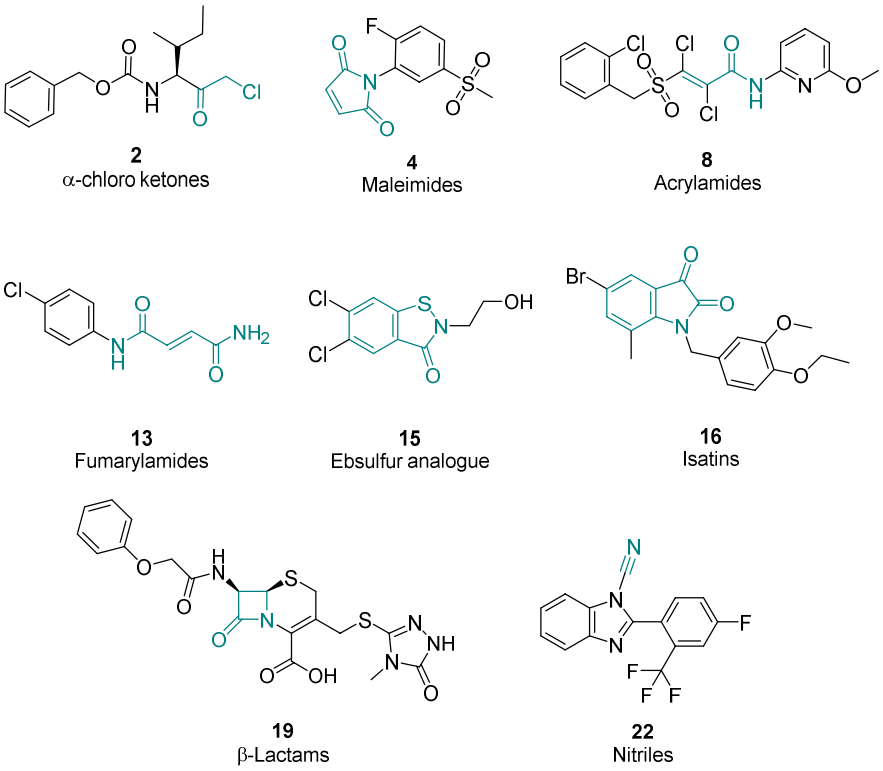

Figure 3.3. Representative examples of hits for the eight identified Ldt_{Mt2} inhibitor classes. The core electrophilic motif is shown in teal.

Notably, two of the identified Ldt_{Mt2} inhibitors belong to the cephalosporin subclass of β-lactams (**19**, **20**); this observation is interesting because cephalosporins have previously been deemed not to be of use for inhibition of Ldt_{Mt2}, potentially because their stereochemistry mimics the D-Ala-D-Ala substrate of PBPs rather than that of Ldts, which accept a substrate with C-terminal L,D-chirality.[23,27,28] However, the Ldt_{Mt2} inhibition observed with cephalosporins **19**-**20** (pIC_{50} 5.55-5.62) is comparable to that observed for the carbapenems biapenem, doripenem and meropenem under the same assay conditions (pIC_{50} 5.54-5.87, Table S1.4). The results thus imply that the cephalosporin scaffold is of considerable interest for inhibition of Ldt_{Mt2} and hence TB treatment. While most compounds showed no significant inhibition of BlaC, cephalosporin **20** was a potent inhibitor (pIC_{50} 7.72, Figure S1.9).

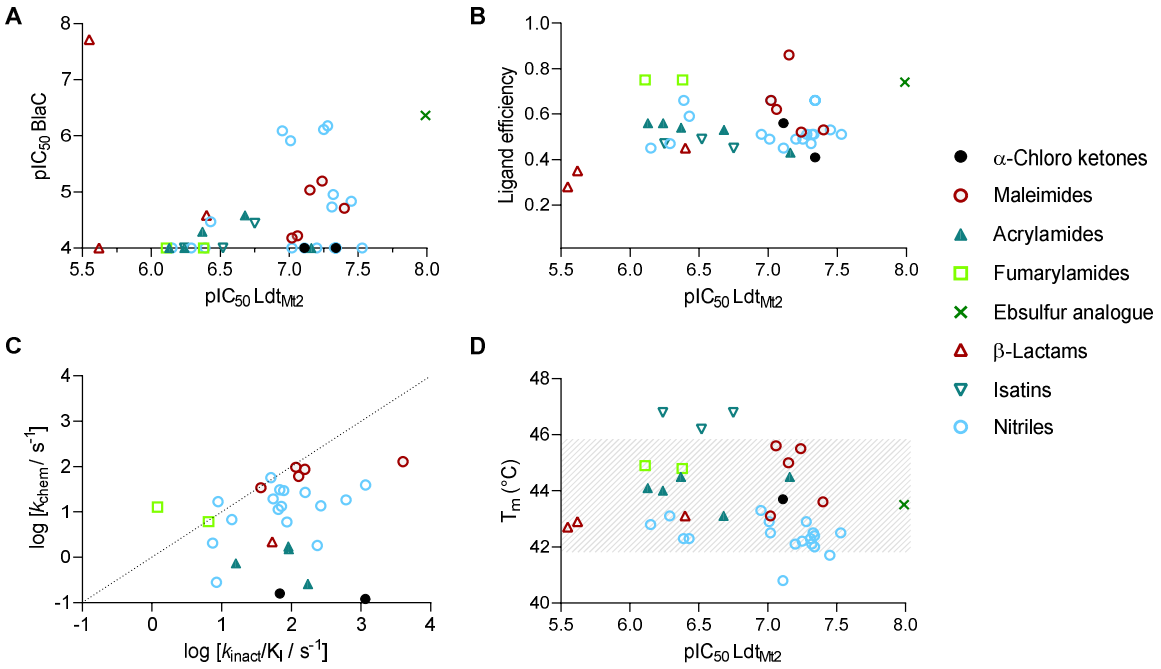

Figure 3.4. Evaluation of the Ldt_{Mt2} HTS inhibitor hits, clustered by compound class. A. Potencies of inhibitors identified from the HTS for Ldt_{Mt2} and for BlaC. Most compounds show higher potency for Ldt_{Mt2} compared to BlaC. **B.** Ligand efficiency of HTS hits plotted *versus* potency against Ldt_{Mt2}. **C.** k_{chem} of the identified compounds plotted *versus* the k_{inact}/K_I for Ldt_{Mt2}. Most compounds show higher reactivity with Ldt_{Mt2} compared to the intrinsic thiol reactivity. **D.** Melting points (T_ms) of Ldt_{Mt2} in the presence of HTS hits plotted *versus* potency against Ldt_{Mt2}. Grey dashes represent the area of non-significant change with respect to the unmodified protein (43.8 ± 2 °C).

3.3.5 Protein observed SPE-MS reveals covalent modification of Ldt_{Mt2}

To investigate the mechanism of Ldt_{Mt2} inhibition by selected inhibitors, protein observed solid phase extraction mass spectrometry (SPE-MS)[29] time course assays were carried out on the reactions of Ldt_{Mt2} with inhibitors **1**-**21** at varied protein-inhibitor ratios (Figure S1.10, Table S1.6). As the SPE-MS procedure involved Ldt_{Mt2} denaturation under acidic conditions (0.1% (*v*/*v*) aqueous formic acid), observation of adduct formation likely reflects covalent reaction. The results therefore imply that most of the tested compounds (**1**-**11**, **13**-**15** and **19**-**21**) covalently modify Ldt_{Mt2}, in most cases leading to an adduct corresponding to apparent irreversible reaction with a single inhibitor molecule (Figure S1.10). An exception was maleimide **6**, which apparently modified Ldt_{Mt2} with the reaction involving multiple inhibitor molecules (Figure S1.10 entry 6).

The SPE-MS results suggest that α-chloro ketones **1**-**2** react with Ldt_{Mt2} with loss of a chloride ion, consistent with a nucleophilic substitution involving Cys354 (Figure S1.10 entries 1-2).

The maleimide derivatives **3**-**7** reacted with Ldt_{Mt2} without fragmentation, resulting in adducts comprising the intact inhibitor mass (Figure S1.10 entries 3-7). Over the course of 24 hours, partial hydrolysis of the ester sidechain of **7** was observed, as manifested by a mass decrease of 106 Da (relative to the modified Ldt_{Mt2}, Figure S1.10 entry 7).

Acrylamide **8** (MW 436 Da), a *trans*-dichloro substituted Michael acceptor, reacted to give covalently modified Ldt_{Mt2} (+399 Da), corresponding to the addition of a single molecule accompanied with loss of one chloride ion (Figure S1.10 entry 8). **9** (MW 306 Da) covalently modified Ldt_{Mt2} (+322 Da, Figure S1.10 entry 9), corresponding to the mass of the inhibitor plus an additional 16 Da. A further +16 Da adduct was observed to accumulate over 21 hours, potentially reflecting slow oxidation of the Cys354 sulphur derived thioester following reaction with the inhibitor. While acrylamides **10**-**12** are structurally closely related, only **10** and **11** were observed to manifest substantial modification of Ldt_{Mt2} (+186 and +298 for **10** and +286 Da for **11**, Figure S1.10 entries 10–11). By contrast, reaction with **12** (MW 268 Da) manifested only low amounts of a +268 Da Ldt_{Mt2} modification (Figure S1.10 entry 12).

Although the fumaryl amides **13** and **14** (MW 225 and 204 Da, respectively) contain a potential Michael acceptor, the SPE-MS experiments solely showed +207 Da and +189 Da adducts on reaction of Ldt_{Mt2} with **13** and **14**, respectively, in agreement with substitution of the terminal amide resulting in loss of NH_3 (Figure S1.10 entries 13-14). Ebsulfur analogue **15** (MW 264 Da) reacted without apparent fragmentation to give a +264 Da adduct (Figure S1.10 entry 15). Isatin derivatives **16** and **17** (MW 404 and 390 Da, respectively) showed only low levels of modification of Ldt_{Mt2} manifesting +404 and +390 Da mass increments, respectively, but addition of 2 molecules of **17** was observed (Figure S1.10 entries 16 and 17). **18** (MW 366 Da) was not observed to modify Ldt_{Mt2} (Figure S1.10 entry 18). β-Lactams **19**-**21** exhibited complex fragmentation patterns, which were observed to vary with time and inhibitor concentration (Figure S1.10 entries **19**-**21**). However, a +626 Da adduct, corresponding to the addition of a non-fragmented molecule of **20** (MW 626 Da), dominated at lower inhibitor to enzyme ratios.

3.3.6 Most hits react selectively with Cys354

Ldt_{Mt2} contains only a single cysteine residue (Cys354). However, as several identified electrophiles are able to react with residues other than cysteine,[30,31] it was assessed whether covalent modification of Ldt_{Mt2} by the inhibitors is related to reaction with Cys354. Thus, Ldt_{Mt2} was preincubated with the non-reversible covalent inhibitor ebselen, which has been shown to react selectively with Cys354.[14] Apparently complete Ldt_{Mt2} modification by a single molecule of ebselen (+274 Da) was observed. Inhibitors **1**-**21** were then added to the ebselen

derived Ldt_{Mt2} complex (Figure S1.11). With Cys354 unavailable, only **6**, **16**, and **17** were observed to react with the Ldt_{Mt2}-ebselen complex. By contrast, **1**-**6**, **7**-**15**, and **19**-**21** no longer reacted with Ldt_{Mt2}, supporting selective binding to Cys354 (or close-by residues in the active site).

3.3.7 Isatins 16-18 are reversibly binding Ldt_{Mt2} inhibitors

As the isatins **16**-**18** showed a lack of clear evidence for irreversible covalent binding to Ldt_{Mt2} in the SPE-MS studies, their mechanism of inhibition was further assessed. By contrast with the SPE-MS studies, nondenaturing MS analysis of Ldt_{Mt2} in the presence of **16**-**18** showed substantial binding, resulting in mass increments of +404 Da and +366 Da for **16** and **18**, respectively, corresponding to binding of a single inhibitor molecule (Figure S1.12A). On incubation with **17**, +390 Da and +780 Da mass adducts were observed, corresponding to binding of 1 or 2 inhibitor molecules, respectively. On increasing the cone voltage from 100 V to 200 V, adducts indicating binding of **16**-**18** were no longer observed, supporting the reversible binding of the isatin inhibitors.

In thermal shift assays[32] stabilisation by isatins **16**-**18** was observed, increasing the melting temperature of Ldt_{Mt2} by 2.4-3 °C (Figure 3.4D and S1.12B). By contrast, the other hits did not show a substantial change in the melting temperatures of Ldt_{Mt2}, apart from nitriles **26** and **36**, which lowered the melting temperature by 2.1 and 3.0 °C, respectively (Table S1.5). The reversibility of isatin binding was assessed by jump dilution studies.[33] While inhibition of the inhibitors **1**-**11**, **13**-**15** and **19**-**39** was found to be irreversible, inhibition by isatins **16**-**18** was reversible with k_{off} values of 103 s^{-1}, 84.6 s^{-1}, and 160 s^{-1}, respectively, resulting in half-lives of the Ldt_{Mt2} inhibitor complexes of 24.6 s, 29.4 s, and 15.6 s, respectively (Figure S1.12C, Table S1.7). Dose-response assays at varying inhibitor pre-incubation times (ranging between 0 min and 2 h) manifested no time-dependency for potency of inhibition by the isatins **16**-**18** (Figure S1.12D, Table S1.8). The reversible binding mode of the isatins, either *via* reversible noncovalent binding, or reversible covalent binding involving reaction of the nucleophilic Cys354 with the C3 isatin ketone, differ from most of the classes identified, which involve irreversible inhibition *via* alkylation, substitution, or acylation mechanisms.

3.3.8 Nitriles 22-36 are electrophilic cyanating agents

SPE-MS assays of the reaction between nitriles **22**-**39** and Ldt_{Mt2} identified cyanamides **22**-**36** as electrophilic cyanating agents (Figure 3.5, Figure S1.13 entries 1–15, Table S1.9), as apparent by a mass shift of +26 Da, reflecting a transfer of a nitrile group. In certain cases, this was accompanied by an additional modification of +17 Da, which likely reflects the addition

of water to the transferred nitrile group to give an *S*-carbamoyl cysteine residue. By contrast, cyanamide **37** – which does not share the benzimidazole core of **22**-**36** – was not observed to cyanate Ldt_{Mt2}, and instead reacted initially without fragmentation, followed by hydrolysis of the ester of **37** (Figure S1.13 entry 16). Reaction of Ldt_{Mt2} with nitriles **38** and **39**, both of which have a benzonitrile core, resulted in complex adduct formation (Figure S1.13 entries 17–18).

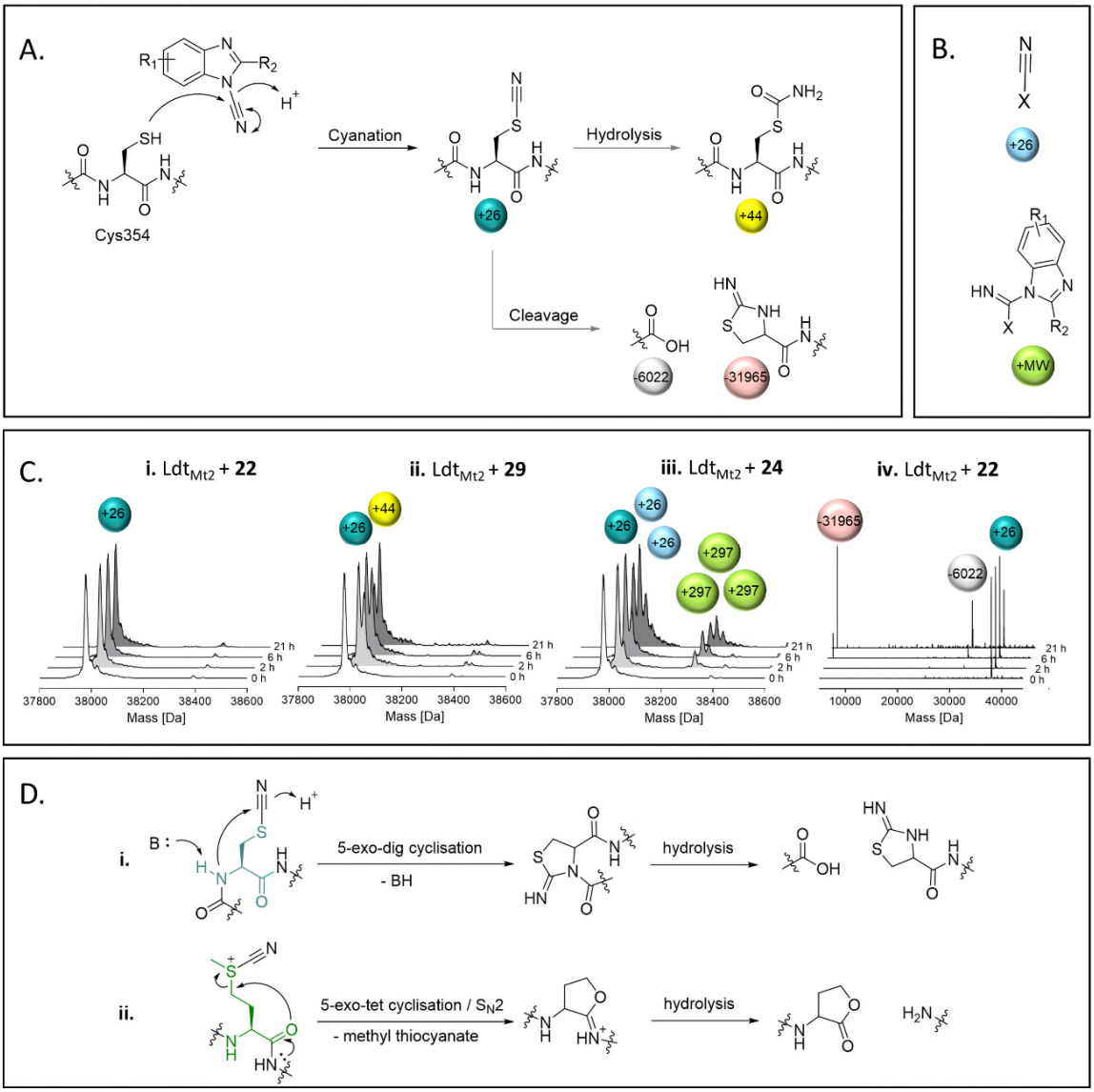

Figure 3.5. Reaction of Ldt_{Mt2} with cyanamides 22-36 as observed by mass spectrometry. A. Cys354 of Ldt_{Mt2} is cyanated by cyanamides **22**-**36**, which can be followed by hydrolysis, or cleavage adjacent to Cys354. **B.** Apparent adducts occasionally observed that cannot be related to reaction with Cys354. The non-Cys354 reacting residue is represented by X. **C.** Representative deconvoluted mass spectra from the reaction between the cyanamides and Ldt_{Mt2}, showing evidence for (i) cyanation, (ii) cyanation followed by hydrolysis, (iii) reaction with multiple molecules of the inhibitor, and (iv) cleavage of Ldt_{Mt2} at Cys354 following cyanation. **D.** Mechanisms for the cleavage of proteins through cyanation of (i) cysteine (N-terminal side; the cysteine residue is in teal) or (ii) methionine (C-terminal side; the methionine residue is in green) residues.

Most of the identified cyanamide inhibitors apparently reacted once with Ldt_{Mt2}, predominantly with Cys354; however, **24**, **33**, **34**, **35** and **37** were observed to react with Ldt_{Mt2} multiple times (Figure S1.13 and S1.14). The latter observation likely relates to reaction with non-cysteine residues, as evidenced by SPE-MS experiments with the Ldt_{Mt2}-ebselen complex (Figure 3.5B and S1.14). The precise reason for the differences in reactivity of the cyanamides is unknown, but it is notable that **33**, **34** and **35** all contain a pyridine ring, and **24** has an analogous pyridazine ring. The extent of cyanation increased with increasing pH (as shown with **22**, **27**, **31** and **36** at pH 5.5-7.5, Figure S1.15). Cyanation appeared to be stable for ~6 hours, after which time backbone cleavage of Ldt_{Mt2} at Cys354 was observed, as previously reported for the known cysteine cyanating agents 2-nitro-5-thiocyanobenzoic acid (NTCB) and 1-cyano-4-dimethylaminopyridinium tetrafluoroborate (CDAP) (Figure 3.5).[34,35] However, β-elimination, which is reported as a side reaction to protein cleavage by NTCB and CDAP,[35,36] was not observed. Additionally, cleavage of methionine residues, as reported for treatment of proteins with cyanogen bromine (Figure 3.5D),[37] was not observed.

The cyanating activity of **22**-**36** was compared to a selection of known electrophilic cyanation agents, including *N*-based cyanating reagents **40**-**43** (including CDAP) and *S*-based cyanating reagents NTCB (**44**) and CDTP (**45**) (Table S1.10).[38,39] SPE-MS studies on Ldt_{Mt2} reaction with **40**-**44** showed comparable results to those for cyanamides **22**-**36**, with predominantly single- or double-cyanation being observed, while **45** did not modify Ldt_{Mt2} (Figure S1.16). The amount of cleavage of Ldt_{Mt2} at Cys354 was comparable for **22**-**36** and **40**-**44** (Figure S1.17). While most of the cyanamides **22**-**36** potently inhibited Ldt_{Mt2} (pIC_{50} values >7.0), cyanating agents **40**-**44** were apparently less potent inhibitors (pIC_{50} values 5.3-6.5), while **45** was inactive (Table S1.10). The intrinsic thiol reactivity of **40**-**42** was generally lower (k_{chem} 0.90 M^{-1} s^{-1}, 0.90 M^{-1} s^{-1}, and 3.69 M^{-1} s^{-1}, respectively, Table S1.10) than observed with **22**-**36** (exceptions being **28** and **32**). Due to assay interference, the intrinsic thiol reactivities of for **43**-**45** could not be determined.

3.3.9 Most hits are more reactive towards Ldt_{Mt2} compared to the intrinsic thiol reactivity

With **1**-**11**, **13**-**14** and **19**-**39** identified as irreversibly binding Ldt_{Mt2} inhibitors, the second-order rate constant k_{inact}/K_I, which describes the efficiency of irreversible reaction,[40] was determined for them. A modified form of a previously reported high-throughput endpoint assay,[41] based on competition for reaction with the active site cysteine between an irreversibly reacting covalent probe and test compounds, was used employing probe **2** (Figure S1.18). The k_{inact}/K_I values were obtained for all identified irreversible inhibitors (Figure S1.19, Table S1.5), with the exceptions of **15**, **19**, **20** and **38**, due to assay interference. Similarly to the results of the HTS assay, compound classes exhibiting high reactivity were the cyanamides, in particular **23** (265

± 17 M^{-1} s^{-1}) and **29**-**31** (1164 ± 105 M^{-1} s^{-1}, 236 ± 9.5 M^{-1} s^{-1} and 609 ± 11 M^{-1} s^{-1}, respectively) and the maleimides **3**-**7** (ranging from 36.5 ± 7.9 M^{-1} s^{-1} to 3991 ± 356 M^{-1} s^{-1}).

The intrinsic reactivity (k_{chem}) with a thiol group was assessed for all the selected compounds **1**-**39** (Table S1.5). Following the same principle as used for the assay determining k_{inact}/K_I, a modified form of a previously reported high-throughput endpoint assay,[42] based on competition for reaction with glutathione between an irreversibly reacting covalent probe and test compounds, was used employing probe **2** (Figure S1.20A).[43] The assay was validated using a small number of thiol-reactive compounds (Figure S1.20B), which show good correlation with reported k_{chem} values (Figure S1.20C, Table S1.11).[42] The irreversibility of the reaction of glutathione with probe **2** was shown over the duration of the measurements (>24 hours) using a displacement assay with *N*-ethylmaleimide (Figure S1.20D and E), as previously reported.[42]

The majority of the compounds showed low to moderate intrinsic thiol (glutathione) reactivity under the tested conditions (k_{chem} < 0.08-13.0 M^{-1} s^{-1}). The maleimide derivatives (**3**-**7**) exhibited relatively higher k_{chem} values (34.2-129.9 M^{-1} s^{-1}), as anticipated based on their known reactivity as alkylating agents and application in thiol-coupling reactions.[44,45] A selection of the nitrile derivatives, i.e., those containing a cyanamide functional group (**22**-**36**), also displayed relatively high k_{chem} values (2.12-61.6 M^{-1} s^{-1}). Comparison of the obtained k_{inact}/K_I values with the k_{chem} values, implies an increased reactivity for Ldt_{Mt2} compared to the intrinsic thiol reactivity for the majority of inhibitors (Figure 3.4C), implying that with appropriate derivatisation, selective inhibition of Ldt_{Mt2} should be possible.[46]

3.3.10 X-ray crystallographic studies

To investigate the molecular interactions between the hits and Ldt_{Mt2}, X-ray crystallographic studies were carried out using reported Ldt_{Mt2} crystallisation conditions.[14] As reported, in most cases, Ldt_{Mt2} crystallised in the $P12_11$ space group with two molecules (chain A and B) in the asymmetric unit (ASU), though the complex with compound **8** was an exception (see below). Crystal structures of Ldt_{Mt2} reacted with α-chloro ketone **2** (PDB 8A1L,[47] 2.30 Å resolution), maleimides **3** (PDB 8A1J, 2.55 Å resolution) and **4** (PDB 8A1M, 2.30 Å resolution), acrylamide **8** (PDB 8A1O, 2.05 Å resolution), fumaryl amide **13** (PDB 8A1N, 2.05 Å resolution), ebsulfur analogue **15** (PDB 8A1K, 1.75 Å resolution), and nitrile **31** (PDB 8AHO, 2.30 Å resolution) were obtained through soaking and were solved by molecular replacement (using PDB 6RRM,[14] as the search model). In all cases, the inhibitors were observed to be covalently bonded to Cys354, and the observed adducts agreed with the MS studies (Figure S1.10 and S1.13).

Overall, the Ldt_{Mt2} fold in the structures of the complexes strongly resembles that of unmodified Ldt_{Mt2} (PDB 6RLG;[14] main chain RMSD: 0.54 Å, 0.37 Å, 0.45 Å, 0.86 Å, 0.7103 Å, and 0.77 Å, for unmodified Ldt_{Mt2} compared to Ldt_{Mt2} reacted with **2**, **3**, **4**, **8**, **13**, and **15**, respectively). As a notable exception, substantial variation of the position of the active site lid (residues 300-323) was observed, resulting in apparent reorientation of various active site residues involved in the binding of the inhibitors, in particular of Tyr308, Met303 and Tyr318 (Figure 3.6).

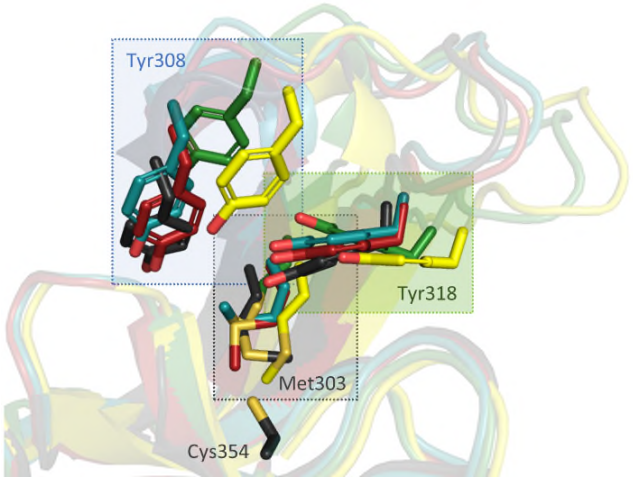

Figure 3.6. Inhibitor binding induces conformational changes in the active site "lid" (residues 300-323) of Ldt_{Mt2}, resulting in reorientation of certain active site residues, in particular Met303, Tyr308, and Tyr318. Superimposition of unmodified Ldt_{Mt2} (dark grey, PDB 6RLG)[14] and Ldt_{Mt2} reacted with **2** (yellow, PDB 8A1L), **4** (teal, PDB 8A1M), **8** (green, PDB 8A1O) and **13** (red, PDB 8A1N). Note that the conformation of Cys354 (shown only for unmodified Ldt_{Mt2}) is very similar in each complex.

While the overall folds of the two Ldt_{Mt2} molecules in the structure of the Ldt_{Mt2}-**2** complex overlay well (main chain RMDS: 0.72 Å), the reacted **2** is observed in two distinct binding modes (Figure 3.7). In the conformation observed in chain B, the ester group of **2** is positioned to engage in polar interactions with the sidechains of Tyr308 (3.5 Å) and Tyr318 (2.7 Å). These residues are disordered in chain A, an observation which can be rationalised by a potential steric clash with the phenyl ring of **2** in chain A. In both binding modes, the carbonyl group of **2** is positioned in the oxyanion hole (the respective distances to the backbone nitrogens of His352, Gly353 and Cys354 in chain A are 3.9 Å, 3.4 Å and 3.4 Å and in chain B are 3.6 Å, 3.0 Å and 3.1 Å). The *sec*-butyl- and phenyl-groups of the inhibitor are oriented towards a hydrophobic pocket made up of the active site residues: Met303, Thr320, Val333, Phe334, His336, Trp340, and His352.

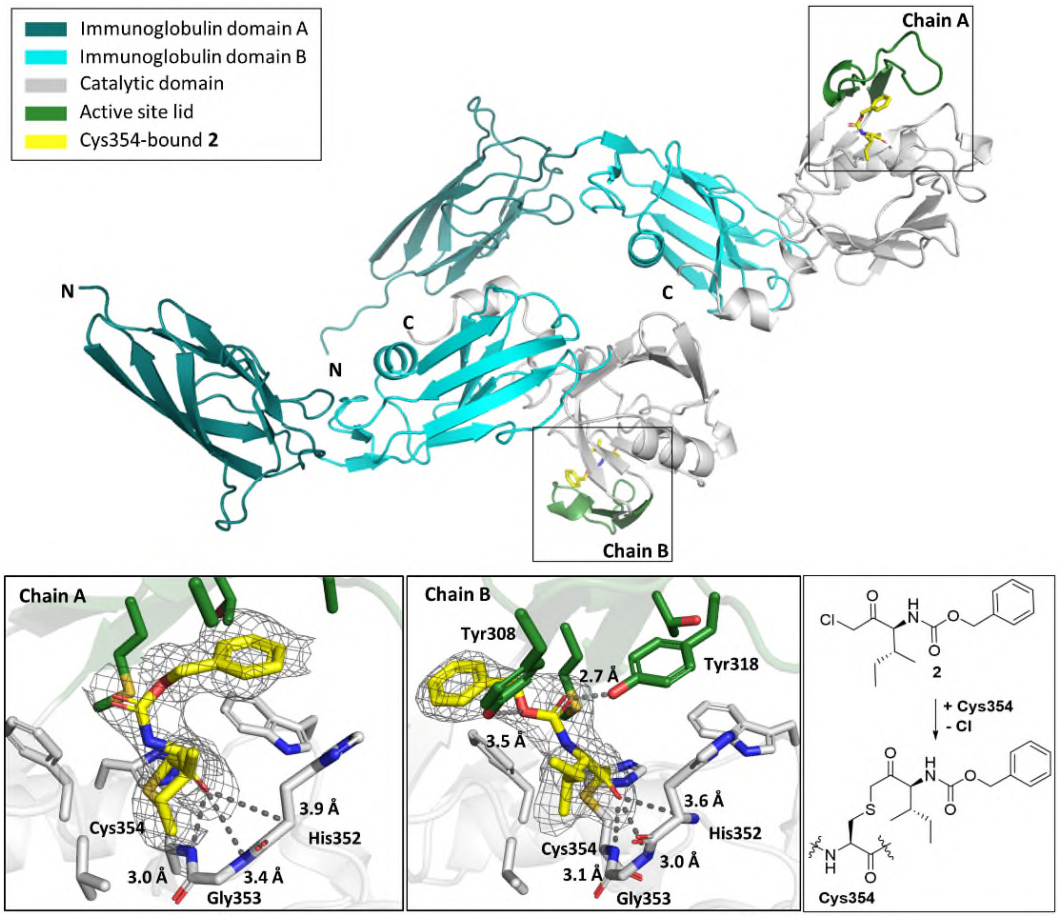

Figure 3.7. Views from a crystal structure derived by reaction of Ldt_{Mt2} with α-chloromethyl ketone 2 (yellow, PDB 8A1L). The immunoglobulin-like domains are in teal and cyan. The catalytic domain is grey, with the active site lid in green. Two different conformations of Ldt_{Mt2}-**2** were observed in chains A and B. $mF_0 - DF_c$ polder OMIT maps[48] are contoured at 3.0 σ, carved around Cys354 bound **2** (shown in grey mesh). Polar interactions are shown in dark grey dashes. The crystallographically assigned product is consistent with that observed by mass spectrometry (Figure S1.10).

The maleimides **3** and **4** are structurally related, but their binding modes differ (Figure 3.8). While the sulfone group on the *N*-phenyl ring of **4** engages in polar interactions with Tyr318 (3.5 Å, Figure 3.8B), the *N*-phenyl ring of **3** is positioned for hydrophobic interactions with Met303, Tyr318, Thr320, and Trp340 (Figure 3.8A). In both binding modes, one of the maleimide carbonyls is positioned in the oxyanion hole (the respective distances to the backbone nitrogens of His352, Gly353 and Cys354 for **3** are 3.4 Å, 3.5 Å and 3.0 Å and for **4** are 2.9 Å, 3.4 Å and 3.4 Å). Additional polar interactions were observed between the second maleimide carbonyl of **4** and the phenolic OH of Tyr318 (2.9 Å). Despite differences in their binding modes, both maleimides bind to Ldt_{Mt2} with the same stereochemical outcome, that is forming the (*R*)-enantiomer.

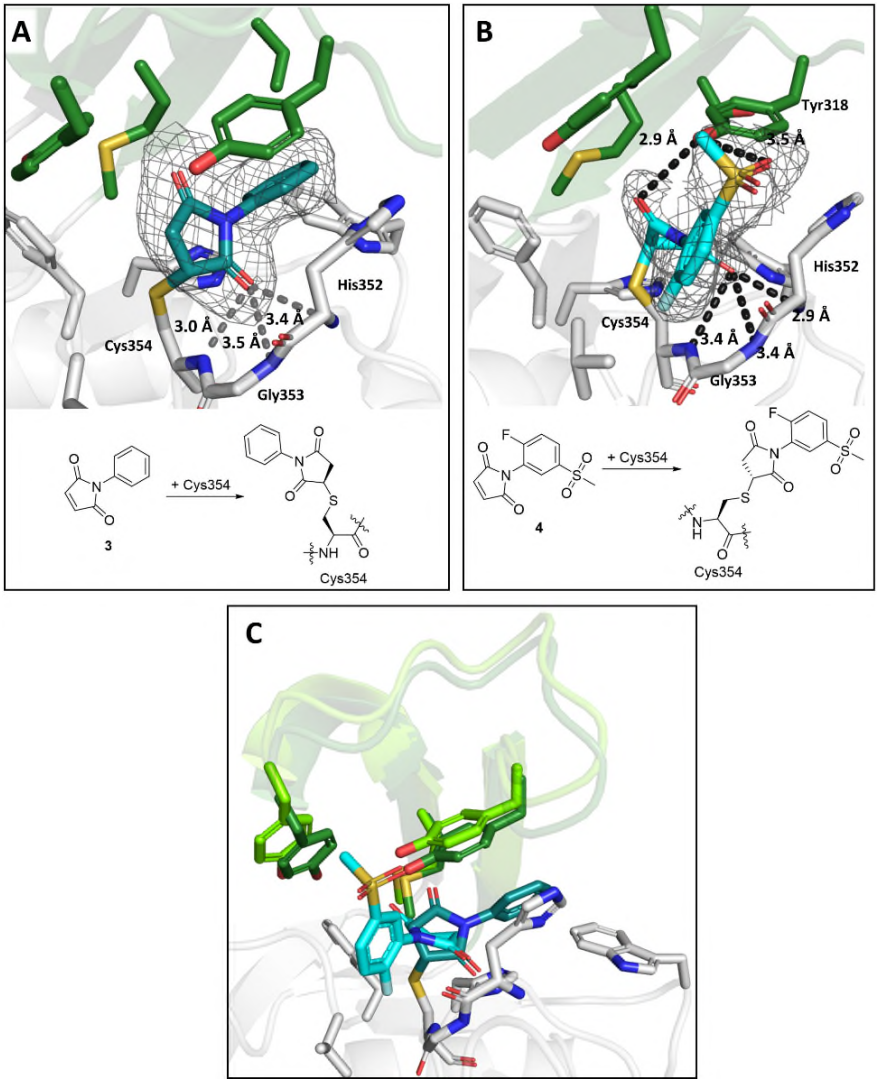

Figure 3.8. Views from crystal structures of the complex derived by reaction of Ldt_{Mt2} with maleimides 3 and 4. A. Active site view of Ldt_{Mt2} reacted with **3** (teal; PDB 8A1J). **B.** Active site view of Ldt_{Mt2} reacted with 4 (cyan; PDB 8A1M). **C.** Superimposition of Ldt_{Mt2} complexes with **3** (teal) and **4** (cyan). Despite close structural similarity between **3** and **4**, different conformations were observed, with variations in the positions of active site "lid" residues Met303, Tyr308 and Tyr318 (dark green for the Ldt_{Mt2}-**3** complex, light green for the Ldt_{Mt2}-**4** complex). Active site views from **A**, **B**, and **C.** are shown as observed in chain A. $mF_0 - DF_c$ polder OMIT maps[48] are contoured at 3.0 σ, and carved around Cys354 bound **3** and **4** (shown in grey mesh). Polar interactions are shown in dark grey dashes. The crystallographically assigned products are consistent with those observed by mass spectrometry (Figure S1.10).

By contrast with the other Ldt_{Mt2} structures reported here, a crystal structure of Ldt_{Mt2} in complex with acrylamide **8** was solved in the $P2_12_12$ space group with a single molecule in the ASU. Inhibitor **8** contains an asymmetric Michael acceptor warhead and has the potential to covalently react with Ldt_{Mt2} either *via* Michael addition to its acrylamide or *via* reaction of its vinyl sulphone group. The obtained structure implies that Ldt_{Mt2} reacts regioselectively by

Michael reaction with the vinyl sulphone of **8** (Figure 3.9A). Polar interactions were observed between the amide carbonyl and backbone nitrogen of His352 (2.8 Å) and the amide nitrogen and the side chain of His336 (3.4 Å). The amide carbonyl of **8** is positioned in the oxyanion hole (the respective distances to the backbone nitrogens of His352, Gly353 and Cys354: 2.8 Å, 3.5 Å and 3.5 Å).

A structure of Ldt_{Mt2} reacted with **13** manifests clear additional electron density at the Ldt_{Mt2} active site in chain A and partial density in chain B. **13** was thus only modelled in chain A. Notably, analysis of the electron density in chain A showed that, in accord with the SPE-MS experiments, **13** covalently modifies Ldt_{Mt2} through reaction of Cys354 with its terminal amide, rather than by Michael reaction with its fumaryl group (Figure 3.9B). Whilst in solution **13** exists as a mixture of *E*/*Z* isomers, the obtained structure implies (at least predominantly) selective reaction of Ldt_{Mt2} with the (*Z*)-stereoisomer of **13**. The nitrogen of **13** is positioned for polar interaction with the Cys354-**13** acyl (2.4 Å), and the Cys354-**13** acyl carbonyl group is positioned in the oxyanion hole (the respective distances of the inhibitor carbonyl oxygen to the backbone nitrogens of His352, Gly353 and Cys354: 3.7 Å, 3.7 Å and 3.0 Å). It cannot be ruled out that the electron density reflects another species with the same mass as the product in the reaction proposed in Figure 3.9B, e.g., as obtained from reaction of Ldt_{Mt2} with the fumaryl group followed by cyclisation (Figure S1.21).

A structure of Ldt_{Mt2} reacted with the ebsulfur analogue **15** revealed the inhibitor covalently bonded to Cys354 *via* reaction of the *N*–*S* bond, analogous to the reaction of Ldt_{Mt2} with ebselen.[14] The inhibitor hydroxy group of the species is positioned to engage in hydrogen-boding interactions with the backbone carbonyl of His352 (3.4 Å) and the inhibitor amide with the sidechain of Tyr318 (2.8 Å, Figure 3.9C). Comparison of the binding mode of **15** with that of ebselen (PDB 6RRM),[14] implies that while both compounds are positioned similarly in the active site, the phenyl ring of ebselen is positioned for π-interactions with Tyr318, while the hydroxy group of **15** is positioned for polar interactions with the backbone carbonyl of His352 (Figure 3.9D), accompanied by reorientation of the active site lid.

A crystal structure of Ldt_{Mt2} reacted with cyanamide **31** manifested covalent modification of Cys354 with formation of a carbamoyl group, likely resulting from initial formation of cyanated cysteine followed by hydrolysis (Figure 3.9E). The carbamoyl group was directed towards the oxyanion hole (the respective distances of the carbonyl oxygen to the backbone nitrogens of His352, Gly353 and Cys354: 3.6 Å, 3.5 Å and 3.1 Å). Further polar interactions were observed between the nitrogen of the carbamoyl group and the sidechain of Tyr318 (3.4 Å in chain A) and the backbone carbonyl of Gly332 (3.4 Å in chain A).

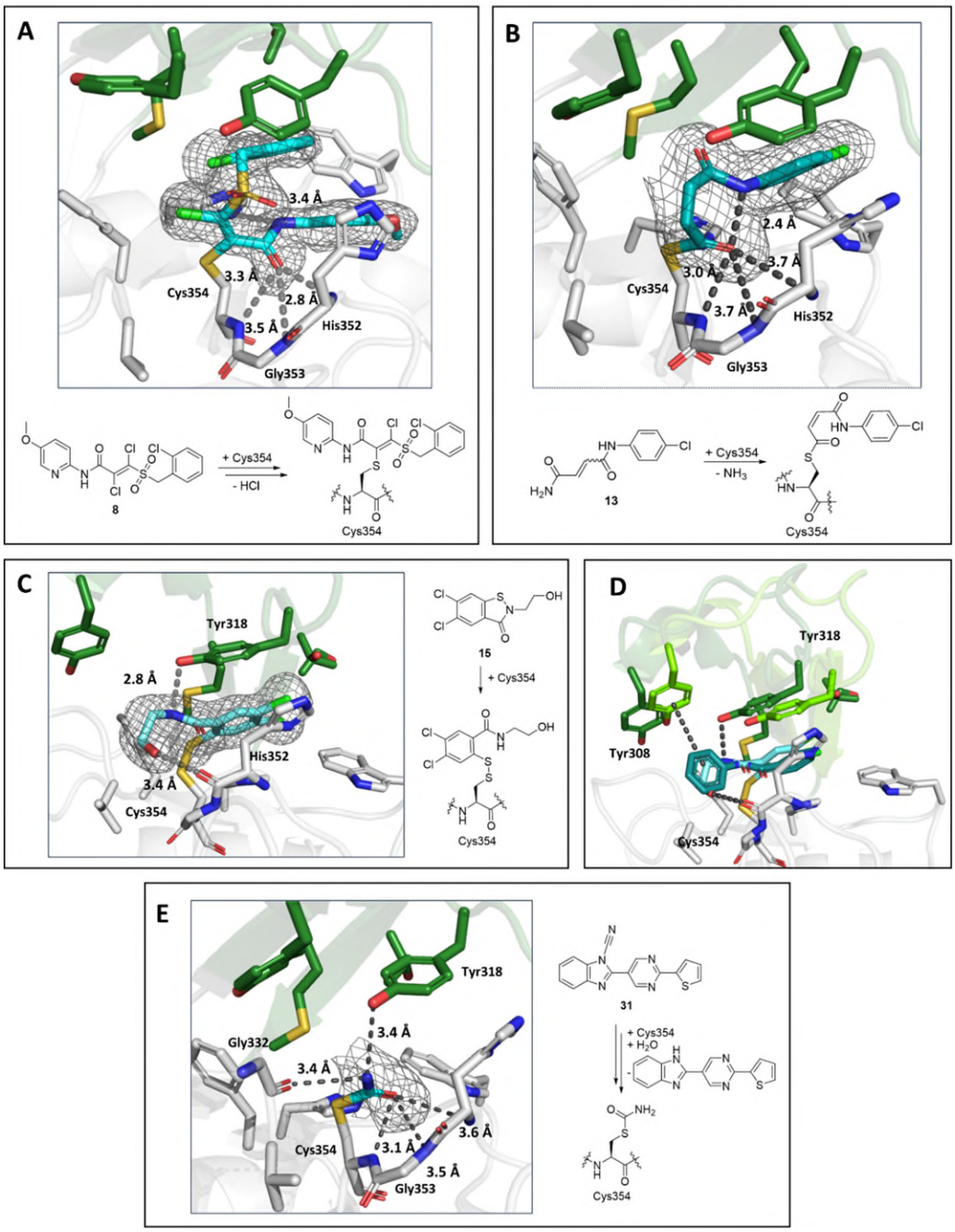

Figure 3.9. Views from crystal structures of the complex derived by reaction of Ldt_{Mt2} with inhibitors 8, 13, 15 and 31. A. Active site view of Ldt_{Mt2} reacted with **8** (cyan, PDB 8A1O). **B.** Active site view of Ldt_{Mt2} reacted with **13** (teal, PDB 8A1N). **C.** Active site view of Ldt_{Mt2} reacted with **15** (cyan; PDB 8A1K). **D.** Superimposition view from crystal structures of Ldt_{Mt2} in complex with **15** (Ldt_{Mt2}-bound **15** in cyan, active site "lid" in dark green; PDB 8A1K) and in complex with ebselen (Ldt_{Mt2}-bound ebselen in teal, active site "lid" in light green; PDB 6RRM).[14] **E.** Active site view of Ldt_{Mt2} reacted with **31** (cyan; PDB 8AHO). Active site views in (**A**–**E**) are shown as observed in chain A. $mF_0 - DF_c$ polder OMIT maps[48] contoured at 3.0 σ, carved around Cys354 bound **8**, **13**, **15**, and **31** are shown in grey mesh. Polar interactions are shown in grey dashes. The crystallographically assigned products are consistent with those observed by mass spectrometry (Figure S1.10 and S1.13).

3.3.11 Selected hit compounds are active in *M. tuberculosis* residing in macrophages

The hit compounds were evaluated for inhibition of *Mtb*, both in medium under replicating conditions and whilst residing in macrophages. The results reveal α-chloro ketone **1**, maleimides **5** and **7**, ebsulfur analogue **15**, isatins **17** and **18**, β-lactam **20**, cyanamides **23**, **30**, **36** and nitrile **39** as inhibitors of *Mtb* residing in macrophages, with MIC_{50} values <50 μM (MIC_{50} values represent the concentration of inhibitor that inhibited bacterial growth by 50%, as obtained from extrapolation of the dose-response curve). None of the tested compounds showed inhibition >100 μM when assessed in medium under replicating conditions (Table S1.12). The most potent inhibitor was nitrile **30** (MIC_{50} 0.98 μM), followed by ebsulfur analogue **15** (MIC_{50} 7.08 μM), cyanamide **23** (MIC_{50} 12.0 μM) and isatin **17** (MIC_{50} 15.1 μM). The MIC_{50} values of the remaining compounds ranged between 25.7-39.8 μM. However, cytotoxicity was observed in HepG2 cells (IC_{50} 2.51-53.5 μM) for all compounds shown in Table S1.12, apart from β-lactam **20** and nitrile **39** (IC_{50} > 100 μM).

3.4 Discussion

Ldt_{Mt2} is reported to be essential for the virulence of *Mtb*,[10] and is mechanistically and functionally related to bacterial PBPs, which are the targets of probably the most important class of all clinically used antibacterials, that is the β-lactams. Ldt_{Mt2} is thus of considerable interest as a drug target for the treatment of *Mtb* infections.

The results of our HTS for inhibitors of Ldt_{Mt2} with ~10 000 electrophilic compounds identified multiple classes of compounds that react covalently with Ldt_{Mt2}, that is: α-chloro ketones, maleimides, acrylamides, fumaryl amides, an ebsulfur analogue, isatins, nitriles (among which a subset of cyanamides), and β-lactams. Several of these functional groups are present in human drugs.[49] The results show that unexpected reaction modes can occur as observed, amongst other compounds, for the fumaryl amides **13** and **14**. Among the most potent identified Ldt_{Mt2} inhibitors were the ebsulfur analogue **15** (pIC_{50} 7.99) and the cyanamides **22**-**36** (pIC_{50} 6.39-7.53).

In most cases inhibition can be related to irreversible covalent reaction with the nucleophilic Cys354, as evidenced by protein observed MS analyses, with an exception being the isatins, which likely react *via* a reversible covalent mechanism. X-ray crystallographic results suggests that, in at least some cases, induced fit occurs during inhibitor binding. In particular, differences in the conformation of the loop that borders the active site (residues 300-323) are observed, leading to variations in the positions of some active site residues (in particular Tyr308, Tyr318 and Met303) that modulate both polar and hydrophobic interactions with the inhibitors. These

observations are in accord with previous observations regarding changes in the conformation of the flexible loop upon binding of β-lactams and ebselen.[13-15] At present, the exact relationship between inhibitor reactions and binding and changes in the conformation of the flexible loop and related residues remain unclear. However, the previous reported structural data[13-15] combined with data reported here forms a basis for detailed biophysical and modelling studies to understand the role of the flexible loop in Ldt_{Mt2} catalysis and inhibition.

Efforts to inhibit Ldt_{Mt2} have thus far focussed on inhibition by β-lactams, in particular by the carbapenem subclass.[15-19] In our HTS campaign we aimed to build on the observation that Ldt_{Mt2} can be inhibited by alternative types of cysteine-reactive compounds.[14] Indeed, the majority of hit compounds that we identified are non-β-lactam covalent inhibitors of Ldt_{Mt2}. Importantly, we identified Ldt_{Mt2} inhibitors from the cephalosporin subclass of β-lactams, which have previously been deemed to be ineffective in the inhibition of Ldt_{Mt2}.[23,27] The identified cephalosporins manifested pIC_{50} values comparable to the observed potencies of carbapenems such as meropenem, doripenem and biapenem (which were included in the HTS as control compounds). This is a notable observation, given that cephalosporins are very widely used antibacterials that are, unlike the intravenously used carbapenems, orally active.[50]

Of the Ldt_{Mt2} inhibitor classes identified here, the cyanamides **22**-**36** are of particular mechanistic interest, as they are electrophilic agents that cyanate Cys354 with high inhibitory potency. The cyanamide series exhibit increased reactivity over the reported cyanating agents **40**-**45**,[34,35,38,39] whilst most derivatives remain selective for reaction with Cys354. Interestingly, in some cases we observed hydrolysis of the *S*-nitrile group to give an *S*-carbamoyl group, as validated by crystallography in the case of **31**. Additionally, we observed cleavage of Ldt_{Mt2} following *S*-cyanation. Such cleavage likely occurs *via* 5-*exo*-dig cyclisation of the Cys354 amide nitrogen onto the carbon of the *S*-nitrile group, followed by hydrolysis on the *N*-terminal side of the cysteine residue.[51] Although not the focus of our work, the results presented here suggest that developing cyanamide type reagents for cleavage at cysteine residues in proteins should be possible. Although it may be challenging to develop cyanamides as drugs due to their reactivity, we also identified nitrile inhibitors (**38**, **39**). The potential of nitriles for the inhibition of nucleophilic cysteine enzymes is highlighted by the recent development of cysteine reacting inhibitor of the main protease (M^{pro}) of SARS-CoV-2.[21]

The HTS approach is validated by the observation that out of the 39 selected hit compounds, 11 were found to have a bactericidal effect on *Mtb* in macrophages. The most potent identified compound was the cyanamide **30** (MIC_{50} of 0.98 μM). Due to environmental factors, such as phagosomal acidification and presence of reactive nitrogen species, *Mtb* residing in macrophages is typically in the nonreplicating or replication-inhibited phase.[52-54] The observed

bactericidal effect of the selected hit compounds on *Mtb* within macrophages, but not *Mtb* under replicating conditions, is thus in accord with the anticipated behaviour of Ldt_{Mt2} inhibition, which is proposed to be essential during the nonreplicating stage.[9,10] However, further research is necessary to confirm the mechanism of action of these compounds.

3.5 Conclusion

The overall results reveal novel classes of electrophilic inhibitors for the promising anti-TB target Ldt_{Mt2}. They provide mechanistic data on the modes of inhibition, so providing leads for the development of potent and selective Ldt_{Mt2} inhibitors. Amongst the inhibitor classes identified, the cephalosporins, the nitriles and the isatins are of particular interest due to their chemical interest and bactericidal effect on *Mtb* residing in macrophages. The results also reveal the power of HTS followed by subsequent protein observed MS analysis focussed on electrophiles to unveil new classes of inhibitors of Ldt_{Mt2} and potentially other classes of nucleophilic enzymes. This aspect of the results, as exemplified by the cyanamides, suggests that there is considerable potential for identifying new types of electrophilic warheads for inhibition of nucleophilic enzymes.

3.6 Methods

3.6.1 Materials

Recombinant Ldt_{Mt2} and BlaC were produced in *E. coli* and purified to <95% purity by SDS-PAGE as described (Appendix V).[55] Probes **1** and **2** and FC-5 were synthesised as reported.[23,26] The HTS library of ~10 000 electrophilic compounds was constructed from the GSK compound collection of ~4 million compounds, by means of 21 different substructure searches using Smart Queries, and a molecular weight filter (MW < 450). Substructures consisting of known, or potential cysteine, binding warheads were identified from literature searches, and datasets from other cysteine and serine protease programmes within GSK.

3.6.2 Ldt_{Mt2} fluorogenic assays

Compounds (in DMSO) were dispensed into a black polystyrene, flat-bottomed, small volume, clear bottomed 384-well microplate (Greiner Bio-One, part number 784076). Single shot assays were performed at a compound concentration of 10 μM (100 nL at 10 mM) and dose-response assays were performed in concentrations ranging from 100 μM to 1.69 nM (11 dilutions of factor 3). Two types of controls were used. In control 1, inhibitors were substituted

with neat DMSO (100 nL) (expected 0% inhibition; 100% fluorescence signal). In control 2, the addition of Ldt_{Mt2} was omitted (expected 100% inhibition; 0% fluorescence signal). Ldt_{Mt2} (final concentration 300 nM) in assay buffer (50 mM sodium phosphate, pH 7.5, 0.007% (*v*/*v*) Tween-20) was added to all wells (except control 2) using a MultiDrop Combi dispenser (ThermoFisher Scientific). In the case of control 2, the Ldt_{Mt2} mixture was substituted with the assay buffer. This mixture was incubated for 30 minutes at room temperature without shaking. Probe **1** (final concentration 15 μM, final assay volume 10 μL) was added using a MultiDrop Combi dispenser (ThermoFisher Scientific). The plate was incubated for 10 minutes at room temperature. The fluorescence intensity was then measured every 5 minutes for 50 minutes using an Envision 2104 Multilabel Reader (PerkinElmer) with λ_{ex} = 485 nm, λ_{em} = 540 nm and an FITC mirror. Data were analysed using ActivityBase (IDBS).

3.6.3 BlaC fluorogenic assays

Compounds (in DMSO, concentrations ranging from 100 μM to 1.69 nM) were dispensed into a black polystyrene, flat-bottomed, small volume, clear bottomed 384-well microplate (Greiner Bio-One, part number 784076). Two types of controls were used. In control 1, inhibitors were substituted with neat DMSO (100 nL) (expected 0% inhibition; 100% fluorescence signal). In control 2, the addition of BlaC was omitted (expected 100% inhibition; 0% fluorescence signal). BlaC (final concentration 2.5 nM) in assay buffer (100 mM sodium phosphate pH 7.5 with 0.01% (*v*/*v*) Triton X-100) was added to all wells (except control 2) using a MultiDrop Combi dispenser (ThermoFisher Scientific). In control 2, the BlaC mixture was substituted with the assay buffer. This mixture was incubated for 30 minutes at room temperature without shaking. FC5 (final concentration 2.5 μM, final assay volume 10 μL) was added using a MultiDrop Combi dispenser (ThermoFisher Scientific). The fluorescence intensity was measured every minute for 10 minutes using an Envision 2104 Multilabel Reader (PerkinElmer) with λ_{ex} = 340 nm, λ_{em} = 480 nm and a general dual mirror. Data were analysed using ActivityBase (IDBS).

3.6.4 HTS interference assay

Compounds (in DMSO, concentrations ranging from 100 μM to 1.69 nM) were dispensed into a black polystyrene, flat-bottomed, small volume, clear bottomed 384-well microplate (Greiner Bio-One, part number 784076). Two types of controls were used. In control 1, inhibitors were substituted with neat DMSO (100 nL) (expected 0% inhibition, 100% fluorescence signal). In control 2, the addition of Ldt_{Mt2} was omitted (expected 100% inhibition, 0% fluorescence signal). Prior to the assay, Ldt_{Mt2} (final concentration 300 nM) was reacted with probe **1** (final concentration 15 μM) in assay buffer (50 mM sodium phosphate, pH 7.5, 0.007% (*v*/*v*) Tween-

20) for 5 hours at room temperature. To all wells except control 2, 10 µL of the reacted Ldt_{Mt2} and the probe **1** mixture were added, using a MultiDrop Combi dispenser (ThermoFisher Scientific). In control 2, the Ldt_{Mt2} mixture was substituted with 5 µL of the assay buffer. The plate was incubated for another 10 minutes at room temperature. The fluorescence intensity was then measured every 5 minutes for 50 minutes using an Envision 2104 Multilabel Reader (PerkinElmer) with λ_{ex} = 485 nm, λ_{em} = 540 nm and an FITC mirror. Data were analysed using ActivityBase (IDBS).

3.6.5 Protein observed solid phase extraction mass spectrometry

Ldt_{Mt2} (1 µM) in buffer (50 mM tris, pH 7.5) was incubated with an inhibitor (100 µM, 10 µM, or 2 µM, as indicated). Mass spectrometry was performed using a RapidFire200 integrated autosampler/solid phase extraction (SPE) system (Agilent Technologies) coupled to an API40000 triple quadrupole mass spectrometer (Applied Biosystems) operating in the positive ionisation mode. Samples were taken after the specified incubation periods, loaded onto a C4 cartridge (Agilent Technologies), and eluted with organic phase (85% (*v*/*v*) acetonitrile, 15% (*v*/*v*) water, 0.1% (*v*/*v*) formic acid). The cartridge was washed with both the organic phase and an aqueous phase (water, 0.1% (*v*/*v*) formic acid). Data were analysed using MassHunter Qualitative Analysis B.07.00 (Agilent Technologies). Spectra were deconvoluted using the maximum entropy algorithm in the same programme.

3.6.6 Rate constant of covalent target inactivation (k_{inact}/K_I)

The second-order rate constant for irreversible inhibition (k_{inact}/K_I) was determined using irreversibly reacting probe **2**.[41] The k_{inact}/K_I of probe **2** was determined through measurement of the fluorescence intensity of the reaction between Ldt_{Mt2} (100 nM) and probe **2** (concentrations ranging between 100 nM and 10 µM) in 50 mM HEPES, pH 7.2, 0.01% (*v*/*v*) Triton X-100 using a PHERAstar plate reader (BMG Labtech) with λ_{ex} = 480 nm and λ_{em} = 520 nm. The observed kinetic rate constant (k_{obs}) was determined using equation 1.

$$Y = (Y_\infty - Y_0)\left[1 - e^{(-k_{obs} \times t)}\right] + Y_0 \quad (1)$$

The $(k_{inact}/K_I)_{probe}$ was derived from k_{obs} using equation 2, yielding a value of 39.8 M^{-1} s^{-1}.

$$k_{obs} = (k_{inact}/K_I)_{probe}[\text{probe } \mathbf{2}] \quad (2)$$

The half-life ($t_{1/2}$) of probe **2** (10 µM), was determined using equation 3 to be 28.7 min. Therefore, an incubation time of 2.4 h should ensure <97% receptor occupancy. With this knowledge, an incubation time of 3 h was selected for the determination of $(k_{inact}/K_I)_{inhibitor}$ values.

$$t_{1/2} = ln2/k_{obs} \quad (3)$$

Ldt_{Mt2} (100 nM) added to a mixture of varying concentrations of inhibitor (400 μM to 20.3 nM) for 10 min in assay buffer (50 mM HEPES, pH 7.2, 0.01% (*v*/*v*) Triton X-100) and probe **2** (10 μM), and incubated for 3 h prior to determination of the fluorescence intensity using a PHERAstar plate reader (BMG Labtech) with λ_{ex} = 480 nm and λ_{em} = 520 nm. Dose-response analyses were performed using a variable slope nonlinear regression model in GraphPad Prism 9 (GraphPad Software). The $(k_{inact}/K_I)_{inhibitor}$ values were derived from the IC_{50} values using equation 4.

$$k_{inact}/K_I = \frac{(k_{inact}/K_I)_{probe} \times [\text{probe } \mathbf{2}]}{IC_{50}} \quad (4)$$

3.6.7 Intrinsic thiol reactivity

In order to obtain the rate constant of probe **2** for reaction with L-glutathione (k_{probe}), L-glutathione (final concentration 500 nM) and probe **2** (final concentration 10 μM) in the assay buffer (50 mM HEPES pH 7.2, 0.01% (*v*/*v*) Triton X-100) were added to a 384-well plate. The fluorescence signal was measured using a PHERAstar plate reader (BMG Labtech) with λ_{ex} = 480 nm and λ_{em} = 520 nm. Readings were taken until apparent completion of the reaction (15 hours). The signal was fitted with a single exponential curve using GraphPad Prism 9 (GraphPad Software) to give the observed kinetic rate constant (k_{obs}), which was then converted to k_{probe} using equation 5.

$$k_{\text{obs}} = k_{\text{probe}}[\text{probe } \mathbf{2}] \quad (5)$$

Inhibitors were serially diluted (by 1/3) across columns 2-10 of a 96-well plate (starting concentration 10 mM). The final two columns of the microplate (11 and 12) were used as inhibitor-free controls and contained only DMSO. To a 384-well plate was added assay buffer (14 μL) using a MultiDrop Combi dispenser (ThermoFisher Scientific). The inhibitor or blank (1 μL) solutions were added using a CyBio liquid handling system (Analytik Jena AG), with 4 replicates per inhibitor concentration. To each well was added probe **2** (5 μL, final concentration 10 μM) using a MultiDrop Combi dispenser (ThermoFisher Scientific). L-Glutathione (5 μL, final concentration 500 nM, final volume 25 μL) was added and the plate was sealed and incubated for 15 h at room temperature. The fluorescence signal was measured using a PHERAstar plate reader (BMG Labtech) with λ_{ex} = 480 nm and λ_{em} = 520 nm and normalised against the mean average of no inhibitor controls and the mean average of no enzyme controls. Nonlinear regression analyses of dose-response were conducted using GraphPad Prism 9 (GraphPad Software) with a variable slope model. The k_{chem} of inhibitors was calculated from the obtained IC_{50} value using equation 6.

$$k_{\text{chem}} = \frac{k_{\text{probe}}\,[\text{probe } \mathbf{2}]}{\text{IC}_{50}} \quad (6)$$

3.6.8 Differential scanning fluorimetry (DSF) thermal shift assays

Ldt_{Mt2} (5 μM) was incubated with the inhibitor (500 μM) in assay buffer (50 mM tris pH 7.5) for 30 minutes at room temperature in 96-well white PCR plates (25 μL final volume, Starlab). SYPRO Orange (final concentration 6x, according to manufacturer's definition, Invitrogen) was then added and the plate was sealed using a transparent plastic film (Polyolefin StarSeal, Starlab). Fluorescence was monitored (with λ_{ex} = 492 nm and λ_{em} = 610 nm) using a CFX96 Touch Real-Time PCR Detection System (Bio-Rad), while the temperature was increased from 20 to 95 °C in increments of 0.2 °C. Melting temperatures (T_ms) were determined using the CFX Maestro Software (Bio-Rad).

3.6.9 Jump dilution assays

Ldt_{Mt2} (10 μM final concentration) was incubated with the inhibitor (100 μM final concentration) in the assay buffer (50 mM HEPES, pH 7.2, 0.01% (*v*/*v*) Triton X-100) for 2 hours at room temperature, then serially diluted 1000x with assay buffer (final Ldt_{Mt2} concentration 10 nM). 20 μL of the diluted mixture was added to a black polystyrene, flat-bottomed 384-well μ-clear plate (clear bottomed, Greiner Bio-One, part number 781096). Probe **2** (final concentration 15 μM) was added using a MultiDrop Combi dispenser (ThermoFisher Scientific). Fluorescence was measured using a PHERAstar plate reader (BMG Labtech) with λ_{ex} = 480 nm and λ_{em} = 520 nm. Readings were taken every 15 s for a period of 5 minutes, using bottom optic measurements. The off rate (k_{off}) was determined using equation 7.

$$P = V_s t + (V_0 - V_s)\frac{\left(1-e^{-k_{off}t}\right)}{k_{off}} + P_0 \quad (7)$$

where, P = formed product; V_s = velocity of no-inhibitor control; V_0 = velocity of no-enzyme control, and P_0 = initial fluorescence.

The half-life of the enzyme–inhibitor complex ($t_{1/2}$) was calculated using equation 8.

$$t_{1/2} = \frac{\ln\,(2)}{k_{off}} \quad (8)$$

3.6.10 Nondenaturing MS assays

Protein samples were prepared by buffer exchange into 500 mM ammonium acetate by dialysis using a Slide-A-Lyser 0.5 mL Dialysis Cassette (Thermo Scientific). Ldt_{Mt2} (final concentration 5 μM) was combined with the inhibitors of interest (final concentration 50 μM).

Mass spectra were acquired using a Waters Synapt Q-TOF machine operating in the positive ionisation mode with extended *m*/*z* range connected to an Advion Triversa Nanomate chip-based electrospray ionisation and autosampler. The cone voltage was as specified, and spectra were accumulated over approximately 50 scans. Data were analysed using MassLynx v4.1 (Waters).

3.6.11 X-ray crystallography

Ldt_{Mt2} (Δ1-55; with the N-terminal HisTag removed, in 50 mM tris, pH 8.0, 100 mM NaCl) was crystallised according to a modified reported procedure.[14] The well solution was composed of 0.2 M ammonium nitrate and 20% (*w*/*v*) PEG 3350. Sitting drop vapor diffusion crystallization plates (low reservoir Intelli-Plate 93–3) were prepared using a Rigaku Phoenix RE Drop setter instrument (Art Robbins Instrument). Crystallisation plates were stored at 4 °C. Inhibitors were introduced through soaking. The crystals were then mounted on nylon loops, cryocooled and stored in liquid nitrogen. Datasets were collected using the MX beamline i03 at Diamond Light Source. Structures were solved by molecular replacement with Phaser,[56] using PDB entry 6RRM,[14] as the search model. Alternating cycles of refinement using PHENIX,[57] and manual model building using COOT,[58] were performed until R_{work} and R_{free} converged. Data collection and refinement statistics are given in Table S1.13.

3.6.12 Bacterial strain

Mtb H37Rv cells expressing the luciferase *luc* gene from *Photinus pyralis* (GenBank Accession Number M15077) inserted in a mycobacterial shuttle plasmid derived from pACE-1 (*Mtb* H37Rv-Luc),[59] was routinely propagated at 37 °C in Middlebrook 7H9 broth (Difco) supplemented with 10% Middlebrook albumin-dextrose-catalase (ADC, Difco), 0.2% glycerol and 0.05% (*v*/*v*) tyloxapol or on Middlebrook 7H10 agar plates (Difco) supplemented with 10% (*v*/*v*) oleic acid-albumin-dextrose-catalase (OADC, Difco). Hygromycin B was added to the medium (50 μg mL^{-1}) to ensure plasmid maintenance when propagating *Mtb* H37Rv-Luc.

3.6.13 Intracellular assays

Frozen stocks of macrophage THP-1 cells (ATCC TIB-202) were thawed in RPMI-1640 medium (Sigma) supplemented with 10% fetal bovine serum (FBS, Gibco), 2 mM l-glutamine (Sigma) and 1 mM sodium pyruvate (Sigma). THP-1 cells were passaged only 5 times and maintained without an antibiotic between 2–10 x 105 cells per mL at 37 °C in a humidified, 5% CO_2 atmosphere. THP-1 cells (3 × 108) were simultaneously differentiated with phorbol myristate acetate (PMA, 40 ng mL^{-1}, Sigma) and infected for 4 hours at a multiplicity of

infection (MOI) of 1 : 1 with a single cell suspension of *Mtb* H37Rv-Luc cells. After incubation, infected cells were washed four times to remove extracellular bacilli and resuspended (2 × 105 cells per mL) in RPMI medium supplemented with 10% FBS (Hyclone), 2 mM L-glutamine and pyruvate and dispensed in white, flat bottom 384-well plates (Greiner) in a final volume of 50 µL containing test compounds (11 serial dilutions of 1/3 with starting concentration 100 µM, max. 0.5% DMSO). Plates were incubated for 5 days under 5% CO_2 atmosphere, 37 °C, 80% relative humidity before growth assessment. The Bright-Glo™ Luciferase Assay System (Promega, Madison, WI) was used as cell growth indicator for the *Mtb* H37Rv-Luc strain. Luminescence was measured in an Envision Multilabel Plate Reader (PerkinElmer) using the opaque 384-plate Ultra-Sensitive luminescence mode, with a measurement time of 50 ms. A reduction in light production was considered growth inhibition and the IC_{50} or IC_{90} value was interpolated from the dose response curve.

3.6.14 Extracellular assays

Mtb H37Rv cells were cultured in Middlebrook 7H9 medium supplied with 10% (*v*/*v*) ADC and 0.025% (*v*/*v*) Tyloxapol, then incubated at 37 °C for approximately 10 days. Following a purity check, subculture was performed in Middlebrook 7H9 medium supplied with 10% (*v*/*v*) ADC and 0.025% (*v*/*v*) Tyloxapol up to OD_{600} = 0.01 and incubated at 37 °C for 4-6 days. The inoculum was adjusted to OD_{600} = 0.00125 (equivalent to 1 x 105 cfu mL^{-1}). 50 µL of the inoculum was dispensed in all wells of a 384-well plate, containing test compounds (11 serial dilutions of 1/3 with starting concentration 100 µM). Plates were placed in a sealed box and incubated at 37 °C for 8 days. The lids were then removed, and the plates were covered with a seal. Absorption was measured at 590 nm using an Envision 2104 Multilabel Reader (PerkinElmer). If the window between negative control (Rifampicin) and positive control (no inhibitor) was not greater than or equal to 3 times, plates were incubated at 37 °C for one or two additional days.

3.6.15 HepG2 cytotoxicity assays

Solutions of the test compounds (250 nL per well; 11 serial dilutions of 1/3 with starting concentration 100 µM) were dispensed in tissue-culture treated black clear-bottomed 384-well plates (Greiner, cat. no. 781091) with an Echo 555 instrument. 25 µL of HepG2 (ATCC HB-8065) cells (~3000 cells per well) grown to confluency in Eagle's Minimal Essential Medium (MEM) supplemented with 10% (*v*/*v*) heat-inactivated FBS, 1% (*v*/*v*) non-essential amino acids (NEAA), and 1% (*v*/*v*) penicillin/streptomycin were added to each well. Plates were incubated at 37 °C with 20% O_2 and 5% CO_2 for 48 h. The plates were then equilibrated to room

temperature. ATP levels, measured with CellTiter Glo kit (Promega), were used as cell viability read-out. 25 µL of CellTiter Glo substrate dissolved in the buffer was added to each well. Plates were incubated at room temperature for 10 min and read on ViewLux (PerkinElmer) with excitation and emission filters of 613 and 655 nm, respectively. The HepG2 IC_{50} value corresponds to the concentration of the compound necessary to inhibit 50% of cell growth.

3.7 Data availability

Crystallographic data has been deposited at the PDB under accession codes 8A1L, 8A1J, 8A1M, 8A1O, 8A1N, 8A1K and 8AHO. Data supporting this manuscript are provided in the Supplementary Information (Appendix I).

3.8 References

1 Global tuberculosis report 2015, 20th ed., (Geneva: World Health Organization, 2015).

2 Sotgiu, G., Centis, R., D'Ambrosio, L. & Migliori, G. B. Tuberculosis Treatment and Drug Regimens. *Cold Spring Harb. Perspect. Med.* **5**, a017822 (2015).

3 Chakaya, J., Khan, M., Ntoumi, F., Aklillu, E., Fatima, R., Mwaba, P., Kapata, N., Mfinanga, S., Hasnain, S. E., Katoto, P. D. M. C., Bulabula, A. N. H., Sam-Agudu, N. A., Nachega, J. B., Tiberi, S., McHugh, T. D., Abubakar, I. & Zumla, A. Global Tuberculosis Report 2020 – Reflections on the Global TB burden, treatment and prevention efforts. *Int J Infect Dis.* **113**, S7-S12 (2021).

4 Finch, R. β-Lactam antibiotics and mycobacteria. *J. Antimicrob. Chemother.* **18**, 6-8 (1986).

5 Story-Roller, E. & Lamichhane, G. Have we realized the full potential of β-lactams for treating drug-resistant TB? *IUBMB Life* **70**, 881-888 (2018).

6 Sauvage, E., Kerff, F., Terrak, M., Ayala, J. A. & Charlier, P. The penicillin-binding proteins: structure and role in peptidoglycan biosynthesis. *FEMS Microbiol. Rev.* **32**, 234-258 (2008).

7 Mainardi, J. L., Fourgeaud, M., Hugonnet, J. E., Dubost, L., Brouard, J. P., Ouazzani, J., Rice, L. B., Gutmann, L. & Arthur, M. A novel peptidoglycan cross-linking enzyme for a beta-lactam-resistant transpeptidation pathway. *J. Biol. Chem.* **280**, 38146-38152 (2005).

8 Mainardi, J. L., Hugonnet, J. E., Rusconi, F., Fourgeaud, M., Dubost, L., Moumi, A. N., Delfosse, V., Mayer, C., Gutmann, L., Rice, L. B. & Arthur, M. Unexpected Inhibition of Peptidoglycan LD-Transpeptidase from *Enterococcus faecium* by the β-Lactam Imipenem. *J. Biol. Chem.* **282**, 30414-30422 (2007).

9 Lavollay, M., Arthur, M., Fourgeaud, M., Dubost, L., Marie, A., Veziris, N., Blanot, D., Gutmann, L. & Mainardi, J. L. The Peptidoglycan of Stationary-Phase *Mycobacterium tuberculosis* Predominantly Contains Cross-Links Generated by L,D-Transpeptidation. *J. Bacteriol.* **190**, 4360-4366 (2008).

10 Gupta, R., Lavollay, M., Mainardi, J. L., Arthur, M., Bishai, W. R. & Lamichhane, G. The *Mycobacterium tuberculosis* protein Ldt_{Mt2} is a nonclassical transpeptidase required for virulence and resistance to amoxicillin. *Nat. Med.* **16**, 466-469 (2010).

11 Böth, D., Steiner, E. M., Stadler, D., Lindqvist, Y., Schnell, R. & Schneider, G. Structure of Ldt_{Mt2}, an L,D-transpeptidase from *Mycobacterium tuberculosis*. *Acta Crystallogr. D* **69**, 432-441 (2013).

12 Erdemli, S. B., Gupta, R., Bishai, W. R., Lamichhane, G., Amzel, L. M. & Bianchet, M. A. Targeting the cell wall of *Mycobacterium tuberculosis*: structure and mechanism of L,D-transpeptidase 2. *Structure* **20**, 2103-2115 (2012).

13 Kim, H. S., Kim, J., Im, H. N., Yoon, J. Y., An, D. R., Yoon, H. J., Kim, J. Y., Min, H. K., Kim, S.-J. & Lee, J. Y. Structural basis for the inhibition of *Mycobacterium tuberculosis* L,D-transpeptidase by meropenem, a drug effective against extensively drug-resistant strains. *Acta Crystallogr. D* **69**, 420-431 (2013).

14 de Munnik, M., Lohans, C. T., Lang, P. A., Langley, G. W., Malla, T. R., Tumber, A., Schofield, C. J. & Brem, J. Targeting the *Mycobacterium tuberculosis* transpeptidase Ldt_{Mt2} with cysteine-reactive inhibitors including ebselen. *Chem. Commun.* **55**, 10214-10217 (2019).

15 Steiner, E. M., Schneider, G. & Schnell, R. Binding and processing of β-lactam antibiotics by the transpeptidase Ldt_{Mt2} from *Mycobacterium tuberculosis*. *FEBS J.* **284**, 725-741 (2017).

16 Li, W. J., Li, D. F., Hu, Y. L., Zhang, X. E., Bi, L. J. & Wang, D. C. Crystal structure of L,D-transpeptidase Ldt_{Mt2} in complex with meropenem reveals the mechanism of carbapenem against *Mycobacterium tuberculosis*. *Cell Res.* **23**, 728-731 (2013).

17 Triboulet, S., Arthur, M., Mainardi, J. L., Veckerlé, C., Dubée, V., Nguekam Moumi, A., Gutmann, L., Rice, L. B. & Hugonnet, J. E. Inactivation Kinetics of a New Target of β-Lactam Antibiotics. *J. Biol. Chem.* **286**, 22777-22784 (2011).

18 Gupta, R., Al-Kharji, N. M. S. A., Alqurafi, M. A., Nguyen, T. Q., Chai, W., Quan, P., Malhotra, R., Simcox, B. S., Mortimer, P., Brammer Basta, L. A., Rohde, K. H. & Buynak, J. D. Atypically Modified Carbapenem Antibiotics Display Improved Antimycobacterial Activity in the Absence of β-Lactamase Inhibitors. *ACS Infect. Dis.* **7**, 2425-2436 (2021).

19 Kumar, P., Kaushik, A., Lloyd, E. P., Li, S.-G., Mattoo, R., Ammerman, N. C., Bell, D. T., Perryman, A. L., Zandi, T. A., Ekins, S., Ginell, S. L., Townsend, C. A., Freundlich, J. S. & Lamichhane, G. Non-classical transpeptidases yield insight into new antibacterials. *Nat. Chem. Biol.* **13**, 54-61 (2017).

20 Powers, J. C., Asgian, J. L., Ekici, Ö. D. & James, K. E. Irreversible inhibitors of serine, cysteine, and threonine proteases. *Chem. Rev.* **102**, 4639-4750 (2002).

21 Owen, D. R., Allerton, C. M. N., Anderson, A. S., Aschenbrenner, L., Avery, M., Berritt, S., Boras, B., Cardin, R. D., Carlo, A., Coffman, K. J., Dantonio, A., Di, L., Eng, H., Ferre, R., Gajiwala, K. S., Gibson, S. A., Greasley, S. E., Hurst, B. L., Kadar, E. P., Kalgutkar, A. S., Lee, J. C., Lee, J., Liu, W., Mason, S. W., Noell, S., Novak, J. J., Obach, R. S., Ogilvie, K., Patel, N. C., Pettersson, M., Rai, D. K., Reese, M. R., Sammons, M. F., Sathish, J. G., Singh, R. S. P., Steppan, C. M., Stewart, A. E., Tuttle, J. B., Updyke, L., Verhoest, P. R., Wei, L., Yang, Q. & Zhu, Y. An oral SARS-CoV-2 M^{pro} inhibitor clinical candidate for the treatment of COVID-19. *Science* **374**, 1586-1593 (2021).

22 Yang, H. & Yang, J. A review of the latest research on M^{pro} targeting SARS-COV inhibitors. *RSC Med. Chem.* **12**, 1026-1036 (2021).

23 de Munnik, M., Lohans, C. T., Langley, G. W., Bon, C., Brem, J. & Schofield, C. J. A Fluorescence-Based Assay for Screening β-Lactams Targeting the *Mycobacterium tuberculosis* Transpeptidase Ldt_{Mt2}. *ChemBioChem* **21**, 368-372 (2020).

24 Zhang, J. H., Chung, T. D. & Oldenburg, K. R. A simple statistical parameter for use in evaluation and validation of high throughput screening assays. *J. Biomol. Screen.* **4**, 67-73 (1999).

25 Iversen, P. W., Eastwood, B. J., Sittampalam, G. S. & Cox, K. L. A comparison of assay performance measures in screening assays: signal window, Z' factor, and assay variability ratio. *J. Biomol. Screen.* **11**, 247-252 (2006).

26 Van Berkel, S. S., Brem, J., Rydzik, A. M., Salimraj, R., Cain, R., Verma, A., Owens, R. J., Fishwick, C. W. G., Spencer, J. & Schofield, C. J. Assay Platform for Clinically Relevant Metallo-β-lactamases. *J. Med. Chem.* **56**, 6945-6953 (2013).

27 Gokulan, K., Khare, S., Cerniglia, C. E., Foley, S. L. & Varughese, K. I. Structure and inhibitor specificity of L, D-transpeptidase (Ldt_{Mt2}) from *Mycobacterium tuberculosis* and antibiotic resistance: calcium binding promotes dimer formation. *AAPS J.* **20**, 1-14 (2018).

28 Wivagg, C. N., Bhattacharyya, R. P. & Hung, D. T. Mechanisms of β-lactam killing and resistance in the context of *Mycobacterium tuberculosis*. *J. Antibiot.* **67**, 645-654 (2014).

29 Lang, P. A., Leissing, T. M., Page, M. G., Schofield, C. J. & Brem, J. Structural Investigations of the Inhibition of *Escherichia coli* AmpC β-Lactamase by Diazabicyclooctanes. *Antimicrob. Agents Chemother.* **65**, e02073 (2020).

30 Brewer, C. F. & Riehm, J. P. Evidence for possible nonspecific reactions between N-ethylmaleimide and proteins. *Anal. Biochem.* **18**, 248-255 (1967).

31 Shaw, E. Cysteinyl proteinases and their selective inactivation. *Adv. Enzymol. Relat. Areas Mol. Biol.* **63**, 271-271 (1993).

32 Huynh, K. & Partch, C. L. Analysis of Protein Stability and Ligand Interactions by Thermal Shift Assay. *Curr. Protoc. Protein Sci.* **79**, 14-21 (2015).

33 Copeland, R. A., Basavapathruni, A., Moyer, M. & Scott, M. P. Impact of enzyme concentration and residence time on apparent activity recovery in jump dilution analysis. *Anal. Biochem.* **416**, 206-210 (2011).

34 Degani, Y. & Patchornik, A. Cyanylation of sulfhydryl groups by 2-nitro-5-thiocyanobenzoic acid. High-yield modification and cleavage of peptides at cysteine residues. *Biochemistry* **13**, 1-11 (1974).

35 Wu, J. & Watson, J. T. A novel methodology for assignment of disulfide bond pairings in proteins. *Protein Sci.* **6**, 391-398 (1997).

36 Wu, J. & Watson, J. T. Optimization of the cleavage reaction for cyanylated cysteinyl proteins for efficient and simplified mass mapping. *Anal. Biochem.* **258**, 268-276 (1998).

37 Villa, S., De Fazio, G. & Canosi, U. Cyanogen bromide cleavage at methionine residues of polypeptides containing disulfide bonds. *Anal. Biochem.* **177**, 161-164 (1989).

38 Schörgenhumer, J. & Waser, M. New strategies and applications using electrophilic cyanide-transfer reagents under transition metal-free conditions. *Org. Chem. Front.* **3**, 1535-1540 (2016).

39 Charpentier, J., Früh, N. & Togni, A. Electrophilic Trifluoromethylation by Use of Hypervalent Iodine Reagents. *Chem. Rev.* **115**, 650-682 (2015).

40 Strelow, J. M. A Perspective on the Kinetics of Covalent and Irreversible Inhibition. *SLAS Discov.* **22**, 3-20 (2017).

41 Miyahisa, I., Sameshima, T. & Hixon, M. S. Rapid Determination of the Specificity Constant of Irreversible Inhibitors (k_{inact}/K_I) by Means of an Endpoint Competition Assay. *Angew Chem. Int. Ed. Engl.* **54**, 14099-14102 (2015).

42 Sameshima, T., Miyahisa, I., Yamasaki, S., Gotou, M., Kobayashi, T. & Sakamoto, J. High-Throughput Quantitative Intrinsic Thiol Reactivity Evaluation Using a Fluorescence-Based Competitive Endpoint Assay. *Adv. Sci. Drug Disc.* **22**, 1168-1174 (2017).

43 Maeda, H., Matsuno, H., Ushida, M., Katayama, K., Saeki, K. & Itoh, N. 2,4-Dinitrobenzenesulfonyl Fluoresceins as Fluorescent Alternatives to Ellman's Reagent in Thiol-Quantification Enzyme Assays. *Angew. Chem. Int. Ed.* **44**, 2922-2925 (2005).

44 Hoyle, C. E. & Bowman, C. N. Thiol-ene click chemistry. *Angew. Chem. Int. Ed.* **49**, 1540-1573 (2010).

45 Mather, B. D., Viswanathan, K., Miller, K. M. & Long, T. E. Michael addition reactions in macromolecular design for emerging technologies. *Prog. Polym. Sci.* **31**, 487-531 (2006).

46 Singh, J., Petter, R. C., Baillie, T. A. & Whitty, A. The resurgence of covalent drugs. *Nat. Rev. Drug Discov.* **10**, 307-317 (2011).

47 Berman, H. M., Westbrook, J., Feng, Z., Gilliland, G., Bhat, T. N., Weissig, H., Shindyalov, I. N. & Bourne, P. E. The protein data bank. *Nucleic Acids Res.* **28**, 235-242 (2000).
48 Liebschner, D., Afonine, P. V., Moriarty, N. W., Poon, B. K., Sobolev, O. V., Terwilliger, T. C. & Adams, P. D. Polder maps: improving OMIT maps by excluding bulk solvent. *Acta Crystallogr. D* **73**, 148-157 (2017).
49 Boike, L., Henning, N. J. & Nomura, D. K. Advances in covalent drug discovery. *Nat. Rev. Drug Discov.*, 881–898 (2022).
50 Lima, L. M., da Silva, B. N. M., Barbosa, G. & Barreiro, E. J. β-lactam antibiotics: An overview from a medicinal chemistry perspective. *Eur. J. Med. Chem.* **208**, 112829 (2020).
51 Baldwin, J. E. Rules for ring closure. *J. Chem. Soc., Chem. Commun.*, 734 (1976).
52 MacMicking, J. D., Taylor, G. A. & McKinney, J. D. Immune control of tuberculosis by IFN-γ-inducible LRG-47. *Science* **302**, 654-659 (2003).
53 MacMicking, J. D., North, R. J., LaCourse, R., Mudgett, J. S., Shah, S. K. & Nathan, C. F. Identification of nitric oxide synthase as a protective locus against tuberculosis. *Proc. Natl. Acad. Sci. U.S.A.* **94**, 5243-5248 (1997).
54 Gold, B., Smith, R., Nguyen, Q., Roberts, J., Ling, Y., Lopez Quezada, L., Somersan, S., Warrier, T., Little, D. & Pingle, M. Novel cephalosporins selectively active on nonreplicating *Mycobacterium tuberculosis*. *J. Med. Chem.* **59**, 6027-6044 (2016).
55 Lohans, C. T., Chan, H. T. H., Malla, T. R., Kumar, K., Kamps, J. J. A. G., McArdle, D. J. B., Van Groesen, E., de Munnik, M., Tooke, C. L., Spencer, J., Paton, R. S., Brem, J. & Schofield, C. J. Non-Hydrolytic β-Lactam Antibiotic Fragmentation by L,D-Transpeptidases and Serine β-Lactamase Cysteine Variants. *Angew. Chem. Int. Ed.* **58**, 1990-1994 (2019).
56 McCoy, A. J., Grosse-Kunstleve, R. W., Adams, P. D., Winn, M. D., Storoni, L. C. & Read, R. J. Phaser crystallographic software. *J. Appl. Crystallogr.* **40**, 658-674 (2007).
57 Adams, P. D., Afonine, P. V., Bunkóczi, G., Chen, V. B., Davis, I. W., Echols, N., Headd, J. J., Hung, L.-W., Kapral, G. J., Grosse-Kunstleve, R. W., McCoy, A. J., Moriarty, N. W., Oeffner, R., Read, R. J., Richardson, D. C., Richardson, J. S., Terwilliger, T. C. & Zwart, P. H. PHENIX: a comprehensive Python-based system for macromolecular structure solution. *Acta Crystallogr. D* **66**, 213-221 (2010).
58 Emsley, P., Lohkamp, B., Scott, W. G. & Cowtan, K. Features and development of Coot. *Acta Crystallogr. D* **66**, 486-501 (2010).
59 Sorrentino, F., Rio, R. G. d., Zheng, X., Matilla, J. P., Gomez, P. T., Hoyos, M. M., Herran, M. E. P., Losana, A. M. & Av-Gay, Y. Development of an Intracellular Screen for New Compounds Able To Inhibit *Mycobacterium tuberculosis* Growth in Human Macrophages. *Antimicrob. Agents Chemother.* **60**, 640-645 (2016).

3.9 Statement of authorship

Title of Paper	High-throughput screen with the L,D-transpeptidases Ldt_{Mt2} of *Mycobacterium tuberculosis* reveals novel classes of covalently reacting inhibitors
Publication Status	■Published □Submitted for Publication □Accepted for Publication □Unpublished and unsubmitted work written in a manuscript style
Publication Details	de Munnik M, Lang PA, De Dios Anton F, Cacho M, Bates RH, Brem J, Rodríguez Miquel B, Schofield CJ. (2023). High-throughput screen with the L,D-transpeptidase Ldt_{Mt2} of *Mycobacterium tuberculosis* reveals novel classes of covalently reacting inhibitors. Chem. Sci., 14(26), 7262-7278.

Student Confirmation

Student Name:	Mariska de Munnik		
Contribution to the Paper	The assay optimisation, high-throughput screen, was supervised by Dr. Beatriz Rodríguez Miquel, Francisco De Dios Anton, Dr. Mónica Cacho and Dr. Robert H. Bates at GSK Tres Cantos. Inhibitor follow-up studies, including inhibitor kinetic, mass-spectrometric and X-ray crystallographic studies were supervised by Dr. Pauline Lang and Dr. Jürgen Brem. GSK Tres Cantos performed the library and inhibitor selection, high-throughput screen data analysis, inhibitor susceptibility studies with *Mycobacterium tuberculosis*, and the cytotoxicity studies. All remaining experimental work described here, data analysis, and preparation of the manuscript were carried out by me.		
Signature		Date	23/01/2024

Supervisor Confirmation

By signing the Statement of Authorship, you are certifying that the candidate made a substantial contribution to the publication, and that the description described above is accurate.

Prof Chris Schofield		
I'm happy to start that the candidate made the major and a very substantial contribution to the publication, and that the description described above is accurate.		
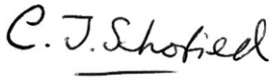	Date	23/01/2024

Chapter 4

αβ,α′β′-Diepoxyketones are mechanism-based inhibitors of nucleophilic cysteine enzymes

Manuscript II

Reproduced from:

Mariska de Munnik, Jasper Lithgow, Lennart Brewitz, Kirsten E. Christensen, Robert H. Bates, Beatriz Rodriguez Miquel, and Christopher J. Schofield. αβ,α'β'-Diepoxyketones are mechanism-based inhibitors of nucleophilic cysteine enzymes. *Chem. Commun.* **59**, 12859-12862 (2023).

with permission from the Royal Society of Chemistry.

Contents

4.1 Abstract 104
4.2 Main text 105
4.3 Data availability 111
4.4 References 111
4.5 Statement of authorship 115

4.1 Abstract

Epoxides are an established class of electrophilic alkylating agents that react with nucleophilic protein residues. We report αβ,α′β′-diepoxyketones (DEKs) as a new type of mechanism-based inhibitors of nucleophilic cysteine enzymes. Studies with the L,D-transpeptidase Ldt_{Mt2} from *Mycobacterium tuberculosis* and the main protease from SARS-CoV-2 (M^{pro}) reveal that following epoxide ring opening by a nucleophilic cysteine, further reactions can occur, leading to irreversible alkylation.

Key words: Covalent inhibitors, mechanism-based enzyme inhibition, nucleophilic enzymes, *Mycobacterium tuberculosis*, L,D-transpeptidases, epoxides, SARS-CoV-2 main protease, M^{pro}.

4.2 Main text

Most covalently reacting enzyme inhibitors bear an electrophilic functional group that reacts with a nucleophile to enable covalent protein modification.[1] Although many such inhibitors work by apparently simple acylation, alkylation or conjugate addition reactions, some undergo further reaction after initial covalent modification. Such mechanism-based inhibitors can be found in drugs,[2-4] with one such example being inhibitors of the nucleophilic serine-β-lactamases, such as clavulanic acid.[5,6]

Despite the long-standing importance of covalently reacting drugs, concerns regarding potential toxicity have hindered their development. Covalently reacting drugs are, however, the subject of recent renewed interest,[1,7] and are currently the basis for multiple drug development programs, including in oncology and antimicrobials.[8-11] Covalent targeting of a prevalent oncogenic mutation in K-Ras (K-Ras^{G12C}) has led to development of sotorasib and adagrasib.[12] Various medicinal chemistry programs targeting the main protease (M^{pro}) of SARS-CoV-2 have focussed on covalent reaction of the catalytic cysteine residue, with nirmatrelvir, a reversibly reacting nitrile-bearing inhibitor, being approved for COVID-19 treatment.[13,14] The L,D-transpeptidase Ldt$_{Mt2}$ of *Mycobacterium tuberculosis*, which is a target for TB treatment,[15] is amenable to covalent inhibition *via* reaction with its catalytic cysteine.[16-18]

Epoxides are an established class of electrophilic alkylating agents, and are used to inhibit nucleophilic cysteine (and serine) proteases.[1,19,20] Many epoxide inhibitors of cysteine or serine proteases contain peptide backbones, e.g., proteasome inhibitors,[21-24] though the small molecule epoxide fosfomycin is a clinically important antibiotic (Figure 4.1A).[25,26]

We are interested in identifying new types of covalently reacting modulators of biological function. Recently, we reported on a high-throughput screen aiming to identify new electrophilic inhibitors of Ldt$_{Mt2}$ and other nucleophilic enzymes.[27] Here, we describe the identification of the small molecule *trans*,*trans* α,β,α′,β′-diepoxyketone (DEK) **1** (Figure 4.1B), and the potency and mechanism of **1** and related DEKs **4**-**12** for Ldt$_{Mt2}$ and SARS-CoV-2 M^{pro} inhibition; the results reveal DEKs as a mechanistically interesting class of electrophile.

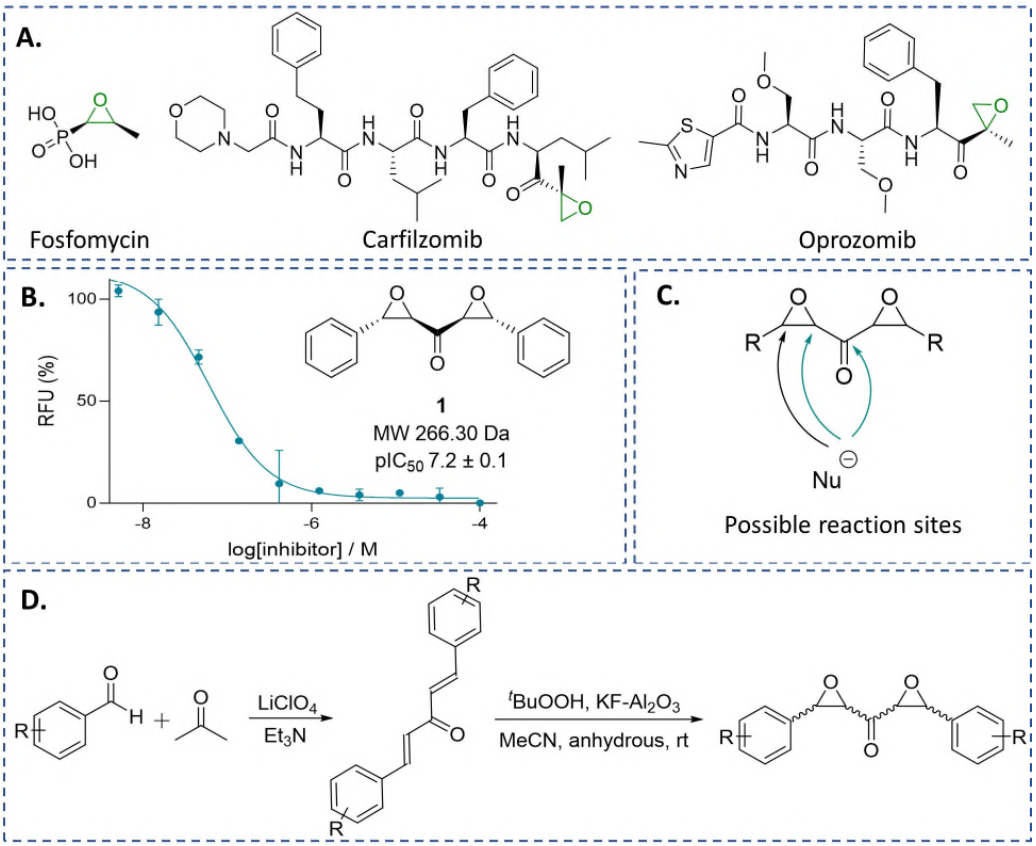

Figure 4.1. αβ,α′β′-Diepoxyketones (DEKs) react with nucleophilic cysteine enzymes. A. Examples of epoxide-bearing drugs. **B.** DEK **1** was identified as a potent inhibitor of Ldt_{Mt2}. **C.** Symmetrical DEKs contain 3 potential sites for interactions with nucleophiles, as well as three oxygens that may react with electrophiles. Arrows in teal represent pathways consistent with mechanistic studies. **D.** Synthesis of DEKs **1** and **4-11**.

Symmetrical DEKs have 3 obvious positions that may react with nucleophiles and have potential to undergo further reactions (Figure 4.1C). DEK **1** exhibited potent inhibition of Ldt_{Mt2}, with a pIC_{50} of 7.2 ± 0.1, with 30 min pre-incubation (Figure 4.1B). To investigate the mode of reaction of **1** with Ldt_{Mt2}, we carried out protein-observed mass spectrometry employing solid-phase extraction (SPE-MS). The results reveal that **1** covalently reacts with Ldt_{Mt2}, giving an initial adduct (**2**) with a +267 Da mass shift relative to unmodified Ldt_{Mt2} (Figure 4.2B, Table S2.1), corresponding to addition of one molecule of **1** to Ldt_{Mt2}, which has a single cysteine (Cys354). This adduct (**2**) was transient, converting within 2 h into one with a mass shift of +160 Da relative to unmodified Ldt_{Mt2}, provisionally assigned as **3**. We proposed the reaction involves nucleophilic attack of Cys354 on the carbonyl-group adjacent carbon of one of the symmetrical epoxides, with ring opening to form **2**, followed by retro-aldol fragmentation, releasing benzaldehyde (Figure 4.2C). Alternatively, the reaction may proceed though reaction at the carbonyl carbon to generate a hemithioketal, after which rearrangement may occur (Figure 4.2C).[28]

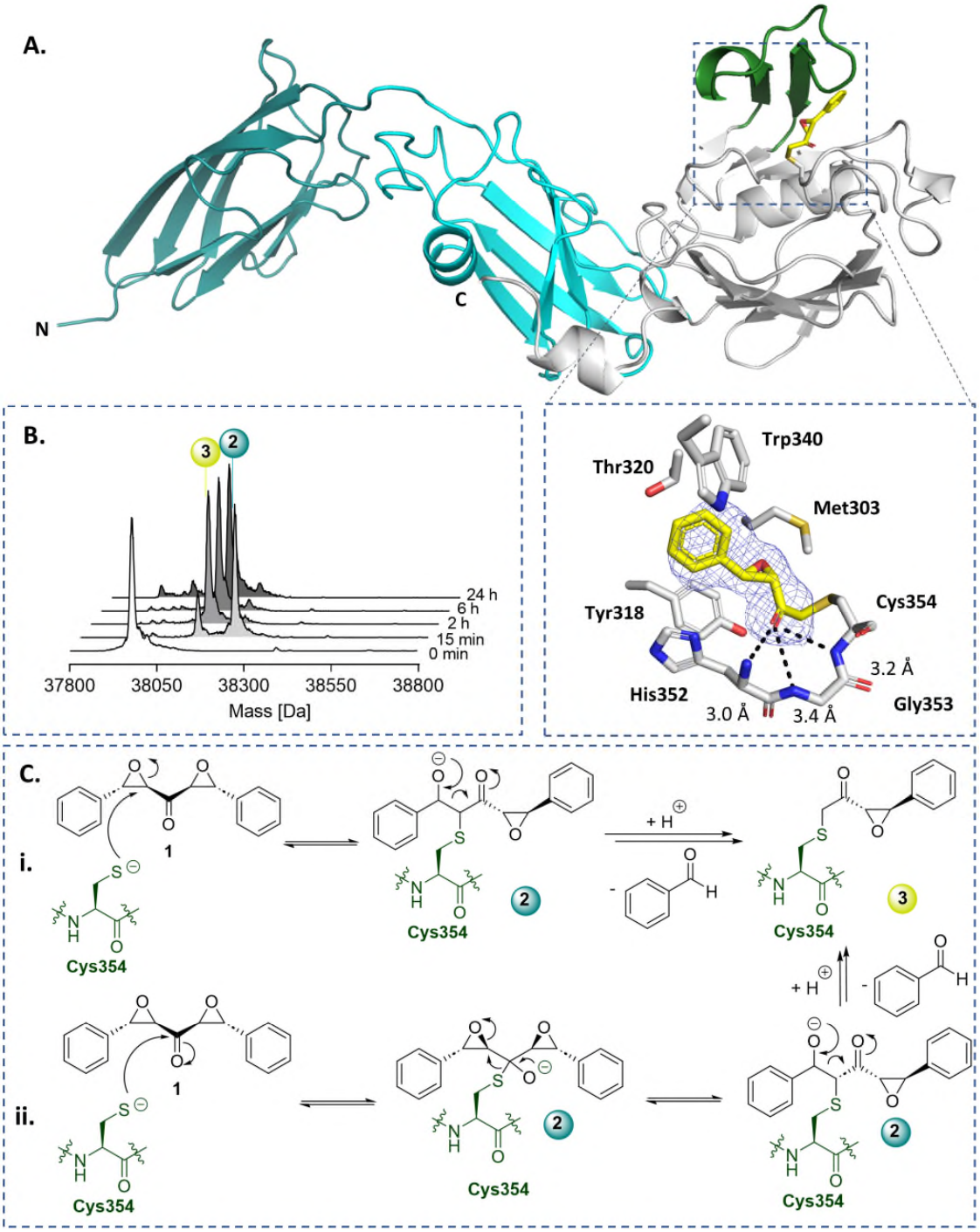

Figure 4.2. X-ray crystallography and protein-observed SPE-MS studies inform on the mechanism of DEK inhibition. A. Views from a crystal structure derived by reaction of Ldt_{Mt2} with DEK **1** (yellow, PDB: 8BK3). The immunoglobulin-like domains are in teal and cyan. The catalytic domain is grey, with the active site lid in green. The mF_o-DF_c polder OMIT map is contoured at 3.0 σ, carved around Cys354 bound **1** (refined as **3**) and shown in blue mesh. Polar interactions are shown in black dashes. **B.** Protein-observed SPE-MS experiments inform on the mechanism of reaction of **1** (20 μM) with Ldt_{Mt2} (1 μM). **C.** The proposed mechanisms for reaction of Cys354 of Ldt_{Mt2} (in green) with **1** *via* reaction with (i) the carbonyl adjacent carbon or (ii) the carbonyl carbon, followed by retro-aldol fragmentation.

The identity of **3** was validated by X-ray crystallography, using reported conditions,[27] wherein **1** was introduced through soaking; a structure of Ldt_{Mt2} reacted with **1** was obtained (2.15 Å resolution, $P12_11$ space group, PDB: 8BK3, Table S2.2). As reported, Ldt_{Mt2} crystallised with two molecules (chains A and B) in the asymmetric unit. While this structure manifested clear additional electron density at the chain A active site, only partial density was observed at that of chain B, thus inhibitor modelling was only performed in chain A. The additional electron density in chain A supports the proposed structure of adduct **3** (Figure 4.2). The carbonyl of **3** projects into the proposed oxyanion hole, formed by the backbone NH groups of His352, Gly353 and Cys354 (distances of 3.0 Å, 3.4 Å, and 3.2 Å, respectively).[29] Extensive hydrophobic interactions of **3** with active site residues Tyr318, His352, Trp340, Thr320, and Met303 were observed.

In aqueous solution, **1** was found to be stable for at least 12 h (Figure S2.3). Cysteine reacted with **1**, apparently yielding a product analogous to adduct **3** (Figure S2.4). No evidence for reaction of **1** with serine, lysine, threonine, tyrosine, arginine, or histidine was observed by ^{1}H NMR or LCMS under the tested conditions (Figure S2.5).

To further analyse the inhibitory potency and mechanism of the DEKs, we prepared derivatives of **1**. Synthesis involved preparation of the diene ketones *via* solvent-free aldol condensation, mediated by lithium perchlorate and Et_3N,[30] followed by epoxidation using ^{t}BuOOH and KF-Al_2O_3,[31,32] to yield stereo-isomeric mixtures of the *trans*,*trans* and *cis*,*cis* isomers of DEKs **1** and **4**-**11** (Figure 4.1D, Figure S2.6, Table S2.3).

No substantial difference in inhibition of Ldt_{Mt2} between the isomerically pure *trans,trans meso* **1** and a mixture of *trans,trans* stereoisomers of **1** was observed. While we did not obtain the pure *cis*,*cis* stereoisomers of **1**, a mixture of the *trans*,*trans* and *cis*,*cis* isomers of **1** (~1 : 3 ratio of *trans*,*trans* : *cis*,*cis* stereoisomers) manifested potent, but decreased, Ldt_{Mt2} inhibition compared to purified *trans,trans* isomers of **1** (pIC_{50} 5.6 ± 0.04 compared to 6.2 ± 0.07 for purified *trans,trans* isomers of **1**, with 15 min preincubation, Figure S2.7). The results imply the importance of the *trans,trans* stereochemistry for potent Ldt_{Mt2} inhibition by the DEKs. Recrystallisation of stereoisomeric mixtures from ethanol afforded the corresponding pure *trans*,*trans* isomers, as supported by ^{1}H NMR analysis and small molecule X-ray diffraction (Table S2.4), except for DEKs **5** and **8**, which were tested as mixtures of *trans,trans* and *cis,cis* isomers (*trans*,*trans*:*cis*,*cis* ratio ~2 : 1 and ~1.2 : 1, respectively).

Dose-response assays of **4**-**11** with Ldt_{Mt2} showed decreased potency compared to **1** (Table S2.3 and Figure S2.1). Determination of the second-order rate constants for covalent target inactivation (k_{inact}/K_I)[33] for Ldt_{Mt2} manifested the highest rate of inhibition for **1** (k_{inact}/K_I of 484.3 ± 28.4 M^{-1} s^{-1}, Table S2.3 and Figure S2.8). DEKs **5**-**7** and **9** were observed to inhibit Ldt_{Mt2},

while no evidence for inhibition was observed with **4**, **8** and **10**. The kinetic rate constant for reactivity with GSH (k_{chem})[27,34] was found to be below the assay limit for all DEKs (k_{chem} of <0.08 M^{-1} s^{-1} and half-life ($t_{1/2}$) >8.7 h), except **7** and **8** (k_{chem} of 1.71 ± 0.24 and 1.11 ± 0.20 M^{-1} s^{-1}, and $t_{1/2}$ of 24 min and 38 min, respectively; Table S2.3 and Figure S2.9). DEKs therefore apparently exhibit lower intrinsic reactivity compared to the common cysteine reactive acrylate, maleimide and isothiocyanate groups ($t_{1/2}$ < 1.0 min), and, with the exceptions of **7** and **8**, chloroacetamide (5.8 h).[35] MS studies of the reaction of GSH and **1** manifested an adduct analogous to **3** (Figure S2.10).

Protein-observed SPE-MS assays of **4**-**11** demonstrated covalent modification of Ldt_{Mt2} with **4**-**10**, which manifested adducts analogous to those with **1** (Figure S2.2 and Table S2.1) supporting the generality of the proposed mechanism. Additional peaks of +18 Da were observed with both unfragmented and fragmented adducts of **4**-**10**, likely due to ring opening of the second epoxide (Figure S2.11). With **1**, **5**, **6** and **7**, over 24 h, a second fragment adduct was observed with a +56 mass shift relative to the unmodified enzyme (Figure S2.11).

DEK **1** apparently displayed a low level of β-elimination of the reacted Cys354 residue, likely to form a dehydroalanine residue (Dha, ~5% in 24 h, as evidenced by a −34 Da mass shift relative to unmodified Ldt_{Mt2}, Figure S2.2 and S2.11).[36-38] Interestingly, the *ortho*-trifluoromethoxy substituents on the phenyl groups of **5** promoted Dha formation (~30% in 24 h). Dha formation was additionally observed following reaction with **4** (~2.5% in 24 h) and **7** (~16% in 24 h). In the cases of **6** and **8**-**10**, no evidence for Dha formation was observed.

While inhibition assays with the α,β-monoepoxyketone **12** did not manifest inhibition of Ldt_{Mt2}, protein-observed SPE-MS assays of Ldt_{Mt2} (1 μM) with **12** (100 μM) evidenced covalent reaction. As with DEKs **1** and **4**-**10**, initial measurements (2 h) showed the most abundant adduct to have a mass shift of +224 Da, corresponding to the addition of a single molecule of **12**. A +119 Da adduct was observed to become abundant after 6 h (Figure S2.2), indicating that the retro-aldol fragmentation is conserved between mono- and diepoxide derivatives.

While Ldt_{Mt2} contains only a single cysteine, in principle, the DEKs may alkylate other nucleophilic residues.[39,40] To investigate whether the DEKs react selectively with Cys354 of Ldt_{Mt2}, we performed protein-observed SPE-MS assays with Ldt_{Mt2} that had been preincubated with ebselen, which is known to selectively and irreversibly react with Cys354.[16] When **1** and **4**-**10** were combined with the Ldt_{Mt2}-ebselen complex, no reaction was observed, evidencing that inhibition arises from at least partially, selective reaction with Cys354 (Figure S2.12).

To further investigate the reactivity of DEKs with nucleophilic cysteine enzymes, dose-response assays of **1** and **4**-**11** were performed with SARS-CoV-2 M^{pro};[41,42] note that the

covalent reaction of SARS-CoV M^{pro} with epoxides has been reported.[43] While DEKs **1** and **9** were inhibitors of M^{pro} (pIC_{50} values of 4.6 ± 0.3 and 5.9 ± 0.2, respectively), no inhibition was observed with **4**-**8** and **10**-**11** (Table S2.3 and Figure S2.13), providing further evidence for potential of the DEKs to react selectively.

Protein-observed SPE-MS experiments with M^{pro} and the DEKs **1** and **9** (Figure S2.14) manifested a +266 Da adduct (analogous to species **2**, Figure 4.2C), with a +160 Da adduct (analogous to species **3**) becoming apparent over time. A second molecule of **1** was observed to bind to M^{pro} after 3 h (as evidenced by a mass shift of +266 Da relative to the +160 adduct), indicating reaction with a second residue, likely with one or more of the 12 cysteine residues of M^{pro}. Notably, the second adduct did not fragment by retro-aldol reaction, implying that this pathway can be promoted by the active site, likely by binding of one of the DEK-derived oxygens in the oxyanion hole of M^{pro}.[44] Incubation of M^{pro} with **9** resulted in a single adduct of +186 Da, which can be assigned to a fragmented species analogous to species **3** (Figure 4.2C).

As epoxide-bearing compounds may inhibit serine proteases, notably including proteasomes,[45,46] we tested the ability of the DEKs to inhibit the nucleophilic serine enzyme BlaC, a class A β-lactamase of *Mtb*. None of compounds **1** and **4**-**12** exhibited inhibitory potency for BlaC (Figure S2.15).

The combined results of the reaction of DEKs with GSH, cysteine, Ldt_{Mt2} and SARS-CoV-2 M^{pro} imply a conserved reaction mechanism, involving epoxide opening followed by retro-aldol reaction. Importantly, the results reveal different reactivity of the 12 M^{pro} cysteine residues with DEKs, indicating that selectivity for some proteins should be achievable; note that previous results showed that excess ebselen reacts covalently with all 12 cysteine residues.[47]

The results identify DEKs as a new class of nucleophilic cysteine reacting covalent ligands. Variations on the DEK functionality can be readily envisaged, e.g., by substituting one or both epoxides for other covalently reacting electrophiles, such as aziridines or acylating agents. Notably, some natural products contain more than one epoxide, sometimes in a contiguous arrangement,[48] though to our knowledge the DEK functional group has not been identified in natural products. Interestingly, DEKs have 5 hypothetical sites for reaction with nucleophiles (Figure 4.1C), and they hold potential for subsequent addition of a second nucleophile. This could be useful in enabling (i) formation of cross-linked enzyme-inhibitor complexes (as can occur with other mechanism-based inhibitors, e.g., certain β-lactamase inhibitors),[49] (ii) labelling of an inhibited protein for analytical or diagnostic purposes, (iii) the capture of enzyme substrates, and (iv) covalent gluing of protein–protein interactions; note that epoxides are used in commonly used polyepoxide glues.[50] The ability of DEKs to fragment after initial covalent

reaction might be useful in releasing a functional fragment, e.g., a cytotoxic agent (the cytotoxicity of benzaldehyde in tumour cells has been reported[51]).

4.3 Data availability

Protein X-ray crystallographic data has been deposited at the PDB under accession code 8BK3. Experimental details, and data supporting this manuscript are provided in the Supplementary Information (Appendix II)

4.4 References

1 Singh, J., Petter, R. C., Baillie, T. A. & Whitty, A. The resurgence of covalent drugs. *Nat. Rev. Drug Discov.* **10**, 307-317 (2011).

2 Robertson, J. G. Mechanistic Basis of Enzyme-Targeted Drugs. *Biochemistry* **44**, 5561-5571 (2005).

3 Walsh, C. T. Suicide Substrates, Mechanism-Based Enzyme Inactivators: Recent Developments. *Annu. Rev. Biochem.* **53**, 493-535 (1984).

4 Silverman, R. B. & Holladay, M. W. *The organic chemistry of drug design and drug action*. (Academic press, 2014).

5 Brown, R. P., Aplin, R. T. & Schofield, C. J. Inhibition of TEM-2 β-lactamase from Escherichia coli by clavulanic acid: observation of intermediates by electrospray ionization mass spectrometry. *Biochemistry* **35**, 12421-12432 (1996).

6 Sulton, D., Pagan-Rodriguez, D., Zhou, X., Liu, Y., Hujer, A. M., Bethel, C. R., Helfand, M. S., Thomson, J. M., Anderson, V. E., Buynak, J. D., Ng, L. M. & Bonomo, R. A. Clavulanic Acid Inactivation of SHV-1 and the Inhibitor-resistant S130G SHV-1 β-Lactamase. *J. Biol. Chem.* **280**, 35528-35536 (2005).

7 Bauer, R. A. Covalent inhibitors in drug discovery: from accidental discoveries to avoided liabilities and designed therapies. *Drug Discov. Today* **20**, 1061-1073 (2015).

8 Dixon, J. M. Exemestane: a potent irreversible aromatase inactivator and a promising advance in breast cancer treatment. *Expert Rev. Anticancer Ther.* **2**, 267-275 (2002).

9 Thomas, D. & Zalcberg, J. 5-Fluorouracil: A pharmacological paradigm in the use of cytotoxics. *Clin. Exp. Pharmacol. Physiol.* **25**, 887-895 (1998).

10 Xu, H., Faber, C., Uchiki, T., Racca, J. & Dealwis, C. Structures of eukaryotic ribonucleotide reductase I define gemcitabine diphosphate binding and subunit assembly. *Proc. Natl. Acad. Sci. U.S.A.* **103**, 4028-4033 (2006).

11 Waxman, D. J. & Strominger, J. L. Penicillin-binding proteins and the mechanism of action of beta-lactam antibiotics. *Annu. Rev. Biochem.* **52**, 825-869 (1983).

12 Liu, J., Kang, R. & Tang, D. The KRAS-G12C inhibitor: activity and resistance. *Cancer Gene Ther.* **29**, 875-878 (2022).

13 Yang, H. & Yang, J. A review of the latest research on M^{pro} targeting SARS-COV inhibitors. *RSC Med. Chem.* **12**, 1026-1036 (2021).

14 Owen, D. R., Allerton, C. M. N., Anderson, A. S., Aschenbrenner, L., Avery, M., Berritt, S., Boras, B., Cardin, R. D., Carlo, A., Coffman, K. J., Dantonio, A., Di, L., Eng, H., Ferre, R., Gajiwala, K. S., Gibson, S. A., Greasley, S. E., Hurst, B. L., Kadar, E. P., Kalgutkar, A. S., Lee, J. C., Lee, J., Liu, W., Mason, S. W., Noell, S., Novak, J. J., Obach, R. S., Ogilvie, K., Patel, N. C., Pettersson, M., Rai, D. K., Reese, M. R., Sammons, M. F., Sathish, J. G., Singh, R. S. P., Steppan, C. M., Stewart, A. E., Tuttle, J. B., Updyke, L., Verhoest, P. R., Wei, L., Yang, Q. & Zhu, Y. An oral SARS-CoV-2 M^{pro}

inhibitor clinical candidate for the treatment of COVID-19. *Science* **374**, 1586-1593 (2021).

15 Gupta, R., Lavollay, M., Mainardi, J.-L., Arthur, M., Bishai, W. R. & Lamichhane, G. The *Mycobacterium tuberculosis* protein Ldt_{Mt2} is a nonclassical transpeptidase required for virulence and resistance to amoxicillin. *Nat. Med.* **16**, 466-469 (2010).

16 de Munnik, M., Lohans, C. T., Lang, P. A., Langley, G. W., Malla, T. R., Tumber, A., Schofield, C. J. & Brem, J. Targeting the *Mycobacterium tuberculosis* transpeptidase Ldt_{Mt2} with cysteine-reactive inhibitors including ebselen. *Chem. Commun.* **55**, 10214-10217 (2019).

17 Steiner, E. M., Schneider, G. & Schnell, R. Binding and processing of β-lactam antibiotics by the transpeptidase Ldt_{Mt2} from *Mycobacterium tuberculosis*. *FEBS J.* **284**, 725-741 (2017).

18 Kumar, P., Kaushik, A., Lloyd, E. P., Li, S.-G., Mattoo, R., Ammerman, N. C., Bell, D. T., Perryman, A. L., Zandi, T. A., Ekins, S., Ginell, S. L., Townsend, C. A., Freundlich, J. S. & Lamichhane, G. Non-classical transpeptidases yield insight into new antibacterials. *Nat. Chem. Biol.* **13**, 54-61 (2017).

19 Powers, J. C., Asgian, J. L., Ekici, Ö. D. & James, K. E. Irreversible inhibitors of serine, cysteine, and threonine proteases. *Chem. Rev.* **102**, 4639-4750 (2002).

20 Boike, L., Henning, N. J. & Nomura, D. K. Advances in covalent drug discovery. *Nat. Rev. Drug Discov.*, 881–898 (2022).

21 Weerapana, E., Simon, G. M. & Cravatt, B. F. Disparate proteome reactivity profiles of carbon electrophiles. *Nat. Chem. Biol.* **4**, 405-407 (2008).

22 Greenbaum, D., Medzihradszky, K. F., Burlingame, A. & Bogyo, M. Epoxide electrophiles as activity-dependent cysteine protease profiling and discovery tools. *Chem. Biol.* **7**, 569-581 (2000).

23 Albeck, A. & Kliper, S. Inactivation of cysteine proteases by peptidyl epoxides: characterization of the alkylation sites on the enzyme and the inactivator. *Biochem. J.* **346**, 71-76 (2000).

24 Kawamura, S., Unno, Y., Asai, A., Arisawa, M. & Shuto, S. Development of a new class of proteasome inhibitors with an epoxyketone warhead: Rational hybridization of non-peptidic belactosin derivatives and peptide epoxyketones. *Bioorg. Med. Chem.* **22**, 3091-3095 (2014).

25 Dijkmans, A. C., Zacarías, N. V. O., Burggraaf, J., Mouton, J. W., Wilms, E., Van Nieuwkoop, C., Touw, D. J., Stevens, J. & Kamerling, I. M. C. Fosfomycin: Pharmacological, Clinical and Future Perspectives. *Antibiotics* **6**, 24 (2017).

26 Silver, L. L. Fosfomycin: Mechanism and Resistance. *Cold Spring Harb. Perspect. Med.* **7**, a025262 (2017).

27 de Munnik, M., Lang, P. A., De Dios Antos, F., Cacho, M., Bates, R. H., Brem, J., Rodríguez-Miquel, B. & Schofield, C. J. High-Throughput Screen with the L,D-transpeptidase Ldt_{Mt2} of *Mycobacterium tuberculosis* Reveals Novel Classes of Covalently Reacting Inhibitors *Chem. Sci.* **14**, 7262-7278 (2023).

28 Krantz, A. Peptidyl (Acyloxy) methanes as quiescent affinity labels for cysteine proteinases. *Methods Enzymol.* **244**, 656-671 (1994).

29 Erdemli, S. B., Gupta, R., Bishai, W. R., Lamichhane, G., Amzel, L. M. & Bianchet, M. A. Targeting the cell wall of *Mycobacterium tuberculosis*: structure and mechanism of L,D-transpeptidase 2. *Structure* **20**, 2103-2115 (2012).

30 Arnold, A., Markert, M. & Mahrwald, R. Amine-Catalyzed Aldol Condensation in the Presence of Lithium Perchlorate. *Synthesis*, 1099-1102 (2006).

31 Weber, W. M., Hunsaker, L. A., Roybal, C. N., Bobrovnikova-Marjon, E. V., Abcouwer, S. F., Royer, R. E., Deck, L. M. & Vander Jagt, D. L. Activation of NFκB is inhibited by curcumin and related enones. *Bioorg. Med. Chem.* **14**, 2450-2461 (2006).

32 Yadav, V. K. & Kapoor, K. K. KF adsorbed on alumina effectively promotes the epoxidation of electron deficient alkenes by anhydrous t-BuOOH. *Tetrahedron* **52**, 3659-3668 (1996).

33 Miyahisa, I., Sameshima, T. & Hixon, M. S. Rapid Determination of the Specificity Constant of Irreversible Inhibitors (k_{inact}/K_I) by Means of an Endpoint Competition Assay. *Angew Chem. Int. Ed. Engl.* **54**, 14099-14102 (2015).

34 Sameshima, T., Miyahisa, I., Yamasaki, S., Gotou, M., Kobayashi, T. & Sakamoto, J. High-Throughput Quantitative Intrinsic Thiol Reactivity Evaluation Using a Fluorescence-Based Competitive Endpoint Assay. *Adv. Sci. Drug Disc.* **22**, 1168-1174 (2017).

35 Petri, L., Ábrányi-Balogh, P., Varga, P. R., Imre, T. & Keserű, G. M. Comparative reactivity analysis of small-molecule thiol surrogates. *Bioorg. Med. Chem.* **28**, 115357 (2020).

36 Holmes, T. J. & Lawton, R. G. Cysteine modification and cleavage of proteins with 2-methyl-N1-benzenesulfonyl-N4-bromoacetylquinonediimide. *J. Am. Chem. Soc.* **99**, 1984-1986 (1977).

37 Bashore, C., Jaishankar, P., Skelton, N. J., Fuhrmann, J., Hearn, B. R., Liu, P. S., Renslo, A. R. & Dueber, E. C. Cyanopyrrolidine Inhibitors of Ubiquitin Specific Protease 7 Mediate Desulfhydration of the Active-Site Cysteine. *ACS Chem. Biol.* **15**, 1392-1400 (2020).

38 Lang, P. A., Raj, R., Tumber, A., Lohans, C. T., Rabe, P., Robinson, C. V., Brem, J. & Schofield, C. J. Studies on enmetazobactam clarify mechanisms of widely used β-lactamase inhibitors. *Proc. Natl. Acad. Sci. U.S.A.* **119**, e2117310119 (2022).

39 Groll, M., Kim, K. B., Kairies, N., Huber, R. & Crews, C. M. Crystal Structure of Epoxomicin:20S Proteasome Reveals a Molecular Basis for Selectivity of α‘,β‘-Epoxyketone Proteasome Inhibitors. *Journal of the American Chemical Society* **122**, 1237-1238 (2000).

40 Grant, S. K., Moore, M. L., Fakhoury, S. A., Tomaszek Jr, T. A. & Meek, T. D. Inactivation of HIV-1 protease by a tripeptidyl epoxide. *Bioorg. Med. Chem. Lett.* **2**, 1441-1445 (1992).

41 Brewitz, L., Dumjahn, L., Zhao, Y., Owen, C. D., Laidlaw, S. M., Malla, T. R., Nguyen, D., Lukacik, P., Salah, E., Crawshaw, A. D., Warren, A. J., Trincao, J., Strain-Damerell, C., Carroll, M. W., Walsh, M. A. & Schofield, C. J. Alkyne Derivatives of SARS-CoV-2 Main Protease Inhibitors Including Nirmatrelvir Inhibit by Reacting Covalently with the Nucleophilic Cysteine. *J. Med. Chem.* **66**, 2663-2680 (2023).

42 Malla, T. R., Brewitz, L., Muntean, D.-G., Aslam, H., Owen, C. D., Salah, E., Tumber, A., Lukacik, P., Strain-Damerell, C., Mikolajek, H., Walsh, M. A. & Schofield, C. J. Penicillin Derivatives Inhibit the SARS-CoV-2 Main Protease by Reaction with Its Nucleophilic Cysteine. *J. Med. Chem.* **65**, 7682-7696 (2022).

43 Lee, T.-W., Cherney, M. M., Huitema, C., Liu, J., James, K. E., Powers, J. C., Eltis, L. D. & James, M. N. G. Crystal Structures of the Main Peptidase from the SARS Coronavirus Inhibited by a Substrate-like Aza-peptide Epoxide. *J. Mol. Biol.* **353**, 1137-1151 (2005).

44 Lee, J., Worrall, L. J., Vuckovic, M., Rosell, F. I., Gentile, F., Ton, A.-T., Caveney, N. A., Ban, F., Cherkasov, A., Paetzel, M. & Strynadka, N. C. J. Crystallographic structure of wild-type SARS-CoV-2 main protease acyl-enzyme intermediate with physiological C-terminal autoprocessing site. *Nat. Commun.* **11** (2020).

45 Meng, L., Mohan, R., Kwok, B. H. B., Elofsson, M., Sin, N. & Crews, C. M. Epoxomicin, a potent and selective proteasome inhibitor, exhibits in vivo antiinflammatory activity. *Proc. Natl. Acad. Sci. U.S.A.* **96**, 10403-10408 (1999).

46 Zhou, H.-J., Aujay, M. A., Bennett, M. K., Dajee, M., Demo, S. D., Fang, Y., Ho, M. N., Jiang, J., Kirk, C. J., Laidig, G. J., Lewis, E. R., Lu, Y., Muchamuel, T., Parlati, F., Ring, E., Shenk, K. D., Shields, J., Shwonek, P. J., Stanton, T., Sun, C. M., Sylvain, C., Woo, T. M. & Yang, J. Design and Synthesis of an Orally Bioavailable and Selective Peptide Epoxyketone Proteasome Inhibitor (PR-047). *J. Med. Chem.* **52**, 3028-3038 (2009).

47 Thun-Hohenstein, S. T., Suits, T. F., Malla, T. R., Tumber, A., Brewitz, L., Choudhry, H., Salah, E. & Schofield, C. J. Structure-Activity Studies Reveal Scope for Optimisation

of Ebselen-Type Inhibition of SARS-CoV-2 Main Protease. *ChemMedChem* **17**, e202100582 (2022).

48 Lu, Q., Harmalkar, D. S., Choi, Y. & Lee, K. An overview of saturated cyclic ethers: Biological profiles and synthetic strategies. *Molecules* **24**, 3778 (2019).

49 Wyrembak, P. N., Babaoglu, K., Pelto, R. B., Shoichet, B. K. & Pratt, R. F. O-Aryloxycarbonyl Hydroxamates: New β-Lactamase Inhibitors That Cross-Link the Active Site. *J. Am. Chem. Soc.* **129**, 9548-9549 (2007).

50 Jin, F.-L., Li, X. & Park, S.-J. Synthesis and application of epoxy resins: A review. *J. Ind. Eng. Chem.* **29**, 1-11 (2015).

51 Ariyoshi-Kishino, K., Hashimoto, K., Amano, O., Saitoh, J., Kochi, M. & Sakagami, H. Tumor-specific cytotoxicity and type of cell death induced by benzaldehyde. *Anticancer Res.* **30**, 5069-5076 (2010).

4.5 Statement of authorship

Title of Paper	αβ,α′β′-Diepoxyketones are mechanism-based inhibitors of nucleophilic cysteine enzymes
Publication Status	■Published □Submitted for Publication □Accepted for Publication □Unpublished and unsubmitted work written in a manuscript style
Publication Details	de Munnik M, Lithgow J, Brewitz L, Christensen KE, Bates RH, Rodriguez-Miquel B, Schofield CJ. (2023). αβ,α′β′-Diepoxyketones are mechanism-based inhibitors of nucleophilic cysteine enzymes. Chem. Commun., 59(86), 12859-12862.

Student Confirmation

Student Name:	Mariska de Munnik		
Contribution to the Paper	The organic synthesis of DEKs was performed by Jasper Lithgow, supervised by Dr. Lennart Brewitz. The inhibition studies of the main protease from SARS-CoV-2 (M^{pro}) were performed by Dr. Lennart Brewitz. Small molecule X-ray diffraction was performed by Dr. Kirsten E. Christensen. All remaining experimental work described here, and preparation of the manuscript were carried out by me.		
Signature		Date	23/01/2024

Supervisor Confirmation

By signing the Statement of Authorship, you are certifying that the candidate made a substantial contribution to the publication, and that the description described above is accurate.

Prof Chris Schofield		
I'm happy to start that the candidate made the major and a very substantial contribution to the publication, and that the description described above is accurate.		
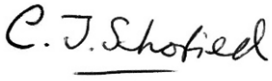	Date	23/01/2024

Chapter 5

Biochemical and crystallographic studies of Ldt_{Mt2} from *Mycobacterium tuberculosis* with its natural monomer substrate

Manuscript III

Submitted manuscript.

Contents

5.1 Abstract 118

5.1 Introduction 119

5.3 Results 122

5.3.1 Isolation of the tetrapeptide monomer 122
5.3.2 Studies of Ldt_{Mt2} activity with peptidoglycan monomers 123
5.3.3 Kinetics of the Ldt_{Mt2} transpeptidase reaction with peptidoglycan monomers 124
5.3.4 X-ray crystallographic studies of the Ldt_{Mt2}-substrate complex 126

5.4 Discussion 129

5.5 Conclusion 132

5.6 Methods 132

5.6.1 Materials 132
5.6.2 Protein production and purification 133
5.6.3 Peptidoglycan fragment isolation 133
5.6.4 Synthesis of 9 and 11 134
5.6.5 Mass spectrometry assays 135
5.6.6 Transpeptidase assays 135
5.6.7 Crystallography 136

5.7 Data availability 136

5.8 References 136

5.9 Statement of authorship 142

5.1 Abstract

The essential L,D-transpeptidase of *Mycobacterium tuberculosis* (Ldt_{Mt2}) catalyses the formation of 3→3 cross-links in cell wall peptidoglycan and is a target for development of antituberculosis therapeutics. Efforts to inhibit Ldt_{Mt2} have been hampered by lack of knowledge of how it binds its substrate. To address this gap, we optimised the isolation of natural disaccharide tetrapeptide monomers from the *Corynebacterium jeikeium* bacterial cell wall through overproduction of peptidoglycan sacculus. The tetrapeptides were used in biochemical and biophysical studies on Ldt_{Mt2}. We determined a crystal structure of wild-type Ldt_{Mt2} reacted with its natural substrate (the tetrapeptide monomer of the peptidoglycan layer). This structure shows formation of a thioester linking the catalytic cysteine and the donor substrate, reflecting an intermediate in the transpeptidase reaction and informs on the mode of entrance of the donor substrate into the Ldt_{Mt2} active site. The results will be useful in design of Ldt_{Mt2} inhibitors, including those based on substrate binding interactions, a strategy successfully employed for other nucleophilic cysteine enzymes.

Key words: *Mycobacterium tuberculosis,* L,D-transpeptidase, Ldt_{Mt2}, bacterial cell wall biosynthesis, β-lactam antibiotic, peptidoglycan, antimicrobial resistance (AMR), nucleophilic cysteine enzyme, carbapenem.

5.1 Introduction

Tuberculosis (TB) imposes a major impact on global health and causes an estimated 1.6 million deaths per year.[1] There is a limited set of drugs for TB treatment; however, the prolonged treatments regimens required for efficacy and increasing resistance mean there is a clear need for new therapeutics targeting *Mycobacterium tuberculosis* (*Mtb*), the causative agent of TB.[2,3]

Disruption of cell wall biosynthesis is arguably the most effective approaches to treatment of bacterial infections, with the cell wall biosynthesis targeting β-lactams being amongst the most successful of antibacterial drug classes.[4] β-Lactams are efficient and safe inhibitors of the penicillin binding proteins (PBPs), a class of nucleophilic serine enzymes that are involved several of the final steps of peptidoglycan synthesis; PBPs include D,D-transpeptidases (some with bifunctional glycosyltransferase activity), D,D-carboxypeptidases, and endopeptidases (Figure 5.1A).[5] To date the application of β-lactams for the treatment of TB has been limited, reflecting challenges including β-lactamase mediated resistance.[6] A further issue with β-lactam based TB treatment is that in addition to the nucleophilic serine PBPs, nucleophilic cysteine enzymes also play a key role in *Mtb* cell wall biosynthesis.[7]

Whereas the PBP D,D-transpeptidases catalyse the formation of 4→3 cross-links between peptidoglycan pentapeptide chains, the functionally related L,D-transpeptidases (Ldts) catalyse the formation of 3→3 cross-links between tetrapeptide chains (Figure 5.1).[8,9] Despite being well conserved between bacterial species,[10] the low abundancy of 3→3 cross-links is proposed to render Ldts redundant in most bacteria, at least in controlled laboratory environments.[11] However, *Mtb* displays up to 80% of 3→3 cross-links during the stationary phase.[7] Hence, the Ldts have been identified as an attractive target for the development of anti-TB treatment.[12] In particular Ldt_{Mt2}, one of five Ldts of *Mtb*, is recognised as being important for virulence.[13-15]

Whereas the D,D-carboxypeptidases and D,D-transpeptidases are nucleophilic serine enzymes (Figure S3.1),[16,17] the Ldts employ a catalytic triad involving the sidechains of a nucleophilic cysteine and a histidine residue, and the backbone carbonyl of a third residue in a characteristic $Hxx_{14–17}$(S/T)HGCZN motif, in which Z represents a hydrophobic residue.[18] Ldts, which do not have structural homology with the PBPs and likely originate from a different evolutionary precursor,[18] share a common YkuD fold (named after the first identified member of this class), distinguished by a β-sandwich with two mixed β-sheets and one helix, and a set of four loops (Figure S3.1).[18-20] One of these loops borders the Ldt_{Mt2} active site,[19] creating two entrances towards the nucleophilic cysteine; the inner cavity and the outer cavity (Figure S3.1).[19]

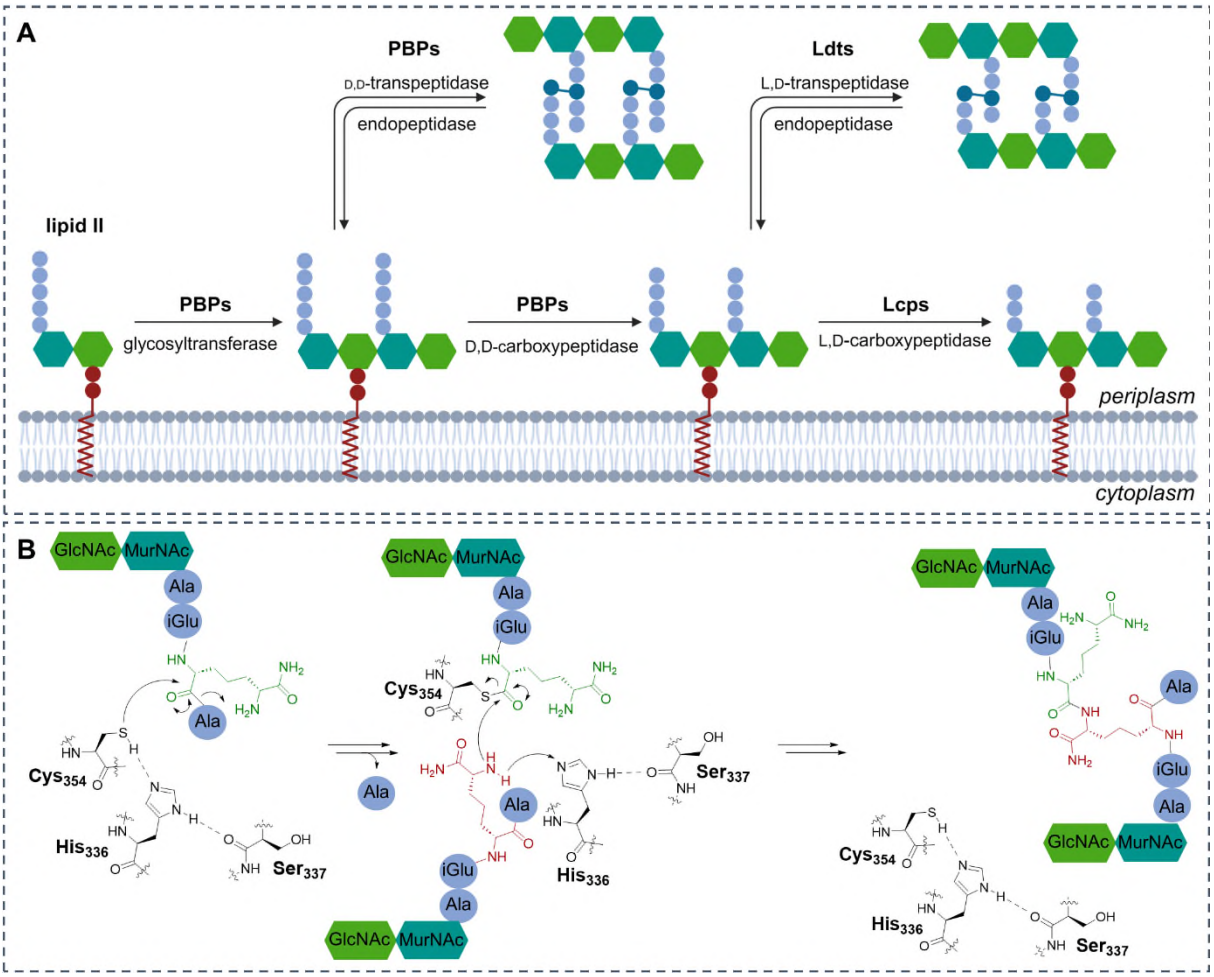

Figure 5.1. Roles of glycosyltransferases, transpeptidases and carboxypeptidases in the final stages of bacterial peptidoglycan synthesis. A. Penicillin binding proteins (PBPs) with glycosyltransferase activity link lipid II to peptidoglycan, PBPs with carboxypeptidase activity cleave peptide strands from pentapeptides to give tetrapeptides and PBPs with transpeptidase activity form 4→3 cross-links between pentapeptide strands. The L,D-transpeptidases (Ldts) form 3→3 cross-links between tetrapeptide strands. The endopeptidases reverse the transpeptidase activity, cleaving the peptide bonds between cross-links. Lcps cleave peptide strands from tetrapeptide to tripeptides. The figure was created using BioRender.com. **B.** Mechanism for the cross-linking reaction between the disaccharide tetrapeptide monomers catalysed by Ldt_{Mt2}.

The established substrate for Ldt_{Mt2} is the disaccharide tetrapeptide monomer **1** (GlcNAc-MurNAc-L-Ala-D-$iGlu_{NH2}$-*m*-DAP_{NH2}-D-Ala; Figure 5.2A).[7,13] The formation of 3→3 crosslinks is proposed to occur through covalent reaction of the amide bond between the 3rd and 4th residue with the nucleophilic cysteine of Ldt_{Mt2}, i.e., Cys354, to give an acyl enzyme complex.[21] The 3rd residue of a second strand of the tetrapeptide chain then reacts with the thioester intermediate to give the 3→3 crosslinked product (Figure 5.1B).[22]

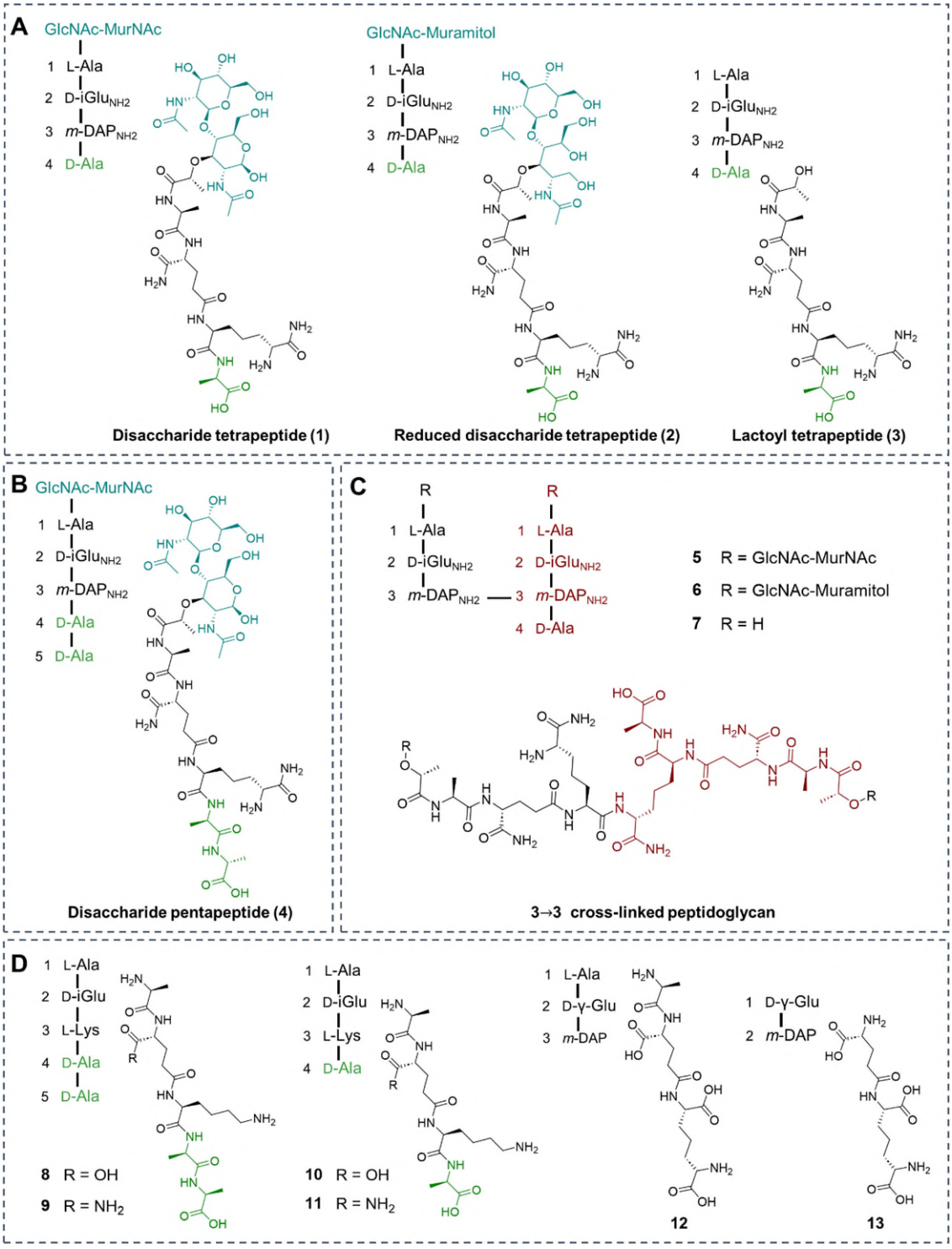

Figure 5.2. Structures of peptidoglycan fragments of *Mycobacterium tuberculosis*. A. Structures of the tetrapeptide substrates of Ldt_{Mt2} **1**-**3**, obtained through isolation of the cell wall of *C. jeikeium*. **B.** Structure of the pentapeptide monomer of peptidoglycan from *Mtb* and *C. jeikeium* **4**, obtained through isolation of the cell wall of *C. jeikeium*. **C.** The structures of the products of transpeptidase activity of Ldt_{Mt2} **5**-**7**, obtained through cross-linking of **1**, **2**, and **3**, respectively. **D.** Peptidoglycan fragments **8**-**13** that do not act as substrates for Ldt_{Mt2}, obtained through solid-phase peptide synthesis (**9** and **11**) or commercial sources (**8**, **10**, **12** and **13**). GlcNAc stands for N-acetylglucosamine, MurNAc stands for N-acetylmuramic acid.

Though traditionally viewed as PBP inhibitors, selected β-lactams also inhibit the Ldts. In particular, carbapenems have been shown to inhibit Ldts,[23-25] and recent work has also shown the potential of cephalosporins to inhibit Ldt_{Mt2}.[26] Additionally, several other classes of electrophilic compounds, e.g., ebselen, nitriles and acrylamides, have been identified to be able to inhibit Ldt_{Mt2} (Chapter 3, Chapter 4).[26,27] Structure based design of Ldt inhibitors has, however, been limited by a lack of detailed knowledge of enzyme-substrate interactions.

Studies of Ldt_{Mt2} in complex with its substrate or acyl-enzyme intermediate have likely been hindered by restricted availability of **1**. Reported studies of the Ldt_{Mt2}-substrate complex have thus far relied on unnatural substrate analogues, e.g., a crystal structure of the peptidoglycan fragment D-γ-Glu-*m*-DAP bound to the Ldt_{Mt2} active site.[22] Efforts to chemically synthesise substrate **3** (lactoyl-L-Ala-D-$iGlu_{NH2}$-*m*-DAP_{NH2}-D-Ala) have yielded low amounts of material.[28] The peptidoglycan substrates **1**, **2** (GlcNAc-Muramitol-L-Ala-D-$iGlu_{NH2}$-*m*-DAP_{NH2}-D-Ala) and **3** can, however, be obtained through isolation of the cell well of *Corynebacterium jeikeium*, which shares an identical peptidoglycan monomer structure with *Mtb*.[7,13,29] Using a variation of this method, we obtained an increased yield of **1**-**3** from the cell wall of *C. jeikeium.* Kinetic and binding studies suggest the isolated Ldt_{Mt2} enzyme has a low affinity for the isolated tetrapeptide peptidoglycan monomer. X-ray crystallographic studies of Ldt_{Mt2} and substrate **3** yielded a structure of the proposed thioester intermediate of the transpeptidase reaction, which suggests the donor substrate enters through the inner cavity, but subsequently interacts with both the inner and outer cavities.

5.3 Results

5.3.1 Isolation of the tetrapeptide monomer

Initially, we isolated the reduced disaccharide tetrapeptide (GlcNAc-Muramitol-L-Ala-D-$iGlu_{NH2}$-*m*-DAP_{NH2}-D-Ala) monomer **2** using reported methods.[29,30] *C. jeikeium* cells were lysed via high-pressure homogenesis, boiled in 8% SDS, then treated with trypsin, pronase, mutanolysin, and lysozyme to yield soluble peptidoglycan monomers (Figure S3.2). MurNAc moieties in peptidoglycan monomers were then reduced to muramitol using sodium borohydride, to improve resolution during HPLC separation (Figure S3.3A).[30] This method was scaled to a dried cell mass of 94.6 g *C. jeikeium* from 21.6 L of culture, which yielded ~4.5 mg of highly purified **2** (<95%, Figures, S3.4A, S3.7). Aiming to improve the yield, we attempted bypassing the reduction of MurNAc in **1**. Decreased separation of peaks was observed by HPLC (Figure S3.3B); however, highly purified (<95%) disaccharide-tetrapeptide **1** (Figure S3.4B) was obtained (~3.6 mg from 61.3 g dried cell mass).

As described,[29] we observed that the distribution between tetrapeptide monomer **1** and pentapeptide monomer **4** favour **1** in crude samples. Addition of ampicillin in apparently subinhibitory concentrations of ampicillin (2 μg/mL)[29] increased the abundance of **4** (Figure S3.3C), likely due to ampicillin mediated inhibition of D,D-carboxypeptidase and D,D-transpeptidase activities, leading to accumulation of their substrate (**4**).[5,17] Subsequent incubation of isolated **4** with the purified recombinant *Escherichia coli* D,D-carboxypeptidase DacA gave **1** (Figure S3.5). This procedure significantly (~10 fold) improved the overall yield of **1** (~20.5 mg from 55.9 g dried cell mass). The disaccharide moiety of **1** was cleaved by reaction with ammonium hydroxide,[29,30] giving lactoyl-tetrapeptide **3** (Figure S3.6). The identities and purities of **1**, **2** and **3** were confirmed by liquid chromatography mass spectrometry (LC-MS; Figure S3.4) and ^{1}H and ^{13}C NMR characterisation (Figure S3.7-8).

5.3.2 Studies of Ldt_{Mt2} activity with peptidoglycan monomers

We assessed Ldt_{Mt2} catalysis via LC-MS analysis of reaction mixtures of recombinant Ldt_{Mt2} with the three variants of L-Ala-D-iGlu$_{NH2}$-*m*-DAP$_{NH2}$-D-Ala: the peptide containing GlcNAc-MurNAc (**1**), the peptide containing GlcNAc-Muramitol (**2**), and the lactoyl peptide (**3**). Incubation of Ldt_{Mt2} (5 μM) with **1**, **2**, or **3** (100 μM) led to the apparent formation of products **5**, **6**, and **7**, as evidenced by the emergence of a species with masses of 1786 Da, 1790 Da, and 974 Da, respectively (Figure S3.9), as previously reported for **2** and **3**.[13,28]

Next, we assessed the structural requirements of the tetrapeptide residues that enable reaction with Ldt_{Mt2}. A previous report identified the importance of sidechain amidation of both the D-iGlu and *m*-DAP residues for turnover.[28] To further investigate the structural requirements for Ldt_{Mt2} substrates, we incubated Ldt_{Mt2} with tetrapeptide **10** (L-Ala-D-iGlu-L-Lys-D-Ala), a peptidoglycan monomer often observed in gram-positive bacteria[11]. We observed no evidence for turnover of **10**. The tetrapeptide **11** (L-Ala-D-iGlu$_{NH2}$-L-Lys-D-Ala), which contains the amidated D-iGlu residue, but wherein *m*-DAP$_{NH2}$ is replaced with L-Lys, was also not a substrate (over 24 h), evidencing the importance of the *m*-DAP$_{NH2}$ residue in peptidoglycan fragments for turnover with isolated Ldt_{Mt2}.

It is reported that the reduced pentapeptide monomer of *Mtb* (GlcNAc-muramitol-L-Ala-D-iGlu$_{NH2}$-*m*-DAP$_{NH2}$-D-Ala-D-Ala) is not a substrate for Ldt_{Mt2}.[13] Consistent with this, incubation of Ldt_{Mt2} with the pentapeptide monomer of *Mtb* **4** (GlcNAc-MurNAc-L-Ala-D-iGlu$_{NH2}$-*m*-DAP$_{NH2}$-D-Ala-D-Ala), or pentapeptide **8** (L-Ala-D-iGlu-L-Lys-D-Ala-D-Ala), did not manifest evidence for reaction, further evidencing that pentapeptide monomers are not Ldt_{Mt2} substrates.

We were interested in assessing the transpeptidase activity of the active site cysteine to serine mutant of Ldt_{Mt2} (Ldt_{Mt2}^{C354S}), in part because previous reports have shown that in contrast to

wildtype Ldt_{Mt2},[13,21] Ldt_{Mt2}^{C354S} is unable to form a covalent complex with several penem and carbapenem derivatives.[23,31] When Ldt_{Mt2}^{C354S} was incubated with **1**, **2**, **3**, or **4**, no product formation could be observed, suggesting the active site cysteine is essential for transpeptidase activity, and cannot be replaced by a potentially nucleophilic serine residue.

Differential scanning fluorometric thermal shift assays[32] (Figure S3.10, Table S3.1) with a 100-fold excess (500 μM) of peptidoglycan fragments showed only pentapeptide **4** induced a modest stabilising effect, as evidenced by a shift in the melting temperature (T_m) of ≥2 °C. With a 200-fold excess (1 mM), stabilisation was observed with tetrapeptides **1**, **3** and **9**, and pentapeptides **4** and **8**, all manifesting a T_m shift of 2–3 °C; no significant shift in melting temperature was observed for **10** and **11**.

Protein-observed solid-phase extraction mass spectrometric (SPE-MS) studies were performed with Ldt_{Mt2} (1 μM) in the presence of substrates **1** and **3** (100 μM). While transpeptidase activity was confirmed under the tested conditions with **1** and **3**, as evidenced by observation of protein unbound species with a masses of 1786 Da, and 974 Da, (correlating to **5** and **7**, respectively), no covalent adducts of Ldt_{Mt2} were observed, suggesting that the lifetime of the covalent thioester intermediate (predicted mass increase of 849 Da in the case of **1** and 443 Da in the case of **3**, relative to unmodified Ldt_{Mt2}) is short-lived in solution (Figure S3.11).

5.3.3 Kinetics of the Ldt_{Mt2} transpeptidase reaction with peptidoglycan monomers

Thus far, Ldt_{Mt2} transpeptidase activity has been measured by LC-MS analysis,[13] and Ldt_{Mt2} inhibition assays have relied on use of unnatural chromogenic or fluorogenic probe substrates,[23,33,34] as employed in an assay suitable for high-throughput screening (Chapter 3).[26] These assays are, however, likely poor mimics of the natural reaction. We therefore developed an efficient, quantitative, and biologically relevant method of determining Ldt_{Mt2} activity and inhibition based on turnover of its natural substrate. A microtiter plate-based assay that determines PBP activity has been reported, based on the detection of D-Ala, which is released upon D,D-transpeptidase and D,D-carboxypeptidase activity (Figure 5.3A).[35-37] D-Ala is converted to pyruvate, ammonia and hydrogen peroxide by D-amino acid oxidase (DAAO). Hydrogen peroxide is then used by horseradish peroxidase (HRP) to oxidise Amplex Red (AR) to form the fluorescent resorufin. We considered that the transpeptidase assay could be extended to monitor Ldt_{Mt2} catalysis.

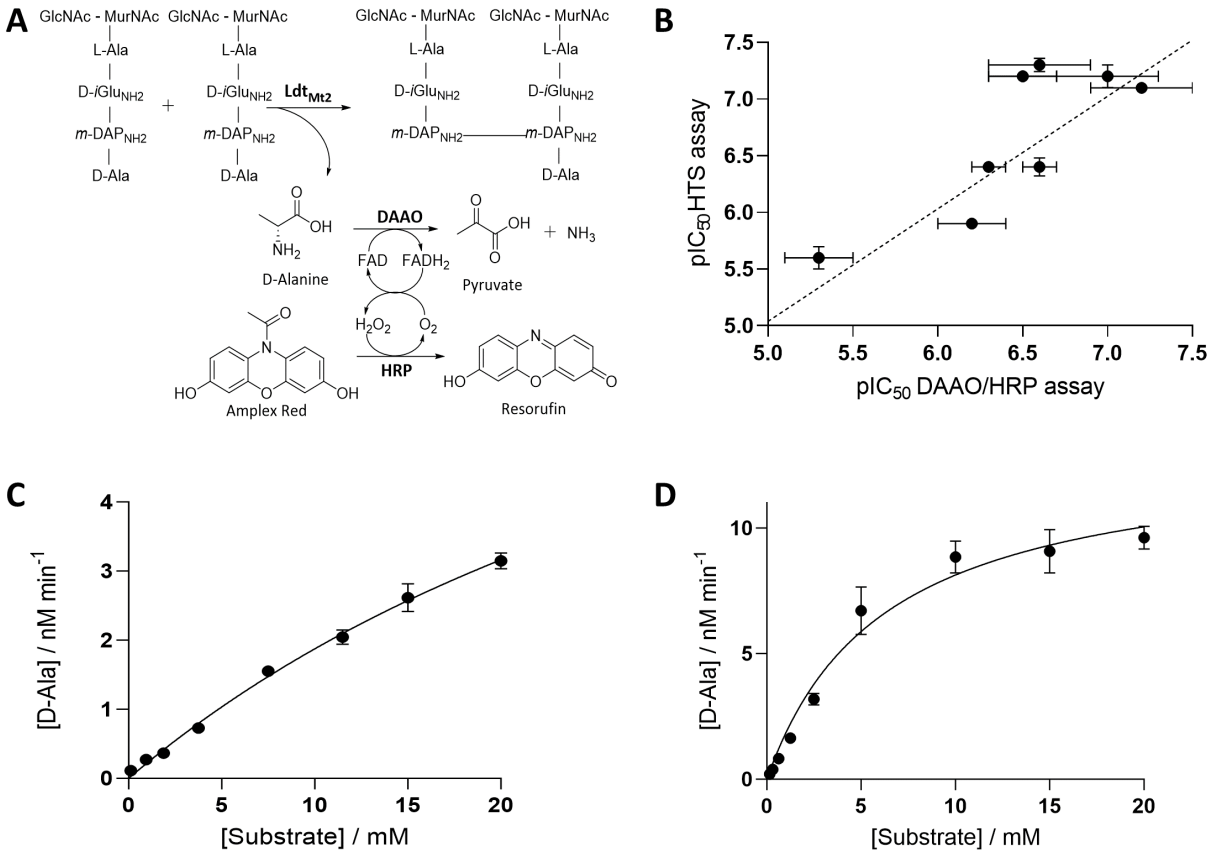

Figure 5.3. A fluorescence-based assay for Ldt_{Mt2} transpeptidase activity. A. Principle of the Ldt_{Mt2} transpeptidase assay, employing D-amino acid oxidase (DAAO) and horseradish peroxidase (HRP) to report on the release of D-Ala. **B.** Correlation between pIC_{50} values obtained with the transpeptidase activity assay and fluorogenic thiol probe assay. **C.** Michaelis-Menten kinetics of Ldt_{Mt2} in reaction with substrate **1**. **D.** Michaelis-Menten kinetics of Ldt_{Mt2} in reaction with substrate **3**.

Optimisation initially involved determination of the optimal DAAO and HRP concentrations, aiming to minimise delay in conversion of D-Ala. When the assay contained an excess of DAAO (2 U/mL) and HRP (2 U/mL), conversion of D-Ala is apparently near instantaneous (Figure S3.12A-B). The assay performed better in the presence of sodium phosphate compared to tris or HEPES buffers (Figure S3.12C), and in the presence of 100 mM NaCl (Figure S3.12D). A higher pH manifested increased Ldt_{Mt2} activity (tested pH range 7.0-8.5; Figure S3.12E) and activity was higher at 37 °C than room temperature (Figure S3.12F). Assays were therefore performed at 37 °C in 50 mM sodium phosphate pH 8.0, 100 mM NaCl and 0.01% (*v*/*v*) Triton X-100, with an Ldt_{Mt2} concentration of 500 nM and substrate (**3**) concentration of 35 µM (Figure S3.12G). Under these conditions, a Z′ value of 0.88 and a signal to background value of 5.0 was obtained. The hydrogen peroxide produced during the assay has the potential to oxidise the catalytic cysteine of Ldt_{Mt2}, however, dose-response studies,[34] manifested no evidence for interference with assay relevant concentrations (Figure S3.12H).

The assay was applied to investigate the inhibition of a variety of reported Ldt_{Mt2} inhibitors (Figure S3.13, Table S3.2).[26,27,33] The results showed good correlation with the reported Ldt_{Mt2} ligand binding assay utilising a fluorogenic thiol reactive probe (Figure 5.3B).[34] The DAAO/HRP method presents an improved assay for inhibitor screening, as the assay more closely resembles the biological process. The possibility for interference through inhibition of DAAO and HRP necessitates use of appropriate controls; indeed, the nonspecific inhibitors ebselen (**24**) and ebsulfur analogue **23** were found to cause interference (Figure S3.14, Table S3.2).

With fixed concentrations of **1** and **3** (35 µM), a substantial difference in reaction rate was observed, with 120.0 ± 1.7 RFU min^{-1} and 224.2 ± 2.6 RFU min^{-1} for **1** and **3**, respectively (Figure S3.15), suggesting that interaction of the GlcNAc-MurNAc moiety of the substrate is not essential for turnover and, at least with isolated components, has the potential to hinder the reaction rate. Increasing concentrations of **1** did not saturate the reaction (up to 20 mM; Figure 5.3C). With **3**, a K_m of 6.2 mM was obtained, indicating low affinity; k_{cat} was 2.6 x 10^2 min^{-1}, providing a k_{cat}/K_m of 4.2 min^{-1} M^{-1} (Figure 5.3D, Table S3.3). Note, that the effective incorporation of fluorescent amino acids and peptidoglycan fragments into the cell wall of *Mtb* suggests more efficient turnover in a cellular context.[38] The difference between isolated activity and cellular activity may suggest a need for complex formation, missing cofactors, or the need for binding of full-length peptidoglycan for optimal Ldt_{Mt2} activity.

The non-substrate peptidoglycan fragments **4**, **8**, **10**, **12**, and **13** showed modest Ldt_{Mt2} inhibition (Figure S3.16). Pentapeptides **8** and **10** and tripeptide **12** were the most potent inhibitors (pIC_{50} 4.8), while dipeptide **13** manifested the lowest potency (pIC_{50} 4.0). The ability of structurally related non-substrate peptides to displace the substrate from the active site shows potential for the development of substrate-like inhibitors, although optimisation to improve affinity will be required.

5.3.4 X-ray crystallographic studies of the Ldt_{Mt2}-substrate complex

To investigate the structural interactions of Ldt_{Mt2} with its substrate, we carried out X-ray crystallographic studies with the peptidoglycan fragments, aiming to obtain a structure of the enzyme-substrate complex; we obtained structures of Ldt_{Mt2} in complex with **1** and **3**.

While in the absence of **3**, Ldt_{Mt2} crystallised in the reported $P12_11$ space group,[26,27] Ldt_{Mt2} crystals grown in the presence of **3** crystallised in the $P2_12_12$ space group with a single protein chain in the asymmetric unit (1.98 Å, Figure 5.4; PDB 8PXZ), using precipitation solutions with a pH range between 7.0-7.5, yielding structures of Ldt_{Mt2} with a molecule of **3** bound to the Ldt_{Mt2} immunoglobulin-like domain 2 (IgD2). Notably, however, when Ldt_{Mt2} and **3** were co-crystallised using precipitation solution at pH 7.0, we observed additional electron density

extending from the sidechain of the nucleophilic residue Cys354. The results are in agreement with formation of the dipeptide (D-iGlu$_{NH2}$-*m*-DAP$_{NH2}$), covalently linked to Ldt$_{Mt2}$ via a thioester with Cys354, apparently reflecting a key intermediate of the transpeptidase reaction with the donor peptide (Figure 5.4A). The thioester has the (*Z*)-stereochemistry, consistent with prior studies on nucleophilic serine and cysteine enzymes, including the SARS-CoV-2 main protease (M^{pro}; Figure S3.17A)[39,40] and porcine pancreatic elastase.[41]

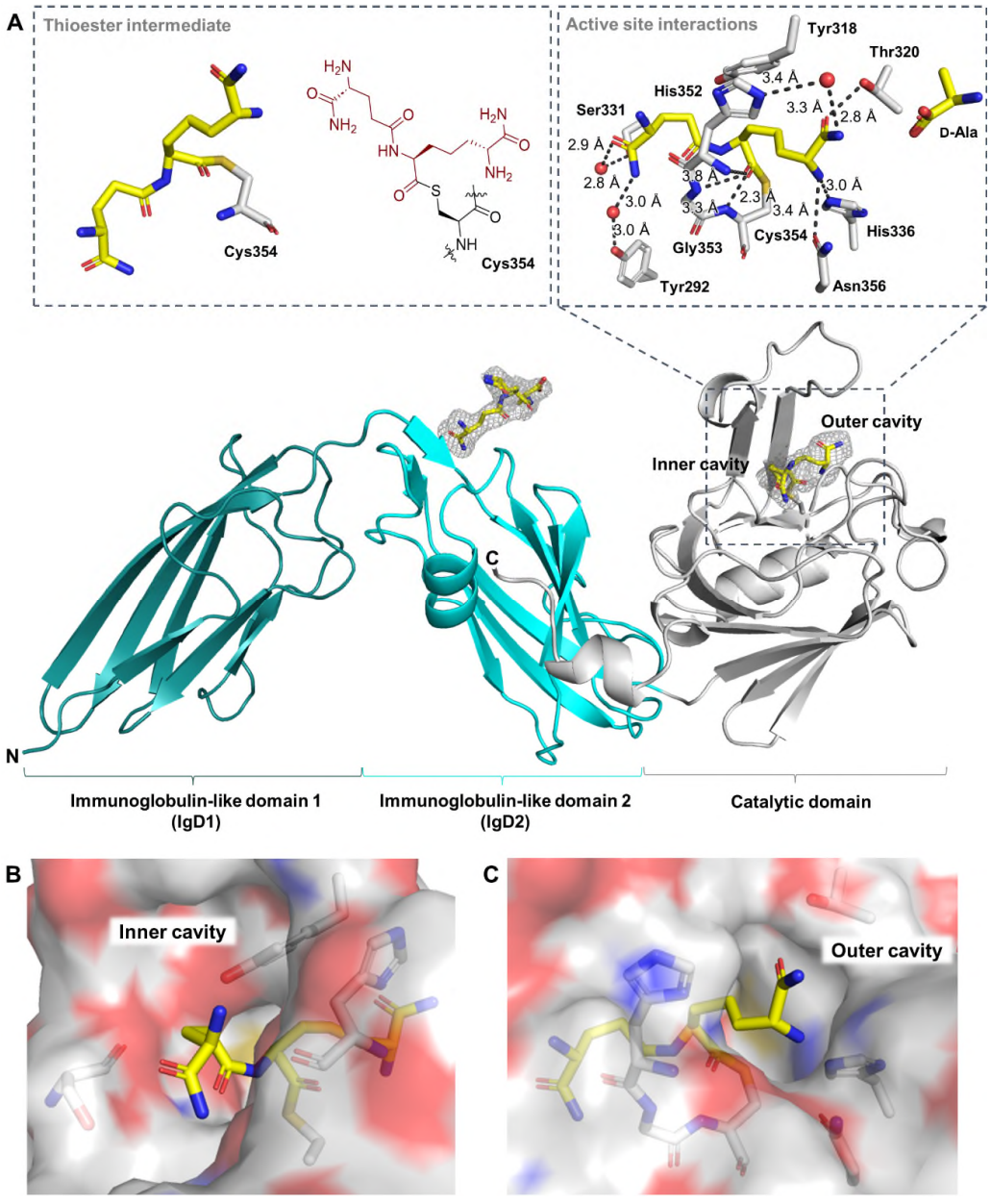

Figure 5.4. Crystallographic studies of Ldt$_{Mt2}$ with peptidoglycan fragment 3 show covalent thioester formation. A. A structure of Ldt$_{Mt2}$ in complex with **3** (PDB: 8PXZ) shows the covalent thioester intermediate structure, and a second molecule of **3** bound to the IgD2 of Ldt$_{Mt2}$. The $mF_0 - DF_c$ polder OMIT map contoured at 3.0 σ, carved around **3** is shown in grey mesh. Polar interactions are shown in grey dashes. **B.** View of the inner cavity, which interacts with the D-iGlu$_{NH2}$ residue. **C.** View of the outer cavity, which interacts with the *m*-DAP$_{NH2}$ residue.

In the Ldt_{Mt2}-**3** complex structure, the *m*-DAP_{NH2} residue sidechain protrudes into the outer cavity, while the D-$iGlu_{NH2}$ sidechain is located in the inner cavity, suggesting that the substrate enters from the inner cavity (Figure 5.4B,C). Note that no electron density was observed corresponding to the L-Ala residue of **3**, which has previously been suggested not to play a significant role in substrate binding.[42] Additional electron density at the entrance of the outer cavity was observed, in which D-Ala, released during the formation of the thioester intermediate, could be modelled (Figure 5.4A). We did not observe density that could reflect binding of an acceptor substrate.

The overall fold of the Ldt_{Mt2}-**3** complex strongly resembles that of unmodified Ldt_{Mt2} (PDB 6RLG;[27] main chain RMSD 0.65 Å). Similarly to unmodified Ldt_{Mt2},[27,43] the S^{γ} atom of Cys354 is positioned 3.9 Å from the $N^{\varepsilon 2}$ atom of His336, and the $N^{\delta 1}$ atom of His336 is positioned for polar interactions with the main-chain carbonyl O of Ser337 at a distance of 2.7 Å. Notably, no conformational changes relative to unmodified Ldt_{Mt2} are observed in loop II (Figure S1) , which encloses the active site (residues 300-323) and which has previously been observed to be flexible upon binding of various inhibitors, and which is proposed to undergo extensive conformational changes upon substrate binding.[26,33,43]

The thioester acyl group, as well as the *m*-DAP_{NH2} residue and the D-$iGlu_{NH2}$ residue of **3** are positioned to engage in interactions with elements in the Ldt_{Mt2} active site (Figures 5.4, S3.18). The oxygen thioester acyl group is located in the proposed oxyanion hole (the backbone NH groups of His352, Gly353 and Cys354) at respective distances of 3.8 Å, 3.3 Å and 2.3 Å, suggesting that, at least in the crystal structure, no strong interactions are made with the backbone NH groups of His352. Polar interactions of *m*-DAP_{NH2} with His336 (3.0 Å), Asn356 (3.4 Å) and Thr320 (2.8 Å), as well as water mediated polar interactions with His352 (3.3 Å to water, 3.4 Å to His352) are observed. The *m*-DAP_{NH2} carbon chain is positioned for hydrophobic interactions with the sidechain of Tyr318. The D-$iGlu_{NH2}$ residue was observed to engage in water mediated polar interactions with His352 (2.7 Å to water and 3.3 Å to His352) and Ser331 (2.9 Å to water and 2.8 Å to Ser331), as well as hydrophobic interactions with Gly332.

Crystallographic studies of Ldt_{Mt2} in the presence of **1** did not manifest evidence for the presence of substrate at the active site; similarly to **3**, however, **1** was observed to bind to the surface of the IgD2 through various polar interactions, as observed with both wildtype Ldt_{Mt2} and with Ldt_{Mt2}^{C354S} (PDB 8PXY, 2.15 Å; Figure S3.19). The GlcNAc moiety of **1**, which is absent in **3**, was observed to interact with the surface the catalytic domain of a second symmetry related molecule of Ldt_{Mt2}, manifesting polar interactions with Asp367 (2.5 Å and 2.8 Å) and with Gln363 (3.0 Å), located ~20 Å away from the nucleophilic cysteine (or serine, in the case

of Ldt_{Mt2}^{C354S}), potentially preventing binding of the second molecule of **1** at the Ldt_{Mt2} active site as observed in the structure of Ldt_{Mt2}.

5.4 Discussion

Targeting bacterial cell wall transpeptidases is a validated method for treating bacterial infections, in particular via β-lactam mediated PBP inhibition.[5] Though a role for β-lactams in the treatment of TB has not been established, promising activity against *Mtb* has been observed, particularly from carbapenems, which inhibit both PBPs and Ldts.[44] Ldts, and specifically Ldt_{Mt2}, are essential for *Mtb*,[13] but have been considerably less studied than the PBPs. Whilst several early-stage studies on inhibitors for Ldt_{Mt2} have been reported,[23,26] the search for potent and clinically useful inhibitors is ongoing. Despite its biological and medicinal importance, the mechanism of the transpeptidase reaction of Ldt_{Mt2} has been the subject of limited studies, in part likely due to the lack of availability of the peptidoglycan monomers. Reported studies on Ldt_{Mt2} have thus mainly relied on the use of relatively simple substrate analogues.[22,45] Our modified procedure for the isolation of peptidoglycan monomers from the *C. jeikeium* cell wall enabled us to obtain a crystal structure of Ldt_{Mt2} reacted with **3** and to obtain insights into the binding and reaction kinetics of Ldt_{Mt2}.

Exposure of *C. jeikeium* cells to subinhibitory concentrations of ampicillin during growth, results in accumulation of peptidoglycan pentapeptide monomer **4**. Ldt_{Mt2} substrate **1** can subsequently be obtained from **4** via enzymatic cleavage of the terminal D-Ala. Via this method, the tetrapeptide monomer was obtained in a yield of ~21 mg from 56 g of dried cell mass. At least presently, this procedure is substantially more efficient than reported synthetic procedures.[28]

X-ray crystallographic studies of Ldt_{Mt2} with substrate **3** yielded a structure of the covalently linked thioester acyl-enzyme complex, likely reflecting the transient intermediate during the Ldt_{Mt2} transpeptidation reaction. Many enzymes employing nucleophilic cysteine or serine residues proceed through covalent acyl-enzyme intermediates; commonly these intermediates are unstable, and therefore structures of them have not often been observed in a form relevant to catalysis with a natural substrate.[46] Crystallographic studies of the (thio)ester intermediates frequently rely on active site mutations (e.g.[47]), the use of substrate mimics(e.g.[48]), or the use of profound rate-reducing conditions (e.g.[41,49]). To our knowledge, the only other nucleophilic cysteine enzyme reported to trap a thioester intermediate of a natural substrate under biologically relevant conditions is the main protease or SARS-CoV-2 main protease (M^{pro}),[39,40] in which a thioester was observed to form *in crystallo* after being presented with the product, resulting from the reverse reaction.

Thioester trapping, as observed in our Ldt_{Mt2}-**3** complex acyl-enzyme crystal structure, could in part be due to the inability of the acceptor substrate to enter the active site in the crystalline state due to reduced flexibility that may be required for acceptor substrate binding. Other factors that may affect the reaction rate and therefore the persistence of the acyl-enzyme intermediate *in crystallo* are the reduced pH (7.0, compared to 7.5) and temperature (4 °C, compared to rt) with respect to the solution-based studies, both of which have been shown to reduce the rate of the Ldt_{Mt2} reaction to some extend (Figure S3.12D-E). It is also important to note that transpeptidation reactions are fundamentally different from hydrolysis reactions, in that during transpeptidation the acyl-enzyme complex is required to be sufficiently stable in order to allow for the *m*-DAP residue of the acceptor substrate to react with the (thio)ester of the donating substrate.

The relative positions of the catalytic residues and oxyanion hole of the Ldt_{Mt2}-**3** complex are similar to those observed in the M^{pro} thioester intermediate structure, and in structures of Ldts in complex β-lactams, e.g., in a structure of the *Enterococcus faecium* Ldt_{fm} complexed with ertapenem,[50] and in structures of Ldt_{Mt2} complexed with meropenem or biapenem (Figure S3.17A-D).[21,51] In all cases the thioester link has the (*Z*)-stereochemistry that is commonly associated with acyl-enzyme intermediates,[46,52] including a structure of PBP4a of *B. subtilis* in complex with a peptidoglycan mimetic (Figure S3.17E).[53]

The structure reported here represents the first reported crystallographic data of Ldt_{Mt2} in complex with a substantial part of its donor substrate. In a structure of a non-substrate peptidoglycan fragment (**13**, D-γ-Glu-*m*-DAP) bound to the Ldt_{Mt2} active site,[22] the *m*-DAP residue faces into the inner cavity, contrasting with our structure, suggesting entrance from the outer cavity (Figures S3.20A-B, S3.21A). Molecular dynamics studies have suggested that entrance of the substrate from the inner cavity of Ldt_{Mt2} will not lead to acylation.[42] Our results suggest that during the initial steps of productive binding via the inner cavity, the substrate may project deeper into the active site than predicted by calculations. In agreement with this proposal, a solid-state NMR structure of the *B. subtilis* L,D-transpeptidase (Ldt_{Bs}) in complex with intact peptidoglycan suggests binding of the donor substrate in the analogous inner cavity (Figures S3.20C, S3.21B).[54]

An allosteric binding pocket of Ldt_{Mt2}, named the S-pocket, has been proposed to bind the sugar-moieties (Figure S3.20E).[45] We did not observe interaction of GlcNAc-MurNAc of **1** in this pocket. Nevertheless, extrapolation of the studies on the *B. subtilis* Ldt_{Bs} bound to intact peptidoglycan suggest that intact peptidoglycan may bind in the S-pocket associated with the IgD2 domain of Ldt_{Mt2}.[54]

A coupled assay for detecting D-Ala was optimised for assessing Ldt_{Mt2} activity. The assay represents an increased throughput method of assessing turnover in comparison with previous LC-MS studies,[13,28] and provides increased biologically relevance over the reported high-throughput assay for inhibition of Ldt_{Mt2}.[26] However, due to the relatively low enzyme effectivity, high concentrations of substrate are required, making the use of this assay in a high-throughput setting challenging without a well-established synthesis route. Additionally, the coupled enzymes DAAO and HRP increase the risk of assay interference. Based on these observations, we recommend that the fluorescence based transpeptidase assay is most suitable for use as a secondary assay to the high-throughput assay for Ldt_{Mt2}, testing identified inhibitors in a more biologically relevant setting.

Although our studies suggest that the isolated recombinant Ldt_{Mt2} has a relatively low affinity and catalytic activity with **1** and **3**, under our conditions the latter is a somewhat more efficient substrate. Interestingly, evidence for efficient transpeptidase activity by Ldts has been observed in *Mtb* cells in a previous report,[38] suggesting the need for increased interactions than present in our assays; potentially these will be achieved with use of full length peptidoglycan. Alternatively, complex formation with related enzymes may increase activity, as observed with the functionally related D,D-transpeptidases and glycosyltransferases PBP1A and PBP2B, which require interactions with lipoprotein cofactors LpoA and LpoB, both in isolated enzyme and cellular systems.[55-58] In *E. coli*, the Ldt YcbB was found to associate with PBP1b and PBP5 revealing links between the two types of peptidoglycan transpeptidases.[59]

Amidation of both D-iGlu and *m*-DAP residues is reported to be required for Ldt_{Mt2} turnover, as well as for growth of *Mtb*.[28] We have shown that **11**, a close analogue of **3**, made up of the D-$iGlu_{NH2}$ but *m*-DAP_{NH2} substituted with L-Lys, is not a substrate for Ldt_{Mt2}. The Ldt_{Mt2}-**3** complex structure suggests that the multiple polar interactions of *m*-DAP_{NH2} with Asn356, His336, Thr320, and His352 are important, as L-Lys is likely only able to interact with Asn356 and His336. By contrast with the high substrate selectivity observed for Ldt_{Mt2}, PBPs have been observed to react with D-Ala-D-Ala peptidoglycan mimetics, suggesting that modified features of the second and third peptide chain residues may not be as important for PBP catalysis as they appears to be for Ldt_{Mt2}.[60,61]

Most reported Ldt_{Mt2} inhibitors interact with the catalytic cysteine (Cys354), and may fill either the inner or the outer active site cavities e.g., Ldt_{Mt2}-bound ertapenem complex occupies the inner cavity, while Ldt_{Mt2}-bound biapenem occupies the outer cavity (Figure S17C-D).[21,43,45,51]. Based on the structure of Ldt_{Mt2} reacted with **3**, elements of which occupies both the inner and outer cavity, improvement of inhibitor potency might be achieved through interactions with both the inner and outer cavities. Design of inhibitors achieving this may be based on the

tetrapeptide structure, but optimisation will be necessary, especially in light of the low affinity of Ldt_{Mt2} for **3** in solution. The structure of Ldt_{Mt2} reacted with **3** suggests that focus of future optimisation studies may be on the D-iGlu$_{NH2}$-*m*-DAP$_{NH2}$-D-Ala residues, in particular the D-iGlu$_{NH2}$-*m*-DAP$_{NH2}$ elements which are observed to interact with Ldt_{Mt2} in the intermediate structure. The addition of an electrophilic group to the *m*-DAP$_{NH2}$ residue *in lieu* of the peptide bond with D-Ala may increase reactivity, e.g., a nitrile group, which has been shown to react with Cys354 of Ldt_{Mt2}.[26] Optimisation of the substrate for inhibition, including the addition of a reversibly covalently reacting nitrile group has been a successful method in the inhibitor development of M^{pro}, with one resulting inhibitor, nirmatrelvir, being approved for COVID-19 treatment.[62,63] Polar interactions with Tyr308 may be achieved through incorporation of a heteroatom in the D-iGlu$_{NH2}$ carbon chain. While the carbon chain of the *m*-DAP$_{NH2}$ does not undergo direct interactions with the active site of Ldt_{Mt2}, the flexibility of this residue may be required to allow for entrance into the active site and the polar interactions observed with His336, Tyr320, and Asn356, as well as the water mediated interactions with His352.

5.5 Conclusion

Ldt_{Mt2} is a promising drug target for TB treatment, though little has been reported on the mechanism of the transpeptidase reaction that it catalyses. We optimised the isolation of the natural disaccharide tetrapeptide monomers **1**-**4** from the *C. jeikeium* bacterial cell wall through overproduction of peptidoglycan sacculus. We explored the interactions of Ldt_{Mt2} with the isolated tetrapeptide monomers **1** and **3** via X-ray crystallographic studies, obtaining a structure of the proposed thioester intermediate in Ldt_{Mt2} catalysis. The structure informs on the mode of entrance of the donor substrate into the Ldt_{Mt2} active site and active site interactions made by it. The combined results will be useful in the design of novel Ldt_{Mt2} inhibitors, including those based on substrate binding interactions, a strategy that has been successfully employed for other nucleophilic cysteine enzymes, including M^{pro}.[62,63]

5.6 Methods

5.6.1 Materials

Faropenem was obtained from Fluorochem Ltd., FAD was from Alfa Aesar, AR was from Cambridge Bioscience Ltd., and Fmoc- D-iGln-OH was from Ambeed, **12** and **13** were from InvivoGen, **16**-**23** were obtained from the GSK HTS compound library. All other compounds were from Merck.

5.6.2 Protein production and purification

Recombinant Ldt_{Mt2} was produced and purified as previously reported.[31] Site-directed mutagenesis was performed as described,[64] with primer sequences shown in Table 5.1 to achieve the C354S mutation of Ldt_{Mt2}. Ldt_{Mt2}^{C354S} was produced and purified as described for the wildtype enzyme.[31] Purity and identity of Ldt_{Mt2}^{C354S} was confirmed by SDS-PAGE (<95% purity) and MS (calculated 37959 Da, observed 37962 Da; Appendix V). Recombinant *E. coli* DacA was produced and purified as previously reported.[65]

Table 5.1. Primers used in the site-directed mutagenesis to achieve the C354S mutation of Ldt_{Mt2}. In bold is the nucleic acid that is changed from the wildtype.

Primer	Sequence
Ldt_{Mt2}^{C354S}-forward	CAGCCATGGT**A**GTCTGAATGTTAGCCCGAGCAATG
Ldt_{Mt2}^{C354S}-reverse	CTAACATTCAGAC**T**ACCATGGCTGGTATTGGTATG

5.6.3 Peptidoglycan fragment isolation

C. jeikeium was grown overnight at 37 °C on Columbia agar supplemented with 5% sheep blood (Scientific Laboratory Supplies Ltd). Cultures were used to inoculate brain heart infusion broth supplemented with 1% (*v/v*) Tween 80 and 2 μg/mL ampicillin.[29] The culture was incubated at 37 °C for 16 hours with shaking.

Cells were collected by centrifugation (15000 x g, 20 min, 4 °C). The cell pellet was resuspended (1 mL/g) in 10 mM sodium phosphate pH 7.0 and lysed using a high-pressure cell disruptor (CF1, Constant Systems, 40 kpsi, 3x). The cell wall was collected by centrifugation (15000 x g, 15 min, 4 °C) and resuspended in 25 mL of 10 mM sodium phosphate pH 7.0. The resulting suspension was added dropwise to 25 mL of 10 mM sodium phosphate pH 7.0 with 8% (*w/v*) SDS and incubated for 30 min at 100 °C. Peptidoglycan was pelleted by centrifugation (45000 x g, 30 min, 15 °C) and washed with 10 mM sodium phosphate pH 7.0 (5x). The peptidoglycan was then treated overnight at 37 °C with shaking with Pronase E (200 μg/mL) in 10 mM Tris-HCl pH 7.4. Peptidoglycan was pelleted by centrifugation (45000 x g, 30 min, 15 °C) and was washed with 20 mM sodium phosphate pH 7.8. Peptidoglycan was treated overnight at 37 °C with shaking with trypsin (200 μg/mL) in 20 mM sodium phosphate pH 7.8. Peptidoglycan was washed twice with water and dissolved in 25 mM sodium phosphate pH 6.0 with 0.1 mM $MgCl_2$ and treated with mutanolysin (200 μg/mL) and lysozyme (200 μg/mL) and incubated overnight at 37 °C with shaking. Insoluble peptidoglycan was pelleted by centrifugation (4000 x g, 30 min, 4 °C). The supernatant containing soluble disaccharide peptides was collected.

The disaccharide peptides were separated via reverse phase high performance liquid chromatography (HPLC) on a C_{18} column (10 µm, 21,2 × 250 mm, Avantor ACE AQ) at a flowrate of 15 mL/min. A gradient of 1-20% (*v*/*v*) of solvent B was applied between 0 and 20 min (solvent A: 0.05% (*v*/*v*) trifluoroacetic acid in water; solvent B: 0.035% (*v*/*v*) trifluoroacetic acid in acetonitrile). Peaks containing **4** were lyophilised and dissolved in 50 mM tris pH 7.5 and DacA (20 µM) was added. The mixture was incubated for 5 h at 37 °C, lyophilised and purified by HPLC on a C_{18} column (10 µm, 21,2 × 250 mm, Avantor ACE AQ) at a flowrate of 15 mL/min. A gradient of 1-5% (*v*/*v*) of solvent B was applied between 0 and 7.5 min, followed by a gradient of 5-7% (*v*/*v*) of solvent B over 40 min to obtain **1** as a white solid.

To obtain **2**, the fragment **1**, purified as above, was dissolved in 0.5 M borate buffer pH 8.0 containing 10 mg/mL sodium borohydride. After 20 min the pH was adjusted to 2-4 with orthophosphoric acid. Purification by HPLC was performed as described above.

To obtain **3**, **1** was dissolved in 25% (*v*/*v*) NH_4OH in H_2O and stirred at 37 °C for 5 hours. Then, the mixture was neutralised via addition of acetic acid and the mixture was lyophilised. Purification by HPLC was performed as described above.

5.6.4 Synthesis of 9 and 11

9 and **11** were synthesised by solid phase peptide synthesis using a Liberty Blue Automated Microwave Peptide Synthesizer. D-Alanine-Wang resin (715 mg, 0.5 mmol) was coupled with Fmoc protected amino acids D-Ala (1.5 mmol, 3 eq.), L-Lys (2.5 mmol, 5 eq.), D-iGlu$_{NH2}$ (2.5 mmol, 5 eq.), and L-Ala (2.5 mmol, 5 eq.), respectively, in the case of **9**, and (L-Lys (2.5 mmol, 5 eq.), D-iGlu$_{NH2}$ (2.5 mmol, 5 eq.), and L-Ala (2.5 mmol, 5 eq.), respectively in the case of **11**). Coupling using the standard procedure was performed with N,N-diisopropylethylamine (DIPEA) in ethyl cyanohydroxyiminoacetate (Oxyma, 1 M; DIPEA/Oxyma 1.5 % (*v*/*v*)) and 7.8% (*v*/*v*) N,N′-diisopropylcarbodiimide (DIC) in DMF. After each coupling step, the resin was washed with DMF and the Fmoc group was deprotected with 20% (*v*/*v*) piperidine in DMF using the standard deprotection procedure. After coupling and deprotection steps were repeated as required, the resin-bound peptide was washed with dichloromethane (DCM), methanol and DCM, and treated with a 5 mL solution of 2:1 TFA/DCM (2 h, rt). Solvent was removed by evaporation *in vacuo* and purified by HPLC on a C_{18} column (5 µm, 10 x 150 mm; SunFire, Waters) at a flowrate of 3 mL/min in 98% (*v*/*v*) buffer A (0.1% (*v*/*v*) formic acid in H_2O) and 2% buffer B (0.1% (*v*/*v*) formic acid in acetonitrile).

5.6.5 Mass spectrometry assays

LC-MS assays were performed using a 1290 Infinity II LC System (Agilent Technologies) equipped with a C_{18} column (3 µm, 50 x 2.1 mm; Ace equivalence) with a gradient of 5-20% (*v*/*v*) acetonitrile:water 0.1% (*v*/*v*) formic acid over 0 and 20 min, coupled to an Agilent 6550 iFunnel Q-TOF mass spectrometer (Agilent Technologies) operating in positive mode. Data were analysed using MassHunter Qualitative Analysis B.07.00 (Agilent Technologies).

Protein-observed SPE-MS assays were performed as reported.[26] In brief, Ldt_{Mt2} (1 µM) in 50 mM tris pH 7.5 was incubated with peptidoglycan fragments (100 µM) and mass spectrometry was performed with a RapidFire200 integrated autosampler/solid phase extraction (SPE) system (Agilent Technologies) coupled to an coupled to an Agilent 6550 iFunnel Q-TOF mass spectrometer (Agilent Technologies) operating in the positive ionisation mode. Data were analysed using MassHunter Qualitative Analysis B.07.00 (Agilent Technologies).

5.6.6 Transpeptidase assays

A transpeptidase assay master mixture was prepared in assay buffer (50 mM sodium phosphate, pH 8.0, 100 mM NaCl, 0.01% (*v/v*) Triton X-100) as described in Table 5.2. The specified master mixture (14 µL) was added to a black polystyrene, clear- and flat-bottomed, 384-well microplate (Greiner Bio-One, part number 781096) using a MultiDrop Combi dispenser (Thermo Fisher Scientific).

Table 5.2. Master mixture for the DAAO assay.

Component	Concentration (1.8x)	Final concentration
DAAO	3.6 U/mL	2.0 U/mL
FAD	72 µM	40 µM
HRP	3.6 U/mL	2.0 U/mL
Amplex red	18 µM	10 µM

Compounds (in DMSO, with final concentrations ranging from 40 µM to 20.3 nM; 10 dilutions of factor 3) were added using a CyBio liquid handling system (Analytik Jena AG), with 4 replicates per inhibitor concentration. In the case of Control 1 (expected 0% inhibition; 100% fluorescence signal) and Control 2 (expected 100% inhibition; 0% fluorescence signal) the compound solution was substituted with neat DMSO. Ldt_{Mt2} (5 µL, 500 nM final concentration) was added to all wells using a MultiDrop Combi dispenser (Thermo Fisher Scientific). In the case of Control 2, Ldt_{Mt2} was substituted with the assay buffer (5 µL). This mixture was incubated for 30 minutes at rt. The substrate (**1** or **3**, as specified, 5 µL, 35 µM final

concentration) was then added to all wells. The fluorescence signal was measured using a PHERAstar plate reader (BMG Labtech) with λ_{ex} = 540 nm and λ_{em} = 590 nm. Data were analysed using Prism 10 (GraphPad).

The transpeptidase interference assay was performed as described above, with the modification that the Ldt_{Mt2} mixture was replaced by 5 µL assay buffer, and the substrate was replaced by D-Ala (500 nM final concentration). Data were analysed using Prism 10 (GraphPad).

5.6.7 Crystallography

Ldt_{Mt2} (Δ1-55; with the N-terminal HisTag removed, in 50 mM tris, pH 8.0, 100 mM NaCl) was incubated with substrate **1** or **3** for 30 minutes on ice, and then crystallised with a well solution consisting of 0.1 M HEPES, pH 7.0, and 25% (*v/v*) Jeffamine ED-2001 pH 7.0, using sitting drop vapor diffusion crystallization plates (low reservoir Intelli-Plate 93-3), with 1 µL of protein-substrate solution and 1 µL of well solution. Crystallisation plates were stored at 4 °C. The crystals were mounted on nylon loops, cryocooled and stored in liquid nitrogen. Datasets were collected using the MX beamline i03 at Diamond Light Source. Datasets were processed using the automated processing pipeline at Diamond Light Source, using xia2.[66] Structures were solved by molecular replacement with Phaser[67], using PDB entry 6RLG[27] as the search model. Ligand restrain files were created using Grade2.[68] Alternating cycles of refinement using PHENIX[69] and manual model building using COOT[70] were performed until no further significant improvement of R_{work} and R_{Free} was achieved. Data collection and refinement statistics are described in Table S3.4.

5.7 Data availability

Crystallographic data that supports the findings of this study have been deposited in the Protein Data Bank (PDB) with the accession codes “8PXY” and “8PXZ”. Data supporting this manuscript are provided in the Supplementary Information (Appendix III).

5.8 References

1 Global tuberculosis report 2022. . Report No. Licence: CC BY-NC-SA 3.0 IGO, (Geneva: World Health Organization, 2022).

2 Sotgiu, G., Centis, R., D'Ambrosio, L. & Migliori, G. B. Tuberculosis Treatment and Drug Regimens. *Cold Spring Harb. Perspect. Med.* **5**, a017822 (2015).

3 Chakaya, J., Khan, M., Ntoumi, F., Aklillu, E., Fatima, R., Mwaba, P., Kapata, N., Mfinanga, S., Hasnain, S. E., Katoto, P. D. M. C., Bulabula, A. N. H., Sam-Agudu, N. A., Nachega, J. B., Tiberi, S., McHugh, T. D., Abubakar, I. & Zumla, A. Global

Tuberculosis Report 2020 – Reflections on the Global TB burden, treatment and prevention efforts. *Int. J. Infect. Dis.* **113**, S7-S12 (2021).

4 Lima, L. M., da Silva, B. N. M., Barbosa, G. & Barreiro, E. J. β-lactam antibiotics: An overview from a medicinal chemistry perspective. *Eur. J. Med. Chem.* **208**, 112829 (2020).

5 Sauvage, E., Kerff, F., Terrak, M., Ayala, J. A. & Charlier, P. The penicillin-binding proteins: structure and role in peptidoglycan biosynthesis. *FEMS Microbiol. Rev.* **32**, 234-258 (2008).

6 Kurz, S. G. & Bonomo, R. A. Reappraising the use of β-lactams to treat tuberculosis. *Expert Rev. Anti-infect. Ther.* **10**, 999-1006 (2012).

7 Lavollay, M., Arthur, M., Fourgeaud, M., Dubost, L., Marie, A., Veziris, N., Blanot, D., Gutmann, L. & Mainardi, J. L. The Peptidoglycan of Stationary-Phase *Mycobacterium tuberculosis* Predominantly Contains Cross-Links Generated by L,D-Transpeptidation. *J. Bacteriol.* **190**, 4360-4366 (2008).

8 Glauner, B., Höltje, J. & Schwarz, U. The composition of the murein of *Escherichia coli*. *J. Biol. Chem.* **263**, 10088-10095 (1988).

9 Aliashkevich, A. & Cava, F. LD-transpeptidases: the great unknown among the peptidoglycan cross-linkers. *FEBS J.* **289**, 4718-4730 (2022).

10 Zandi, T. A., Marshburn, R. L., Stateler, P. K. & Brammer Basta, L. A. Phylogenetic and Biochemical Analyses of Mycobacterial L,D-Transpeptidases Reveal a Distinct Enzyme Class That Is Preferentially Acylated by Meropenem. *ACS Infect. Dis.* **5**, 2047-2054 (2019).

11 Vollmer, W., Blanot, D. & De Pedro, M. A. Peptidoglycan structure and architecture. *FEMS Microbiol. Rev.* **32**, 149-167 (2008).

12 Mainardi, J., Hugonnet, J., Gutmann, L. & Arthur, M. Fighting resistant tuberculosis with old compounds: the carbapenem paradigm. *Clin. Microbiol. Infect.* **17**, 1755-1756 (2011).

13 Gupta, R., Lavollay, M., Mainardi, J.-L., Arthur, M., Bishai, W. R. & Lamichhane, G. The *Mycobacterium tuberculosis* protein Ldt_{Mt2} is a nonclassical transpeptidase required for virulence and resistance to amoxicillin. *Nat. Med.* **16**, 466-469 (2010).

14 Schoonmaker, M. K., Bishai, W. R. & Lamichhane, G. Nonclassical Transpeptidases of *Mycobacterium tuberculosis* Alter Cell Size, Morphology, the Cytosolic Matrix, Protein Localization, Virulence, and Resistance to β-Lactams. *J. Bacteriol.* **196**, 1394-1402 (2014).

15 Sanders, A. N., Wright, L. F. & Pavelka, M. S. Genetic characterization of mycobacterial L,D-transpeptidases. *Microbiology* **160**, 1795-1806 (2014).

16 Andreeva, A., Howorth, D., Brenner, S. E., Hubbard, T. J., Chothia, C. & Murzin, A. G. SCOP database in 2004: refinements integrate structure and sequence family data. *Nucleic acids res.* **32**, D226-D229 (2004).

17 Goffin, C. & Ghuysen, J.-M. Multimodular penicillin-binding proteins: an enigmatic family of orthologs and paralogs. *Microbiol. Mol. Biol. Rev.* **62**, 1079-1093 (1998).

18 Biarrotte-Sorin, S., Hugonnet, J.-E., Delfosse, V., Mainardi, J.-L., Gutmann, L., Arthur, M. & Mayer, C. Crystal structure of a novel β-lactam-insensitive peptidoglycan transpeptidase. *J. Mol. Biol.* **359**, 533-538 (2006).

19 Böth, D., Steiner, E. M., Stadler, D., Lindqvist, Y., Schnell, R. & Schneider, G. Structure of Ldt_{Mt2}, an L,D-transpeptidase from *Mycobacterium tuberculosis*. *Acta Crystallogr. D* **69**, 432-441 (2013).

20 Bielnicki, J., Devedjiev, Y., Derewenda, U., Dauter, Z., Joachimiak, A. & Derewenda, Z. S. *B. subtilis* ykuD protein at 2.0 Å resolution: insights into the structure and function of a novel, ubiquitous family of bacterial enzymes. *Proteins* **62**, 144-151 (2006).

21 Li, W. J., Li, D. F., Hu, Y. L., Zhang, X. E., Bi, L. J. & Wang, D. C. Crystal structure of L,D-transpeptidase Ldt_{Mt2} in complex with meropenem reveals the mechanism of carbapenem against *Mycobacterium tuberculosis*. *Cell Res.* **23**, 728-731 (2013).

22 Erdemli, S. B., Gupta, R., Bishai, W. R., Lamichhane, G., Amzel, L. M. & Bianchet, M. A. Targeting the cell wall of *Mycobacterium tuberculosis*: structure and mechanism of L,D-transpeptidase 2. *Structure* **20**, 2103-2115 (2012).

23 Kumar, P., Kaushik, A., Lloyd, E. P., Li, S.-G., Mattoo, R., Ammerman, N. C., Bell, D. T., Perryman, A. L., Zandi, T. A., Ekins, S., Ginell, S. L., Townsend, C. A., Freundlich, J. S. & Lamichhane, G. Non-classical transpeptidases yield insight into new antibacterials. *Nat. Chem. Biol.* **13**, 54-61 (2017).

24 Cordillot, M., Dubée, V., Triboulet, S., Dubost, L., Marie, A., Hugonnet, J.-E., Arthur, M. & Mainardi, J.-L. In vitro cross-linking of *Mycobacterium tuberculosis* peptidoglycan by L,D-transpeptidases and inactivation of these enzymes by carbapenems. *Antimicrob. Agents Chemother.* **57**, 5940-5945 (2013).

25 Triboulet, S., Arthur, M., Mainardi, J. L., Veckerlé, C., Dubée, V., Nguekam Moumi, A., Gutmann, L., Rice, L. B. & Hugonnet, J. E. Inactivation Kinetics of a New Target of β-Lactam Antibiotics. *J. Biol. Chem.* **286**, 22777-22784 (2011).

26 de Munnik, M., Lang, P. A., De Dios Antos, F., Cacho, M., Bates, R. H., Brem, J., Rodríguez-Miquel, B. & Schofield, C. J. High-Throughput Screen with the L,D-transpeptidase Ldt_{Mt2} of *Mycobacterium tuberculosis* Reveals Novel Classes of Covalently Reacting Inhibitors *Chem. Sci.* **14**, 7262-7278 (2023).

27 de Munnik, M., Lohans, C. T., Lang, P. A., Langley, G. W., Malla, T. R., Tumber, A., Schofield, C. J. & Brem, J. Targeting the *Mycobacterium tuberculosis* transpeptidase Ldt_{Mt2} with cysteine-reactive inhibitors including ebselen. *Chem. Commun.* **55**, 10214-10217 (2019).

28 Ngadjeua, F., Braud, E., Saidjalolov, S., Iannazzo, L., Schnappinger, D., Ehrt, S., Hugonnet, J.-E., Mengin-Lecreulx, D., Patin, D., Ethève-Quelquejeu, M., Fonvielle, M. & Arthur, M. Critical Impact of Peptidoglycan Precursor Amidation on the Activity of L,D-Transpeptidases from *Enterococcus faecium* and *Mycobacterium tuberculosis*. *Chem. Eur. J.* **24**, 5743-5747 (2018).

29 Lavollay, M., Arthur, M., Fourgeaud, M., Dubost, L., Marie, A., Riegel, P., Gutmann, L. & Mainardi, J.-L. The β-lactam-sensitive D,D-carboxypeptidase activity of Pbp4 controls the L,D and D,D transpeptidation pathways in *Corynebacterium jeikeium*. *Mol. Microbiol.* **74**, 650-661 (2009).

30 Arbeloa, A., Hugonnet, J.-E., Sentilhes, A.-C., Josseaume, N., Dubost, L., Monsempes, C., Blanot, D., Brouard, J.-P. & Arthur, M. Synthesis of Mosaic Peptidoglycan Cross-bridges by Hybrid Peptidoglycan Assembly Pathways in Gram-positive Bacteria. *J. Biol. Chem.* **279**, 41546-41556 (2004).

31 Lohans, C. T., Chan, H. T. H., Malla, T. R., Kumar, K., Kamps, J. J. A. G., McArdle, D. J. B., Van Groesen, E., de Munnik, M., Tooke, C. L., Spencer, J., Paton, R. S., Brem, J. & Schofield, C. J. Non-Hydrolytic β-Lactam Antibiotic Fragmentation by L,D-Transpeptidases and Serine β-Lactamase Cysteine Variants. *Angew. Chem. Int. Ed.* **58**, 1990-1994 (2019).

32 Huynh, K. & Partch, C. L. Analysis of Protein Stability and Ligand Interactions by Thermal Shift Assay. *Curr. Protoc. Protein Sci.* **79**, 14-21 (2015).

33 Steiner, E. M., Schneider, G. & Schnell, R. Binding and processing of β-lactam antibiotics by the transpeptidase Ldt_{Mt2} from *Mycobacterium tuberculosis*. *FEBS J.* **284**, 725-741 (2017).

34 de Munnik, M., Lohans, C. T., Langley, G. W., Bon, C., Brem, J. & Schofield, C. J. A Fluorescence-Based Assay for Screening β-Lactams Targeting the *Mycobacterium tuberculosis* Transpeptidase Ldt_{Mt2}. *ChemBioChem* **21**, 368-372 (2020).

35 Gutheil, W. G., Stefanova, M. E. & Nicholas, R. A. Fluorescent coupled enzyme assays for D-alanine: application to penicillin-binding protein and vancomycin activity assays. *Anal. Biochem.* **287**, 196-202 (2000).

36 Frére, J.-M., Leyh-Bouille, M., Ghuysen, J.-M., Nieto, M. & Perkins, H. R. in *Meth. Enzymol.* Vol. 45 *Exocellular dd-carboxypeptidases-transpeptidases from Streptomyces* Ch. 51, 610-636 (Elsevier, 1976).

37 Catherwood, A. C., Lloyd, A. J., Tod, J. A., Chauhan, S., Slade, S. E., Walkowiak, G. P., Galley, N. F., Punekar, A. S., Smart, K., Rea, D., Evans, N. D., Chappell, M. J., Roper, D. I. & Dowson, C. G. Substrate and Stereochemical Control of Peptidoglycan Cross-Linking by Transpeptidation by *Escherichia coli* PBP1B. *J. Am. Chem. Soc.* **142**, 5034-5048 (2020).

38 Pidgeon, S. E., Apostolos, A. J., Nelson, J. M., Shaku, M., Rimal, B., Islam, M. N., Crick, D. C., Kim, S. J., Pavelka, M. S., Kana, B. D. & Pires, M. M. L,D-Transpeptidase Specific Probe Reveals Spatial Activity of Peptidoglycan Cross-Linking. *ACS Chem. Biol.* **14**, 2185–2196 (2019).

39 Lee, J., Worrall, L. J., Vuckovic, M., Rosell, F. I., Gentile, F., Ton, A.-T., Caveney, N. A., Ban, F., Cherkasov, A., Paetzel, M. & Strynadka, N. C. J. Crystallographic structure of wild-type SARS-CoV-2 main protease acyl-enzyme intermediate with physiological C-terminal autoprocessing site. *Nat. Commun.* **11** (2020).

40 Lee, J., Kenward, C., Worrall, L. J., Vuckovic, M., Gentile, F., Ton, A.-T., Ng, M., Cherkasov, A., Strynadka, N. C. J. & Paetzel, M. X-ray crystallographic characterization of the SARS-CoV-2 main protease polyprotein cleavage sites essential for viral processing and maturation. *Nat. Commun.* **13** (2022).

41 Wilmouth, R. C., Clifton, I. J., Robinson, C. V., Roach, P. L., Aplin, R. T., Westwood, N. J., Hajdu, J. & Schofield, C. J. Structure of a specific acyl-enzyme complex formed between β-casomorphin-7 and porcine pancreatic elastase. *Nat. Struct. Biol.* **4**, 456-462 (1997).

42 Baldin, S., Misiura, N. & Švedas, V. Building a full-atom model of L,D-transpeptidase 2 from *Mycobacterium tuberculosis* for screening new inhibitors. *Acta Nat.* **9**, 44-51 (2017).

43 Kim, H. S., Kim, J., Im, H. N., Yoon, J. Y., An, D. R., Yoon, H. J., Kim, J. Y., Min, H. K., Kim, S.-J. & Lee, J. Y. Structural basis for the inhibition of *Mycobacterium tuberculosis* L,D-transpeptidase by meropenem, a drug effective against extensively drug-resistant strains. *Acta Crystallogr. D* **69**, 420-431 (2013).

44 Jaganath, D., Lamichhane, G. & Shah, M. Carbapenems against *Mycobacterium tuberculosis*: a review of the evidence. *Int. J. Tuberc. Lung Dis.* **20**, 1436-1447 (2016).

45 Ahmad, N., Dugad, S., Chauhan, V., Ahmed, S., Sharma, K., Kachhap, S., Zaidi, R., Bishai, W. R., Lamichhane, G. & Kumar, P. Allosteric cooperation in β-lactam binding to a non-classical transpeptidase. *eLife* **11**, e73055 (2022).

46 Yang, W. & Drueckhammer, D. G. Understanding the relative acyl-transfer reactivity of oxoesters and thioesters: computational analysis of transition state delocalization effects. *J. Am. Chem. Soc.* **123**, 11004-11009 (2001).

47 Huguenin-Dezot, N., Alonzo, D. A., Heberlig, G. W., Mahesh, M., Nguyen, D. P., Dornan, M. H., Boddy, C. N., Schmeing, T. M. & Chin, J. W. Trapping biosynthetic acyl-enzyme intermediates with encoded 2,3-diaminopropionic acid. *Nature* **565**, 112-117 (2019).

48 Macheboeuf, P., Lemaire, D., Martins, A. D. S., Dideberg, O., Jamin, M. & Dessen, A. Trapping of an acyl–enzyme intermediate in a penicillin-binding protein (PBP)-catalyzed reaction. *J. Mol. Biol.* **376**, 405-413 (2008).

49 Alber, T., Petsko, G. A. & Tsernoglou, D. Crystal structure of elastase–substrate complex at −55 °C. *Nature* **263**, 297-300 (1976).

50 Lecoq, L., Dubée, V., Triboulet, S., Bougault, C., Hugonnet, J.-E., Arthur, M. & Simorre, J.-P. Structure of *Enterococcus faecium* L,D-Transpeptidase Acylated by Ertapenem Provides Insight into the Inactivation Mechanism. *ACS Chem. Biol.* **8**, 1140-1146 (2013).

51 Bianchet, M. A., Pan, Y. H., Basta, L. A. B., Saavedra, H., Lloyd, E. P., Kumar, P., Mattoo, R., Townsend, C. A. & Lamichhane, G. Structural insight into the inactivation of *Mycobacterium tuberculosis* non-classical transpeptidase Ldt_{Mt2} by biapenem and tebipenem. *BMC Biochem.* **18** (2017).

52 Liu, B., Schofield, C. J. & Wilmouth, R. C. Structural Analyses on Intermediates in Serine Protease Catalysis. *J. Biol. Chem.* **281**, 24024-24035 (2006).

53 Sauvage, E., Duez, C., Herman, R., Kerff, F., Petrella, S., Anderson, J. W., Adediran, S. A., Pratt, R. F., Frère, J.-M. & Charlier, P. Crystal Structure of the *Bacillus subtilis* Penicillin-binding Protein 4a, and its Complex with a Peptidoglycan Mimetic Peptide. *J. Mol. Biol.* **371**, 528-539 (2007).

54 Schanda, P., Triboulet, S., Laguri, C., Bougault, C. M., Ayala, I., Callon, M., Arthur, M. & Simorre, J.-P. Atomic Model of a Cell-Wall Cross-Linking Enzyme in Complex with an Intact Bacterial Peptidoglycan. *J. Am. Chem. Soc.* **136**, 17852-17860 (2014).

55 Paradis-Bleau, C., Markovski, M., Uehara, T., Lupoli, T. J., Walker, S., Kahne, D. E. & Bernhardt, T. G. Lipoprotein cofactors located in the outer membrane activate bacterial cell wall polymerases. *Cell* **143**, 1110-1120 (2010).

56 Typas, A., Banzhaf, M., van Saparoea, B. v. d. B., Verheul, J., Biboy, J., Nichols, R. J., Zietek, M., Beilharz, K., Kannenberg, K. & von Rechenberg, M. Regulation of peptidoglycan synthesis by outer-membrane proteins. *Cell* **143**, 1097-1109 (2010).

57 Egan, A. J., Jean, N. L., Koumoutsi, A., Bougault, C. M., Biboy, J., Sassine, J., Solovyova, A. S., Breukink, E., Typas, A. & Vollmer, W. Outer-membrane lipoprotein LpoB spans the periplasm to stimulate the peptidoglycan synthase PBP1B. *Proc. Natl. Acad. Sci. U.S.A.* **111**, 8197-8202 (2014).

58 Lupoli, T. J., Lebar, M. D., Markovski, M., Bernhardt, T., Kahne, D. & Walker, S. Lipoprotein activators stimulate *Escherichia coli* penicillin-binding proteins by different mechanisms. *J. Am. Chem. Soc.* **136**, 52-55 (2014).

59 Caveney, N. A., Caballero, G., Voedts, H., Niciforovic, A., Worrall, L. J., Vuckovic, M., Fonvielle, M., Hugonnet, J.-E., Arthur, M. & Strynadka, N. C. J. Structural insight into YcbB-mediated beta-lactam resistance in *Escherichia coli*. *Nat. Commun.* **10**, 1849 (2019).

60 Anderson, J. W., Adediran, S. A., Charlier, P., Nguyen-Distèche, M., Frère, J.-M., Nicholas, R. A. & Pratt, R. F. On the substrate specificity of bacterial DD-peptidases: evidence from two series of peptidoglycan-mimetic peptides. *Biochem. J.* **373**, 949-955 (2003).

61 Stefanova, M. E., Tomberg, J., Olesky, M., Höltje, J.-V., Gutheil, W. G. & Nicholas, R. A. *Neisseria gonorrhoeae* penicillin-binding protein 3 exhibits exceptionally high carboxypeptidase and β-lactam binding activities. *Biochemistry* **42**, 14614-14625 (2003).

62 Yang, H. & Yang, J. A review of the latest research on M^{pro} targeting SARS-COV inhibitors. *RSC Med. Chem.* **12**, 1026-1036 (2021).

63 Owen, D. R., Allerton, C. M. N., Anderson, A. S., Aschenbrenner, L., Avery, M., Berritt, S., Boras, B., Cardin, R. D., Carlo, A., Coffman, K. J., Dantonio, A., Di, L., Eng, H., Ferre, R., Gajiwala, K. S., Gibson, S. A., Greasley, S. E., Hurst, B. L., Kadar, E. P., Kalgutkar, A. S., Lee, J. C., Lee, J., Liu, W., Mason, S. W., Noell, S., Novak, J. J., Obach, R. S., Ogilvie, K., Patel, N. C., Pettersson, M., Rai, D. K., Reese, M. R., Sammons, M. F., Sathish, J. G., Singh, R. S. P., Steppan, C. M., Stewart, A. E., Tuttle, J. B., Updyke, L., Verhoest, P. R., Wei, L., Yang, Q. & Zhu, Y. An oral SARS-CoV-2 M^{pro} inhibitor clinical candidate for the treatment of COVID-19. *Science* **374**, 1586-1593 (2021).

64 Zheng, L. An efficient one-step site-directed and site-saturation mutagenesis protocol. *Nucleic Acids Research* **32**, e115-e115 (2004).

65 Inglis, S. R., Strieker, M., Rydzik, A. M., Dessen, A. & Schofield, C. J. A boronic-acid-based probe for fluorescence polarization assays with penicillin binding proteins and β-lactamases. *Anal. Biochem.* **420**, 41-47 (2012).

66 Winter, G. xia2: an expert system for macromolecular crystallography data reduction. *J. Appl. Crystallogr.* **43**, 186-190 (2010).

67 McCoy, A. J., Grosse-Kunstleve, R. W., Adams, P. D., Winn, M. D., Storoni, L. C. & Read, R. J. Phaser crystallographic software. *J. Appl. Crystallogr.* **40**, 658-674 (2007).

68 Grade2 version 1.5.0. (Cambridge, United Kingdom: Global Phasing Ltd., 2021).

69 Adams, P. D., Afonine, P. V., Bunkóczi, G., Chen, V. B., Davis, I. W., Echols, N., Headd, J. J., Hung, L.-W., Kapral, G. J., Grosse-Kunstleve, R. W., McCoy, A. J., Moriarty, N.

W., Oeffner, R., Read, R. J., Richardson, D. C., Richardson, J. S., Terwilliger, T. C. & Zwart, P. H. PHENIX: a comprehensive Python-based system for macromolecular structure solution. *Acta Crystallogr. D* **66**, 213-221 (2010).

Emsley, P., Lohkamp, B., Scott, W. G. & Cowtan, K. Features and development of Coot. *Acta Crystallogr. D* **66**, 486-501 (2010).

5.9 Statement of authorship

Title of Paper	Biochemical and crystallographic studies of Ldt_{Mt2} from *Mycobacterium tuberculosis* with its natural monomer substrate
Publication Status	□Published ■Submitted for Publication □Accepted for Publication □Unpublished and unsubmitted work written in a manuscript style
Publication Details	Manuscript submitted to Communications Biology.

Student Confirmation

Student Name:	Mariska de Munnik		
Contribution to the Paper	Conceptualisation and supervision of the cell wall isolation of the Ldt_{Mt2} substrates **1**-**3** was supported by Dr. Jürgen Brem (University of Oxford) and Dr. Pauline A. Lang (University of Oxford). DacA of *E. coli* was provided by Dr. Jürgen Brem. X-ray crystallography was supported by Dr. Pauline A. Lang. The bacterial growth conditions of *C. jeikeium* were determined by Dr. Karina Cavopiña Tapia (University of Oxford). Site-directed mutagenesis and synthesis of the peptidoglycan analogues **9** and **11** was supervised by Dr. Patrick Rabe (University of Oxford). All experimental work described here, data analysis, and preparation of the manuscript were carried out by me.		
Signature		Date	23/01/2024

Supervisor Confirmation

By signing the Statement of Authorship, you are certifying that the candidate made a substantial contribution to the publication, and that the description described above is accurate.

Prof Chris Schofield		
I'm happy to start that the candidate made the major and a very substantial contribution to the publication, and that the description described above is accurate.		
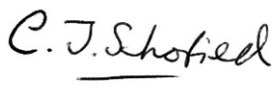	Date	23/01/2024

Chapter 6

How inhibition of L,D-transpeptidases and penicillin binding proteins leads to inhibition of mycobacteria

Manuscript IV

Unpublished manuscript.

Contents

6.1 Abstract 145

6.2 Introduction 146

6.3 Results 148

6.3.1 Inhibition of M*ycobacterium smegmatis* by inhibitors of Ldt_{Mt2} 148
6.3.2 Inhibition of *Mycobacterium smegmatis* by β-lactams 148
6.3.3 Dual treatment of *Mycobacterium smegmatis* with Ldt_{Mt2} inhibitors and β-lactams 149
6.3.4 Inhibition of the incorporation of fluorescent peptides 149
6.3.5 Biochemical inhibition of the *Mycobacterium tuberculosis* PBP3 153
6.3.6 Sulfonyl pyridines exhibit promising anti-mycobacterial activity 153

6.4 Discussion 154

6.5 Conclusion 157

6.6 Methods 157

6.6.1 Materials 157
6.6.2 Synthesis of fluorescent peptides 157
6.6.3 Recombinant protein production and purification 158
6.6.4 Bacterial strain and growth conditions 159
6.6.5 Susceptibility testing 159
6.6.6 Fluorescent peptide incorporation assays 159
6.6.7 Biochemical inhibition assays 160
6.6.8 Mass spectrometry assays 160

6.7 Data availability 161

6.8 References 161

6.9 Statement of authorship 165

6.1 Abstract

β-Lactams exhibit promising *in vitro* activity against mycobacteria, and have been considered for the treatment of tuberculosis, though evidence of *in vivo* efficacy is limited. Optimisation of β-lactams, or non-β-lactam inhibitors targeting the same cellular targets, will likely be required to obtain clinically relevant potency. In mycobacteria, relevant targets of β-lactams include the L,D-transpeptidases (Ldts), as well as the penicillin binding proteins (PBPs). Literature reports have suggested that dual inhibition of Ldts and PBPs may be required to reach potent antimycobacterial activity, though evidence for the precise roles of Ldt and PBP inhibition in the mechanism of β-lactams killing is limited. This report describes studies on the inhibition of *Mycobacterium smegmatis* (*Msm*) by β-lactams and reported inhibitors of Ldt_{Mt2} from *Mycobacterium tuberculosis*, and their inhibition of transpeptidase activity of Ldts and PBPs in live cells using fluorogenic substrate mimics. The apparent inhibition of transpeptidase activity of PBPs cannot be directly correlated to inhibition of *Msm* growth, while partial Ldt inhibition in combination with varying levels of PBP inhibition can putatively be correlated to inhibition of *Msm* growth. In addition, it was observed that the combination of the β-lactams meropenem or faropenem with selected Ldt_{Mt2} inhibitors increased activity against *Msm*. Further, sulfonyl pyridines were found to be promising inhibitors of *Msm*, though the activity of this compound class could not be related to inhibition of transpeptidase activity of Ldts or PBPs.

Key words: *Mycobacterium tuberculosis, Mycobacterium smegmatis*, L,D-transpeptidase, Penicillin Binding Protein, Ldt_{Mt2}, PBP3, bacterial cell wall biosynthesis, beta-lactam antibiotic, peptidoglycan, antimicrobial resistance (AMR).

6.2 Introduction

The discovery of β-lactam antibiotics represented a revolution in the treatment of infections, and still they are the most important class of antibiotics in clinical use.[1] β-Lactams act as mechanism based inhibitors of the penicillin-binding proteins (PBPs), a class of essential enzymes involved in the biosynthesis of the peptidoglycan layer which is present in every bacterial species, which have D,D-transpeptidase or D,D-carboxypeptidase activities (Figure 6.1A).[2,3] However, the effectivity of the β-lactams, including the penicillins, cephalosporins, carbapenems, penems, and monobactams (Figure 6.1B), is increasingly compromised by resistance, such as by the β-lactamases, a class of enzymes that catalyse hydrolysis of β-lactams (Figure 6.1A).[1] The presence of the chromosomally encoded Ambler class A β-lactamase BlaC is commonly accredited to be responsible for the historical view that *Mycobacterium tuberculosis* (*Mtb*), the causative agent of tuberculosis (TB) that is estimated to cause 1.6 million deaths per year,[4] is resistant to β-lactams.[5] However, promising *in vitro* activity of carbapenems in combination with the β-lactamase inhibitor clavulanic acid against *Mtb* have generated interest in reappraising β-lactams for the treatment of TB.[6-9]

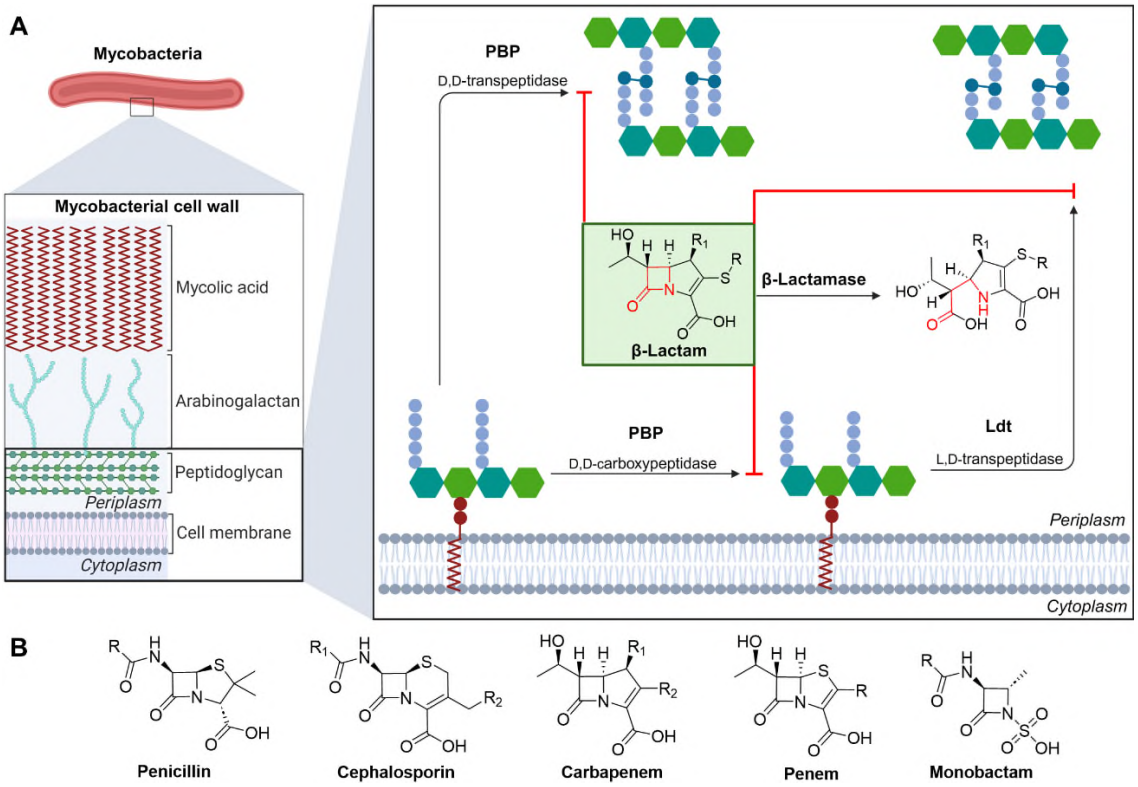

Figure 6.1. Inhibition of mycobacterial cell wall biosynthesis by β-lactams. A. Cross-links in the peptidoglycan layer of the mycobacterial cell wall can be inhibited by β-lactams, but β-lactamases confer resistance. Hexagons in green are GlcNAc, hexagons in teal are MurNAc, blue circles are amino acids, dark blue circles are cross-linked amino acids. The figure was created using BioRender.com. **B.** Core motifs of clinically relevant classes of β-lactams.

In addition to the presence of BlaC, the activity of β-lactams against *Mtb* is complicated by another class of enzymes important to the biosynthesis of the bacterial cell wall, that is the L,D-transpeptidases (Ldts). It was found that mycobacteria display an exceptionally high quantity of 3→3 cross-links in the peptidoglycan layer, catalysed by the Ldts, as opposed to the 4→3 cross-links catalysed by the PBPs (Figure 6.1A).[10] In *Mtb*, Ldt_{Mt2} has been identified as the Ldt that is essential for cell morphology and virulence, as well as resistance to β-lactams;[11] Ldts are not generally susceptible to inhibition by most β-lactams, though carbapenems and selected cephalosporins have been observed to inhibit Ldts.[12-15]

Mtb contains at least seven PBPs, as well as five Ldts.[16] It has been suggested that inhibition of just Ldt_{Mt2} should be sufficient to treat *Mtb*,[17] and in addition, several PBPs been identified as individually essential for growth (PBP3) and/or infection (e.g., PonA1, PonA2, and PBPA).[18,19] However, there is evidence that inhibition of both Ldts and PBPs may be required for therapeutically relevant inhibition of *Mtb*.[7-9] Dual treatment of amoxicillin/clavulanic acid and meropenem improved inhibition in both *Mtb* and *Mycobacterium smegmatis* (*Msm*).[20,21] An anecdotal report of a patient treated with the meropenem and amoxicillin/clavulanic acid combination describes the early clearance of *Mtb* from the sputum.[22] The effectivity of the combination of meropenem and amoxicillin may be attributed to the inhibition of both PBPs and Ldts. However, its place in the treatment of TB has not been established, with clinical trials yielding inconclusive results.[22-24] Findings suggest that for clinically relevant inhibition of *Mtb* via inhibition of PBPs and Ldts, inhibitors tailored towards these *Mtb* targets will be required.

Fluorescent derivatives of β-lactams have been used to identify the targets of β-lactams in the lysate of *Mtb*, revealing binding to both PBPs and Ldts.[25] Pidgeon *et al.* (2019) demonstrated the use of fluorescent substrate mimics of Ldts (TetraRh) and PBPs (PentaFl) to assess inhibition by β-lactams in whole cells of *Msm*.[26] Differentiating between Ldt and PBP inhibition, and correlating the enzymatic inhibition to the inhibition of growth may provide further insights into the essential targets in mycobacteria, and lead to focussed inhibitor optimisation efforts.

We were interested in further investigating the inhibition of mycobacteria by different classes of β-lactams, as well as selected Ldt_{Mt2} inhibitors recently reported by us.[27] We made use of *Msm*, a well validated model organism for *Mtb*,[28] which contains at least five PBPs and six Ldts, as well as the Ambler class A β-lactamase BlaS,[29-31] to assess the activity of β-lactams and Ldt_{Mt2} inhibitors, and their ability to inhibit PBPs and Ldts in live *Msm* cells, using PentaFl and TetraRh, respectively. The combination of selected Ldt_{Mt2} inhibitors with β-lactams yielded improved inhibitory results. Correlation of *Msm* inhibition to inhibition of PentaFl incorporation yielded inconclusive results, yet a modest correlation between the MIC and ~50% inhibition of Ldts was observed for all tested inhibitors except for the penicillins and sulfonyl pyridines.

6.3 Results

6.3.1 Inhibition of M*ycobacterium smegmatis* by inhibitors of Ldt_{Mt2}

A high-throughput screen for Ldt_{Mt2} identified a variety of diverse potent electrophilic compounds (Chapters 3 and 4).[27,32] Despite not being optimised for pharmacokinetic properties, a selection of the inhibitors were active against *Mtb* in macrophages.[27] We set out to assess the activities of these inhibitors against *Msm*, as well as representative Ldt_{Mt2} inhibitors that did not show activity against *Mtb*, the results of which are summarised in Table S4.1. Further, we included the established anti-TB therapeutics ethambutol, isoniazid, and rifampicin as control compounds, which manifested inhibition within reported values (Table S4.2);[28,33] note that the MIC value of isoniazid reported in literature varies significantly, and that MIC determination of *Msm* has thus far not been standardised by the Clinical & Laboratory Standards Institute (CLSI) or the European Committee on Antimicrobial Susceptibility Testing (EUCAST).[34]

The most potent activity against of *Msm* was observed with the sulfonyl pyridine **14**, with an MIC of 8 µg/mL. Interestingly, **14** was also among the most potent compounds tested against *Mtb*, though was not active against intracellular *Mtb*.[27] Cyanamide **9** exhibited promising activity with an MIC of 16 µg/mL. Ebsulfur **4** and cyanamide **8** manifested MICs of 32 µg/mL and 48 µg/mL, respectively. Poor activity against *Msm* was observed with **2**, **3**, **7** and **10** (MIC of 64 µg/mL). No inhibition of *Msm* was detected with **1**, **5** and **6** (MIC >128 µg/mL), despite exhibiting moderate inhibition of *Mtb*, while **11**-**13** were inactive both in *Msm* and *Mtb*.

6.3.2 Inhibition of *Mycobacterium smegmatis* by β-lactams

Next, we aimed to assess the activity of β-lactams from different classes against *Msm*. The penem faropenem, the carbapenems meropenem and imipenem, the cephalosporins ceftazidime and ceftriaxone, the penicillins ampicillin and amoxicillin, and the monobactam aztreonam were selected. The results are summarised in Table S4.3.

No significant activity was observed with the cephalosporins ceftazidime and ceftriaxone, the penicillins ampicillin and amoxicillin, and the monobactam aztreonam. This can likely be attributed to β-lactamase activity, as addition of clavulanic acid (100 µg/mL), which by itself did not inhibit *Msm* (MIC >128 µg/mL), significantly improved the activity of ampicillin and amoxicillin (MICs of 2 µg/mL and 1 µg/mL, respectively). However, little improvement of cephalosporin activity against *Msm* was observed. The carbapenems meropenem and imipenem manifested potent inhibition of *Msm* without the presence of clavulanic acid (MICs of 2 µg/mL and 0.125 µg/mL, respectively). The penem faropenem as well manifested

inhibition of *Msm* without the presence of clavulanic acid, though less potent than the carbapenems (MIC of 16 µg/mL).

6.3.3 Dual treatment of *Mycobacterium smegmatis* with Ldt_{Mt2} inhibitors and β-lactams

Aiming to assess whether synergy exist between the inhibition by the Ldt_{Mt2} inhibitors and the β-lactams, we tested the effect of dual treatment with the two inhibitor classes. Ldt_{Mt2} inhibitors with varying activity against *Msm* were selected (**2**, **4**, **7**-**9**, and **14**), and the inactive compounds **12** and **13** were as well included. Meropenem and faropenem were selected as representative β-lactams, based on their inhibitory potency against *Msm* in the absence of clavulanic acid, limiting the potential for interference.

Initially, three concentrations of Ldt_{Mt2} inhibitors were assessed (64 µg/mL, 16 µg/mL, and 4 µg/mL; Table S4.4) with selected β-lactams. The presence of **4**, **8** and **14**, increased the observed activities of both faropenem and meropenem. The increase in activity was apparently more pronounced with the combinations with faropenem, as evidenced by a decrease in the MIC of faropenem when combined with 4 µg/mL of **4** and **8**, which did not alter the MIC of meropenem. Further, in the presence of **9** (4 µg/mL), the MIC of faropenem was halved, but **9** (4 µg/mL) did not influence the MIC of meropenem. The presence of **2**, **7**, **12** and **14** had no effect on the MIC of faropenem or meropenem.

In particular, since compounds **4**, **8** and **14** exhibited increased antibacterial activity in combination with the β-lactams, a checkerboard analysis of these compounds in combination with faropenem or meropenem was performed (Table 6.1, Figure S4.1). In all cases, evidence for increased activity of the Ldt_{Mt2} inhibitor-β-lactam combination was observed against *Msm*. Based on the recommended interpretation of the determined Fractional Inhibitory Concentration (FIC) indexes of the assessed inhibitor combinations,[35] the results suggest that the combinations of Ldt_{Mt2} inhibitors with faropenem manifest a synergistic effect, with FIC indexes between 0.4-0.5, while the combinations with meropenem leads to an additive effect, with FIC indexes between 0.6-0.7.

6.3.4 Inhibition of the incorporation of fluorescent peptides

With the aim of investigating a potential correlation between inhibition of *Msm* growth and the inhibition of PBPs and Ldts, we employed the fluorescent probes PentaFl and TetraRh, which mimic the substrates for PBPs and Ldts, respectively (Figure 6.2A-B), as reported by Pidgeon *et al.* (2019).[26] Incubation of *Msm* with both the inhibitor of interest and PentaFl or TetraRh may lead to a dose-dependent reduction in fluorescent signal as a result of inhibition of PBPs or Ldts, respectively, as demonstrated with meropenem and ampicillin with *Msm*.[26]

Table 6.1. The combined effect of Ldt_{Mt2} inhibitors 4, 8, and 14 with faropenem (FAR) or meropenem (MER). FIC index represents the Fractional Inhibitory Concentration index of the indicated combinations of inhibitors, calculated using $FIC\ index = \frac{MIC\ A_{combination}}{MIC\ A_{alone}} + \frac{MIC\ B_{combination}}{MIC\ B_{alone}}$.

Ldt_{Mt2} inhibitor		MIC alone (μg/mL)	MIC combined with FAR (μg/mL)			MIC combined with MER (μg/mL)		
			Ldt_{Mt2} inhibitor	FAR	FIC index	Ldt_{Mt2} inhibitor	MER	FIC index
4	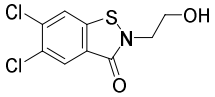	32	8	4	0.5	16	0.25	0.6
8	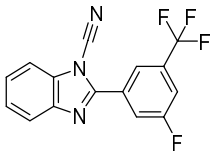	48	8	4	0.4	8	1	0.7
14	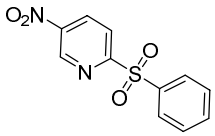	8	2	4	0.5	4	0.25	0.6
FAR	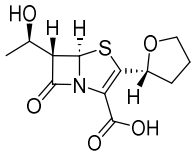	16	-	-	-	-	-	-
MER	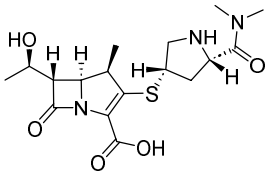	2	-	-	-	-	-	-

Optimisation of this assay was initiated by assessing the time-dependent incorporation of PentaFI and TetraRh into *Msm*. Upon incubation with 50 μM Penta-FI, a time-dependant increase in fluorescent signal was observed over 24 h; this was not present in the negative control, which consisted of a sample treated with meropenem-clavulanic acid (100 μg/mL; Figure S4.2A). Incubation with 50 μM Tetra-Rh exhibited high levels of fluorescent incorporation within 1 h, with little increase over 24 h, and a sample containing 100 μg/mL meropenem-clavulanic acid showed remaining fluorescence, albeit reduced (Figure S4.2B). When the concentration of TetraRh was reduced to 0.5 μM, a time-dependant increase in fluorescent signal could be observed over 24 h, and addition of 100 μg/mL meropenem-clavulanic acid led to samples devoid of a significant fluorescent signal (Figure S4.2D). As reported,[26] upon incubation of both TetraRh (50 μM) and PentaFI (50 μM), only incorporation of TetraRh was observed.

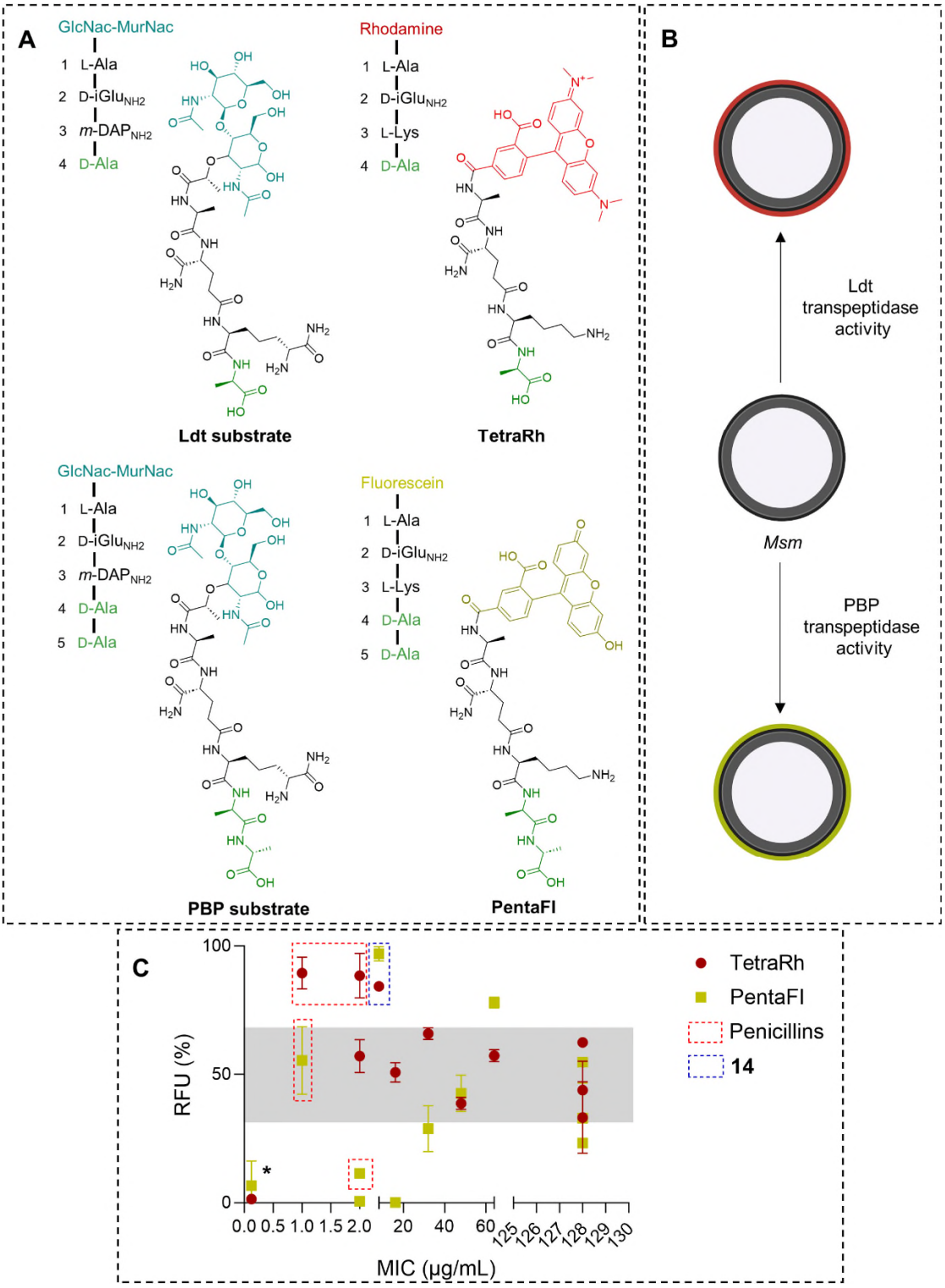

Figure 6.2. Fluorescent peptide incorporation assay investigating the inhibition of Ldts and PBPs in live *Mycobacterium smegmatis* cells. A. The fluorescent probes TetraRh and PentaFl, reported by Pidgeon *et al* (2019),[26] are based on the substrates of Ldts and PBPs, respectively. **B.** The fluorescent probes are incorporated upon Ldts and PBPs activity. **C**. When cells are treated with the inhibitors MIC, most compounds exhibit ~50% Ldt inhibition in combination with varying PBP inhibition. Exceptions are the penicillins (red borders) and **14** (blue borders). *Note that the MIC of imipenem was lower than the lowest tested concentration.

Out of all tested compounds, the carbapenem imipenem manifested the most potent apparent inhibition of both Ldts and PBPs in *Msm* (Figure S4.2A), abolishing incorporation of both TetraRh and PentaFl to the lowest tested concentration (0.5 µg/mL). Compared to imipenem, meropenem and faropenem exhibited equally potent inhibition of PBPs, though decreased inhibition of TetraRh incorporation. Meropenem exhibited slightly increased inhibition of Ldts over faropenem (40% inhibition by 2 µg/mL meropenem, and no inhibition by 2 µg/mL faropenem).

The cephalosporins ceftazidime and ceftriaxone manifested limited inhibition of TetraRh or PentaFl incorporation (Figure S4.2B), despite the presence of clavulanic acid (100 µg/mL); inhibition of TetraRh and PentaFl incorporation was only observed at concentrations above 64 µg/mL (38% and 39% inhibition, respectively). Ceftriaxone manifested inhibition of PentaFl incorporation at concentrations ≤ 8 µg/mL (27%), though 32 µg/mL was required to significantly inhibit TetraRh incorporation (42%). The cephalosporin **7** manifested 21% and 28% inhibition of PentaFl and TetraRh incorporation, respectively, at 32 µg/mL. Ampicillin and amoxicillin, tested also in the presence of clavulanic acid (100 µg/mL), exhibited potent inhibition of PentaFl incorporation, but required a concentration of 16 µg/mL to inhibit TetraRh incorporation (59% and 43% inhibition, respectively; Figure S4.2C). Clavulanic acid by itself exhibited limited apparent PBP (67% at 128 µg/mL) and Ldt inhibition (38% at 128 µg/mL; Figure S4.2D).

Ldt_{Mt2} inhibitors exhibited limited inhibition of TetraRh incorporation (Figure S4.2E), though when treated with the MIC substantial Ldt_{Mt2} inhibition was observed, for **4** and **8** (34% and 61%, respectively). An exception to this was **14**, which was a significantly more potent inhibitor of *Msm* with an MIC of 8 µg/mL, while only limited inhibition of Ldts was observed. Surprisingly, with both **4** and **8**, inhibition of PBPs (71% and 57%, respectively) was comparable to inhibition of Ldts.

Overall, no apparent correlation between PBP inhibition and activity against *Msm* was observed. When assessing the inhibition of PentaFl and TetraRh incorporation at the concentration of inhibitor corresponding to the MIC, the PentaFl incorporation manifest particularly varied levels of inhibition. Interestingly, however, the Ldts appear to be relatively consistently inhibited by most assessed inhibitors to an extent of approximately 50% (Figure 6.2C). Exceptions to this are the penicillins ampicillin and amoxicillin, as well as sulfonyl pyridine **14**. Note that the lowest concentration by which inhibition of fluorescent peptide incorporation by imipenem was assessed (0.5 µg/mL) was higher than the MIC (0.125 µg/mL), and was therefore not considered in this analysis. The combined results suggest that inhibition of PentaFl incorporation alone is apparently insufficient to prevent *Msm* growth, as in the case

of faropenem, meropenem, and ampicillin (nearly) complete inhibition is observed at significantly lower concentrations compared to the MIC. However, without access to a specific Ldt inhibitor it remains unclear if partial inhibition of Ldts alone is sufficient to prevent *Msm* growth.

6.3.5 Biochemical inhibition of the *Mycobacterium tuberculosis* PBP3

Following the observation that PBPs are apparently cellularly inhibited by the Ldt_{Mt2} inhibitors, particularly ebsulfur derivative **4**, we assessed the biochemical inhibition of the essential PBP of *Mtb*, that is PBP3,[18,36,37] by **1**-**14** (Table S4.5, Figure S4.4). Interestingly, despite cellular inhibition of PBPs of *Msm*, most assessed compounds manifested limited inhibitory potency ($pIC_{50} \leq 4.5$ for **2**-**4** and **9**) to no apparent inhibition ($pIC_{50} < 3.4$ for **1**, **5**, **8**, and **11**-**14**) of PBP3. An exception was the cephalosporin **7** (pIC_{50} of 6.1 ± 0.089). Interestingly, **7** has been shown to additionally be an inhibitor of Ldt_{Mt2} as well as BlaC, though not exhibiting potent anti-TB activity (Chapter 3, Chapter 7).[27]

Next, the inhibitory potency of the selected β-lactams considered here against *Msm* were assessed for inhibition of PBP3 of *Mtb* (Table S4.5, Figure S4.4). Most β-lactams potently inhibited PBP3, with pIC_{50} values around the upper assay limit (pIC_{50} of 6.8). Ceftazidime, known for potent inhibition of PBP3 from gram-negative bacteria,[38] was a slightly less potent inhibitor (pIC_{50} of 5.5). In addition, aztreonam, known for potent inhibition of PBP3 in gram-negative, but not gram-positive bacteria,[39] manifested low inhibition of *Mtb* PBP3 (pIC_{50} of 3.8).

6.3.6 Sulfonyl pyridines exhibit promising anti-mycobacterial activity

Of the Ldt_{Mt2} inhibitors, the sulfonyl pyridine **14** manifested the most potent inhibition of *Msm*, though in fluorescent peptide incorporation assays limited evidence for inhibition of PBPs and Ldts was observed, suggesting an alternative mechanism of action. However, as the activity was notable, we assessed the activity of a set of derivatives of **14** against *Msm* (Figure 6.3A, Table S4.6). In the case of **15**, the position of the nitrogen atom in the pyridine ring was altered, leading to a decrease of the MIC to 4 µg/mL. Derivatisation of the phenyl ring with a methyl (**16**) or bromide (**18**) did not affect the MIC, though derivatisation with a chloride (**17**) decreased the MIC to 4 µg/mL. Moving of the nitro group from *para* to *ortho* position (**19**) doubled the MIC to 16 µg/mL. Removing the nitro group abolished activity against *Msm*, regardless of the position of the nitrogen atom on the pyridine ring (**20**-**22**), or substitution of the nitro group with a methoxy group (**23**) or a nitrile in *para* (**24**) or *ortho* (**25**) position. Substitution of the phenylsulfonyl group with a chloride increased the MIC to 32 µg/mL (**26**),

and elimination of the nitro group in that moiety abolished activity against *Msm* (**27**). Nitrophenyl sulfonyl derivatives **28** and **29** did not exhibit activity against *Msm*.

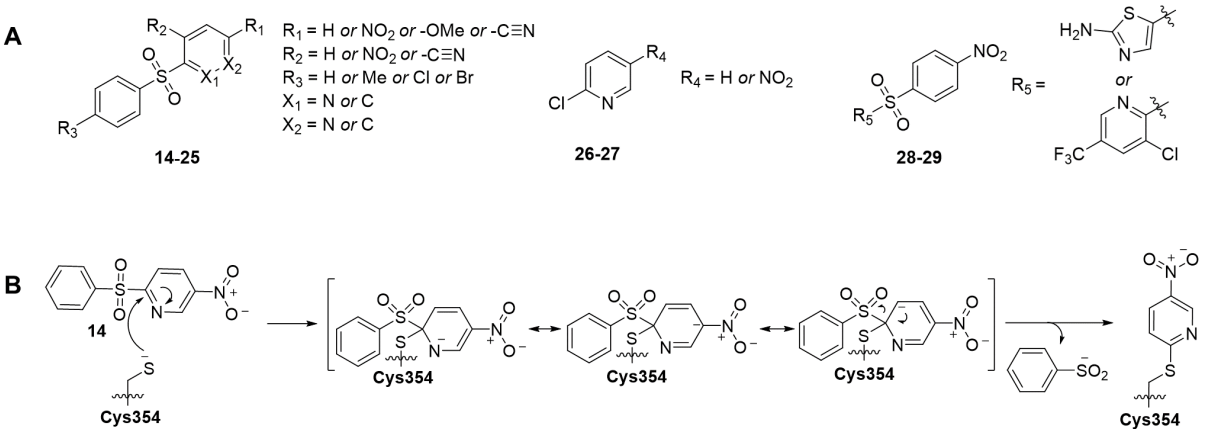

Figure 6.3. Sulfonyl pyridines are inhibitors of *Mycobacterium smegmatis*. A. Sulfonyl pyridines tested against *Msm*. Full compound structures and MICs can be found in Table S4.6. **B.** Mass spectrometry studies suggest selected sulfonyl pyridines to react with the nucleophilic cysteine of Ldt_{Mt2} via nucleophilic aromatic substitution, as exemplified with **14**.

Despite Ldts likely not being the target of the sulfonyl pyridines, their reactivity with the nucleophilic thiols of Ldt_{Mt2} (Table S4.6, Figure S4.5, S4.6), as well as with L-glutathione (GSH; Table S4.6, Figure S4.7) was examined, aiming to profile the electrophilic reactivity of this class of inhibitors. No correlation between reactivity with Ldt_{Mt2} or GSH and activity against *Msm* was observed, e.g., **15** was significantly less reactive with both Ldt_{Mt2} and GSH compared to **14**, while exhibiting increased activity against *Msm*. Alternatively, **24** manifested similar levels of reactivity as **15**, but no activity against *Msm* was observed. Protein-observed solid-phase extraction MS (SPE-MS) assays with Ldt_{Mt2} showed that **14**, **16**-**19**, **24**, **25** and **29** all reacted with Ldt_{Mt2} through nucleophilic aromatic substitution of the sulfonyl group on the pyridine ring (Figure 6.3B, Table S4.6, Figure S4.8). By contrast, the mass shift observed upon incubation with **15** corresponds to nucleophilic substitution at the nitro group instead of the sulfonyl group. The derivatives **20**-**23**, **26** and **27** did not react with Ldt_{Mt2}; of these only **26** exhibited moderate activity against *Msm* (MIC 32 µg/mL).

6.4 Discussion

Though historically β-lactams have not been deemed useful in the treatment of TB, promising *in vitro* activity against *Mtb* have led to the re-examination of this paradigm.[7-9] However, clinical studies have been inconclusive on the place of β-lactam antibiotics in the treatment of TB.[22,24,40] The results imply that optimisation of inhibitors tailored towards *Mtb* may be required. Due to the high level of 3→3 cross-links in the peptidoglycan layer catalysed by the Ldts, Ldts

are a promising target for the development of inhibitors, though reports suggest that inhibition of both Ldts and PBPs may be required.[20] Insights into the mechanism of action of β-lactams will enable targeted efforts into the optimisation of β-lactams, as well as towards the development of non-β-lactam inhibitors against *Mtb*.

We performed studies with *Msm*, a validated model organism for *Mtb*.[28] The main Ldt of *Msm*, LdtC,[41] which is additionally the main contributor to TetraRh incorporation,[26] is a close homolog to Ldt_{Mt5}, while in *Mtb* Ldt_{Mt2} is the main Ldt, which is a close homolog to *Msm* LdtB.[42] However, superimposition of Ldt_{Mt2} with a structural prediction model of LdtC created with AlphaFold,[43] manifest great structural resemblance of the active site domains (RMSD 0.75 Å) and key residues (Figure S4.9A). PBP3 of *Msm* and *Mtb* share 79% sequence similarity, and prominent structural resemblance of the active site domains (RMSD 0.48 Å; Figure S4.9B).[44] It has yet to be determined which PBPs in *Msm* contribute to the incorporation of PentaFl into the cell wall, as the third residue of PentaFl differs from the natural substrate (an L-Lysine residue rather than a *m*-DAP residue) and it is unknown if all PBPs of *Msm* can accept this as a substrate. However, considering the assay principle, it can be assumed that only PBPs with D,D-transpeptidase activity are assessed, and not those with D,D-carboxypeptidase activity.

Carbapenems and penems are known for being able to inhibit both Ldts and PBPs.[45-48] We observed evidence that faropenem and meropenem inhibit the Ldts as well as PBPs, though more potent inhibition of PBPs was observed. However, the MICs manifested a modest correlation to (partial) inhibition of Ldts, which was not established with PBPs, putatively suggesting Ldts to be a better target, though further research will be needed to establish this. Faropenem has been identified as the most potent inhibitor of Ldts,[13,42,49] though we observe reduced effectivity over meropenem, and particularly imipenem against Ldts in live *Msm* cells. We observed that against *Msm*, imipenem was the most potent inhibitor of Ldts, as well as manifesting the lowest MIC out of the tested compounds.

Interestingly, the penicillins exhibit significant inhibition of *Msm* in the presence of clavulanic acid, though the fluorescent peptide incorporation assays exhibit a different pattern to the other inhibitors assessed (apart from **14**), particularly exhibiting significantly less inhibition of Ldts. Amoxicillin displayed increased activity against *Msm* over ampicillin (MIC of 1 µg/mL and 2 µg/mL, respectively), though treatment of 1 µg/mL amoxicillin to *Msm* led to ~50% inhibition of PentaFl incorporation and no inhibition of TetraRh incorporation. This may suggest that inhibition of mycobacteria by penicillins follow a different mechanism of action than the targeting of transpeptidases. Previously, the added effect of meropenem and amoxicillin and clavulanic acid has been attributed to the inhibition of Ldts and PBPs.[20] Our results suggest that meropenem alone is a potent inhibitor of the transpeptidase activity of PBPs and Ldts,

while penicillins are less potent inhibitors of transpeptidase PBPs and do not inhibit Ldts, and the apparent (possible) synergistic effect may be due to the combination with an alternative mechanism of action, such as inhibition of D,D-carboxypeptidases, or other mechanisms of β-lactam killing.[5]

Interestingly, while we observed that **4** and **8** apparently inhibit both Ldts and PBPs in *Msm* whereas **14** apparently functions via an alternative mechanism of action, **4**, **8**, and **14** all manifested similar levels of synergistic or additive inhibition in the dual treatment with faropenem or meropenem. Further research will need to be done to elucidate the mechanism behind the benefit of dual treatment of β-lactams and **14**, while in the case of **4** and **8** the increased inhibition of Ldts and PBPs in the presence of β-lactams is likely to play a role. However, both **4** and **8** contain a reactive functional group, and are likely non-specific compounds, and the development of highly potent and specific inhibitors for Ldts will aid the elucidation of their interplay with PBPs in the inhibition of mycobacteria.

The major β-lactamase of *Msm*, BlaS, has ~40% sequence similarity and high structural homology with BlaC, the major β-lactamase of *Mtb*, and exhibits particularly efficient penicillinase and cephalosporinase activity.[31] Similarly to BlaC, BlaS can be inhibited by clavulanic acid.[31] However, *Msm* also expresses a cephalosporinase, BlaE, which is less sensitive to clavulanic acid inhibition,[31] which may explain the resistance to cephalosporins as observed by us, despite the presence of clavulanic acid.

Following the observation that Ldt_{Mt2} inhibitors were able to inhibit both Ldts and PBPs in *Msm*, we assessed the biochemical inhibition of the essential PBP3 of *Mtb*. Interestingly, inhibition of PBP3 by the Ldt_{Mt2} inhibitors was limited. Potent inhibition was observed with most tested β-lactams, apart from aztreonam, which has previously reported to interact with PBP3 in a crystal structure.[44] Aztreonam is known as a potent inhibitor of gram-negative, but not gram-positive bacteria.[39] *Mtb*, as an acid-fast bacterium, falls in neither these categories, though they can be considered a subclass of gram-positive bacteria.[50]

The inhibition of sulfonyl pyridine **14** could not be linked to inhibition of PBPs or Ldts, but did exhibit surprisingly potent inhibition of *Msm*, though likely through a different mechanism of action. Inhibitory studies with derivatives of **14** suggest that the nitropyridine sulfonyl moiety was particularly important to inhibitory activity against *Msm*, as removal of the nitro group or exchange with other electron withdrawing groups, or exchange of the pyridine ring for a phenyl ring, abolished activity. Reactivity with nucleophilic cysteine residues (as evidenced through reactivity with GSH and Ldt_{Mt2}) could not be correlated to activity against *Msm*. Identification of the mechanism of action of the sulfonyl pyridine compounds is of interest.

6.5 Conclusion

The results presented here (and described in Chapter 2) show that certain β-lactams exhibit promising activity against mycobacteria, though optimisation will likely be required to obtain clinically relevant potency. Relevant targets for β-lactams in mycobacteria include the PBPs and the Ldts. Reports have suggested that dual inhibition of Ldts and PBPs may be required. Our results suggest that inhibition of transpeptidase activity of PBPs cannot be directly correlated to inhibition of *Msm* growth, while partial Ldt inhibition in combination with varying levels of PBP inhibition can be putatively correlated to inhibition of *Msm* growth. In addition, we identified the sulfonyl pyridines as promising inhibitors of *Msm*, though they could not be related to inhibition of transpeptidase activity of Ldts or PBPs.

6.6 Methods

6.6.1 Materials

S2d and 2-(6-(((2,4-dinitrophenyl)sulfonyl)oxy)-3-oxo-3H-xanthen-9-yl)benzoic acid (Probe **1**) were synthesised as described.[51-53] **1**-**14** were obtained from the GSK HTS compound library. **15**, **19**, and **21**-**25** were from Cortex Organics, **20** and Fmoc- D-iGln-OH were from AmBeed, **16**-**18** and **29** were from Key Organics, **27** and **28** were from Enamine, and 5(6)-TAMRA was from MedChemExpress. Faropenem was from Fluorochem Ltd, meropenem was from Glentham Life Sciences, ceftazidime was from TOKU-E, ceftriaxone and aztreonam were from Molekula Ltd, ampicillin was from Apollo Scientific, and ampicillin was from Alfa Aesar. Isoniazid, ethambutol, and rifampicin were from Cambridge Bioscience Ltd; all other compounds were from Merck.

6.6.2 Synthesis of fluorescent peptides

PentaFl (D-Ala-D-Ala-L-Lys-D-iGln-L-Ala-Fluorescein) and TetraRh (D-Ala-L-Lys-D-iGln-L-Ala-Rhodamine) were synthesised by solid phase peptide synthesis using a Liberty Blue Automated Microwave Peptide Synthesiser, following stepwise coupling reactions to D-Alanine-Wang resin (715 mg, 0.5 mmol). The respective amino acids D-Ala (1.5 mmol, 3 eq.), L-Lys (2.5 mmol, 5 eq.), D-iGln (2.5 mmol, 5 eq.), and L-Ala (2.5 mmol, 5 eq.), were coupled using the standard procedure with N,N-diisopropylethylamine (DIPEA) in ethyl cyanohydroxyiminoacetate (Oxyma, 1 M; DIPEA/Oxyma 1.5 % (*v*/*v*)) and 7.8% (*v*/*v*) N,N′-diisopropylcarbodiimide (DIC) in DMF. After each coupling step, the resin was washed with DMF and the Fmoc group was deprotected with 20% (*v*/*v*) piperidine in DMF using the

standard deprotection procedure. The fluorescent tags 5(6)-carboxyfluorescein (2 eq) and 5(6)-TAMRA (2 eq) were coupled manually, using hexafluorophosphate benzotriazole tetramethyl uronium (HBTU; 2 eq) and DIPEA (6 eq). The resin bound TetraRh and PentaFl were washed with dichloromethane (DCM), methanol and DCM, and treated with a 5 mL solution of 2:1 TFA/DCM (2 h, rt). Solvents were removed by evaporation *in vacuo* and purified by HPLC on a C_{18} column (5 µm, 10 x 150 mm; SunFire, Waters) at a flowrate of 3 mL/min with a gradient of 98% (*v*/*v*) buffer A (0.1% (*v*/*v*) formic acid in H_2O) and 2% buffer B (0.1% (*v*/*v*) formic acid in acetonitrile) to 50% buffer A and 50% buffer B. TetraRh and PentaFl eluted after 18.8 min and 22.1 min, respectively. TetraRh and PentaFl were characterised by ^{1}H and ^{13}C NMR (Figure S4.11-12, Table S4.7-8).

6.6.3 Recombinant protein production and purification

Ldt_{Mt2} was produced in *Escherichia coli* and purified (>95% purity by SDS-PAGE analysis) as previously described.[54]

A codon-optimised synthetic gene (GeneArt, Thermo Fisher Scientific) encoding for *Mtb* PBP3 Δ1-122 was amplified and cloned into the expression vector pCold using Sal1-HF (New England BioLabs) and Not1-HF (New England BioLabs) digestion and ligation using T4 DNA ligase (New England BioLabs) according to the manufacturer's protocol. The ampicillin resistance gene of the vector was exchanged for the kanamycin resistance gene using Gibson Assembly,[55] and transformed with *Escherichia coli* BL21(DE3).

A culture of *E. coli* BL21(DE3) pCold-PBP3 Δ1-122 was grown at 37 °C at 180 rpm in 2xTY media (with 50 µg/mL kanamycin) to OD_{600} of 0.6. Isopropyl β-D-thiogalactopyranoside (IPTG) (0.5 mM) was then added and the culture was incubated at 15 °C at 180 rpm for an additional 16 h. Cells were collected by centrifugation (11,000 x g, 8 min), and stored at -80 °C. The cell pellet was resuspended in HisTrap Buffer A (50 mM Tris-HCl pH 7.5, 500 mM NaCl, 20 mM imidazole) in the presence of DNase I, and lysed using a Continuous Flow Cell Disruptor (Constant Systems, 25 kpsi). The lysates were centrifuged (32,000 x g, 20 min), passed through a 0.45 µm filter, and loaded onto a 5 mL HisTrap column (GE Life Sciences) that had been pre-equilibrated in HisTrap Buffer A. The column was washed with HisTrap Buffer A, followed by a gradient running from 0 % to 100 % (*v*/*v*) HisTrap Buffer B (50 mM Tris-HCl pH 7.5, 500 mM NaCl, 500 mM imidazole). Fractions containing PBP3 (as observed by SDS-PAGE) were combined, the buffer was exchanged to HisTrap Buffer A, and the HisTag was cleaved using recombinant 3C protease at 4 °C, over 12 h. The HisTag cleaved PBP3 was passed through a 5 mL HisTrap column (GE Life Sciences) and subsequently loaded onto a 300 mL Superdex 75 column (GE Life Sciences) pre-equilibrated in gel filtration buffer (50 mM

Tris-HCl pH 7.5, 500 mM NaCl), and eluted over 1 column volume in gel filtration buffer. The identity and purity of PBP3 was confirmed by mass spectrometry (calculated mass 60148 Da, observed deconvoluted mass 60152 Da) and SDS-PAGE (>95% purity; Appendix V).

6.6.4 Bacterial strain and growth conditions

All experiments using *Msm* refer to strain ATCC 607. *Msm* was grown on Columbia blood agar supplemented with 5% sheep blood at 37 °C. Liquid cultures of *Msm* were grown in Middlebrook 7H9 broth supplemented with 0.1% (*v*/*v*) Tween-80, 0.5 % (*w*/*v*) bovine albumin fraction V, 0.2% (*w*/*v*) dextrose, and 0.3 % (*v*/*v*) catalase (beef).

6.6.5 Susceptibility testing

Antibiotic susceptibility was assessed using the broth microdilution method for MIC determination. The effect of two combined inhibitors was determined using a checkerboard assay.[56] A liquid culture of *Msm* was incubated at 37 °C with aeration for 48 h, after which the culture had reached the stationary phase (Figure S4.10), and subsequently diluted in media containing diverse concentrations of the compound of interest (final concentrations of 0.25 - 128 µg/mL, total volume 200 µL) to OD_{600} 0.05 in a sterile 96-well plate (Corning Costar, flat-bottom, cell culture-treated). Positive controls consisted of samples containing only *Msm* culture in media and negative controls omitted *Msm* inoculation and contained only media. In line with reported procedures for *Msm* MIC assays,[28,33,57] we applied an incubation period of 4 days to all MIC experiments. Then, resazurin (20 µL of a 150 µg/mL stock solution) was added to all wells, and incubated at 37 °C for 12 h. The MIC was defined as the lowest concentration at which no resazurin colour change was observed. All assays were performed in triplicate.

6.6.6 Fluorescent peptide incorporation assays

A 5 mL culture of *Msm* was grown at 37 °C to an OD_{600} of 0.8. This culture (196 µL) was added to a sterile 96-well plate (Corning Costar, flat-bottom, cell culture-treated). To this was added either TetraRh (2 µL, to a final concentration of 0.5 µM) or PentaFI (2 µL, to a final concentration of 5 µM), and varying concentrations of the compound of interest (2 µL, final concentrations ranging from 0.5 µg/mL to 256 µg/mL). A positive control (no inhibitor) and a negative control (addition of 100 µg/mL meropenem and 100 µg/mL clavulanic acid) were included. This was incubated at 37 °C for 24 h. Then, samples were washed in PBS (200 µL, 3x), and fixated with 2% (*v*/*v*) in PBS for 30 min. The *Msm* cells were washed PBS (200 µL, 3x), and resuspended in 200 µL PBS. The fluorescence of the *Msm* cells was analysed using

an LSRFortessa™ X-20 (BD Biosciences). Cells treated with TetraRh were assessed using a 561 nm laser and a 586/15 bandpass filter. Cells treated with PentaFl were assessed using a 488 nm laser and a 530/30 bandpass filter. For each dataset 10,000 events were counted. Data were analysed using FlowJo™ Software. All assays were performed in duplicate.

6.6.7 Biochemical inhibition assays

Ldt_{Mt2} dose-response assays were performed as described.[51] In brief, Ldt_{Mt2} (100 nM) was incubated with varying concentrations of the compound of interest (final concentrations ranging between 400 µM and 20.3 nM) for 10 min in the assay buffer (50 mM HEPES, pH 7.2, 0.01% (*v*/*v*) Triton X-100) and then assayed using Probe **1** (25 µM).

The 'intrinsic' thiol reactivity (k_{chem}) was determined as described.[27] In brief, L-Glutathione (500 nM) was incubated with varying concentrations of the compound of interest (final concentrations ranging between 400 µM and 20.3 nM) and Probe **1** (10 µM) for 15 h in assay buffer (50 mM HEPES, pH 7.2, 0.01% (*v*/*v*) Triton X-100).

The second-order rate constant of covalent target inactivation (k_{inact}/K_I) of Ldt_{Mt2} was determined as described.[27] In brief, Ldt_{Mt2} (100 nM) was incubated with varying concentrations of the compound of interest (final concentrations ranging between 400 µM and 20.3 nM) and Probe **1** (10 µM) for 3.5 h in assay buffer (50 mM HEPES, pH 7.2, 0.01% (*v*/*v*) Triton X-100).

Dose-response assays of PBP3 were assessed using the fluorometric S2d assay.[58-60] PBP3 (300 nM) in assay buffer (50 mM HEPES pH 7.4, 100 mM NaCl, 0.01% (*v*/*v*) Triton X-100) was incubated with varying concentrations of the compound of interest (final concentrations ranging between 400 µM and 20.3 nM) for 10 minutes in a black polystyrene, flat-bottomed 384-well µ-clear plate (clear bottomed, Greiner Bio-One, part number 781096). Then, a mixture containing S2d (1.5 mM), monobromobimane (mBBr; 0.05 mM), and D-Ala (1 mM) in assay buffer was added (final volume 25 µL). The fluorescence signal was measured using a BMG Labtech CLARIOstar instrument with λ_{ex}=394 nm and λ_{em}=490 nm. Data were analysed using Prism (GraphPad).

6.6.8 Mass spectrometry assays

Protein-observed SPE-MS experiments with Ldt_{Mt2} were performed as described.[27] In brief, Ldt_{Mt2} (1 µM) in 50 mM tris, pH 7.5 was incubated with an inhibitor (100 µM) at room temperature. Mass spectrometry was performed using a RapidFire200 integrated autosampler/solid phase extraction (SPE) system (Agilent Technologies) employing a C4

cartridge (Agilent Technologies), coupled to an API40000 triple quadrupole mass spectrometer (Applied Biosystems) operating in the positive ionisation mode.

6.7 Data availability

Data supporting this manuscript are provided in the Supplementary Information (Appendix IV).

6.8 References

1 Bush, K. & Bradford, P. A. β-Lactams and β-Lactamase Inhibitors: An Overview. *Cold Spring Harb. Perspect. Med.* **6** (2016).

2 Georgopapadakou, N. H. & Liu, F. Y. Penicillin-binding proteins in bacteria. *Antimicrob. Agents Chemother.* **18**, 148-157 (1980).

3 Sauvage, E., Kerff, F., Terrak, M., Ayala, J. A. & Charlier, P. The penicillin-binding proteins: structure and role in peptidoglycan biosynthesis. *FEMS Microbiol. Rev.* **32**, 234-258 (2008).

4 Global tuberculosis report 2022. . Report No. Licence: CC BY-NC-SA 3.0 IGO, (Geneva: World Health Organization, 2022).

5 Wivagg, C. N., Bhattacharyya, R. P. & Hung, D. T. Mechanisms of β-lactam killing and resistance in the context of *Mycobacterium tuberculosis*. *J. Antibiot.* **67**, 645-654 (2014).

6 Hugonnet, J.-E., Tremblay, L. W., Boshoff, H. I., Barry, C. E. & Blanchard, J. S. Meropenem-Clavulanate Is Effective Against Extensively Drug-Resistant *Mycobacterium tuberculosis*. *Science* **323**, 1215-1218 (2009).

7 Gun, M. A., Bozdogan, B. & Coban, A. Y. Tuberculosis and beta-lactam antibiotics. *Future Microbiol.* **15**, 937-944 (2020).

8 Story-Roller, E. & Lamichhane, G. Have we realized the full potential of β-lactams for treating drug-resistant TB? *IUBMB Life* **70**, 881-888 (2018).

9 Jaganath, D., Lamichhane, G. & Shah, M. Carbapenems against *Mycobacterium tuberculosis*: a review of the evidence. *Int. J. Tuberc. Lung Dis.* **20**, 1436-1447 (2016).

10 Lavollay, M., Arthur, M., Fourgeaud, M., Dubost, L., Marie, A., Veziris, N., Blanot, D., Gutmann, L. & Mainardi, J. L. The Peptidoglycan of Stationary-Phase *Mycobacterium tuberculosis* Predominantly Contains Cross-Links Generated by L,D-Transpeptidation. *J. Bacteriol.* **190**, 4360-4366 (2008).

11 Gupta, R., Lavollay, M., Mainardi, J.-L., Arthur, M., Bishai, W. R. & Lamichhane, G. The *Mycobacterium tuberculosis* protein Ldt_{Mt2} is a nonclassical transpeptidase required for virulence and resistance to amoxicillin. *Nat. Med.* **16**, 466-469 (2010).

12 Kumar, P., Kaushik, A., Lloyd, E. P., Li, S.-G., Mattoo, R., Ammerman, N. C., Bell, D. T., Perryman, A. L., Zandi, T. A., Ekins, S., Ginell, S. L., Townsend, C. A., Freundlich, J. S. & Lamichhane, G. Non-classical transpeptidases yield insight into new antibacterials. *Nat. Chem. Biol.* **13**, 54-61 (2017).

13 Steiner, E. M., Schneider, G. & Schnell, R. Binding and processing of β-lactam antibiotics by the transpeptidase Ldt_{Mt2} from *Mycobacterium tuberculosis*. *FEBS J.* **284**, 725-741 (2017).

14 Cordillot, M., Dubée, V., Triboulet, S., Dubost, L., Marie, A., Hugonnet, J.-E., Arthur, M. & Mainardi, J.-L. In vitro cross-linking of *Mycobacterium tuberculosis* peptidoglycan by L,D-transpeptidases and inactivation of these enzymes by carbapenems. *Antimicrob. Agents Chemother.* **57**, 5940-5945 (2013).

15 Triboulet, S., Arthur, M., Mainardi, J. L., Veckerlé, C., Dubée, V., Nguekam Moumi, A., Gutmann, L., Rice, L. B. & Hugonnet, J. E. Inactivation Kinetics of a New Target of β-Lactam Antibiotics. *J. Biol. Chem.* **286**, 22777-22784 (2011).

16 Cole, S. T., Brosch, R., Parkhill, J., Garnier, T., Churcher, C., Harris, D., Gordon, S. V., Eiglmeier, K., Gas, S., Barry, C. E., Tekaia, F., Badcock, K., Basham, D., Brown, D., Chillingworth, T., Connor, R., Davies, R., Devlin, K., Feltwell, T., Gentles, S., Hamlin, N., Holroyd, S., Hornsby, T., Jagels, K., Krogh, A., McLean, J., Moule, S., Murphy, L., Oliver, K., Osborne, J., Quail, M. A., Rajandream, M. A., Rogers, J., Rutter, S., Seeger, K., Skelton, J., Squares, R., Squares, S., Sulston, J. E., Taylor, K., Whitehead, S. & Barrell, B. G. Deciphering the biology of *Mycobacterium tuberculosis* from the complete genome sequence. *Nature* **393**, 537-544 (1998).

17 Gupta, R., Lavollay, M., Mainardi, J. L., Arthur, M., Bishai, W. R. & Lamichhane, G. The *Mycobacterium tuberculosis* protein Ldt_{Mt2} is a nonclassical transpeptidase required for virulence and resistance to amoxicillin. *Nat. Med.* **16**, 466-469 (2010).

18 Botta, G. A. & Park, J. T. Evidence for involvement of penicillin-binding protein 3 in murein synthesis during septation but not during cell elongation. *J. bacteriol.* **145**, 333-340 (1981).

19 DeJesus, M. A., Gerrick, E. R., Xu, W., Park, S. W., Long, J. E., Boutte, C. C., Rubin, E. J., Schnappinger, D., Ehrt, S., Fortune, S. M., Sassetti, C. M. & Ioerger, T. R. Comprehensive Essentiality Analysis of the *Mycobacterium tuberculosis* Genome via Saturating Transposon Mutagenesis. *mBio* **8**, 10.1128/mbio.02133-02116 (2017).

20 Baranowski, C., Welsh, M. A., Sham, L. T., Eskandarian, H. A., Lim, H. C., Kieser, K. J., Wagner, J. C., McKinney, J. D., Fantner, G. E., Ioerger, T. R., Walker, S., Bernhardt, T. G., Rubin, E. J. & Rego, E. H. Maturing *Mycobacterium smegmatis* peptidoglycan requires non-canonical crosslinks to maintain shape. *Elife* **7** (2018).

21 Gonzalo, X. & Drobniewski, F. Is there a place for β-lactams in the treatment of multidrug-resistant/extensively drug-resistant tuberculosis? Synergy between meropenem and amoxicillin/clavulanate. *J. Antimicrob. Chemother.* **68**, 366-369 (2013).

22 Diacon, A. H., van der Merwe, L., Barnard, M., von Groote-Bidlingmaier, F., Lange, C., García-Basteiro, A. L., Sevene, E., Ballell, L. & Barros-Aguirre, D. β-Lactams against Tuberculosis — New Trick for an Old Dog? *N. Engl. J. Med.* **375**, 393-394 (2016).

23 Sotgiu, G., D'Ambrosio, L., Centis, R., Tiberi, S., Esposito, S., Dore, S., Spanevello, A. & Migliori, G. B. Carbapenems to Treat Multidrug and Extensively Drug-Resistant Tuberculosis: A Systematic Review. *Int. J. Mol. Sci.* **17**, 373 (2016).

24 Tiberi, S., Sotgiu, G., D'Ambrosio, L., Centis, R., Abdo Arbex, M., Alarcon Arrascue, E., Alffenaar, J. W., Caminero, J. A., Gaga, M., Gualano, G., Skrahina, A., Solovic, I., Sulis, G., Tadolini, M., Alarcon Guizado, V., De Lorenzo, S., Roby Arias, A. J., Scardigli, A., Akkerman, O. W., Aleksa, A., Artsukevich, J., Auchynka, V., Bonini, E. H., Chong Marín, F. A., Collahuazo López, L., de Vries, G., Dore, S., Kunst, H., Matteelli, A., Moschos, C., Palmieri, F., Papavasileiou, A., Payen, M. C., Piana, A., Spanevello, A., Vargas Vasquez, D., Viggiani, P., White, V., Zumla, A. & Migliori, G. B. Comparison of effectiveness and safety of imipenem/clavulanate- versus meropenem/clavulanate-containing regimens in the treatment of MDR- and XDR-TB. *Eur. Respir. J.* **47**, 1758-1766 (2016).

25 Levine, S. R. & Beatty, K. E. Investigating β-Lactam Drug Targets in *Mycobacterium tuberculosis* Using Chemical Probes. *ACS Infect. Dis.* **7**, 461-470 (2021).

26 Pidgeon, S. E., Apostolos, A. J., Nelson, J. M., Shaku, M., Rimal, B., Islam, M. N., Crick, D. C., Kim, S. J., Pavelka, M. S., Kana, B. D. & Pires, M. M. L,D-Transpeptidase Specific Probe Reveals Spatial Activity of Peptidoglycan Cross-Linking. *ACS Chem. Biol.* **14**, 2185–2196 (2019).

27 de Munnik, M., Lang, P. A., De Dios Antos, F., Cacho, M., Bates, R. H., Brem, J., Rodríguez-Miquel, B. & Schofield, C. J. High-Throughput Screen with the L,D-transpeptidase Ldt_{Mt2} of *Mycobacterium tuberculosis* Reveals Novel Classes of Covalently Reacting Inhibitors *Chem. Sci.* **14**, 7262-7278 (2023).

28 Lelovic, N., Mitachi, K., Yang, J., Lemieux, M. R., Ji, Y. & Kurosu, M. Application of Mycobacterium smegmatis as a surrogate to evaluate drug leads against Mycobacterium tuberculosis. *J. Antibiot.* **73**, 780-789 (2020).

29 Yabu, K., Ochiai, T. & Kaneda, S. Penicillin-binding proteins in *Mycobacterium smegmatis*. *FEMS Microbiol. Lett.* **25**, 307-310 (1984).

30 Sanders, A. N., Wright, L. F. & Pavelka, M. S. Genetic characterization of mycobacterial L,D-transpeptidases. *Microbiology* **160**, 1795-1806 (2014).

31 Flores, A. R., Parsons, L. M. & Pavelka, M. S. Genetic analysis of the beta-lactamases of *Mycobacterium tuberculosis* and *Mycobacterium smegmatis* and susceptibility to beta-lactam antibiotics. *Microbiology (Reading, Engl.)* **151**, 521-532 (2005).

32 de Munnik, M., Lithgow, J., Brewitz, L., Christensen, K. E., Bates, R. H., Rodriguez-Miquel, B. & Schofield, C. J. αβ,α'β'-Diepoxyketones are mechanism-based inhibitors of nucleophilic cysteine enzymes. *Chem. Commun. (Camb)* **59**, 12859-12862 (2023).

33 Agrawal, P., Miryala, S. & Varshney, U. Use of Mycobacterium smegmatis Deficient in ADP-Ribosyltransferase as Surrogate for Mycobacterium tuberculosis in Drug Testing and Mutation Analysis. *PloS one* **10**, e0122076 (2015).

34 CLSI. Performance Standards for Susceptibility Testing of Mycobacteria, Nocardia spp., and Other Aerobic Actinomycetes., (Clinical and Laboratory Standards Institute, 2018).

35 van Vuuren, S. & Viljoen, A. Plant-based antimicrobial studies--methods and approaches to study the interaction between natural products. *Planta Med.* **77**, 1168-1182 (2011).

36 Plocinska, R., Martinez, L., Gorla, P., Pandeeti, E., Sarva, K., Blaszczyk, E., Dziadek, J., Madiraju, M. V. & Rajagopalan, M. *Mycobacterium tuberculosis* MtrB Sensor Kinase Interactions with FtsI and Wag31 Proteins Reveal a Role for MtrB Distinct from That Regulating MtrA Activities. *J. Bacteriol.* **196**, 4120-4129 (2014).

37 Datta, P., Dasgupta, A., Singh, A. K., Mukherjee, P., Kundu, M. & Basu, J. Interaction between FtsW and penicillin-binding protein 3 (PBP3) directs PBP3 to mid-cell, controls cell septation and mediates the formation of a trimeric complex involving FtsZ, FtsW and PBP3 in mycobacteria. *Mol. Microbiol.* **62**, 1655-1673 (2006).

38 Hayes, M. V. & Orr, D. C. Mode of action of ceftazidime: affinity for the penicillin-binding proteins of *Escherichia coli* K12, *Pseudomonas aeruginosa* and *Staphylococcus aureus*. *J. Antimicrob. Chemother.* **12**, 119-126 (1983).

39 Georgopapadakou, N. H., Smith, S. A. & Sykes, R. B. Mode of action of azthreonam. *Antimicrob. Agents Chemother.* **21**, 950-956 (1982).

40 Sotgiu, G., Centis, R., D'Ambrosio, L. & Migliori, G. B. Tuberculosis Treatment and Drug Regimens. *Cold Spring Harb. Perspect. Med.* **5**, a017822 (2015).

41 Francis, Z. K., Sanders, A. N., Crick, D. C., Mahapatra, S., Islam, M. N. & Pavelka, M. S. LdtC Is a Key L,D-Transpeptidase for Peptidoglycan Assembly in *Mycobacterium smegmatis*. *J. Bacteriol.* **205**, e00424-00422 (2023).

42 Zandi, T. A., Marshburn, R. L., Stateler, P. K. & Brammer Basta, L. A. Phylogenetic and Biochemical Analyses of Mycobacterial L,D-Transpeptidases Reveal a Distinct Enzyme Class That Is Preferentially Acylated by Meropenem. *ACS Infect. Dis.* **5**, 2047-2054 (2019).

43 Jumper, J., Evans, R., Pritzel, A., Green, T., Figurnov, M., Ronneberger, O., Tunyasuvunakool, K., Bates, R., Žídek, A., Potapenko, A., Bridgland, A., Meyer, C., Kohl, S. A. A., Ballard, A. J., Cowie, A., Romera-Paredes, B., Nikolov, S., Jain, R., Adler, J., Back, T., Petersen, S., Reiman, D., Clancy, E., Zielinski, M., Steinegger, M., Pacholska, M., Berghammer, T., Bodenstein, S., Silver, D., Vinyals, O., Senior, A. W., Kavukcuoglu, K., Kohli, P. & Hassabis, D. Highly accurate protein structure prediction with AlphaFold. *Nature* **596**, 583-589 (2021).

44 Lu, Z., Wang, H., Zhang, A., Liu, X., Zhou, W., Yang, C., Guddat, L., Yang, H., Schofield, C. J. & Rao, Z. Structures of *Mycobacterium tuberculosis* Penicillin-Binding Protein 3 in Complex with Five β-Lactam Antibiotics Reveal Mechanism of Inactivation. *Mol. Pharmacol.* **97**, 287-294 (2020).

45 Chambers, H. F., Moreau, D., Yajko, D., Miick, C., Wagner, C., Hackbarth, C., Kocagöz, S., Rosenberg, E., Hadley, W. K. & Nikaido, H. Can penicillins and other beta-lactam antibiotics be used to treat tuberculosis? *Antimicrob. Agents Chemother.* **39**, 2620-2624 (1995).

46 Kim, H. S., Kim, J., Im, H. N., Yoon, J. Y., An, D. R., Yoon, H. J., Kim, J. Y., Min, H. K., Kim, S.-J. & Lee, J. Y. Structural basis for the inhibition of *Mycobacterium tuberculosis* L,D-transpeptidase by meropenem, a drug effective against extensively drug-resistant strains. *Acta Crystallogr. D* **69**, 420-431 (2013).

47 Dubée, V., Triboulet, S., Mainardi, J. L., Ethève-Quelquejeu, M., Gutmann, L., Marie, A., Dubost, L., Hugonnet, J. E. & Arthur, M. Inactivation of *Mycobacterium tuberculosis* L,D-transpeptidase $LdtMt_1$ by carbapenems and cephalosporins. *Antimicrob. Agents Chemother.* **56**, 4189-4195 (2012).

48 Kumar, G., Galanis, C., Batchelder, H. R., Townsend, C. A. & Lamichhane, G. Penicillin Binding Proteins and β-Lactamases of *Mycobacterium tuberculosis*: Reexamination of the Historical Paradigm. *mSphere* **7**, e0003922 (2022).

49 Dhar, N., Dubée, V., Ballell, L., Cuinet, G., Hugonnet, J. E., Signorino-Gelo, F., Barros, D., Arthur, M. & McKinney, J. D. Rapid cytolysis of *Mycobacterium tuberculosis* by faropenem, an orally bioavailable β-lactam antibiotic. *Antimicrob. Agents Chemother.* **59**, 1308-1319 (2015).

50 Bishop, P. J. & Neumann, G. The history of the Ziehl-Neelsen stain. *Tubercle* **51**, 196-206 (1970).

51 de Munnik, M., Lohans, C. T., Langley, G. W., Bon, C., Brem, J. & Schofield, C. J. A Fluorescence-Based Assay for Screening β-Lactams Targeting the *Mycobacterium tuberculosis* Transpeptidase Ldt_{Mt2}. *ChemBioChem* **21**, 368-372 (2020).

52 Adam, M., Damblon, C., Plaitin, B., Christiaens, L. & Frere, J. M. Chromogenic depsipeptide substrates for beta-lactamases and penicillin-sensitive DD-peptidases. *Biochem. J.* **270**, 525 (1990).

53 Schwyzer, R. Preparation of thio esters of amino acids and of peptides *Helvetica Chimica Acta* **37**, 647-649 (1954).

54 Lohans, C. T., Chan, H. T. H., Malla, T. R., Kumar, K., Kamps, J. J. A. G., McArdle, D. J. B., Van Groesen, E., de Munnik, M., Tooke, C. L., Spencer, J., Paton, R. S., Brem, J. & Schofield, C. J. Non-Hydrolytic β-Lactam Antibiotic Fragmentation by L,D-Transpeptidases and Serine β-Lactamase Cysteine Variants. *Angew. Chem. Int. Ed.* **58**, 1990-1994 (2019).

55 Gibson, D. G., Young, L., Chuang, R.-Y., Venter, J. C., Hutchison, C. A. & Smith, H. O. Enzymatic assembly of DNA molecules up to several hundred kilobases. *Nat. Methods* **6**, 343-345 (2009).

56 Bellio, P., Fagnani, L., Nazzicone, L. & Celenza, G. New and simplified method for drug combination studies by checkerboard assay. *MethodsX* **8**, 101543 (2021).

57 Piddock, L. J., Williams, K. J. & Ricci, V. Accumulation of rifampicin by Mycobacterium aurum, Mycobacterium smegmatis and Mycobacterium tuberculosis. *J. Antimicrob. Chemother.* **45**, 159-165 (2000).

58 Adam, M., Fraipont, C., Rhazi, N., Nguyen-Distèche, M., Lakaye, B., Frère, J. M., Devreese, B., Van Beeumen, J., van Heijenoort, Y., van Heijenoort, J. & Ghuysen, J. M. The bimodular G57-V577 polypeptide chain of the class B penicillin-binding protein 3 of *Escherichia coli* catalyzes peptide bond formation from thiolesters and does not catalyze glycan chain polymerization from the lipid II intermediate. *J. Bacteriol.* **179**, 6005-6009 (1997).

59 Inglis, S. R., Zervosen, A., Woon, E. C. Y., Gerards, T., Teller, N., Fischer, D. S., Luxen, A. & Schofield, C. J. Synthesis and Evaluation of 3-(Dihydroxyboryl)benzoic Acids as d,d-Carboxypeptidase R39 Inhibitors. *J. Med. Chem.* **52**, 6097-6106 (2009).

60 Jamin, M., Damblon, C., Millier, S., Hakenbeck, R. & Frère, J. M. Penicillin-binding protein 2x of *Streptococcus pneumoniae*: enzymic activities and interactions with β-lactams. *Biochem. J.* **292**, 735-741 (1993).

6.9 Statement of authorship

Title of Paper	How inhibition of L,D-transpeptidases and D,D-transpeptidases leads to inhibition of mycobacteria
Publication Status	□Published □Submitted for Publication □Accepted for Publication ■Unpublished and unsubmitted work written in a manuscript style
Publication Details	Manuscript in preparation

Student Confirmation

Student Name:	Mariska de Munnik		
Contribution to the Paper	The microbiological work described in this manuscript, including the inhibitor susceptibility studies with *Mycobacterium smegmatis*, and the fluorescent peptidoglycan incorporation assays, was supervised by Dr. Karina Cavopiña Tapia (University of Oxford). Synthesis of the fluorescent substrate mimics was supervised by Dr. Patrick Rabe (University of Oxford). Flow cytometry experiments were performed with support from Dr. Robert Hedley and Vasiliki Tsioligka at The Don Mason Facility of Flow Cytometry, Sir William Dunn School of Pathology, University of Oxford. Optimisation of the fluorogenic microplate assay for recombinant PBPs, applied to PBP3 of *Mtb*, was performed by Dr. Helen Smith (University of Oxford), synthesis of S2d was performed by Dr. Victor Aniebok (University of Oxford). Dr. Alistair Farley (University of Oxford) provided expertise on the selection of sulfonyl pyridines. All experimental work described here, data analysis, and preparation of the manuscript were carried out by me.		
Signature 		Date	23/01/2024

Supervisor Confirmation

By signing the Statement of Authorship, you are certifying that the candidate made a substantial contribution to the publication, and that the description described above is accurate.

Prof Chris Schofield		
I'm happy to start that the candidate made the major and a very substantial contribution to the publication, and that the description described above is accurate.		
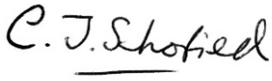	Date	23/01/2024

Chapter 7

Studies on inhibition of the β-lactamase BlaC from *Mycobacterium tuberculosis*

Contents

7.1 Introduction 168

7.2 Production, purification, and characterisation of BlaC 170

7.2.1 Cloning of BlaC 170
7.2.2 Expression of BlaC 170
7.2.3 Production and purification of BlaC 171

7.3 Steady-state kinetics 172

7.3.1 Michaelis-Menten kinetics 172
7.3.2 Detailed kinetical analysis of inhibition 174

7.4. Covalent interactions of BlaC with cephalosporins 175

7.5 Discussion 178

7.6 Summary and conclusions 179

7.7 Methods 180

7.7.1 Materials 180
7.7.2 Steady-state kinetics 180
7.7.2.1 Michaelis-Menten kinetics 180
7.7.2.2 Apparent inhibition constants and pseudo first order rate constants 181
7.7.2.3 Dissociation rate constants 182
7.7.3 Mass spectrometry 182

7.8 References 182

7.1 Introduction

Resistance to β-lactams is a continuously escalating threat to public health, rendering one of the most important classes of antibiotics increasingly ineffective.[1] Resistance to β-lactam antibiotics is commonly accredited to bacterial production of β-lactamases, a class of enzymes that are able to react with the β-lactam core, leading to hydrolysis and thereby inactivation of the antibiotic (Figure 7.1A).[2] The β-lactamases may be grouped into four classes, referred to as Ambler class A-D.[3,4] Ambler classes A, C, and D employ a nucleophilic serine residue in catalysis, and are therefore referred to as serine β-lactamases (SBLs), and Ambler class B β-lactamases employ one or two zinc ions in catalysis, and are correspondingly referred to as metallo-β-lactamases (MBLs).[5]

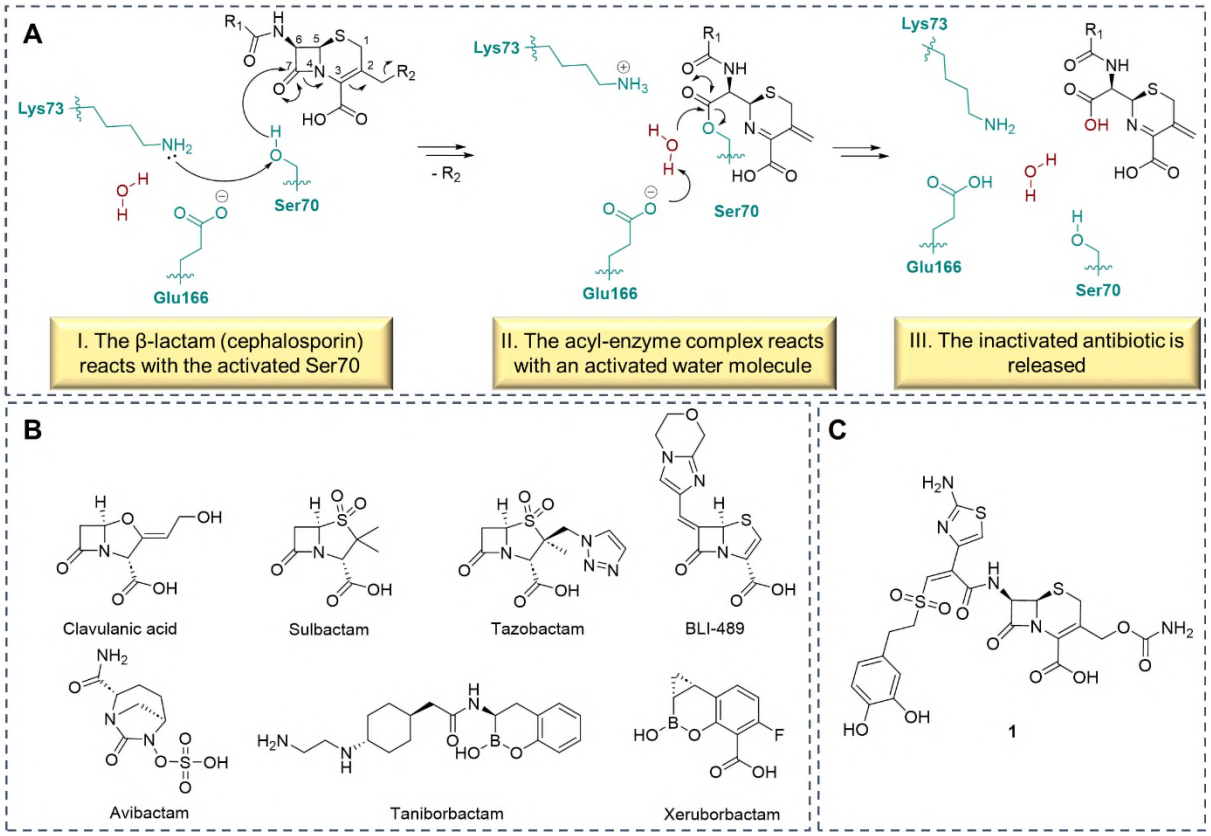

Figure 7.1. Catalysis and inhibition of the serine β-lactamase BlaC of *Mycobacterium tuberculosis*. A. Outline of the mechanism of hydrolysis of β-lactams, exemplified with a cephalosporin, which is likely accompanied by fragmentation of the C2 sidechain. The BlaC residues are in teal and the hydrolytic water is in red. **B.** Structures of β-lactamase inhibitors. **C.** Structure of cephalosporin **1**.

Mycobacterium tuberculosis (*Mtb*) is intrinsically resistant to most β-lactams, in part due to the presence of the Ambler class A β-lactamase BlaC.[6,7] BlaC follows a catalytic mechanism of β-lactam hydrolysis similar to that commonly observed in SBLs (Figure 7.1A).[8] Initially, the reactive β-lactam ring becomes positioned in close proximity to the catalytic serine residue

(Ser70), which is likely activated by the base Lys73. This allows Ser70 to react with the β-lactam ring, forming a covalently linked acyl-enzyme intermediate which, in the case of cephalosporins, is likely accompanied by fragmentation of the C2 sidechain.[9,10] A strategically placed activated water molecule is then utilised to hydrolyse the acyl-enzyme intermediate, releasing the inactivated antibiotic. The hydrolytic water, which is replaced in every catalytic cycle, has been observed by crystallography as a proton bridge from Glu166 and Lys73 to the nucleophilic Ser70, where Glu166 acts as general base to activate the water molecule.[8]

BlaC is known for its wide substrate profile, having been observed to be able to hydrolyse all classes of β-lactams.[11] However, increased catalytic efficiency is observed with penicillins and cephalosporins,[12] while carbapenems are relatively more resistant to BlaC hydrolysis.[11] Overall, however, BlaC has lower catalytic efficiency as observed in other class A SBLs, such as SHV and TEM-1.[13,14]

Inactivation of β-lactams due to β-lactamase catalysis can be prevented through coadministration of a β-lactamase inhibitor.[3] SBL inhibition often involves the formation of an acyl-enzyme complex that manifests increased stability in comparison to that observed with the rapidly hydrolysed acyl-enzyme intermediate of β-lactam catalysis, and such inhibitors may therefore be regarded as very slow substrates. β-Lactamase inhibitors containing a β-lactam core, such as clavulanic acid (CLAV),[15] and the penam sulfones sulbactam (SUL),[16] and tazobactam (TAZ),[17] are commonly used as class A SBL inhibitors (Figure 7.1B). In addition, diazabicyclooctanes such as avibactam (AVI),[18] and cyclic boronates, such as taniborbactam (TAN, formerly VNRX-5133) and xeruborbactam (XER, formerly QPX7728),[19-21] may also exhibit inhibition of class A SBLs (Figure 7.1B). BlaC inhibition by CLAV has been established; the combination between clavulanic acid and β-lactams such as meropenem or imipenem leads to *in vitro* and *in vivo* activity against *Mtb*.[12,22,23] In addition, SUL, TAZ, and AVI have previously been shown to manifest inhibition of BlaC.[24,25]

Despite generally being a potent cephalosporinase, evidence that optimisation of the cephalosporin core may lead to resistance to BlaC hydrolysis has been reported; a screen of β-lactams led to the identification of cephalosporins that were active against *Mtb* in the absence of a β-lactamase inhibitor.[26] A high-throughput screen aimed towards the identification of inhibitors of Ldt_{Mt2}, an L,D-transpeptidase of *Mtb*, applied a BlaC inhibition assay as secondary assay (Chapter 3), and identified a cephalosporin (**1**; Figure 7.1C) that has activity against Ldt_{Mt2} (pIC_{50} 5.55 ± 0.05), as well as potent inhibition of BlaC (pIC_{50} 7.72 ± 0.02).[27] Detailed kinetic analysis of the inhibition and hydrolysis of this cephalosporin is described here, and compared to the inhibitory potency of reported β-lactamase inhibitors, as well as being compared to the interaction of BlaC with a selection of additional cephalosporins.

7.2 Production, purification, and characterisation of BlaC

7.2.1 Cloning of BlaC

Previous attempts in our laboratory to express recombinant BlaC using a pET28a vector have yielded low expression levels. Hence, a novel expression vector was prepared. The *blaC* gene was acquired from Invitrogen™ GeneArt™, codon optimised for expression in *Escherichia coli*, and synthesised to present Not1 and Sal1 restriction sites. The gene was designed to lack the first 40 amino acids (Δ40), as a previous report has described full-length BlaC to be insoluble.[12] Both the expression gene and the expression vector pCold (containing an ampicillin resistance gene) were digested by Not1 and Sal1, and purified and extracted from 1% agarose gel electrophoresis. Ligation of the digested gene and plasmid was performed at a ratio of 3:1 and 5:1, to maximise the potential of annealing, and incubated at 37 °C for 24 h prior to transformation into XL 10-Gold ultracompetent *E. coli*. Transformed *E. coli* was propagated on ampicillin imbedded agar. The ampicillin resistance gene of the pCold vector was exchanged for a kanamycin resistance gene, to avoid contamination of BlaC with the SBL encoded by the pCold vector, as well as inactivation of ampicillin by BlaC. The *blaC*-pCold vector and the kanamycin resistance gene were amplified and linearised by PCR. The PCR products were purified and extracted from 1% agarose gel, and cloned following the Gibson Assembly procedure.[28] Once completed, the obtained product was transformed into XL 10-Gold ultracompetent *E. coli*, with propagation of transformed *E. coli* on kanamycin imbedded agar. The plasmids were extracted from the resulting colonies and sequenced to confirm the presence of the retained *blaC* gene (Appendix VI).

7.2.2 Expression of BlaC

The *blaC*-pCold plasmid was transformed into competent *E. coli* BL21(DE3) expression cells, and cultures of liquid media containing kanamycin were grown to OD_{600}, and then induced using several different conditions; isopropyl β-D-1-thiogalactopyranoside (IPTG) concentrations were varied between 0 and 1 mM, and temperatures were varied between 15 and 37 °C (Figure 7.2). The expression of soluble BlaC was assessed after 16 h of induction, via nickel resin purification of the cell lysate. Expression was observed at 15 °C and 18 °C at all tested IPTG concentrations, with little variance between the conditions.

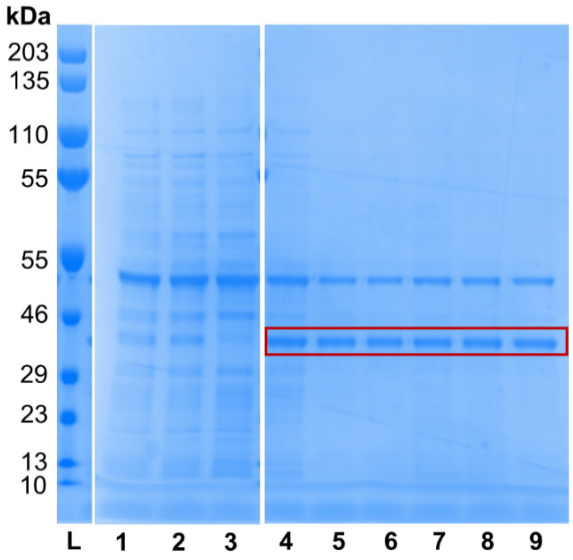

Figure 7.2. SDS-PAGE analysis of expression trials of BlaC. Recombinant BlaC was expressed in *E. coli* BL21(DE3) under varying conditions; 37 °C with 0 mM IPTG (**1**), 0.5 mM IPTG (**2**), or 1 mM IPTG (**3**), 18 °C with 0 mM IPTG (**4**), 0.5 mM IPTG (**5**), or 1 mM IPTG (**6**), 15 °C with 0 mM IPTG (**7**), 0.5 mM IPTG (**8**), or 1 mM IPTG (**9**). The protein ladder is labelled as "L". Significant presence of BlaC (MW 32.7 Da) is detected in samples **4**-**9**, indicated in red.

7.2.3 Production and purification of BlaC

Recombinant BlaC (Δ40) was purified via HisTag affinity chromatography (Figure 7.3A) followed by size-exclusion chromatography (Figure 7.3B), following the reported procedure (Appendix II).[29] BlaC was obtained in high purity (as observed by SDS-PAGE; Figure 7.3C), with a mass of 28740 Da (calculated mass: 28740 Da; Figure 7.3D) in total yield of 48.9 mg.

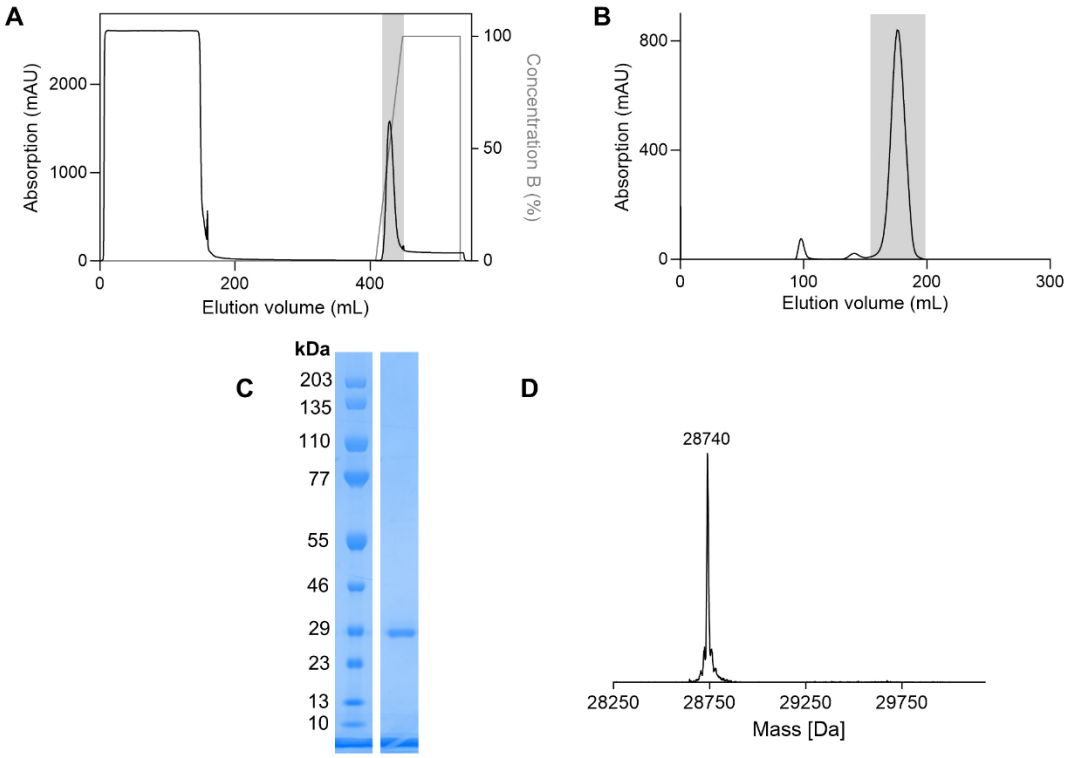

Figure 7.3. Purification of recombinant BlaC. A. HisTag affinity chromatography purification of BlaC. The area in grey represents BlaC containing fractions. **B.** Size-exclusion chromatography of BlaC, with the HisTag cleaved. The area in grey represents BlaC containing fractions. **C.** SDS-PAGE analysis of purified BlaC. **D.** MS analysis of purified BlaC. The deconvoluted spectrum is shown.

7.3 Steady-state kinetics

7.3.1 Michaelis-Menten kinetics

BlaC is known for its wide substrate profile; it has particularly potent penicillinase, and cephalosporinase activity.[12] Wang *et al.* (2009) reported variable catalytic efficiency between cephalosporin derivatives, observing potent hydrolysis of cephalothin (103 mM^{-1} s^{-1}), but modest hydrolysis of ceftazidime hydrolysis (0.4 mM^{-1} s^{-1}; Table 7.1).[12] Here, the Michaelis-Menten kinetics of BlaC catalysis were determined for **1**, the fluorescent cephalosporin substrate FC5,[30] and cephalothin, which was included as positive control (Figure 7.4, Table 7.1). As reported, efficient hydrolysis of cephalothin was observed, though due to a higher reaction rate constant (k_{cat} 25.2 ± 0.9 s^{-1}, compared to the reported k_{cat} 12.1 ± 1.1 s^{-1}) the catalytic efficiency (k_{cat}/K_m) was higher (215 mM^{-1} s^{-1}) than the reported value (Table 7.1). FC5 was a potent substrate for BlaC (k_{cat}/K_m 81 mM^{-1} s^{-1}), while **1** was apparently a poor substrate for BlaC. The K_m and k_{cat} of **1** could not be determined with high certainty, due to apparently low hydrolytic activity. While the concentration of **1** could not be increased due to low solubility in aqueous solutions, findings suggest a catalytic efficiency of 0.022 mM^{-1} s^{-1}.

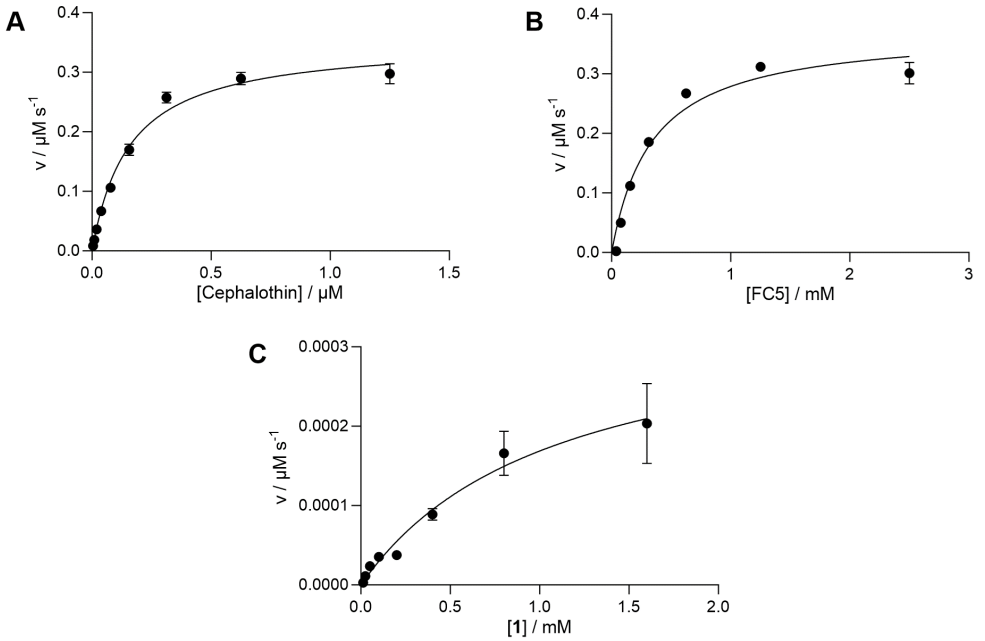

Figure 7.4. Kinetic characterisation of BlaC catalysed hydrolysis of the cephalosporins cephalothin (A) FC5 (B) and 1 (C). Assays were performed with 14 nM BlaC in 100 mM sodium phosphate pH 7.5. Error bars represent standard deviation (n = 4).

Table 7.1. Steady-state kinetics for BlaC catalysed hydrolysis of the cephalosporins FC5, 1, and cephalothin. Errors represent standard deviation (n = 4). For reference, reported values for cephalothin and ceftazidime are shown here.

Substrate		k_{cat} (s^{-1})	K_m (μM)	k_{cat}/K_m (mM^{-1} s^{-1})
1	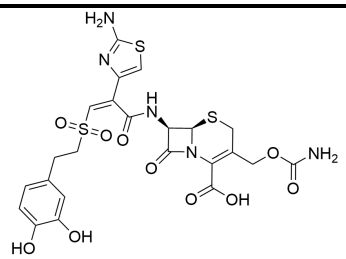	0.025 ± 0.009	1128 ± 329	0.022
FC5	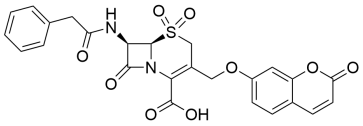	27.6 ± 0.6	342.5 ± 24	81
Cephalothin	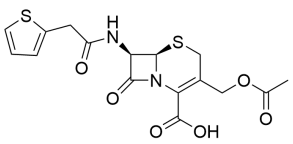	25.2 ± 0.9 12.1 ± 1.1*	157.3 ± 46 117 ± 12*	215 103*
Ceftazidime	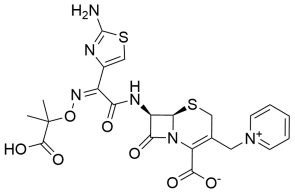	0.2 ± 0.1*	593 ± 29*	0.4*

*Values reported by Wang *et al*. (2009).[12]

7.3.2 Detailed kinetical analysis of inhibition

The inhibition of **1** was further assessed via the determination of kinetic determinants of inhibition; the apparent inhibition constant ($K_{i,app}$), the association constant (k_2/K), and the dissociation constant (k_{off}; Figure 7.5, Table 7.2). In addition to **1**, inhibition of CLAV, the approved β-lactamase inhibitor in the treatment of TB, was assessed, as well as SUL, TAZ, and AVI, which have previously been shown to manifest inhibition of BlaC.[24,25] Further, the methylidene penem β-lactamase inhibitor BLI-489 (BLI) and the cyclic boronates XER and TAN were assessed for inhibition of BlaC.

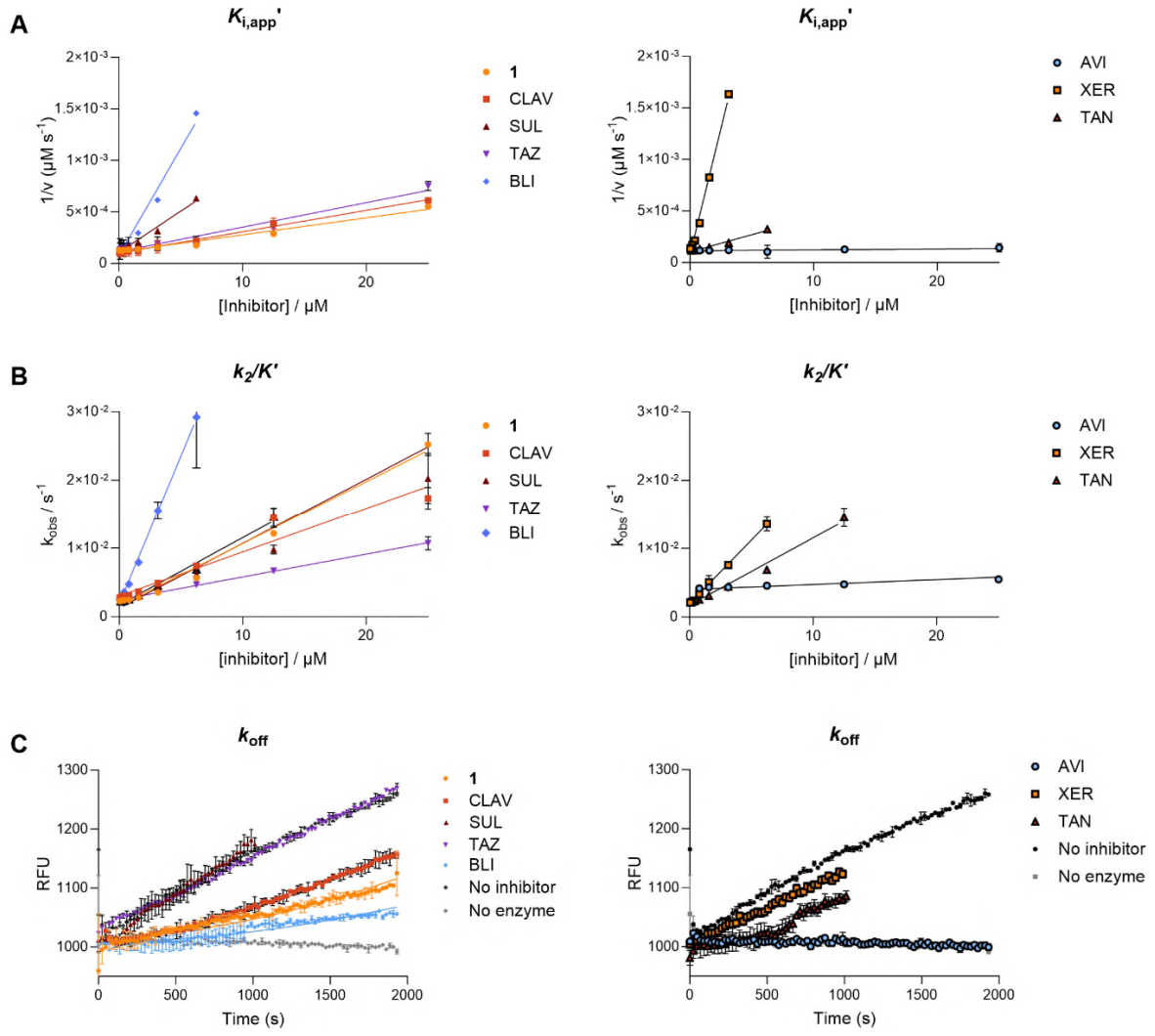

Figure 7.5. Kinetic characterisation of BlaC inhibition. A. Determination of $K_{i,app}$ values. **B.** Determination of k_2/K values. **C.** Determination of k_{off} values using the jump-dilution method,[31] with 30 minutes inhibitor pre-incubation, followed by a 1000-fold dilution, and assayed with FC5. CLAV = clavulanic acid, SUL = sulbactam, TAZ = tazobactam, BLI = BLI-489, AVI = avibactam, XER = xeruborbactam, TAN = taniborbactam. All assays were performed at room temperature in 100 mM sodium phosphate, pH 7.5, 0.01% (*v*/*v*) Triton X-100. Error bars represent standard deviation (n = 4). Compound structures are given in Figure 7.1.

Table 7.2. Kinetic characterisation of BlaC inhibition by 1 and clavulanic acid. Errors represent standard deviation (n = 4). Compound structures are given in Figure 7.1.

Inhibitor	$K_{i,app}$ (μM)	k_2/K (M^{-1} s^{-1}) x 10^{-2}	k_{off} (s^{-1}), x 10^{-3}	$t_{1/2}$ (min)
1	6.7 ± 0.2	9.3 ± 0.4	0.43 ± 0.05	26.9
Clavulanic acid	4.8 ± 0.2	6.5 ± 0.6	0.86 ± 0.03	13.4
Tazobactam	4.8 ± 0.1	3.4 ± 0.01	2.7 ± 0.02	4.4 ± 1
Sulbactam	1.3 ± 0.03	9.6 ± 0.5	N.D.*	N.D.*
BLI-489	0.37 ± 0.01	44 ± 0.8	0.17 ± 0.01	68 ± 1
Xeruborbactam	0.15 ± 0.01	18 ± 0.3	3.3 ± 0.6	1.0 ± 0.6
Taniborbactam	3.1 ± 0.1	10 ± 0.5	1.4 ± 0.2	8.8 ± 1
Avibactam	134 ± 5	0.73 ± 0.03	N.D.**	N.D.**

*k_{off} could not be determined for sulbactam due to rapid dissociation. **k_{off} could not be determined due no observed dissociation throughout the duration of the assay.

The $K_{i,app}$ of **1** (6.7 ± 0.2 μM) was similar to that for CLAV (4.8 ± 0.2 μM). In addition, **1** exhibited similar, but slightly increased acylation efficiency compared to CLAV (k_2/K 9.3 ± 0.4 M^{-1} s^{-1}, and 6.52 ± 0.6 M^{-1} s^{-1}, respectively), and slightly increased stability of the acyl-enzyme complex, as evidenced by a doubled half-life of the enzyme-inhibitor complex (26.9 min and 12.4 min, respectively. Note that it has been reported that the phosphate ions present in the assay buffer promote the recovery of active BlaC upon inhibition by CLAV.[32] As reported, AVI exhibited the lowest inhibitory efficiency ($K_{i,app}$ 134 ± 5 μM) and low acylation efficiency (k_2/K 0.73 ± 0.03 M^{-1} s^{-1}) of the tested β-lactamase inhibitors, but did exhibit increased stability of the BlaC-avibactam complex, manifesting no measurable dissociation.[25] The inhibition of TAZ, SUL, and taniborbactam (TAN) were all similar to that of clavulanic acid, though the enzyme-inhibitor complexes exhibited reduced stability, in line with reported studies of the recovery of BlaC activity.[11]

Particularly potent inhibition was observed with the cyclic boronate XER, and the penem BLI, with $K_{i,app}$ < 1 μM. Remarkably, BLI exhibited increased efficiency of acylation (44 ± 0.8 M^{-1} s^{-1}) in comparison to other assessed inhibitors, and among the longest residency time (k_{off} 0.17 ± 0.01 x 10^{-3} s^{-1} and $t_{1/2}$ 68 ± 1 min). The inhibition of BlaC by BLI has not previously been reported, though the inhibition of a close methylidene penem derivative yielded similar results (K_i 0.2 μM).[33]

7.4. Covalent interactions of BlaC with cephalosporins

The covalent interaction of **1** with BlaC was investigated by protein-observed solid-phase extraction (SPE) MS. At an inhibitor to enzyme ratio of 100:1, an adduct with a mass shift of

+565 Da compared to the unmodified BlaC was obtained (Figure 7.6A), supporting fragmentation of the C2 sidechain (Figure 7.6B). The formed adduct was observed for 24 h, with no evidence for unmodified BlaC, in early and late timepoints. This observation supports the notion that **1** is an inhibitor of BlaC, acting via formation of an unexpectedly stable acyl-enzyme complex, in line with the Michaelis-Menten kinetics (Figure 7.4C), and the inhibition kinetics (Figure 7.5), which suggested slow hydrolysis, but efficient acylation.

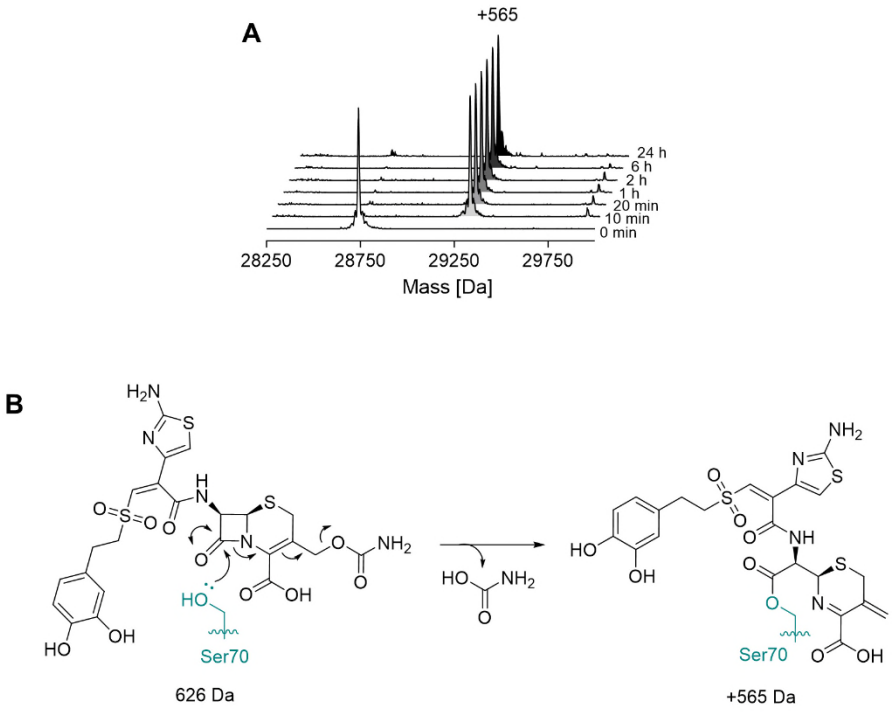

Figure 7.6. Protein-observed SPE-MS informs in the mechanism of BlaC inhibition by 1. A. Protein observed SPE-MS assays of BlaC (5 µM) with **1** (100 µM) in 50 mM tris pH 7.5. **B.** The mechanism of inhibition, as suggested by the protein observed SPE-MS assays, following C2 fragmentation upon covalent interaction with BlaC.

By contrast with the continued presence of the adduct obtained with **1**, a selection of first to fourth generation cephalosporins did not manifest formation of a stable covalently modified form of BlaC, i.e., a BlaC modification lasting >2 h (Figure 7.7). Ceftiofur, ceftriaxone, cefdinir, and cefepime all did not manifest significant evidence for covalent modification of BlaC, suggesting efficient deacylation. Interestingly, these cephalosporins share an identical or near identical C6 sidechain, involving a 2-amino-4-thiazolyl methoxyimino group. Cefditoren (MW 507 Da), which equally shares this sidechain, manifested a limited BlaC modification over 24 hours, with a mass shift of +525 Da, coinciding with the mass of the hydrolysed, unfragmented molecule. Similar observations could be made with cefuroxime (MW 424 Da) and cephalothin (MW 396 Da) as well exhibited limited BlaC modification, though the mass shifts of +381 Da and +354 Da, respectively, suggest C2 fragmentation. Cefmetazole (MW 472 Da) exhibited a

significant amount of modification of BlaC (+355 Da, apparently correlating to the C2 fragmented covalent intermediate) at 10 min incubation, but no longer after 20 min incubation. Ceftazidime (MW 547 Da) manifested an adduct of the apparent C2 fragmented covalent intermediate (+467 Da), which was observed for at least 2 h. This is in accordance with the reported relatively lower k_{cat}/K_m,[12] which has been suggested to be due to increased bulkiness of the C6 sidechain.[34]

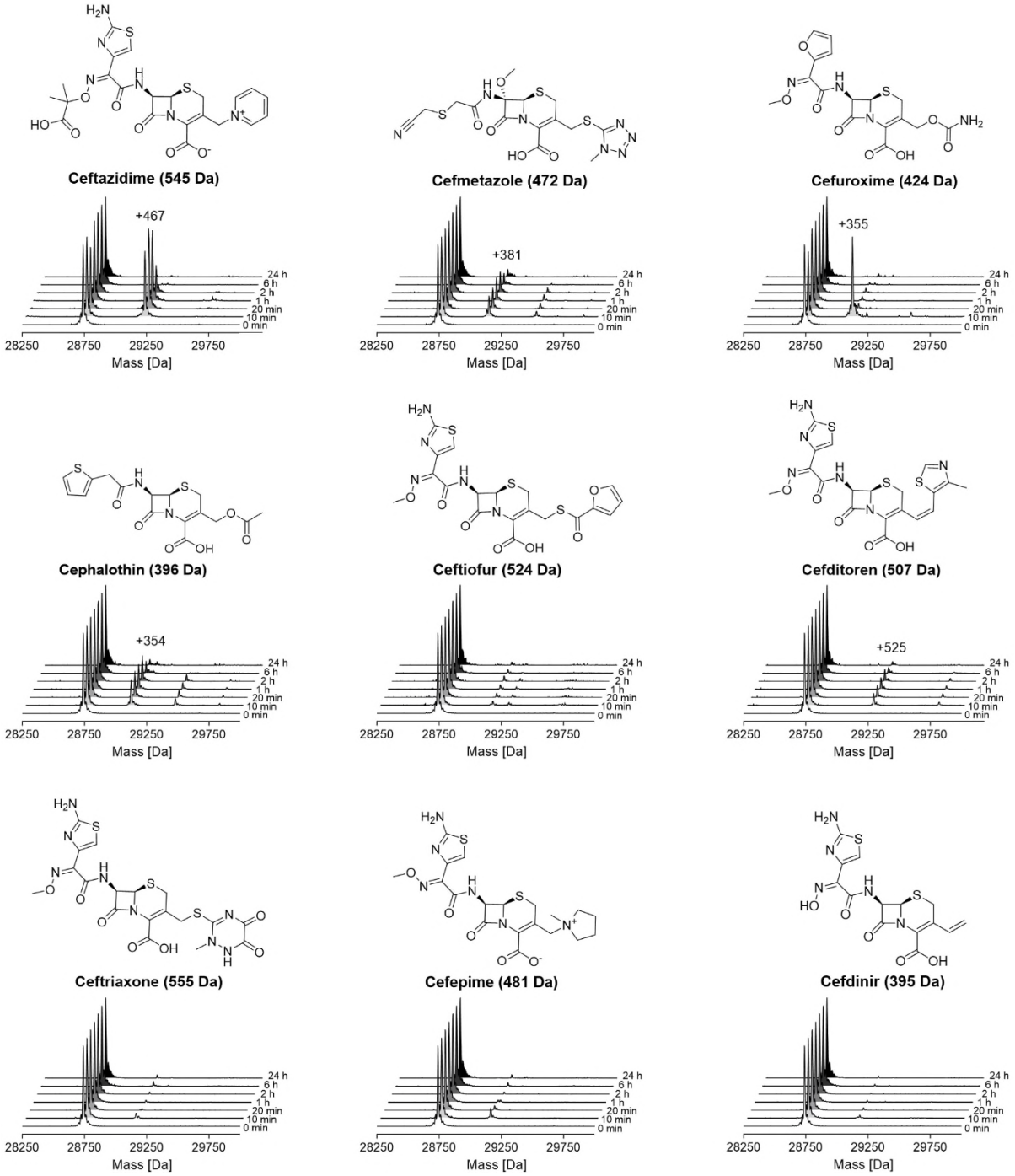

Figure 7.7. Protein-observed SPE-MS assays of BlaC with a selection of first to fourth generation cephalosporins. BlaC (5 µM) was incubated with the indicated cephalosporin (500 µM) in 50 mM tris, pH 7.5.

7.5 Discussion

The inhibition studies described here suggest that the acyl-enzyme complex of **1** exhibits notable and unusual stability, an increased half-life in comparison to CLAV under the same conditions, and clear increased stability over other cephalosporins assessed here. The acyl-enzyme complex between BlaC and **1** (Figure 7.8) was observed to involve C2 fragmentation. A clear difference between **1** and the other cephalosporins is the larger, bulky C6 sidechain of **1**, as shown in Figure 7.8, in comparison with the acyl-enzyme intermediate of ceftriaxone, whose acyl-enzyme complex was barely perceivable in the SPE-MS studies, but has been studied via time-resolved crystallography by Olmos *et al.* (2018).[35] The increased bulkiness of **1** may lead to displacement of Glu166, the residue which has been determined to be essential for deacylation, and plays an important role in the coordination of the hydrolytic water.[36] The effect of bulky C6 sidechains to confer increased resistance to the Ambler class C β-lactamase AmpC via steric hindrance of the deacylation step has been previously observed in several third-generation cephalosporins with SBLs, such as ceftazidime.[34] While ceftazidime is a relatively slower substrate of BlaC, the relatively large active site of BlaC compared to most class A SBLs may require further increased bulk of the sidechain.[12]

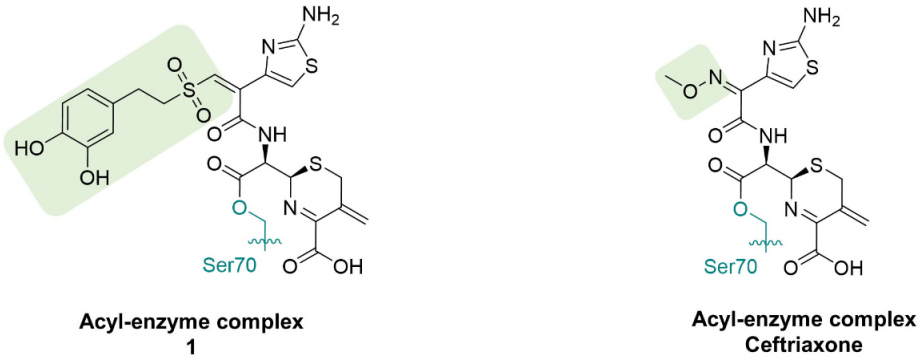

Figure 7.8. Structures of the acyl-enzyme complex of BlaC with 1 and ceftriaxone. The BlaC residue Ser70 is represented in teal. The structural differences are highlighted in green.

Similarly to **1**, carbapenems are known to be relatively resistant to BlaC hydrolysis. While hydrolysis with this compound class has been observed, carbapenems such as meropenem,[22] doripenem, ertapenem,[37] and tebipenem,[38] are slow BlaC substrates that are able to act is inhibitors of BlaC. Kinetic analysis revealed that these carbapenems are able to potently acylate BlaC through reaction with Ser70, though rate of deacylation was low. Structural studies of BlaC in complex with carbapenems reveal that the adduct is positioned in such a way that hydrogen bonds are formed between the C6-hydroxyethyl group with Glu166 and Lys73, leading to a modest shift of these residues away from the catalytic water (2.4 Å to 2.7 Å), making water activation less probable, hence increasing the stability of the acyl-enzyme

complex.[37] Whether this mechanism correlated to the increased stability of the BlaC-**1** complex in comparison to other cephalosporins is unknown, given the significant structural differences, though it is possible that the bulky C6 sidechain confers interaction, or movement of Glu166, leading to altered interaction with the hydrolytic water.

Previous reports of cephalosporins resistant to BlaC hydrolysis (as evidenced by activity against *Mtb* independent from the presence of absence of CLAV) have been described,[26] though they are structurally different from cephalosporin **1**; in these compounds, the C3 carboxylic acid has been exchanged for an ester or oxadiazole isostere. Further studies of the interactions of these cephalosporins with BlaC have not been reported.

Stability of other inhibitors of SBLs, such as CLAV, SUL, and TAZ are thought to arise through further reactions of the acyl-enzyme complex following covalent modification of SBLs to give a relatively stable complex.[24,39] Similar mechanisms were not observed with **1**, as the C2-fragmented acyl-enzyme complex was observed to be stable for at least 24 h, not manifesting evidence for further fragmentation.

Notable is the C6 sidechain of **1**, which contains a 1,2-benzenedial (or catechol) group, and may therefore act as a siderophore, similarly to the siderophore cephalosporin cefiderocol, which contains a chlorocatechol group on its C2 sidechain. Cefiderocol has been reported to exhibit notable resistance to hydrolysis by β-lactamases and exhibit particular transportation into the periplasmic space, and potent antibacterial potency against both gram-positive and gram-negative pathogens.[40,41] While **1** exhibits only moderate activity against *Mtb* (MIC_{50} 38.9 µM, Chapter 3) and limited activity against *Mycobacterium smegmatis* (MIC 64 µg/mL, Chapter 6), the scaffold is of interest for optimisation studies, considering its inhibition of both the essential transpeptidases Ldt_{Mt2} (pIC_{50} 5.55; Chapter 3), and PBP3 (pIC_{50} 6.1; Chapter 6), as well as resistance to BlaC hydrolysis.

7.6 Summary and conclusions

Cephalosporins are of considerable interest for the optimisation for use in *Mtb*, but are generally hydrolysed by BlaC. Understanding of structural modification of cephalosporins to lead to decreased hydrolysis, or inhibition of BlaC, is therefore of interest. Cephalosporin **1**, which was identified initially as an inhibitor of Ldt_{Mt2} has been observed to form a stable acyl-enzyme complex with BlaC leading to increased resistance to hydrolysis. The inhibitory potency of **1** was found to be similar to that of CLAV. The notion that **1** is additionally an inhibitor of Ldt_{Mt2}, and an inhibitor of PBP3, makes it a particularly interesting compound, despite exhibiting limited inhibition of *Mtb* (MIC_{50} 38.9 µM, Chapter 3).

Further research is warranted towards the properties of **1** that lead to the increase stability, though this may be related to the bulky C6 sidechain. X-ray crystallography studies of BlaC in combination with **1** ought to be performed to obtain structural insights into the relative resistance of **1** against BlaC hydrolysis, as findings may guide the design of cephalosporins with activity against *Mtb*. Given the inhibition of **1** is very similarly to the commonly used CLAV, *in vitro* studies of the recovery of β-lactam activity in *Mtb* are of interest, when used in combination with **1**.

The inhibition of BlaC with CLAV, SUL, TAZ, and AVI, which are all in clinical use, is well established, both in biochemical inhibition studies and *in vitro* assays of β-lactam activity. In addition, BlaC can be inhibited by cyclic boronates and penems. Through a systematic analysis of seven β-lactamase inhibitors of diverse compound classes, BLI is identified as the most potent inhibitor, exhibiting $K_{i,app} < 1$ µM, efficient acylation, and slow deacylation. Studies of the recovery of β-lactam activity in *Mtb* when used in combination with BLI may therefore be of interest.

7.7 Methods

7.7.1 Materials

Ceftazidime, cephalothin, cefmetazole, and cefditoren were from TOKU-E, ceftriaxone, ceftiofur, and SUL were from Molekula Ltd, cefepime was from Alfa Aesar, XER, TAN, and AVI were from MedChemExpress, **1** was obtained from the GSK HTS compound library. All other compounds were from Merck. Primers and template DNA for the kanamycin resistance gene were provided by Dr. Freddy Foster (University of Oxford). The pCold expression vector was supplied by Dr. Patrick Rabe (University of Oxford). Recombinant BlaC was cloned, produced, and purified using the procedure described in Appendix II.[29] FC5 was synthesised as decribed.[30]

7.7.2 Steady-state kinetics

7.7.2.1 Michaelis-Menten kinetics

Michaelis-Menten kinetics with BlaC (14 nM) and FC5 (39 µM – 2.5 mM) were determined in 100 mM sodium phosphate, pH 7.5, 0.01% (*v*/*v*) Triton X-100 (total volume 25 µL). Fluorescence intensity was measured using a PHERAstar plate reader (BMG Labtech) with λ_{ex} = 380 nm and λ_{em} = 460 nm. Michaelis-Menten kinetics with BlaC (14 nM) and **1** (12.5 µM – 1.6 mM) or cephalothin (4.9 µM – 1.25 mM) were determined in 100 mM sodium phosphate,

pH 7.5 (total volume 200 µL). Absorbance was measured using a CLARIOstar plate reader (BMG Labtech) with ε = 346 nm and ε = 262 nm for **1** and cephalothin, respectively.

The reaction velocities were determined from regression of the initial linear slope, and used to determine the kinetic parameters V_{max} and K_m using the Michaelis-Menten equation (1).

$$v = V_{max} \frac{[S]}{K_m + [S]} \quad (1)$$

where, v = reaction velocity; V_{max} = maximum reaction velocity; [S] = substrate concentration; and K_m = Michaelis constant.

The reaction rate constant (k_{cat}) was determined using equation 2.

$$k_{cat} = \frac{V_{max}}{[E]} \quad (2)$$

where, V_{max} = maximum reaction velocity; and [E] = enzyme concentration.

7.7.2.2 Apparent inhibition constants and pseudo first order rate constants

The pseudo first order rate constant (k_2/K) and the apparent inhibition constant ($K_{i,app}$) were determined using reported methods.[42,43] BlaC (100 nM) was added to a solution of FC5 (5 µM) and various concentrations of inhibitors in 100 mM sodium phosphate, pH 7.5, 0.01% (*v*/*v*) Triton X-100 (total volume 25 µL) and fluorescent intensity was immediately measured using a PHERAstar plate reader (BMG Labtech) with λ_{ex} = 380 nm and λ_{em} = 460 nm until a plateau was reached.

The reciprocal of the initial linear slope was determined and fitted against the inhibitor concentration, and $K_{i,app}$' was determined from the intercept divided by the slope. $K_{i,app}$ was determined from correction of $K_{i,app}$' for FC5 concentration and K_m, using equation 3.

$$K_{i,app} = \frac{K_{i,app}'}{1 + (\frac{[S]}{K_m})} \quad (3)$$

The observed rate constant (k_{obs}) was determined by fitting of the fluorescence intensity to equation 4.

$$P = V_s t + (V_0 - V_s) \frac{(1 - e^{-k_{obs} t})}{k_{obs}} + P_0 \quad (4)$$

where, P = formed product; V_s = velocity of no-inhibitor control; V_0 = velocity of no-enzyme control, and P_0 = initial fluorescence.

The resulting k_{obs} was then fitted against the inhibitor concentration (I), and fitted to equation 5, to give k_2/K'.

$$k_{obs} = k_2 + \frac{k_2}{K'} \times [I] \quad (5)$$

k_2/K could then be obtained from correction for FC5 concentration and K_m, using equation 6.

$$k_2/K = \frac{k_2/K'}{1+(\frac{[S]}{K_m})} \quad (6)$$

7.7.2.3 Dissociation rate constants

Dissociation rate constants (k_{off}) were determined using the jump dilution method.[31] BlaC (1 µM) was incubated with inhibitor (10 µM, or 100 µM in the case of AVI) for 10 minutes at room temperature in 100 mM sodium phosphate, pH 7.5, 0.01% (*v*/*v*) Triton X-100, and then diluted 1000x and immediately assayed using 125 µM FC5 using a PHERAstar plate reader (BMG Labtech) with λ_{ex} = 380 nm and λ_{em} = 460 nm. The obtained data was fitted with equation 4. The half-life ($t_{1/2}$) of the enzyme-inhibitor complex could then be determined using equation 7.

$$t_{1/2} = \frac{\ln(2)}{k_{off}} \quad (7)$$

7.7.3 Mass spectrometry

Protein-observed SPE-MS experiments were performed as previously described for Ldt_{Mt2},[27] where BlaC (5 µM) in 50 mM tris, pH 7,5, was incubated with a cephalosporin (500 µM) at room temperature, and samples were measured after the specified incubation periods.

7.8 References

1 Collaborators, A. R. Global burden of bacterial antimicrobial resistance in 2019: a systematic analysis. *Lancet* **399**, 629-655 (2022).

2 Bush, K. & Bradford, P. A. β-Lactams and β-Lactamase Inhibitors: An Overview. *Cold Spring Harb. Perspect. Med.* **6** (2016).

3 Drawz, S. M. & Bonomo, R. A. Three decades of beta-lactamase inhibitors. *Clin. Microbiol. Rev.* **23**, 160-201 (2010).

4 Bush, K. & Jacoby, G. A. Updated Functional Classification of β-Lactamases. *Antimicrobial Agents & Chemotherapy* **54**, 969-976 (2010).

5 Bush, K. Past and Present Perspectives on β-Lactamases. *Antimicrob. Agents Chemother.* **62** (2018).

6 Flores, A. R., Parsons, L. M. & Pavelka, M. S. Genetic analysis of the beta-lactamases of *Mycobacterium tuberculosis* and *Mycobacterium smegmatis* and susceptibility to beta-lactam antibiotics. *Microbiology (Reading, Engl.)* **151**, 521-532 (2005).

7 Kurz, S. G. & Bonomo, R. A. Reappraising the use of β-lactams to treat tuberculosis. *Expert Rev. Anti Infect. Ther.* **10**, 999-1006 (2012).

8 Fisher, J. F. & Mobashery, S. Three decades of the class A beta-lactamase acyl-enzyme. *Curr. Protein Pept. Sci.* **10**, 401-407 (2009).

9 Dubée, V., Triboulet, S., Mainardi, J. L., Ethève-Quelquejeu, M., Gutmann, L., Marie, A., Dubost, L., Hugonnet, J. E. & Arthur, M. Inactivation of *Mycobacterium tuberculosis*

L,D-transpeptidase LdtMt$_1$ by carbapenems and cephalosporins. *Antimicrob. Agents Chemother.* **56**, 4189-4195 (2012).

10 Boyd, D. B. & Lunn, W. H. Electronic structures of cephalosporins and penicillins. 9. Departure of a leaving group in cephalosporins. *J. Med. Chem.* **22**, 778-784 (1979).

11 Hugonnet, J.-E. & Blanchard, J. S. Irreversible Inhibition of the *Mycobacterium tuberculosis* β-Lactamase by Clavulanate. *Biochemistry* **46**, 11998-12004 (2007).

12 Wang, F., Cassidy, C. & Sacchettini, J. C. Crystal structure and activity studies of the *Mycobacterium tuberculosis* beta-lactamase reveal its critical role in resistance to beta-lactam antibiotics. *Antimicrob. Agents Chemother.* **50**, 2762-2771 (2006).

13 Helfand, M. S., Bethel, C. R., Hujer, A. M., Hujer, K. M., Anderson, V. E. & Bonomo, R. A. Understanding resistance to beta-lactams and beta-lactamase inhibitors in the SHV beta-lactamase: lessons from the mutagenesis of SER-130. *J. Biol. Chem.* **278**, 52724-52729 (2003).

14 Thomas, V. L., Golemi-Kotra, D., Kim, C., Vakulenko, S. B., Mobashery, S. & Shoichet, B. K. Structural consequences of the inhibitor-resistant Ser130Gly substitution in TEM beta-lactamase. *Biochemistry* **44**, 9330-9338 (2005).

15 Reading, C. & Cole, M. Clavulanic acid: a beta-lactamase-inhiting beta-lactam from *Streptomyces clavuligerus*. *Antimicrob. Agents Chemother.* **11**, 852-857 (1977).

16 English, A. R., Retsema, J. A., Girard, A. E., Lynch, J. E. & Barth, W. E. CP-45,899, a beta-lactamase inhibitor that extends the antibacterial spectrum of beta-lactams: initial bacteriological characterization. *Antimicrob. Agents Chemother.* **14**, 414-419 (1978).

17 Aronoff, S. C., Jacobs, M. R., Johenning, S. & Yamabe, S. Comparative activities of the beta-lactamase inhibitors YTR 830, sodium clavulanate, and sulbactam combined with amoxicillin or ampicillin. *Antimicrob. Agents Chemother.* **26**, 580-582 (1984).

18 Ehmann, D. E., Jahić, H., Ross, P. L., Gu, R. F., Hu, J., Kern, G., Walkup, G. K. & Fisher, S. L. Avibactam is a covalent, reversible, non-β-lactam β-lactamase inhibitor. *Proc. Natl. Acad. Sci. U.S.A.* **109**, 11663-11668 (2012).

19 Liu, B., Trout, R. E. L., Chu, G.-H., McGarry, D., Jackson, R. W., Hamrick, J. C., Daigle, D. M., Cusick, S. M., Pozzi, C., De Luca, F., Benvenuti, M., Mangani, S., Docquier, J.-D., Weiss, W. J., Pevear, D. C., Xerri, L. & Burns, C. J. Discovery of Taniborbactam (VNRX-5133): A Broad-Spectrum Serine- and Metallo-β-lactamase Inhibitor for Carbapenem-Resistant Bacterial Infections. *J. Med. Chem.* **63**, 2789-2801 (2020).

20 Hecker, S. J., Reddy, K. R., Lomovskaya, O., Griffith, D. C., Rubio-Aparicio, D., Nelson, K., Tsivkovski, R., Sun, D., Sabet, M., Tarazi, Z., Parkinson, J., Totrov, M., Boyer, S. H., Glinka, T. W., Pemberton, O. A., Chen, Y. & Dudley, M. N. Discovery of Cyclic Boronic Acid QPX7728, an Ultrabroad-Spectrum Inhibitor of Serine and Metallo-β-lactamases. *J. Med. Chem.* **63**, 7491-7507 (2020).

21 Hecker, S. J., Reddy, K. R., Totrov, M., Hirst, G. C., Lomovskaya, O., Griffith, D. C., King, P., Tsivkovski, R., Sun, D., Sabet, M., Tarazi, Z., Clifton, M. C., Atkins, K., Raymond, A., Potts, K. T., Abendroth, J., Boyer, S. H., Loutit, J. S., Morgan, E. E., Durso, S. & Dudley, M. N. Discovery of a Cyclic Boronic Acid β-Lactamase Inhibitor (RPX7009) with Utility vs Class A Serine Carbapenemases. *J. Med. Chem.* **58**, 3682-3692 (2015).

22 Hugonnet, J.-E., Tremblay, L. W., Boshoff, H. I., Barry, C. E. & Blanchard, J. S. Meropenem-Clavulanate Is Effective Against Extensively Drug-Resistant *Mycobacterium tuberculosis*. *Science* **323**, 1215-1218 (2009).

23 Gonzalo, X. & Drobniewski, F. Is there a place for β-lactams in the treatment of multidrug-resistant/extensively drug-resistant tuberculosis? Synergy between meropenem and amoxicillin/clavulanate. *J. Antimicrob. Chemother.* **68**, 366-369 (2013).

24 Tassoni, R., Blok, A., Pannu, N. S. & Ubbink, M. New Conformations of Acylation Adducts of Inhibitors of β-Lactamase from *Mycobacterium tuberculosis*. *Biochemistry* **58**, 997-1009 (2019).

25 Xu, H., Hazra, S. & Blanchard, J. S. NXL104 Irreversibly Inhibits the β-Lactamase from *Mycobacterium tuberculosis*. *Biochemistry* **51**, 4551-4557 (2012).

26 Gold, B., Smith, R., Nguyen, Q., Roberts, J., Ling, Y., Lopez Quezada, L., Somersan, S., Warrier, T., Little, D. & Pingle, M. Novel cephalosporins selectively active on nonreplicating *Mycobacterium tuberculosis*. *J. Med. Chem.* **59**, 6027-6044 (2016).

27 de Munnik, M., Lang, P. A., De Dios Antos, F., Cacho, M., Bates, R. H., Brem, J., Rodríguez-Miquel, B. & Schofield, C. J. High-Throughput Screen with the L,D-transpeptidase Ldt_{Mt2} of *Mycobacterium tuberculosis* Reveals Novel Classes of Covalently Reacting Inhibitors *Chem. Sci.* **14**, 7262-7278 (2023).

28 Gibson, D. G., Young, L., Chuang, R.-Y., Venter, J. C., Hutchison, C. A. & Smith, H. O. Enzymatic assembly of DNA molecules up to several hundred kilobases. *Nat. Methods* **6**, 343-345 (2009).

29 de Munnik, M., Lithgow, J., Brewitz, L., Christensen, K. E., Bates, R. H., Rodriguez-Miquel, B. & Schofield, C. J. αβ,α'β'-Diepoxyketones are mechanism-based inhibitors of nucleophilic cysteine enzymes. *Chem. Commun. (Camb)* **59**, 12859-12862 (2023).

30 Van Berkel, S. S., Brem, J., Rydzik, A. M., Salimraj, R., Cain, R., Verma, A., Owens, R. J., Fishwick, C. W. G., Spencer, J. & Schofield, C. J. Assay Platform for Clinically Relevant Metallo-β-lactamases. *J. Med. Chem.* **56**, 6945-6953 (2013).

31 Copeland, R. A., Basavapathruni, A., Moyer, M. & Scott, M. P. Impact of enzyme concentration and residence time on apparent activity recovery in jump dilution analysis. *Anal. Biochem.* **416**, 206-210 (2011).

32 Elings, W., Tassoni, R., van der Schoot, S. A., Luu, W., Kynast, J. P., Dai, L., Blok, A. J., Timmer, M., Florea, B. I., Pannu, N. S. & Ubbink, M. Phosphate Promotes the Recovery of *Mycobacterium tuberculosis* β-Lactamase from Clavulanic Acid Inhibition. *Biochemistry* **56**, 6257-6267 (2017).

33 Hazra, S., Kurz, S. G., Wolff, K., Nguyen, L., Bonomo, R. A. & Blanchard, J. S. Kinetic and Structural Characterization of the Interaction of 6-Methylidene Penem 2 with the β-Lactamase from *Mycobacterium tuberculosis*. *Biochemistry* **54**, 5657-5664 (2015).

34 Trehan, I., Morandi, F., Blaszczak, L. C. & Shoichet, B. K. Using Steric Hindrance to Design New Inhibitors of Class C β-Lactamases. *Chem. Biol.* **9**, 971-980 (2002).

35 Olmos, J. L., Pandey, S., Martin-Garcia, J. M., Calvey, G., Katz, A., Knoska, J., Kupitz, C., Hunter, M. S., Liang, M., Oberthuer, D., Yefanov, O., Wiedorn, M., Heyman, M., Holl, M., Pande, K., Barty, A., Miller, M. D., Stern, S., Roy-Chowdhury, S., Coe, J., Nagaratnam, N., Zook, J., Verburgt, J., Norwood, T., Poudyal, I., Xu, D., Koglin, J., Seaberg, M. H., Zhao, Y., Bajt, S., Grant, T., Mariani, V., Nelson, G., Subramanian, G., Bae, E., Fromme, R., Fung, R., Schwander, P., Frank, M., White, T. A., Weierstall, U., Zatsepin, N., Spence, J., Fromme, P., Chapman, H. N., Pollack, L., Tremblay, L., Ourmazd, A., Phillips, G. N. & Schmidt, M. Enzyme intermediates captured “on the fly” by mix-and-inject serial crystallography. *BMC Biol.* **16**, 59 (2018).

36 Tremblay, L. W., Xu, H. & Blanchard, J. S. Structures of the Michaelis Complex (1.2 Å) and the Covalent Acyl Intermediate (2.0 Å) of Cefamandole Bound in the Active Sites of the *Mycobacterium tuberculosis* β-Lactamase K73A and E166A Mutants. *Biochemistry* **49**, 9685-9687 (2010).

37 Tremblay, L. W., Fan, F. & Blanchard, J. S. Biochemical and structural characterization of *Mycobacterium tuberculosis* beta-lactamase with the carbapenems ertapenem and doripenem. *Biochemistry* **49**, 3766-3773 (2010).

38 Hazra, S., Xu, H. & Blanchard, J. S. Tebipenem, a New Carbapenem Antibiotic, Is a Slow Substrate That Inhibits the β-Lactamase from *Mycobacterium tuberculosis*. *Biochemistry* **53**, 3671-3678 (2014).

39 Lang, P. A., Raj, R., Tumber, A., Lohans, C. T., Rabe, P., Robinson, C. V., Brem, J. & Schofield, C. J. Studies on enmetazobactam clarify mechanisms of widely used β-lactamase inhibitors. *Proc. Natl. Acad. Sci. U.S.A.* **119**, e2117310119 (2022).

40 Aoki, T., Yoshizawa, H., Yamawaki, K., Yokoo, K., Sato, J., Hisakawa, S., Hasegawa, Y., Kusano, H., Sano, M., Sugimoto, H., Nishitani, Y., Sato, T., Tsuji, M., Nakamura, R., Nishikawa, T. & Yamano, Y. Cefiderocol (S-649266), A new siderophore cephalosporin exhibiting potent activities against Pseudomonas aeruginosa and other gram-negative

pathogens including multi-drug resistant bacteria: Structure activity relationship. *Eur. J. Med. Chem.* **155**, 847-868 (2018).

41 Sato, T. & Yamawaki, K. Cefiderocol: Discovery, Chemistry, and In Vivo Profiles of a Novel Siderophore Cephalosporin. *Clin. Infect. Dis.* **69**, S538-s543 (2019).

42 Morrison, J. F. & Walsh, C. T. The behavior and significance of slow-binding enzyme inhibitors. *Adv. Enzymol. Relat. Areas Mol. Biol.* **61**, 201-301 (1988).

43 Lang, P. A., Parkova, A., Leissing, T. M., Calvopiña, K., Cain, R., Krajnc, A., Panduwawala, T. D., Philippe, J., Fishwick, C. W. G., Trapencieris, P., Page, M. G. P., Schofield, C. J. & Brem, J. Bicyclic Boronates as Potent Inhibitors of AmpC, the Class C β-Lactamase from *Escherichia coli*. *Biomolecules* **10**, 899 (2020).

Chapter 8

Discussion and Conclusion

Contents

8.1 L,D-Transpeptidases are promising drug targets for tuberculosis 188
8.2 Novel inhibitors for Ldt_{Mt2} have been identified 189
8.3 Insights into the mechanism of Ldt_{Mt2} 191
8.4 Cellular inhibition of L,D-transpeptidases and penicillin binding proteins 192
8.5 Inhibition of BlaC 193
8.6 Future perspectives 194
8.7 Conclusions 196
8.8 References 197

8.1 L,D-Transpeptidases are promising drug targets for tuberculosis

Despite being a curable and preventable infective disease, tuberculosis (TB) continues to impose major impact on global health, with an estimated annual mortality rate of 1.6 million in 2021.[1] Current treatment regimens typically consist of combinatorial treatment with four anti-TB drugs, taken for the duration of 4-6 months.[2] Efficacy, however, is impaired due to various factors such as toxicity, treatment nonadherence, and the emergence of drug resistance.[3-5] The unmet need for novel anti-TB therapeutics is evident, however, the development of therapeutics targeting *Mycobacterium tuberculosis* (*Mtb*), the causative agent of TB, has been proven to be challenging, as only a limited number of new anti-TB drugs have emerged in the last 50 years (Chapter 1).[6,7] In particular, *Mtb* residing in dormancy have demonstrated resistance to drug treatment.[8-11]

The inhibition of the transpeptidases involved in peptidoglycan biosynthesis is an antibiotic target with great, broad-spectrum success: the β-lactam antibiotics, which are target the D,D-transpeptidases (also known as penicillin binding proteins, or PBPs), are amongst the most prescribed drugs.[12] While *Mtb* is generally considered to be resistant to β-lactams due to the presence of the β-lactamases, in particular BlaC,[13] combinations of β-lactams and β-lactamase inhibitors show promise for the treatment of TB,[14-16] though optimisation will likely be required in order to reach clinically relevant activity (Chapter 2).[15]

Mtb contains multiple transpeptidases (Figure 8.1), involving at least seven PBPs, and five L,D-transpeptidases (Ldts), many of which are apparently redundant.[17] However, reports suggest that while PBP and Ldt paralogs have apparently similar functions, complex dynamically interacting networks exist,[18-20] and different paralogs are likely to play specific roles in diverse metabolic states of *Mtb*, with Ldts are being important in the aging cell wall and in the maintenance of peptidoglycan in dormancy (Chapter 2).[21-26] It has not been fully elucidated which PBPs and Ldts are essential to obtain therapeutically useful inhibition of *Mtb in vivo*. However, since the majority of cross-links during the stationary phase are catalysed by Ldts, they have emerged as drug targets of considerable interest.[27,28] The majority of the 3→3 cross-linking is catalysed by Ldt_{Mt2}, which is therefore considered as the main Ldt of *Mtb*.[25] It has been suggested that inhibition of Ldt_{Mt2} alone may be sufficient to inhibit all 3→3 cross-linking activity,[25] though dual inhibition of Ldt_{Mt1} and Ldt_{Mt2} has an additive effect on *Mtb* growth and susceptibility to β-lactam antibiotics.[29]

The work described in this thesis aimed to study the mechanism and inhibition of Ldt_{Mt2}, and aimed to further elucidate the effect of Ldt inhibition on *Mtb*, using a variety of biochemical, biophysical, and microbiological techniques.

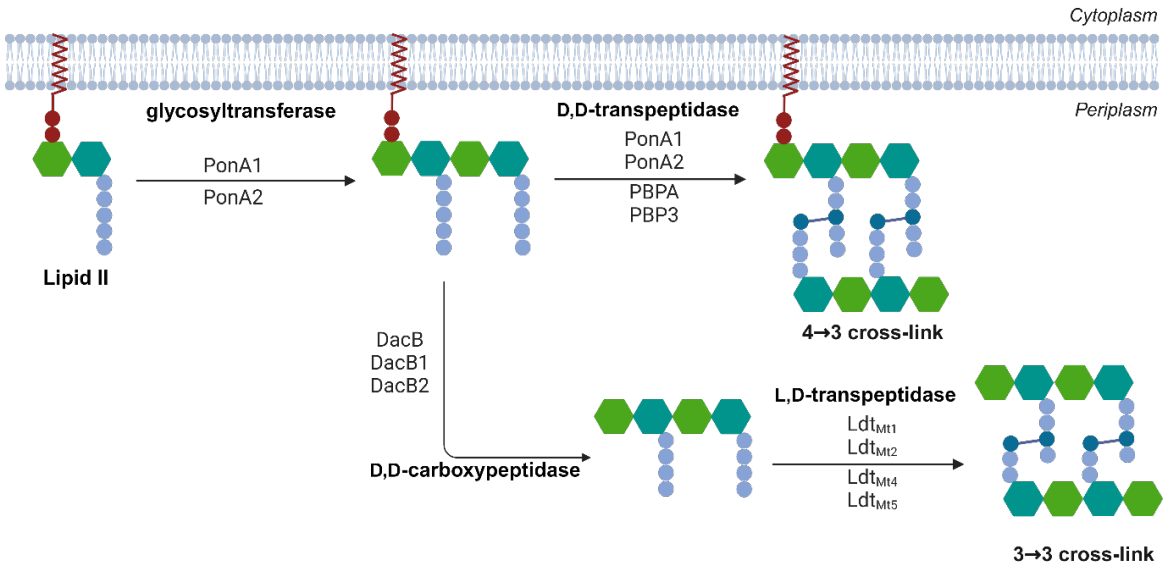

Figure 8.1. Summary of the reactions of the penicillin binding proteins (PBPs) and the L,D-transpeptidases (Ldts) in *Mycobacterium tuberculosis*. The PBPs have D,D-transpeptidase (some with additional glycosyltransferase activity), forming 4→3 cross-links, or D,D-carboxypeptidase activity. Ldts are responsible for the formation of 3→3 cross-links. Note that the function of the Ldt$_{Mt3}$ has not been elucidated. The figure was created using BioRender.com.

8.2 Novel inhibitors for Ldt$_{Mt2}$ have been identified

Inhibition of Ldt$_{Mt2}$ has thus far mainly focussed on inhibition by β-lactams, in particular by penem and carbapenem β-lactams,[30,31] which inhibit Ldt$_{Mt2}$ through covalent reaction with its nucleophilic cysteine (Cys354), forming a thioester adduct.[32] However, the nucleophilic cysteine is able to react with a larger variety of electrophilic compounds, as has been demonstrated with a small library of cysteine reactive agents, such as ebselen.[33] Therefore, a high-throughput screen (HTS) for the identification of Ldt$_{Mt2}$ inhibitors, making use of a targeted library of diverse electrophilic compounds, was performed (Figure 8.2; Chapter 3).[34]

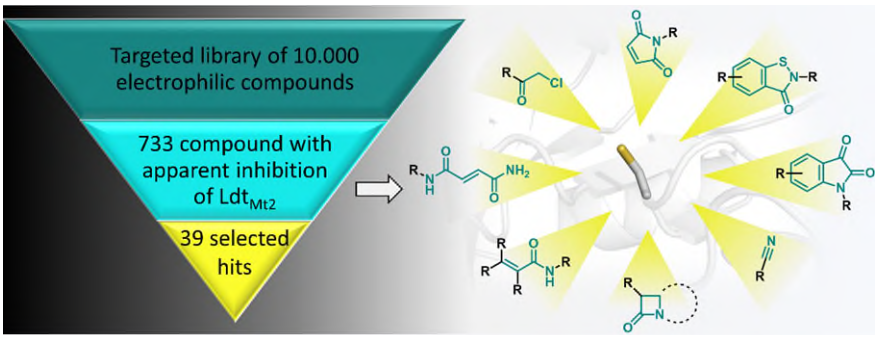

Figure 8.2. A high-throughput screen for the identification of Ldt$_{Mt2}$ inhibitors has yielded 39 potent inhibitors of Ldt$_{Mt2}$. Hit compounds contained a variety of electrophilic groups, that react with the nucleophilic cysteine of Ldt$_{Mt2}$.

A variety of potent inhibitors were identified, including two novel cephalosporins (pIC_{50}s 5.55-5.62; Figure 8.3), a β-lactam class which has previously been considered to not be able to inhibit Ldt_{Mt2}. The cephalosporins were surprisingly reaching inhibitory potency similar to that of the known Ldt_{Mt2} inhibitors meropenem,[35] biapenem,[36] and doripenem[37] (pIC_{50}s 5.54-5.87).

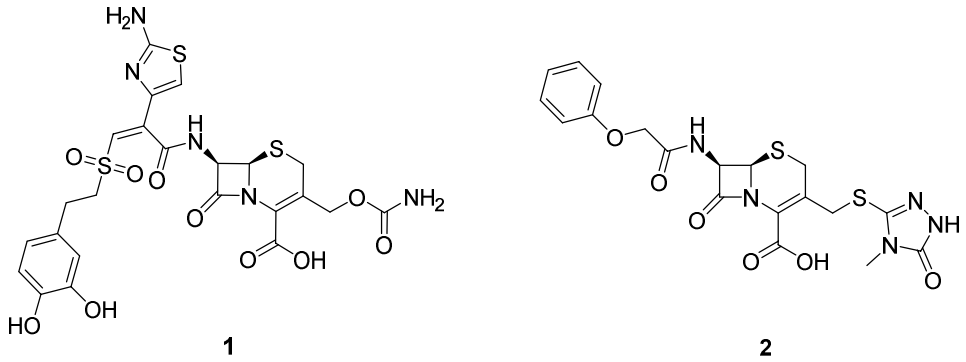

Figure 8.3. Structures of the cephalosporins 1 and 2, identified as inhibitors of Ldt_{Mt2}.

Mass spectrometric (MS) and X-ray crystallographic studies revealed that the majority of hit compounds react covalently with the nucleophilic cysteine of Ldt_{Mt2}, which was apparently able to react with a large variety of established (e.g., the β-lactams and maleimides) and novel electrophilic reacting groups (e.g., the cyanamides). The cyanamides are of particular interest due to their potency (pIC_{50} 6.39-7.53), and notable mechanism of inhibition, as the cyanamides were observed (in MS and X-ray crystallographic studies) to cyanate the nucleophilic cysteine of Ldt_{Mt2}. Out of the 39 HTS hit compounds selected for follow-up studies, 11 compounds were found to inhibit *Mtb* while residing in macrophages (MIC_{50} 0.98 – 38.9 μM), though no inhibitory activity of *Mtb* in media was obtained, suggesting that the activity of the inhibitors is dependent on the metabolic state of *Mtb*, which are likely to be dormant when residing in macrophages.[38-40]

The αβ,α′β′-diepoxyketones (DEKs) represent another novel class of mechanism-based covalently binding inhibitors identified in the HTS (Figure 8.4; Chapter 4).[41] The DEKs were found to inhibit Ldt_{Mt2} via reaction with one of the symmetrical epoxide groups, leading to ring opening, followed by retro-aldol reaction, leading to apparently irreversible alkylation. This reaction was as well observed in the main protease of SARS-CoV-2 (M^{pro}), another nucleophilic cysteine enzyme.

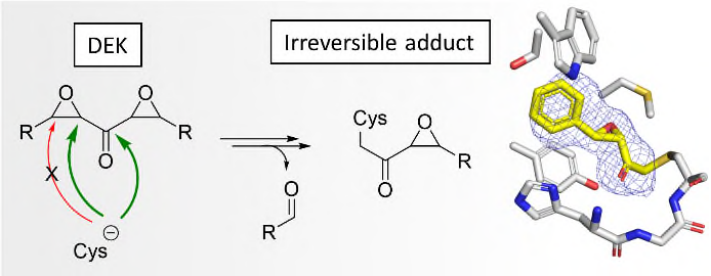

Figure 8.4. αβ,α′β′-Diepoxyketones (DEKs) are inhibitors of nucleophilic cysteine enzymes. DEKs initially react with a nucleophilic cysteine (evidenced with Ldt_{Mt2} and the SARS-CoV-2 main protease) via epoxide ring opening. Subsequently, retro-aldol and other reactions can occur, leading to apparently irreversible alkylation.

8.3 Insights into the mechanism of Ldt_{Mt2}

Despite the biological importance of Ldt_{Mt2}, studies of the 3→3 cross-linking reaction catalysed by Ldt_{Mt2} have been limited, likely (at least partially) due to the limited availability of the disaccharide tetrapeptide (GlcNAc-MurNAc-L-Ala-D-$iGlu_{NH2}$-*m*-DAP_{NH2}-D-Ala) monomer, which has been identified as the substrate of Ldt_{Mt2}.[25] The chemical synthesis of this substrate has been reported to yield low amounts of material.[42] Optimisation of the isolation of this Ldt_{Mt2} from the cell wall of *Corynebacterium jeikeium*, using subinhibitory concentrations of ampicillin to allow for overproduction of peptidoglycan, yielded increased amounts of the Ldt_{Mt2} substrate (~20.5 mg per 55.9 g dried cell mass; Chapter 5).

X-ray crystallographic studies provided a crystal structure of Ldt_{Mt2} in complex with its substrate. In the structure, the substrate is covalently linked to Ldt_{Mt2} by a thioester unit, apparently reflecting the thioester intermediate during the catalysis of the transpeptidase reaction (Chapter 5). This structure suggests that the donor substrate of Ldt_{Mt2} enters the active site via the inner cavity of the catalytic domain, positioning *m*-DAP_{NH2} into the outer cavity to allow a covalent reaction with the nucleophilic Cys354 (Figure 8.5). This crystal structure provides insights into the active site interactions of Ldt_{Mt2} and its substrate, which will be used in the design of novel inhibitors, including those based on the substrate structure, a method which has been effective in the inhibitor development for M^{pro}.[43,44] However, experiments determining enzyme kinetics suggest that the isolated Ldt_{Mt2} has low affinity with the isolated substrate, suggesting that optimisation of interactions will be required, and cellular inhibition assays of substrate-based Ldt_{Mt2} inhibitors in cells may be essential.

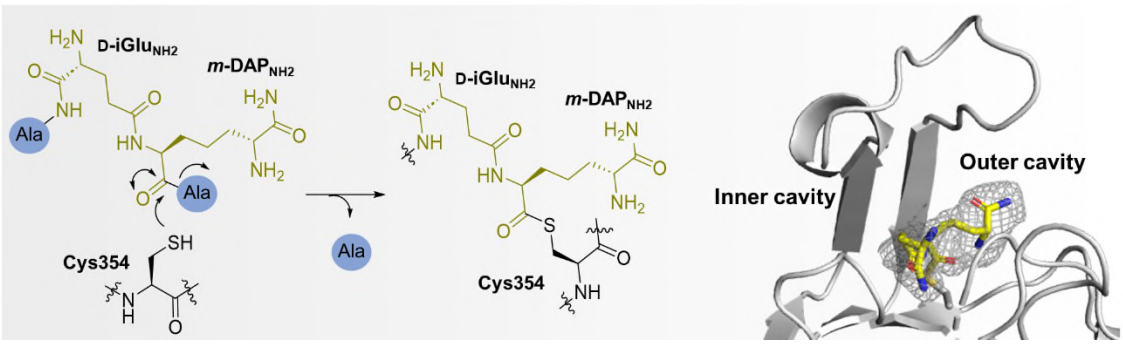

Figure 8.5. The first step of the 3→3 cross-linking reaction involves reaction between the tetrapeptide L-Ala-D-iGlu$_{NH2}$-*m*-DAP$_{NH2}$-D-Ala and the nucleophilic cysteine of Ldt$_{Mt2}$ (Cys354) to form a thioester intermediate, as observed in X-ray crystallographic studies.

8.4 Cellular inhibition of L,D-transpeptidases and penicillin binding proteins

Due to the intricate network of interactions partners of β-lactams (Chapter 2), it is challenging to assign the precise roles of PBPs and Ldts on mycobacterial inhibition. An assay to assess Ldt and PBP transpeptidase activity individually in live cells has been reported, making use of fluorescent mimics of substrates for Ldts and PBPs.[45] Applying this assay, PBP and Ldt inhibition by a selection of β-lactams and Ldt$_{Mt2}$ inhibitors was assessed with *Mycobacterium smegmatis* (*Msm*), a validated model organism of *Mtb*,[46] and related to the minimum inhibitory concentration (MIC) of the same inhibitor (Figure 8.6; Chapter 6). Notably, inhibition of D,D-transpeptidases could not be related to inhibition of growth. Several penicillins, penems, and carbapenems, were able to fully inhibit incorporation of the fluorescent substrate mimic while not inhibiting growth at the same concentration, putatively suggesting that PBP inhibition alone is not the optimal strategy for mycobacterial inhibition, at least under the tested conditions. Alternatively, Ldts were often partially (~50%) inhibited at the concentrations which inhibit growth, as observed with penems, carbapenems, cephalosporins, and two Ldt$_{Mt2}$ inhibitors, putatively suggesting that partial Ldt inhibition, perhaps in combination of D,D-transpeptidase inhibition, leads to inhibition of growth. This observation is in line with reported proposals that Ldt inhibition, in combination with PBP inhibition, leads to efficient inhibition of mycobacterial growth.[25,47] The development of inhibitors selective for Ldts that do not inhibit PBPs should enable further understanding into role of Ldt inhibition in relation to inhibition of growth.

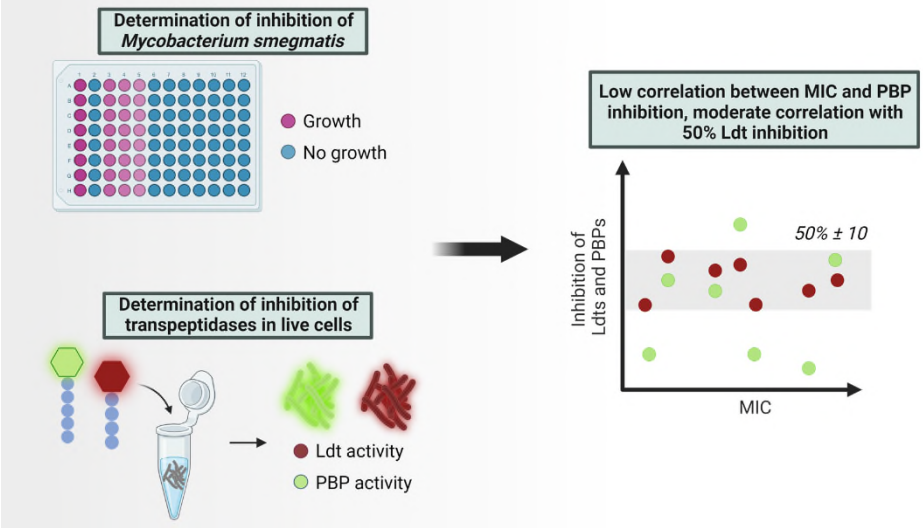

Figure 8.6. The cellular inhibition of the transpeptidases of *Mycobacterium smegmatis* and the inhibition of growth were evaluated with β-lactams and Ldt_{Mt2} inhibitors. Inhibition of PBPs could not be related to inhibition of growth, while inhibition of ~50% of Ldts could be related to inhibition of growth in with most tested inhibitors. The figure was created using BioRender.com.

Interestingly, a sulfonyl pyridine identified in the HTS for Ldt_{Mt2} exhibited potent inhibition of *Msm* (8 µg/mL). This observation, however, could not be related to inhibition of Ldts or PBPs in the cellular inhibition experiments, and likely acts through a different mechanism of action. Though this compound (as well as a selection of derivatives) was able to inhibit Ldt_{Mt2} via nucleophilic aromatic substitution (pIC_{50} 4.6-6.1), the electrophilic reactivity of derivatives did not appear to correlate to inhibition of *Msm*, which was particularly dependent on the presence of a nitro group on the pyridine ring.

8.5 Inhibition of BlaC

BlaC, the Ambler class A β-lactamase of *Mtb*, was used as a secondary assay of the HTS for Ldt_{Mt2}, and interestingly identified cephalosporin **1** as a potent inhibitor of BlaC (pIC_{50} 7.72; Figure 8.7). This is an interesting observations, not least because BlaC is generally considered to be a cephalosporinase.[48,49] Detailed studies of the inhibition kinetics suggested notable and unusual stability of the acyl-enzyme complex resulting from reaction with **1** (Chapter 7). Inhibition of BlaC by **1** was similar to that observed with clavulanic acid, which is approved for clinical use in combination with meropenem or imipenem in the treatment of drug-resistant TB.[50] It is particularly noteworthy that **1** was a moderate inhibitor of Ldt_{Mt2} (pIC_{50} 5.55) and a potent inhibitor of the essential PBP3 (pIC_{50} 6.14), though had poor activity against *Msm* (MIC 64 µg/mL; Chapter 6), and moderate antibiotic activity against *Mtb* residing in macrophages (MIC_{50} 38.9 µM; Chapter 3). However, **1** may provide a starting point for targeted optimisation

efforts. Structural studies with Ldt_{Mt2}, PBP3, and BlaC may provide further insights into the essential interactions with the respective enzymes.

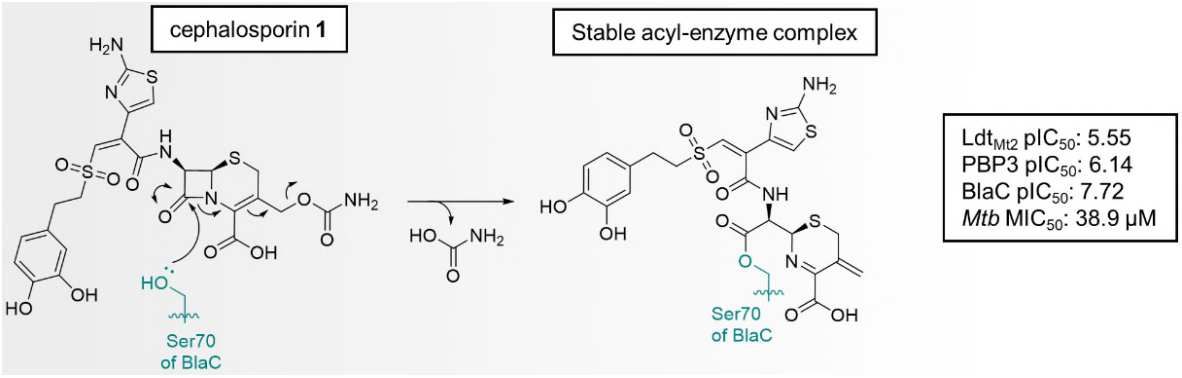

Figure 8.7. Cephalosporin 1 reacts with BlaC to form an acyl-enzyme complex that exhibits notable and unusual stability. In addition to inhibiting BlaC, **1** is an inhibitor of Ldt_{Mt2} and PBP3, but displays only moderate inhibition of *Mtb* residing in macrophages.

It should also be noted that **1** contains a catechol in its sidechain. Catechols have been exploited to promote penetration into gram-negative bacteria, with the siderophore cephalosporin cefiderocol (Figure 8.8) being an important new medicine.[51,52] There is no evidence that the catechol of **1** is relevant to the moderate cellular activity against *Mtb* and *Msm*, though further investigations towards the merit of catechol sidechains in mycobacterial treatments is warranted.

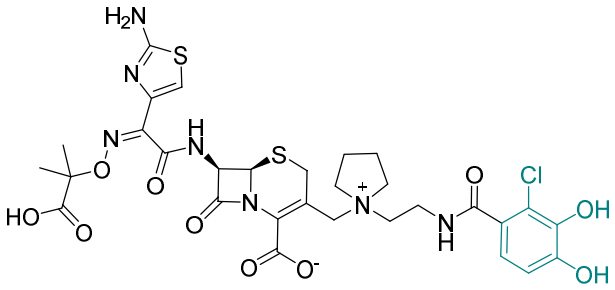

Figure 8.8. Structure of the cefiderocol. The catechol moiety is in teal.

8.6 Future perspectives

The development of inhibitors selective for Ldt_{Mt2} should aid in the elucidation of the effect of its inhibition on *Mtb*, and support in the identification of essential targets within the assemble of mycobacterial transpeptidases. The Ldt_{Mt2} inhibitors identified in the HTS (Chapter 3) are generally small (MW 200-350 Da), reactive compounds that would require optimisation to reach selectivity towards Ldt_{Mt2}. Studies with a small selection of cell active Ldt_{Mt2} inhibitors

exhibited inhibition of both Ldts and PBPs in live *Msm* cells (Chapter 6). β-Lactams may inhibit Ldts, (Chapter 2, Chapter 3, Chapter 6), but will likely also inhibit PBPs. Evidence for the possibility to develop β-lactams as specific Ldt inhibitors has not been reported. Another approach may be the development of inhibitors based on the structure of the substrate for Ldts, the disaccharide tetrapeptide monomer, optimised for increased interactions based on the structure of the thioester intermediate of the transpeptidase reaction with Ldt_{Mt2} (Chapter 5), which should hold potential for selectivity for Ldts over PBPs.

Inhibition of both Ldts and PBPs is likely required to inhibit both replicating and non-replicating *Mtb*, presenting interest in the targeted development of dual inhibitors. Currently, research suggests that the β-lactam classes of (carba)penems and cephalosporins are of particular interest for optimisation for inhibition of the PBPs and Ldts of mycobacteria (Chapter 2, Chapter 6). The carbapenems are particularly potent for the inhibition of Ldts, PBPs, and exhibit increased stability against BlaC. In MIC studies with *Mtb*, they have often been identified as the most potent in comparison to other β-lactam classes.[14-16] The cellular inhibition assays with *Msm* described in Chapter 6 reflected particularly potent inhibition of both PBPs and Ldts by imipenem. However, downsides of carbapenems include low stability in aqueous solutions and low oral bioavailability.[15] By contrast, some cephalosporins are used orally; indeed, the cephalosporins are probably the most important class of antibacterials.[12]

Early inhibition studies of Ldt_{Mt2} with cephalosporins suggested this compound class does not potently inhibit Ldt_{Mt2}.[31,53] This proposal is contradicted by the results of the HTS for Ldt_{Mt2}, which identified cephalosporins **1** and **2** (Figure 8.3) with inhibitory potency similar to meropenem under the same assay conditions (Chapter 3), evidencing the potential for sidechain optimisation to enable inhibition of Ldts by cephalosporins. Cephalosporin **1** has been identified as particularly interesting in biochemical inhibition studies, exhibiting inhibition of both Ldt_{Mt2} and PBP3 of *Mtb*, while being a very slow substrate of BlaC. Unfortunately, the biochemical inhibition did not translate to potent inhibition of *Mtb*, though targeted SAR studies of **1** may reveal highly potent inhibitors of *Mtb*.

An interesting feature of cephalosporins is that the formation of an acyl-enzyme complex leading to β-lactam ring opening is often accompanied with fragmentation of the C2 sidechain. Cephalosporins may therefore be utilised to carry small compounds into the periplasmic space, where they are released upon β-lactamase (and potentially PBP) mediated hydrolysis and present further cytotoxic functions, exhibited by cephalosporins releasing a pyrithione moiety.[54] The same principle may be applied to transport highly potent Ldt_{Mt2} inhibitors, e.g., the cyanamides (Chapter 3) into the periplasmic space (Figure 8.9).

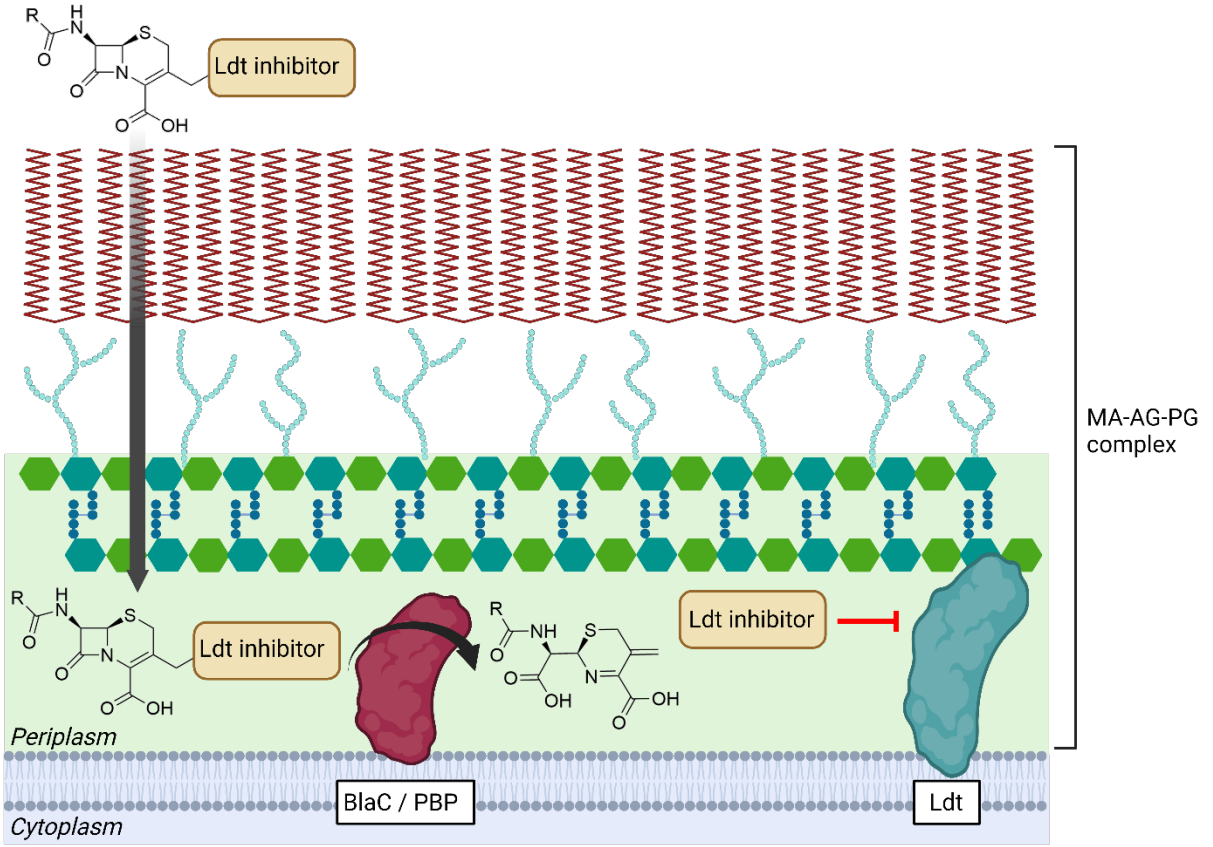

Figure 8.9. Cephalosporins may enable the transportation of a small, L,D-transpeptidase (Ldt) reactive compound into the periplasmic space of *Mycobacterium tuberculosis* through loss of the C2 sidechain upon reaction with BlaC and/or penicillin binding proteins (PBPs).

Studies have shown that the *Mtb* strains lacking both Ldt_{Mt1} and Ldt_{Mt2} leads to an increased impact on *Mtb* compared to strains lacking only Ldt_{Mt2}.[29] Therefore, dual inhibitors of Ldt_{Mt1} and Ldt_{Mt2} may be actively pursued. Testing the Ldt_{Mt2} inhibitors presented in this thesis against Ldt_{Mt1}, as well as other Ldt paralogs is therefore of interest in future studies.

8.7 Conclusions

Overall, the work presented in this thesis reports on the identification of novel inhibitors of Ldt_{Mt2}, a promising drug target of *Mtb*, and studies of their mechanism of inhibition at the molecular level, and at the cellular level in the model organism *Msm*. Further, mechanistic studies on the Ldt_{Mt2} catalysis of 3→3 cross-linking of the disaccharide tetrapeptide monomer of the peptidoglycan layer of *Mtb* are presented in this thesis. The work may inform on the design and development of novel inhibitors of Ldt_{Mt2}, as well as dual inhibitors of Ldts and PBPs.

8.8 References

1 Global tuberculosis report 2022. . Report No. Licence: CC BY-NC-SA 3.0 IGO, (Geneva: World Health Organization, 2022).

2 *Treatment of tuberculosis: guidelines*. (World Health Organization, 2010).

3 Rabahi, M. F., Silva Júnior, J., Ferreira, A. C. G., Tannus-Silva, D. G. S. & Conde, M. B. Tuberculosis treatment. *J. Bras. Pneumol.* **43**, 472-486 (2017).

4 Tola, H. H., Tol, A., Shojaeizadeh, D. & Garmaroudi, G. Tuberculosis Treatment Non-Adherence and Lost to Follow Up among TB Patients with or without HIV in Developing Countries: A Systematic Review. *Iran J. Public Health* **44**, 1-11 (2015).

5 Seung, K. J., Keshavjee, S. & Rich, M. L. Multidrug-Resistant Tuberculosis and Extensively Drug-Resistant Tuberculosis. *Cold Spring Harb. Perspect. Med.* **5**, a017863 (2015).

6 Ginsberg, A. M. & Spigelman, M. Challenges in tuberculosis drug research and development. *Nature Med.* **13**, 290-294 (2007).

7 Dartois, V. A. & Rubin, E. J. Anti-tuberculosis treatment strategies and drug development: challenges and priorities. *Nature Rev. Microbiol.* **20**, 685-701 (2022).

8 Zhang, Y., Yew, W. W. & Barer, M. R. Targeting persisters for tuberculosis control. *Antimicrob. Agents Chemother.* **56**, 2223-2230 (2012).

9 Zhang, Y. Persisters, persistent infections and the Yin-Yang model. *Emerg. Microbes Infect.* **3**, e3 (2014).

10 Gomez, J. E. & McKinney, J. D. *M. tuberculosis* persistence, latency, and drug tolerance. *Tuberculosis (Edinb.)* **84**, 29-44 (2004).

11 Monack, D. M., Mueller, A. & Falkow, S. Persistent bacterial infections: the interface of the pathogen and the host immune system. *Nat. Rev. Microbiol.* **2**, 747-765 (2004).

12 Bush, K. & Bradford, P. A. β-Lactams and β-Lactamase Inhibitors: An Overview. *Cold Spring Harb. Perspect. Med.* **6** (2016).

13 Chambers, H. F., Moreau, D., Yajko, D., Miick, C., Wagner, C., Hackbarth, C., Kocagöz, S., Rosenberg, E., Hadley, W. K. & Nikaido, H. Can penicillins and other beta-lactam antibiotics be used to treat tuberculosis? *Antimicrob. Agents Chemother.* **39**, 2620-2624 (1995).

14 Gun, M. A., Bozdogan, B. & Coban, A. Y. Tuberculosis and beta-lactam antibiotics. *Future Microbiol.* **15**, 937-944 (2020).

15 Jaganath, D., Lamichhane, G. & Shah, M. Carbapenems against *Mycobacterium tuberculosis*: a review of the evidence. *Int. J. Tuberc. Lung Dis.* **20**, 1436-1447 (2016).

16 Story-Roller, E. & Lamichhane, G. Have we realized the full potential of β-lactams for treating drug-resistant TB? *IUBMB Life* **70**, 881-888 (2018).

17 Cole, S. T., Brosch, R., Parkhill, J., Garnier, T., Churcher, C., Harris, D., Gordon, S. V., Eiglmeier, K., Gas, S., Barry, C. E., Tekaia, F., Badcock, K., Basham, D., Brown, D., Chillingworth, T., Connor, R., Davies, R., Devlin, K., Feltwell, T., Gentles, S., Hamlin, N., Holroyd, S., Hornsby, T., Jagels, K., Krogh, A., McLean, J., Moule, S., Murphy, L., Oliver, K., Osborne, J., Quail, M. A., Rajandream, M. A., Rogers, J., Rutter, S., Seeger, K., Skelton, J., Squares, R., Squares, S., Sulston, J. E., Taylor, K., Whitehead, S. & Barrell, B. G. Deciphering the biology of *Mycobacterium tuberculosis* from the complete genome sequence. *Nature* **393**, 537-544 (1998).

18 Kieser, K. J., Baranowski, C., Chao, M. C., Long, J. E., Sassetti, C. M., Waldor, M. K., Sacchettini, J. C., Ioerger, T. R. & Rubin, E. J. Peptidoglycan synthesis in *Mycobacterium tuberculosis* is organized into networks with varying drug susceptibility. *Proc. Natl. Acad. Sci. U.S.A.* **112**, 13087-13092 (2015).

19 Kieser, K. J., Boutte, C. C., Kester, J. C., Baer, C. E., Barczak, A. K., Meniche, X., Chao, M. C., Rego, E. H., Sassetti, C. M., Fortune, S. M. & Rubin, E. J. Phosphorylation of the Peptidoglycan Synthase PonA1 Governs the Rate of Polar Elongation in Mycobacteria. *PLoS Pathog* **11**, e1005010 (2015).

20 Vandal, O. H., Roberts, J. A., Odaira, T., Schnappinger, D., Nathan, C. F. & Ehrt, S. Acid-susceptible mutants of *Mycobacterium tuberculosis* share hypersusceptibility to cell wall and oxidative stress and to the host environment. *J. Bacteriol.* **191**, 625-631 (2009).

21 Arora, D., Chawla, Y., Malakar, B., Singh, A. & Nandicoori, V. K. The transpeptidase PbpA and noncanonical transglycosylase RodA of *Mycobacterium tuberculosis* play important roles in regulating bacterial cell lengths. *J. Biol. Chem.* **293**, 6497-6516 (2018).

22 DeJesus, M. A., Gerrick, E. R., Xu, W., Park, S. W., Long, J. E., Boutte, C. C., Rubin, E. J., Schnappinger, D., Ehrt, S., Fortune, S. M., Sassetti, C. M. & Ioerger, T. R. Comprehensive Essentiality Analysis of the *Mycobacterium tuberculosis* Genome via Saturating Transposon Mutagenesis. *mBio* **8**, 10.1128/mbio.02133-02116 (2017).

23 Bourai, N., Jacobs, W. R. & Narayanan, S. Deletion and overexpression studies on DacB2, a putative low molecular mass penicillin binding protein from *Mycobacterium tuberculosis* H37Rv. *Microb. Pathog.* **52**, 109-116 (2012).

24 Kandasamy, S., Palaniyandi, K., Gupta, U. D. & Narayanan, S. Double deletion of PknI/DacB2 leads to attenuation of *Mycobacterium tuberculosis* for growth and virulence. *Tuberculosis* **123**, 101957 (2020).

25 Gupta, R., Lavollay, M., Mainardi, J.-L., Arthur, M., Bishai, W. R. & Lamichhane, G. The *Mycobacterium tuberculosis* protein Ldt_{Mt2} is a nonclassical transpeptidase required for virulence and resistance to amoxicillin. *Nat. Med.* **16**, 466-469 (2010).

26 Brammer Basta, L. A., Ghosh, A., Pan, Y., Jakoncic, J., Lloyd, E. P., Townsend, C. A., Lamichhane, G. & Bianchet, M. A. Loss of a Functionally and Structurally Distinct L,D-Transpeptidase, Ldt_{Mt5}, Compromises Cell Wall Integrity in *Mycobacterium tuberculosis*. *J. Biol. Chem.* **290**, 25670-25685 (2015).

27 Seiler, P., Ulrichs, T., Bandermann, S., Pradl, L., Jörg, S., Krenn, V., Morawietz, L., Kaufmann, S. H. & Aichele, P. Cell-wall alterations as an attribute of *Mycobacterium tuberculosis* in latent infection. *J. Infect. Dis.* **188**, 1326-1331 (2003).

28 Bacon, J., Alderwick, L. J., Allnutt, J. A., Gabasova, E., Watson, R., Hatch, K. A., Clark, S. O., Jeeves, R. E., Marriott, A., Rayner, E., Tolley, H., Pearson, G., Hall, G., Besra, G. S., Wernisch, L., Williams, A. & Marsh, P. D. Non-replicating *Mycobacterium tuberculosis* elicits a reduced infectivity profile with corresponding modifications to the cell wall and extracellular matrix. *PLoS One* **9**, e87329 (2014).

29 Schoonmaker, M. K., Bishai, W. R. & Lamichhane, G. Nonclassical Transpeptidases of *Mycobacterium tuberculosis* Alter Cell Size, Morphology, the Cytosolic Matrix, Protein Localization, Virulence, and Resistance to β-Lactams. *J. Bacteriol.* **196**, 1394-1402 (2014).

30 Kumar, P., Kaushik, A., Lloyd, E. P., Li, S.-G., Mattoo, R., Ammerman, N. C., Bell, D. T., Perryman, A. L., Zandi, T. A., Ekins, S., Ginell, S. L., Townsend, C. A., Freundlich, J. S. & Lamichhane, G. Non-classical transpeptidases yield insight into new antibacterials. *Nat. Chem. Biol.* **13**, 54-61 (2017).

31 Steiner, E. M., Schneider, G. & Schnell, R. Binding and processing of β-lactam antibiotics by the transpeptidase Ldt_{Mt2} from *Mycobacterium tuberculosis*. *FEBS J.* **284**, 725-741 (2017).

32 Li, W. J., Li, D. F., Hu, Y. L., Zhang, X. E., Bi, L. J. & Wang, D. C. Crystal structure of L,D-transpeptidase Ldt_{Mt2} in complex with meropenem reveals the mechanism of carbapenem against *Mycobacterium tuberculosis*. *Cell Res.* **23**, 728-731 (2013).

33 de Munnik, M., Lohans, C. T., Lang, P. A., Langley, G. W., Malla, T. R., Tumber, A., Schofield, C. J. & Brem, J. Targeting the *Mycobacterium tuberculosis* transpeptidase Ldt_{Mt2} with cysteine-reactive inhibitors including ebselen. *Chem. Commun.* **55**, 10214-10217 (2019).

34 de Munnik, M., Lang, P. A., De Dios Antos, F., Cacho, M., Bates, R. H., Brem, J., Rodríguez-Miquel, B. & Schofield, C. J. High-Throughput Screen with the L,D-transpeptidase Ldt_{Mt2} of *Mycobacterium tuberculosis* Reveals Novel Classes of Covalently Reacting Inhibitors *Chem. Sci.* **14**, 7262-7278 (2023).

35 Kim, H. S., Kim, J., Im, H. N., Yoon, J. Y., An, D. R., Yoon, H. J., Kim, J. Y., Min, H. K., Kim, S.-J. & Lee, J. Y. Structural basis for the inhibition of *Mycobacterium tuberculosis* L,D-transpeptidase by meropenem, a drug effective against extensively drug-resistant strains. *Acta Crystallogr. D* **69**, 420-431 (2013).

36 Bianchet, M. A., Pan, Y. H., Basta, L. A. B., Saavedra, H., Lloyd, E. P., Kumar, P., Mattoo, R., Townsend, C. A. & Lamichhane, G. Structural insight into the inactivation of *Mycobacterium tuberculosis* non-classical transpeptidase Ldt_{Mt2} by biapenem and tebipenem. *BMC Biochem.* **18** (2017).

37 Tremblay, L. W., Fan, F. & Blanchard, J. S. Biochemical and structural characterization of *Mycobacterium tuberculosis* beta-lactamase with the carbapenems ertapenem and doripenem. *Biochemistry* **49**, 3766-3773 (2010).

38 MacMicking, J. D., Taylor, G. A. & McKinney, J. D. Immune control of tuberculosis by IFN-γ-inducible LRG-47. *Science* **302**, 654-659 (2003).

39 MacMicking, J. D., North, R. J., LaCourse, R., Mudgett, J. S., Shah, S. K. & Nathan, C. F. Identification of nitric oxide synthase as a protective locus against tuberculosis. *Proc. Natl. Acad. Sci. U.S.A.* **94**, 5243-5248 (1997).

40 Gold, B., Smith, R., Nguyen, Q., Roberts, J., Ling, Y., Lopez Quezada, L., Somersan, S., Warrier, T., Little, D. & Pingle, M. Novel cephalosporins selectively active on nonreplicating *Mycobacterium tuberculosis*. *J. Med. Chem.* **59**, 6027-6044 (2016).

41 de Munnik, M., Lithgow, J., Brewitz, L., Christensen, K. E., Bates, R. H., Rodriguez-Miquel, B. & Schofield, C. J. αβ,α'β'-Diepoxyketones are mechanism-based inhibitors of nucleophilic cysteine enzymes. *Chem. Commun. (Camb)* **59**, 12859-12862 (2023).

42 Ngadjeua, F., Braud, E., Saidjalolov, S., Iannazzo, L., Schnappinger, D., Ehrt, S., Hugonnet, J.-E., Mengin-Lecreulx, D., Patin, D., Ethève-Quelquejeu, M., Fonvielle, M. & Arthur, M. Critical Impact of Peptidoglycan Precursor Amidation on the Activity of L,D-Transpeptidases from *Enterococcus faecium* and *Mycobacterium tuberculosis*. *Chem. Eur. J.* **24**, 5743-5747 (2018).

43 Yang, H. & Yang, J. A review of the latest research on M^{pro} targeting SARS-COV inhibitors. *RSC Med. Chem.* **12**, 1026-1036 (2021).

44 Owen, D. R., Allerton, C. M. N., Anderson, A. S., Aschenbrenner, L., Avery, M., Berritt, S., Boras, B., Cardin, R. D., Carlo, A., Coffman, K. J., Dantonio, A., Di, L., Eng, H., Ferre, R., Gajiwala, K. S., Gibson, S. A., Greasley, S. E., Hurst, B. L., Kadar, E. P., Kalgutkar, A. S., Lee, J. C., Lee, J., Liu, W., Mason, S. W., Noell, S., Novak, J. J., Obach, R. S., Ogilvie, K., Patel, N. C., Pettersson, M., Rai, D. K., Reese, M. R., Sammons, M. F., Sathish, J. G., Singh, R. S. P., Steppan, C. M., Stewart, A. E., Tuttle, J. B., Updyke, L., Verhoest, P. R., Wei, L., Yang, Q. & Zhu, Y. An oral SARS-CoV-2 M^{pro} inhibitor clinical candidate for the treatment of COVID-19. *Science* **374**, 1586-1593 (2021).

45 Pidgeon, S. E., Apostolos, A. J., Nelson, J. M., Shaku, M., Rimal, B., Islam, M. N., Crick, D. C., Kim, S. J., Pavelka, M. S., Kana, B. D. & Pires, M. M. L,D-Transpeptidase Specific Probe Reveals Spatial Activity of Peptidoglycan Cross-Linking. *ACS Chem. Biol.* **14**, 2185–2196 (2019).

46 Lelovic, N., Mitachi, K., Yang, J., Lemieux, M. R., Ji, Y. & Kurosu, M. Application of Mycobacterium smegmatis as a surrogate to evaluate drug leads against Mycobacterium tuberculosis. *J. Antibiot.* **73**, 780-789 (2020).

47 Baranowski, C., Welsh, M. A., Sham, L. T., Eskandarian, H. A., Lim, H. C., Kieser, K. J., Wagner, J. C., McKinney, J. D., Fantner, G. E., Ioerger, T. R., Walker, S., Bernhardt, T. G., Rubin, E. J. & Rego, E. H. Maturing *Mycobacterium smegmatis* peptidoglycan requires non-canonical crosslinks to maintain shape. *Elife* **7** (2018).

48 Hugonnet, J.-E. & Blanchard, J. S. Irreversible Inhibition of the *Mycobacterium tuberculosis* β-Lactamase by Clavulanate. *Biochemistry* **46**, 11998-12004 (2007).

49 Wang, F., Cassidy, C. & Sacchettini, J. C. Crystal structure and activity studies of the *Mycobacterium tuberculosis* beta-lactamase reveal its critical role in resistance to beta-lactam antibiotics. *Antimicrob. Agents Chemother.* **50**, 2762-2771 (2006).

50 WHO consolidated guidelines on tuberculosis. Report No. ISBN-13: 978-92-4-006312-9, (Geneva: World Health Organization, 2022).

51 Sato, T. & Yamawaki, K. Cefiderocol: Discovery, Chemistry, and In Vivo Profiles of a Novel Siderophore Cephalosporin. *Clin. Infect. Dis.* **69**, S538-s543 (2019).

52 Aoki, T., Yoshizawa, H., Yamawaki, K., Yokoo, K., Sato, J., Hisakawa, S., Hasegawa, Y., Kusano, H., Sano, M., Sugimoto, H., Nishitani, Y., Sato, T., Tsuji, M., Nakamura, R., Nishikawa, T. & Yamano, Y. Cefiderocol (S-649266), A new siderophore cephalosporin exhibiting potent activities against Pseudomonas aeruginosa and other gram-negative pathogens including multi-drug resistant bacteria: Structure activity relationship. *Eur. J. Med. Chem.* **155**, 847-868 (2018).

53 de Munnik, M., Lohans, C. T., Langley, G. W., Bon, C., Brem, J. & Schofield, C. J. A Fluorescence-Based Assay for Screening β-Lactams Targeting the *Mycobacterium tuberculosis* Transpeptidase Ldt_{Mt2}. *ChemBioChem* **21**, 368-372 (2020).

54 Lopez Quezada, L., Li, K., McDonald, S. L., Nguyen, Q., Perkowski, A. J., Pharr, C. W., Gold, B., Roberts, J., McAulay, K., Saito, K., Somersan Karakaya, S., Javidnia, P. E., Porras De Francisco, E., Amieva, M. M., DíAz, S. P., Mendoza Losana, A., Zimmerman, M., Liang, H.-P. H., Zhang, J., Dartois, V., Sans, S., Lagrange, S., Goullieux, L., Roubert, C., Nathan, C. & Aubé, J. Dual-Pharmacophore Pyrithione-Containing Cephalosporins Kill Both Replicating and Nonreplicating *Mycobacterium tuberculosis*. *ACS Infectious Diseases* **5**, 1433-1445 (2019).

Appendix

Contents

Appendix I. Supplementary information for Chapter 3. 203
Appendix II. Supplementary information for Chapter 4. 263
Appendix III. Supplementary information for Chapter 5. 305
Appendix IV. Supplementary information for Chapter 6. 338
Appendix V. Protein purification..... 368
Appendix VI. Sequences of protein constructs 371

Appendix I. Supplementary information for Chapter 3.

High-throughput screen with the L,D-transpeptidase Ldt_{Mt2} of *Mycobacterium tuberculosis* reveals novel classes of covalently reacting inhibitors

Manuscript I

Reproduced from

Mariska de Munnik, Pauline A. Lang, Francisco De Dios Anton, Mónica Cacho, Robert H. Bates, Jürgen Brem, Beatriz Rodríguez Miquel, and Christopher J. Schofield. High-throughput screen with the L,D-transpeptidase Ldt_{Mt2} of *Mycobacterium tuberculosis* reveals novel classes of covalently reacting inhibitors. *Chem. Sci.* **14**, 7262-7278 (2023).

with permission from the Royal Society of Chemistry.

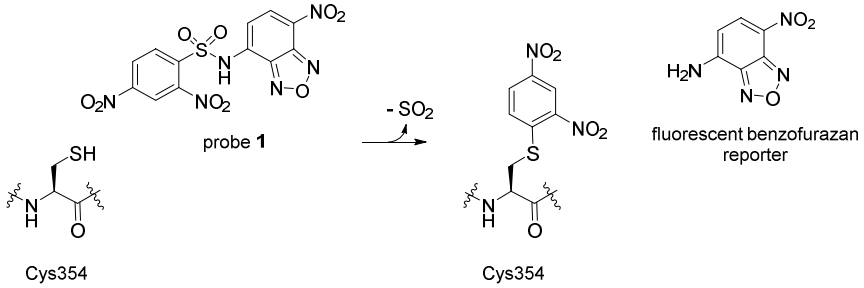

Figure S1.1. Basis of the high-throughput screen assay for Ldt_{Mt2} inhibitors. Reaction of the Ldt_{Mt2} nucleophilic Cys354 with probe **1** releases a fluorescent benzofurazan reporter molecule.[1]

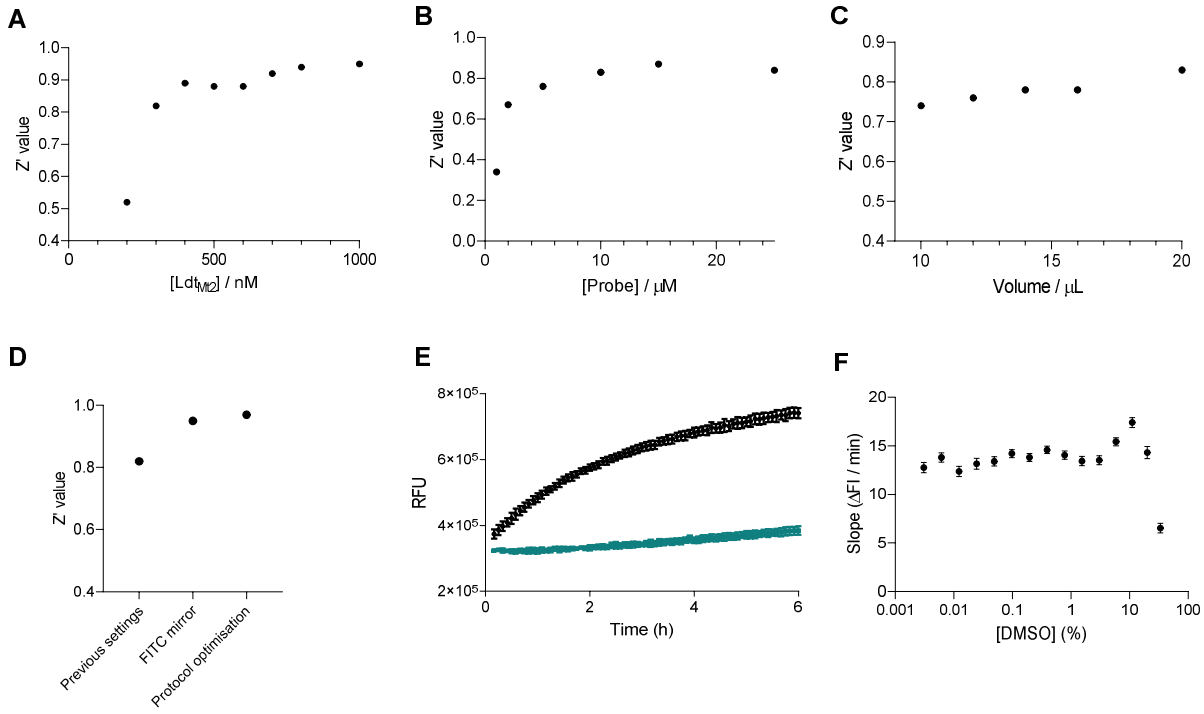

Figure S1.2. Optimisation of the HTS assay for Ldt$_{Mt2}$. A. Z' values obtained with varying concentrations of Ldt$_{Mt2}$ at a fixed probe **1** concentration (20 µM). The Z' values were ≥ 0.8 for Ldt$_{Mt2}$ concentrations ≥ 300 nM. **B.** Z' values obtained with varying concentrations of probe **1** at a fixed Ldt$_{Mt2}$ concentration (300 nM). The optimal Z' value (0.87) was obtained with probe **1** at 15 µM. **C.** Z' values obtained with varying reaction volumes, using fixed Ldt$_{Mt2}$ (300 nM) and probe **1** (15 µM) concentrations. A lower reaction volume decreased the Z' value, but up to a volume of 10 µL, the Z' values are sufficiently high (≥ 0.40). **D.** Optimisation of the plate reader settings improved the Z' values of the assay. The optimisation protocol included exchanging the general dual mirror to a FITC mirror increases the Z' value from 0.82 to 0.95. Optimising the plate reader protocol in terms of coordinates of corners, measurement height and gain further improved the Z' value to 0.97. **E.** Time-course of the relative fluorescence units (RFU) measured on reaction of probe **1** (15 µM) with (300 nM, black) and without (teal) Ldt$_{Mt2}$ at room temperature in (error bars; SD, n=32). The reaction between probe **1** and Ldt$_{Mt2}$ was shown to reach completion after 5 hours, with the initial linear phase lasting **1** hour. **F.** DMSO interference assay. Assays were performed at varied DMSO concentrations (error bars; SD, n=4). Up to a concentration of 3% (*v/v*) DMSO did not affect the assay. Assays were carried out with 300 nM Ldt$_{Mt2}$ and 15 µM probe **1** at room temperature. Assays were carried out at room temperature in 50 mM sodium phosphate pH 7.5 with 0.01% (*v/v*) Triton X-100. Assays in **A** and **B** used reaction volumes of 25 µL. Assays in **D** - **F** used reaction volumes of 10 µL.

Table S1.1. Influence of detergents on Z' and signal to background ratio (S/B). The reaction between Ldt_{Mt2} (300 nM) and probe **1** (15 µM) was monitored at room temperature in 50 mM sodium phosphate pH 7.5 in the presence of the indicated detergents. The maximum tolerated concentrations of each detergent were determined in interference assays at varying detergent concentrations and were defined as the highest tested concentration at which no interference was observed.

Detergent	Maximum tolerated concentration (*v/v*)	Z'	S/B
Triton X-100	0.03%	0.77	2.5
Triton X-114	0.02%	0.77	2.3
Tween-20	0.007%	0.82	3.2
Tween-80	0.001%	0.66	2.2
MEGA-8	1.25%	0.77	3.3
CHAPS	0.245%	0.76	2.8
BRIJ-35	0.000054%	N.D.	N.D.
IPEGAL-630	0.00028%	N.D.	N.D.
DDM	0.00014%	N.D.	N.D.
BSA	<0.00064%	N.D.	N.D.
dBSA	<0.00064%	N.D.	N.D.

Table S1.2. Stability analysis of Ldt_{Mt2} and probe 1 stock solutions. The stabilities of stock solutions of Ldt_{Mt2} and probe **1** were assessed by comparing the Z' and signal to background ratios (S/B) of the assay using fresh and aged (7 h, on ice) stock solutions. The results show very similar Z' and S/B values. Assays were carried out with 300 nM Ldt_{Mt2} and 15 µM probe **1** at room temperature in 50 mM sodium phosphate pH 7.5 with 0.007% (*v/v*) Tween-20.

	Z'	S/B
Fresh stocks	0.97	14.5
7 hours old stocks	0.96	14.4

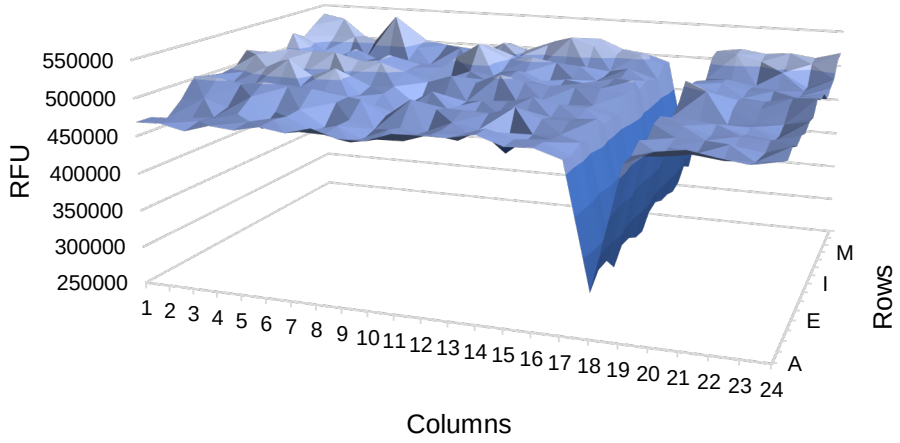

Figure S1.3. Analysis of a 384-well plate to test for variance in plate patterns. The full plate analysis using final assay conditions (300 nM Ldt_{Mt2} and 15 µM probe **1** at room temperature in 50 mM sodium phosphate pH 7.5 with 0.007% (*v/v*) Tween-20) shows no evidence for non-specific patterns across the assay plate, as measured 1 h after start of the reaction. Column 18 represents the no enzyme control.

Table S1.3. Dose-response analysis results for tool compounds. Compounds were incubated with Ldt_{Mt2} or Blac (10 min), then assayed using the optimised assay conditions (see Experimental Details). Inhibition assays of Ldt_{Mt2} were carried out with 300 nM Ldt_{Mt2} and 15 µM probe **1** at room temperature in 50 mM sodium phosphate pH 7.5 with 0.007% (*v/v*) Tween-20. Inhibition assays of BlaC were carried out with 2.5 nM BlaC and 2.5 µM FC5 at room temperature in 100 mM sodium phosphate pH 7.5 with 0.01% (*v/v*) Triton X-100. pIC_{50}s were determined via non-linear regression in Graphpad Prism. (n=4, mean ± SD)

Compound	Structure	pIC_{50} Ldt_{Mt2} (mean ± SD)	pIC_{50} BlaC (mean ± SD)
Faropenem	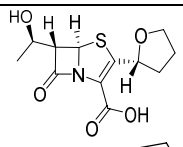	6.5 ± 0.04	6.35 ± 0.03
Sulopenem	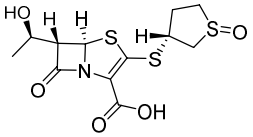	6.2 ± 0.03	6.60 ± 0.12
Panipenem	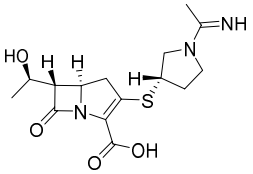	6.5 ± 0.05	6.78 ± 0.01
Ertapenem	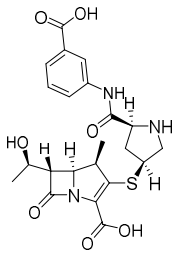	5.8 ± 0.08	6.75 ± 0.03
Doripenem	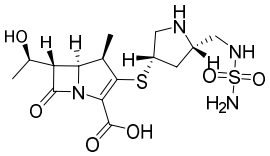	5.3 ± 0.16	7.38 ± 0.04
Meropenem	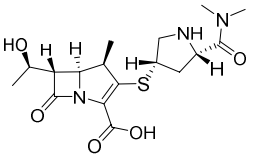	5.0 ± 0.11	6.85 ± 0.05
Biapenem	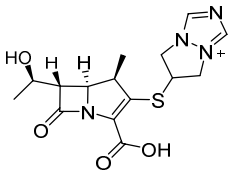	4.1 ± 0.03	5.51 ± 0.09
Flucloxacillin	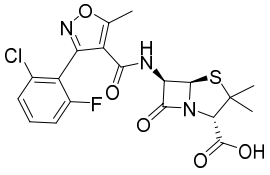	4.6 ± 0.09	6.87 ± 0.03

Compound	Structure	pIC_{50} Ldt_{Mt2} (mean ± SD)	pIC_{50} BlaC (mean ± SD)
Oxacillin	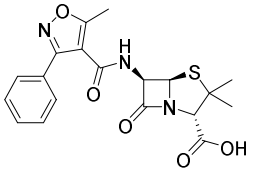	4.2 ± 0.03	6.80 ± 0.01
Ticarcillin	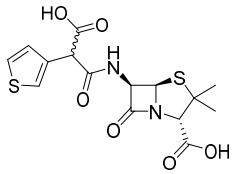	<4.0	4.93 ± 0.01
Carbenicillin	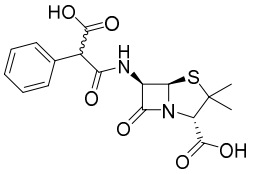	<4.0	<4.0
Sulbactam	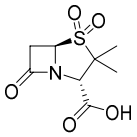	<4.0	5.12 ± 0.01
Zidebactam	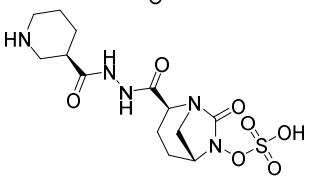	4.0 ± 0.02	4.15 ± 0.10
Relebactam	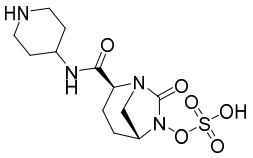	<4.0	4.48 ± 0.01
Ceftazidime	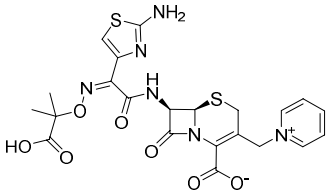	<4.0	4.40 ± 0.01
Cefminox	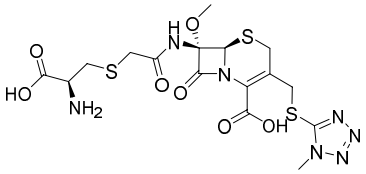	<4.0	4.50 ± 0.01
Cefotaxime	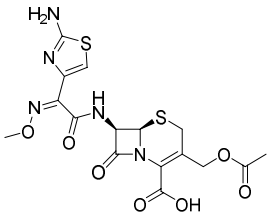	<4.0	<4.0
Ceftiofur	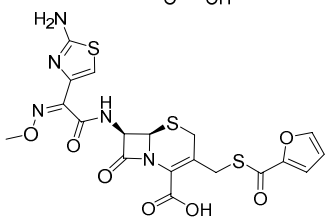	<4.0	<4.0

Compound	Structure	pIC_{50} Ldt_{Mt2} (mean ± SD)	pIC_{50} BlaC (mean ± SD)
Iodoacetamide	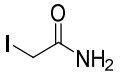	5.8 ± 0.03	<4.0
Maleimide	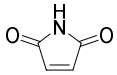	5.4 ± 0.04	<4.0
Ebselen	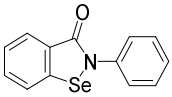	6.8 ± 0.03	5.82 ± 0.09
Benzeneseleninic acid	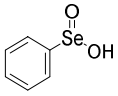	5.0 ± 0.06	<4.0
Thiram	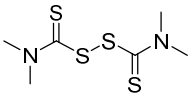	6.8 ± 0.03	<4.0
PX-12	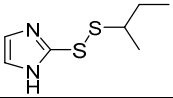	5.9 ± 0.01	<4.0

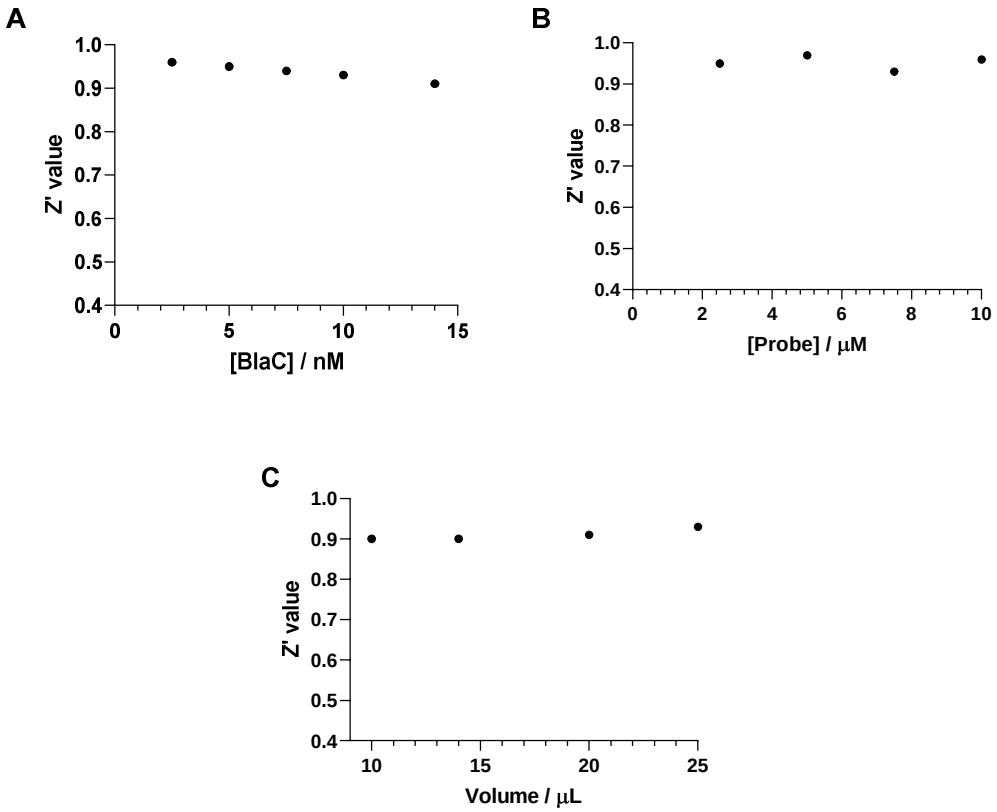

Figure S1.4. Optimisation of the HTS assay for BlaC. A. Z' values obtained with varying concentrations of BlaC using a fixed concentration of probe FC5[2] (10 μM). **B.** Z' values obtained with varying concentrations of FC5 using a fixed BlaC concentration (2.5 nM). A Z' value of 0.95 was obtained at a FC5 concentration of 2.5 μM. **C.** Z' values obtained with varying reaction volumes using fixed BlaC and FC5 concentrations (2.5 nM and 2.5 μM, respectively). Assays in **A** and **B** used reaction volumes of 25 μL. Assays were performed at room temperature in 100 mM sodium phosphate pH 7.5 with 0.01% (*v/v*) Triton X-100.

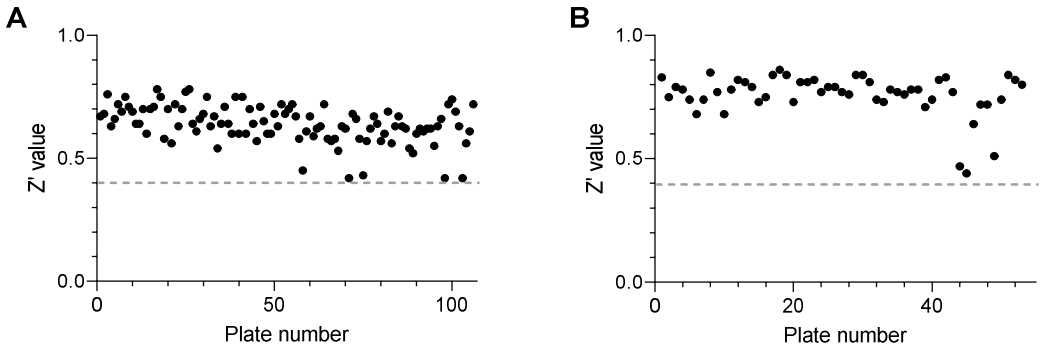

Figure S1.5. Z' values of the plates throughout the HTS campaign. A. Z' values for the Ldt_{Mt2} HTS assay. **B.** Z' values for the HTS assay for the BlaC HTS assay. The cut-off value for plate acceptance is indicated at Z' > 0.4.

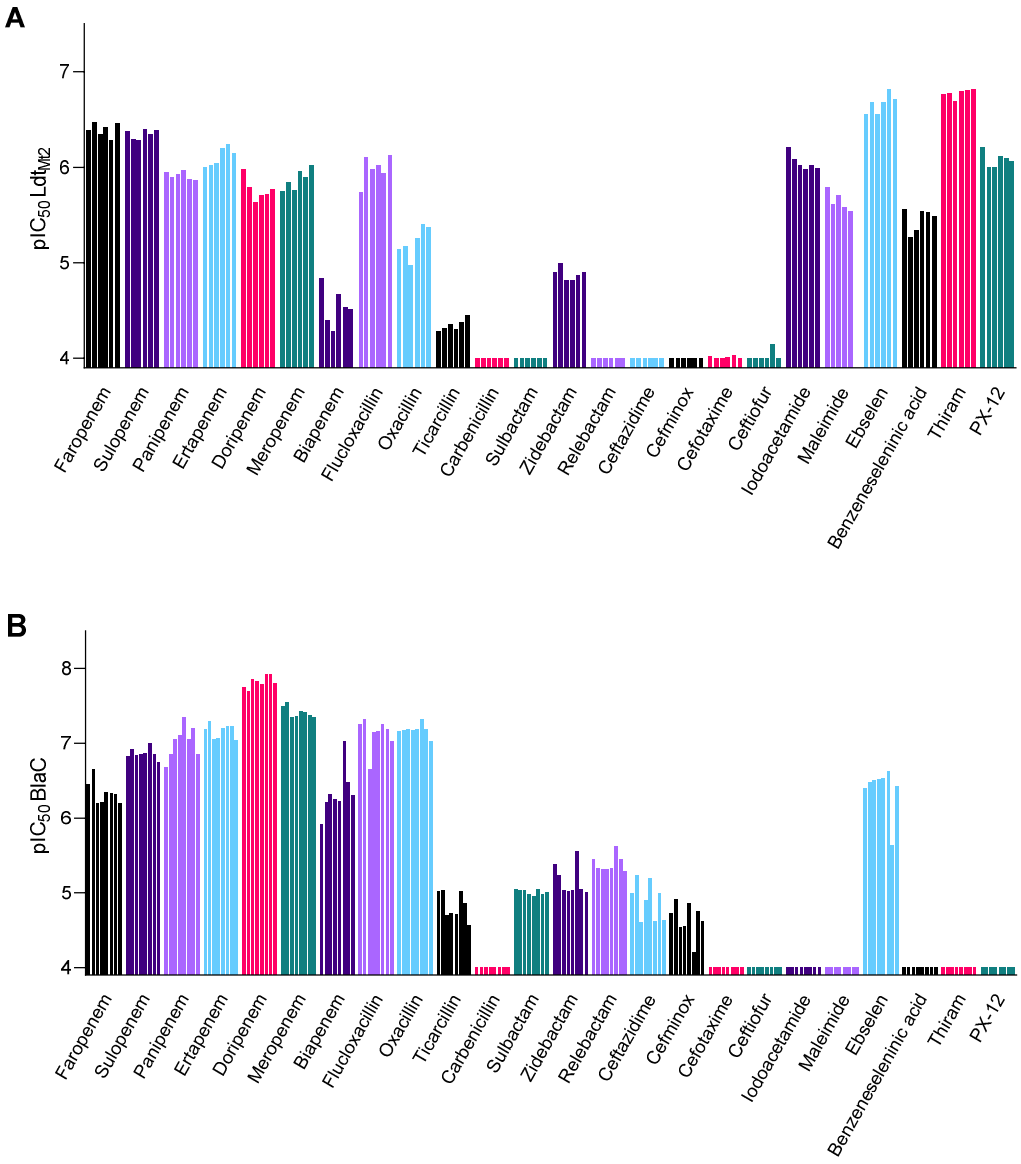

Figure S1.6. Dose response assay results of tool compounds as HTS validation. pIC_{50} values for Ldt_{Mt2} inhibition (**A**) and BlaC inhibition (**B**) were measured on different days, and show good reproducibility for the tested compounds. Inhibition assays of Ldt_{Mt2} were carried out with 300 nM Ldt_{Mt2} and 15 µM probe **1** with 30 minutes inhibitor pre-incubation at room temperature in 50 mM sodium phosphate pH 7.5 with 0.007% (*v/v*) Tween-20. Inhibition assays of BlaC were carried out with 2.5 nM BlaC and 2.5 µM FC5 with 30 minutes inhibitor pre-incubation at room temperature in 100 mM sodium phosphate pH 7.5 with 0.01% (*v/v*) Triton X-100. Average pIC_{50} values and compound structures are given in Table S1.4.

Table S1.4. Validation of the HTS assay using tool compounds. pIC_{50} values for Ldt_{Mt2} and BlaC inhibition, as obtained from independent repeats of technical duplicates during the HTS validation. Errors given are SD of the independent repeats (Ldt_{Mt2} assay n=6, BlaC assay n=8). Inhibition assays of Ldt_{Mt2} were carried out with 300 nM Ldt_{Mt2} and 15 µM probe **1** with 30 minutes inhibitor pre-incubation at room temperature in 50 mM sodium phosphate pH 7.5 with 0.007% (*v/v*) Tween-20. Inhibition assays of BlaC were carried out with 2.5 nM BlaC and 2.5 µM FC5 with 30 minutes inhibitor pre-incubation at room temperature in 100 mM sodium phosphate pH 7.5 with 0.01% (*v/v*) Triton X-100.

Compound	Structure	pIC_{50} Ldt_{Mt2} (mean ± SD)	pIC_{50} BlaC (mean ± SD)
Faropenem	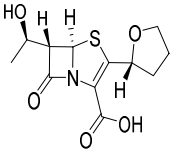	6.39 ± 0.03	6.33 ± 0.06
Sulopenem	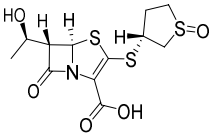	6.35 ± 0.02	6.86 ± 0.02
Panipenem	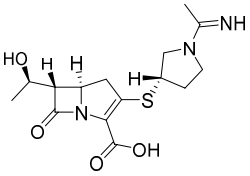	5.91 ± 0.02	7.03 ± 0.06
Ertapenem	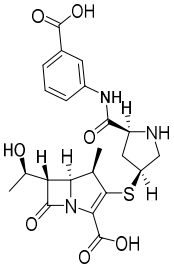	6.11 ± 0.04	7.17 ± 0.03
Doripenem	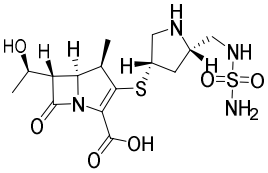	5.77 ± 0.04	7.85 ± 0.02
Meropenem	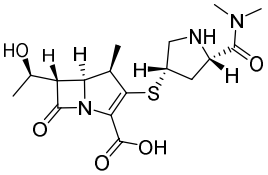	5.87 ± 0.04	7.39 ± 0.03
Biapenem	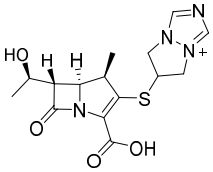	5.54 ± 0.07	6.32 ± 0.11
Flucloxacillin	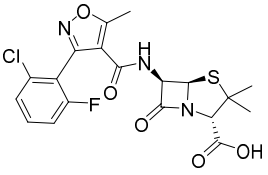	5.98 ± 0.06	7.11 ± 0.07

Compound	Structure	pIC_{50} Ldt_{Mt2} (mean ± SD)	pIC_{50} BlaC (mean ± SD)
Oxacillin	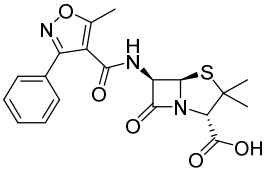	5.22 ± 0.06	7.17 ± 0.03
Ticarcillin	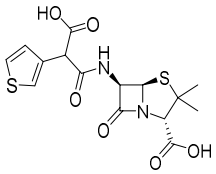	4.35 ± 0.02	4.84 ± 0.06
Carbenicillin	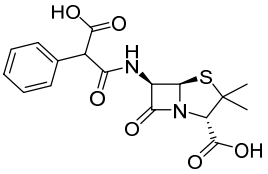	<4.0	<4.0
Sulbactam	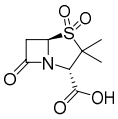	<4.0	5.02 ± 0.03
Zidebactam	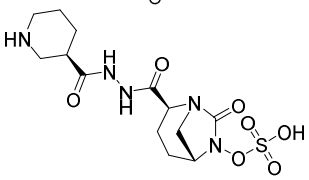	4.88 ± 0.02	5.14 ± 0.10
Relebactam	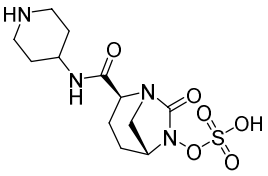	<4.0	5.40 ± 0.04
Ceftazidime	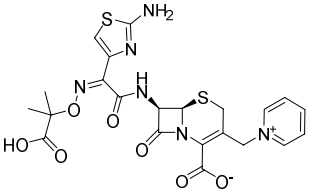	<4.0	4.92 ± 0.07
Cefminox	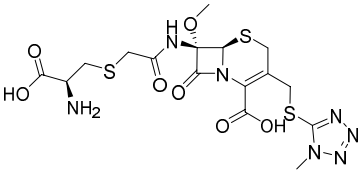	<4.0	4.66 ± 0.08
Cefotaxime	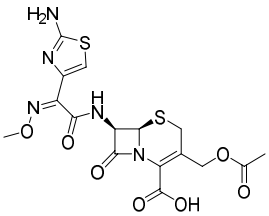	<4.0	<4.0
Ceftiofur	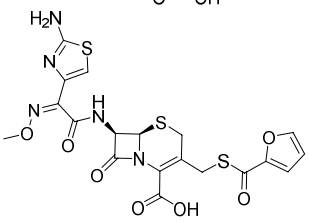	<4.0	<4.0

Compound	Structure	pIC_{50} Ldt_{Mt2} (mean ± SD)	pIC_{50} BlaC (mean ± SD)
Iodoacetamide	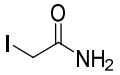	6.05 ± 0.03	<4.0
Maleimide	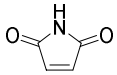	5.65 ± 0.04	<4.0
Ebselen	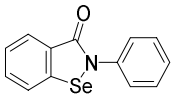	6.67 ± 0.04	6.52 ± 0.04
Benzeneseleninic acid	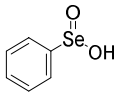	5.45 ± 0.05	<4.0
Thiram	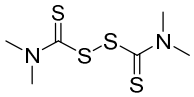	6.77 ± 0.02	<4.0
PX-12	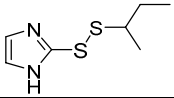	6.09 ± 0.03	<4.0

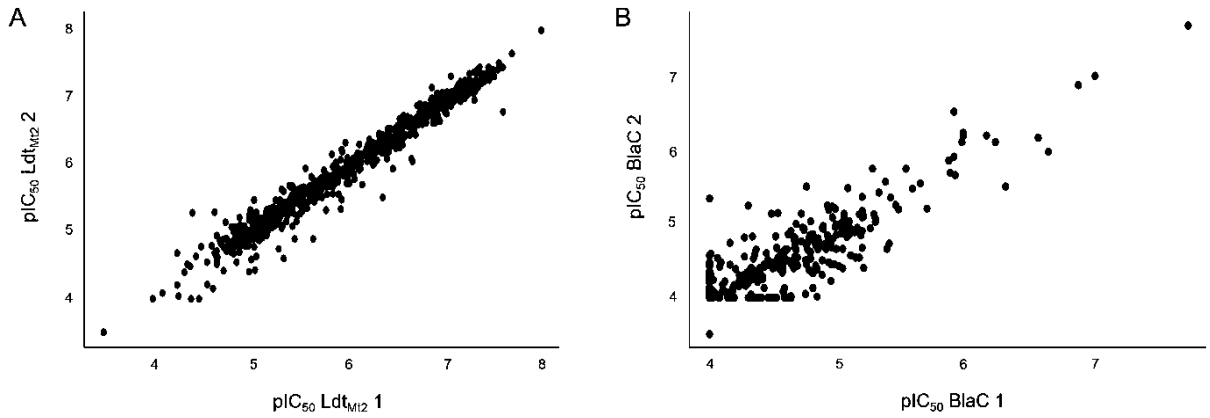

Figure S1.7. Correlation between pIC_{50} values from two independent repeats in the HTS for Ldt_{Mt2} (A) and for BlaC (B) using the standard assay conditions (Figure S1.2E, Figure S1.4C).

Table S1.5. Eight classes of compounds identified from the Ldt_{Mt2} HTS. MW: Molecular weight. LE: Ligand efficiency. T_m: Melting point (°C) of Ldt_{Mt2} after pre-incubation with the compound as measured using SYPRO Orange (6 x concentrated, according to the manufacturer's (Invitrogen) protocol) in 50 mM Tris pH 7.5. ΔT_m: Difference in melting point (T_m) of Ldt_{Mt2} after pre-incubation with the compound relative to unreacted Ldt_{Mt2} (43.8 °C). k_{chem}: apparent intrinsic thiol reactivity as measured with L-glutathione and probe **2** (Figure S1.20).

Class		Compound	MW (Da)	pIC_{50}		LE	T_m (ΔT_m)	k_{inact}/K_I (M^{-1} s^{-1})	k_{chem} (M^{-1} s^{-1})
				Ldt_{Mt2}	BlaC				
α-chloro ketone	**1**	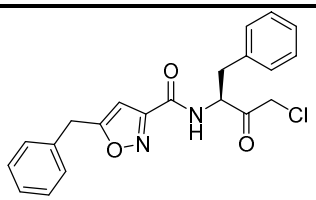	382.85	7.34 ± 0.045	<4.0	0.41	N.D.	1152 ± 87	0.11 ± 0.02
	2	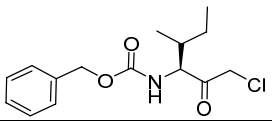	297.78	7.11 ± 0.010	<4.0	0.56	43.7 ± 0.09 (-0.1)	68.4 ± 3.5	0.15 ± 0.02
Maleimides	**3**	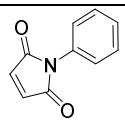	173.17	7.15 ± 0.030	5.03 ± 0.045	0.86	45.0 ± 0.16 (+1.2)	3991 ± 356	129.9 ± 9.9
	4	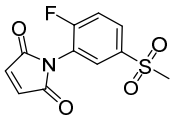	269.25	7.06 ± 0.035	4.22 ± 0.060	0.62	45.6 ± 0.28 (+1.8)	36.5 ± 7.9	34.2 ± 1.0
	5	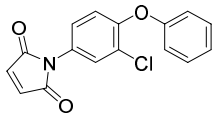	299.71	7.40 ± 0.010	4.71 ± 0.055	0.53	43.6 ± 0.16 (-0.2)	116 ± 6.2	91.8 ± 1.8
	6	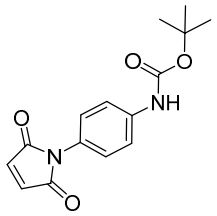	288.30	7.24 ± 0.005	5.19 ± 0.005	0.52	45.5 ± 0.09 (+1.7)	127 ± 7.7	61.6 ± 0.78
	7	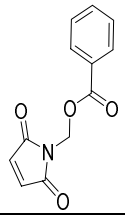	231.21	7.02 ± 0.000	4.18 ± 0.175	0.66	43.1 ± 0.09 (-0.7)	156 ± 5.1	91.7 ± 4.5
Acrylamides	**8**	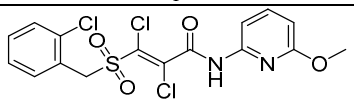	435.71	7.16 ± 0.035	<4.0	0.43	44.5 ± 1.23 (+0.7)	91.6 ± 2.0	1.53 ± 0.15
	9	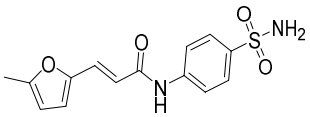	306.34	6.68 ± 0.025	4.58 ± 0.010	0.53	43.1 ± 0.09 (-0.7)	90.7 ± 4.7	1.76 ± 0.20
	10	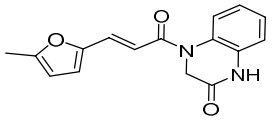	282.30	6.37 ± 0.005	4.29 ± 0.290	0.54	44.5 ± 0.19 (-0.7)	16.0 ± 0.75	0.79 ± 0.02

Class		Compound	MW (Da)	pIC_{50}		LE	T_m (ΔT_m)	k_{inact}/K_I (M^{-1} s^{-1})	k_{chem} (M^{-1} s^{-1})
				Ldt_{Mt2}	BlaC				
Acrylamides (continued)	**11**	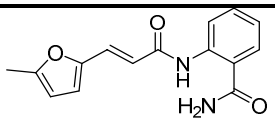	270.29	6.24 ± 0.030	<4.0	0.56	44.0 ± 0.16 (+0.2)	172 ± 6.0	0.27 ± 0.05
	12	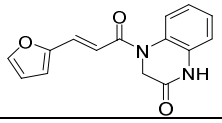	268.27	6.13 ± 0.115	<4.0	0.56	44.1 ± 0.09 (+0.3)	N.D.	0.55 ± 0.11
Fumaryl-amides	**13**	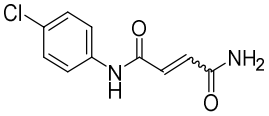	224.65	6.38 ± 0.080	<4.0	0.75	44.8 ± 0.00 (+1.0)	6.48 ± 0.11	6.1 ± 0.52
	14	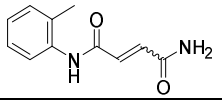	204.23	6.11 ± 0.020	<4.0	0.75	44.9 ± 0.09 (+1.1)	1.20 ± 0.15	13.0 ± 1.0
Ebsulfur analogue	**15**	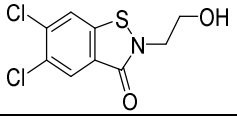	264.13	7.99 ± 0.040	6.37 ± 0.175	0.74	43.5 ± 0.09 (-0.3)	N.D.	N.D.
Isatins	**16**	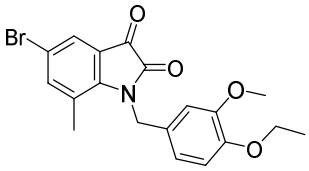	404.26	6.75 ± 0.015	4.44 ± 0.015	0.45	46.8 ± 0.00 (+3.0)	N.D.	<0.08
	17	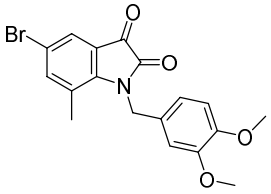	390.23	6.24 ± 0.140	<4.0	0.47	46.8 ± 0.00 (+3.0)	N.D.	<0.08
	18	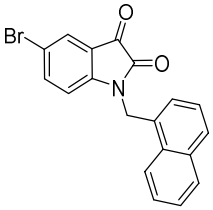	366.21	6.52 ± 0.005	<4.0	0.49	46.2 ± 0.00 (+2.4)	N.D.	<0.08
β-Lactams	**19**	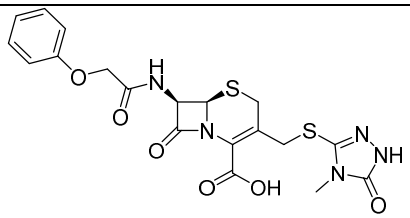	477.52	5.62 ± 0.100	<4.0	0.35	42.9 ± 0.09 (-0.9)	N.D.	N.D.
	20	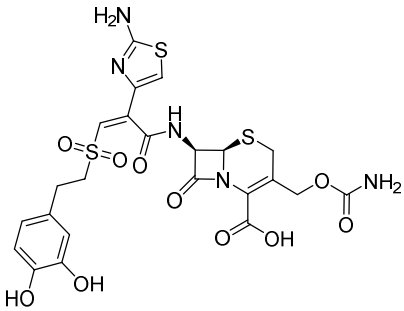	625.66	5.55 ± 0.045	7.72 ± 0.015	0.28	42.7 ± 0.25 (-1.1)	N.D.	N.D.

Class		Compound	MW (Da)	pIC_{50}		LE	T_m (ΔT_m)	k_{inact}/K_I (M^{-1} s^{-1})	k_{chem} (M^{-1} s^{-1})
				Ldt_{Mt2}	BlaC				
β-Lactams (continued)	**21**	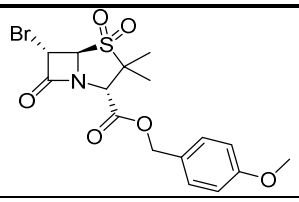	432.29	6.40 ± 0.035	4.58 ± 0.195	0.45	43.1 ± 0.09 (-0.7)	53.2 ± 4.7	2.03 ± 0.76
Nitriles	**22**	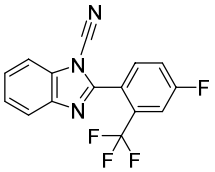	305.23	7.53 ± 0.010	<4.0	0.51	42.5 ± 0.09 (-1.3)	55.1 ± 3.0	20.3 ± 0.9
	23	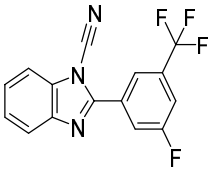	305.23	7.33 ± 0.065	<4.0	0.51	42.5 ± 0.09 (-1.3)	265 ± 17	15.0 ± 0.41
	24	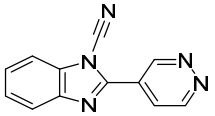	221.22	7.34 ± 0.030	<4.0	0.66	42.0 ± 0.00 (-1.8)	158 ± 5.7	27.1 ± 2.3
	25	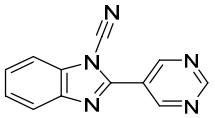	221.22	7.34 ± 0.050	<4.0	0.66	42.4 ± 0.00 (-1.8)	77.5 ± 6.0	28.7 ± 1.9
	26	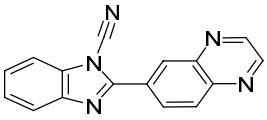	271.28	7.45 ± 0.015	4.83 ± 0.110	0.53	41.7 ± 0.09 (-2.1)	65.0 ± 4.4	11.4 ± 0.62
	27	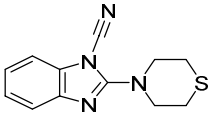	244.32	7.02 ± 0.025	<4.0	0.66	42.5 ± 0.09 (-1.3)	14.0 ± 0.73	6.50 ± 0.25
	28	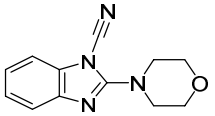	228.25	6.39 ± 0.120	<4.0	0.66	42.3 ± 0.09 (-1.5)	7.41 ± 0.40	2.12 ± 0.15
	29	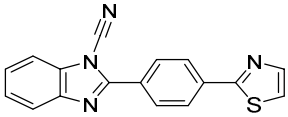	302.36	7.28 ± 0.010	6.18 ± 0.040	0.51	42.9 ± 0.19 (-0.9)	1164 ± 105	42.1 ± 0.82
	30	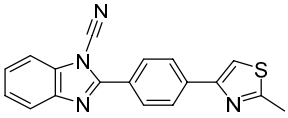	316.39	7.25 ± 0.065	6.11 ± 0.150	0.49	42.2 ± 0.00 (-1.6)	236 ± 9.5	N.D.
	31	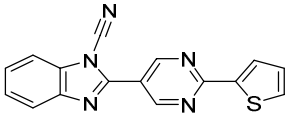	303.35	7.32 ± 0.055	4.95 ± 0.070	0.51	42.1 ± 0.10 (-1.7)	609 ± 11	21.0 ± 1.4
	32	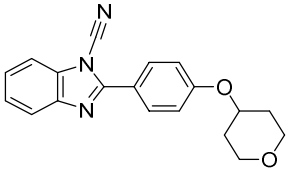	319.36	7.31 ± 0.045	4.73 ± 0.080	0.47	42.3 ± 0.09 (-1.5)	86.3 ± 2.6	3.58 ± 0.19
Nitriles (continued)	**33**	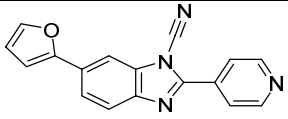	286.29	6.95 ± 0.045	6.09 ± 0.125	0.51	43.3 ± 0.09 (-0.5)	71.8 ± 1.1	12.9 ± 0.67

Class	Compound		MW (Da)	pIC_{50}		LE	T_m (ΔT_m)	k_{inact}/K_I (M^{-1} s^{-1})	k_{chem} (M^{-1} s^{-1})
				Ldt_{Mt2}	BlaC				
	34	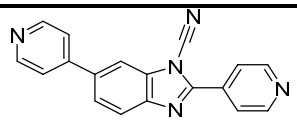	297.32	7.20 ± 0.080	<4.0	0.49	42.1 ± 0.09 (-1.7)	68.4 ± 2.7	31.0 ± 1.6
	35	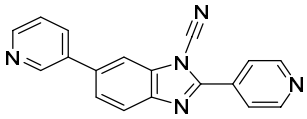	297.32	7.01 ± 0.015	5.91 ± 0.385	0.49	42.9 ± 0.34 (-0.9)	8.88 ± 0.39	16.8 ± 0.61
	36	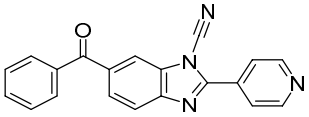	324.34	7.11 ± 0.050	<4.0	0.45	40.8 ± 0.59 (-3.0)	51.0 ± 3.4	61.6 ± 2.7
	37	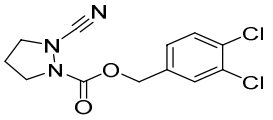	300.14	6.43 ± 0.025	4.47 ± 0.075	0.59	42.3 ± 0.09 (-1.5)	8.44 ± 1.2	0.30 ± 0.03
	38	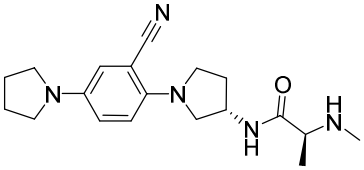	341.46	6.15 ± 0.010	<4.0	0.45	42.8 ± 0.00 (-1.0)	N.D.	N.D.
	39	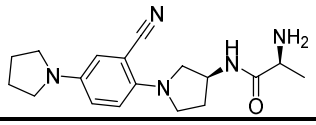	327.43	6.29 ± 0.065	<4.0	0.47	43.1 ± 0.10 (-0.7)	N.D.	N.D.

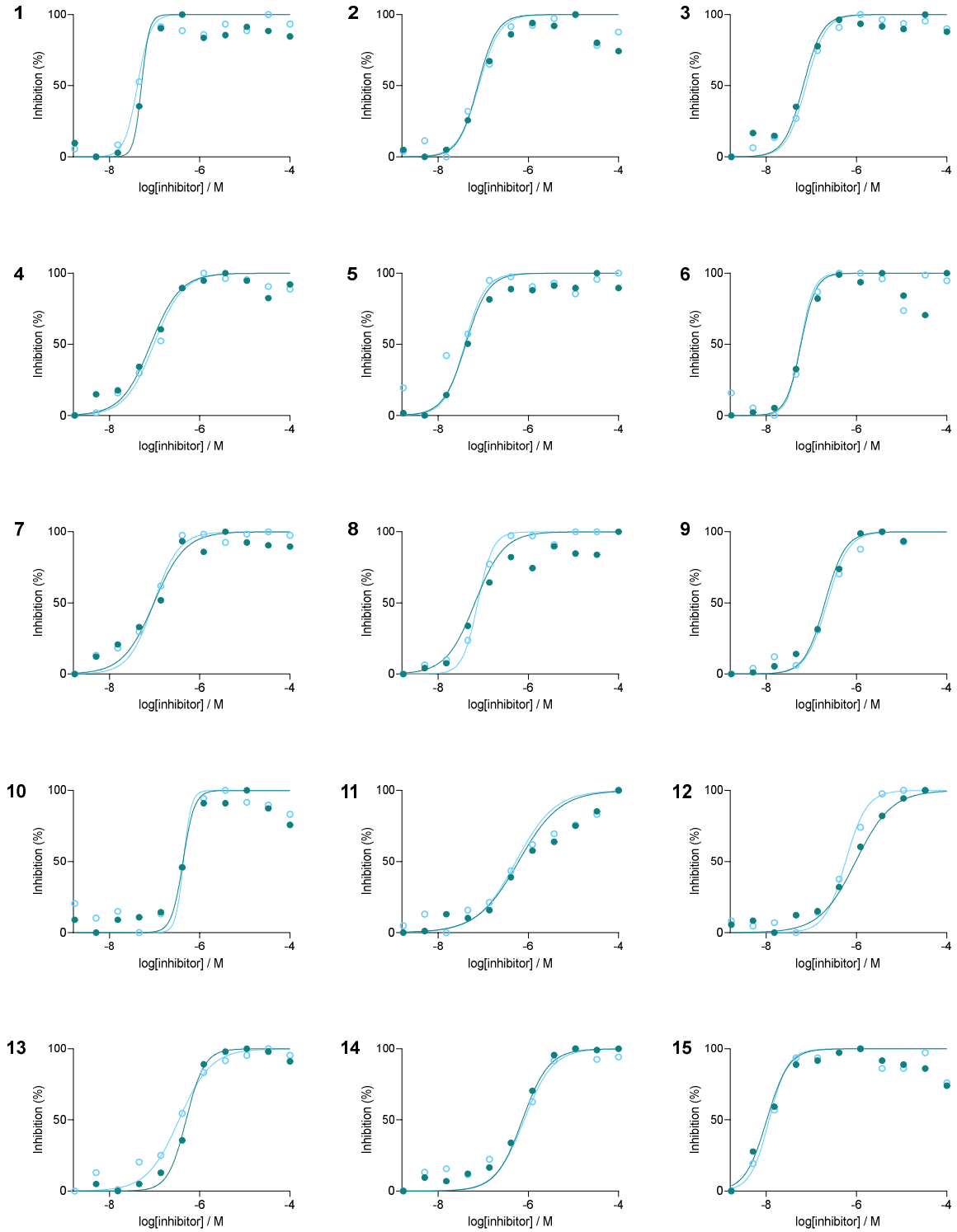

Figure S1.8. Dose-response curves for compounds 1-39 with Ldt_{Mt2} (figure continues).

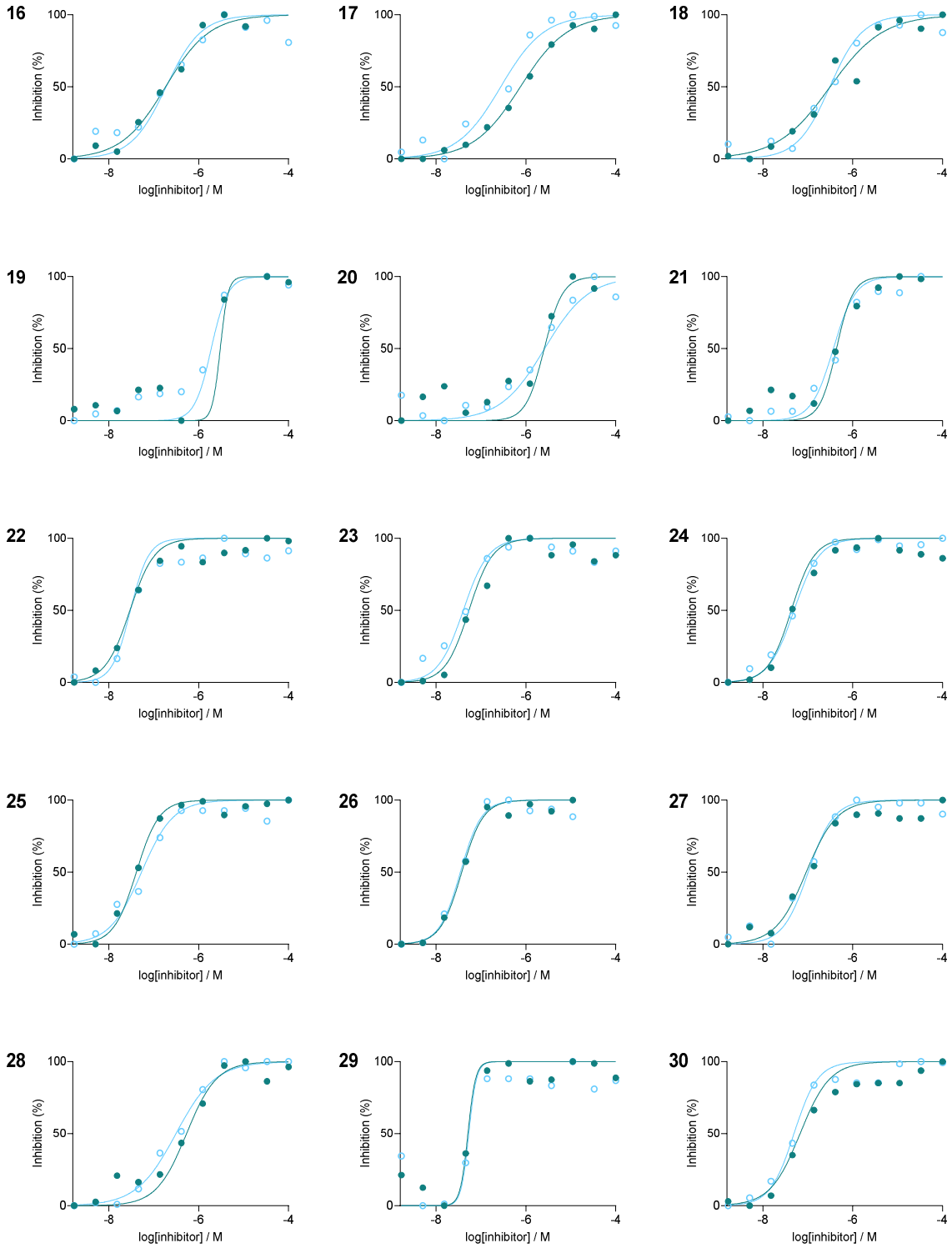

Figure S1.8. Dose-response curves for compounds 1-39 with Ldt_{Mt2} (figure continues).

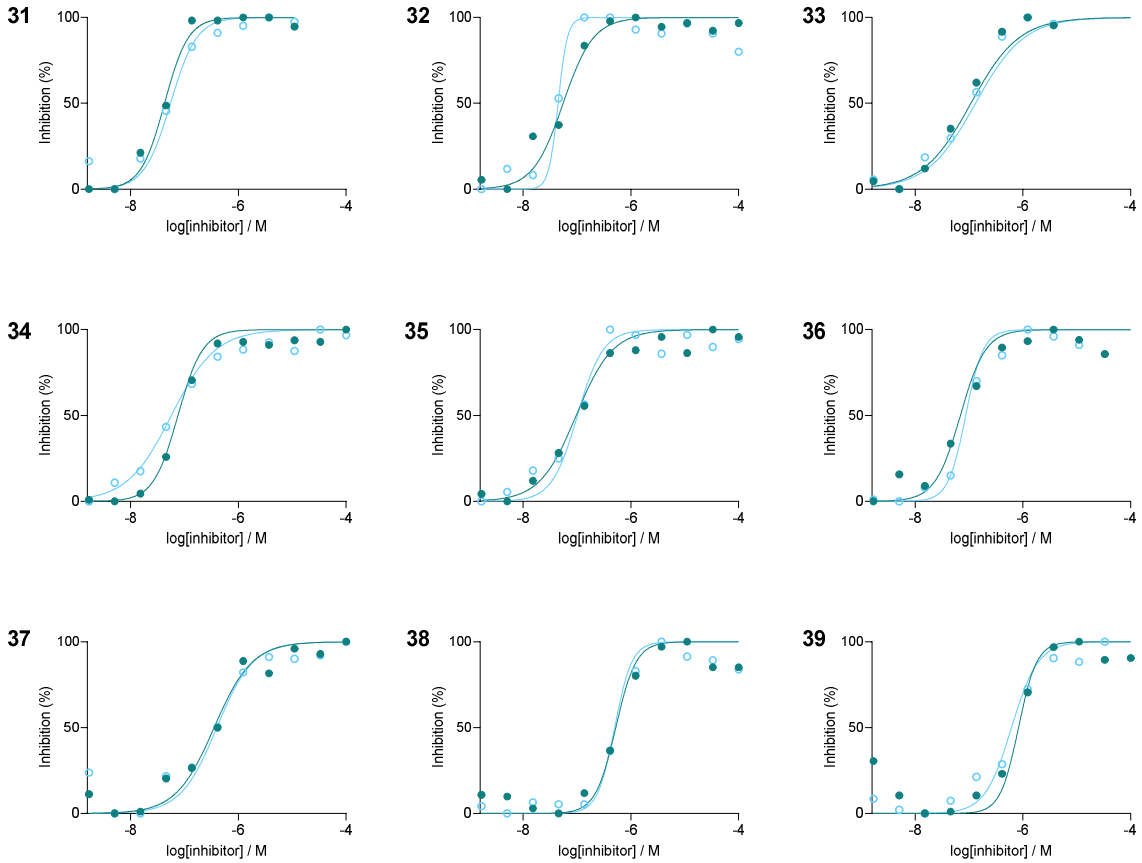

Figure S1.8. Dose-response curves for compounds 1-39 with Ldt_{Mt2}. Inhibition assays of Ldt_{Mt2} were carried out with 300 nM Ldt_{Mt2} and 15 µM probe **1** with a 30 minute inhibitor pre-incubation at room temperature in 50 mM sodium phosphate pH 7.5 with 0.007% (*v/v*) Tween-20. Two independent repeats are shown in teal and cyan. Average pIC_{50} values and compound structures are given in Table S1.5.

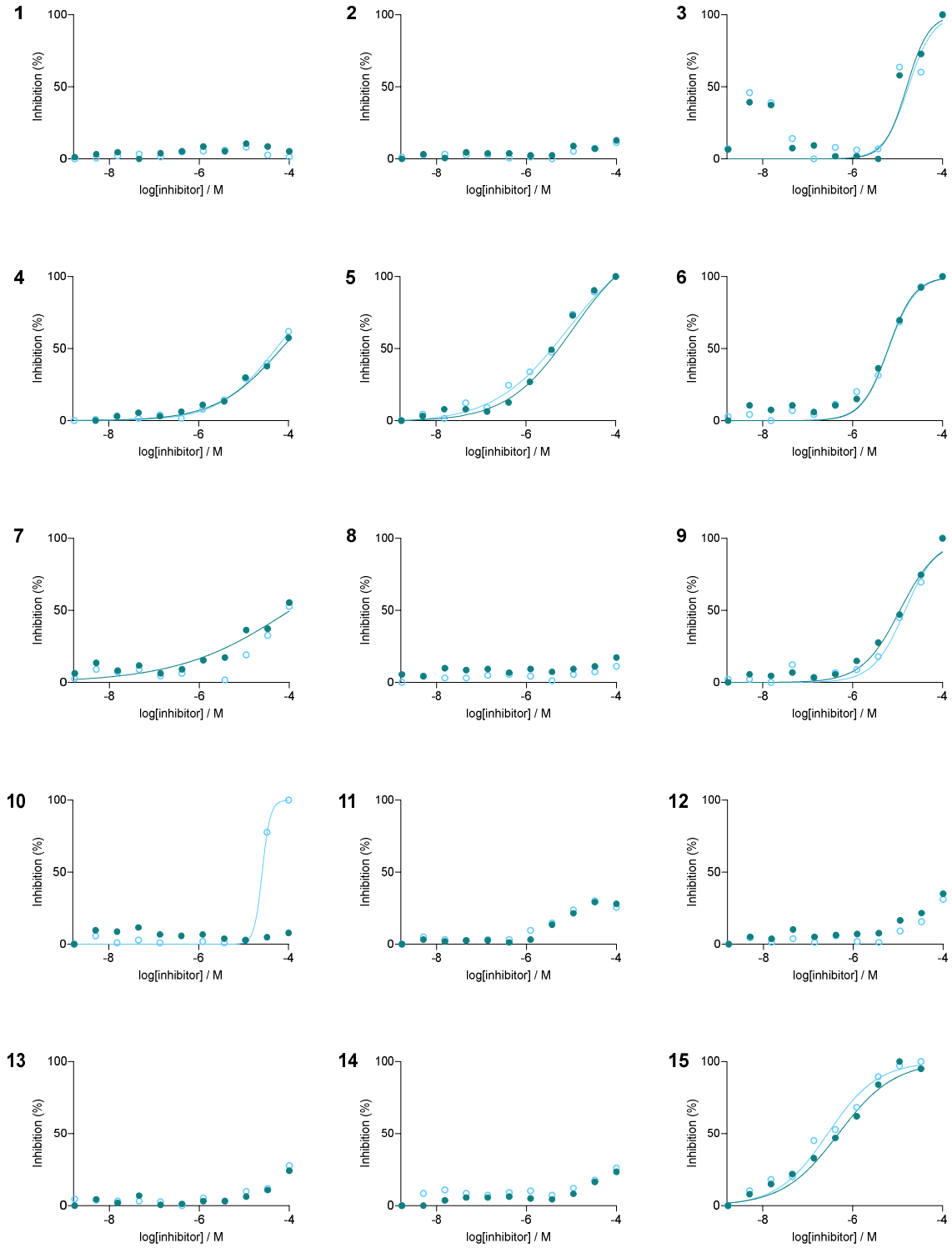

Figure S1.9. Dose-response curves for compounds 1-39 with BlaC (figure continues).

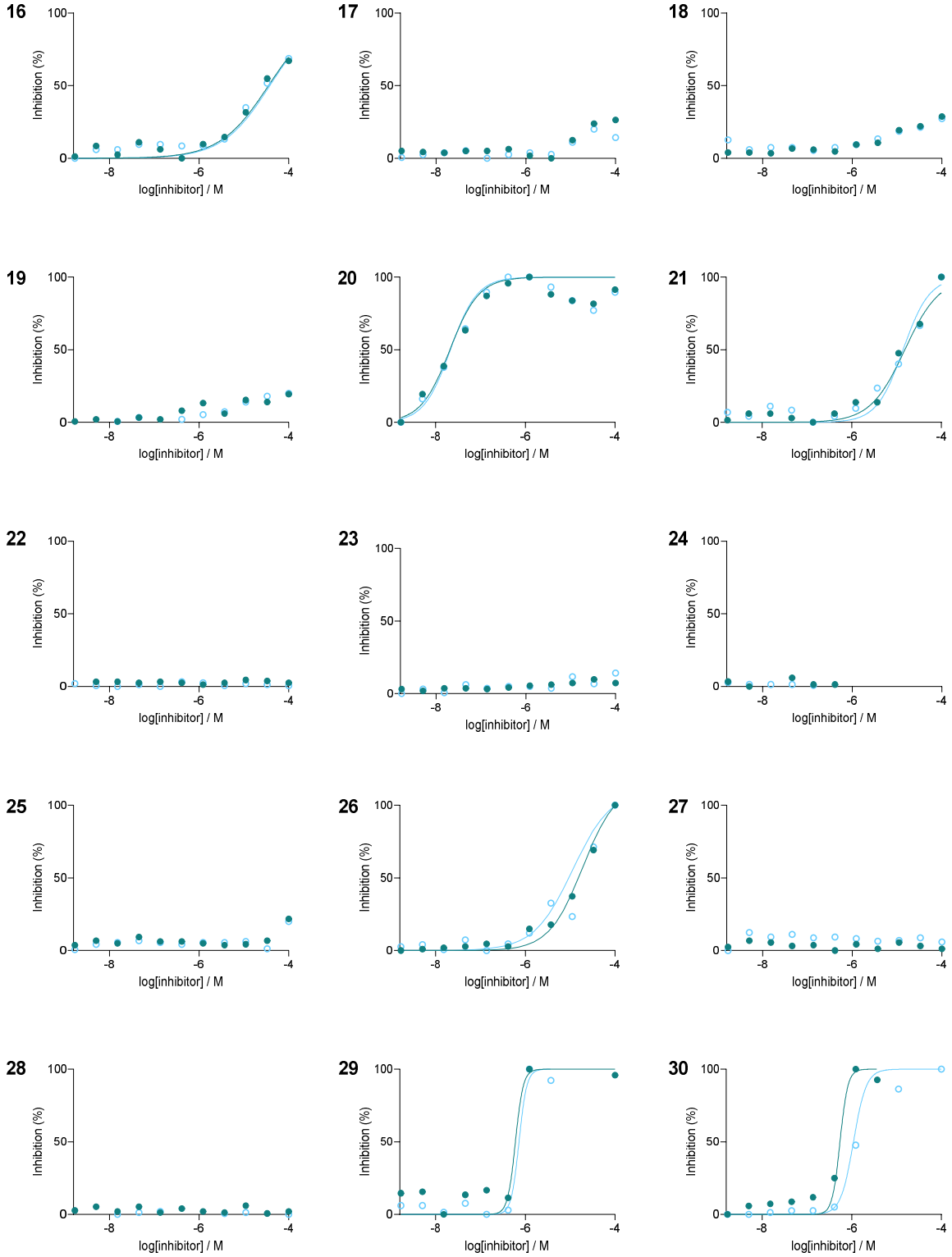

Figure S1.9. Dose-response curves for compounds 1-39 with BlaC (figure continues).

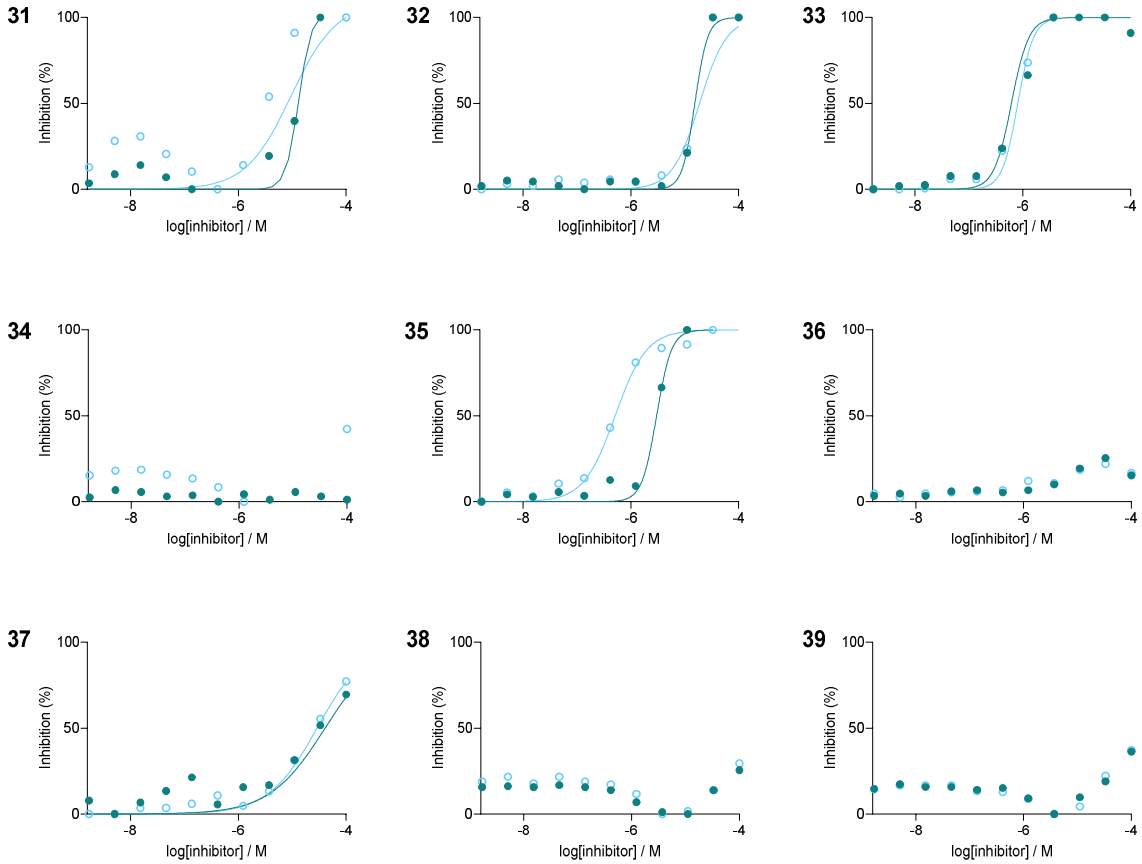

Figure S1.9. Dose-response curves for compounds 1-39 with BlaC. Inhibition assays of BlaC were carried out with 2.5 nM BlaC and 2.5 µM FC5 with a 30 minute inhibitor pre-incubation at room temperature in 100 mM sodium phosphate pH 7.5 with 0.01% (*v/v*) Triton X-100. Two independent repeats are shown in teal and cyan. Average pIC_{50} values and compound structures are given in Table S1.5.

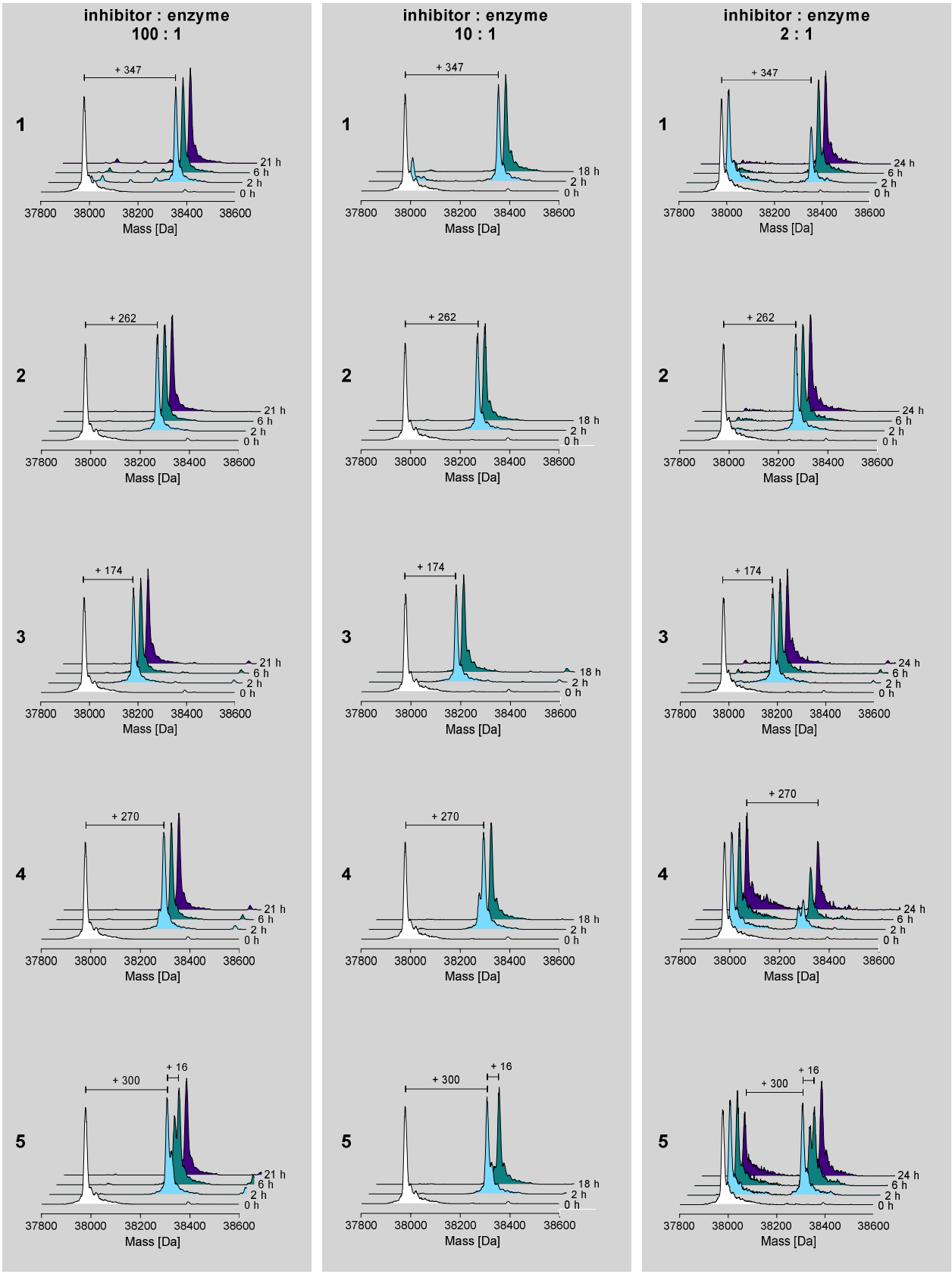

Figure S1.10. Protein observed SPE-MS analysis for the reaction of Ldt_{Mt2} with inhibitors 1-21 (figure continues).

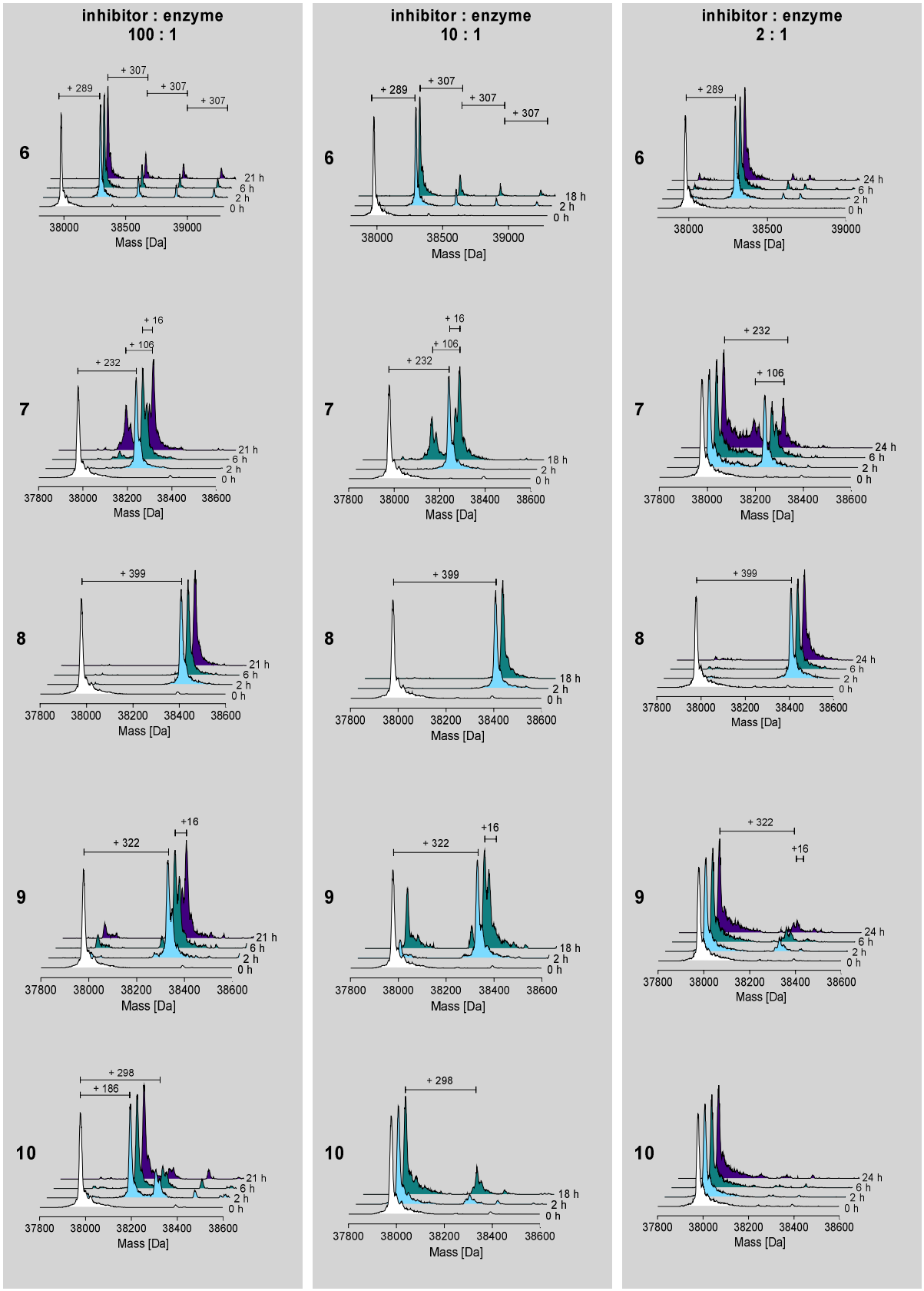

Figure S1.10. Protein observed SPE-MS analysis for the reaction of Ldt_{Mt2} with inhibitors 1-21 (figure continues).

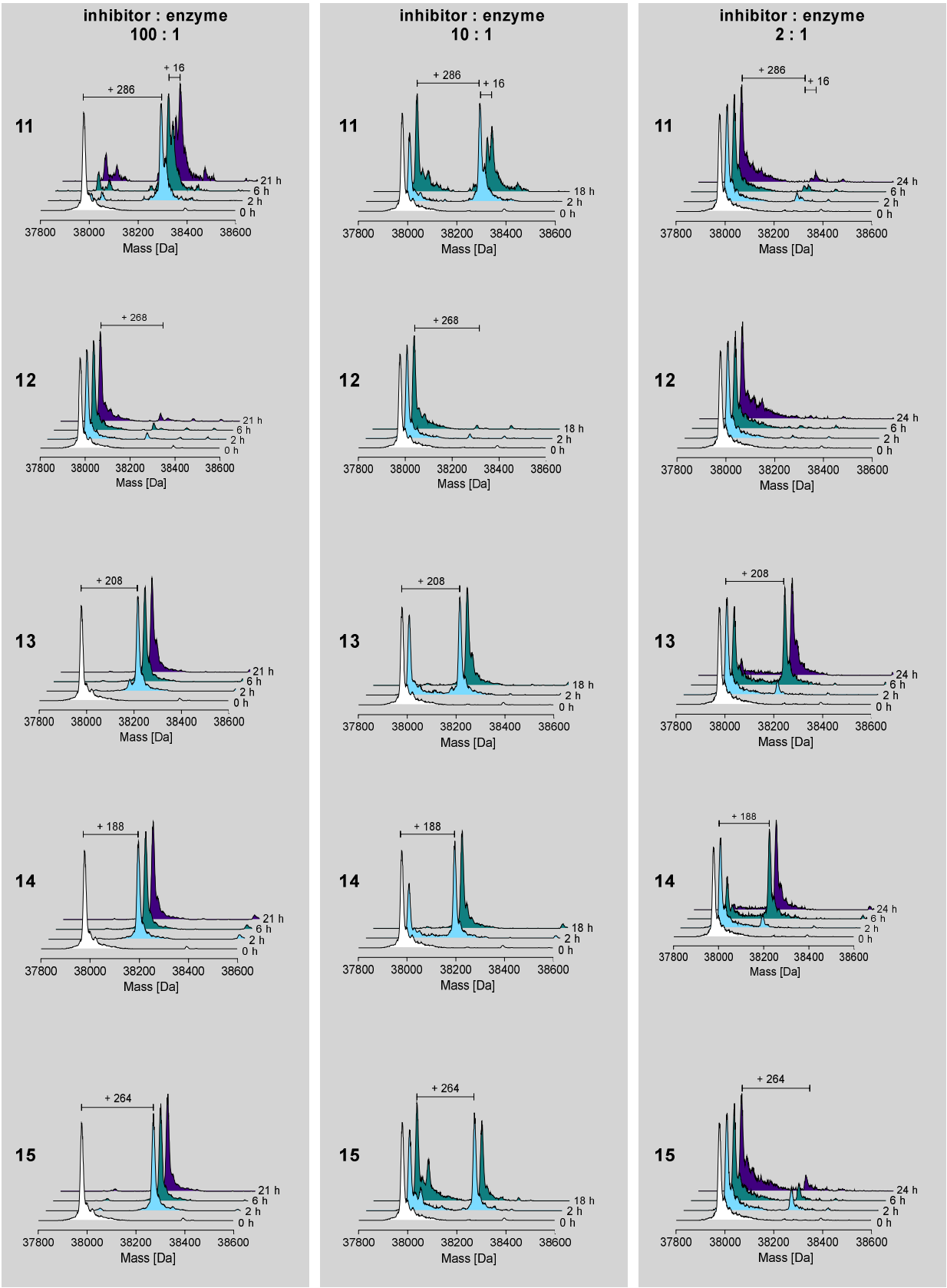

Figure S1.10. Protein observed SPE-MS analysis for the reaction of Ldt_{Mt2} with inhibitors 1-21 (figure continues).

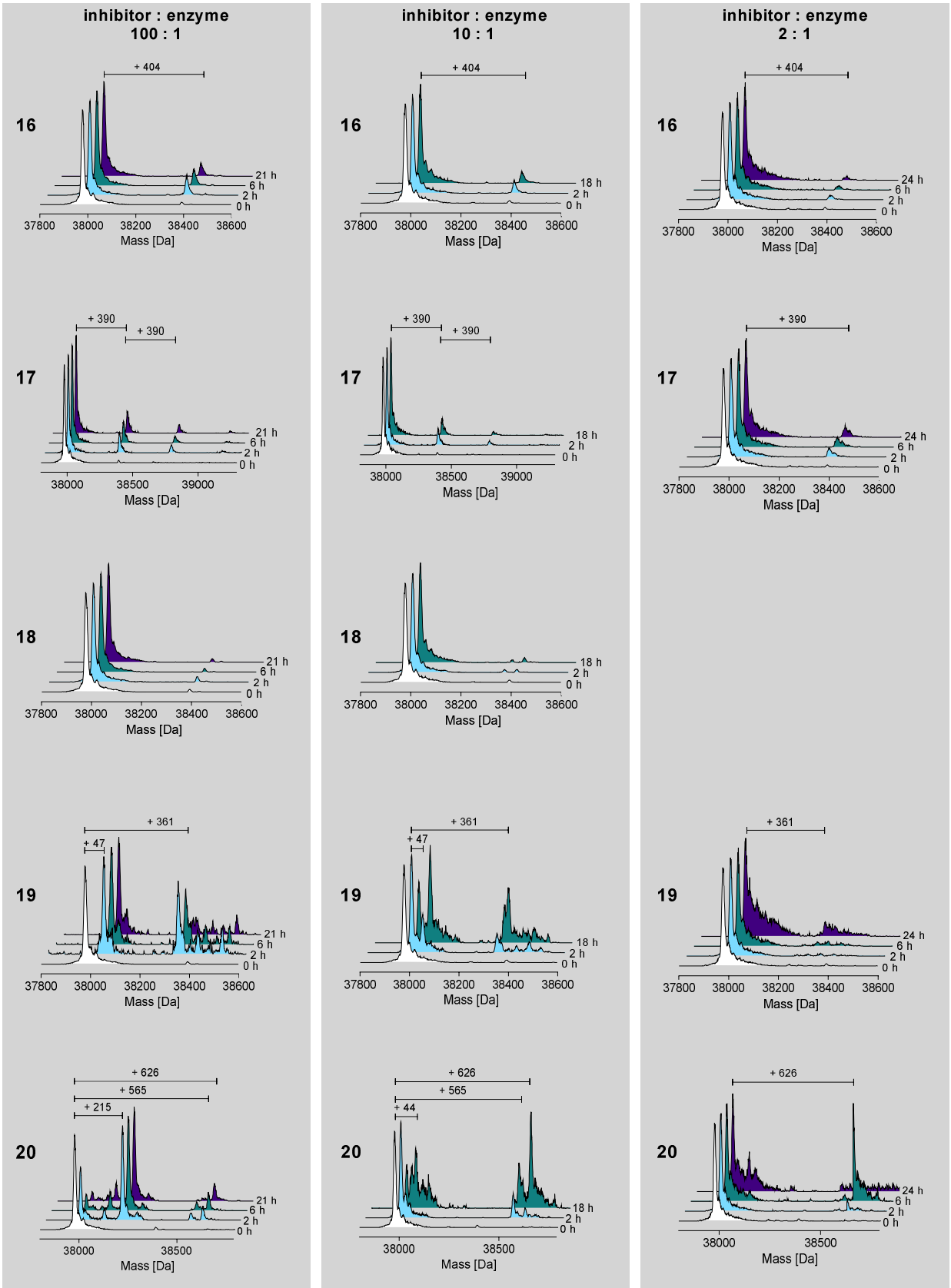

Figure S1.10. Protein observed SPE-MS analysis for the reaction of Ldt_{Mt2} with inhibitors 1-21 (figure continues).

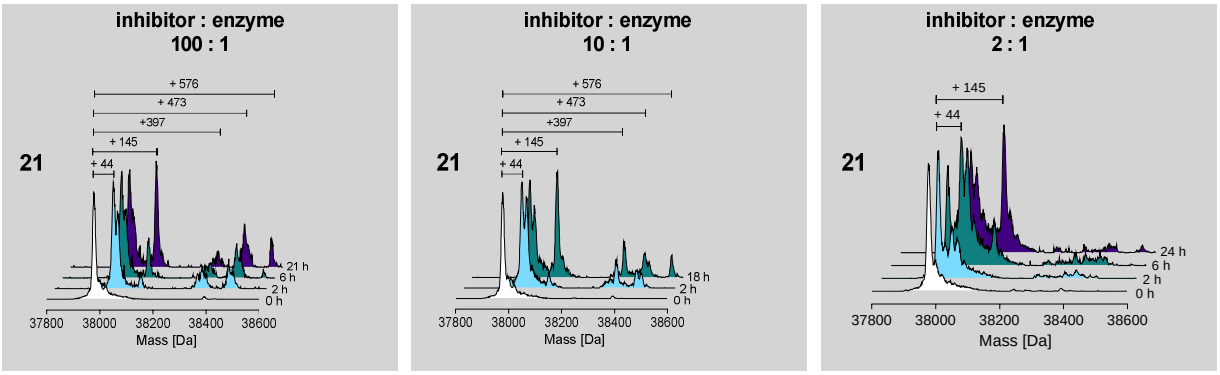

Figure S1.10. Protein observed SPE-MS analysis for the reaction of Ldt_{Mt2} with inhibitors 1-21. 1 µM Ldt_{Mt2} was incubated with the inhibitors at the specified ratio at room temperature in 50 mM Tris, pH 7.5. Samples were analysed after the indicated times. Compound structures are given in Table S1.5. Deconvoluted spectra, obtained using the maximum entropy algorithm in the MassHunter Workstation Qualitative Analysis B.07.00 program (Agilent), are shown.

Table S1.6. Calculated (based on anticipated binding mode) and observed masses (Da) and mass shifts (Da) for protein observed SPE-MS experiments with Ldt_{Mt2} and the indicated inhibitors. Mass shifts are relative to unmodified Ldt_{Mt2}. * Calculated mass for reaction at the inhibitor terminal amide group. ** Calculated mass for reaction at the inhibitor acrylamide group. Compound structures are given in Table S1.5. Deconvoluted SPE-MS spectra are shown in Figure S1.10.

Compound	Calculated mass (Da)	Observed mass (Da)
1	38334 (+347)	38334 (+347)
2	38249 (+262)	38249 (+262)
3	38161 (+174)	38161 (+174)
4	38257 (+270)	38257 (+270)
5	38287 (+300)	38287 (+300), 38303 (+316)
6	38276 (+289)	38276 (+289), 38582 (+595), 38889 (+902), 39196 (+1209)
7	38219 (+232)	38113 (+126), 38219 (+232), 38235 (+248)
8	38386 (+399)	38386 (+399)
9	38293 (+306)	38309 (+322), 38325 (+338)
10	38269 (+282)	38173 (+186), 38285 (+298)
11	38257 (+270)	38273 (+286), 38289 (+302)
12	38255 (+268)	38255 (+268)
13	38195 (+208)*, 38212 (+225)**	38195 (+208)
14	38175 (+188)*, 38191 (+204)**	38175 (+188)
15	38251 (+264)	38251 (+264)
16	38391 (+404)	38391 (+404)
17	38377 (+390)	38377 (+390), 38767 (+780)
18	38353 (+366)	37987 (+0)
19	38465 (+478)	38034 (+47), 38348 (+361)
20	38613 (+626)	38031 (+44), 38202 (+215), 38552 (+565), 38613 (+626)
21	38419 (+432)	38031 (+44), 38132 (+145), 38384 (+397), 38460 (+473), 38565 (+578)

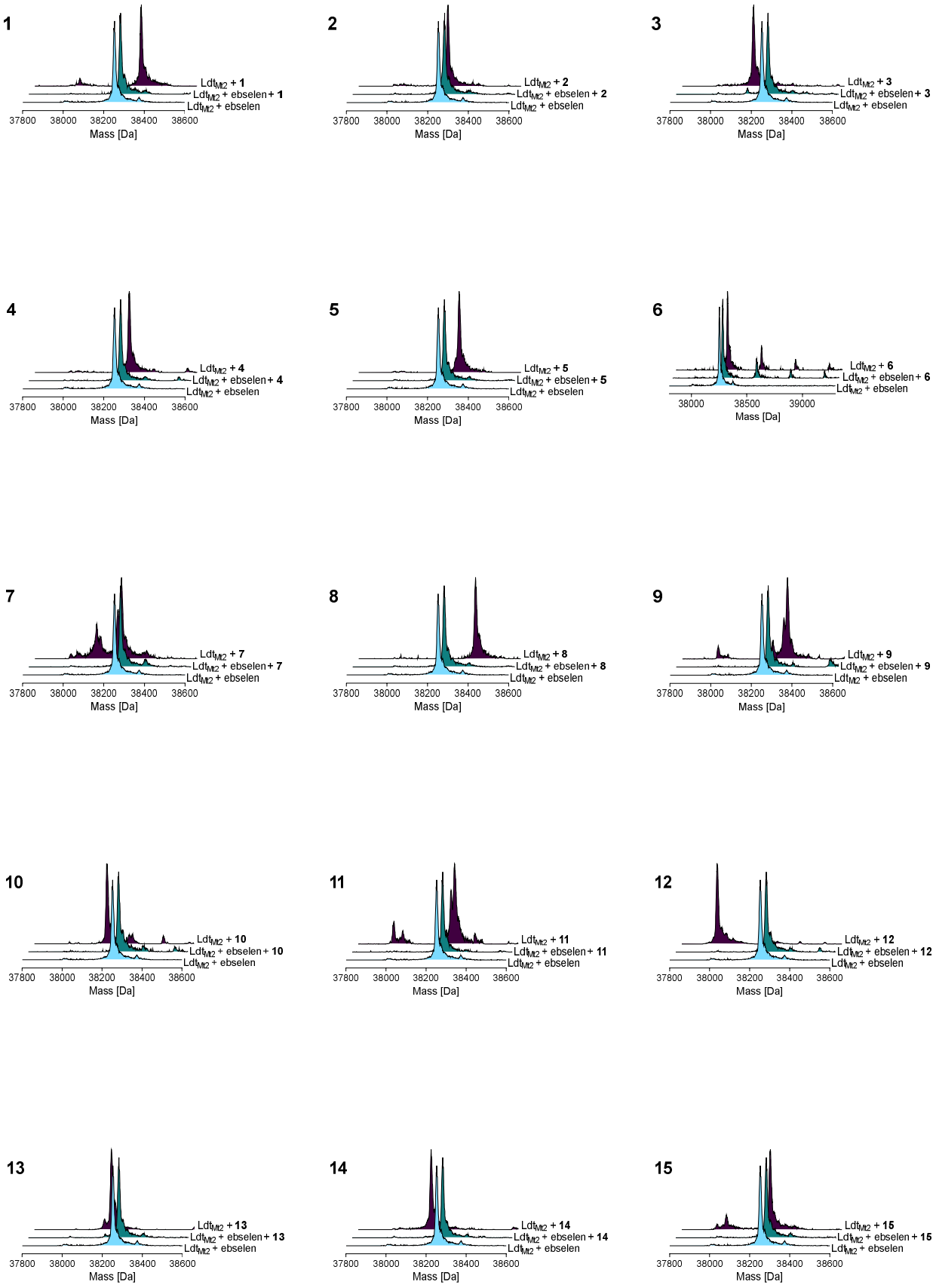

Figure S1.11. Protein observed SPE-MS based active-site selectivity assays (figure continues).

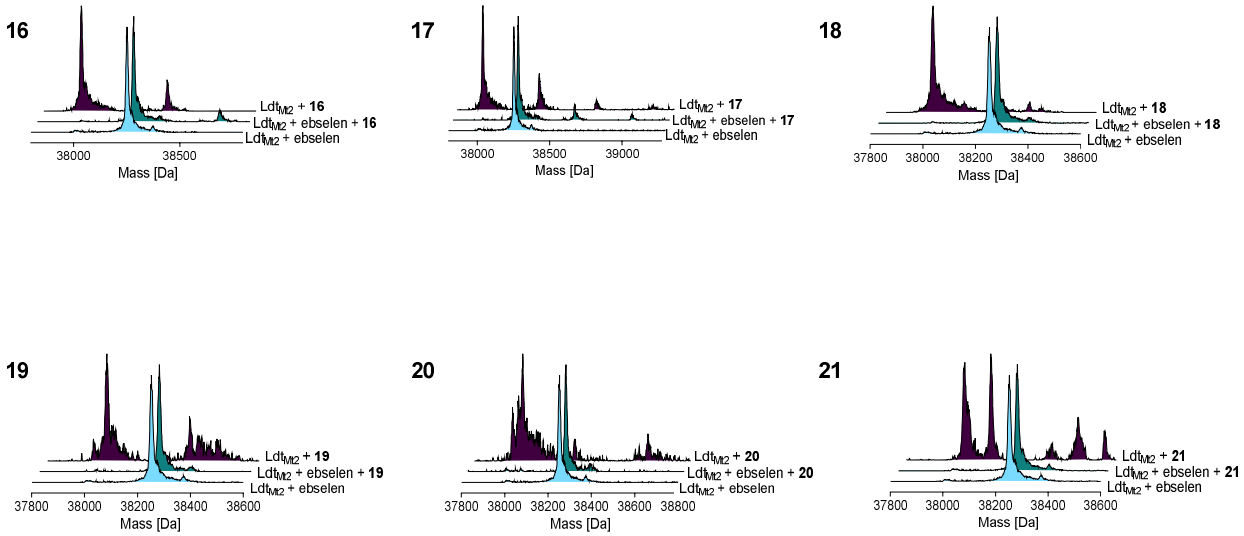

Figure S1.11. Protein observed SPE-MS based active-site selectivity assays. Ldt_{Mt2} (1 µM) was preincubated with ebselen (10 µM, a known Ldt_{Mt2} inhibitor,[3] which reacts with the nucleophilic Cys354) for 1 h in 50 mM Tris, pH 7.5, prior to addition of inhibitors **1-15** (100 µM). Samples were analysed after an additional 24 h incubation at room temperature. The spectrum in blue corresponds to Ldt_{Mt2} reacted with ebselen. The spectrum in green corresponds to Ldt_{Mt2} reacted with the specified inhibitor, following preincubation with ebselen. The spectrum in purple corresponds to Ldt_{Mt2} reacted with the specified inhibitor. Deconvoluted spectra, obtained using the maximum entropy algorithm in the MassHunter Workstation Qualitative Analysis B.07.00 program (Agilent), are shown.

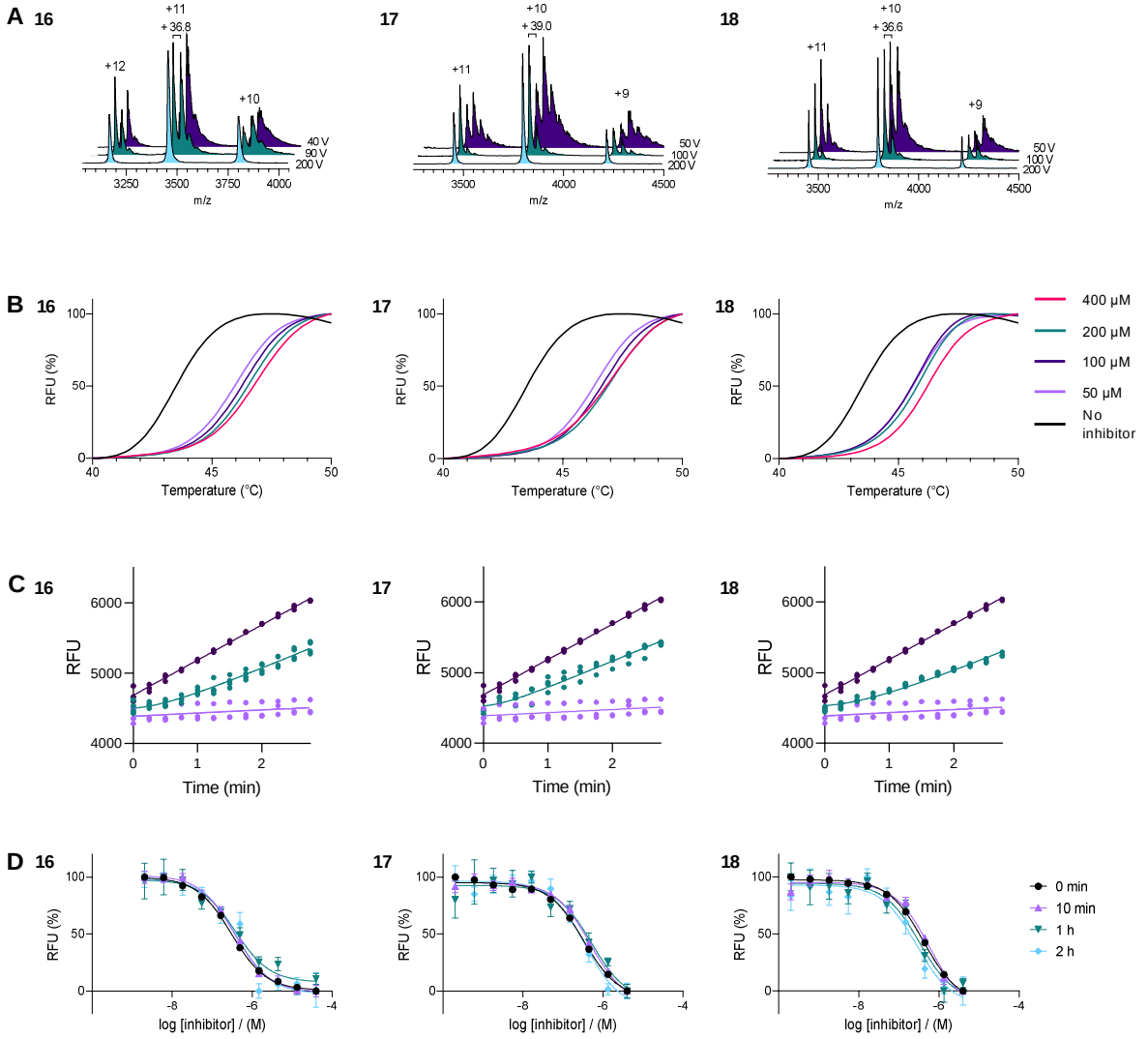

Figure S1.12. Characterisation of the inhibition of Ldt_{Mt2} by isatins 16-18. A. Non-denaturing MS analyses of Ldt_{Mt2} reaction with isatins **16**, **17**, and **18**. Ldt_{Mt2} (5 µM) was combined with **16**, **17** or **18** (500 µM) in 500 mM ammonium acetate. Mass spectra were recorded at cone voltages ranging from 40 V to 200 V. The mass shifts induced by inhibitor binding are shown for the +11 charge state (**16**) or the +10 charge state (**17** and **18**) and correspond to the binding of a single inhibitor molecule. **B.** Thermal shift assays with isatins **16-18**. Ldt_{Mt2} (5 µM) and the specified inhibitor (500 µM) were preincubated for 30 minutes prior to addition of SYPRO Orange (6 x concentrated, according to the manufacturer's (Invitrogen) protocol) in 50 mM Tris, pH 7.5. **C.** Jump dilution assays with isatins **16-18**. Ldt_{Mt2} (10 µM) and the specified inhibitor (100 µM) in 50 mM HEPES, pH 7.2, 0.01% (*v/v*) Triton X-100 were incubated for 2 hours at room temperature, then 1000 x diluted and assayed with probe **2** (15 µM). The results imply that binding of the tested isatin inhibitors is reversible. The k_{off} and $t_{1/2}$ values are given in Table S1.7. **D.** Dose-response assays with isatins **16**-**18** at varying inhibitor pre-incubation times. Assays of Ldt_{Mt2} were carried out with 300 nM Ldt_{Mt2} and 15 µM probe **1** at room temperature in 50 mM sodium phosphate pH 7.5 with 0.007% (*v/v*) Tween-20. Average pIC_{50} values are given in Table S1.8.

Table S1.7. Off rate (k_{off}) and half-life ($t_{1/2}$) of isatins 16 – 18 in complex with Ldt_{Mt2}, as determined by jump dilution assays.

Compound	k_{off} (s^{-1})	$t_{1/2}$ (min)
16	103 ± 16.5	0.41 ± 0.17
17	84.6 ± 6.03	0.49 ± 0.094
18	160 ± 15.5	0.26 ± 0.17

Table S1.8. Dose-response assays with isatins 16-18 at varying inhibitor pre-incubation times.

Compound	pIC_{50}			
	0 min	**10 min**	**60 min**	**120 min**
16	6.52 ± 0.06	6.44 ± 0.11	6.43 ± 0.32	6.39 ± 0.37
17	6.48 ± 0.14	6.33 ± 0.14	6.28 ± 0.45	6.45 ± 0.26
18	6.39 ± 0.07	6.24 ± 0.23	6.49 ± 0.35	6.56 ± 0.35

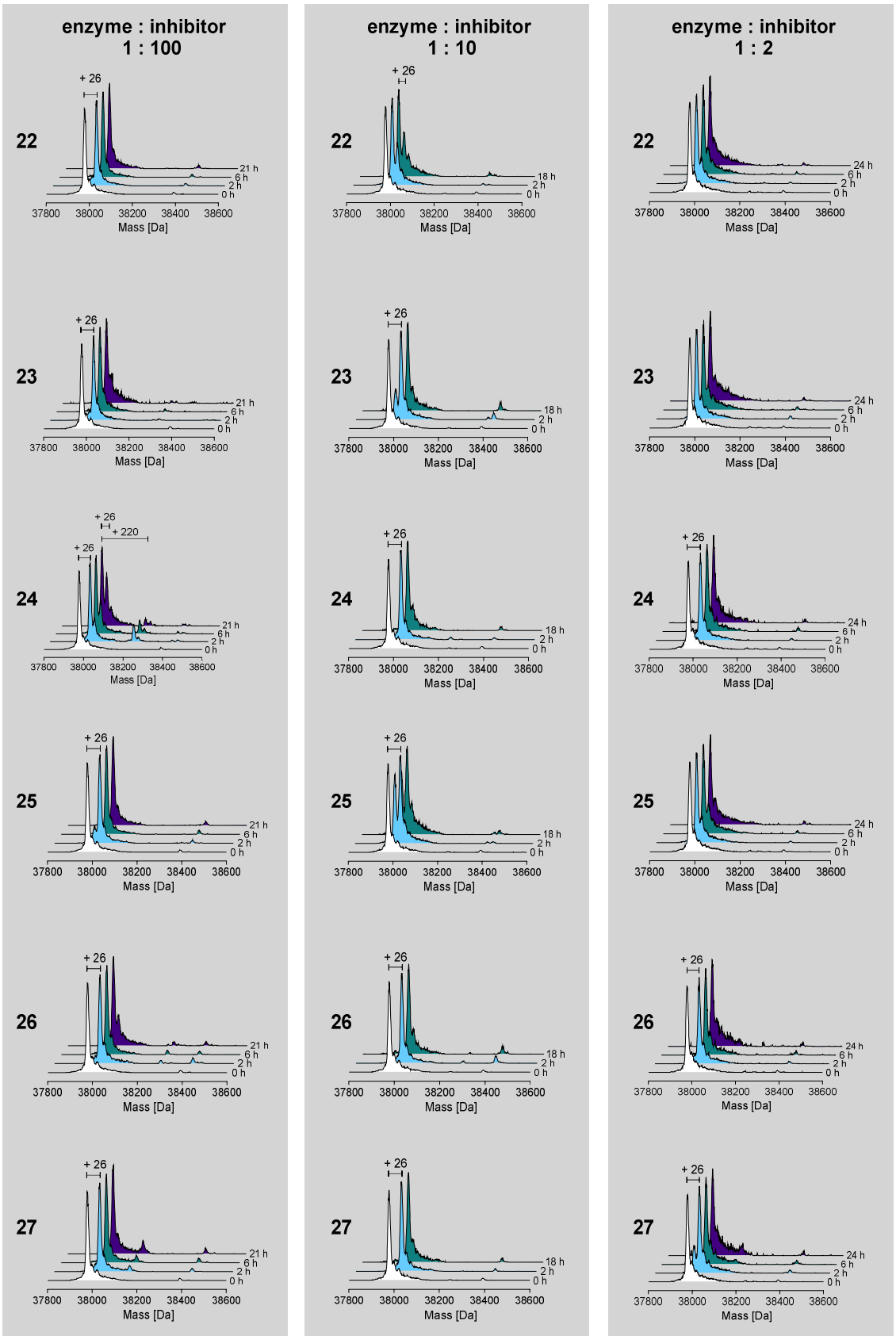

Figure S1.13. Protein observed SPE-MS analysis for the reaction of Ldt_{Mt2} with inhibitors 22-39 (figure continues).

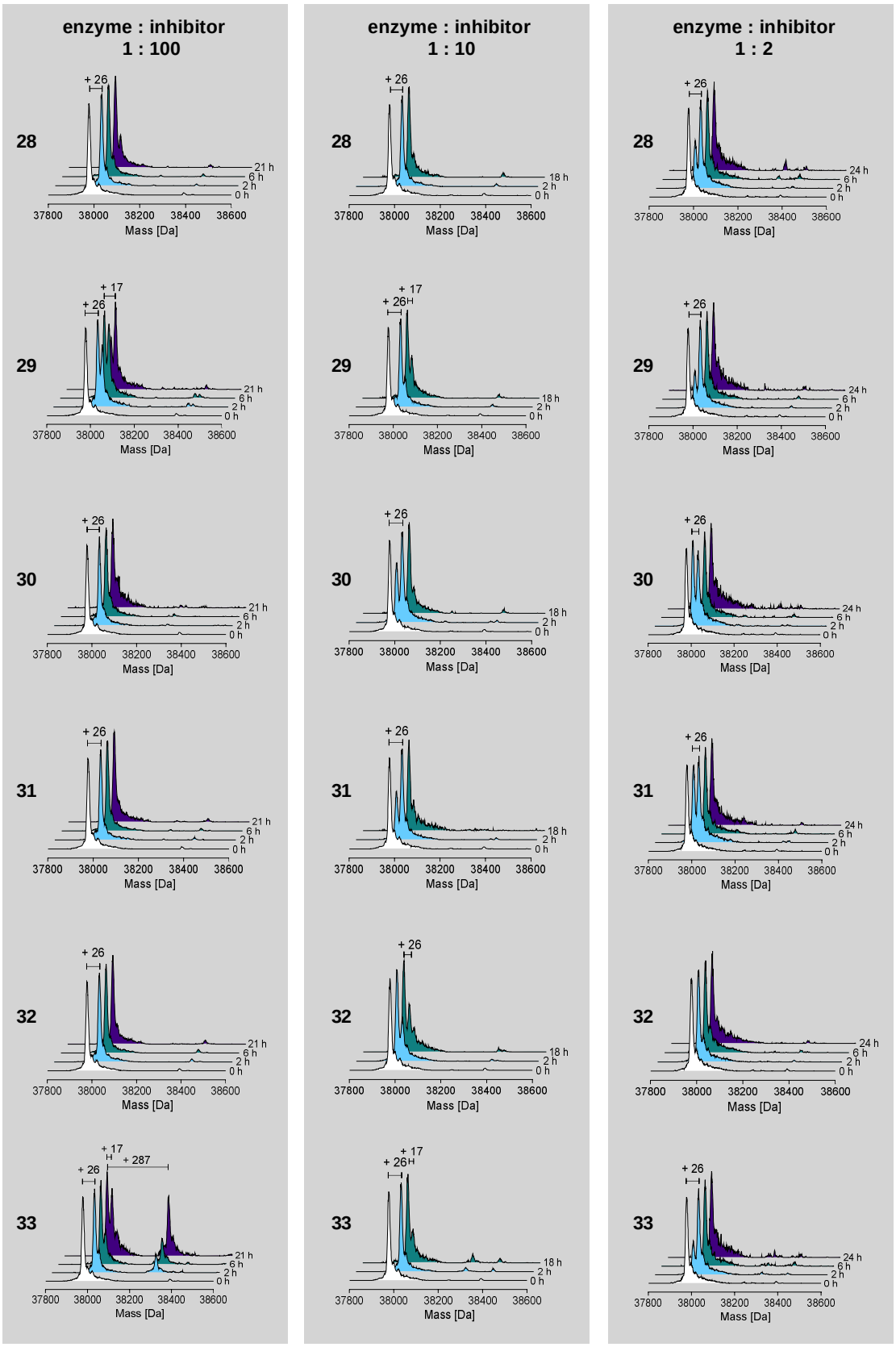

Figure S1.13. Protein observed SPE-MS analysis for the reaction of Ldt_{Mt2} with inhibitors 22-39 (figure continues).

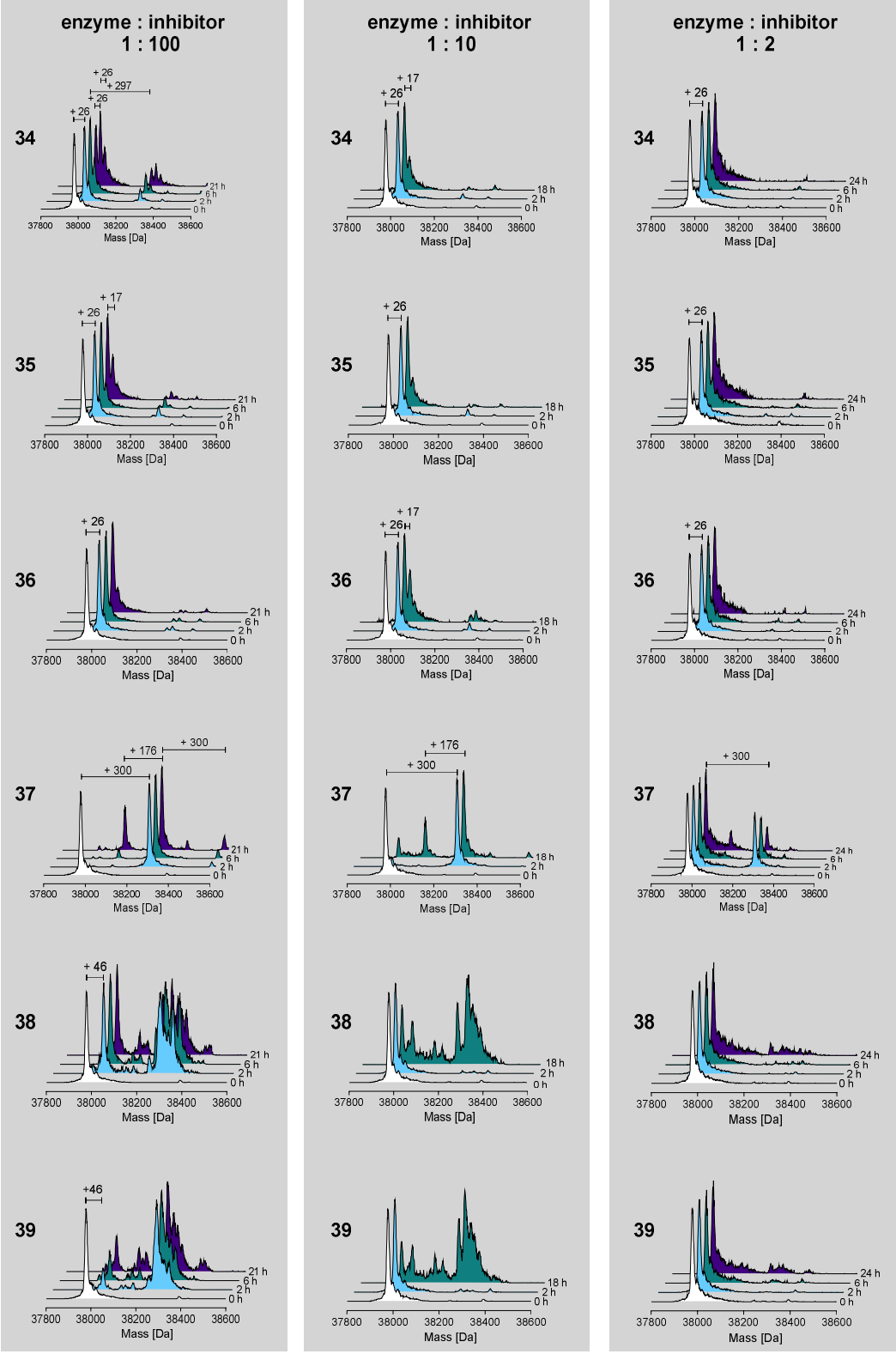

Figure S1.13. Protein observed SPE-MS analysis for the reaction of Ldt_{Mt2} with inhibitors 22-39. 1 µM Ldt_{Mt2} was incubated with the inhibitor at the specified ratio at room temperature in 50 mM Tris, pH 7.5. Samples were analysed after the indicated times. Compound structures are given in Table S1.5. Deconvoluted spectra, obtained using the maximum entropy algorithm in the MassHunter Workstation Qualitative Analysis B.07.00 program (Agilent), are shown.

Table S1.9. Calculated* and observed masses (Da) and mass shifts (Da) from protein observed SPE-MS experiments with Ldt_{Mt2} (1 µM) and the indicated nitrile inhibitors. Mass shifts are relative to unmodified Ldt_{Mt2}. *Calculated mass for cyanation of Ldt_{Mt2}. **Calculated mass for unfragmented adduct formation. ***Due to complexity of the obtained mass spectra, only major observed peaks are provided.

Compound	Calculated mass (Da)	Observed mass (Da)
22	38004 (+26)*, 38283 (+305)**	38004 (+26)
23	38004 (+26)*, 38283 (+305)**	38004 (+26)
24	38004 (+26)*, 38199 (+221)**	38004 (+26), 38030 (+52), 38224 (+246)
25	38004 (+26)*, 38199 (+221)**	38004 (+26)
26	38004 (+26)*, 38249 (+271)**	38004 (+26)
27	38004 (+26)*, 38222 (+244)**	38004 (+26)
28	38004 (+26)*, 38206 (+228)**	38004 (+26)
29	38004 (+26)*, 38280 (+302)**	38004 (+26), 38022 (+44)
30	38004 (+26)*, 38294 (+316)**	38004 (+26)
31	38004 (+26)*, 38281 (+303)**	38004 (+26)
32	38004 (+26)*, 38297 (+319)**	38004 (+26)
33	38004 (+26)*, 38264 (+286)**	38004 (+26), 38022 (+44), 38291 (+313)
34	38004 (+26)*, 38275 (+297)**	38004 (+26), 38030 (+52), 38056 (+78), 38301 (+323), 38327 (+349), 38353 (+375)
35	38004 (+26)*, 38275 (+297)**	38004 (+26), 38022 (+44)
36	38004 (+26)*, 38302 (+324)**	38004 (+26), 38022 (+44)
37	38004 (+26)*, 38278 (+300)**	38102 (+124), 38278 (+300), 38402 (+424), 38578 (+ 600)
38	38319 (+341)**	38024 (+46), 38277 (+299), 38293 (+315), 38331 (+353)***
39	38305 (+327)**	38024 (+46), 38125 (+147), 38157 (+179), 38252 (+274), 38277 (+299), 38296 (+318), 38316 (+338)***

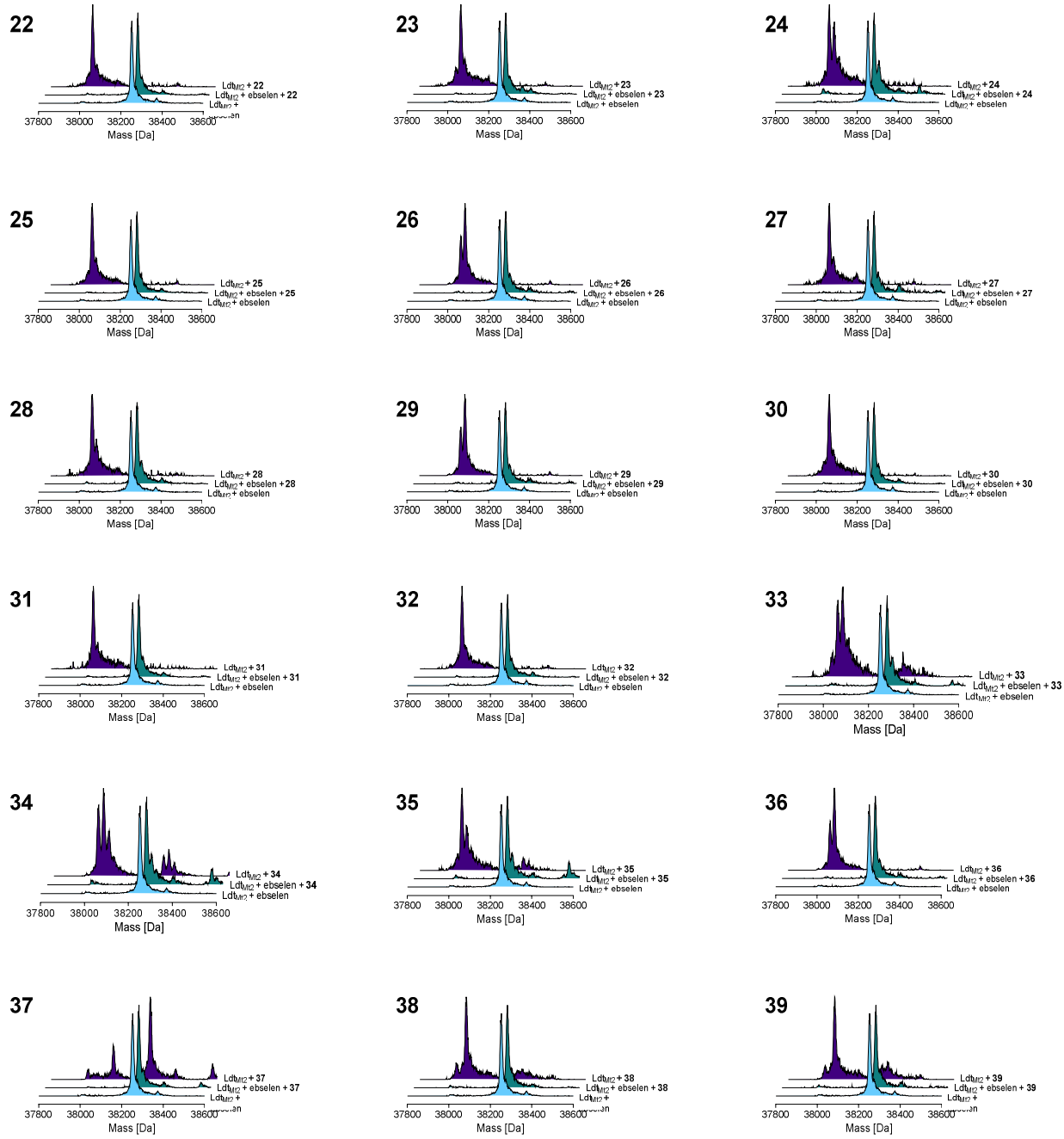

Figure S1.14. Protein observed SPE-MS based active-site selectivity assays with nitriles 22-36. Ldt_{Mt2} (1 µM) was preincubated with ebselen (10 µM, a known Ldt_{Mt2} inhibitor,[3] which reacts with the nucleophilic Cys354) for 1 h in 50 mM Tris, pH 7.5, prior to addition of inhibitors **22**-**36** (100 µM). Samples were analysed after an additional 24 h incubation at room temperature. The spectrum in blue corresponds to Ldt_{Mt2} in complex with ebselen. The spectrum in green corresponds to Ldt_{Mt2} and the specified inhibitor upon preincubation with ebselen. The spectrum in purple corresponds to Ldt_{Mt2} in complex with the specified inhibitor. Deconvoluted spectra, obtained using the maximum entropy algorithm in the MassHunter Workstation Qualitative Analysis B.07.00 program (Agilent), are shown.

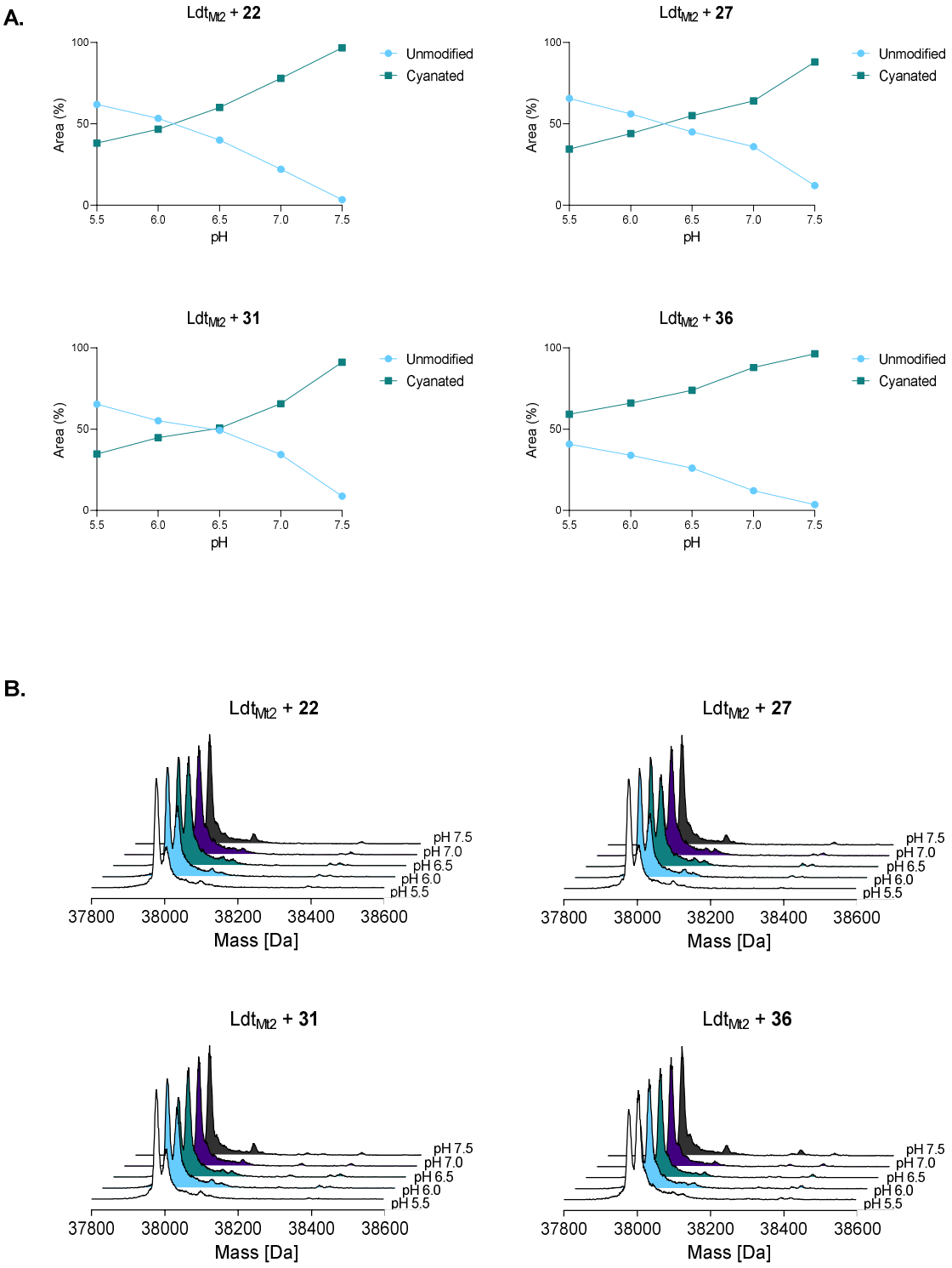

Figure S1.15. pH dependence of the cyanation of Ldt$_{Mt2}$ by representative cyanamides 22, 27, 31 and 36. A. Area of cyanated and unmodified Ldt$_{Mt2}$ peaks at the specified pH. **B.** MS spectra of Ldt$_{Mt2}$ following reaction with selected cyanamides at the specified pH values. MS spectra were taken 15 min after addition of the nitrile (10 μM) to Ldt$_{Mt2}$ (1 μM) in 50 mM Tris, pH 7.5.

Table S1.10. Inhibition of Ldt_{MT2} by known cyanating compounds.[4,5] MW: Molecular weight. k_{chem}: apparent intrinsic thiol reactivity as measured with L-glutathione and probe **2**.

	Structure	MW	pIC_{50} Ldt_{Mt2}	k_{chem}
40	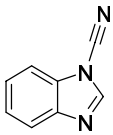	143.15	6.31 ± 0.03	0.90 ± 0.05
41	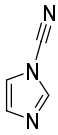	93.09	6.54 ± 0.01	3.69 ± 0.11
42	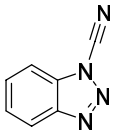	144.14	6.02 ± 0.05	0.90 ± 0.08
43 (CDAP)	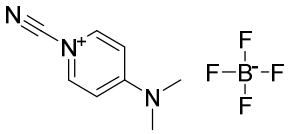	234.99	5.30 ± 0.08	N.D.
44 (NTCB)	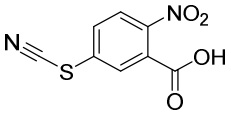	224.19	5.84 ± 0.04	N.D.
45 (CDTP)	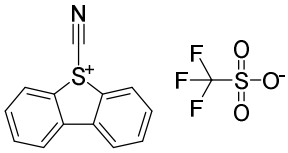	359.34	<4.4	N.D.

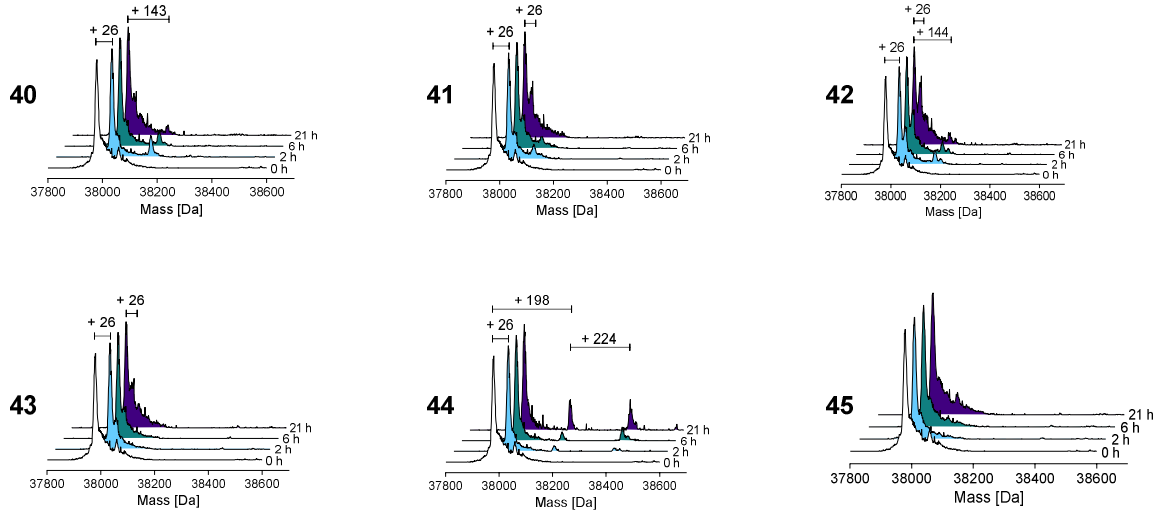

Figure S1.16. Protein observed SPE-MS analysis for the reaction of Ldt_{Mt2} with cyanating agents 40-45. 1 µM Ldt_{Mt2} was incubated with 100 µM cyanating agent at room temperature in 50 mM Tris, pH 7.5. Samples were analysed after the indicated times. Compound structures are given in Table S1.10. Deconvoluted spectra, obtained using the maximum entropy algorithm in the MassHunter Workstation Qualitative Analysis B.07.00 program (Agilent), are shown.

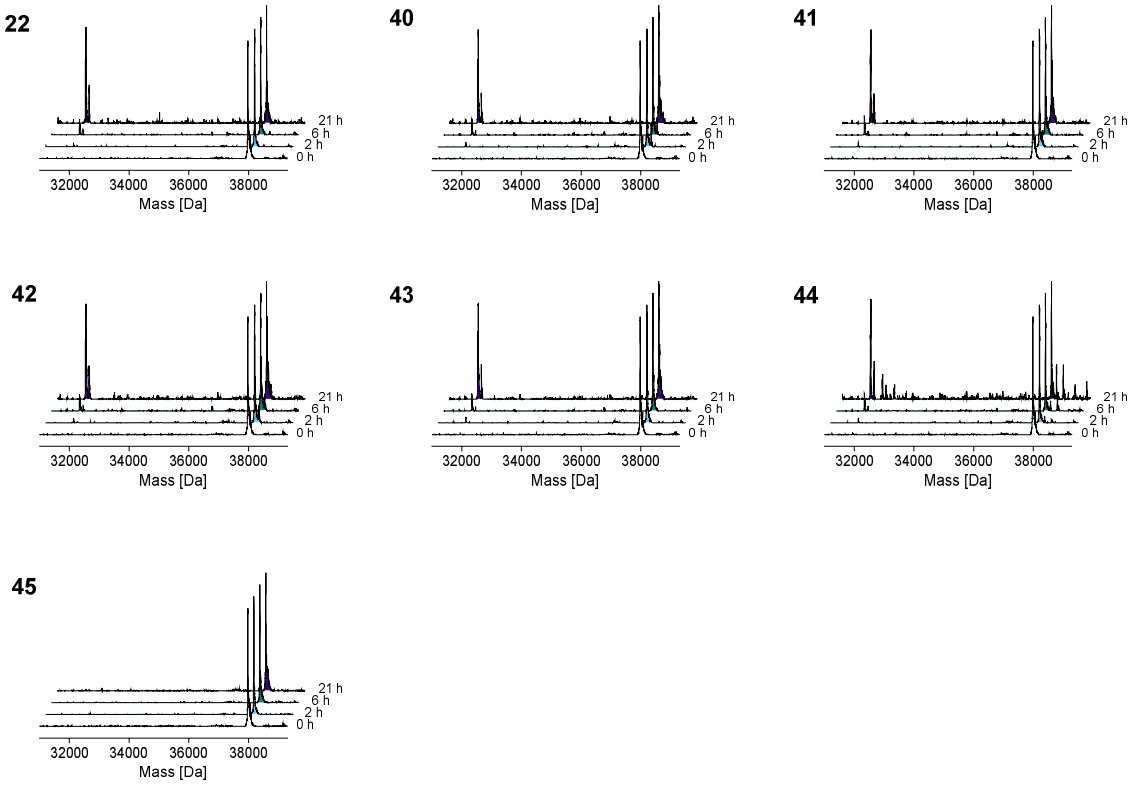

Figure S1.17. Protein observed SPE-MS analysis of the reaction of Ldt_{Mt2} with 22 (a representative of cyanamides 22-36) and 40-45, showing evidence for cleavage of Ldt_{Mt2} at Cys354 after prolonged incubation for 22 and 40-44. 1 µM Ldt_{Mt2} was incubated with the inhibitor at a 1 to 100 ratio at room temperature in 50 mM Tris, pH 7.5. Samples were analysed after the indicated times. Compound structures are given in Table S1.5 and Table S1.9. Deconvoluted spectra, obtained using the maximum entropy algorithm in the MassHunter Workstation Qualitative Analysis B.07.00 program (Agilent), are shown. Note, cleavage was not observed in the case of compound **45**.

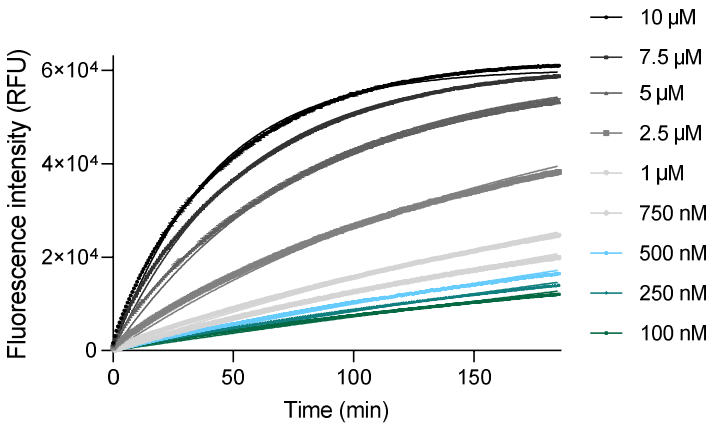

Figure S1.18. Assay set up for the determination of the second-order rate constant k_{inact}/K_I for irreversible inactivation of Ldt_{Mt2} via an endpoint assay using irreversibly reacting Probe 2. A. Determination of the observed kinetic rate constant (k_{obs}). Assays were carried out using 100 nM Ldt_{Mt2} at room temperature in 50 mM HEPES, pH 7.2 with 0.01% (*v/v*) Triton X-100, using varying Probe **2** concentrations, as specified. **B.** The obtained k_{obs} values at various Probe **2** concentrations were used to provide the $(k_{inact}/K_I)_{probe}$ value.

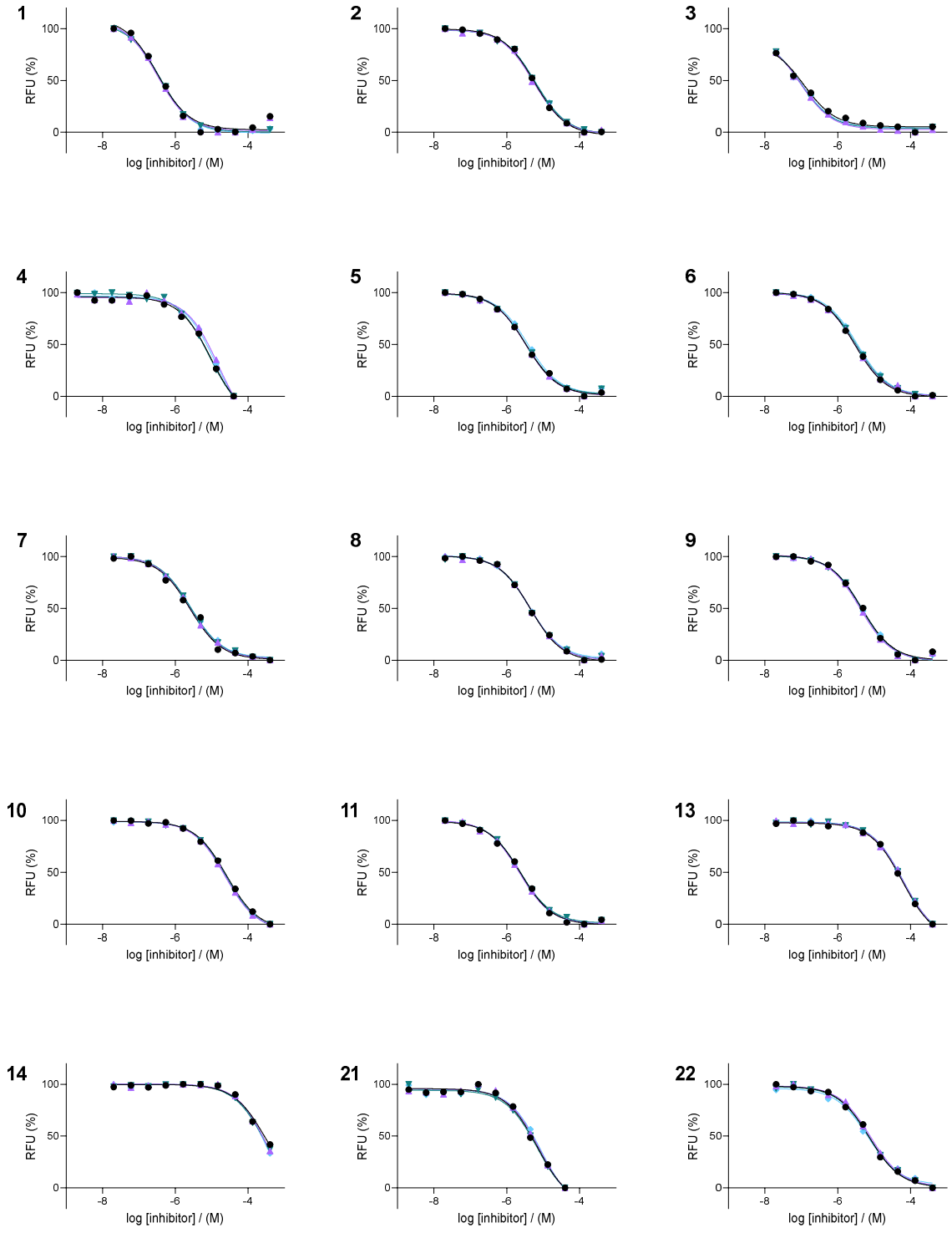

Figure S1.19. Determination of the second-order rate constant for covalent target inactivation (k_{inact}/K_I) of covalent inhibitors 1-11, 13-14 and 21-37 (figure continues).

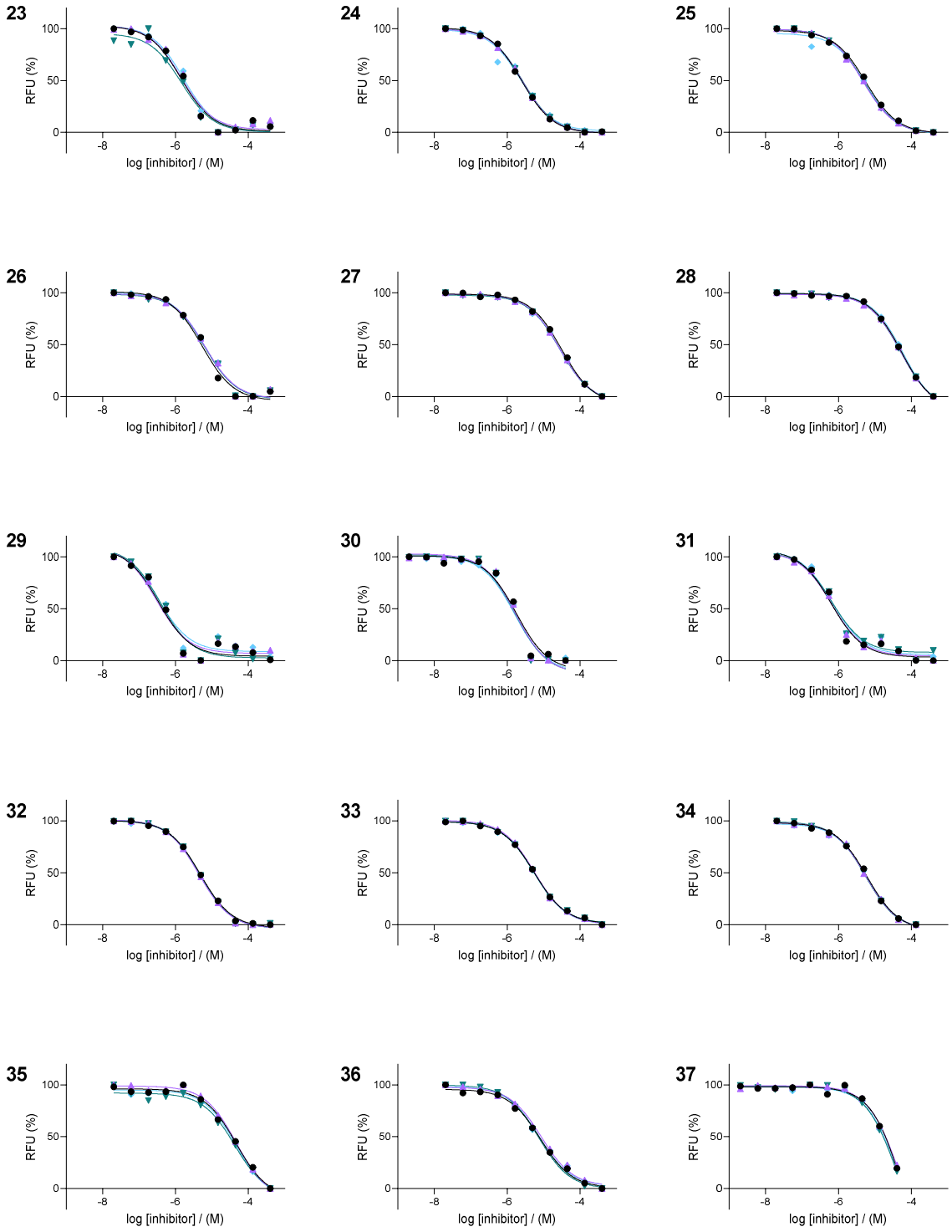

Figure S1.19. Determination of the second-order rate constant for covalent target inactivation (k_{inact}/K_I) of covalent inhibitors 1-11, 13-14 and 21-37. Inhibition assays were carried out using 100 nM Ldt_{Mt2} and 10 µM Probe **2** with 3 h incubation at rt in 50 mM HEPES, pH 7.2 with 0.01% (*v/v*) Triton X-100. Data points represent values of independent repeats (n=4). Average $(k_{inact}/K_I)_{inhibitor}$ values and compound structures are given in Table S1.5.

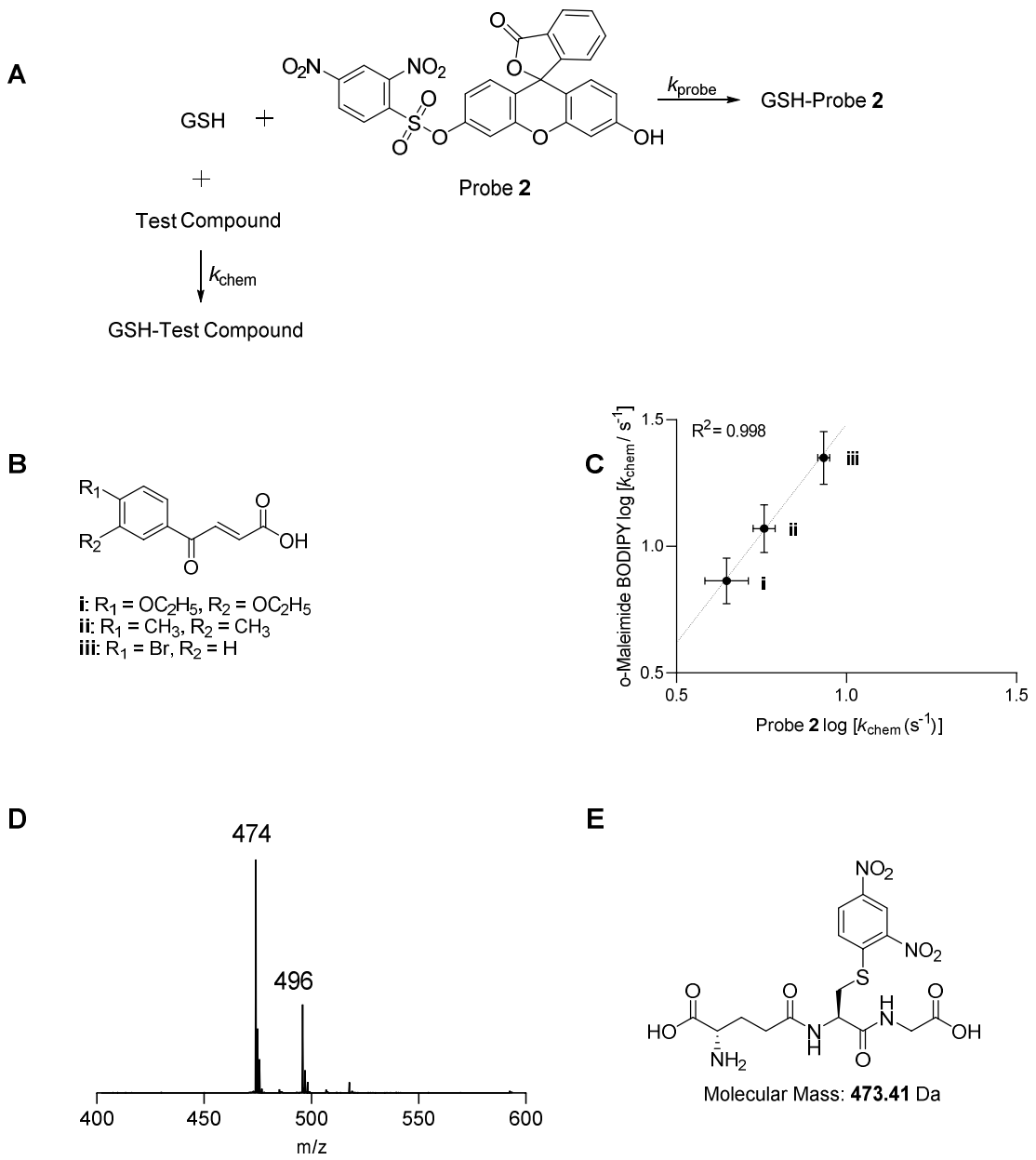

Figure S1.20. Analysis of the intrinsic thiol reactivity (k_{chem}) assay. A. The assay measures competition between glutathione (GSH) and test compounds for reaction with probe **2**. **B.** Compounds i-iii used for validation of the k_{chem} assay. **C.** k_{chem} of i-iii obtained from the fluorogenic assay with probe **2** versus the k_{chem} values reported from the fluorogenic assay with *o*-maleimide BODIPY.[6] **D.** GSH reacts covalently and irreversibly with probe **2** under the tested conditions. GSH (2 µM) was incubated with probe **2** (200 µM) for 16 hours in 50 mM tris, pH 7.5, prior to addition of *N*-ethylmaleimide (2 mM) and incubation of an additional 24 h. Only the mass of GSH modified with probe **2** ($[M+H]^+$ 474, $[M+Na]^+$ 496) was observed. **E.** Structure and molecular mass of the anticipated product from the reaction of GSH and probe **2**.

Table S1.11. k_{chem} of i-iii obtained from the fluorogenic assay with probe 2 versus the k_{chem} values reported from the fluorogenic assay with *o*-maleimide BODIPY.[6]

Compound	log(k_{chem}) probe 2 (mean ± SD)	log(k_{chem}) *o*-maleimide BODIPY (mean ± SD)
i	0.65 ± 0.06	0.86 ± 0.09
ii	0.76 ± 0.03	1.07 ± 0.09
iii	0.93 ± 0.02	1.34 ± 0.10

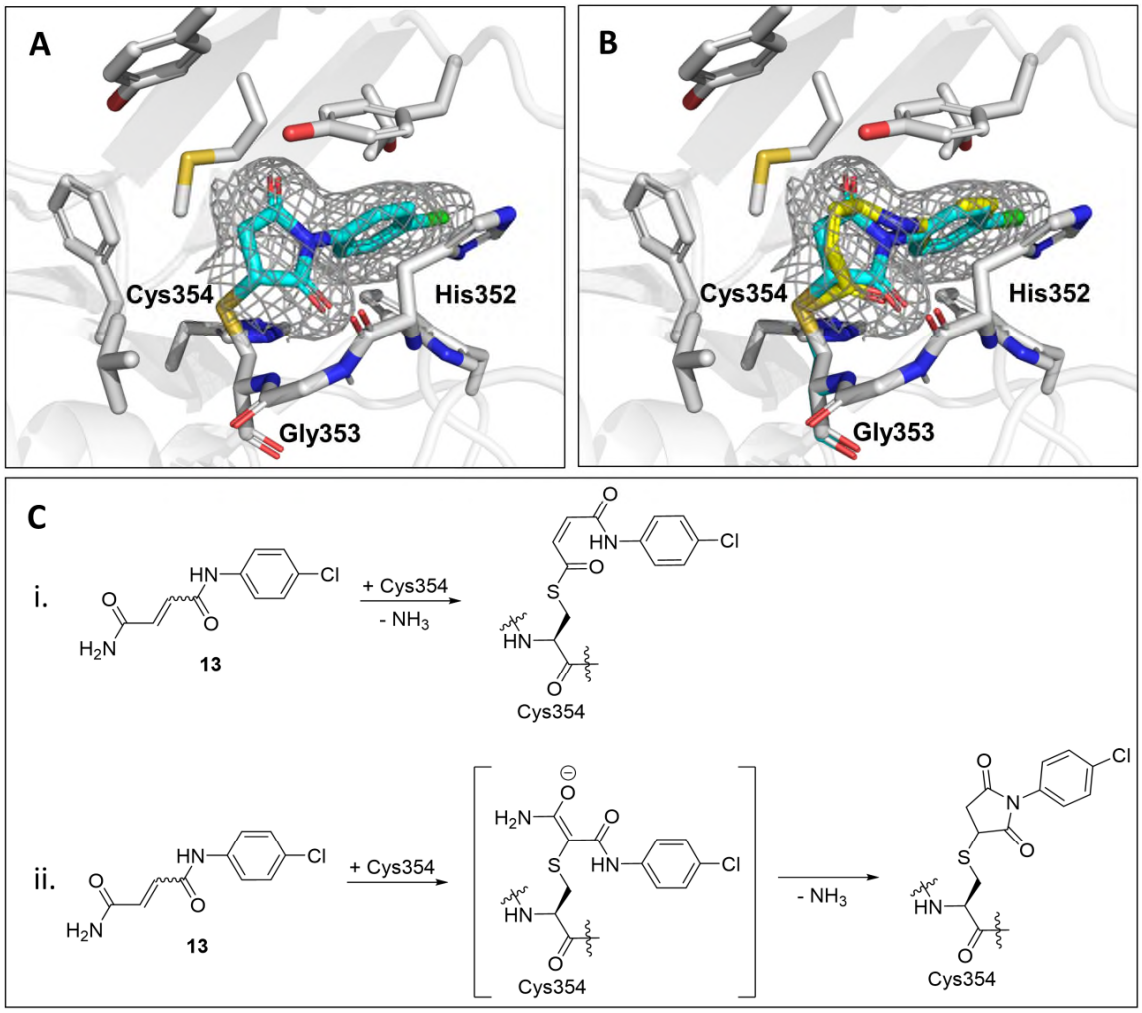

Figure S1.21. Alternative reaction mechanism for 13 in reaction with Cys354 of Ldt_{Mt2}. A. A view of the potential Ldt_{Mt2}-**13** adduct, which can be obtained via reaction with the fumaryl group, followed by ring closure. **B.** Overlay of the two proposed adducts in the crystal structure obtained from Ldt_{Mt2} in reaction with **13** (PDB 8A1K). Both proposed adducts can be modelled in the electron density in the Ldt_{Mt2} active site. **C**. Reaction schemes for the two proposed adducts: (i) reaction with the terminal amide of **13**, and (ii) reaction with the fumaryl group, followed by ring closure. Note that the identity and purity of **13** used in the MS and crystallographic studies was confirmed by NMR and MS (Figure S1.22).

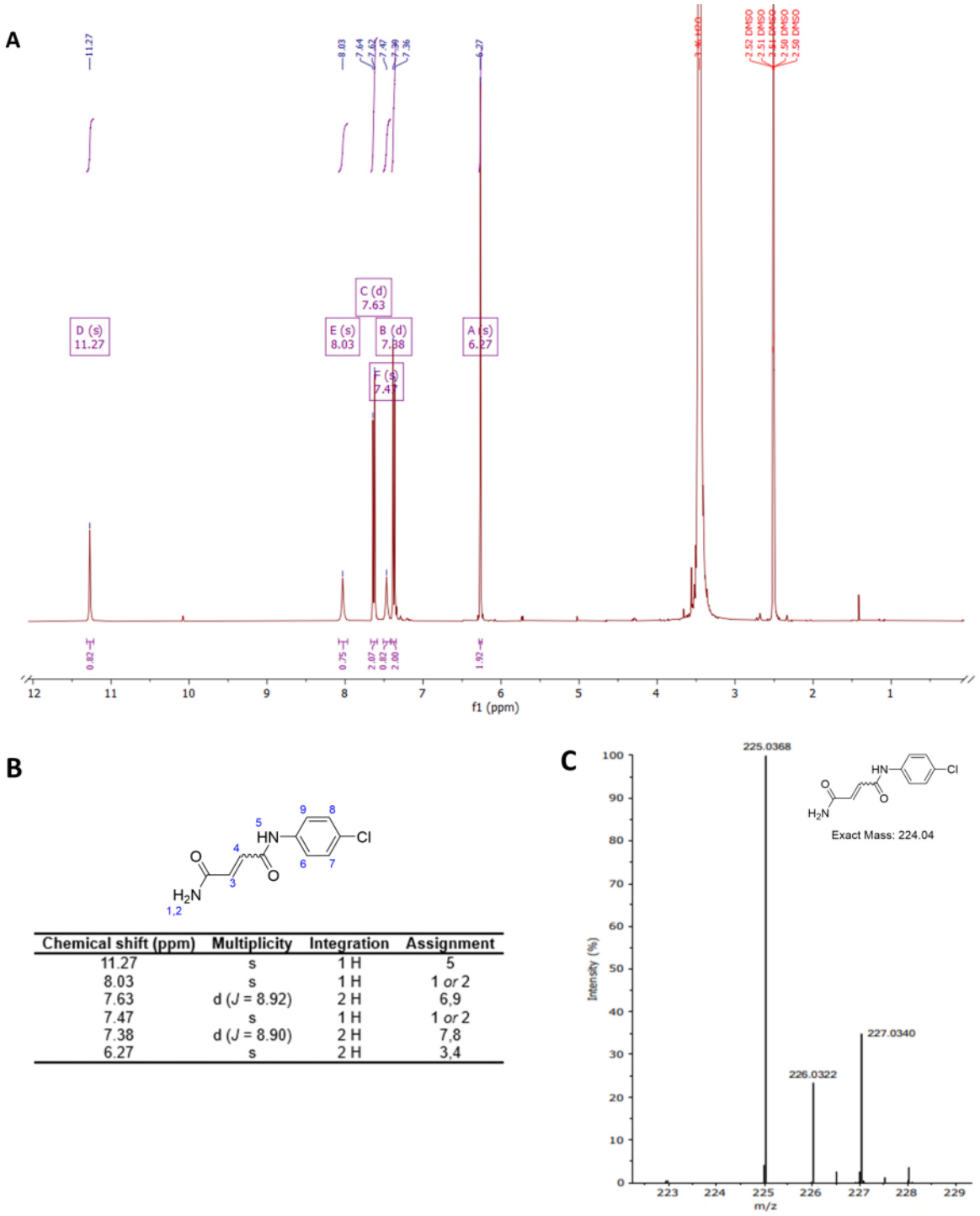

Chemical shift (ppm)	Multiplicity	Integration	Assignment
11.27	s	1 H	5
8.03	s	1 H	1 *or* 2
7.63	d (*J* = 8.92)	2 H	6,9
7.47	s	1 H	1 *or* 2
7.38	d (*J* = 8.90)	2 H	7,8
6.27	s	2 H	3,4

Figure S1.22. Characterisation of the structure and purity of 13 by NMR (400 MHz) and MS. A. ^{1}H NMR (400 MHz) spectrum of **13** in DMSO-d6. **B.** Structure of **13** labelled with assignments. **C**. Mass spectrum of **13**, revealing the expected mass of [M+H] = 225.04.

Table S1.12. Inhibitory activity of selected hit compounds against *Mycobacterium tuberculosis* and cytotoxicity in HepG2 cells. MIC_{50} intracellular values represent the concentration of inhibitor that inhibited *Mtb* (strain H37Rv) growth in THP1 cells by 50%, as obtained from extrapolation of the dose-response curve. MIC_{50} extracellular values represent the concentration of inhibitor that inhibited *Mtb* (strain H37Rv) growth by 50%, as obtained from extrapolation of the dose-response curve.

	Structure	MIC_{50} intracellular (µM)	MIC_{50} extracellular (µM)	HepG2 IC_{50} (µM)
1	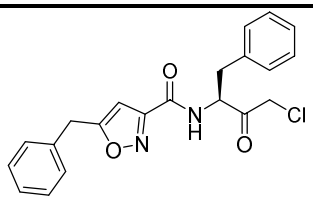	35.5 ± 4.9	>100	N.D.
5	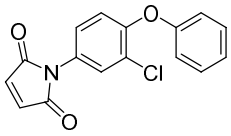	25.7 ± 0.30	>100	2.51 ± 0.12
7	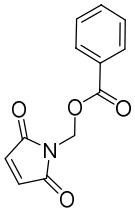	39.8 ± 0.0	>100	3.90 ± 0.88
15	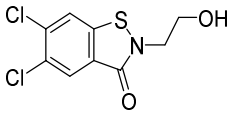	7.08 ± 0.16	>100	9.55 ± 0.22
17	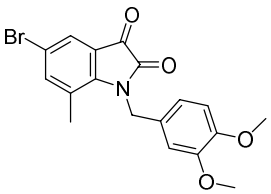	15.1 ± 0.70	>100	53.5 ± 6.7
18	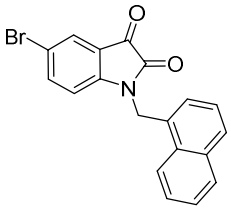	35.5 ± 5.4	>100	42.3 ± 3.4
20	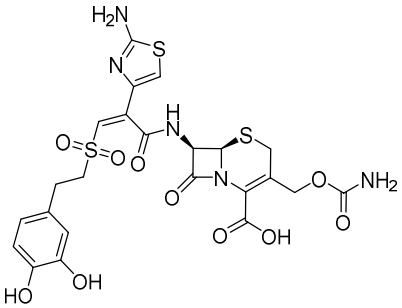	38.9 ± 1.8	>100	>100
23	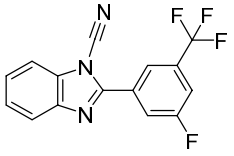	12.0 ± 1.5	>100	28.8 ± 0.0

	Structure	MIC_{50} intracellular (μM)	MIC_{50} extracellular (μM)	HepG2 IC_{50} (μM)
30	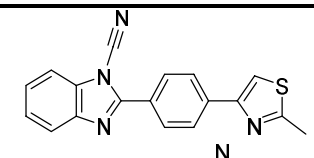	0.98 ± 1.2	>100	3.98 ± 0.10
36	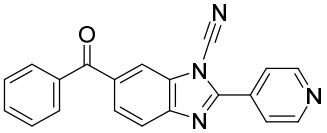	29.5 ± 0.0	>100	32.7 ± 0.38
39	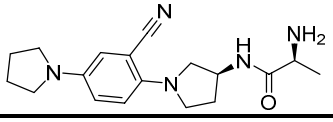	28.8 ± 0.0	>100	>100

Table S1.13. Data collection and refinement statistics for Ldt_{Mt2} inhibitor crystal structures.

Datasets	Ldt_{Mt2} – 2 (PDB: 8A1L)	Ldt_{Mt2} – 3 (PDB: 8A1J)	Ldt_{Mt2} – 4 (PDB: 8A1M)
Data Collection			
Beamline (Wavelength, Å)	DLS I03 (0.9763)	DLS I03 (0.9763)	DLS I03 (0.9763)
Detector	Eiger2 XE 16M	Eiger2 XE 16M	Eiger2 XE 16M
Data Processing	Xia2 dials	Xia2 3dii	Xia2 3dii
Space group	*P* 1 2_1 1	*P* 1 2_1 1	*P* 1 2_1 1
Cell dimensions			
a,b,c (Å)	61.76, 94.77, 75.74	61.19, 94.02, 75.29	61.70, 95.07, 75.45
α, β, γ (°)	90.00, 92.90, 90.00	90.00, 92.61, 90.00	90.00, 92.22, 90.00
No. of molecules/ASU	2	2	2
No. reflections	38420 (1817)*	27561 (1234)*	38184 (1886)*
Resolution (Å)	61.68-2.30 (2.34-2.30)*	47.01-2.54 (2.58-2.54)*	48.66-2.30 (2.34-2.30)*
R_{merge} (I)	0.162 (1.331)*	0.237 (1.859)*	0.131 (1.291)*
I/σI	9.8 (1.0)*	7.4 (1.0)*	9.6 (1.4)*
CC-1/2	1.0 (0.8)*	1.0 (0.6)*	1.0 (0.6)*
Completeness (%)	99.6 (96.1)*	97.9 (89.7)*	98.5 (98.7)*
Multiplicity	6.9 (7.2)*	6.8 (5.8)*	6.9 (6.8)*
Wilson B value ($Å^2$)	33.84	31.08	40.55
Refinement	PHENIX	PHENIX	PHENIX
R_{work}/R_{free}	0.2146/0.2476	0.2346/0.2663	0.2179/0.2501
No. atoms	5775	5616	5782
- Enzyme	5276	5231	5319
- Ligand	76	46	81
- Water	423	339	382
Average B-factors	47.06	52.20	53.20
- Enzyme	46.99	52.46	53.17
- Ligand	55.35	58.79	66.73
- Water	46.40	47.23	50.85
RMS[$] deviations			
- Bond lengths (Å)	0.003	0.003	0.003
- Bond angles (°)	0.51	0.58	0.53

[#] ASU = asymmetric unit.

[$] RMS = root mean square.

*Highest resolution shell in parentheses.

Datasets	**Ldt_{Mt2} – 8 (PDB: 8A1O)**	**Ldt_{Mt2} – 13 (PDB: 8A1N)**	**Ldt_{Mt2} – 15 (PDB: 8A1K)**
Data Collection			
Beamline (Wavelength, Å)	DLS I03 (0.9763)	DLS I03 (0.9763)	DLS I03 (0.9763)
Detector	Eiger2 XE 16M	Eiger2 XE 16M	Eiger2 XE 16M
Data Processing	Xia2 dials	Xia2 dials	Xia2 dials
Space group	*P* 2_1 2_1 2	*P* 1 2_1 1	*P* 1 2_1 1
Cell dimensions			
a,b,c (Å)	76.87, 93.00, 61.40	60.93, 94.63, 75.36	60.98, 95.17, 75.62
α, β, γ (°)	90.00, 90.00, 90.00	90.00, 92.35, 90.00	90.00, 92.35, 90.00
No. of molecules/ASU	1	2	2
No. reflections	31561 (1582)*	53680 (2613)*	86822 (4298)*
Resolution (Å)	46.50-1.95 (1.98-1.95)*	75.29-2.05 (2.08-2.05)*	60.93-1.75 (1.78-1.75)*
R_{merge}(I)	0.066 (0.593)*	0.090 (0.826)*	0.063 (0.759)*
I/σI	24.2 (3.5)*	13.2 (1.1)*	17.7 (1.0)*
CC-1/2	1.0 (0.9)*	1.0 (0.8)*	1.0 (0.8)*
Completeness (%)	96.2 (97.1)*	99.9 (97.9)*	100.0 (99.3)*
Multiplicity	12.6 (11.5)*	6.8 (6.8)*	6.6 (6.6)*
Wilson B value ($Å^2$)	24.43	31.68	23.14
Refinement	PHENIX	PHENIX	PHENIX
R_{work}/R_{free}	0.1939/0.2228	0.1954/0.2379	0.1837/0.2107
No. atoms	3166	5937	6401
- Enzyme	2696	5296	5367
- Ligand	42	42	43
- Water	428	599	991
Average B-factors	37.22	44.34	34.55
- Enzyme	35.97	44.07	32.96
- Ligand	58.19	53.53	40.01
- Water	43.07	46.05	42.92
RMS[$] deviations			
- Bond lengths (Å)	0.010	0.003	0.011
- Bond angles (°)	0.88	0.58	0.94

[#] ASU = asymmetric unit.

[$] RMS = root mean square.

*Highest resolution shell in parentheses.

Datasets	**Ldt_{Mt2} – 31 (PDB: 8AHO)**
Data Collection	
Beamline (Wavelength, Å)	DLS I03 (0.9763)
Detector	Eiger2 XE 16M
Data Processing	Xia2 dials
Space group	*P* 1 2_1 1
Cell dimensions	
a,b,c (Å)	61.25, 94.26, 75.67
α, β, γ (°)	90.00, 92.69, 90.00
No. of molecules/ASU	2
No. reflections	38141 (3764)*
Resolution (Å)	48.69-2.30 (2.38-2.30)*
R_{merge}(I)	0.136 (0.781)*
I/σI	8.9 (1.3)*
CC-1/2	1.0 (0.9)*
Completeness (%)	99.8 (98.4)*
Multiplicity	6.9 (6.8)*
Wilson B value ($Å^2$)	39.27
Refinement	PHENIX
R_{work}/R_{free}	0.2101/0.2495
No. atoms	5701
- Enzyme	5267
- Ligand	41
- Water	393
Average B-factors	45.27
- Enzyme	45.18
- Ligand	66.22
- Water	44.40
RMS[$] deviations	
- Bond lengths (Å)	0.002
- Bond angles (°)	0.54

[#] ASU = asymmetric unit.

[$] RMS = root mean square.

*Highest resolution shell in parentheses.

Experimental details for the HTS assay optimisation process

Optimisation of reagent concentrations and reaction volume

The specified volume of assay buffer (50 mM sodium phosphate pH 7.5 with 0.01% (*v/v*) Triton X-100) was added to a black polystyrene, flat-bottomed, small volume, clear bottomed 384-well microplate (Greiner Bio-One, part number 784076) using a MultiDrop Combi dispenser (ThermoFisher Scientific). To this was added the specified concentrations of Ldt_{Mt2} and probe **1**.[1] The fluorescence intensity was measured for the specified time using an Envision 2104 Multilabel Reader (Perkin Elmer) with λ_{ex}=485 nm, λ_{em}=540 nm and a general dual mirror. All reactions were carried out in quadruplicate, with no-enzyme control measurements included.

DMSO tolerance assay

A Ldt_{Mt2} stock solution of 600 nM (2x final concentration 300 nM) was prepared in the assay buffer (50 mM sodium phosphate pH 7.5 with 0.01% (*v/v*) Triton X-100). A solution of probe **1** (30 µM, 2x final concentration 15 µM) was prepared in the assay buffer. A dilution series of DMSO ranging from 33.3% to 0.003% (*v/v*) was added to a black polystyrene, flat-bottomed, small volume, clear bottomed 384-well microplate (Greiner Bio-One, part number 784076) using a HP D300 Digital Dispenser. To each well was added 5 µL of the 2x Ldt_{Mt2} stock and 5 µL of the 2x probe **1** stock using a MultiDrop Combi dispenser (ThermoFisher Scientific). The fluorescence intensity was measured every minute for 60 minutes using an Envision 2104 Multilabel Reader (Perkin Elmer) with λ_{ex}=485 nm, λ_{em}=540 nm and a general dual mirror. All reactions were carried out in quadruplicate, with no-enzyme control and no DMSO control measurements included.

Detergent optimisation

An Ldt_{Mt2} stock solution of 600 nM (2x final concentration 300 nM) was prepared in the assay buffer (50 mM sodium phosphate pH 7.5). Stock solutions of 20 x critical micelle concentration (CMC) of the detergents Triton X-100, Triton X-114, Tween-20 (Thermo Scientific), Tween-80, MEGA-8, CHAPS, BRIJ-35, IPEGAL-630, n-dodecyl-β-D-maltose, BSA and dBSA (prepared by incubation of BSA for 15 minutes at 80 °C, followed by 2 hours at room temperature and stored at -20 °C) were prepared. Using a HP D300 Digital Dispenser 11 concentrations of ½ step dilutions were added to a black polystyrene, flat-bottomed, small volume, clear bottomed 384-well microplate (Greiner Bio-One, part number 784076). To each well was added 5 µL of the 2x Ldt_{Mt2} stock and 5 µL of the 2x probe **1** stock solution using a MultiDrop Combi dispenser (ThermoFisher Scientific). The fluorescence intensity was measured every minute for 60 minutes using an Envision 2104 Multilabel Reader (Perkin Elmer) with λ_{ex}=485 nm, λ_{em}=540 nm and a general dual mirror. All reactions were carried out in quadruplicate, with no-enzyme

control and no detergent control measurements included. Maximum tolerated concentrations were calculated by analysing the resulting slopes using Microsoft Excel. Buffers of the detergents in maximum tolerated concentrations, or 1 x CMC where no interference was observed, in 50 mM sodium phosphate pH 7.5 were prepared, omitting BRIJ-35, IPEGAL-630, BSA and dBSA due to interference at all concentrations. With each buffer, a Ldt_{Mt2} stock of 600 nM (2x final concentration 300 nM) and a probe **1** stock solution of 30 µM (2x final concentration 15 µM) was prepared. To each well was added 5 µL of the 2x Ldt_{Mt2} stock solution and 5 µL of the 2x probe **1** stock solution using a MultiDrop Combi dispenser (ThermoFisher Scientific). The fluorescence intensity was measured every minute for 60 minutes using a Envision 2104 Multilabel Reader (Perkin Elmer) with λ_{ex}=485 nm, λ_{em}=540 nm and a general dual mirror. All reactions were carried out in quadruplicate, with no-enzyme control measurements included.

Plate reader protocol optimisation

A stock solution of Ldt_{Mt2} of 600 nM (2x final concentration 300 nM) was prepared in the assay buffer (50 mM sodium phosphate pH 7.5 with 0.007% (*v/v*) Tween-20). A stock solution of probe **1** of 30 µM (2x final concentration 15 µM) was prepared in the assay buffer. To each well was added 5 µL of the 2x Ldt_{Mt2} stock solution and 5 µL of the 2x probe **1** stock solution using a MultiDrop Combi dispenser (ThermoFisher Scientific). The fluorescence intensity was measured every minute for 60 minutes using a Envision 2104 Multilabel Reader (Perkin Elmer) with λ_{ex}=485 nm, λ_{em}=540 nm and a FITC mirror. The plate reader protocol was optimised for the coordinates of the corners, measurement height and gain.

Stability of stock solution concentrations

A stock solution of Ldt_{Mt2} of 600 nM (2x final concentration 300 nM) was prepared in the assay buffer (50 mM sodium phosphate pH 7.5 with 0.007% (*v/v*) Tween-20). A stock solution of probe **1** of 30 µM (2x final concentration 15 µM) was prepared in the assay buffer. The stock solutions were kept on ice for 7 hours, after which time 5 µL of the 2x Ldt_{Mt2} solution and 5 µL of the 2x probe **1** solution were added to a black polystyrene, flat-bottomed, small volume, clear bottomed 384-well microplate (Greiner Bio-One, part number 784076) using a MultiDrop Combi dispenser (ThermoFisher Scientific). The fluorescence intensity was measured every minute for 60 minutes using an Envision 2104 Multilabel Reader (Perkin Elmer) with λ_{ex}=485 nm, λ_{em}=540 nm and a FITC mirror.

Full plate analysis

A stock solution of Ldt_{Mt2} of 600 nM (2x final concentration 300 nM) was prepared in the assay buffer (50 mM sodium phosphate pH 7.5 with 0.007% (*v/v*) Tween-20). A stock solution of probe **1** of 30 µM (2x final concentration 15 µM) was prepared in the assay buffer. To a black

polystyrene, flat-bottomed, small volume, clear bottomed 384-well microplate (Greiner Bio-One, part number 784076) was added 100 nL of DMSO to all wells using a HP D300 Digital Dispenser. To this was added 5 µL of the 2x Ldt_{Mt2} stock solution and 5 µL of the 2x probe **1** stock solution using a MultiDrop Combi dispenser (ThermoFisher Scientific). The fluorescence intensity was measured every 5 minutes for 10 hours using a Envision 2104 Multilabel Reader (Perkin Elmer) with λ_{ex}=485 nm, λ_{em}=540 nm and a FITC mirror.

Dose-response analysis with tool compounds

Inhibitor solutions (in DMSO, concentrations ranging from 100 µM to 1.69 nM)) were added to a black polystyrene, flat-bottomed, small volume, clear bottomed 384-well microplate (Greiner Bio-One, part number 784076), with DMSO concentrations normalised to 1% (100 nL) in each well using a Hewlett-Packard D300 Digital Dispenser.

The so obtained plates were stored at -20 °C until use. A stock solution of Ldt_{Mt2} of 600 nM (2x final concentration 300 nM) was prepared in the assay buffer (50 mM sodium phosphate pH 7.5 with 0.007% (*v/v*) Tween-20). A stock solution of probe **1** of 30 µM (2x final concentration 15 µM) was prepared in the assay buffer. To the inhibitor plates was added 5 µL of the 2x Ldt_{Mt2} stock solution using a MultiDrop Combi dispenser (ThermoFisher Scientific). The resulting solution was incubated for 10 minutes at room temperature without shaking. 5 µL of the 2x probe **1** stock solution was then added using a MultiDrop Combi dispenser (ThermoFisher Scientific). The plate was incubated for another 10 minutes at room temperature. The fluorescence intensity was then measured 5 minute intervals for 50 minutes using an Envision 2104 Multilabel Reader (Perkin Elmer) with λ_{ex}=485 nm, λ_{em}=540 nm and a FITC mirror. The slope was calculated using linear regression analysis. The normalised response was calculated using the following formula: Normalized response = 100 * ((slope – slope control 2) / (slope control 1 – slope control 2)). The dose-response analysis was performed in Prism (GraphPad), using the log(inhibitor) versus normalized response− variable slope function.

References

1 de Munnik, M., Lohans, C. T., Langley, G. W., Bon, C., Brem, J. & Schofield, C. J. A Fluorescence-Based Assay for Screening β-Lactams Targeting the *Mycobacterium tuberculosis* Transpeptidase Ldt_{Mt2}. *ChemBioChem* **21**, 368-372 (2020).

2 Van Berkel, S. S., Brem, J., Rydzik, A. M., Salimraj, R., Cain, R., Verma, A., Owens, R. J., Fishwick, C. W. G., Spencer, J. & Schofield, C. J. Assay Platform for Clinically Relevant Metallo-β-lactamases. *J. Med. Chem.* **56**, 6945-6953 (2013).

3 de Munnik, M., Lohans, C. T., Lang, P. A., Langley, G. W., Malla, T. R., Tumber, A., Schofield, C. J. & Brem, J. Targeting the *Mycobacterium tuberculosis* transpeptidase Ldt_{Mt2} with cysteine-reactive inhibitors including ebselen. *Chem. Commun.* **55**, 10214-10217 (2019).

4 Schörgenhumer, J. & Waser, M. New strategies and applications using electrophilic cyanide-transfer reagents under transition metal-free conditions. *Org. Chem. Front.* **3**, 1535-1540 (2016).

5 Charpentier, J., Früh, N. & Togni, A. Electrophilic Trifluoromethylation by Use of Hypervalent Iodine Reagents. *Chem. Rev.* **115**, 650-682 (2015).

6 Sameshima, T., Miyahisa, I., Yamasaki, S., Gotou, M., Kobayashi, T. & Sakamoto, J. High-Throughput Quantitative Intrinsic Thiol Reactivity Evaluation Using a Fluorescence-Based Competitive Endpoint Assay. *Adv. Sci. Drug Disc.* **22**, 1168-1174 (2017).

Appendix II. Supplementary information for Chapter 4.

αβ,α′β′-Diepoxyketones are mechanism-based inhibitors of nucleophilic cysteine enzymes

Manuscript II

Reproduced from:

Mariska de Munnik, Jasper Lithgow, Lennart Brewitz, Kirsten E. Christensen, Robert H. Bates, Beatriz Rodriguez Miquel, and Christopher J. Schofield. αβ,α'β'-Diepoxyketones are mechanism-based inhibitors of nucleophilic cysteine enzymes. *Chem. Commun.* **59**, 12859-12862 (2023).

with permission from the Royal Society of Chemistry.

Experimental details

Materials

Recombinant Ldt_{Mt2} was produced in *Escherichia coli* and purified (>95% purity by SDS-PAGE analysis) as reported.[1] Recombinant SARS-CoV-2 M^{pro} was produced by Eidarus Salah and purified as reported.[2] Probe 1 (2-(6-(((2,4-dinitrophenyl)sulfonyl)oxy)-3-oxo-3H-xanthen-9-yl)benzoic acid) and FC-5 was synthesised as reported.[3,4] DEK **1** was initially obtained from the GSK compound collection in enantiopure form, and then synthesised as a single diastereomer as outlined below. Epoxide **12** was purchased from Enamine in diastereomerically pure from. All reagents for the preparation of **1** and **4** – **11** were from commercial sources (Sigma-Aldrich, Inc.; Fluorochem Ltd; Alfa Aesar; Manchester Organics) and were used as received. Purifications by column chromatography were performed using an automated Biotage® Selekt instrument (wavelengths monitored: 254 and 280 nm) equipped with pre-packed Biotage® Sfär Silica D chromatography cartridges. Thin layer chromatography (TLC) was carried out using Merck Silica gel 60 F254 TLC plates. Melting points (m.p.) were determined using a Stuart SMP-40 automated melting point apparatus. Infrared (IR) spectroscopy was performed using a Bruker Tensor-27 Fourier transform infrared (FT-IR) spectrometer. High-resolution mass spectrometry (HRMS) was performed using electro-spray ionization (ESI) mass spectrometry (MS) in the positive ionisation mode employing a Thermo Scientific Exactive mass spectrometer (ThermoFisher Scientific). Nuclear magnetic resonance (NMR) spectroscopy was performed using a Bruker AVANCE AVIIIHD 400 instrument.

Inhibition studies

Ldt_{Mt2} fluorogenic assays were performed as described.[3] Ldt_{Mt2} (100 nM) was incubated with varying concentrations of a potential inhibitor (400 µM – 20.3 nM) for 10 min in the assay buffer (50 mM HEPES, pH 7.2, 0.01% (*v*/*v*) Triton X-100) and then assayed using Probe 1 (25 µM).

SARS-CoV-2 M^{pro} inhibition assays were performed as described.[5] M^{pro} (150 nM) was incubated with varying concentrations of inhibitor (100 µM – 1.7 nM) for 15 min in assay buffer (20 mM HEPES, pH 7.5, 50 mM NaCl) and then assayed using a 37mer peptide as the substrate (ALNDFSNSGSDVLYQPPQTSITSAVLQSGFRKMAFPS-NH_2, 2 µM).

BlaC fluorogenic assays were performed as described.[4,6] BlaC (14 nM) was incubated with varying concentrations of inhibitor (400 µM – 20.3 nM) for 10 min in assay buffer (100 mM sodium phosphate pH 7.5, 0.01% (*v*/*v*) Triton X-100) and then assayed using FC5 (10 µM).

The 'intrinsic' thiol reactivity (k_{chem}) was determined as described.[6] *L*-Glutathione (500 nM) was incubated with varying concentrations of inhibitor (400 µM – 20.3 nM) and Probe 1 (10 µM) for 15 h in assay buffer (50 mM HEPES, pH 7.2, 0.01% (*v*/*v*) Triton X-100).

The second-order rate constant of covalent target inactivation (k_{inact}/K_I) was determined as described.[6] Ldt_{Mt2} (100 nM) was incubated with varying concentrations of inhibitor (400 µM – 20.3 nM) and Probe 1 (10 µM) for 3.5 h in assay buffer (50 mM HEPES, pH 7.2, 0.01% (*v*/*v*) Triton X-100).

Protein observed SPE-MS assays

Protein-observed SPE-MS experiments with Ldt_{Mt2} were performed as described.[6] Ldt_{Mt2} (1 µM) in 50 mM tris, pH 7.5 was incubated with an inhibitor (20 µM) at room temperature.

SARS-CoV-2 M^{pro} protein-observed SPE-MS experiments were performed as described.[2,5]

X-ray crystallography

Recombinant Ldt_{Mt2} (Δ1-55; with the N-terminal His_6-Tag removed, in 50 mM tris, pH 8.0, 100 mM NaCl) was crystallised using sitting drop vapor diffusion at 4 °C, according to a reported procedure.[6] The inhibitor was introduced to the crystals through soaking (1.5 mM, 24 h), after which time the crystals were cryocooled and stored in liquid nitrogen. Datasets were collected using the MX beamline I03 at the Diamond Light Source synchrotron (Harwell, United Kingdom). Structures were solved by molecular replacement using Phaser[7], using PDB entry 6RRM[8] as the search model. Alternating cycles of refinement using PHENIX[9] and manual model building using COOT[10] were performed until R_{work} and R_{Free} converged. Data collection and refinement statistics can be found in Table S2. Ligands were visualised by mF_o-DF_c polder OMIT map.[11]

Single crystal X-ray diffraction data were collected for **1** at 150 K using a (Rigaku) Oxford Diffraction SuperNova diffractometer and CrysAlisPro. The structure was solved using 'Superflip'[12] before refinement with CRYSTALS[13,14] as described in the SI (CIF). The crystallographic data have been deposited with the Cambridge Crystallographic Data Centre (CCDC 2262059), and copies of these data can be obtained free of charge from The Cambridge Crystallographic Data Centre via www.ccdc.cam.ac.uk/data_request/cif.

Preparation of recombinant BlaC protein

A codon-optimised synthetic gene (GeneArt, Thermo Fisher Scientific) encoding for BlaC Δ1-40 was amplified and cloned into the expression vector pCold using SalI-HF (New England

BioLabs) and Not1-HF (New England BioLabs) digestion and ligation using T4 DNA ligase (New England BioLabs) according to the manufacturer's protocol. The ampicillin resistance gene of the vector was exchanged for the kanamycin resistance gene using Gibson Assembly,[15] and transformed with *Escherichia coli* BL21(DE3). An overnight culture of *E. coli* BL21(DE3) pCold-BlaC Δ1-40 was grown at 37 °C at 180 rpm in 2xTY media (with 50 µg/mL kanamycin). This culture was used to inoculate fresh 2xTY media containing 50 µg/mL kanamycin (1% (*v/v*)), which was grown at 37 °C at 180 rpm to OD_{600} of 0.6. Then, 0.5 mM Isopropyl β-D-thiogalactopyranoside (IPTG) was added and the culture was incubated at 18 °C at 180 rpm for an additional 16 h. Cells were collected by centrifugation (11,000 x g, 8 min), and stored at -80 °C.

The cell pellet was resuspended in HisTrap Buffer A (25 mM Tris-HCl pH 8.0, 500 mM NaCl, 0.5 mM tris(2-carboxyethyl)phosphine) (TCEP), 5% (*v/v*) glycerol, 20 mM imidazole) in the presence of DNase I, and lysed using a Continuous Flow Cell Disruptor (Constant Systems, 20 kpsi). The lysates were centrifuged (32,000 x g, 20 min), passed through a 0.45 µm filter, and loaded onto a 5 mL HisTrap column (GE Life Sciences) that had been pre-equilibrated in HisTrap Buffer A. The column was washed with HisTrap Buffer A, followed by a gradient running from 0 % to 100 % (*v/v*) HisTrap Buffer B (25 mM Tris-HCl pH 8.0, 500 mM NaCl, 0.5 mM TCEP, 5% (*v/v*) glycerol, 250 mM imidazole). Fractions containing BlaC (as observed by SDS-PAGE) were combined, the buffer was exchanged to HisTrap Buffer A, and the HisTag was cleaved using recombinant 3C protease at 4 °C, over 12 h. The HisTag cleaved BlaC was passed through a 5 mL HisTrap column (GE Life Sciences) and washed with HisTrap Buffer A. The BlaC containing fractions (as observed by NanoDrop (Thermo Scientific) analysis) were concentrated and loaded onto a 300 mL Superdex 75 column (GE Life Sciences) pre-equilibrated in gel filtration buffer (25 mM Tris-HCl pH 8.0, 500 mM NaCl, 0.5 mM TCEP, 5% (*v/v*) glycerol). BlaC was eluted using the gel filtration buffer. Fractions containing BlaC (as observed by SDS-PAGE) were combined, concentrated, and frozen using liquid nitrogen. The identity and purity of BlaC was confirmed by mass spectrometry (calculated mass 28740 Da, observed deconvoluted mass 28740 Da) and SDS-PAGE (>95% purity).

Procedure for the synthesis of the diene precursors of 1 and 4-11 (General Procedure A)

A modified literature procedure was followed to prepare the αβ,α′β′-dienone precursors of **1** and **4**-**11**, i.e., **13**-**18**.[16] To a neat solution of lithium perchlorate ($LiClO_4$) (20 mmol, 2 equiv.), benzaldehyde (or a benzaldehyde derivative, as specified; 20 mmol, 2 equiv.), and the requisite ketone (10 mmol, 1 equiv.) was added triethylamine (Et_3N) (0.3 mL, 2 mmol, 0.1 equiv.). The mixture was stirred at room temperature (rt) and the reaction progress was

monitored by thin layer chromatography (TLC). Upon completion of the reaction, a saturated aqueous ammonium chloride (NH_4Cl) solution was added, and the resulting mixture was extracted with dichloromethane. The organic extracts were dried over anhydrous sodium sulfate (Na_2SO_4) and concentrated under reduced pressure. The crude mixture was purified by flash column chromatography.

Procedure for the synthesis of DEKs 1 and 4-11 (General Procedure B)

A modified literature procedure was followed to prepare αβ,α′β′-diepoxide ketones **1** and **4-11**.[17] To a stirred suspension of potassium fluoride supported on alumina ($KF\text{-}Al_2O_3$) (prepared as described[18]) in *tert*-butyl hydroperoxide (^{t}BuOOH; 5.0-6.0 M in decane, 3.8 mL, ~21 mmol) under N_2 was added a solution of the specified αβ,α′β′-dienone (2 mmol) in anhydrous acetonitrile (10 mL). The mixture was stirred at rt, and the reaction progress was monitored by TLC. Upon completion of the reaction, the mixture was filtered with a sintered funnel *in vacuo*. The filtrate was washed with brine and extracted with ethyl acetate. The combined organic extracts were dried over anhydrous Na_2SO_4 and concentrated *in vacuo*. The crude residue was purified by recrystallisation from ethanol to afford the *trans/trans*-αβ,α′β′-diepoxide ketone.

(1*E*,4*E*)-1,5-Bis(4-(trifluoromethoxy)phenyl)penta-1,4-dien-3-one (13)

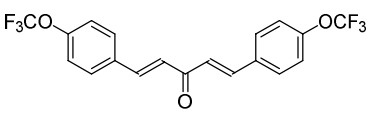

According to General Procedure A, diene **13** (2.37 g, 59%) was obtained from 4-(trifluoromethoxy)benzaldehyde (3.80 g, 20 mmol) and acetone (0.58 g, 10 mmol), following column chromatography [50 g Sfär Silica D; 120 mL/min, 100% cyclohexane (2 CV (column volumes)), followed by a linear gradient (12 CV): 0%→10% acetone in cyclohexane]. The analytical data for **13** were in agreement with those reported.[19]

Yellow solid, m.p.: 119-121 °C; ^{1}H NMR (400 MHz, 300 K, $CDCl_3$): δ = 7.73 (d, *J* = 15.9 Hz, 2H), 7.70 – 7.61 (m, 4H), 7.27 (d, *J* = 8.0 Hz, 4H), 7.06 ppm (d, *J* = 16.0 Hz, 2H); ^{13}C NMR (100 MHz, 300 K, $CDCl_3$): δ = 188.2, 150.6 (q, *J* = 1.9 Hz), 141.8, 133.2, 129.8, 126.0, 121.2, 120.3 ppm (q, *J* = 258.2 Hz); ^{19}F NMR (376 MHz, 300 K, $CDCl_3$): δ = -57.8 ppm (s, 6F); IR (film): $\tilde{\nu}$ = 1651, 1580, 1508, 1263, 1214, 1190, 1164, 1109 cm^{-1}; HRMS (ESI): *m/z* calculated for $C_{19}H_{13}O_3F_6$ $[M+H]^+$: 403.0763, found: 403.0760.

(1*E*,4*E*)-1,5-Bis(2-methoxyphenyl)penta-1,4-dien-3-one (14)

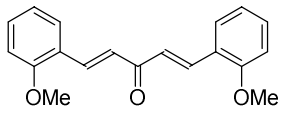

According to General Procedure A, diene **14** (2.29 g, 78%) was obtained from 2-methoxybenzaldehyde (2.72 g, 20 mmol) and acetone (0.58 g, 10 mmol), following column chromatography [50 g Sfär Silica D; 120 mL/min, 100% cyclohexane (2 CV), followed by a linear gradient (12 CV): 0%→20% acetone in cyclohexane]. The analytical data for **14** were in agreement with those reported.[20]

Yellow solid, m.p.: 125-128 °C; ^{1}H NMR (400 MHz, 300 K, $CDCl_3$): δ = 8.08 (d, *J* = 16.1 Hz, 2H), 7.62 (dd, *J* = 7.7, 1.6 Hz, 2H), 7.36 (ddd, *J* = 8.3, 7.4, 1.7 Hz, 2H), 7.18 (d, *J* = 16.1 Hz, 2H), 6.98 (t, *J* = 7.5 Hz, 2H), 6.92 (d, *J* = 7.9 Hz, 2H), 3.90 ppm (s, 6H); ^{13}C NMR (100 MHz, 300 K, $CDCl_3$): δ = 189.9, 158.5, 138.1, 131.5, 128.6, 126.1, 123.9, 120.6, 111.1, 55.4 ppm; IR (film): ṽ = 2838, 1666, 1647, 1612, 1598, 1573, 1487, 1464, 1437, 1336, 1296, 1274, 1246, 1184, 1163, 1106, 1049, 1026 cm^{-1}; HRMS (ESI): *m/z* calculated for $C_{19}H_{19}O_3$ $[M+H]^+$: 295.1329, found: 295.1330.

(1*E*,4*E*)-1,5-Bis(2-(trifluoromethoxy)phenyl)penta-1,4-dien-3-one (15)

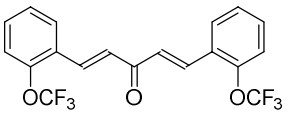

According to General Procedure A, diene **15** (2.53 g, 63%) was obtained from 2-(trifluoromethoxy)benzaldehyde (3.80 g, 20 mmol) and acetone (0.58 g, 10 mmol), following column chromatography [100 g Sfär Silica D; 120 mL/min, 100% cyclohexane (2 CV), followed by a linear gradient (12 CV): 0%→10% acetone in cyclohexane].

Yellow solid, m.p.: 75-78 °C; ^{1}H NMR (400 MHz, 300 K, $CDCl_3$): δ = 7.94 (d, *J* = 16.1 Hz, 2H), 7.74 (dd, *J* = 7.8, 1.7 Hz, 2H), 7.46 – 7.42 (m, 2H), 7.37 – 7.30 (m, 4H), 7.13 ppm (d, *J* = 16.1 Hz, 2H); ^{13}C NMR (100 MHz, 300 K, $CDCl_3$): δ = 188.5, 147.9, 136.3, 131.5, 128.4, 128.0, 127.8, 127.1, 121.3, 120.5 ppm (q, *J* = 258.6 Hz); ^{19}F NMR (376 MHz, 300 K, $CDCl_3$): δ = -57.3 ppm (s, 6F); IR (film) ṽ = 1660, 1623, 1603, 1487, 1457, 1334, 1248, 1210, 1170, 1098 cm^{-1}; HRMS (ESI): *m/z* calculated for $C_{19}H_{13}O_3F_6$ $[M+H]^+$: 403.0763, found: 403.0754.

(1*E*,4*E*)-1,5-Bis(3,5-dimethylphenyl)penta-1,4-dien-3-oneone (16)

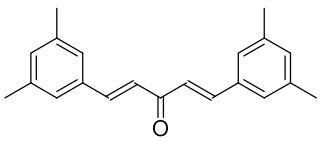

According to General Procedure A, diene **16** (0.64 g, 22%) was obtained from 3,5-dimethylbenzaldehyde (2.68 g, 20 mmol) and acetone (0.58 g, 10 mmol), following column chromatography [25 g Sfär Silica D; 80 mL/min, 100% cyclohexane (2 CV), followed by a linear gradient (12 CV): 0%→15% acetone in cyclohexane].

Yellow solid, m.p.: 109-111 °C; ^{1}H NMR (400 MHz, 300 K, $CDCl_3$): δ = 7.71 (d, *J* = 15.9 Hz, 2H), 7.27 – 7.25 (m, 4H), 7.13 – 7.05 (m, 4H), 2.38 ppm (s, 12H); ^{13}C NMR (100 MHz, 300 K, $CDCl_3$): δ = 188.9, 143.3, 138.3, 134.7, 132.2, 126.2, 125.1, 21.1 ppm; IR (film): ṽ = 2980, 2918, 1652, 1620, 1604, 1439, 1341, 1287, 1255, 1188, 1161, 1105 cm^{-1}; HRMS (ESI): *m/z* calculated for $C_{21}H_{23}O$ $[M+H]^+$: 291.1743, found: 291.1743.

(1*E*,4*E*)-1,5-Bis(2,6-dimethylphenyl)penta-1,4-dien-3-oneone (17)

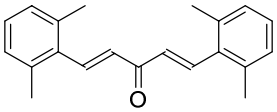

According to General Procedure A, diene **17** (0.20 g, 7%) was obtained from 2,6-dimethylbenzaldehyde (2.68 g, 20 mmol), and acetone (0.58 g, 10 mmol), following recrystallisation from *n*-pentane.

Yellow solid, m.p.: 150-153 °C; ^{1}H NMR (400 MHz, 300 K, $CDCl_3$): δ = 7.92 (d, *J* = 16.3 Hz, 2H), 7.19 – 7.09 (m, 6H), 6.74 (d, *J* = 16.3 Hz, 2H), 2.43 ppm (s, 12H); ^{13}C NMR (100 MHz, 300 K, $CDCl_3$): δ = 189.0, 142.1, 136.8, 134.4, 131.1, 128.4, 128.3, 21.1 ppm; IR (film): ṽ = 2981, 1650, 1625, 1591, 1467, 1446, 1382, 1355, 1291, 1192, 1165, 1004 cm^{-1}; HRMS (ESI): *m/z* calculated for $C_{21}H_{23}O$ $[M+H]^+$: 291.1743, found: 291.1743.

2,7-Di((*E*)-benzylidene)cycloheptan-1-one (18)

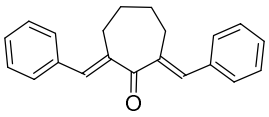

According to General Procedure A, diene **18** (0.78 g, 27%) was obtained from benzaldehyde (2.12 g, 20 mmol) and cycloheptanone (1.12 g, 10 mmol) following column chromatography [25 g Sfär Silica D; 80 mL/min, 100% cyclohexane (2 CV), followed by a linear gradient (12 CV): 0%→10% acetone in cyclohexane]. The analytical data for **18** were in agreement with those reported.[21,22]

Yellow solid, m.p.: 104-108 °C; ^{1}H NMR (400 MHz, 300 K, $CDCl_3$): δ = 7.53 – 7.33 (m, 12H), 2.78 – 2.70 (m, 4H), 2.04 – 1.99 ppm (m, 4H); ^{13}C NMR (100 MHz, 300 K, $CDCl_3$): δ = 199.4, 141.7, 135.9, 135.6, 129.4, 128.4, 128.1, 28.8, 28.0 ppm; IR (film): ṽ = 2927, 1667, 1623, 1604, 1492, 1455, 1446, 1306, 1291, 1228, 1190, 1144, 1021 cm^{-1}; HRMS (ESI): *m/z* calculated for $C_{21}H_{21}O$ $[M+H]^+$: 289.1587, found: 289.1586.

(*trans*-3-Phenyloxiran-2-yl)(*trans*-3-phenyloxiran-2-yl)methanone (1)

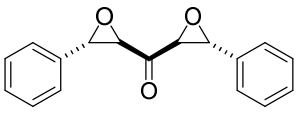

According to General Procedure B, DEK **1** (180 mg, 35%) was obtained as a single *trans*,*trans*-diastereomer from (1*E*,4*E*)-1,5-diphenylpenta-1,4-dien-3-one[16] (0.47 g, 2 mmol) following recrystallisation from ethanol. The stereochemistry of **1** was assigned as *trans*,*trans* by X-ray diffraction analysis of a single crystal obtained after recrystallisation (Table S4; CCDC

2262059). Note that the analysis of the crude reaction mixture using ^{1}H NMR analysis indicated that two diastereomers are formed during the reaction, one of which was assigned as the *trans*,*trans*-diastereomer; the other diastereomer formed is likely the *cis*,*cis*-diastereomer (*cis*,*trans*-diastereomeric mixtures should manifest in an additional set of signals for the epoxide protons and were not detected using ^{1}H NMR analysis). Note that both the *trans*,*trans*-diastereomer and the *cis*,*cis*-diastereomer are *meso*-compounds. The analytical data for **1** were in agreement with those reported.[23]

White crystals, m.p.: 119-120 °C. ^{1}H NMR (400 MHz, 300 K, $CDCl_3$): δ = 7.40 – 7.37 (m, 6H), 7.32 – 7.29 (m, 4H), 4.10 (d, *J* = 1.8 Hz, 2H), 3.81 ppm (d, *J* = 1.8 Hz, 2H); ^{13}C NMR (100 MHz, 300 K, $CDCl_3$): δ = 199.2, 134.6, 129.3, 128.8, 125.8, 60.9, 59.0 ppm; IR (film): ṽ = 3062, 1721, 1458, 1428, 1410, 1117, 1084 cm^{-1}; HRMS (ESI): *m/z* calculated for $C_{17}H_{15}O_3$ $[M+H]^+$: 267.1016, found: 267.1015.

Purification of the mother liquor obtained after recrystallization using column chromatography (10 g Sfär Silica D; 40 mL/min, 100% cyclohexane (2 CV), followed by a linear gradient (12 CV): 0%→20% ethyl acetate in cyclohexane) afforded a 3:1 mixture of *cis*,*cis*:*trans*,*trans*-**1** (37 mg, 7%) as an orange oil. Note that *cis*,*cis*-enriched **1** appears to be an oil and not a solid like *trans*,*trans* **1**; as yet *cis*,*cis*-enriched **1** has not been further purified by recrystallisation or trituration. By implication, subsequently acquired diastereomerically pure αβ,α′β′-diepoxides obtained by crystallisation were *tentatively* assigned as the *trans*,*trans*-diastereomers if they were obtained as pure solids. ^{1}H and ^{13}C NMR signals observed for *cis*,*cis*-enriched **1**: ^{1}H NMR (400 MHz, 300 K, $CDCl_3$): δ = 4.20 (d, *J* = 1.7 Hz, 2H), 3.74 ppm (d, *J* = 1.7 Hz, 2H); ^{13}C NMR(100 MHz, 300 K, $CDCl_3$): δ = 199.2, 134.5, 129.2, 128.7, 125.8, 60.3, 58.8 ppm.

(*trans*-3-(4-(Trifluoromethoxy)phenyl)oxiran-2-yl)(*trans*-3-(4-(trifluoromethoxy)phenyl)oxiran-2-yl)methanone (4)

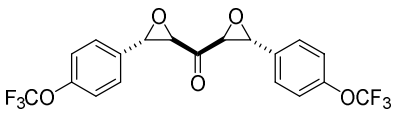

According to General Procedure B, DEK **4** (95 mg, 11%) was obtained as a single diastereomer from diene **13** (0.81 g, 2 mmol) following recrystallisation from ethanol. DEK **4** was *tentatively* assigned as the *trans*,*trans*-diastereomer, in part because it was obtained as a solid after recrystallization; *trans*,*trans*-**1** was a solid and its stereochemistry was assigned by crystallographic analysis, whereas *cis*,*cis*-**1b** manifested as an oil.

White crystals, m.p.: 95-97 °C; ^{1}H NMR (400 MHz, 300 K, $CDCl_3$): δ = 7.38 – 7.34 (m, 4H), 7.28 – 7.25 (m, 4H), 4.16 (d, *J* = 1.8 Hz, 2H), 3.79 ppm (d, *J* = 1.8 Hz, 2H); ^{13}C NMR (100 MHz, 300 K, $CDCl_3$): δ = 198.4, 149.9 (q, *J* = 1.9 Hz), 133.2, 127.3, 121.4, 120.6 (q, *J* = 257.8 Hz), 60.9, 58.1 ppm; ^{19}F NMR (376 MHz, 300 K, $CDCl_3$): δ = -57.9 ppm (s, 6F); IR (film): ṽ =

1718, 1514, 1260, 1210, 1162 cm^{-1}; HRMS (ESI): *m/z* calculated for $C_{19}H_{12}O_5F_6Na$ $[M+Na]^+$: 457.0481, found: 457.0481.

(3-(2-Methoxyphenyl)oxiran-2-yl)(3-(2-methoxyphenyl)oxiran-2-yl)methanone (5)

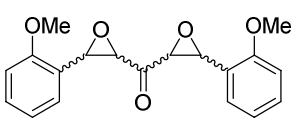

According to General Procedure B, DEK **5** (189 mg, 29%) was obtained from diene **14** (0.59 g, 2 mmol) as a 2:1 mixture of diastereomers (likely the *trans*,*trans*- and *cis*,*cis*-diastereomers) following column chromatography (10 g Sfär Silica D; 40 mL/min, 100% cyclohexane (2 CV), followed by a linear gradient (12 CV): 0%→20% ethyl acetate in cyclohexane).

Analytical data for the ~2:1 mixture of diastereomers: ^{1}H NMR (400 MHz, 300 K, $CDCl_3$): δ = 7.36 – 7.31 (m, 6H), 7.23 – 7.18 (m, 6H), 7.00 – 6.91 (m, 12H), 4.51 (d, *J* = 1.8 Hz, 2H), 4.48 (d, *J* = 1.9 Hz, 4H), 3.90 (s, 12H), 3.88 (s, 6H), 3.74 (d, *J* = 1.8 Hz, 4H), 3.67 ppm (d, *J* = 1.8 Hz, 2H); ^{13}C NMR (100 MHz, 300 K, $CDCl_3$): δ = 200.1, 200.0, 158.3, 158.0, 129.8(4), 129.8, 125.3, 125.2, 123.6, 123.2, 120.8, 120.6, 110.4, 110.2, 60.3, 59.8, 55.4, 55.3(2), 55.3, 55.0 ppm; HRMS (ESI): *m/z* calculated for $C_{19}H_{19}O_5$ $[M+H]^+$: 327.1227, found: 327.1227.

(*trans*-3-(2-(Trifluoromethoxy)phenyl)oxiran-2-yl)(*trans*-3-(2-(trifluoromethoxy)phenyl)oxiran-2-yl)methanone (6)

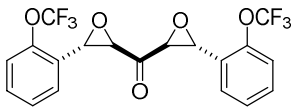

According to General Procedure B, DEK **6** (191 mg, 22%) was obtained as a single diastereomer from diene **15** (0.81 g, 2 mmol) following recrystallisation from ethanol. DEK **6** was *tentatively* assigned as the *trans*,*trans*-diastereomer, in part because it was obtained as a solid after recrystallization (as described above).

White crystals, m.p.: 136-139 °C. ^{1}H NMR (400 MHz, 300 K, $CDCl_3$): δ = 7.43 – 7.27 (m, 8H), 4.40 (d, *J* = 1.8 Hz, 2H), 3.71 ppm (d, *J* = 1.8 Hz, 2H); ^{13}C NMR (100 MHz, 300 K, $CDCl_3$): δ = 198.0, 147.8, 130.2, 128.0, 127.5, 125.8, 121.1, 120.5 (q, *J* = 257.6 Hz), 60.1, 54.0 ppm; ^{19}F NMR (376 MHz, 300 K, $CDCl_3$): δ = -57.9 ppm (s, 6F); IR (film): $\tilde{\nu}$ = 1720, 1274, 1252, 1207, 1183, 1165, 1100, 1077 cm^{-1}; HRMS (ESI): *m/z* calculated for $C_{19}H_{12}O_5F_6Na$ $[M+Na]^+$: 457.0481, found: 457.0479.

(*trans*-3-(3,5-Dimethylphenyl)oxiran-2-yl)(*trans*-3-(3,5-dimethylphenyl)oxiran-2-yl)methanone (7)

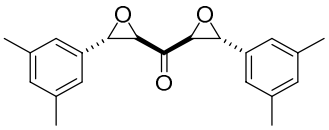

According to General Procedure B, DEK **7** (100 mg, 16%) was obtained as a single diastereomer from diene **16** (0.59 g, 2 mmol) following recrystallisation from ethanol. DEK **7** was *tentatively* assigned as the *trans*,*trans*-diastereomer, in part because it was obtained as a solid after recrystallization (as described above).

White crystals, m.p.: 124-128 °C. ^{1}H NMR (400 MHz, 300 K, $CDCl_3$): δ = 6.99 (s, 2H), 6.92 (s, 4H), 4.09 (d, *J* = 1.7 Hz, 2H), 3.69 (d, *J* = 1.7 Hz, 2H), 2.32 ppm (s, 12H); ^{13}C NMR (100 MHz, 300 K, $CDCl_3$): δ = 199.5, 138.5, 134.4, 130.9, 123.5, 60.2, 58.9, 21.2 ppm; IR (film): ṽ = 2920, 1716, 1609, 1470, 1408, 1225, 1189, 1071, 1038 cm^{-1}; HRMS (ESI): *m/z* calculated for $C_{21}H_{22}O_3Na$ $[M+Na]^+$: 345.1461, found: 345.1463.

(3-(2,6-Dimethylphenyl)oxiran-2-yl)(3-(2,6-dimethylphenyl)oxiran-2-yl)methanone (8)

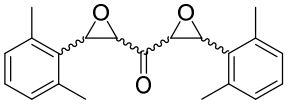

According to General Procedure B, DEK **8** (38 mg, 24%) was obtained from diene **17** (145 mg, 0.5 mmol) as a 1.2:1 mixture of diastereomers (likely the *trans*,*trans*- and *cis*,*cis*-diastereomers) following column chromatography (5 g Sfär Silica D; 18 mL/min, 100% cyclohexane (2 CV), followed by a linear gradient (12 CV): 0%→10% ethyl acetate in cyclohexane).

Analytical data of the ~1.2:1 mixture of diastereomers: ^{1}H NMR (400 MHz, 300 K, $CDCl_3$): δ = 7.17 (t, *J* = 7.6 Hz, 4H), 7.03 (d, *J* = 7.6 Hz, 8H), 4.32 (d, *J* = 2.0 Hz, 2H), 4.24 (d, *J* = 1.9 Hz, 2H), 3.78 (d, *J* = 2.1 Hz, 2H), 3.68 (d, *J* = 2.0 Hz, 2H), 2.43 (s, 12H), 2.42 ppm (s, 12H); ^{13}C NMR (100 MHz, 300 K, $CDCl_3$): δ = 201.9, 201.8(5), 137.2, 136.9, 131.5, 131.4(7), 128.5, 128.3, 128.2, 58.6, 58.3, 57.9, 57.8(6), 19.9, 19.7 ppm; HRMS (ESI): *m/z* calculated for $C_{21}H_{23}O_3$ $[M+H]^+$: 323.1642, found: 323.1642.

(*trans*)-2,7-Diphenyl-1,6-dioxadispiro[2.1.2^5.2^3]nonan-4-one (9)

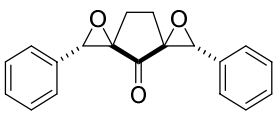

According to General Procedure B, DEK **9** (300 mg, 52%) was obtained as a single diastereomer from 2,5-di((*E*)benzylidene)-cyclopentan-1-one[16] (0.52 g, 2 mmol) without further purification. DEK **9** was *tentatively* assigned as the *trans*,*trans*-diastereomer, in part because it was obtained as a solid.

White solid, m.p.: 115-118 °C. ^{1}H NMR (400 MHz, 300 K, $CDCl_3$): δ = 7.35 – 7.27 (m, 6H), 7.21 – 7.18 (m, 4H), 4.34 (s, 2H), 1.97 – 1.87 (m, 2H), 1.79 – 1.70 ppm (m, 2H); ^{13}C NMR (100 MHz, 300 K, $CDCl_3$): δ = 208.6, 133.4, 128.8, 128.5, 126.6, 66.1, 65.2, 19.9 ppm; IR (film): ṽ = 1762, 1410 cm^{-1}; HRMS (ESI): *m/z* calculated for $C_{19}H_{16}O_3Na$ [M+Na]$^{+}$: 315.0992, found: 315.0991.

(*trans*)-2,7-Diphenyl-1,6-dioxadispiro[2.1.2^5.2^3]decan-4-one (10)

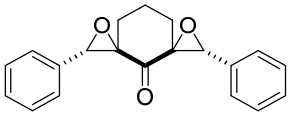

According to General Procedure B, DEK **10** (270 mg, 44%) was obtained as a single diastereomer from 2,6-di((*E*)-benzylidene)-cyclohexan-1-one[16] (0.55 g, 2 mmol) without further purification. DEK **10** was *tentatively* assigned as the *trans*,*trans*-diastereomer, in part because it was obtained as a solid.

White solid, m.p.: >230 °C (decomposition). ^{1}H NMR (400 MHz, 300 K, $CDCl_3$): δ = 7.44 – 7.30 (m, 10H), 4.15 (s, 2H), 2.15 – 2.07 (m, 2H), 1.65 – 1.58 (m, 3H), 1.25 – 1.11 ppm (m, 1H); ^{13}C NMR (100 MHz, 300 K, $CDCl_3$): δ = 203.1, 133.1, 128.6, 128.5, 126.6, 66.1, 65.5, 26.0, 19.4 ppm; IR (film): ṽ = 1716, 1453, 1407 cm^{-1}; HRMS (ESI): *m/z* calculated for $C_{20}H_{18}O_3Na$ [M+Na]$^{+}$: 329.1148, found: 329.1148.

(*trans*)-2,7-Diphenyl-1,6-dioxadispiro[2.1.2^5.2^3]undecan-4-one (11)

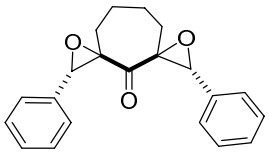

According to General Procedure B, DEK **11** (260 mg, 41%) was obtained as a single diastereomer from diene **18** (0.58 g, 2 mmol) without further purification. DEK **11** was *tentatively* assigned as the *trans*,*trans*-diastereomer, in part because it was obtained as a solid.

White solid, m.p.: 147-150 °C. ^{1}H NMR (400 MHz, 300 K, $CDCl_3$): δ = 7.40 – 7.32 (m, 10H), 4.23 (s, 2H), 1.90 – 1.79 (m, 4H), 1.49 – 1.46 (m, 2H), 1.35 – 1.31 ppm (m, 2H); ^{13}C NMR (100 MHz, 300 K, $CDCl_3$): δ = 203.6, 133.6, 128.4, 128.3, 126.6, 67.7, 63.9, 26.9, 24.4 ppm; IR (film): ṽ = 1718, 1454 cm^{-1}; HRMS (ESI): *m/z* calculated for $C_{21}H_{20}O_3Na$ [M+Na]$^{+}$: 343.1305, found: 345.1306.

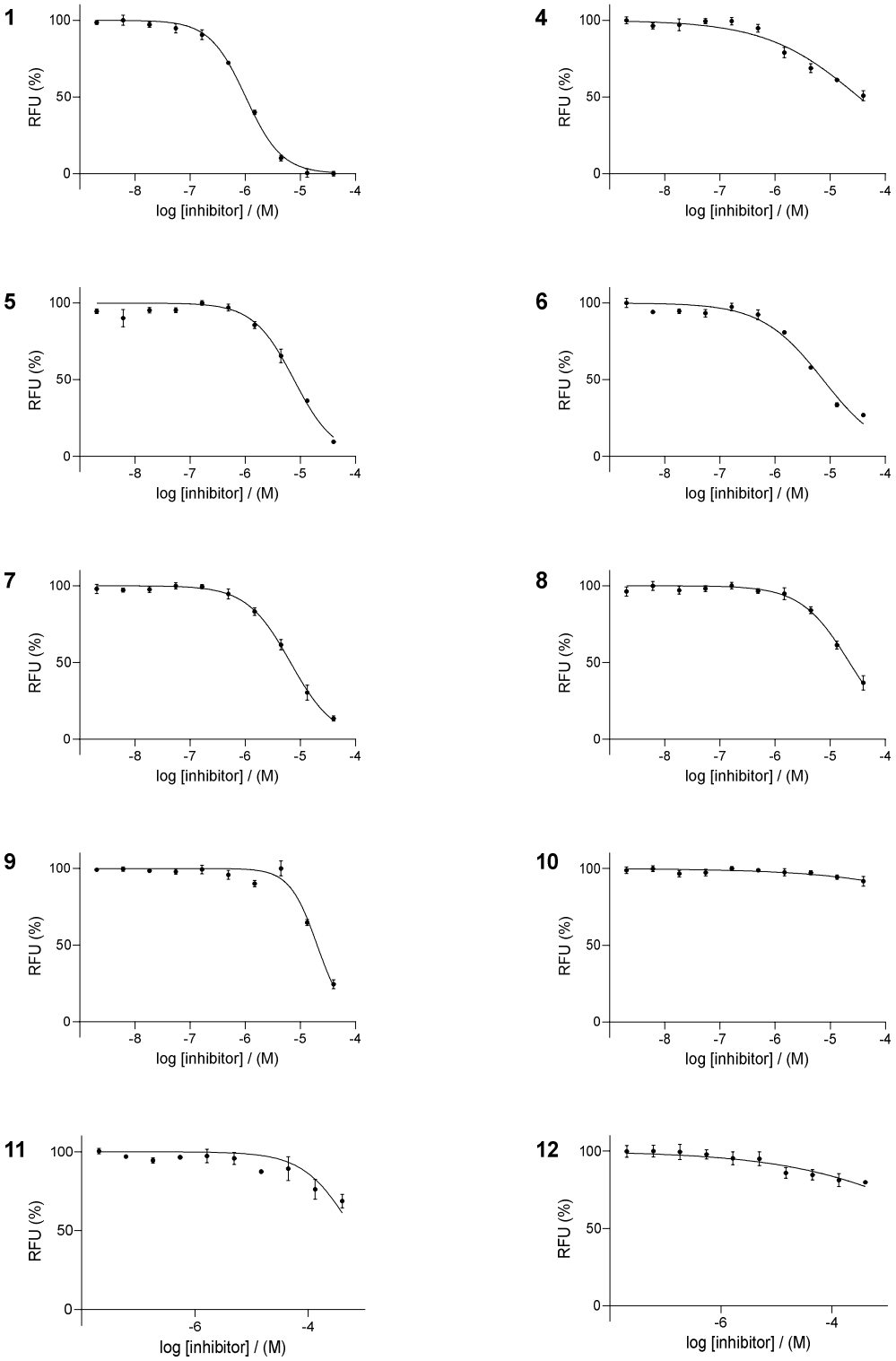

Figure S2.1. Dose-response curves for the DEKs 1 and 4-11 and mono-epoxide ketone 12 with Ldt_{Mt2}. Inhibition assays were carried out using 100 nM Ldt_{Mt2} and 25 µM Probe **1** with 10 min pre-incubation at room temperature in 50 mM HEPES, pH 7.2 with 0.01% (*v/v*) Triton X-100. Error bars represent standard deviation (n=4). Average pIC_{50} values and compound structures are given in Table S2.3.

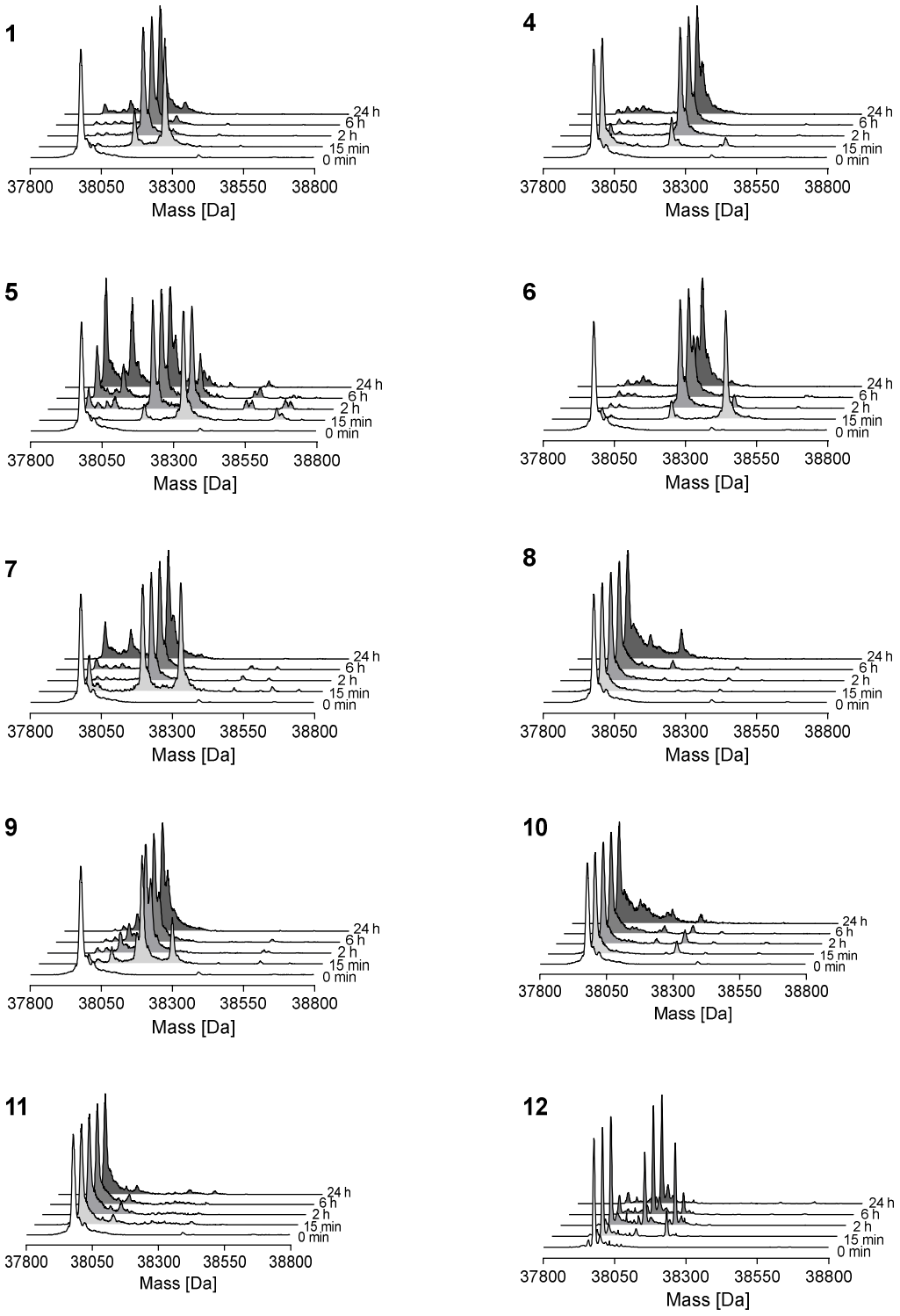

Figure S2.2. Protein observed SPE-MS analysis for the reaction of Ldt_{Mt2} with DEKs 1 and 4-11 and mono-epoxide ketone 12. 1 µM Ldt_{Mt2} was incubated with the inhibitors (20 µM for 1 and 4 – 11, 100 µM for 12) at rt in 50 mM Tris, pH 7.5. Samples were analysed after the indicated times. Deconvoluted spectra, obtained using the maximum entropy algorithm in the MassHunter Workstation Qualitative Analysis B.07.00 program (Agilent), are shown. Mass shifts and assignments are given in Table S2.1.

Table S2.1. Calculated and observed masses (Da) and mass shifts (Da) for protein-observed SPE-MS experiments with Ldt_{Mt2} and inhibitors 1 and 4-12, and their assignments. Mass shifts are relative to unmodified Ldt_{Mt2}. The observed mass of the most abundant adduct at 24h is in blue. *Calculated mass for the fragmented adduct **3** (as shown in Figure 4.2). **Calculated mass for the unfragmented adduct **2** (as shown in Figure 4.2). Deconvoluted SPE-MS spectra are shown in Figure S2.2.

Compound	Calculated mass (Da)	Observed mass (Da)	Area (%) 15 min	Area (%) 24 h	Assignment
1	39139 (+161)* 38245 (+267)**	37944 (-34)	0.0	5.0	Dha
		37978 (+0)	2.0	0.0	Unmodified
		38034 (+56)	0.0	5.9	Unassigned fragment[1]
		38138 (+160)	23.3	82.0	Retro-aldol fragment (**3**)
		38245 (+267)	74.7	7.2	Unfragmented (**2**)
4	38223 (+245)* 38413 (+435)**	37944 (-34)	0.0	2.4	Dha
		37978 (+0)	76.5	0.0	Unmodified
		38221 (+244)	18.1	97.6	Retro-aldol fragment (**3**)
		38412 (+434)	5.41	0.0	Unfragmented (**2**)
5	38169 (+191)* 38305 (+327)**	37944 (-34)	0.0	30.4	Dha
		37978 (+0)	2.5	0.0	Unmodified
		38035 (+57)	0.0	25.8	Unassigned fragment[1]
		38169 (+191)	9.0	39.6	Retro-aldol fragment (**3**)
		38287 (+309)	0.0	4.22	N.D.
		38306 (+328)	77.9	0.0	Unfragmented (**2**)
6	38223 (+245)* 38413 (+435)**	37978 (+0)	7.2	2.6	Unmodified
		38032 (+56 Da)	0.0	4.2	Fragment II[1]
		38221 (+243)	11.6	93.2	Retro-aldol fragment (**3**)
		38413 (+435)	81.2	0.0	Unfragmented (**2**)
7	38167 (+189)* 38210 (+232)**	37944 (-34)	0.0	16.2	Dha
		37978 (+0)	11.5	0.0	Unmodified
		38034 (+56)	0.0	13.5	Unassigned fragment[1]
		38166 (+188)	43.7	70.3	Retro-aldol fragment (**3**)
		38301 (+232)	44.8	0.0	Unfragmented (**2**)
8	38167 (+189)* 38210 (+232)**	37978 (+0)	100.0	68.8	Unmodified
		38058 (+80)	0.0	14.9	N.D.
		38166 (+188)	0.0	16.3	Retro-aldol fragment (**3**)
9	38165 (+187)* 38271 (+293)**	37978 (+0)	3.3	0.0	Unmodified
		38058 (+80)	6.9	9.1	N.D.
		38163 (+185)[2]	68.8	90.9	Retro-aldol fragment (**3**)
		38271 (+293)	21.0	0.0	Unfragmented (**2**)
10	38179 (+201)* 38285 (+307)**	37978 (+0)	100.0	90.2	Unmodified
		38285 (+307)	0.0	9.8	Unfragmented (**2**)
11	38193 (+215)* 38299 (+321)**	37978 (+0)	100.0	100.0	Unmodified
12	38097 (+119)* 38202 (+224)**	37978 (+0)	91.4%	12.8%	Unmodified
		38097 (+119)	0.0%	87.2%	Retro-aldol fragment (**3**)
		38202 (+224)	8.6%	0.0%	Unfragmented (**2**)

[1] See Figure S2.6 for possible structures of the unassigned fragment.
[2] The 38163 (+185) Da adduct was observed to shift to a mass of 38146 (+168) Da over the course of 24h, suggesting further fragmentation.

Table S2.2. Data collection and refinement statistics for the crystal structure of Ldt_{Mt2} reacted with 1.

Datasets	**Ldt_{Mt2} – 1 (PDB: 8BK3)**
Data Collection	
Beamline (Wavelength, Å)	DLS I03 (0.9763)
Detector	Eiger2 XE 16M
Data Processing	Xia2 dials
Space group	*P* 1 2_1 1
Cell dimensions	
a,b,c (Å)	60.93, 95.06, 75.53
α, β, γ (°)	90.00, 92.60, 90.00
No. of molecules/ASU	2
No. reflections	46835 (4654)*
Resolution (Å)	75.46-2.15 (2.23-2.15)*
R_{merge} (I)	0.167 (1.351)*
I/σI	10.2 (1.1)*
CC-1/2	0.97 (0.7)*
Completeness (%)	100.0 (99.5)*
Multiplicity	7.0 (7.0)*
Wilson B value ($Å^2$)	28.02
Refinement	PHENIX
R_{work}/R_{free}	0.2176/0.2487
No. atoms	6129
- Enzyme	5340
- Ligand	46
- Water	743
Average B-factors	36.62
- Enzyme	36.27
- Ligand	40.92
- Water	38.86
RMS[$] deviations	
- Bond lengths (Å)	0.005
- Bond angles (°)	0.58

[#] ASU = asymmetric unit.

[$] RMS = root mean square.

*Highest resolution shell in parentheses.

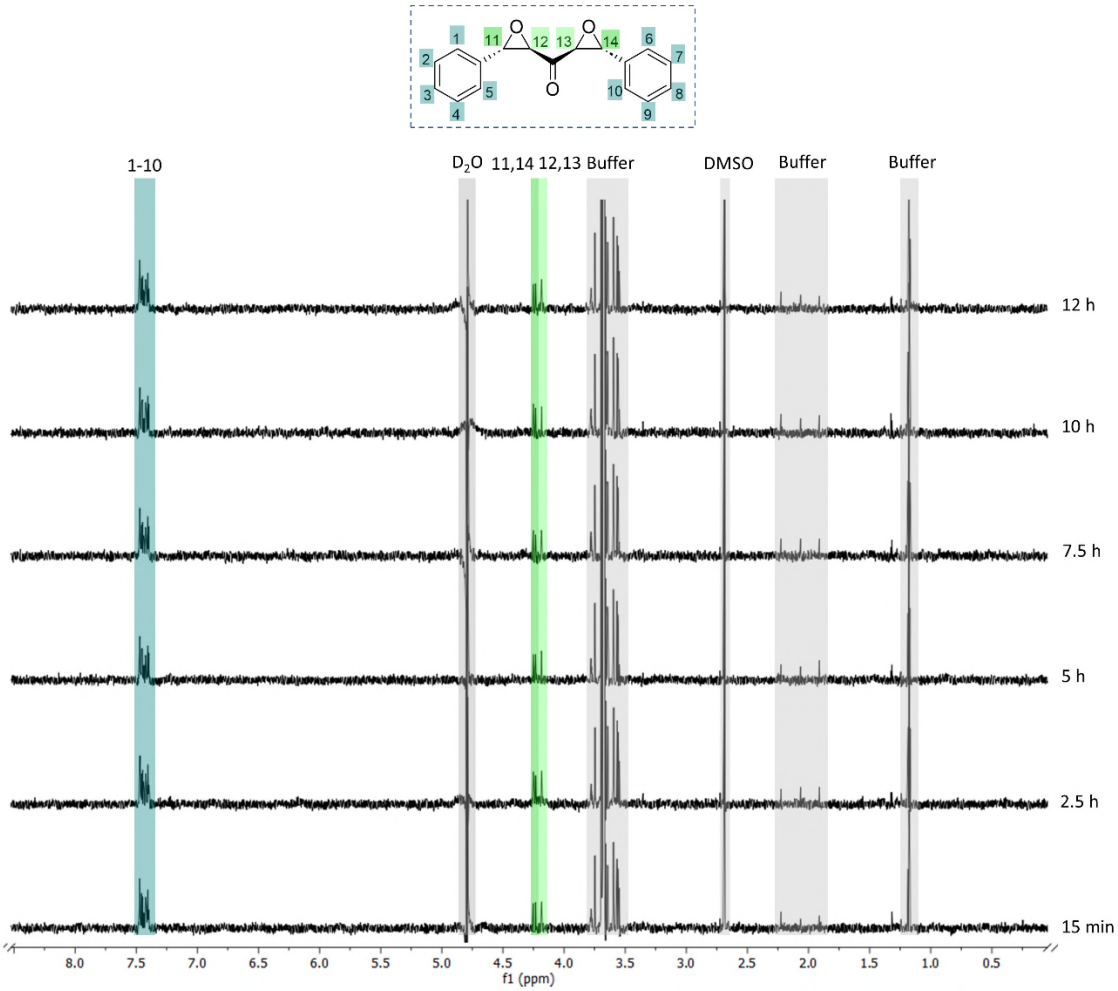

Figure S2.3. Stability of DEK 1 in aqueous solution. A solution of DEK **1** (250 µM) in 50 mM tris-d11, pH 7.5, 10% D_2O, was analysed by ^{1}H-NMR (950 MHz) for up to 12 h. No changes in peaks corresponding to **1** (in blue and green) in spectra were observed. Buffer and solvent peaks are in grey.

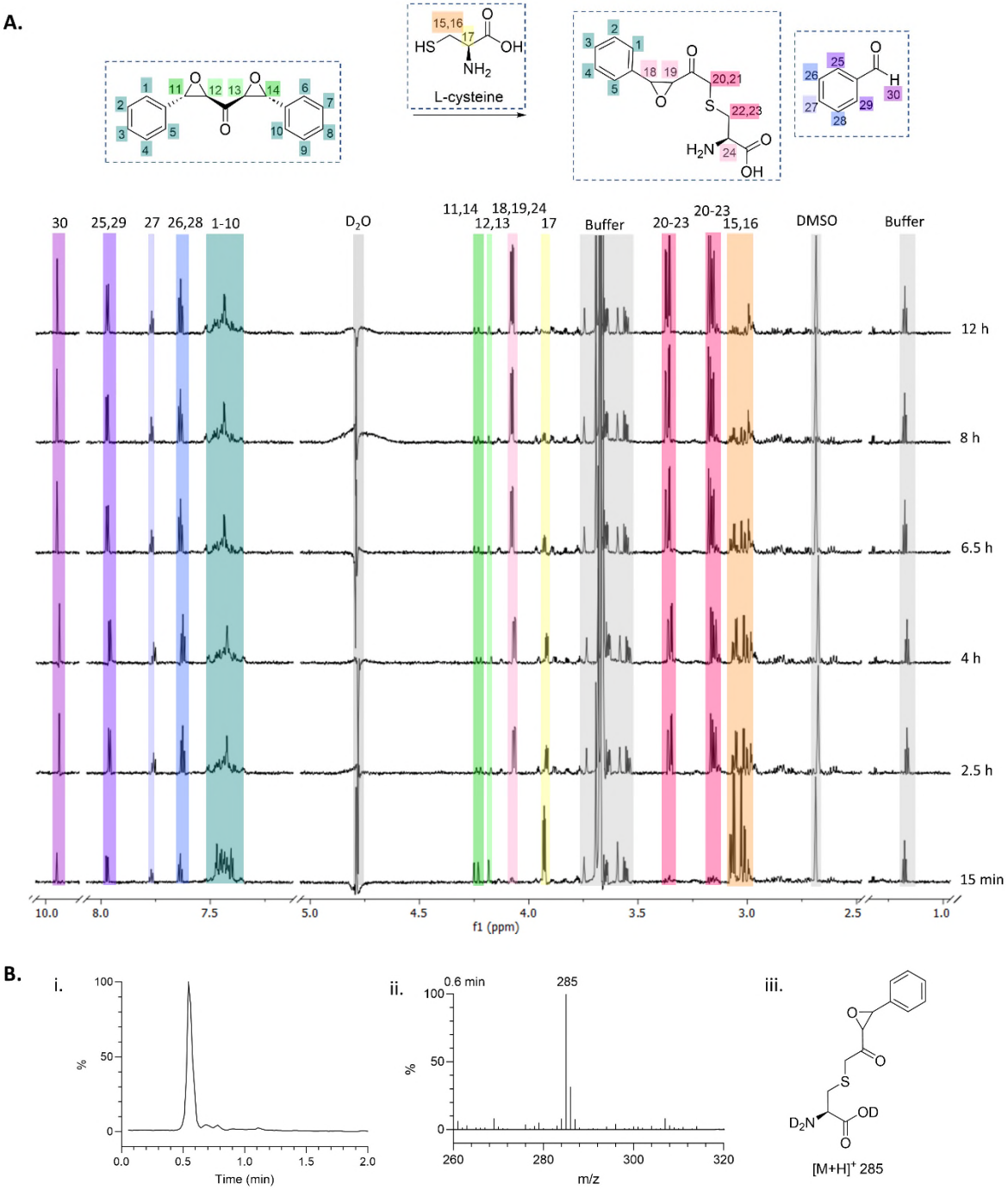

Figure S2.4. Reactivity of 1 with L-cysteine. A solution of **1** (250 µM) was incubated with L-cysteine (250 µM) in 50 mM tris-d11, pH 7.5, 10% D_2O. **A.** The reaction was analysed by ^{1}H-NMR (950 MHz) for up to 12 h. **B.** The reaction was analysed by LCMS, 16 h after initiation of the reaction.

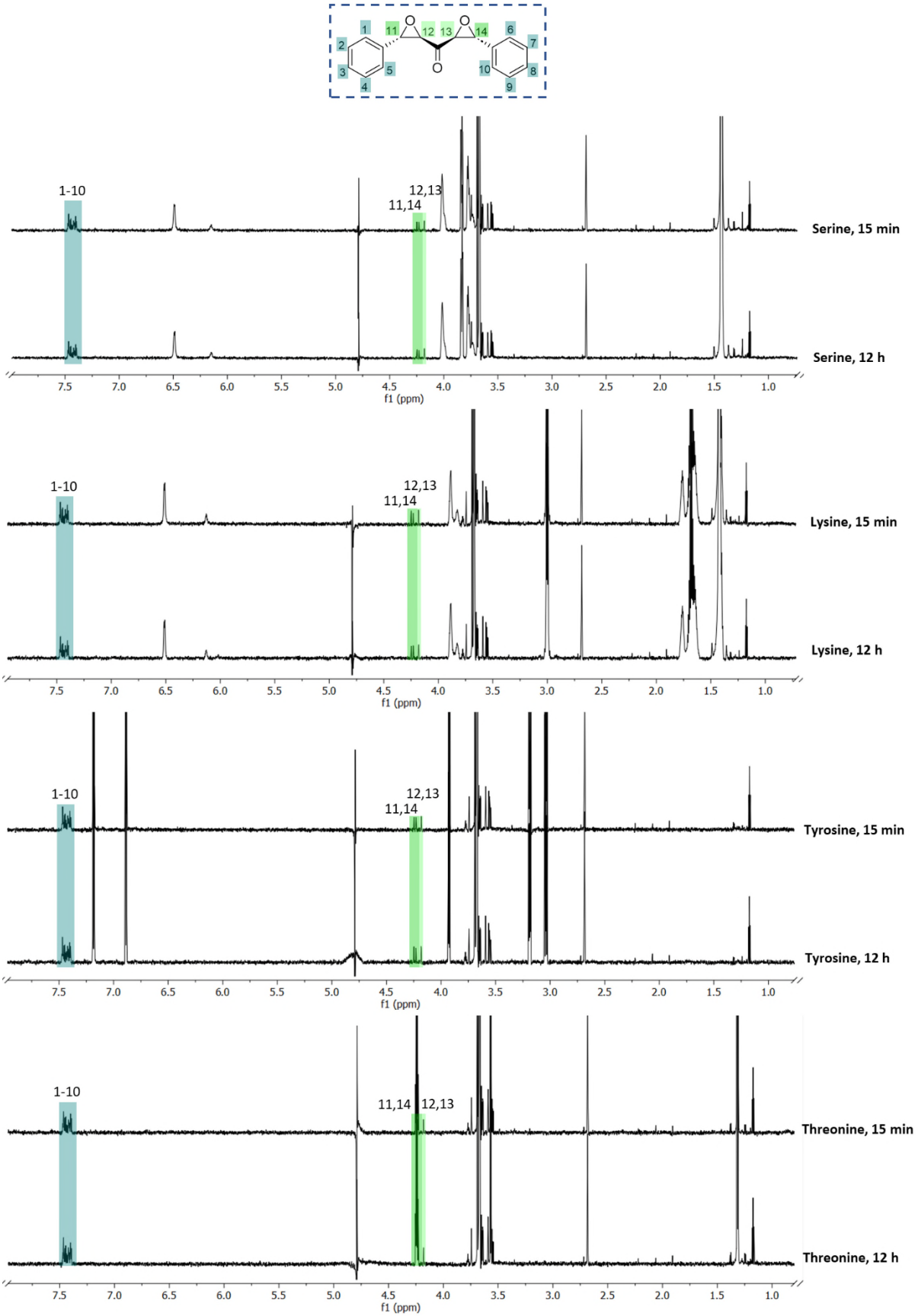

Figure S2.5. Reactivity of 1 with serine, lysine, tyrosine, threonine, arginine, and histidine. [Continues]

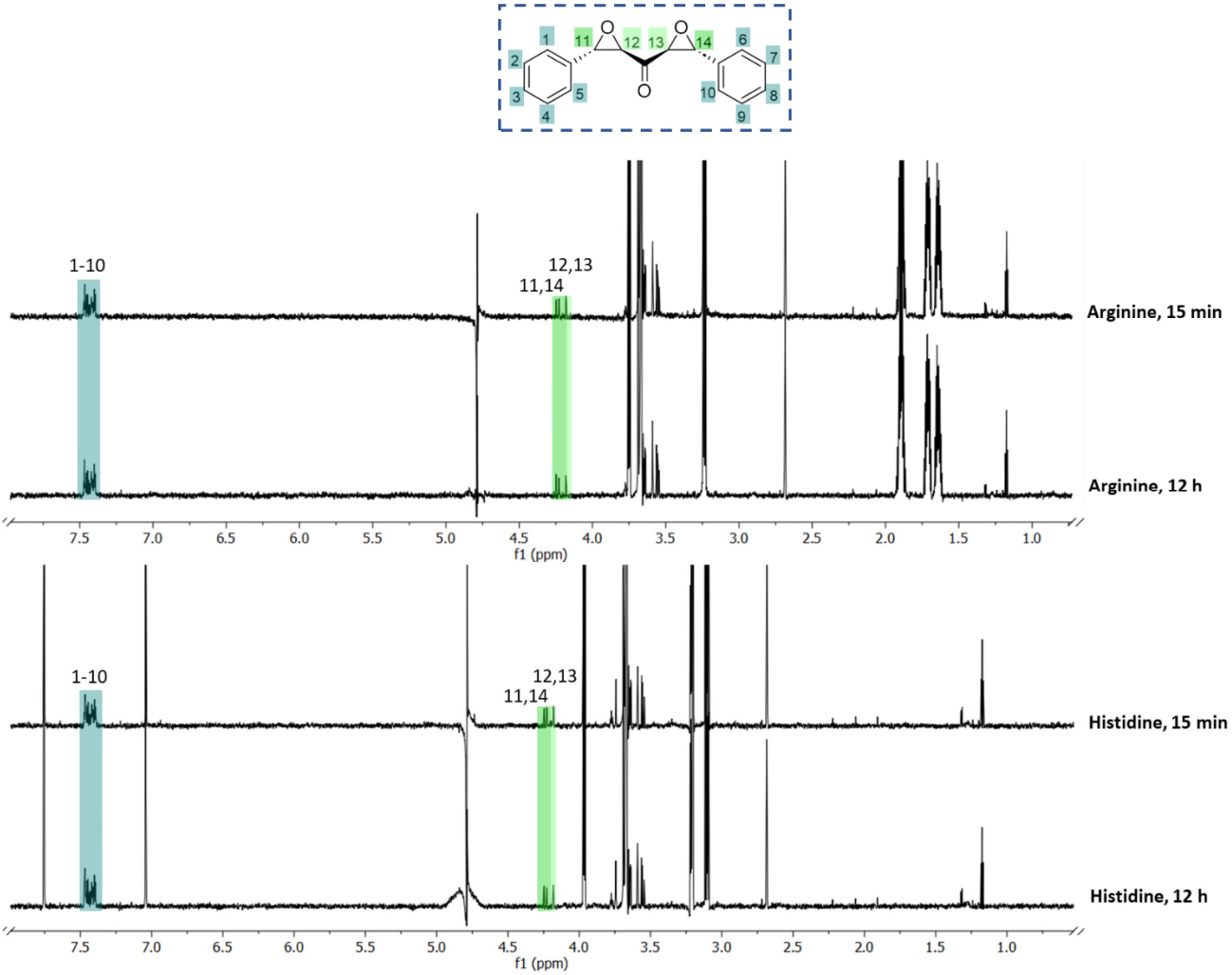

Figure S2.5. Reactivity of 1 with serine, lysine, tyrosine, threonine, arginine, and histidine. A solution of **1** (250 µM) was incubated with Boc-Ser-OH, Boc-Lys-OH, Tyr, Thr, Arg, or His, (250 µM) in 50 mM tris-d11, pH 7.5, 10% D_2O. The reaction was analysed by ^{1}H-NMR (950 MHz) up to 12 h. DEK **1** apparently did not react with the tested amino acids under the tested conditions.

***trans,trans*-isomers**

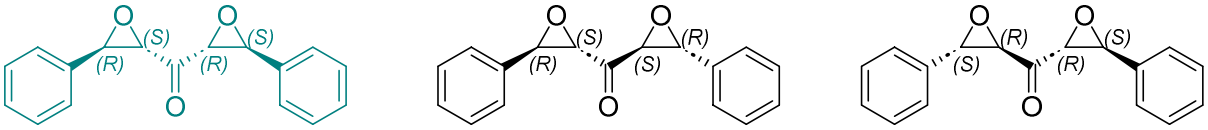

***cis,cis*-isomers**

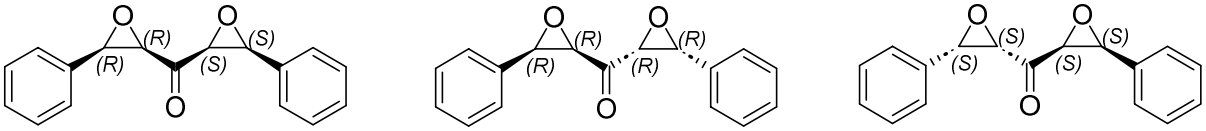

Figure S2.6. Synthesised stereoisomers of 1, which is equally representative for compounds 4-11. 1 was synthesised as a mixture of three *trans,trans* isomers and three *cis,cis* isomers. Note that no evidence for the formation of the *trans,cis* isomers was observed by ^{1}H NMR analysis. In some cases, the *trans,trans* isomers could be isolated from the *cis,cis* isomers via recrystallisation, as specified in Table S2.3. The *trans,trans* isomer in teal represents the hit compound from the HTS, which was obtained as a pure stereoisomer from the GSK compound library.

Table S2.3. Synthesis and inhibitory characterisation of DEKs 1 and 4-12 with the nucleophilic cysteine enzymes Ldt_{Mt2} and SARS-CoV-2 M^{pro} and with the nucleophilic serine enzyme BlaC.

	Structure	Synthetic yield (%)		pIC_{50}		k_{inact}/K_I (M^{-1} s^{-1}) Ldt_{Mt2}	k_{chem} (M^{-1} s^{-1})
		Step 1[a]	Step 2 (dr)[a,b]	Ldt_{Mt2}	M^{pro}		
1	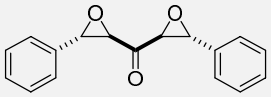	96	35 (1:0)	6.0 ± 0.03	4.6 ± 0.3	484.3 ± 28.4	<0.8
4	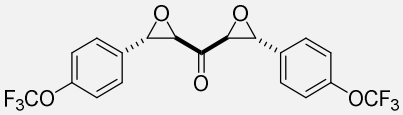	59	11 (1:0)	4.5 ± 0.1	<4.4	<10.0	<0.8
5	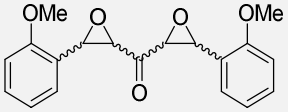	78	29 (2:1)	5.1 ± 0.05	<4.4	61.1 ± 2.78	<0.8
6	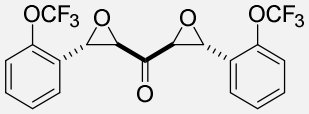	63	22 (1:0)	5.1 ± 0.06	<4.4	140.6 ± 17.1	<0.8
7	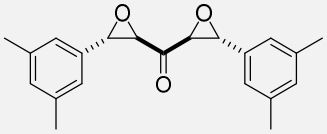	22	16 (1:0)	5.2 ± 0.03	<4.4	80.9 ± 6.74	1.7 ± 0.2
8	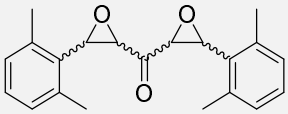	7	24 (1.2:1)	4.7 ± 0.04	<4.4	<10.0	1.1 ± 0.2
9	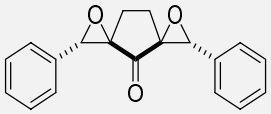	94	52 (1:0)	4.7 ± 0.04	5.9 ± 0.2	25.8 ± 1.41	<0.8
10	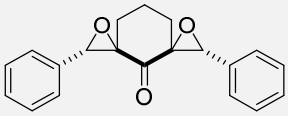	58	44 (1:0)	<4.4	<4.4	<10.0	<0.8
11	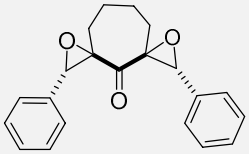	27	41 (1:0)	<4.4	<4.4	N.D.	N.D.
12	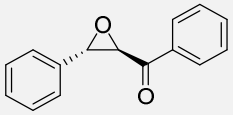	-	- (1:0)	<4.4	<4.4	N.D.	N.D.

[a] The 2-step synthesis involved the formation of the diene ketones (Step 1) followed by epoxidation (Step 2), to yield stereoisomeric mixtures (Figure 4.1D).

[b] Diastereomeric ratio (*trans*,*trans*:*cis*,*cis*) following purification, as determined by ^{1}H NMR analysis.

Table S2.4. Crystal data and structure refinement for 1.

Datasets	**1 (CCDC 2262059)**	
Empirical formula	C17 H14 O3	
Formula weight	266.30	
Temperature	150 K	
Wavelength	1.54184 Å	
Crystal system	Monoclinic	
Space group	C 2/c	
Cell dimensions	a = 28.7921(3) Å	α = 90°
	b = 5.34270(10) Å	β = 92.7637(11)°
	c = 8.59030(10) Å	γ = 90°
Volume	1319.89(3) $Å^3$	
Z	4	
Density (calculated)	1.340 Mg/m^3	
Absorption coefficient	0.742 mm^{-1}	
F(000)	560	
Crystal size	0.28 x 0.11 x 0.02 mm^3	
Theta range for data collection	3.073 to 75.928°	
Index ranges	-36<=h<=36, -6<=k<=6, -10<=l<=10	
Reflections collected	16701	
Independent reflections	1381 [R(int) = 0.024]	
Completeness to theta = 75.928°	99.9 %	
Absorption correction	Semi-empirical from equivalents	
Max. and min. transmission	0.99 and 0.71	
Refinement method	Full-matrix least-squares on F^2	
Data / restraints / parameters	1381 / 0 / 93	
Goodness-of-fit on F^2	0.9994	
Final R indices [I>2sigma(I)]	R1 = 0.0294, wR2 = 0.0777	
R indices (all data)	R1 = 0.0303, wR2 = 0.0786	
Extinction coefficient	12(2)	
Largest diff. peak and hole	0.25 and -0.13 $e.Å^{-3}$	

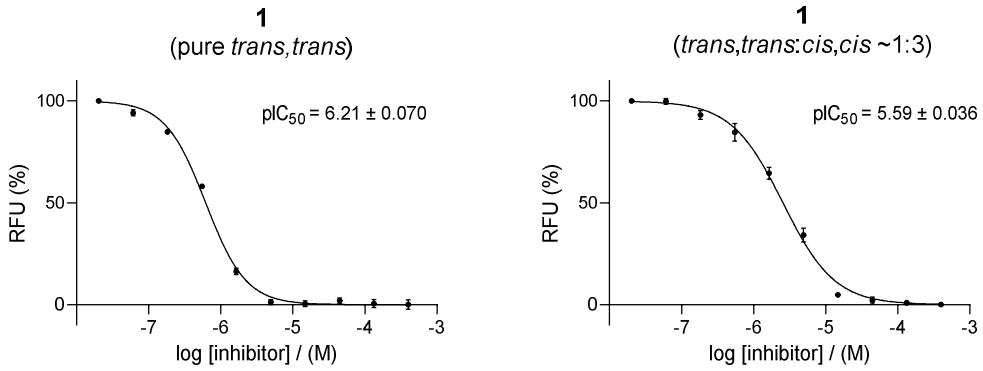

Figure S2.7. Dose-response curves for the pure *trans*,*trans* isomers of 1 and an isomeric mixture of 1 (*trans*,*trans*:*cis*,*cis* of ~1:3). Inhibition assays were carried out using 100 nM Ldt_{Mt2} and 25 µM Probe **1** with 15 min pre-incubation at rt in 50 mM HEPES, pH 7.2 with 0.01% (*v/v*) Triton X-100. Error bars represent the standard deviation (n=4). Note that pIC_{50} values are similar, but imply that the pure *trans*,*trans* isomer of **1** is the most active stereoisomer.

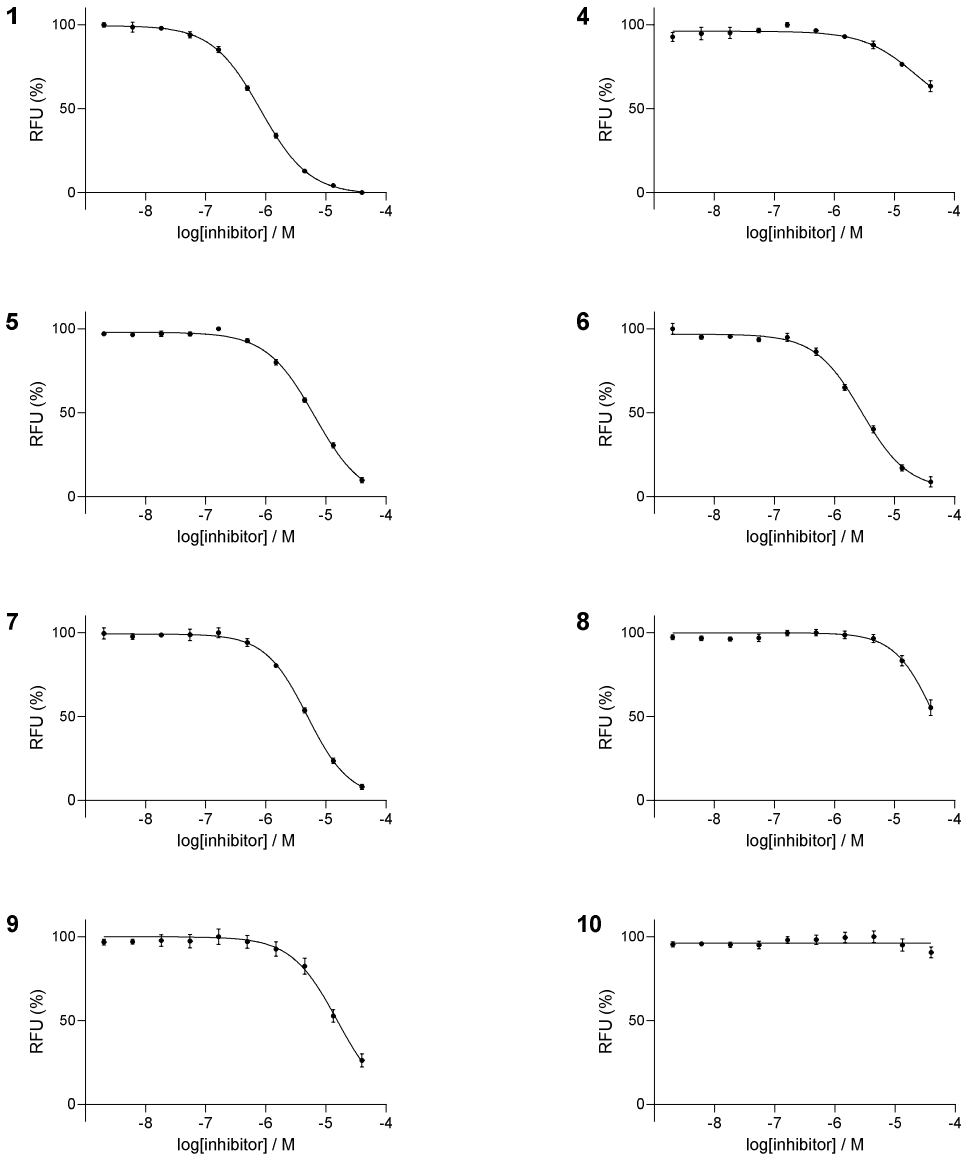

Figure S2.8. Determination of the second-order rate constant for irreversible inhibition (k_{inact}/K_I) of Ldt_{Mt2} by DEKs 1 and 4-10. Inhibition assays were carried out using 100 nM Ldt_{Mt2} and 10 µM Probe **1** with 3 h incubation at rt in 50 mM HEPES, pH 7.2 with 0.01% (*v/v*) Triton X-100. Error bars represent the standard deviation (n=4). Average $(k_{inact}/K_I)_{inhibitor}$ values and compound structures are given in Table S2.3.

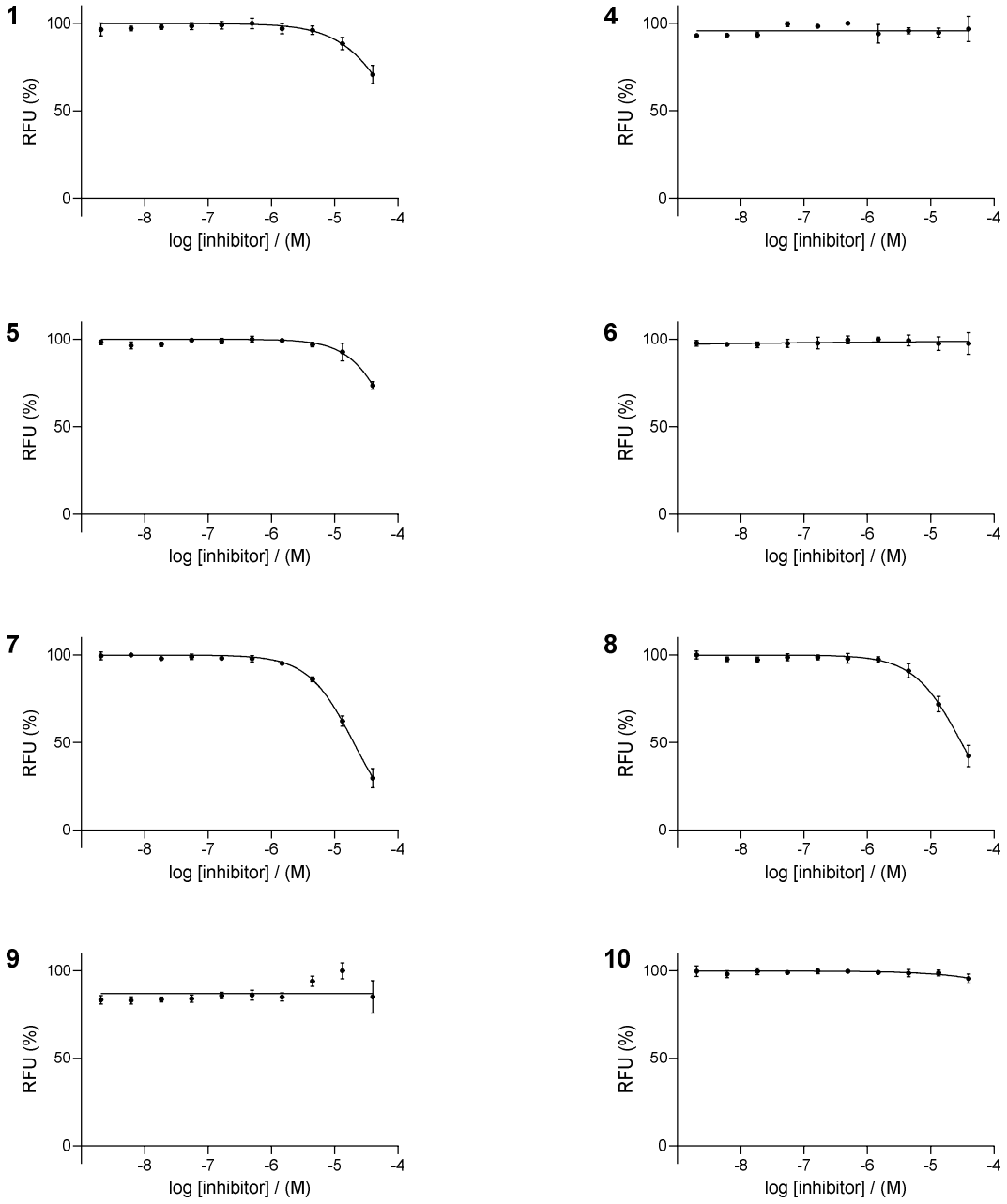

Figure S2.9. Determination of the intrinsic thiol reactivity rate constant (k_{chem}) for DEKs 1 and 4-10. Assays were carried out using 500 nM L-glutathione and 10 µM Probe **1** with 16 h incubation at room temperature in 50 mM HEPES, pH 7.2 with 0.01% (*v/v*) Triton X-100. Error bars represent the standard deviation (n=4). Average k_{chem} values and compound structures are given in Table S2.3.

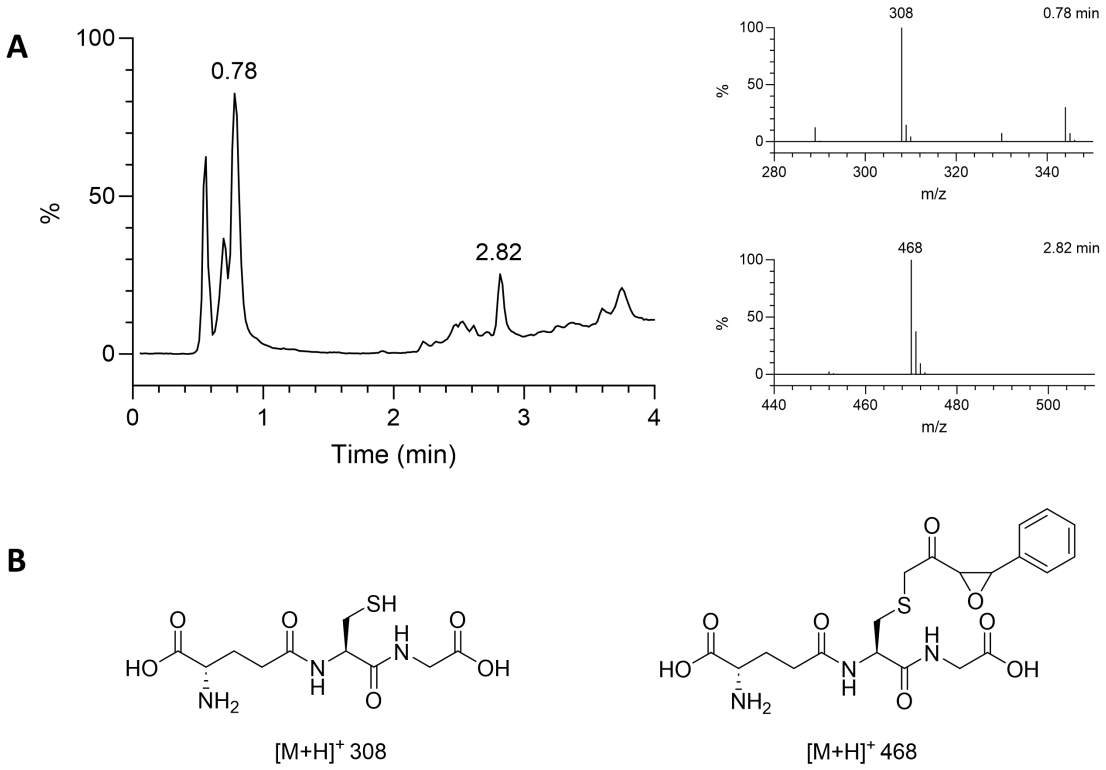

Figure S2.10. LCMS studies of the reaction between GSH and 1. A. A solution of **1** (250 µM) and GSH (250 µM) in 50 mM tris pH 7.5 was incubated for 16 h in the presence of TCEP (250 µM), then analysed by LCMS operating in the positive ion mode. **B.** The compounds eluting at 0.78 min and 2.82 min correspond to unreacted GSH and GSH reacted with **1** (apparently leading to the fragmented species analogous to **3**), respectively.

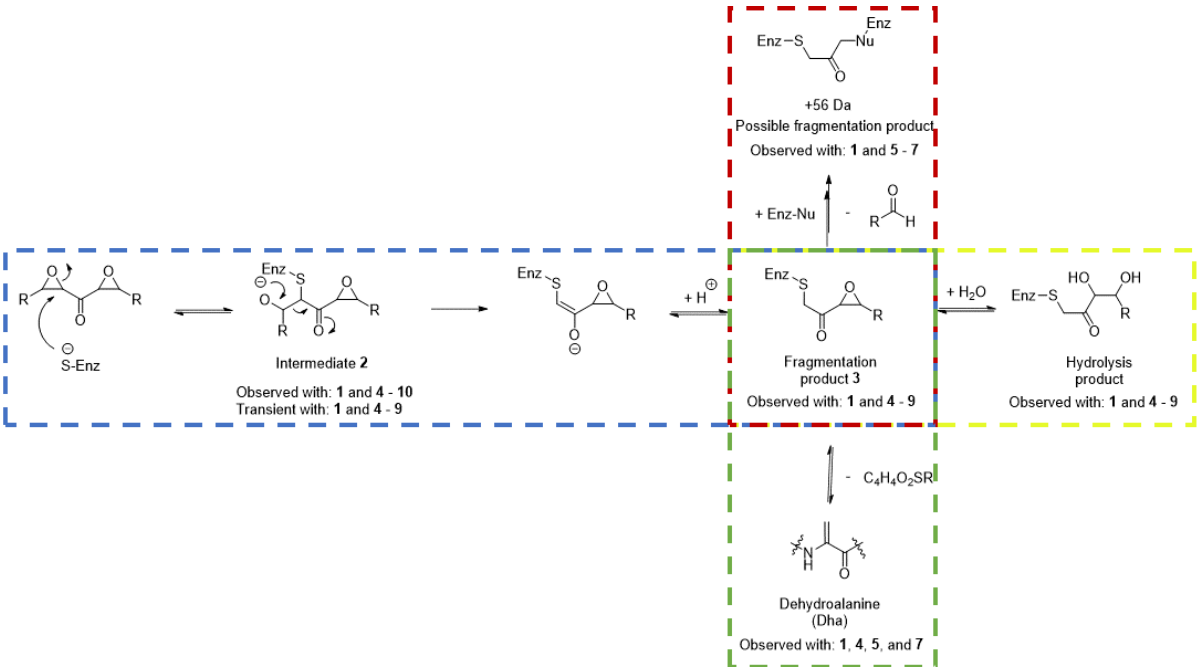

Figure S2.11. Summary of the reactions of DEKs with nucleophilic cysteine enzymes. The DEKs are proposed to inhibit nucleophilic cysteine enzymes via initial reaction of the nucleophilic cysteine with one of the epoxides, followed by retro-aldol reaction (blue outline). Initial reaction at the DEK carbonyl followed by rearrangement is also possible (Figure 4.2C). The fragmentation product **3** (Figure 4.2) obtained after retro-aldol reaction was sometimes (as indicated by compound numbers) observed (by MS analysis) to further react to give: (i) the corresponding hydrolysis product, likely through hydrolytic ring opening of its epoxide (yellow outline), or (ii) a dehydroalanine (Dha) residue (green outline). Another unassigned product corresponding to a mass shift of +57 Da compared to the unmodified enzyme was (sometimes) observed (red outline). Among other possibilities, the +57 Da fragmentation product(s) may arise through reaction with another nucleophilic residue in the active site, leading to a cross-linked adduct.

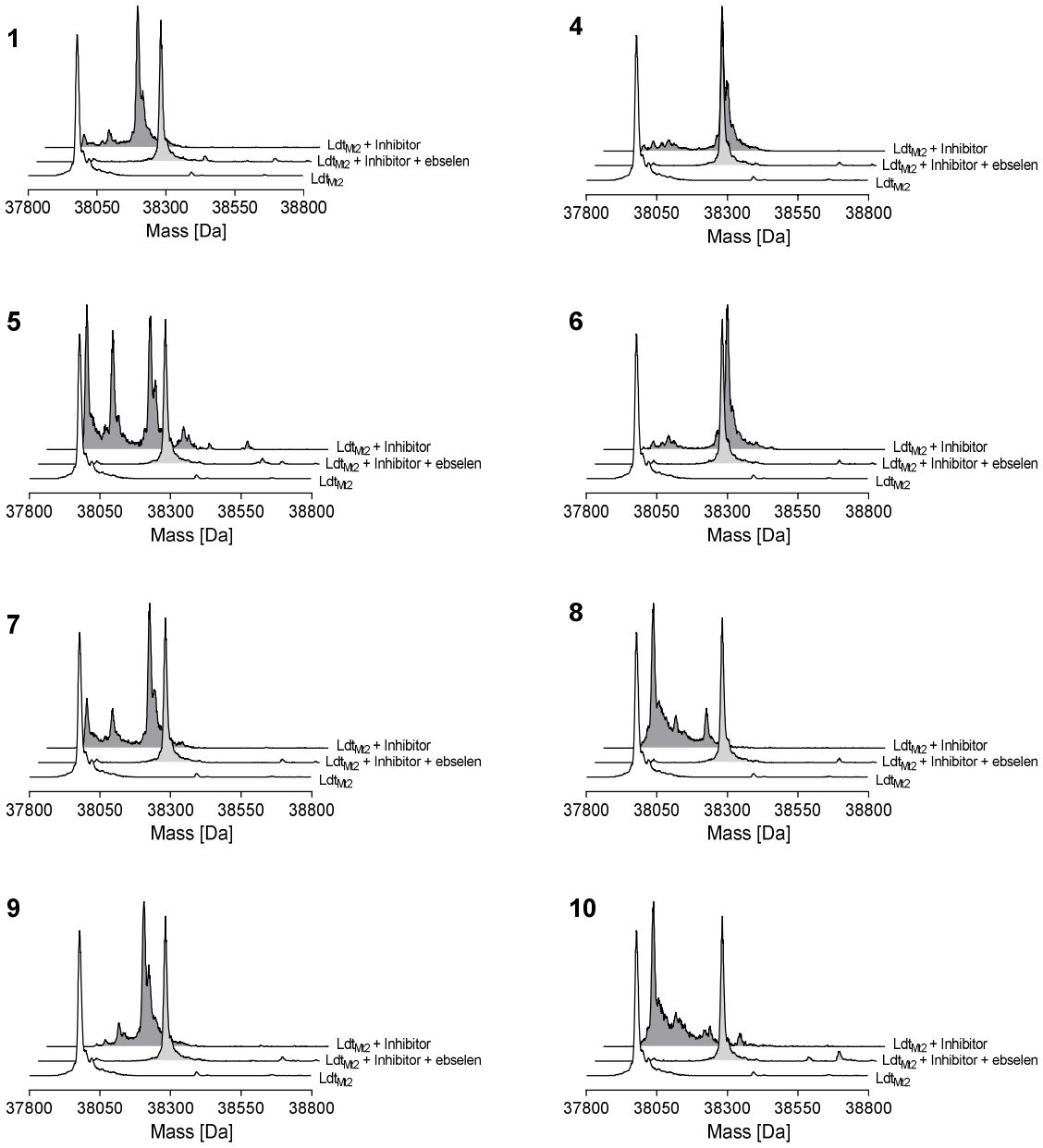

Figure S2.12. Protein-observed SPE-MS based Cys354 selectivity assays. Ldt_{Mt2} (1 µM) was preincubated with ebselen (a reported Ldt_{Mt2} inhibitor[8] which reacts with the nucleophilic Cys354, 10 µM) for 1 h in 50 mM Tris, pH 7.5. Inhibitors **1** and **4** – **10** (100 µM) were then added and samples were analysed after an additional 24 h incubation at room temperature using SPE-MS. The spectrum in white corresponds to Ldt_{Mt2} reacted with ebselen. The spectrum in light grey corresponds to Ldt_{Mt2} reacted with the specified inhibitor, following preincubation with ebselen. The spectrum in dark grey corresponds to Ldt_{Mt2} reacted with the specified inhibitor. Deconvoluted spectra, obtained using the maximum entropy algorithm in the MassHunter Workstation Qualitative Analysis B.07.00 program (Agilent), are shown.

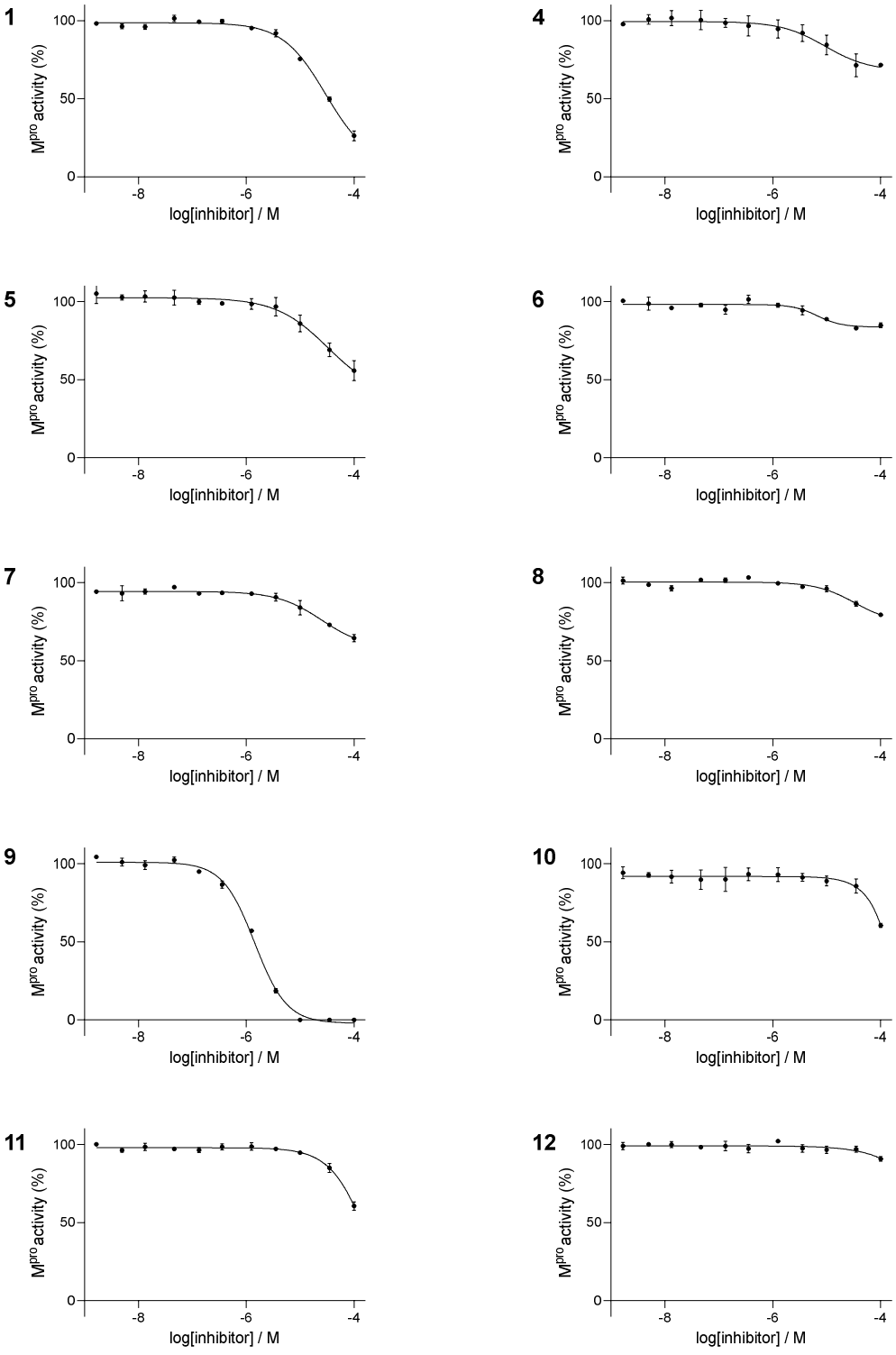

Figure S2.13. Representative dose-response curves for DEKs 1 and 4-11 and the mono-epoxide ketone 12 with SARS-CoV-2 M^{pro}. Inhibition assays were carried out using 150 nM M^{pro} and 2 µM 37mer peptide, with 15 min pre-incubation at rt in 20 mM HEPES, pH 7.5, 50 mM NaCl and M^{pro} activity was determined by SPE-MS.[5] Error bars represent the standard deviation of technical duplicates (n=2). Assays were performed in independent duplicates, each composed of technical duplicates; average pIC_{50} values and compound structures are given in Table S2.3.

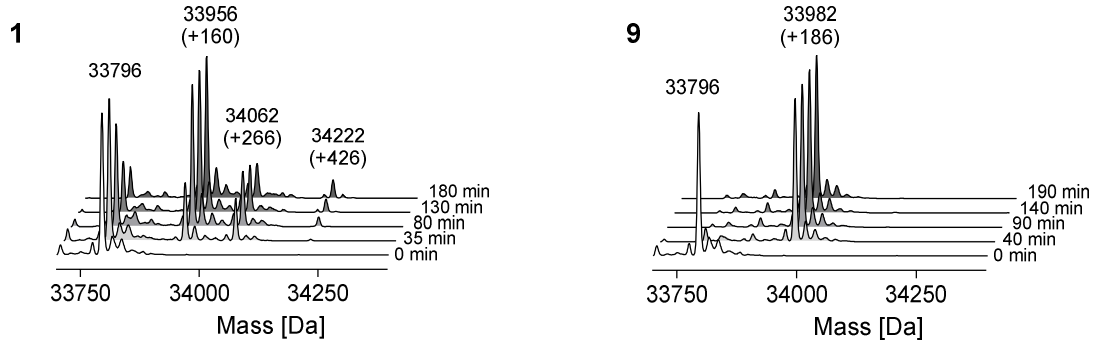

Figure S2.14. Protein observed SPE-MS analysis for the reaction of SARS-CoV-2 M^{pro} with DEKs 1 and 9. M^{pro} (2 µM) was incubated with DEKs **1** and **9** (20 µM) at rt in 20 mM HEPES, pH 7.5. Samples were analysed after the indicated times. Deconvoluted spectra, obtained using the maximum entropy algorithm in the MassHunter Workstation Qualitative Analysis B.07.00 program (Agilent), are shown. Mass shifts and assignments are analogous to those described in Table S2.1 for **1** and **9** for reaction with Ldt_{Mt2}.

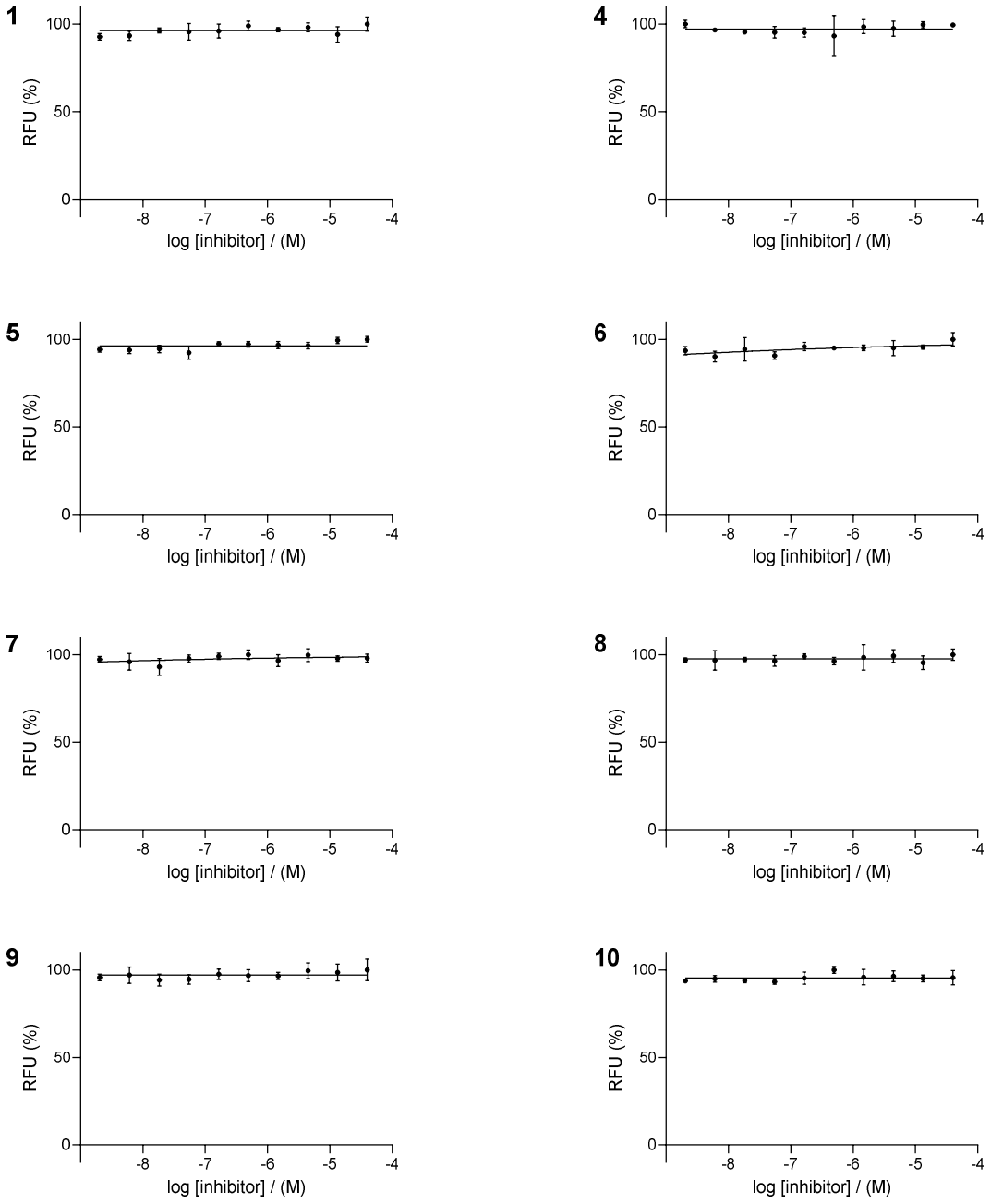

Figure S2.15. Dose-response curves for DEKs 1 and 4-10 with BlaC. Inhibition assays were carried out using 14 nM BlaC and 10 µM FC5[4] with a 10 min pre-incubation at rt in 100 mM sodium phosphate pH 7.5 with 0.01% (*v/v*) Triton X-100. Error bars represent the standard deviation (n=4). Average pIC_{50} values and compound structures are given in Table S2.3.

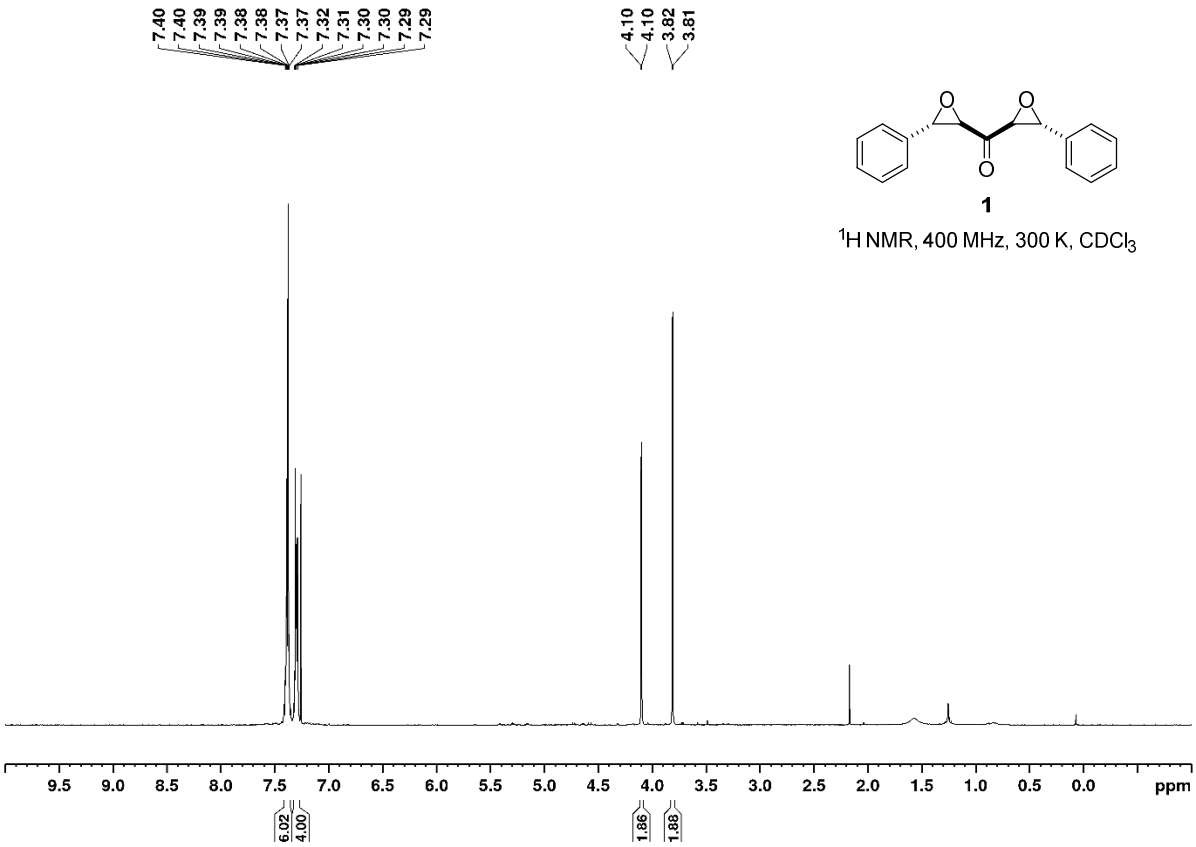
7.40
7.40
7.39
7.39
7.38
7.38
7.37
7.37
7.32
7.31
7.30
7.30
7.29
7.29
4.10
4.10
3.82
3.81
1
^{1}H NMR, 400 MHz, 300 K, $CDCl_3$
9.5 9.0 8.5 8.0 7.5 7.0 6.5 6.0 5.5 5.0 4.5 4.0 3.5 3.0 2.5 2.0 1.5 1.0 0.5 0.0 ppm
6.02
4.00
1.86
1.88

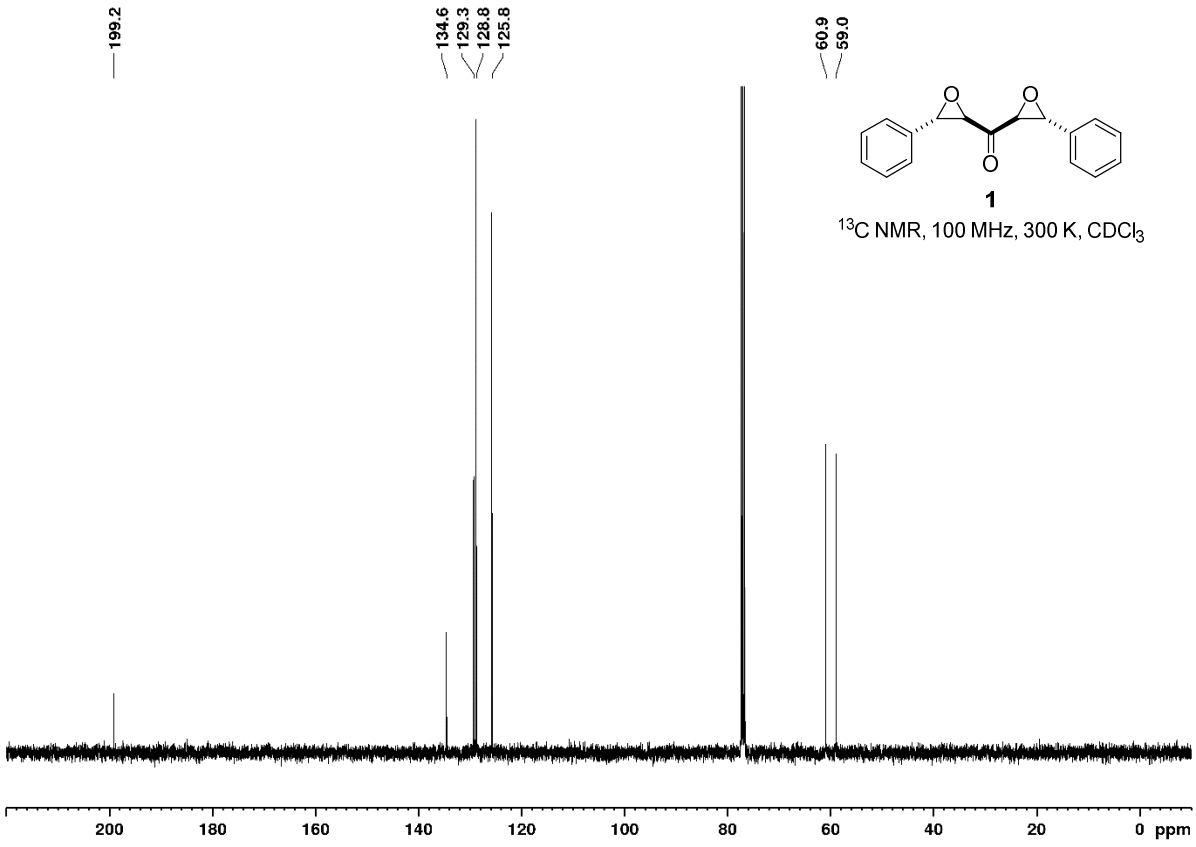
199.2
134.6
129.3
128.8
125.8
60.9
59.0
1
^{13}C NMR, 100 MHz, 300 K, $CDCl_3$
200 180 160 140 120 100 80 60 40 20 0 ppm

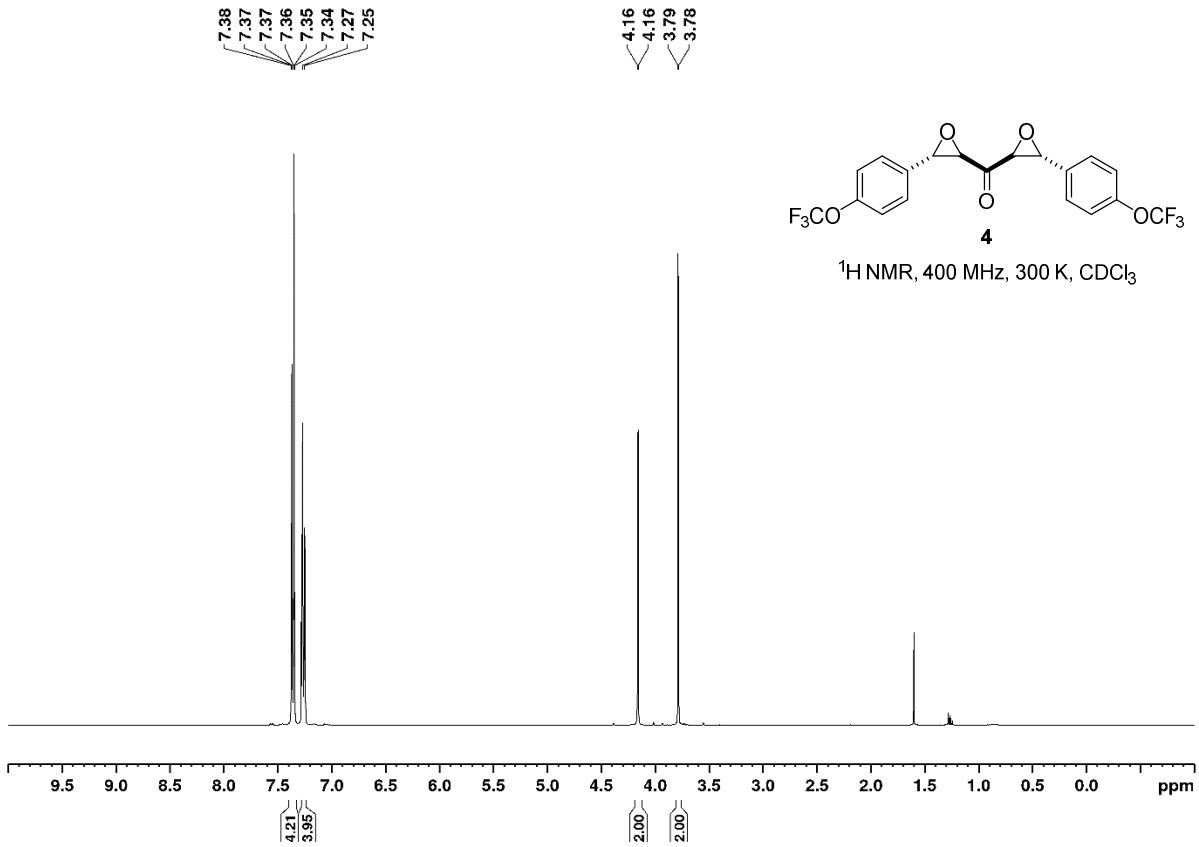
7.38
7.37
7.37
7.36
7.35
7.34
7.27
7.25
4.16
4.16
3.79
3.78
F3CO
OCF3
4
1H NMR, 400 MHz, 300 K, CDCl3
9.5 9.0 8.5 8.0 7.5 7.0 6.5 6.0 5.5 5.0 4.5 4.0 3.5 3.0 2.5 2.0 1.5 1.0 0.5 0.0 ppm
4.21
3.95
2.00
2.00

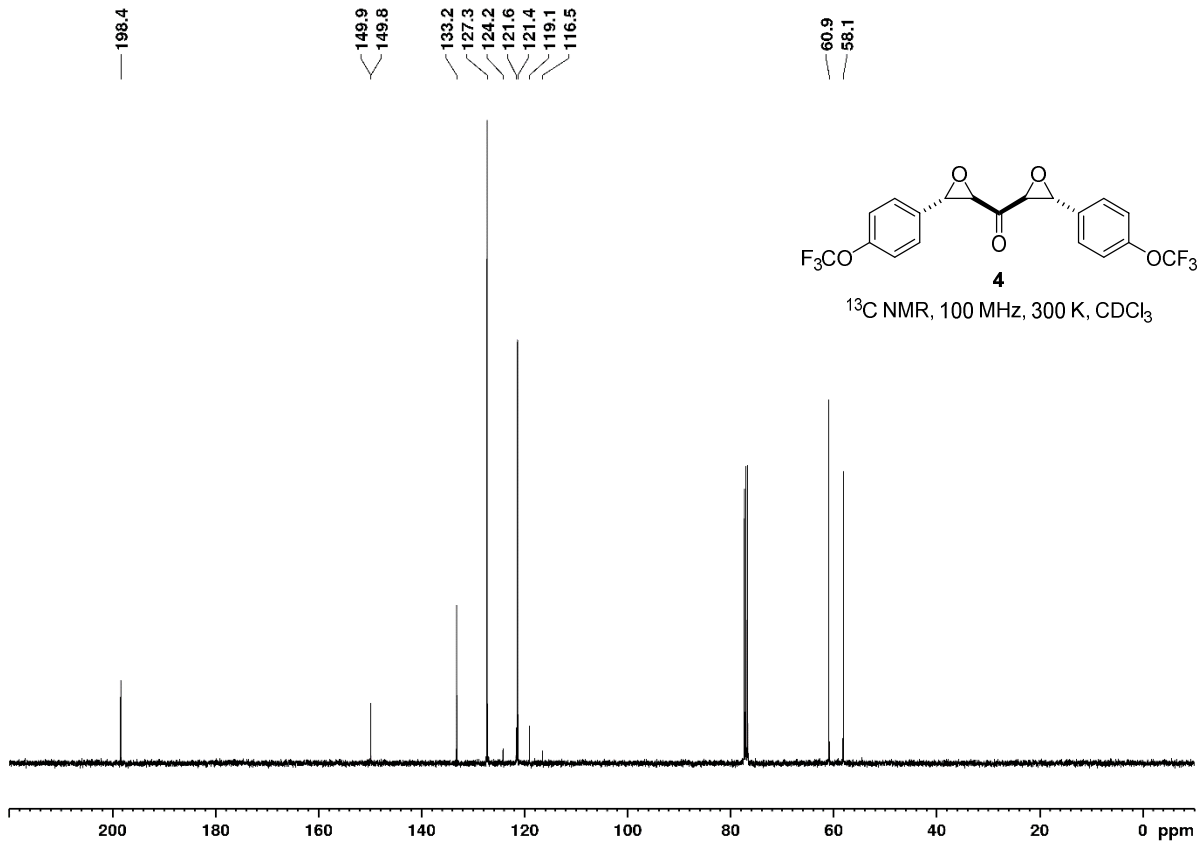
198.4
149.9
149.8
133.2
127.3
124.2
121.6
121.4
119.1
116.5
60.9
58.1
F3CO
OCF3
4
13C NMR, 100 MHz, 300 K, CDCl3
200 180 160 140 120 100 80 60 40 20 0 ppm

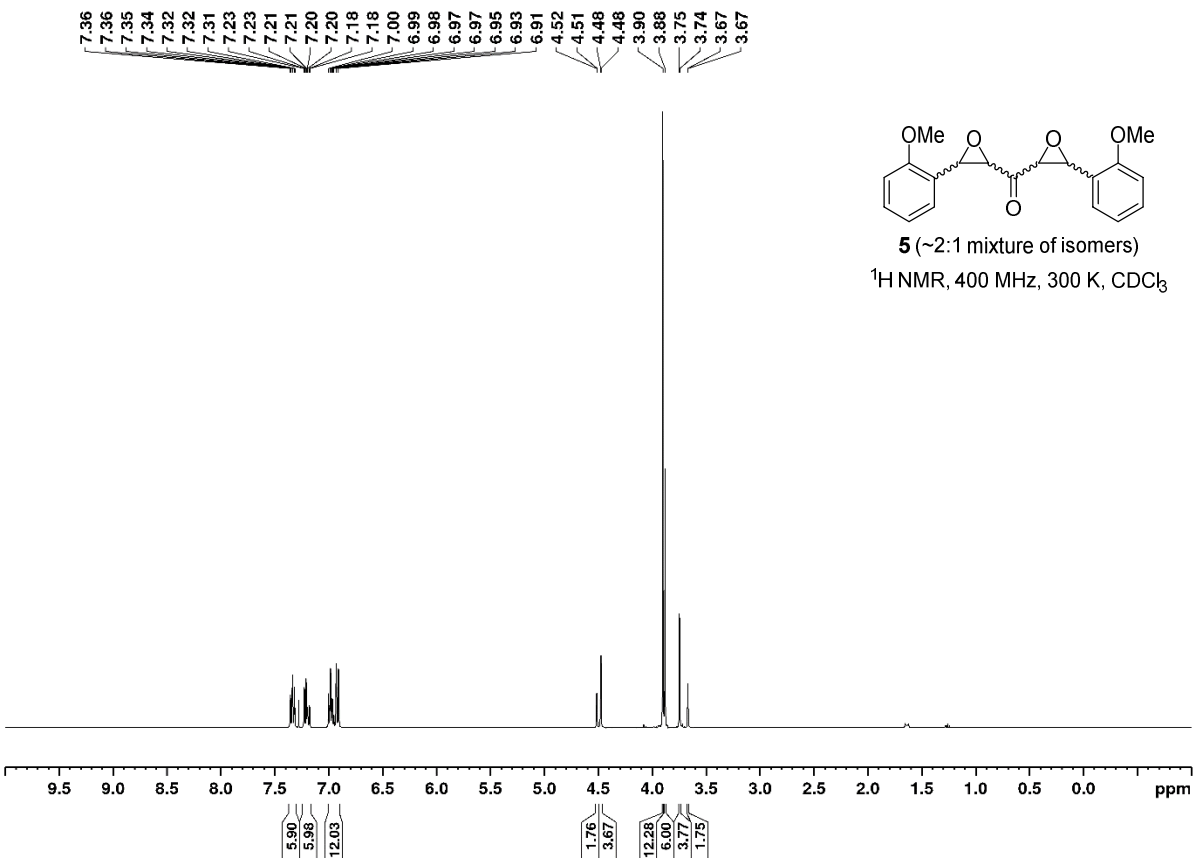
7.36
7.36
7.35
7.34
7.32
7.32
7.31
7.23
7.23
7.21
7.21
7.20
7.20
7.18
7.18
7.00
6.99
6.98
6.97
6.97
6.95
6.93
6.91
4.52
4.51
4.48
4.48
3.90
3.88
3.75
3.74
3.67
3.67
OMe
O
O
OMe
O
5 (~2:1 mixture of isomers)
1H NMR, 400 MHz, 300 K, CDCl3
9.5
9.0
8.5
8.0
7.5
7.0
6.5
6.0
5.5
5.0
4.5
4.0
3.5
3.0
2.5
2.0
1.5
1.0
0.5
0.0
ppm
5.90
5.98
12.03
1.76
3.67
12.28
6.00
3.77
1.75

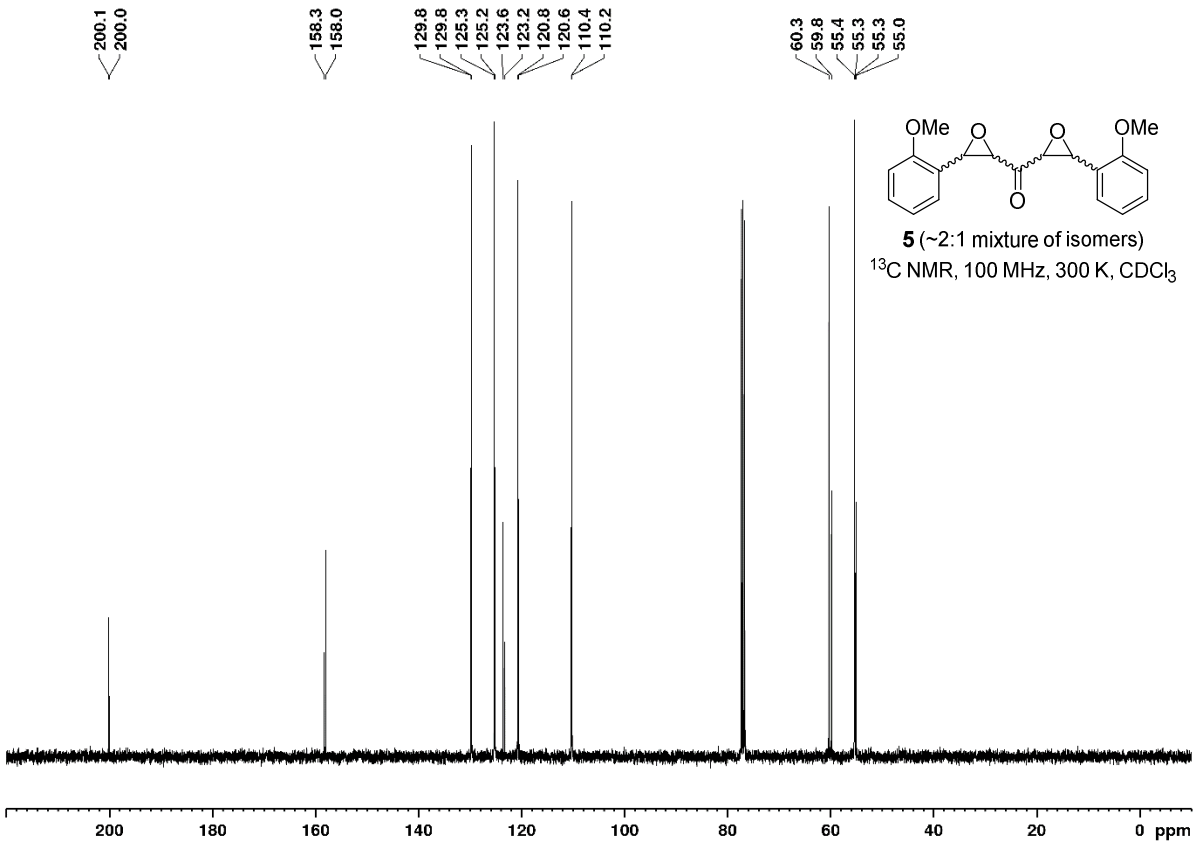
200.1
200.0
158.3
158.0
129.8
129.8
125.3
125.2
123.6
123.2
120.8
120.6
110.4
110.2
60.3
59.8
55.4
55.3
55.3
55.0
OMe
O
O
OMe
O
5 (~2:1 mixture of isomers)
13C NMR, 100 MHz, 300 K, CDCl3
200
180
160
140
120
100
80
60
40
20
0 ppm

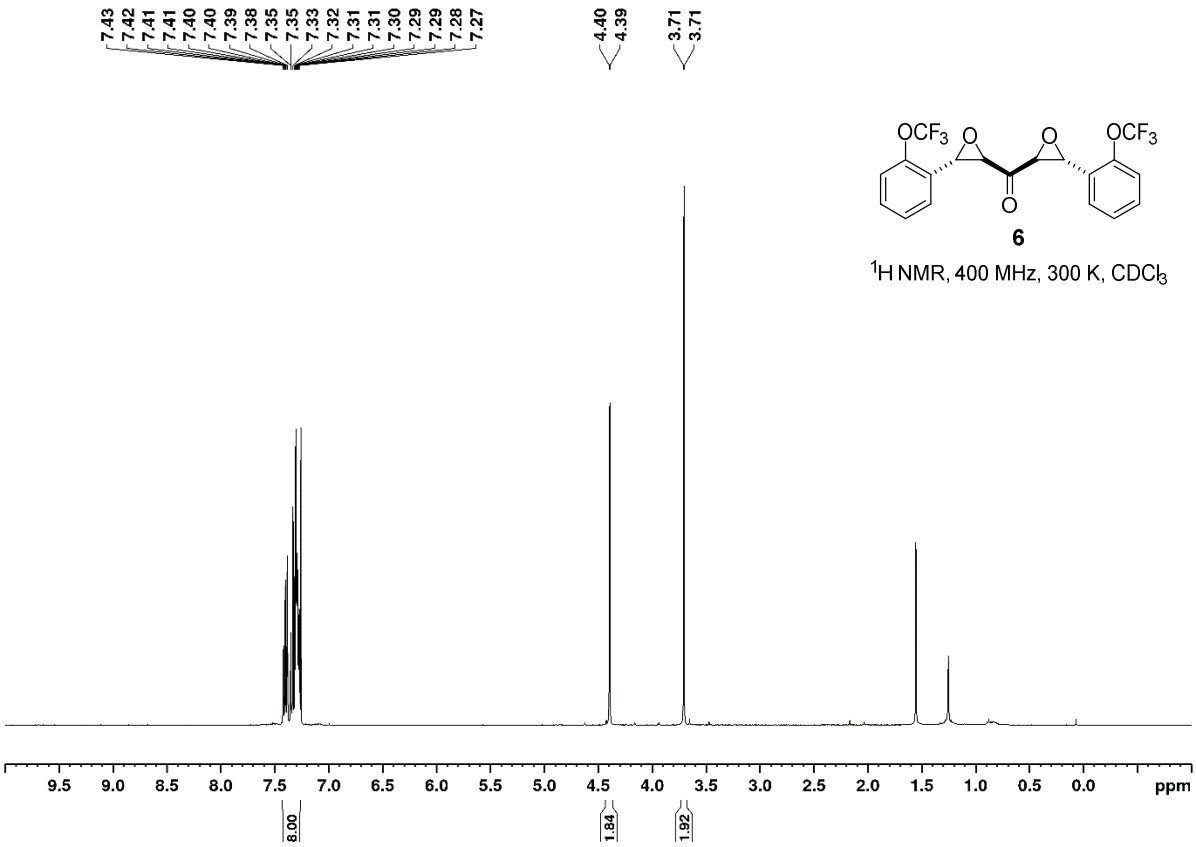
7.43
7.42
7.41
7.41
7.40
7.40
7.39
7.38
7.35
7.35
7.33
7.32
7.31
7.31
7.30
7.29
7.29
7.28
7.27
4.40
4.39
3.71
3.71
OCF3
O
O
OCF3
O
6
1H NMR, 400 MHz, 300 K, CDCl3
9.5
9.0
8.5
8.0
7.5
7.0
6.5
6.0
5.5
5.0
4.5
4.0
3.5
3.0
2.5
2.0
1.5
1.0
0.5
0.0
ppm
8.00
1.84
1.92

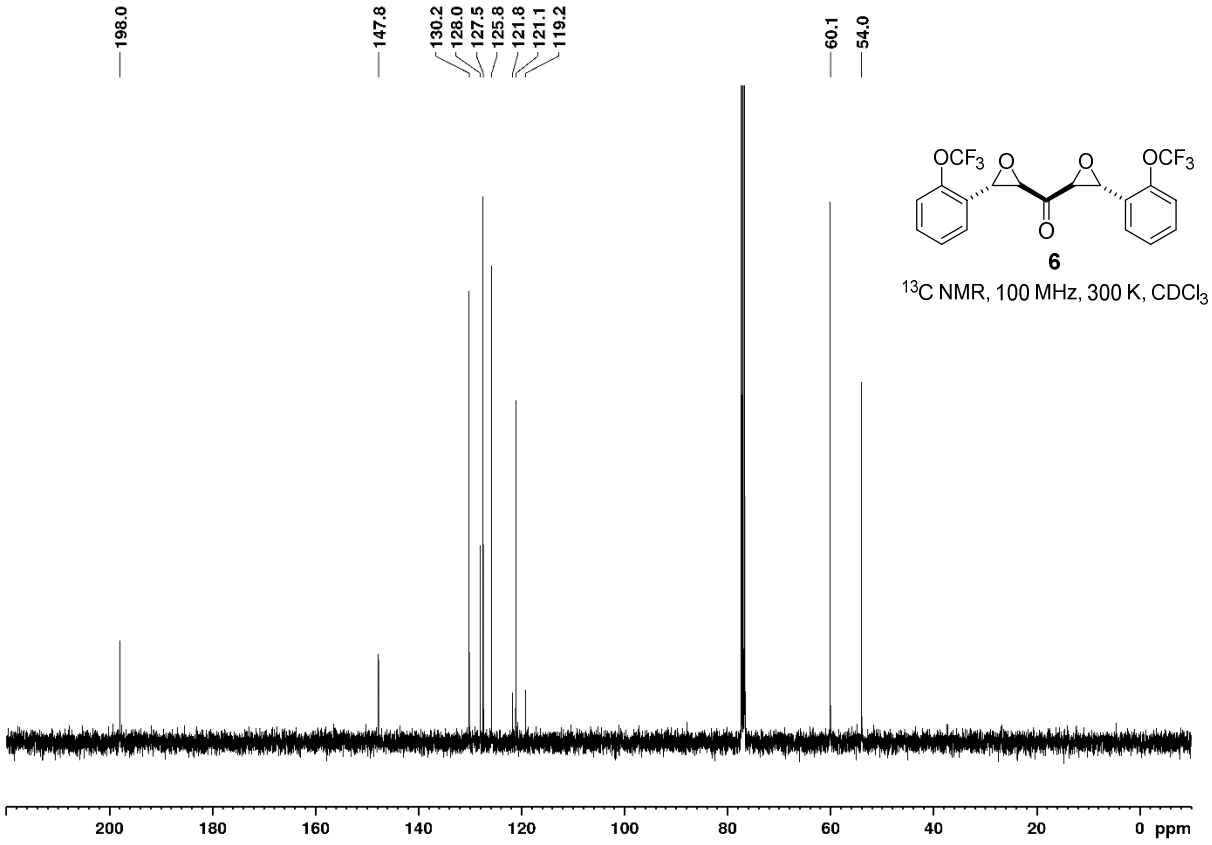
198.0
147.8
130.2
128.0
127.5
125.8
121.8
121.1
119.2
60.1
54.0
OCF3
O
O
OCF3
O
6
13C NMR, 100 MHz, 300 K, CDCl3
200
180
160
140
120
100
80
60
40
20
0 ppm

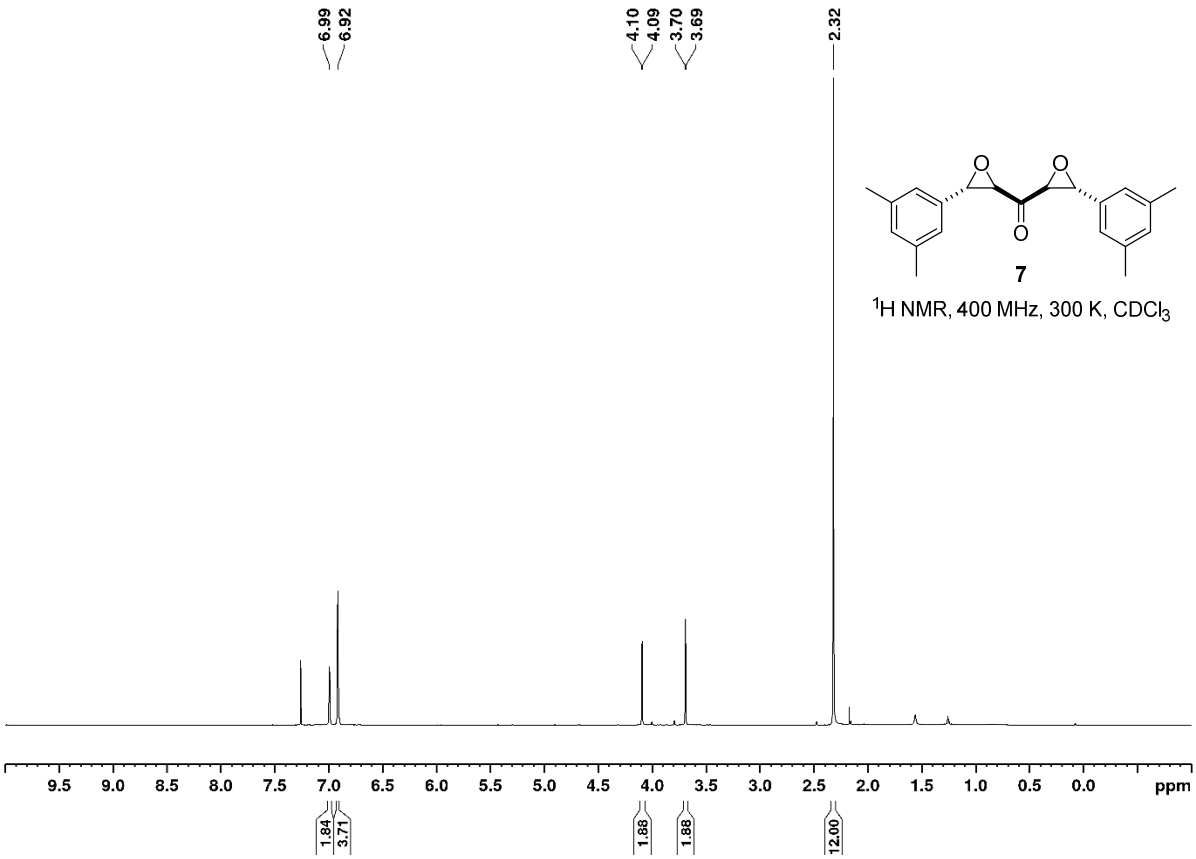

7

^{1}H NMR, 400 MHz, 300 K, $CDCl_3$

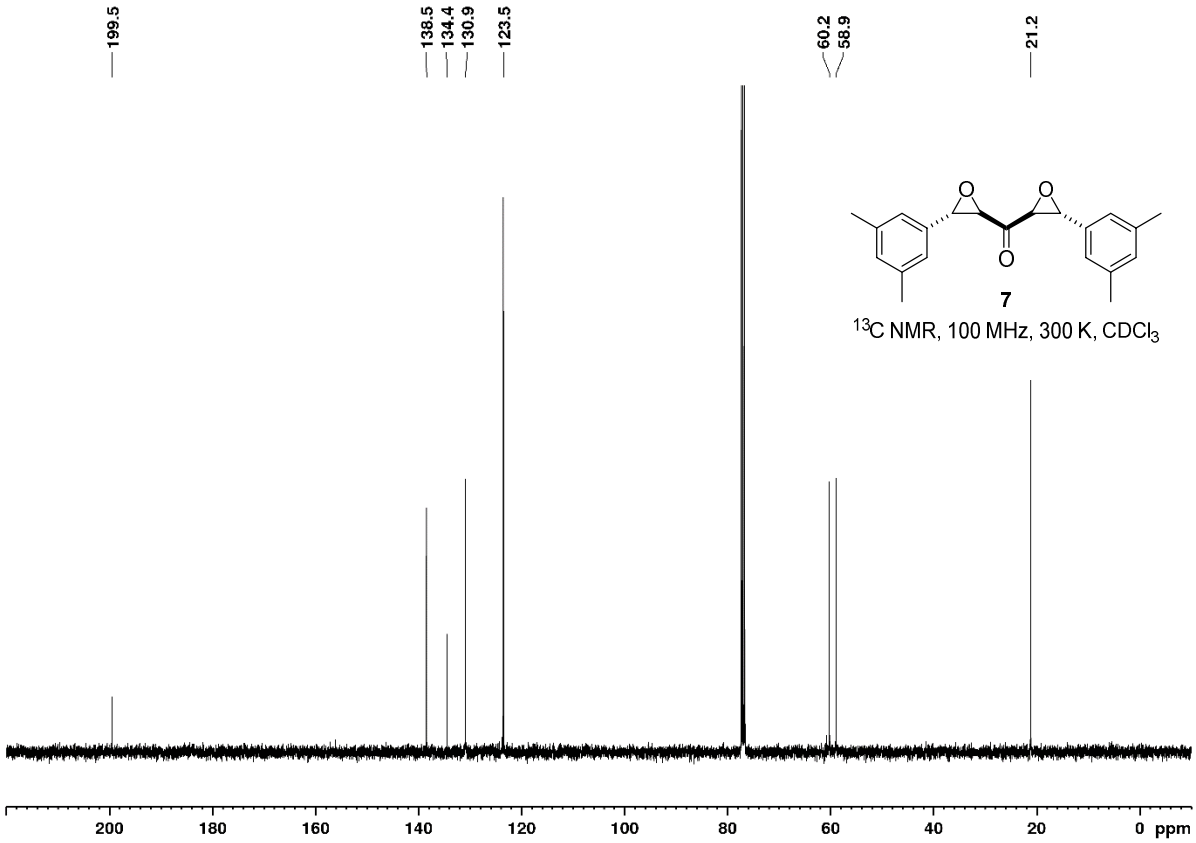

7

^{13}C NMR, 100 MHz, 300 K, $CDCl_3$

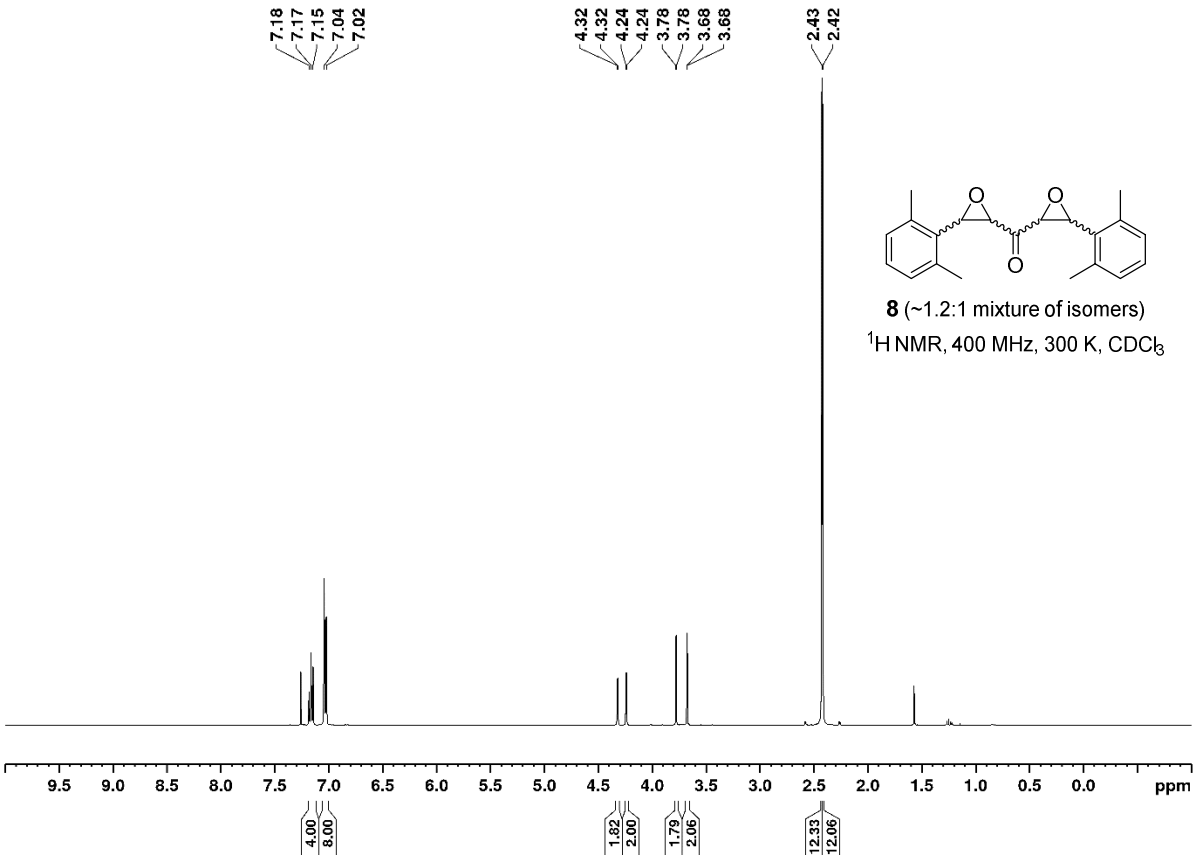
7.18
7.17
7.15
7.04
7.02
4.32
4.32
4.24
4.24
3.78
3.78
3.68
3.68
2.43
2.42
8 (~1.2:1 mixture of isomers)
1H NMR, 400 MHz, 300 K, CDCl3
9.5 9.0 8.5 8.0 7.5 7.0 6.5 6.0 5.5 5.0 4.5 4.0 3.5 3.0 2.5 2.0 1.5 1.0 0.5 0.0 ppm
4.00
8.00
1.82
2.00
1.79
2.06
12.33
12.06

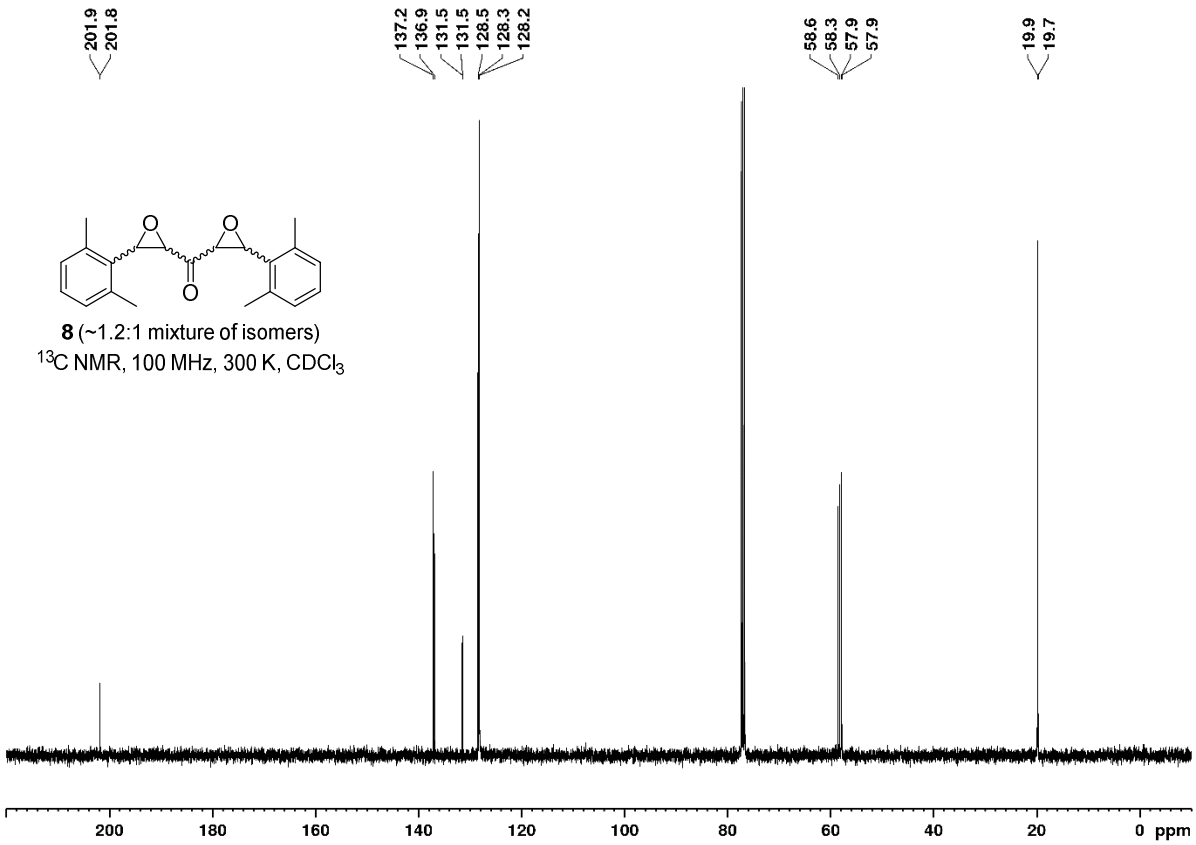
201.9
201.8
137.2
136.9
131.5
131.5
128.5
128.3
128.2
58.6
58.3
57.9
57.9
19.9
19.7
8 (~1.2:1 mixture of isomers)
13C NMR, 100 MHz, 300 K, CDCl3
200 180 160 140 120 100 80 60 40 20 0 ppm

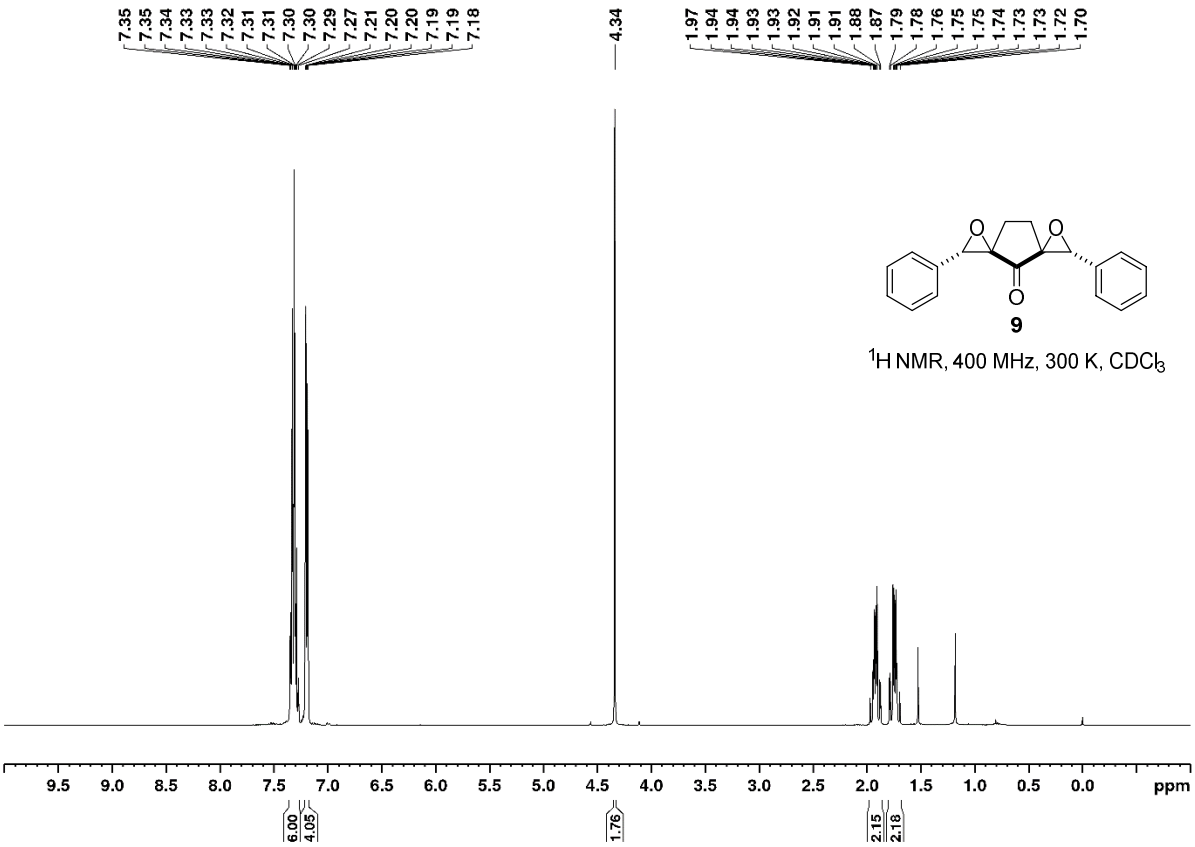

9

^{1}H NMR, 400 MHz, 300 K, $CDCl_3$

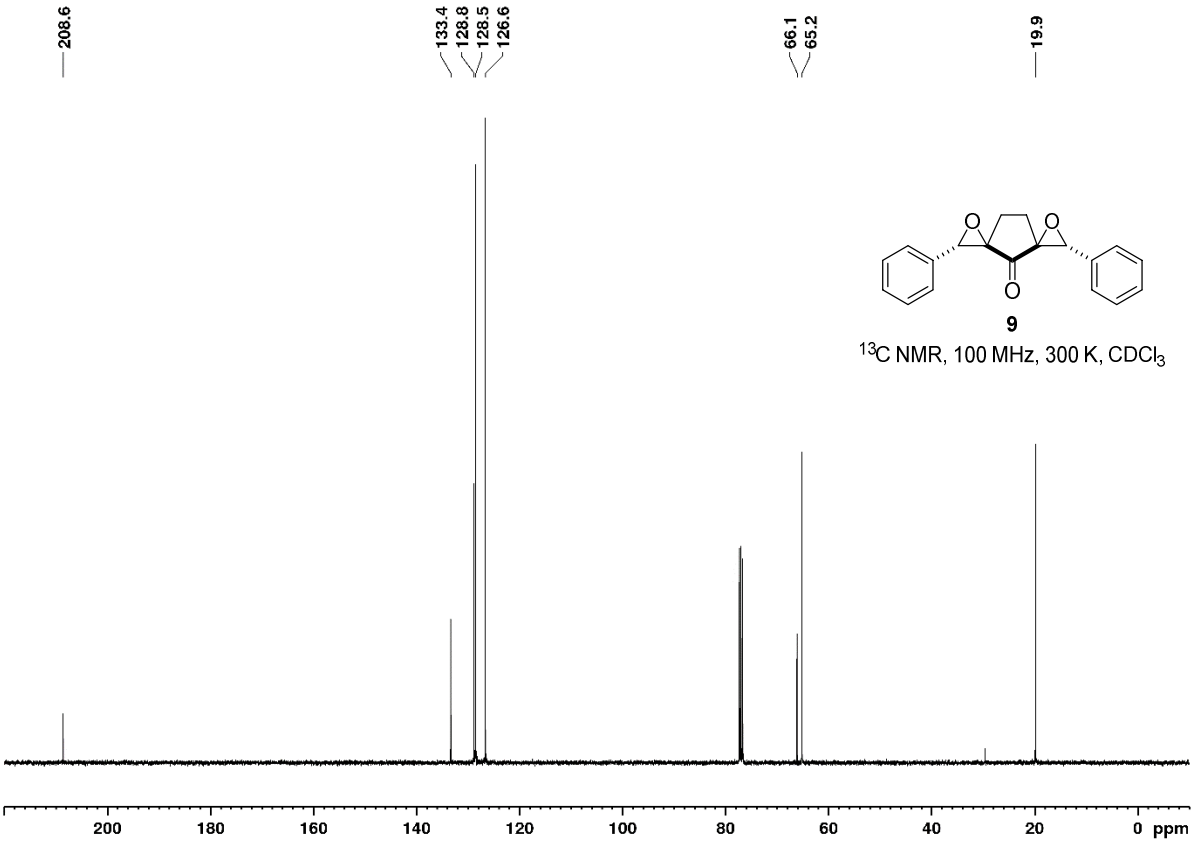

9

^{13}C NMR, 100 MHz, 300 K, $CDCl_3$

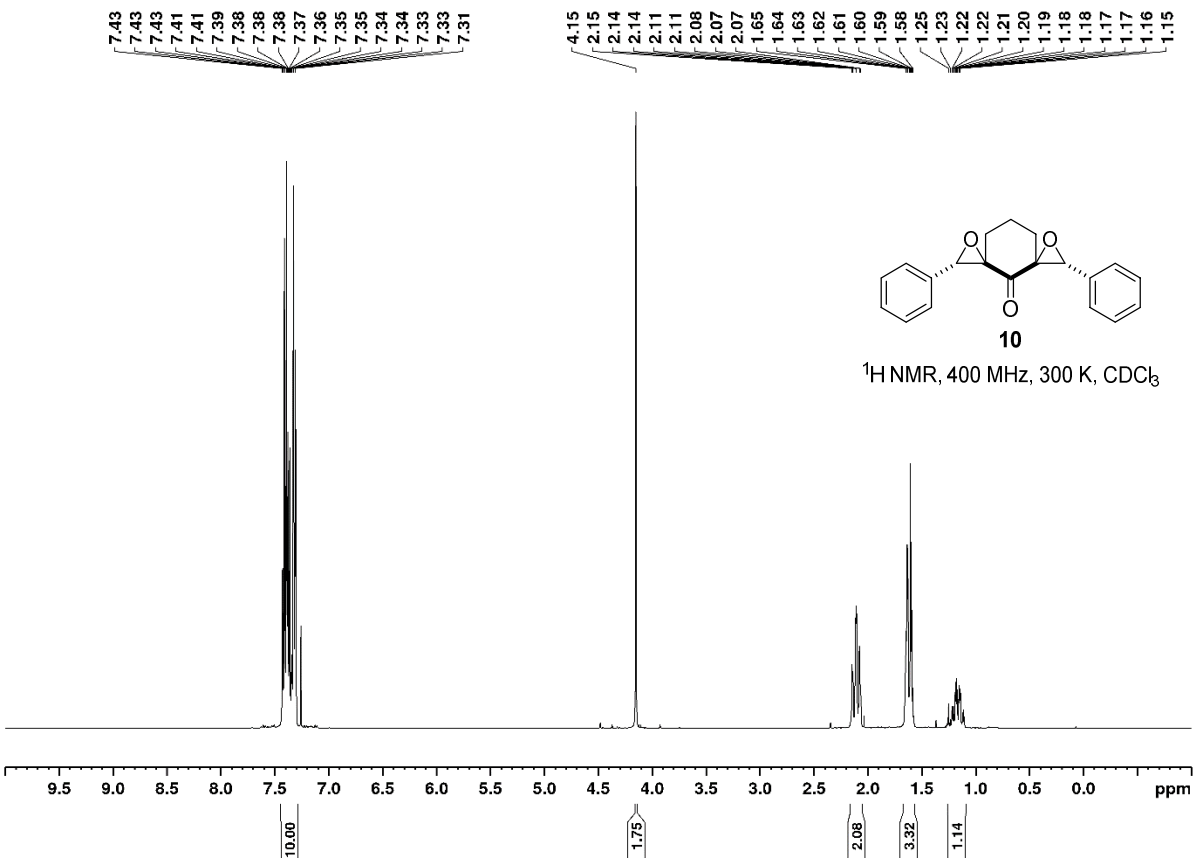

10

^{1}H NMR, 400 MHz, 300 K, $CDCl_3$

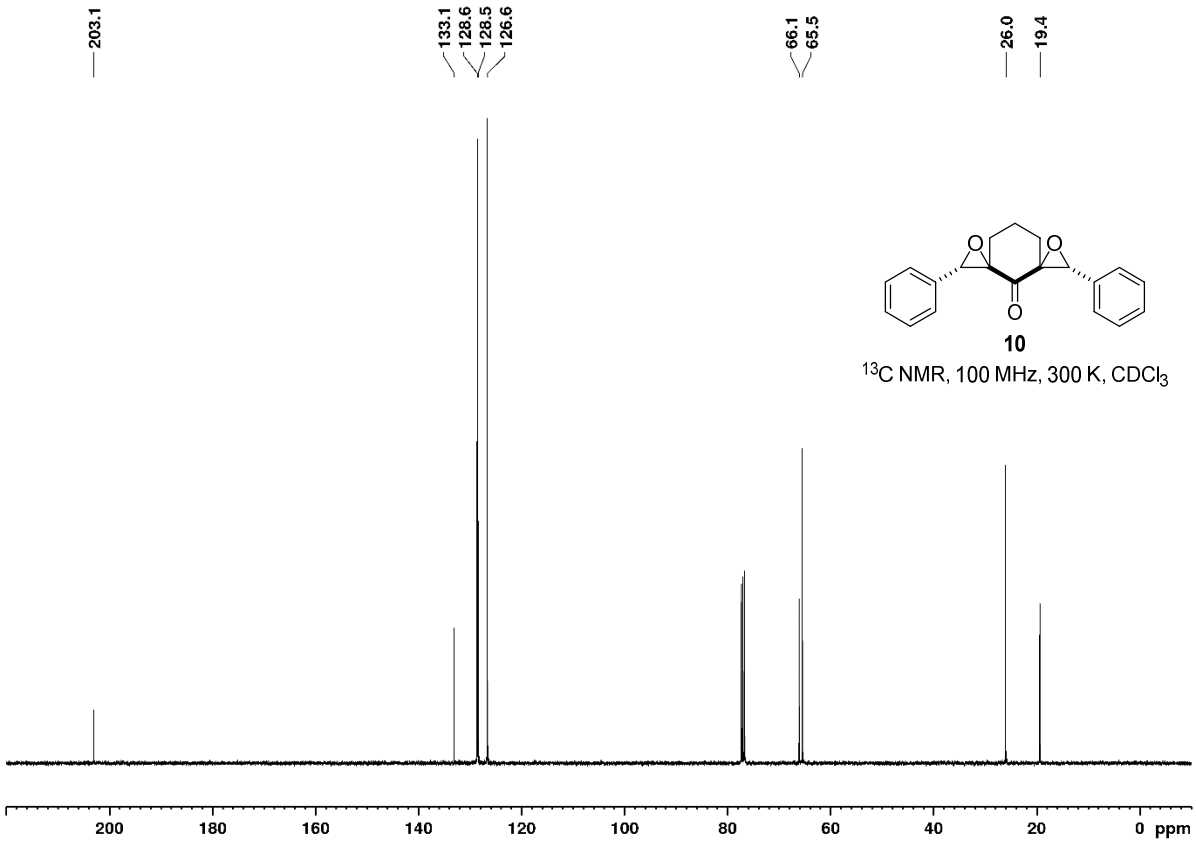

10

^{13}C NMR, 100 MHz, 300 K, $CDCl_3$

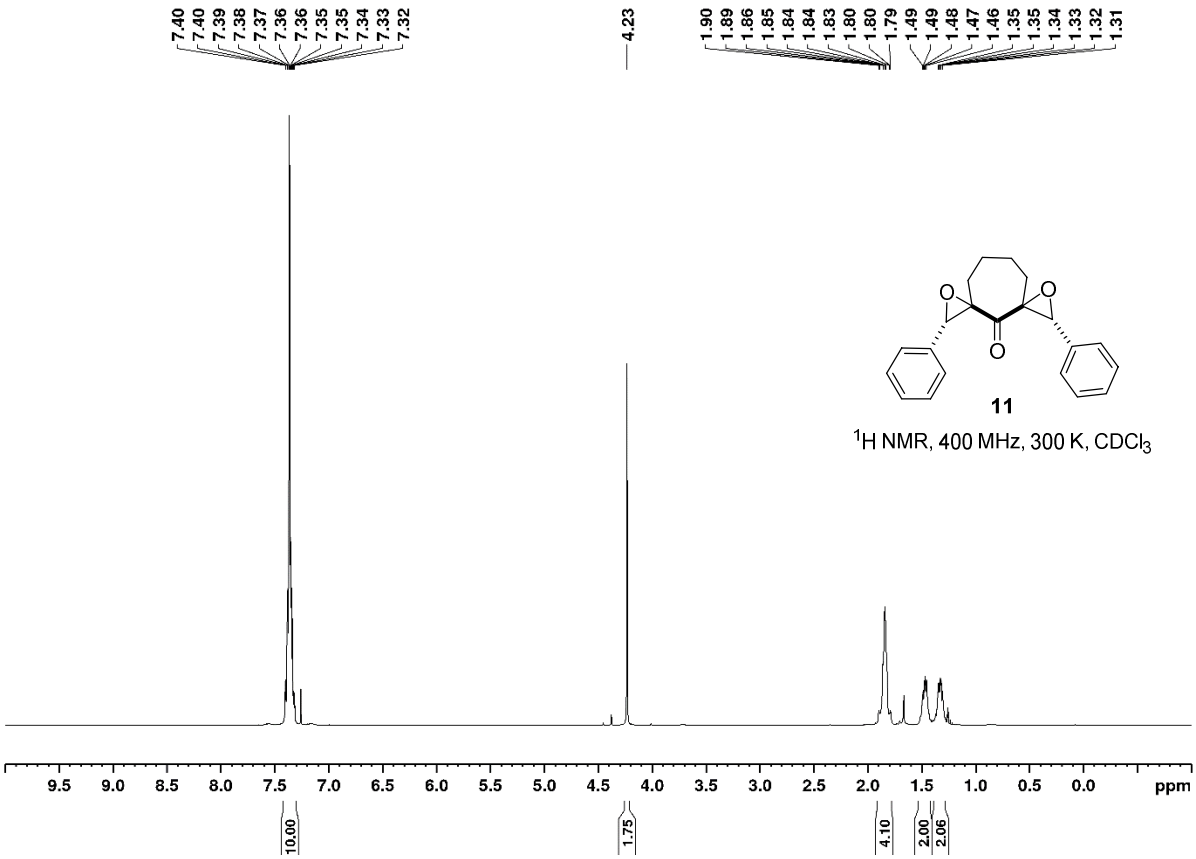

11

^{1}H NMR, 400 MHz, 300 K, $CDCl_3$

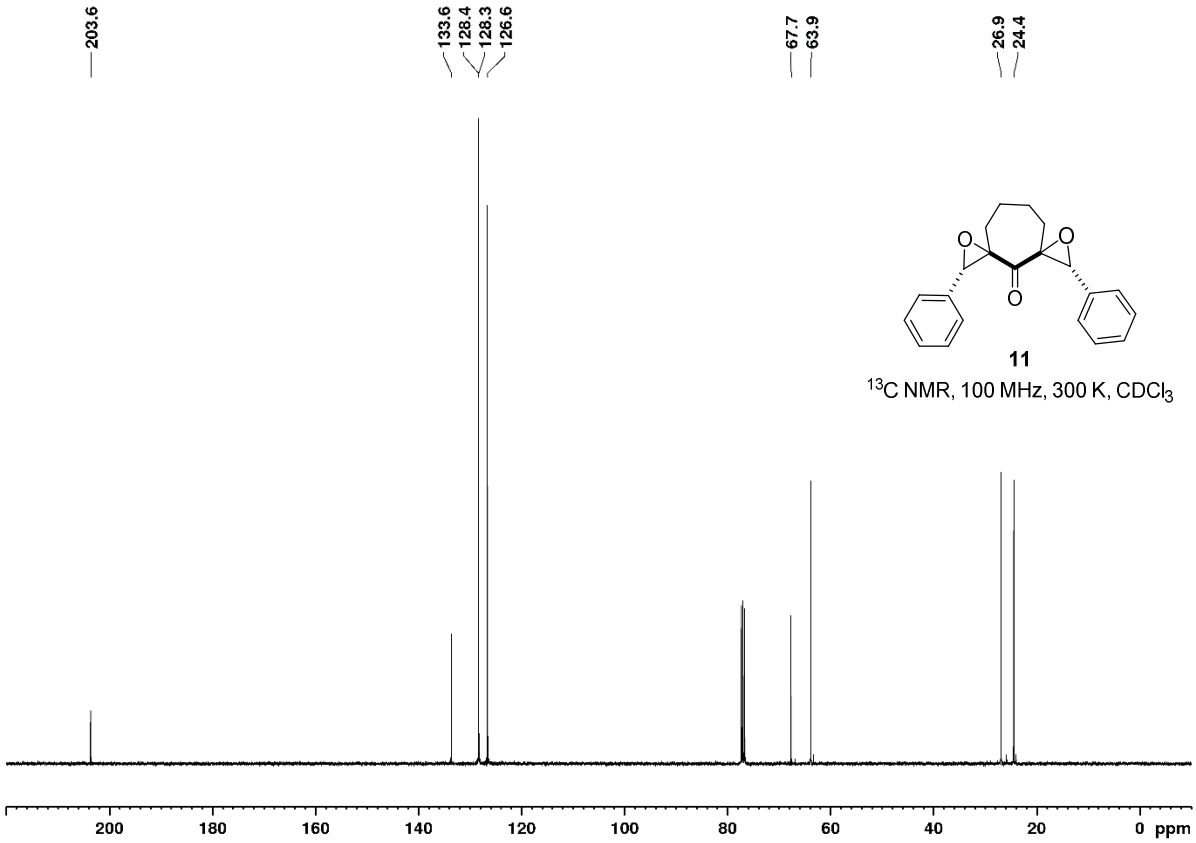

11

^{13}C NMR, 100 MHz, 300 K, $CDCl_3$

References

1 Lohans, C. T., Chan, H. T. H., Malla, T. R., Kumar, K., Kamps, J. J. A. G., McArdle, D. J. B., Van Groesen, E., de Munnik, M., Tooke, C. L., Spencer, J., Paton, R. S., Brem, J. & Schofield, C. J. Non-Hydrolytic β-Lactam Antibiotic Fragmentation by L,D-Transpeptidases and Serine β-Lactamase Cysteine Variants. *Angew. Chem. Int. Ed.* **58**, 1990-1994 (2019).

2 Malla, T. R., Tumber, A., John, T., Brewitz, L., Strain-Damerell, C., Owen, C. D., Lukacik, P., Chan, H. T. H., Maheswaran, P., Salah, E., Duarte, F., Yang, H., Rao, Z., Walsh, M. A. & Schofield, C. J. Mass spectrometry reveals potential of β-lactams as SARS-CoV-2 Mpro inhibitors. *Chem. Commun.* **57**, 1430-1433 (2021).

3 de Munnik, M., Lohans, C. T., Langley, G. W., Bon, C., Brem, J. & Schofield, C. J. A Fluorescence-Based Assay for Screening β-Lactams Targeting the *Mycobacterium tuberculosis* Transpeptidase Ldt_{Mt2}. *ChemBioChem* **21**, 368-372 (2020).

4 Van Berkel, S. S., Brem, J., Rydzik, A. M., Salimraj, R., Cain, R., Verma, A., Owens, R. J., Fishwick, C. W. G., Spencer, J. & Schofield, C. J. Assay Platform for Clinically Relevant Metallo-β-lactamases. *J. Med. Chem.* **56**, 6945-6953 (2013).

5 Malla, T. R., Brewitz, L., Muntean, D.-G., Aslam, H., Owen, C. D., Salah, E., Tumber, A., Lukacik, P., Strain-Damerell, C., Mikolajek, H., Walsh, M. A. & Schofield, C. J. Penicillin Derivatives Inhibit the SARS-CoV-2 Main Protease by Reaction with Its Nucleophilic Cysteine. *J. Med. Chem.* **65**, 7682-7696 (2022).

6 de Munnik, M., Lang, P. A., De Dios Antos, F., Cacho, M., Bates, R. H., Brem, J., Rodríguez-Miquel, B. & Schofield, C. J. High-Throughput Screen with the L,D-transpeptidase Ldt_{Mt2} of *Mycobacterium tuberculosis* Reveals Novel Classes of Covalently Reacting Inhibitors *Chem. Sci.* **14**, 7262-7278 (2023).

7 McCoy, A. J., Grosse-Kunstleve, R. W., Adams, P. D., Winn, M. D., Storoni, L. C. & Read, R. J. Phaser crystallographic software. *J. Appl. Crystallogr.* **40**, 658-674 (2007).

8 de Munnik, M., Lohans, C. T., Lang, P. A., Langley, G. W., Malla, T. R., Tumber, A., Schofield, C. J. & Brem, J. Targeting the *Mycobacterium tuberculosis* transpeptidase Ldt_{Mt2} with cysteine-reactive inhibitors including ebselen. *Chem. Commun.* **55**, 10214-10217 (2019).

9 Adams, P. D., Afonine, P. V., Bunkóczi, G., Chen, V. B., Davis, I. W., Echols, N., Headd, J. J., Hung, L.-W., Kapral, G. J., Grosse-Kunstleve, R. W., McCoy, A. J., Moriarty, N. W., Oeffner, R., Read, R. J., Richardson, D. C., Richardson, J. S., Terwilliger, T. C. & Zwart, P. H. PHENIX: a comprehensive Python-based system for macromolecular structure solution. *Acta Crystallogr. D* **66**, 213-221 (2010).

10 Emsley, P., Lohkamp, B., Scott, W. G. & Cowtan, K. Features and development of Coot. *Acta Crystallogr. D* **66**, 486-501 (2010).

11 Liebschner, D., Afonine, P. V., Moriarty, N. W., Poon, B. K., Sobolev, O. V., Terwilliger, T. C. & Adams, P. D. Polder maps: improving OMIT maps by excluding bulk solvent. *Acta Crystallogr. D* **73**, 148-157 (2017).

12 Palatinus, L. & Chapuis, G. SUPERFLIP – a computer program for the solution of crystal structures by charge flipping in arbitrary dimensions. *J. Appl. Crystallogr.* **40**, 786-790 (2007).

13 Parois, P., Cooper, R. I. & Thompson, A. L. Crystal structures of increasingly large molecules: meeting the challenges with CRYSTALS software. *Chem. Cent. J.* **9** (2015).

14 Cooper, R. I., Thompson, A. L. & Watkin, D. J. CRYSTALS enhancements: dealing with hydrogen atoms in refinement. *J. Appl. Crystallogr.* **43**, 1100-1107 (2010).

15 Gibson, D. G., Young, L., Chuang, R.-Y., Venter, J. C., Hutchison, C. A. & Smith, H. O. Enzymatic assembly of DNA molecules up to several hundred kilobases. *Nat. Methods* **6**, 343-345 (2009).

16 Arnold, A., Markert, M. & Mahrwald, R. Amine-Catalyzed Aldol Condensation in the Presence of Lithium Perchlorate. *Synthesis*, 1099-1102 (2006).

17 Weber, W. M., Hunsaker, L. A., Roybal, C. N., Bobrovnikova-Marjon, E. V., Abcouwer, S. F., Royer, R. E., Deck, L. M. & Vander Jagt, D. L. Activation of NFκB is inhibited by curcumin and related enones. *Bioorg. Med. Chem.* **14**, 2450-2461 (2006).

18 Yadav, V. K. & Kapoor, K. K. KF adsorbed on alumina effectively promotes the epoxidation of electron deficient alkenes by anhydrous t-BuOOH. *Tetrahedron* **52**, 3659-3668 (1996).

19 Davioud-Charvet, E., Wenzel, I. N., Muller, T. J. J., Hanquet, G., Lanfranchi, D. A., Leroux, F. & Gendron, T. Compounds useful against kinetoplastideae parasites. US9174960B2 (2015).

20 Ashtekar, K. D., Ding, X., Toma, E., Sheng, W., Gholami, H., Rahn, C., Reed, P. & Borhan, B. Mechanistically Inspired Route toward Hexahydro-2H-chromenes via Consecutive [4 + 2] Cycloadditions. *Org. Lett.* **18**, 3976-3979 (2016).

21 Aguilera, E., Varela, J., Birriel, E., Serna, E., Torres, S., Yaluff, G., De Bilbao, N. V., Aguirre-López, B., Cabrera, N., Díaz Mazariegos, S., De Gómez-Puyou, M. T., Gómez-Puyou, A., Pérez-Montfort, R., Minini, L., Merlino, A., Cerecetto, H., González, M. & Alvarez, G. Potent and Selective Inhibitors ofTrypanosoma cruziTriosephosphate Isomerase with Concomitant Inhibition of Cruzipain: Inhibition of Parasite Growth through Multitarget Activity. *ChemMedChem* **11**, 1328-1338 (2016).

22 Hasaninejad, A., Zare, A., Balooty, L., Mehregan, H. & Shekouhy, M. Solvent-Free, Cross-Aldol Condensation Reaction Using Silica-Supported, Phosphorus-Containing Reagents Leading to α,α′-Bis(arylidene)cycloalkanones. *Synth. Commun.* **40**, 3488-3495 (2010).

23 Weber, W. M., Hunsaker, L. A., Abcouwer, S. F., Deck, L. M. & Vander Jagt, D. L. Anti-oxidant activities of curcumin and related enones. *Bioorg. Med. Chem.* **13**, 3811-3820 (2005).

Appendix III. Supplementary information for Chapter 5.

Biochemical and crystallographic studies on the mechanism of the transpeptidase Ldt_{Mt2} from *Mycobacterium tuberculosis*

Manuscript III

Submitted manuscript.

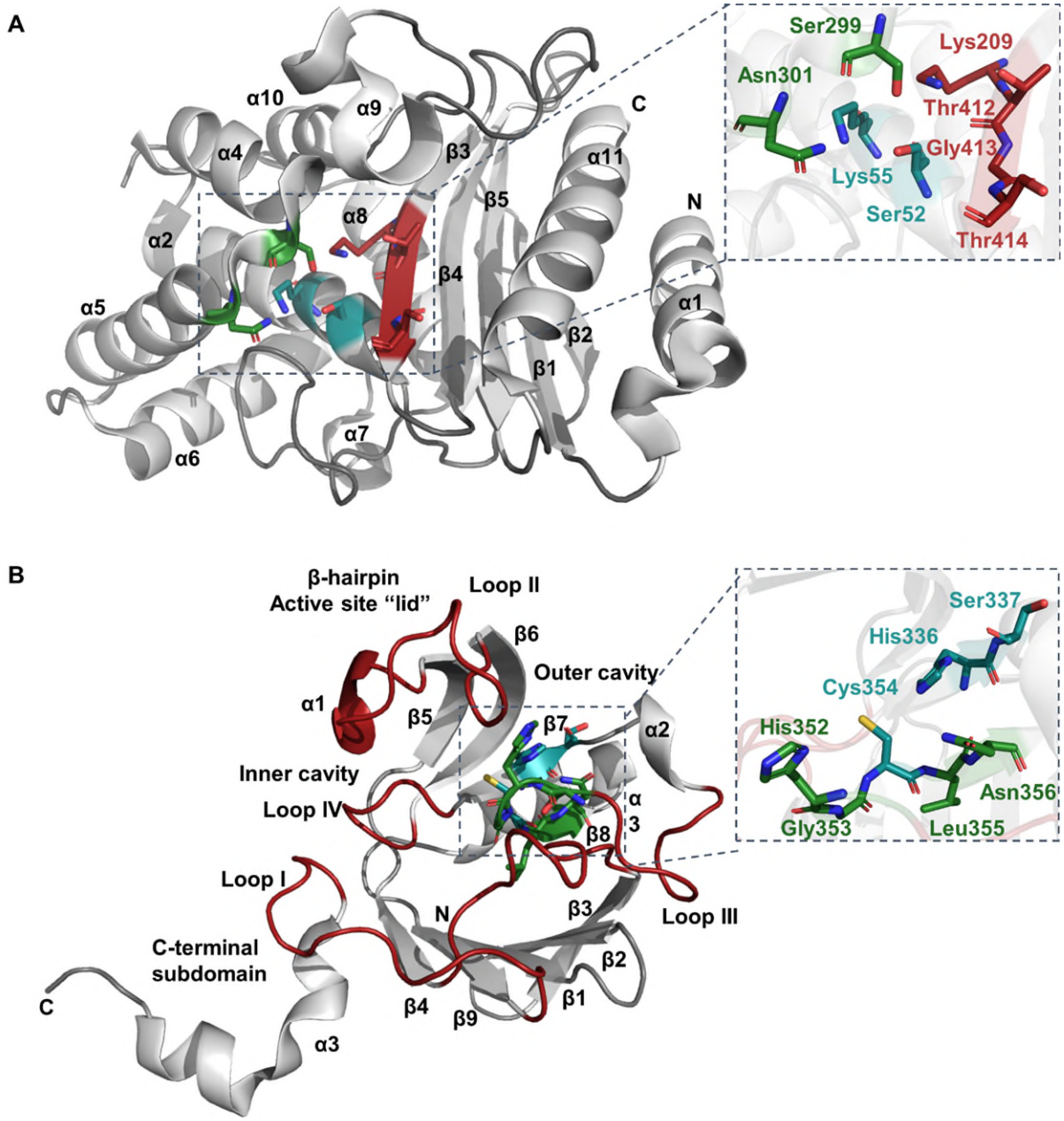

Figure S3.1. Views from structures of the transpeptidase domain of a representative D,D-transpeptidase (*B. subtilis* PBP4a) and a representative L,D-transpeptidase (*Mycobacterium tuberculosis* Ldt_{Mt2}). A. View of the *B. subtilis* PBP4a (PDB: 1W5D),[1] showing the common peptidase domain fold of PBPs (grey), as described by Sauvage *et al.*[2] The close up shows the highly conserved catalytic dyad SxxK motif (cyan) containing the nucleophilic serine, the SxN motif (green) that is involved in protonation of the β-lactam leaving group, and the KTG(S/T) motif (red) that is involved in substrate binding and forming an oxyanion hole. **B.** View of the *Mtb* Ldt_{Mt2} (PDB: 6RLG),[3] showing the common YkuD catalytic domain fold of Ldts (grey), the conserved $Hxx_{14–17}$(S/T)HGChN motif (green) with the catalytic triad residues (nucleophilic Cys354, His336 and Ser337) highlighted in teal, and loops I-IV (red), which are not highly conserved between Ldt variants.

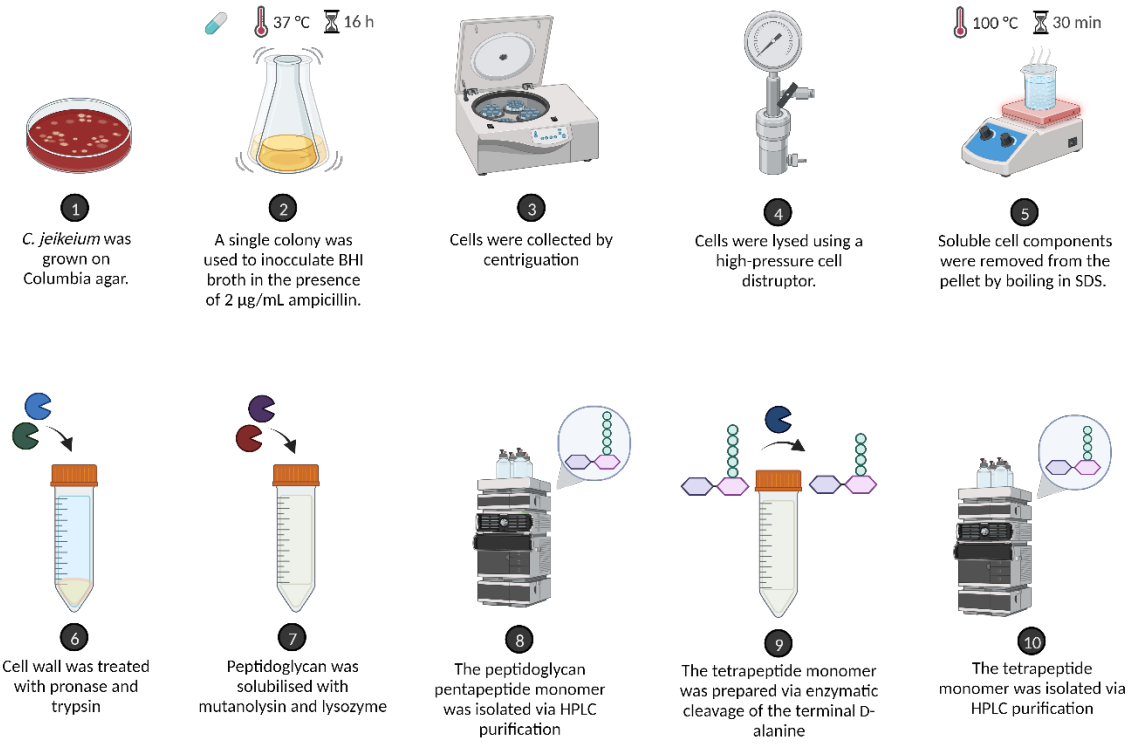

Figure S3.2. Method for the isolation of the tetrapeptide disaccharide monomer from the cell wall of *Corynebacterium jeikeium*. See Methods for experimental details.

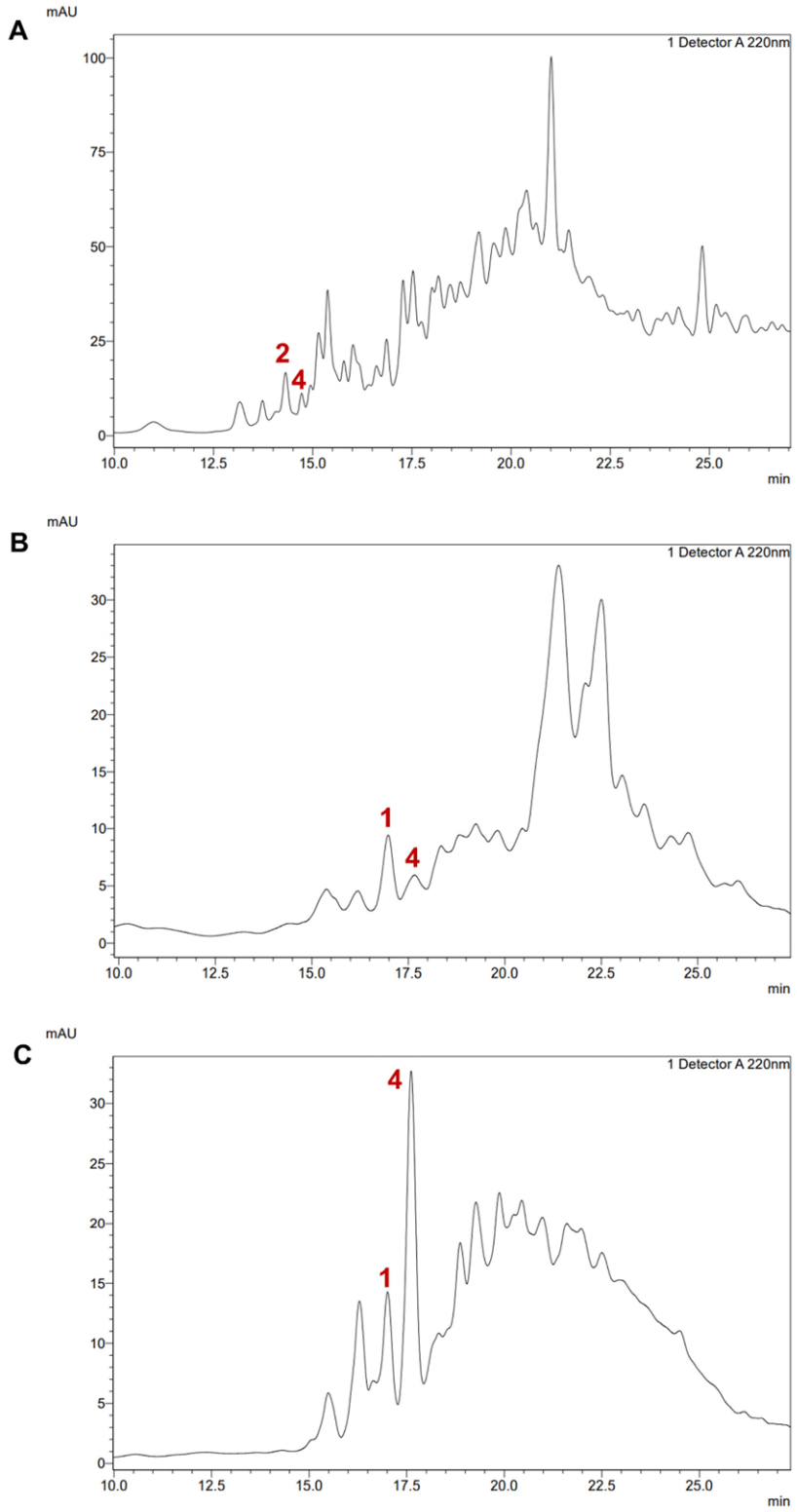

Figure S3.3. HPLC profiles of isolated peptidoglycan from lysed *Corynebacterium jeikeium* cells. **A.** HPLC profile of soluble peptidoglycan, where MurNAc has been reduced to muramitol via treatment of soluble peptidoglycan with sodium borohydride. **B.** HPLC profile of soluble peptidoglycan, omitting the MurNAc reduction step. **C.** HPLC profile of soluble peptidoglycan, when *C. jeikeium* was exposed to ampicillin, leading to overproduction of disaccharide pentapeptide. Structures of the numbered fragments are given in Figure 5.2. See Methods for experimental details.

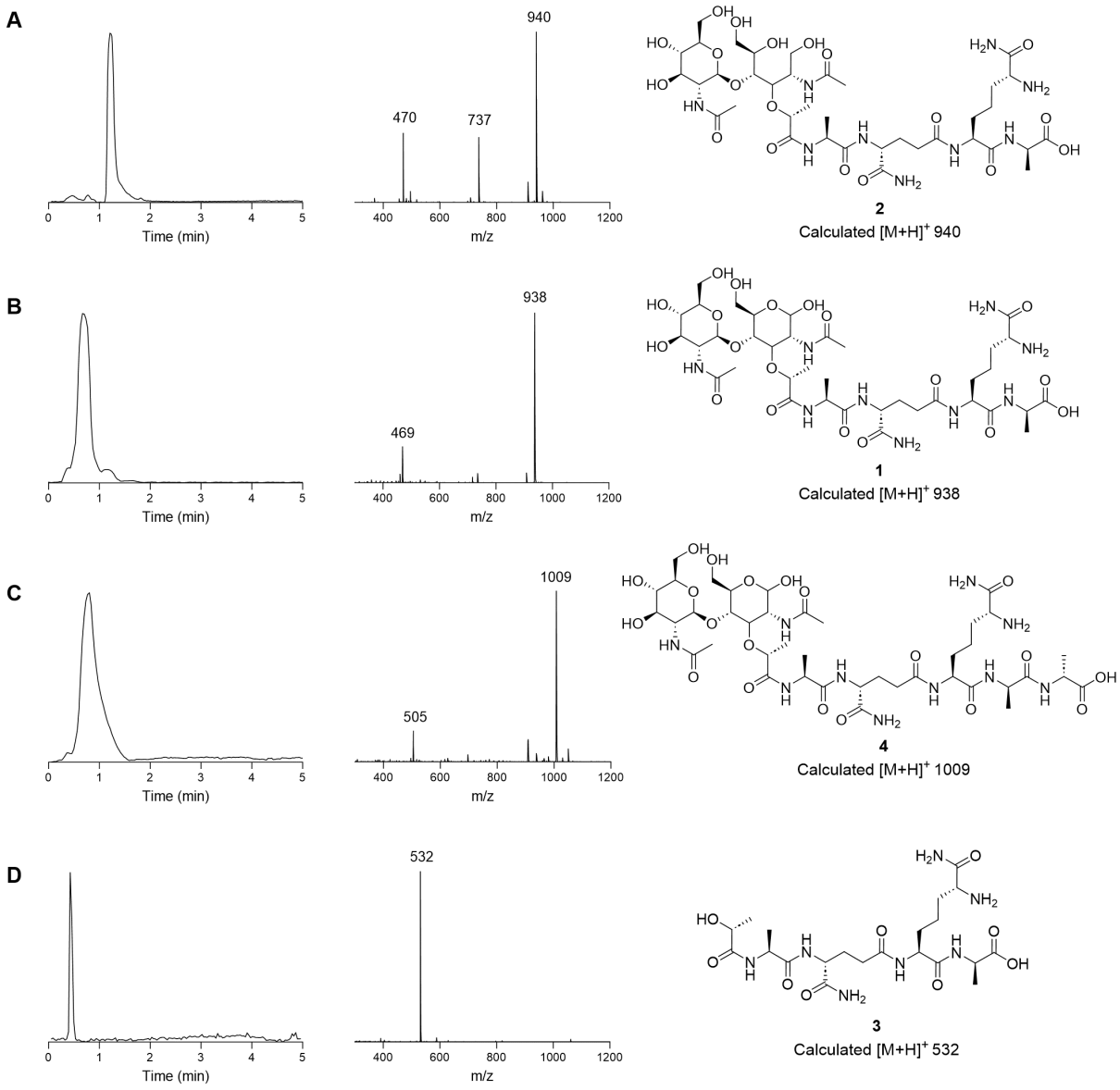

Figure S3.4. Liquid chromatography-mass spectrometry (LCMS) of peptidoglycan fragments isolated from lysed *Corynebacterium jeikeium* cells. A. LC (left) and MS (right) analyses of the isolated reduced disaccharide tetrapeptide **2**. **B.** LC (left) and MS (right) analyses of the isolated disaccharide tetrapeptide **1**. **C.** LC (left) and MS (right) analyses of the isolated disaccharide pentapeptide **4**. **D.** LC (left) and MS (right) analyses of the lactoyl tetrapeptide **3**, obtained from reaction with **1** (Figure S3.6). See Methods for experimental details.

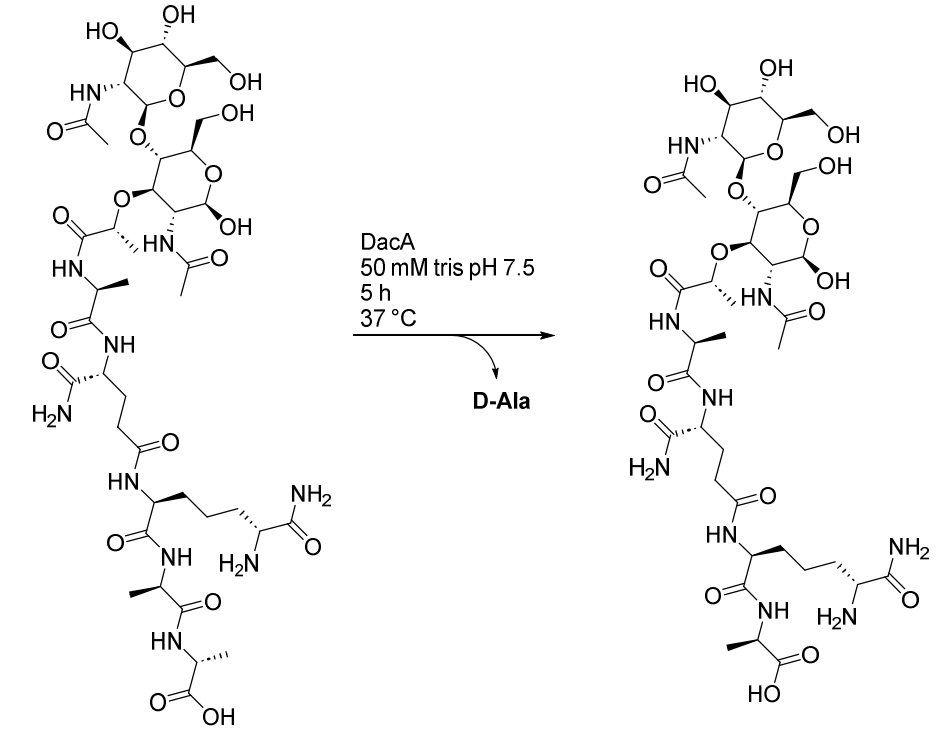

Disaccharide pentapeptide (4) **Disaccharide tetrapeptide (1)**

Figure S3.5. Reaction scheme for the formation of disaccharide tetrapeptide 1 from disaccharide pentapeptide 4. The disaccharide pentapeptide **4** was dissolved in 50 mM tris buffer, pH 7.5. To this solution was added the *E. coli* D,D-carboxypeptidase DacA (20 µM). This was incubated for 5 h at 37 °C. See Methods for experimental details.

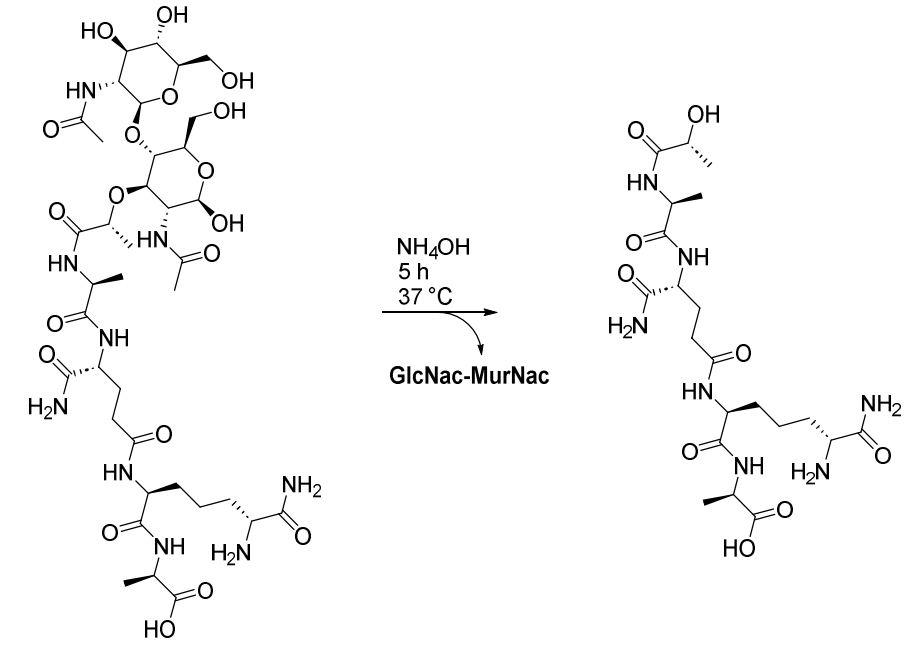

Figure S3.6. Reaction scheme for the formation of lactoyl tetrapeptide 3 from disaccharide tetrapeptide 1. The disaccharide tetrapeptide **1** was dissolved in 25% (*v/v*) NH_4OH in H_2O and incubated for 5 h at 37 °C. See Methods for experimental details.

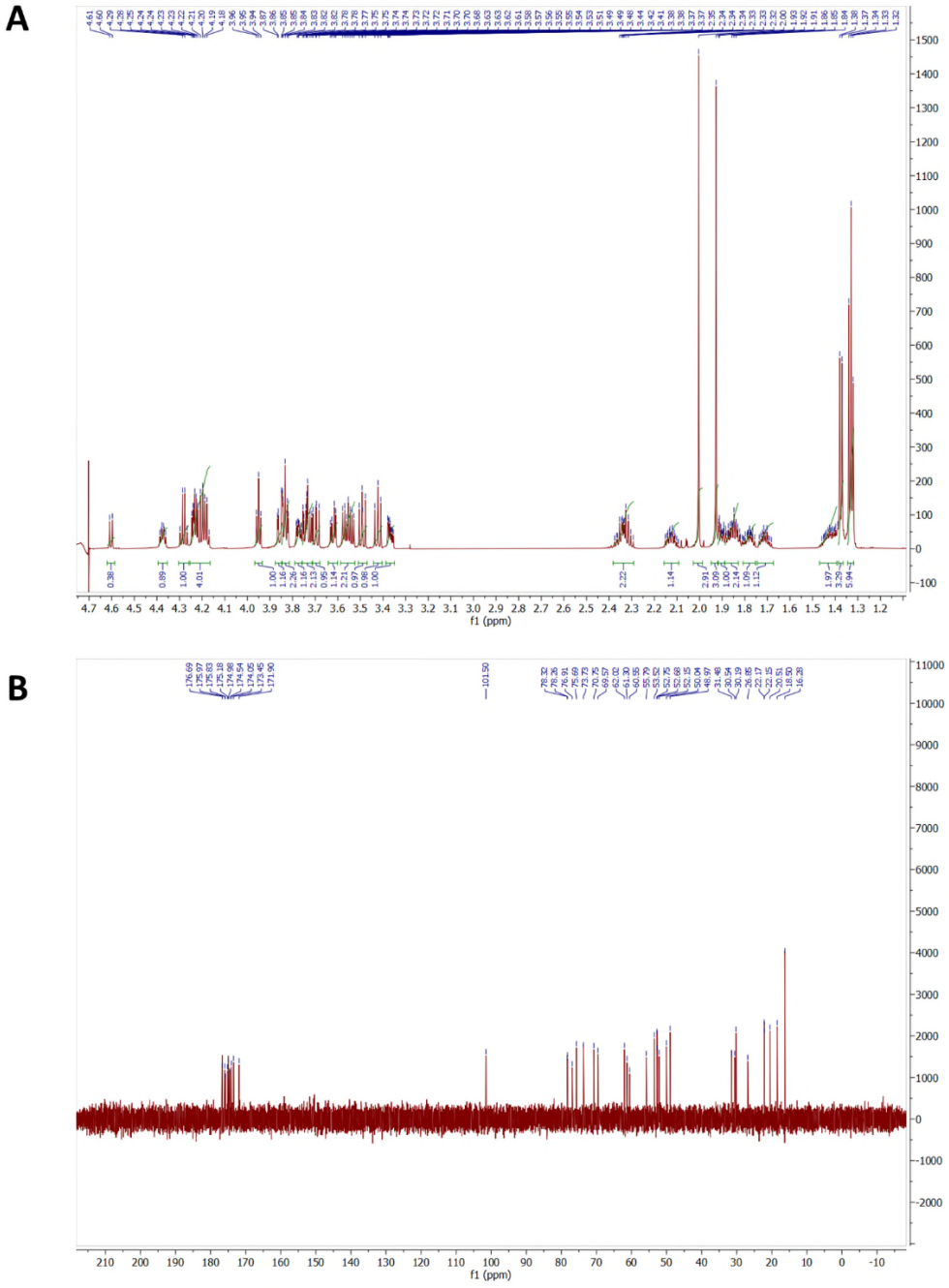

Figure S3.7. NMR characterisation (700 MHz) of substrate 2 in D_2O. [continues]

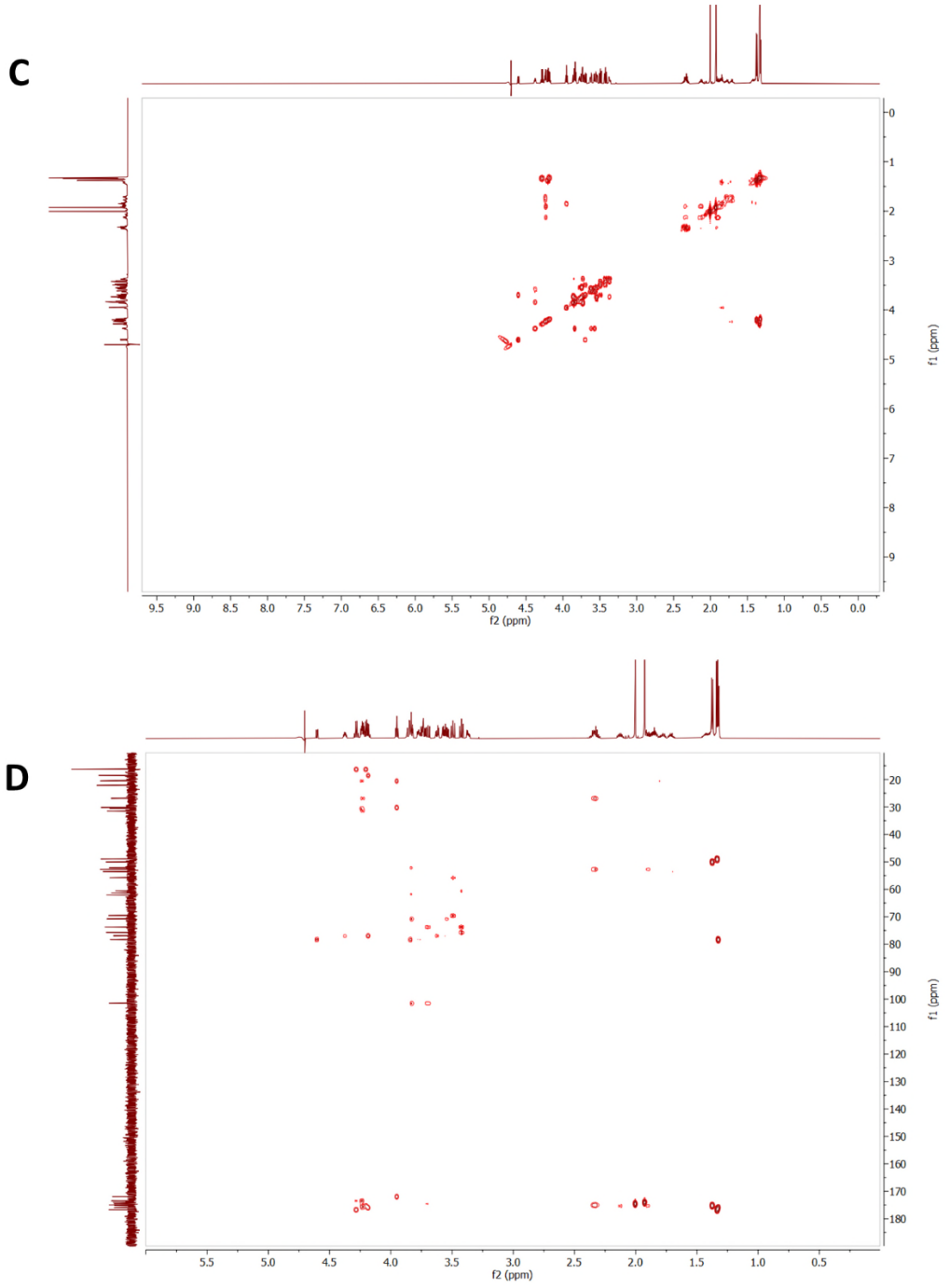

Figure S3.7. NMR characterisation (700 MHz) of substrate 2 in D_2O. [continues]

E

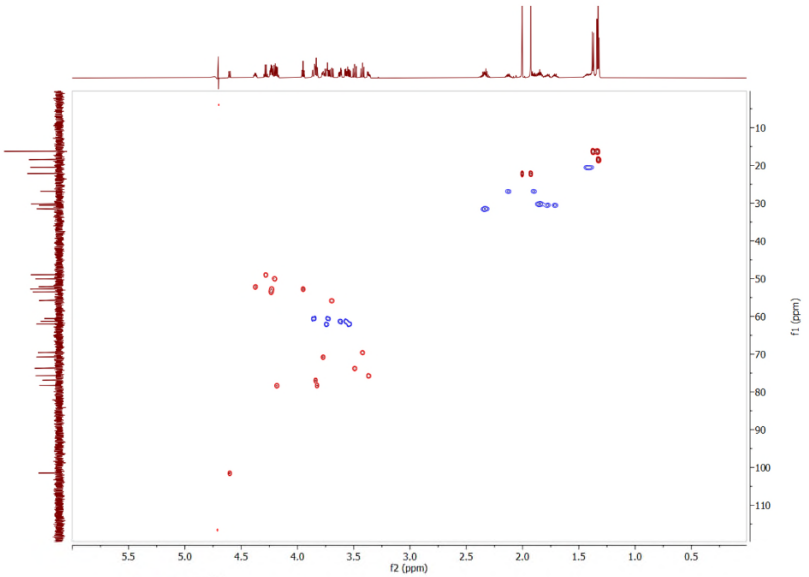

F

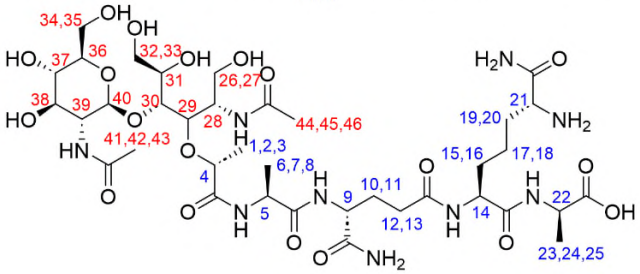

2

Chemical shift (ppm)	Multiplicity	Integration	Assignment
4.39 – 4.36	m	1H	28,29,30,31
4.28	q (*J* = 7.3 Hz)	1H	22
4.25 – 4.16	m	4H	4,5,9,14
3.95	t (*J* = 6.6 Hz)	1H	21
3.88 – 3.81	m	3H	28,29,30,31,34,35
3.79 – 3.76	m	1H	28,29,30,31
3.75 – 3.71	m	2H	26,27,32,33,34,35
3.71 – 3.68	m	1H	28,29,30,31
3.64 – 3.60	m	1H	26,27,32,33
3.59 – 3.53	m	2H	26,27,32,33,34,35
3.49	dd (*J* = 11.9, 4.4 Hz)	1H	36,37,38,39,40
3.44 – 3.40	m	1H	36,37,38,39,40
3.38 – 3.35	m	1H	36,37,38,39,40
2.38 – 2.29	m	2H	10,11
2.16 – 2.09	m	1H	12,13
2.00	s	3H	41,42,43,44,45,46
1.93	s	3H	41,42,43,44,45,46
1.92 – 1.89	m	1H	12,13
1.88 – 1.82	m	2H	19,20
1.81 – 1.75	m	1H	15,16
1.74 – 1.68	m	1H	15,16
1.47 – 1.39	m	2H	17,18
1.38	d (*J* = 7.3 Hz)	3H	6,7,8
1.35 – 1.32	m	6H	1,2,3,23,24,25

Figure S3.7. NMR characterisation (700 MHz) of substrate 2 in D_2O. NMR analyses of **2**, obtained from isolation of the cell wall of *C. jeikeium*, comprised of ^{1}H (**A**), ^{13}C (**B**), COSY (**C**), HMBC (**D**) and HSQC (**E**). **F.** Structure of **2** labelled with assignments. Note that assignment of the GlcNAc-muramitol unit (red) is complicated by overlapping peaks. See Methods for experimental details.

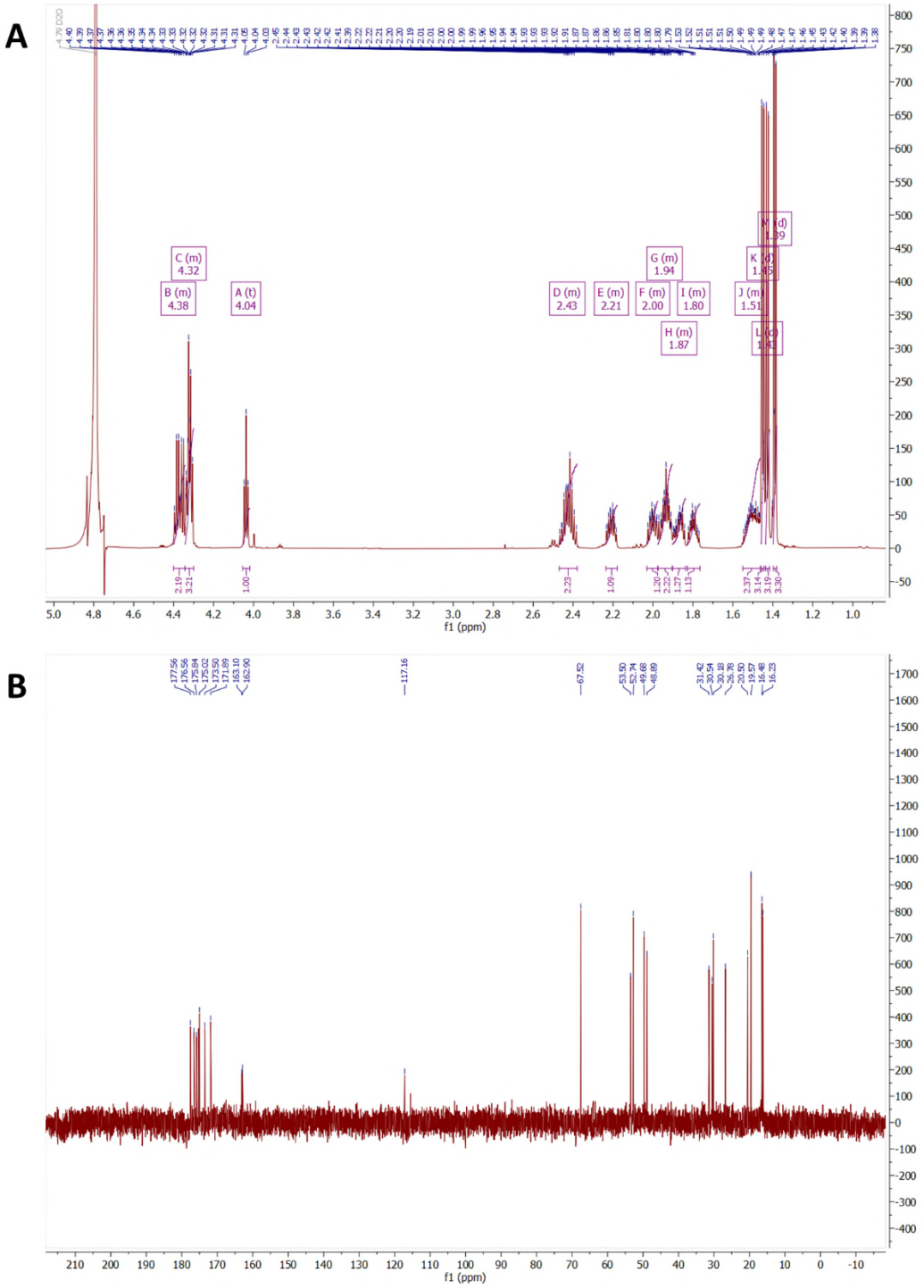

Figure S3.8. NMR characterisation (700 MHz) of substrate 3 in D_2O. [continues]

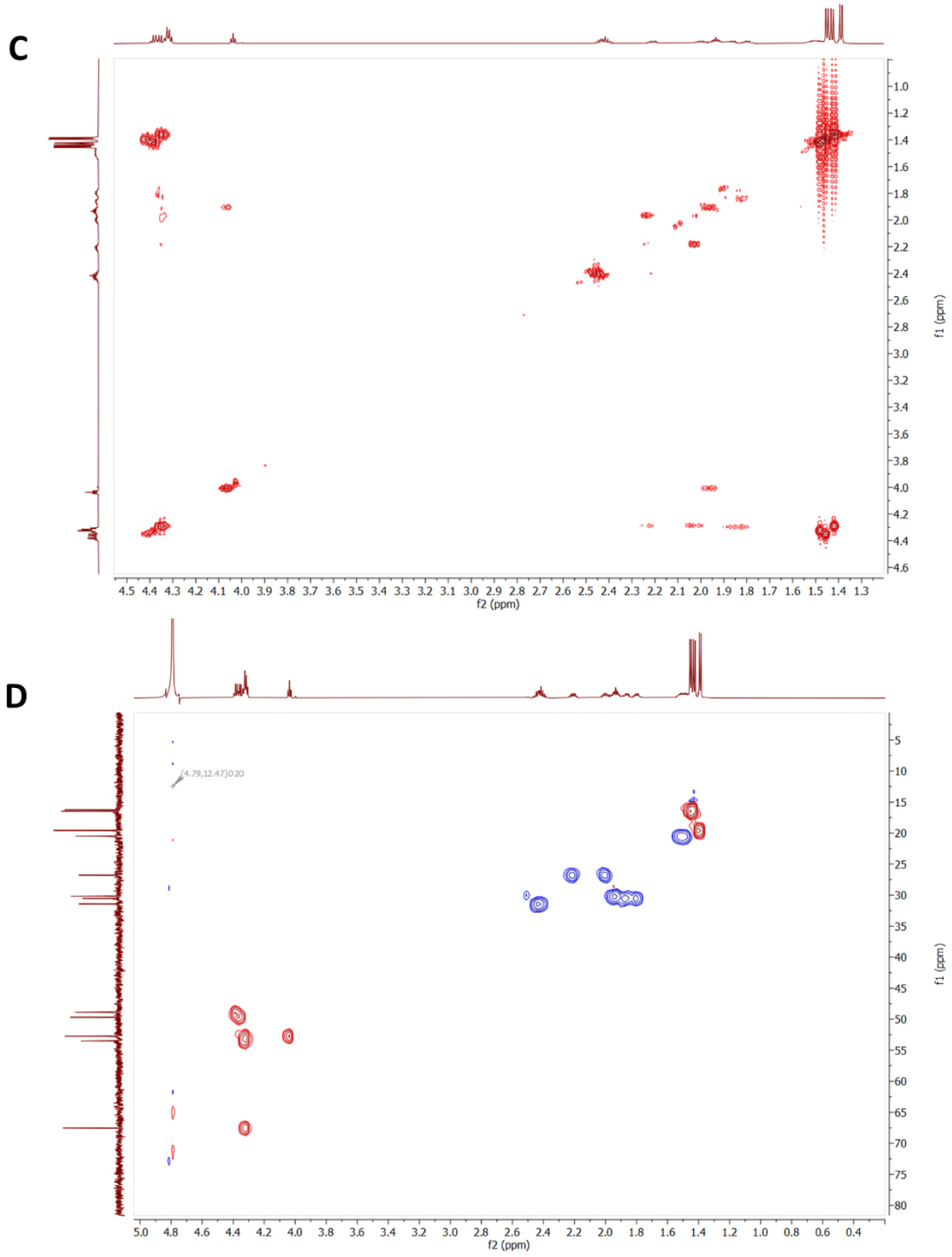

Figure S3.8. NMR characterisation (700 MHz) of substrate 3 in D_2O. [continues]

E

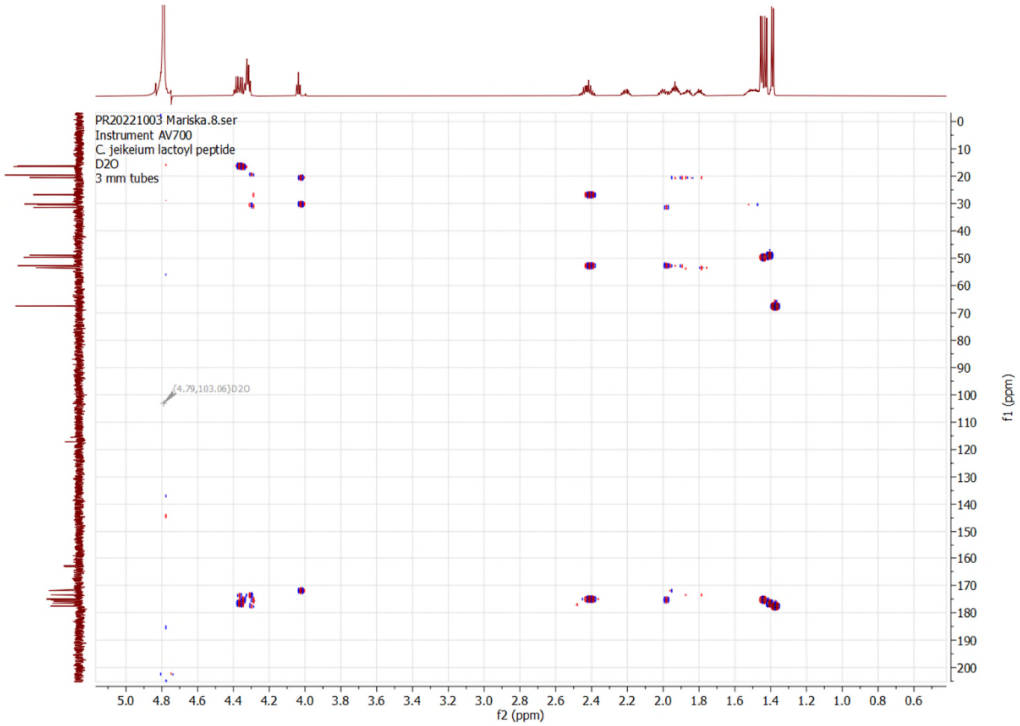

F

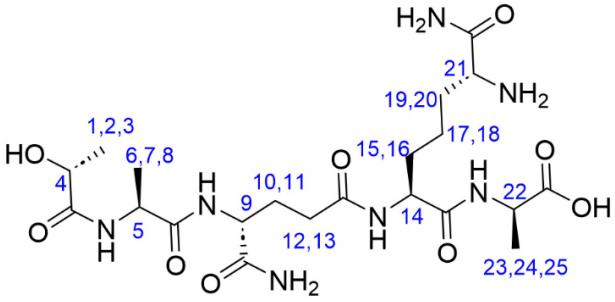

3

Chemical shift (ppm)	Multiplicity	Integration	Assignment
4.40 – 4.35	m	2H	5,22
4.35 – 4.30	m	3H	4,9,14
4.04	t (*J* = 6.6 Hz)	1H	21
2.47 – 2.38	m	2H	10,11
2.23 – 2.18	m	1H	12,13
2.03 – 1.98	m	1H	12,13
1.97 – 1.91	m	2H	19,20
1.90 – 1.84	m	1H	15,16
1.82 – 1.77	m	1H	15,16
1.55 – 1.47	m	2H	17,18
1.45	d (*J* = 7.21 Hz)	3H	6,7,8
1.43	d (*J* = 7.32 Hz)	3H	23,24,25
1.39	d (*J* = 6.91 Hz)	3H	1,2,3

Figure S3.8. NMR characterisation (700 MHz) of substrate 3 in D_2O. NMR analyses of **3**, obtained from isolation of the cell wall of *C. jeikeium*, comprised of ^{1}H (**A**), ^{13}C (**B**), COSY (**C**), HMBC (**D**) and HSQC (**E**). **F.** Structure of **3** labelled with assignments. See Methods for experimental details.

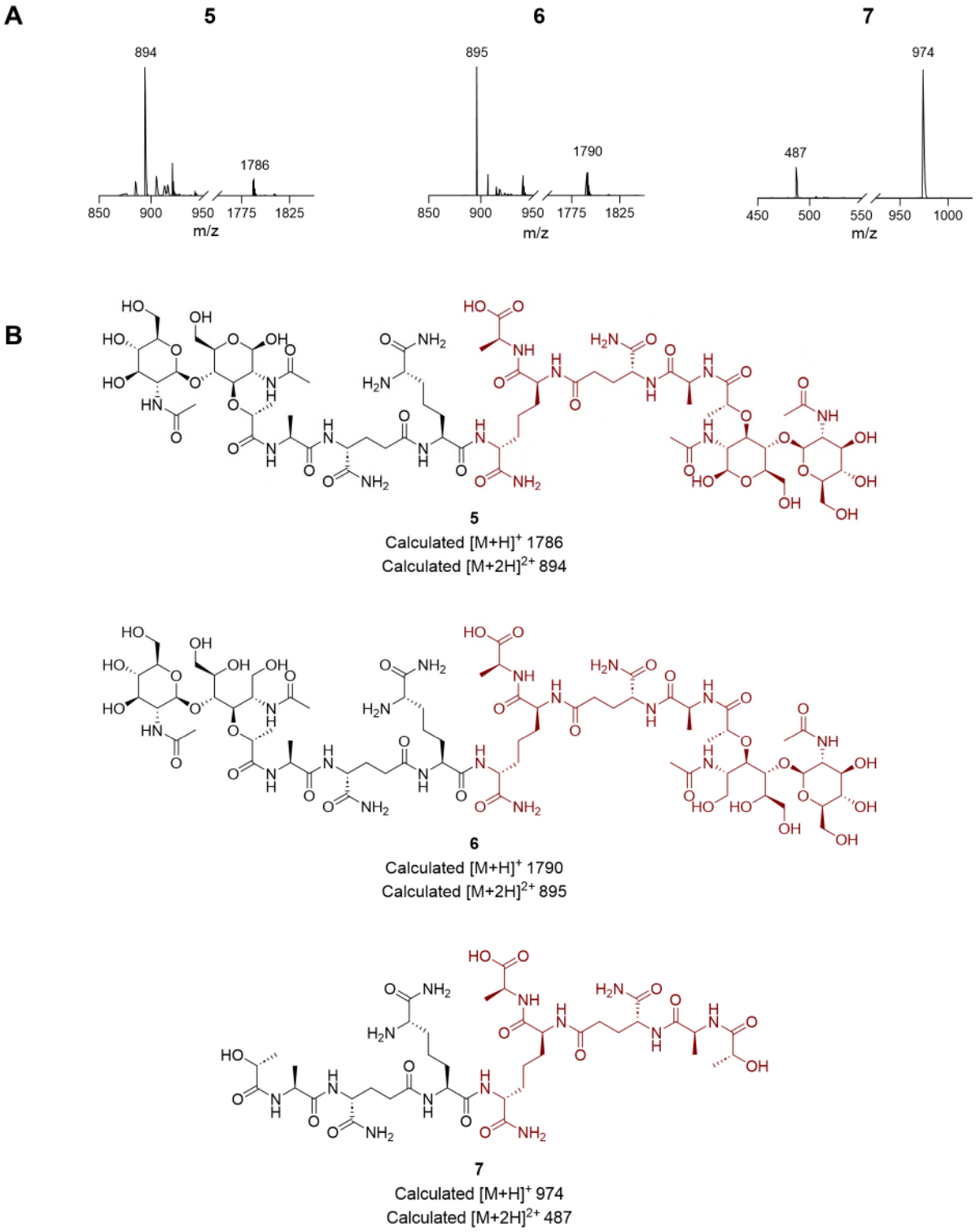

Figure S3.9. Mass spectrometric analyses of transpeptidase activity of Ldt_{Mt2}. A. MS analysis of Ldt_{Mt2} (5 µM) and **1**, **2** or **3** (100 µM) in 50 mM tris pH 7.5, after 2 hours of incubation at 37 °C show the formation of transpeptidase products **5**, **6**, and **7**, respectively. For **5**, **6** and **7**, both the $[M+H]^+$ and $[M+2H]^{2+}$ masses were observed. See the Methods section for details. Structures of **1**, **2** and **3** are given in Figure 5.2. **B.** Structures and calculated masses for **5**, **6** and **7**.

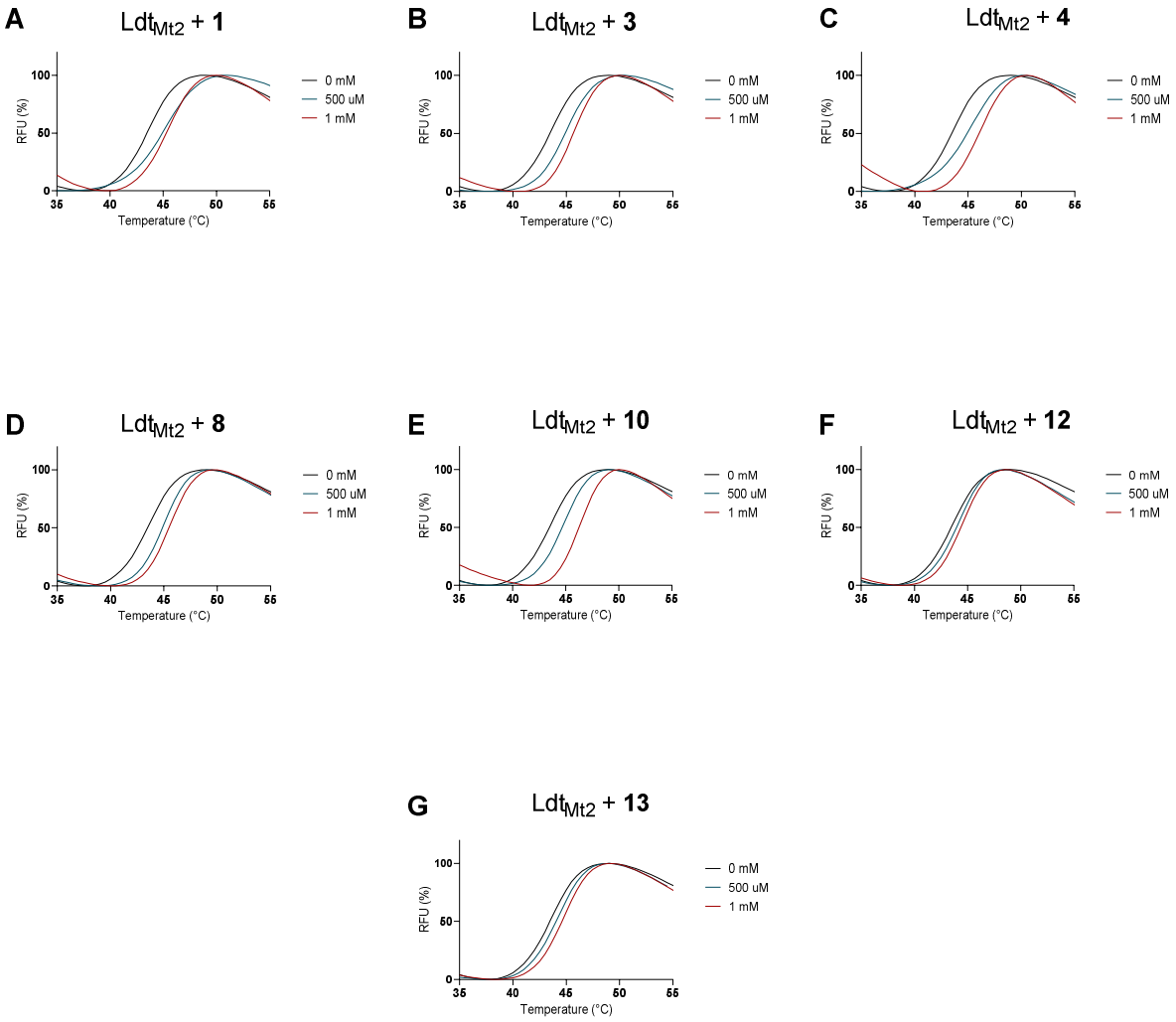

Figure S3.10. Differential scanning fluorimetry thermal shift curves for Ldt_{Mt2} in the presence of 1, 3, 4, 8, 10, 12, and 13. Ldt_{Mt2} (5 µM) was incubated with peptidoglycan fragments (500 µM or 1 mM), or only in buffer (50 mM tris pH 7.5) for unmodified Ldt_{Mt2}, for 30 minutes at room temperature, after which SYPRO Orange (final concentration 6x, according to manufacturer's definition, Invitrogen) was added. Melting temperatures (T_ms) are provided in Table S3.1. Structures of **1**, **3**, **4**, **8**, **10**, **12** and **13** are given in Figure 5.2. See Methods for experimental details.

Table S3.2. Melting temperatures of Ldt_{Mt2} when treated with 1, 3, 4, 8, 10, 12 or 13. The melting temperatures were obtained in three independent repeats, all of which yielded equal results. Values in brackets represent the shift in melting temperature compared to unmodified Ldt_{Mt2}. Values in blue represent a significant change in melting temperature compared to unmodified Ldt_{Mt2} (Δ 2°C).[4] Structures of **1**, **3**, **4**, **8**, **10**, **12** and **13** are given in Figure 5.2.

Compound	T_m 500 µM	T_m 1 mM
1	45 (+1.5)	45.5 (+2.0)
3	45 (+1.5)	45.5 (+2.0)
4	45.5 (+2.0)	46 (+2.5)
8	45 (+1.5)	45.5 (+2.0)
10	45 (+1.5)	46.5 (+3.0)
12	44 (+0.5)	44.5 (+1.0)
13	44.5 (+1.0)	45 (+1.5)

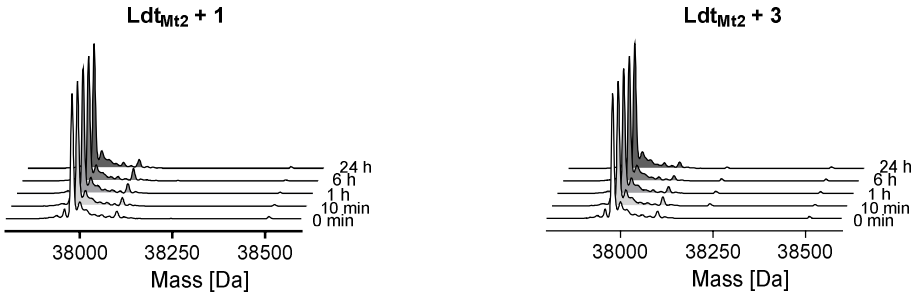

Figure S3.11. Protein-observed solid-phase extraction mass spectrometric studies of the covalent interaction between Ldt$_{Mt2}$ and tetrapeptides 1 or 3. Ldt$_{Mt2}$ (1 µM) was combined with tetrapeptide **1** or **3** (100 µM), and samples were analysed after the indicated times. Deconvoluted spectra, obtained using the maximum entropy algorithm in the MassHunter Workstation Qualitative Analysis B.07.00 program (Agilent), are shown.

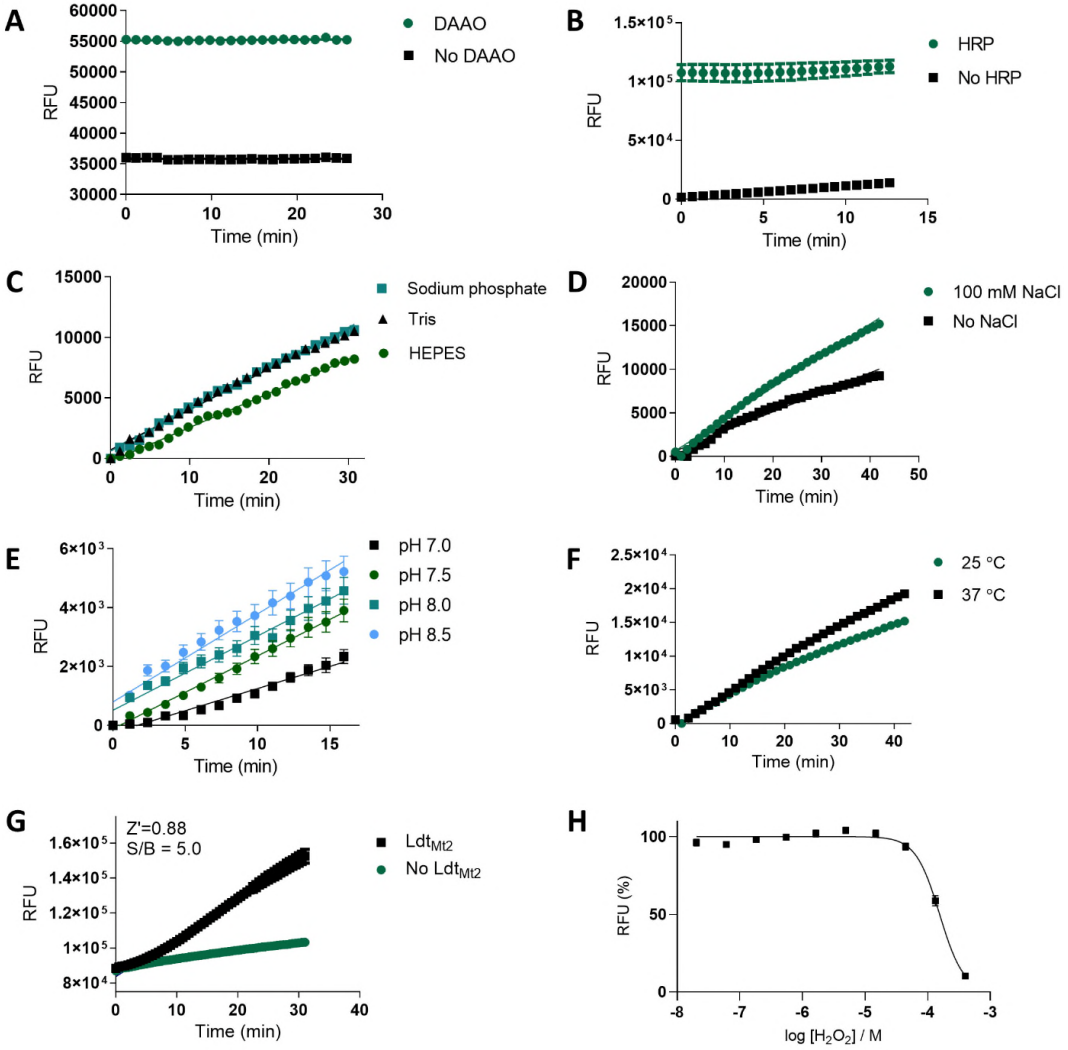

Figure S3.12. Transpeptidase assay optimisation. A. D-Ala (1 nM) is efficiently oxidised in the presence of D-amino acid oxidase (DAAO; 2 U/mL), horseradish peroxidase (HRP; 2 U/mL), flavin adenine dinucleotide (FAD; 40 μM) and Amplex red (10 μM) in 50 mM sodium phosphate pH 7.5. **B.** H_2O_2 was rapidly converted in the presence of HRP (2 U/mL) and Amplex red (10 μM) in 50 mM sodium phosphate pH 7.5. **C.** The transpeptidase activity of Ldt$_{Mt2}$ (500 nM) with substrate **1** (35 μM) was assessed in sodium phosphate, tris, and HEPES (50 mM pH 7.5). **D.** The transpeptidase activity of Ldt$_{Mt2}$ (500 nM) with substrate **1** (35 μM) was assessed in 50 mM sodium phosphate pH 7.5, with and without the presence of 100 mM NaCl. **E.** The transpeptidase activity of Ldt$_{Mt2}$ (500 nM) with substrate **1** (35 μM) was assessed in 50 mM sodium phosphate pH with 100 mM NaCl, at pH 7.0-8.5. **F.** The transpeptidase activity of Ldt$_{Mt2}$ (500 nM) with substrate **1** (35 μM) was assessed in 50 mM sodium phosphate pH with 100 mM NaCl, pH 8.0 with incubation temperatures of 25 °C or 37 °C. **G.** The transpeptidase assay of Ldt$_{Mt2}$ (500 nM) with substrate **1** (35 μM) in 50 mM sodium phosphate pH 8.0 with 100 mM NaCl, with incubation at 37 °C. **H.** Dose-response assay of Ldt$_{Mt2}$ with H_2O_2, using the thiol-reactive fluorogenic probe assay for Ldt$_{Mt2}$.[5] Assays in **C**-**G** were performed in the presence of DAAO (2 U/mL), HRP (2 U/mL), FAD (40 μM) and Amplex red (10 μM). See Methods for experimental details.

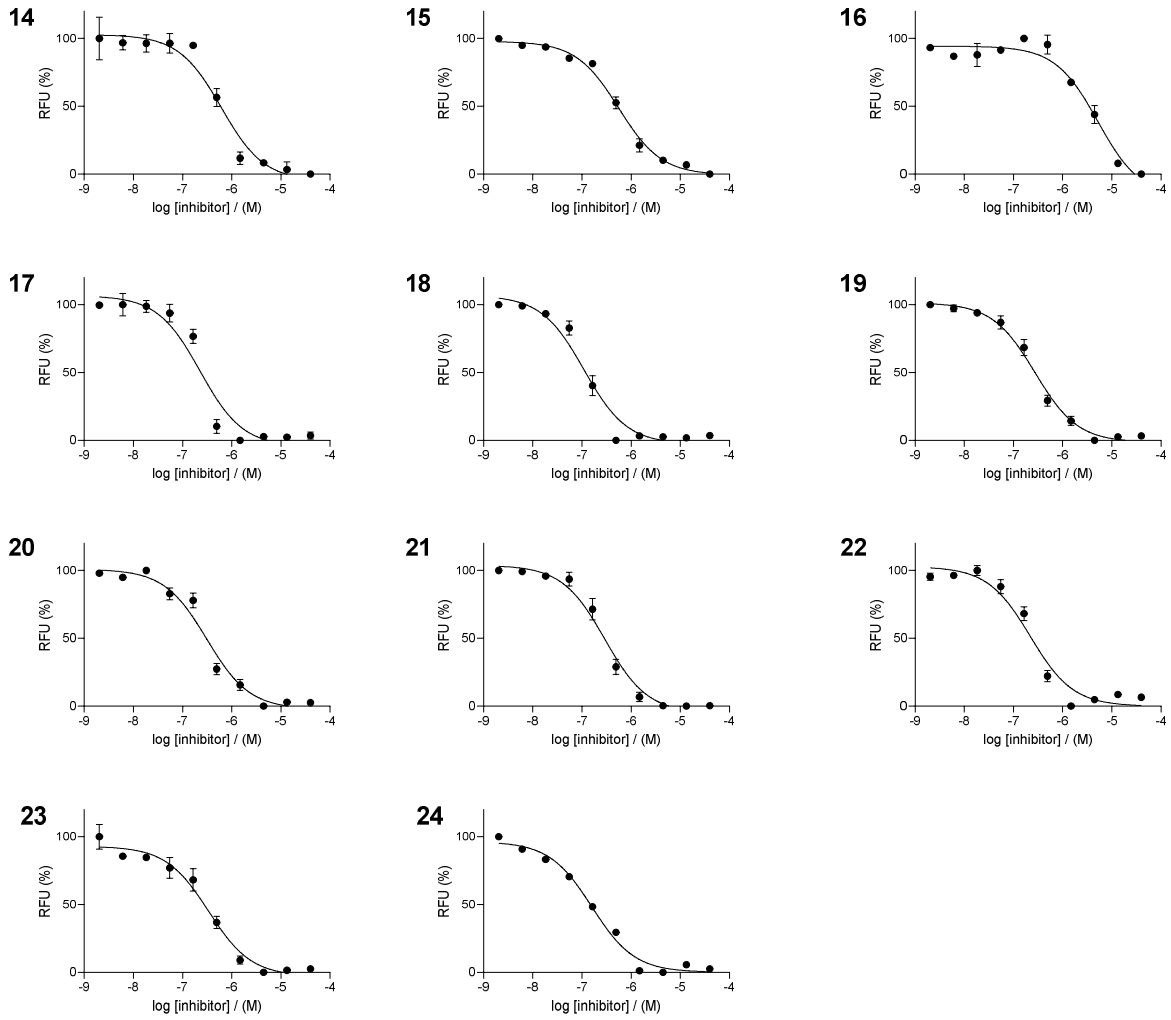

Figure S3.13. Dose-response curves for inhibition of Ldt_{Mt2} using the transpeptidase assay with compounds 14-24. Ldt_{Mt2} (500 nM) was incubated with the specified inhibitor for 30 minutes at room temperature, after which time the activity was assessed using **1** (35 μM) in the presence of DAAO (2 U/mL), HRP (2 U/mL), FAD (40 μM) and Amplex red (10 μM) in 50 mM sodium phosphate pH 8.0 with 100 mM NaCl at 37 °C. The pIC_{50} values and structures of the compounds are provided in Table S3.2. See Methods for experimental details.

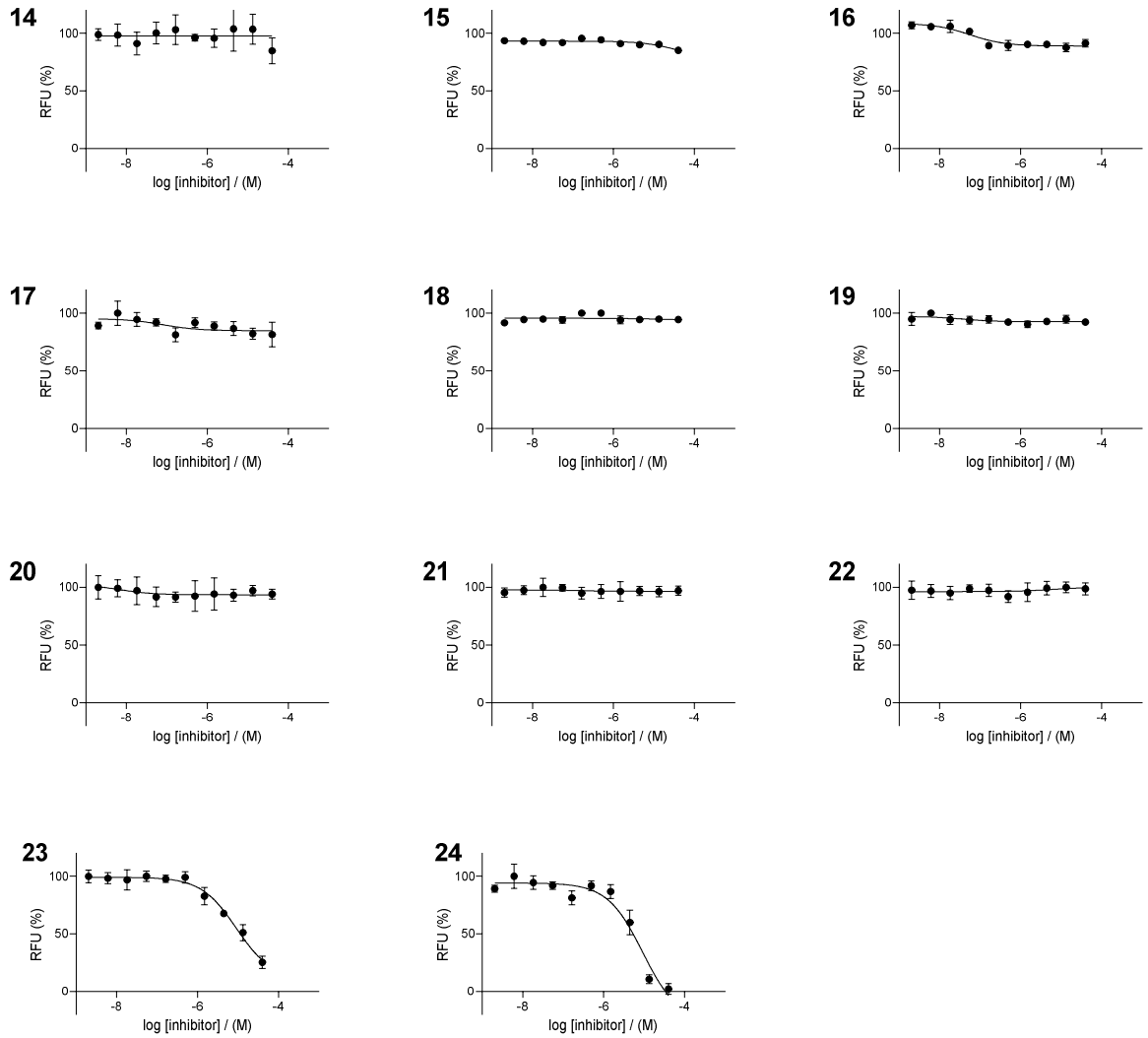

Figure S3.14. Dose-response curves of the transpeptidase interference assay with compounds 14-24. The specified inhibitors were incubated with DAAO (2 U/mL), HRP (2 U/mL), FAD (40 μM) and Amplex red (10 μM) in 50 mM sodium phosphate pH 8.0 with 100 mM NaCl at room temperature for 30 minutes, after which time D-alanine (500 nM) was added. The pIC_{50} values and compound structures are shown in Table S3.2. See Methods for experimental details.

Table S3.2. pIC_{50} values of 14-24 for Ldt_{Mt2} obtained using: (i) the transpeptidase activity assay, (ii) the thiol-reactive fluorescent probe assay,[6] and (iii) the transpeptidase interference assay. Assays were performed in quadruplicate. Errors represent standard deviation. See Methods for experimental details.

Compound	Structure	Transpeptidase activity assay pIC_{50} (mean ± SD)	Fluorogenic probe assay pIC_{50} (mean ± SD)	Transpeptidase interference assay pIC_{50} (mean ± SD)
14 (Meropenem)	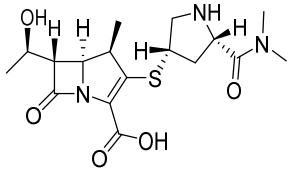	6.2 ± 0.2	5.9 ± 0.04	<4.0
15 (Faropenem)	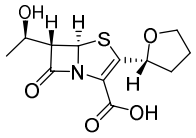	6.3 ± 0.1	6.4 ± 0.03	<4.0
16	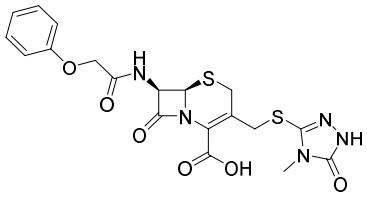	5.3 ± 0.2	5.6 ± 0.1	<4.0
17	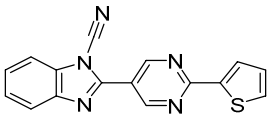	6.6 ± 0.3	7.3 ± 0.06	<4.0
18	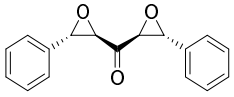	6.9 ± 0.3	7.2 ± 0.1	<4.0
19	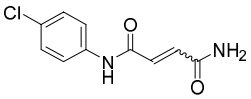	6.6 ± 0.1	6.4 ± 0.08	<4.0
20	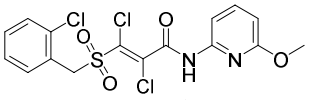	6.5 ± 0.3	7.2 ± 0.04	<4.0
21	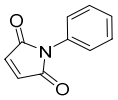	6.5 ± 0.2	7.2 ± 0.03	<4.0
22	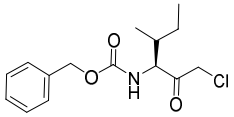	6.7 ± 0.3	7.1 ± 0.01	<4.0
23	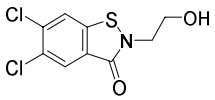	6.5 ± 0.2	8.0 ± 0.04	5.0 ± 0.2
24 (Ebselen)	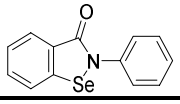	6.8 ± 0.2	6.7 ± 0.04	5.0 ± 0.4

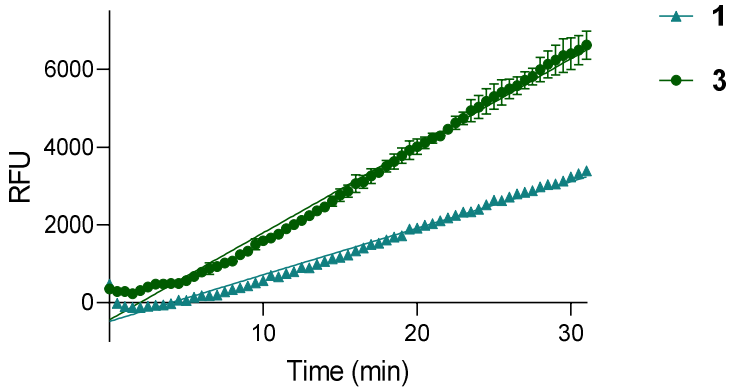

Figure S3.15. Activity of Ldt_{Mt2} with 1 and 3 assessed using the transpeptidase fluorescence assay. Ldt_{Mt2} (500 nM) activity was assayed using **1** or **3** (35 μM) in the presence of DAAO (2 U/mL), HRP (2 U/mL), FAD (40 μM) and Amplex red (10 μM) in 50 mM sodium phosphate pH 8.0 with 100 mM NaCl at 37 °C. Assays were performed in quadruplicate. Errors represent standard deviation. See Methods for experimental details.

Table S3.3. Enzyme kinetics of Ldt_{Mt2} with substrates 1 and 3. Ldt_{Mt2} (500 nM) activity was assayed using varying concentrations of **1** or **3** in the presence of DAAO (2 U/mL), HRP (2 U/mL), FAD (40 μM) and Amplex red (10 μM) in 50 mM sodium phosphate pH 8.0 with 100 mM NaCl at 37 °C. See Methods for experimental details.

	K_m (M), x 10^{-3}	V_{max} (M min^{-1}), x 10^{-8}	k_{cat} (min^{-1}), x 10^{-2}	k_{cat}/K_M (min^{-1} M^{-1})
1	Ambiguous	Ambiguous	-	-
3	6.2 ± 1.3	1.4 ± 0.5	2.6 ± 0.9	4.2

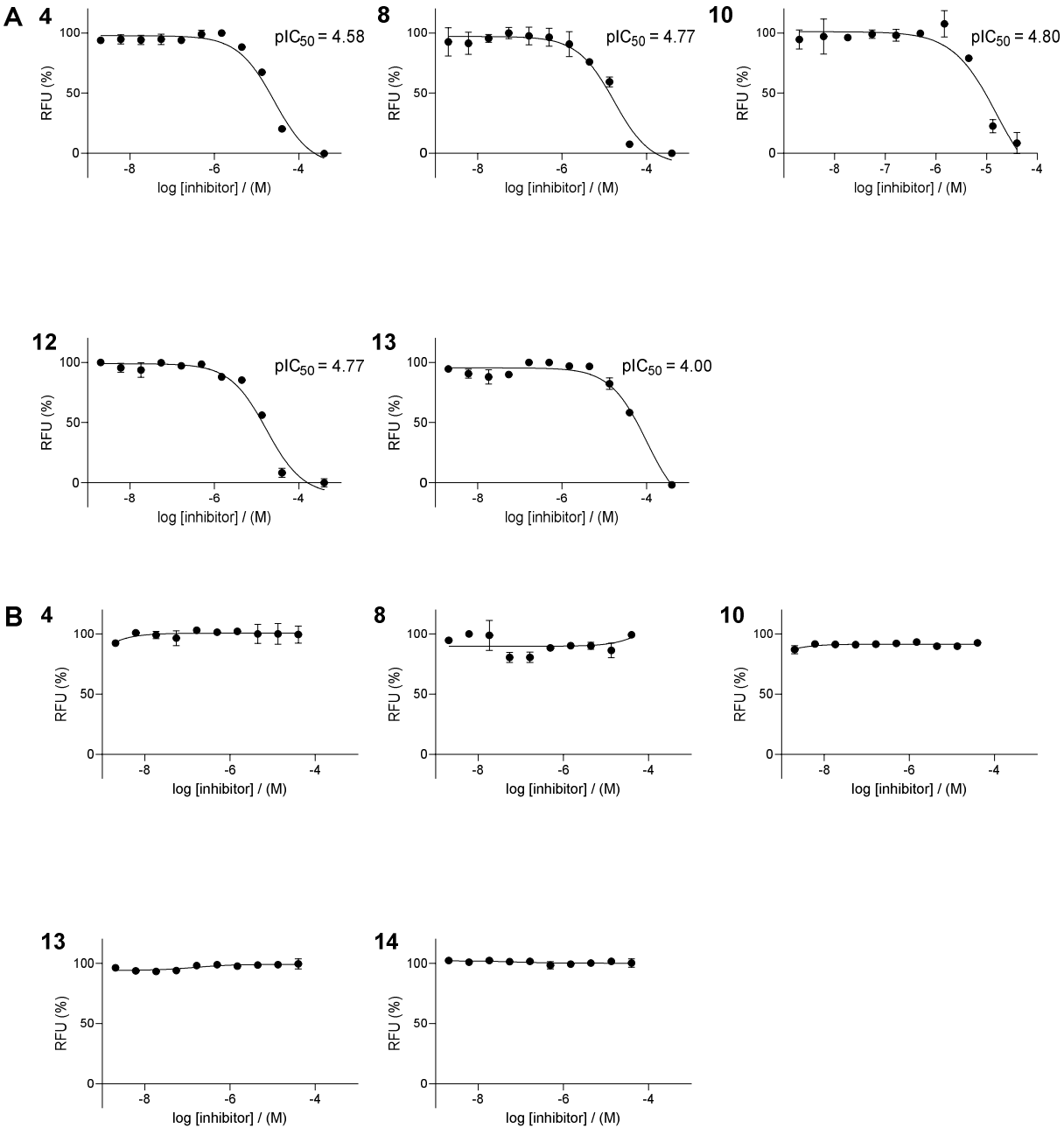

Figure S3.16. Inhibition studies of Ldt_{Mt2} with non-substrate peptidoglycan fragments. A. Ldt_{Mt2} (500 nM) was incubated with the specified peptidoglycan fragments (**4**, **8**, **10**, **13**, and **14**) for 30 minutes at room temperature, after which time activity was assessed using **1** (35 μM) in the presence of DAAO (2 U/mL), HRP (2 U/mL), FAD (40 μM) and Amplex red (10 μM) in 50 mM sodium phosphate pH 8.0 with 100 mM NaCl at 37 °C. **B.** Transpeptidase interference assay for peptidoglycan fragments. The specified peptidoglycan fragments (**4**, **8**, **10**, **13**, or **14**) were incubated with DAAO (2 U/mL), HRP (2 U/mL), FAD (40 μM) and Amplex red (10 μM) in 50 mM sodium phosphate pH 8.0 with 100 mM NaCl at room temperature for 30 minutes, after which D-alanine (500 nM) was added. See Methods for experimental details.

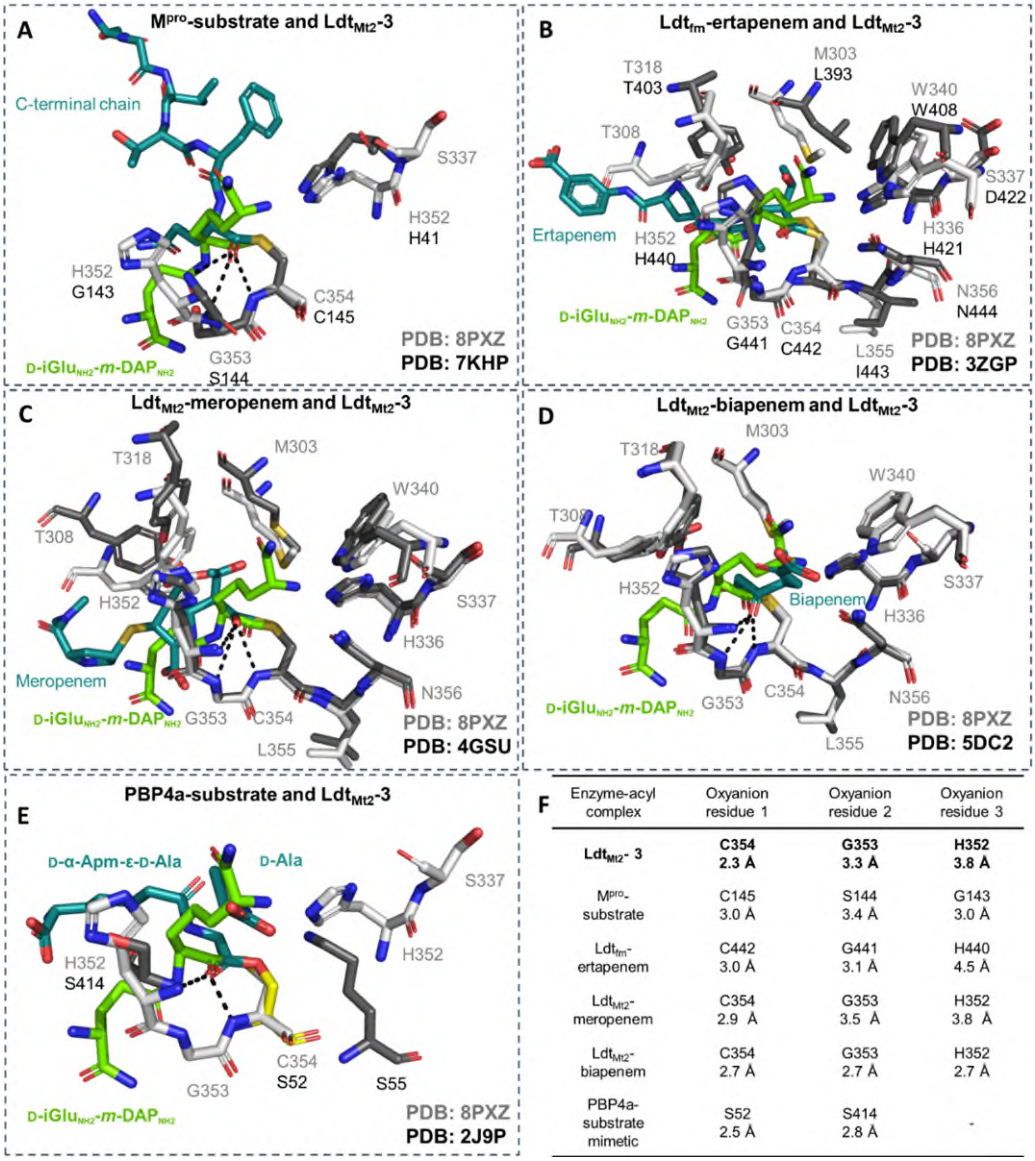

F

Enzyme-acyl complex	Oxyanion residue 1	Oxyanion residue 2	Oxyanion residue 3
Ldt$_{Mt2}$- 3	**C354 2.3 Å**	**G353 3.3 Å**	**H352 3.8 Å**
M^{pro}-substrate	C145 3.0 Å	S144 3.4 Å	G143 3.0 Å
Ldt$_{fm}$-ertapenem	C442 3.0 Å	G441 3.1 Å	H440 4.5 Å
Ldt$_{Mt2}$-meropenem	C354 2.9 Å	G353 3.5 Å	H352 3.8 Å
Ldt$_{Mt2}$-biapenem	C354 2.7 Å	G353 2.7 Å	H352 2.7 Å
PBP4a-substrate mimetic	S52 2.5 Å	S414 2.8 Å	-

Figure S3.17. Comparison of active site views of different nucleophilic cysteine acyl-enzyme complexes with that of Ldt$_{Mt2}$ in complex with 3. A. View of the oxyanion hole and catalytic residues of the SARS-CoV-2 main protease (M^{pro}) in complex with the C-terminal chain (dark grey and teal; PDB 7KHP)[7] overlaid with one of Ldt$_{Mt2}$ in complex with **3** (light grey and green; PDB 8PXZ). **B.** View of the active site of the *E. faecium* Ldt$_{fm}$ in complex with ertapenem (dark grey and teal; PDB 3ZGP)[8] overlaid with one of Ldt$_{Mt2}$ in complex with **3** (light grey and green; PDB 8PXZ). **C.** View of the active site of Ldt$_{Mt2}$ in complex with meropenem (dark grey and teal; PDB 4GSU)[9] overlaid with one of Ldt$_{Mt2}$ in complex with **3** (light grey and green; PDB 8PXZ). **D.** View of the active site of Ldt$_{Mt2}$ in complex with biapenem (dark grey and teal; PDB 5DC2)[10] overlaid with one of Ldt$_{Mt2}$ in complex with **3** (light grey and green; PDB 8PXZ). **E.** View of the oxyanion hole and catalytic residues of the *B. subtilis* PBP4a in complex with the D-α-aminopimelyl-ε-D-alanine dipeptide (dark grey and green, with Ser52 in yellow; PDB 2J9P)[1] overlaid with one of Ldt$_{Mt2}$ in complex with **3** (light grey and green; PDB 8PXZ). **F.** Distance information defining the position of the acyl group oxygen with respect to the nitrogens of oxyanion hole residues of the corresponding enzyme. The structure of **3** is given in Figure 5.2.

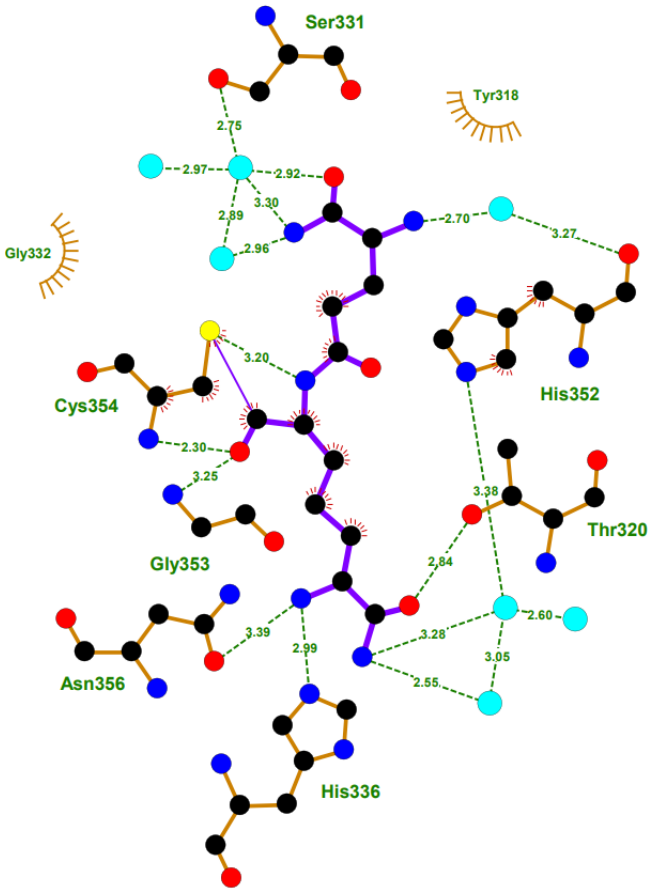

Figure S3.18. Interactions of the thioester complex of 3 with Ldt_{Mt2}. Hydrogen bonds are shown as green dotted lines and covalent bonds are shown as purple lines. **3** is shown in purple. The figure was generated using LigPlot+ from the crystal structure of Ldt_{Mt2} in complex with **3** (PDB 8PXZ).[11]

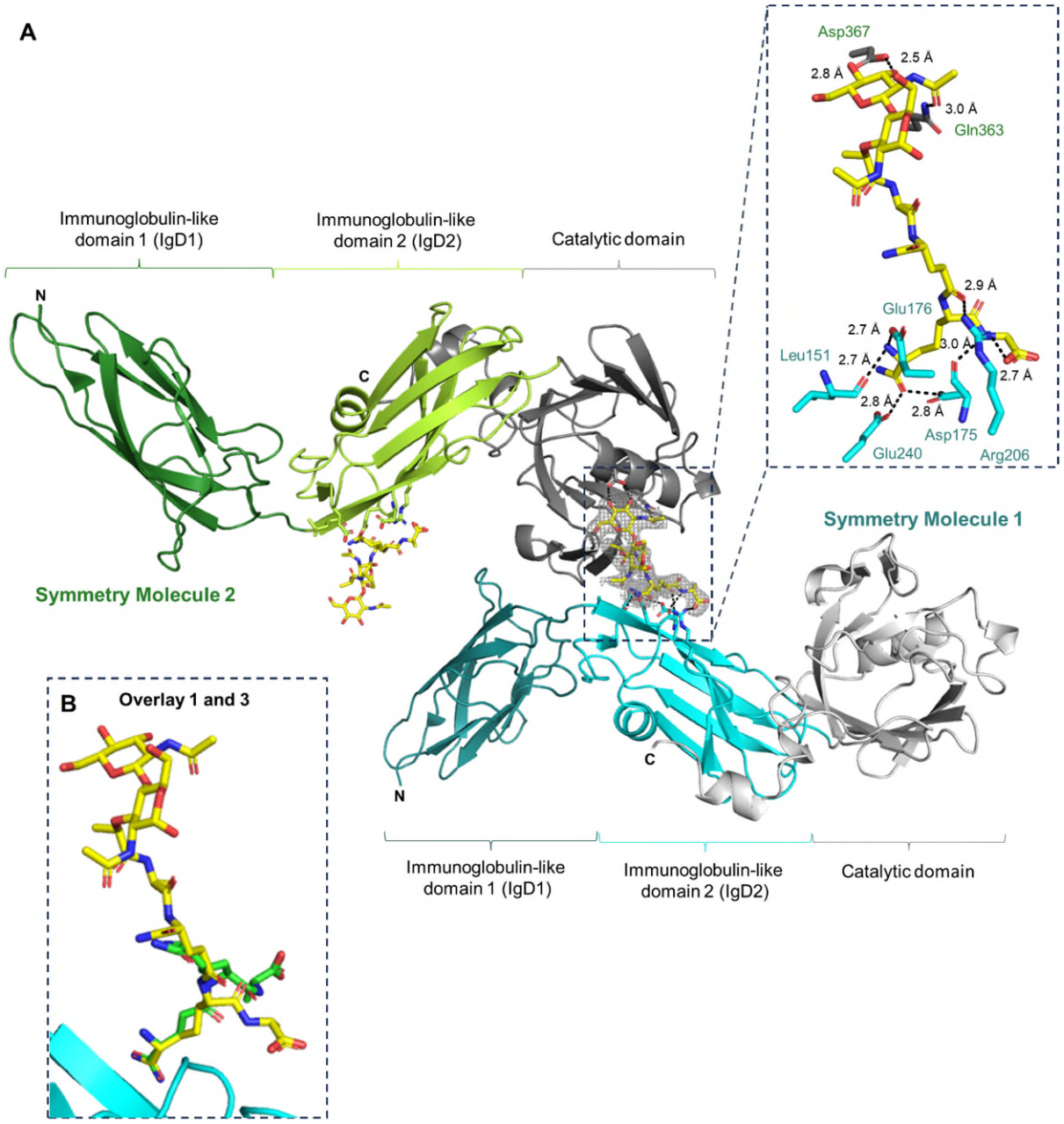

Figure S3.19. Views from a crystal structure of Ldt_{Mt2}^{C354S} in complex with peptidoglycan monomer 1 (yellow, PDB 8PXY) showing interactions with two symmetry related molecules of Ldt_{Mt2}^{C354S}. A. The $mF_0 - DF_c$ polder OMIT map[12] contoured at 3.0 σ, and carved around **1** is in grey mesh for symmetry molecule 1. Polar interactions are shown in grey dashes. Labels of residues interacting with symmetry molecule 1 are in teal, and labels of residues interacting with symmetry molecule 2 are in green. The crystallographically assigned structure of **1** is consistent with the structure shown in Figure 5.2A. **B.** Overlay of the IgD2 bound substrates **1** (yellow, PDB 8PXY), and **3** (green, PDB 8PXZ).

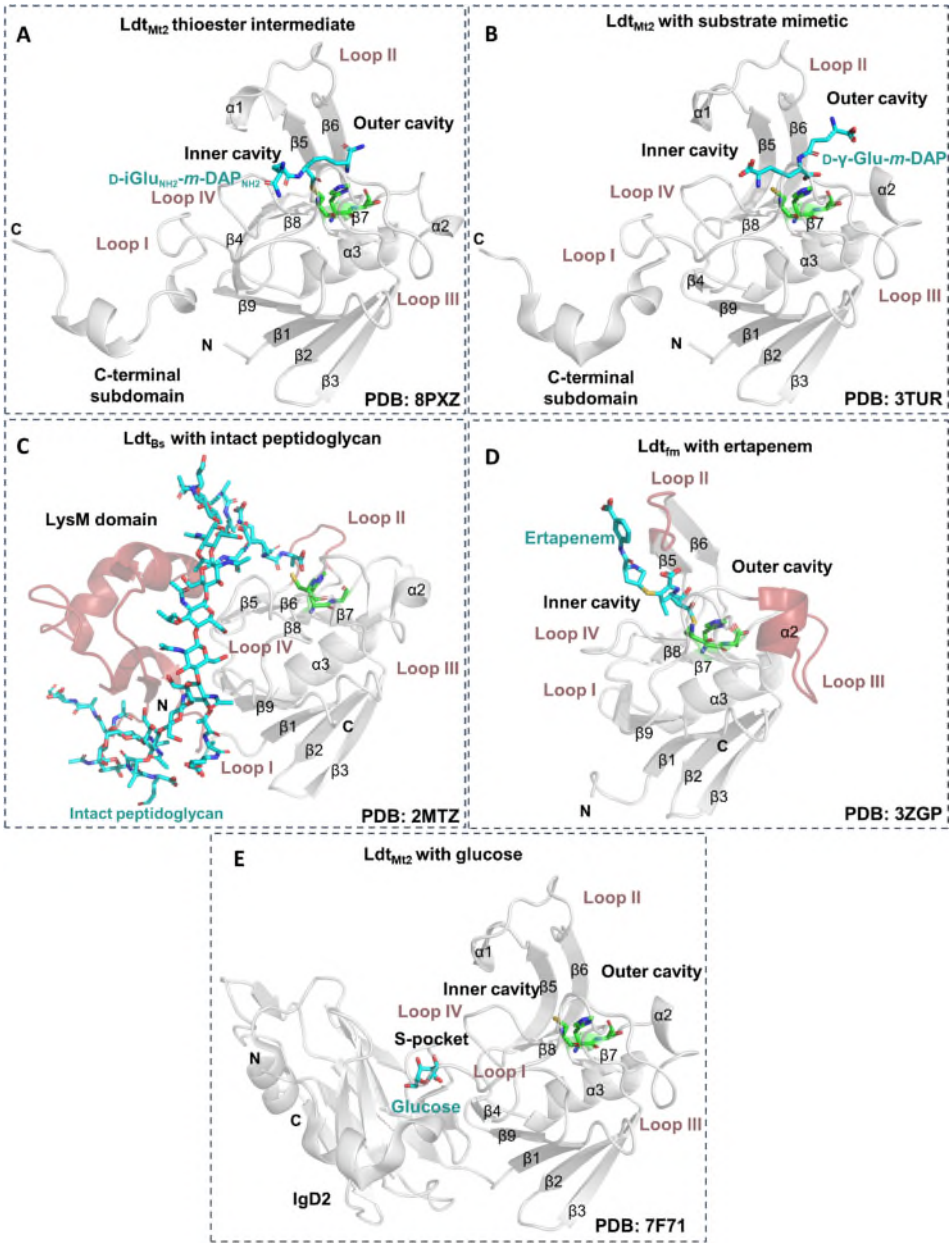

Figure S3.20. Comparison views of structures of L,D-transpeptidases in complex with various peptidoglycan fragments. A. View from our X-ray structure of the catalytic domain Ldt_{Mt2} in complex with **3** (PDB:8PXZ). **B.** View of the catalytic domain from the X-ray structure of Ldt_{Mt2} in complex with the substrate analogue D-γ-Glu-*m*-DAP (**13**, PDB: 3TUR).[13] **C.** View from a solid-state NMR derived structure of the catalytic domain of Ldt_{Bs} from *Bacillus subtilis* in complex with intact peptidoglycan (PDB: 2MTZ).[14] **D.** View from an NMR structure of the catalytic domain of Ldt_{fm} of *Enterococcus faecium* in complex with ertapenem (PDB: 3ZGP).[8] **E.** View of the catalytic domain and IgD2 from an X-ray crystal structure of Ldt_{Mt2} in complex with glucose (PDB: 7F71).[15] All structural views are oriented following alignment with Ldt_{Mt2}. Proteins are shown in grey, ligands in cyan and catalytic triads in green. Areas in red in **C** and **D** represent significant structural differences with Ldt_{Mt2}. The structures of **3** and 13 are given in Figure 5.2.

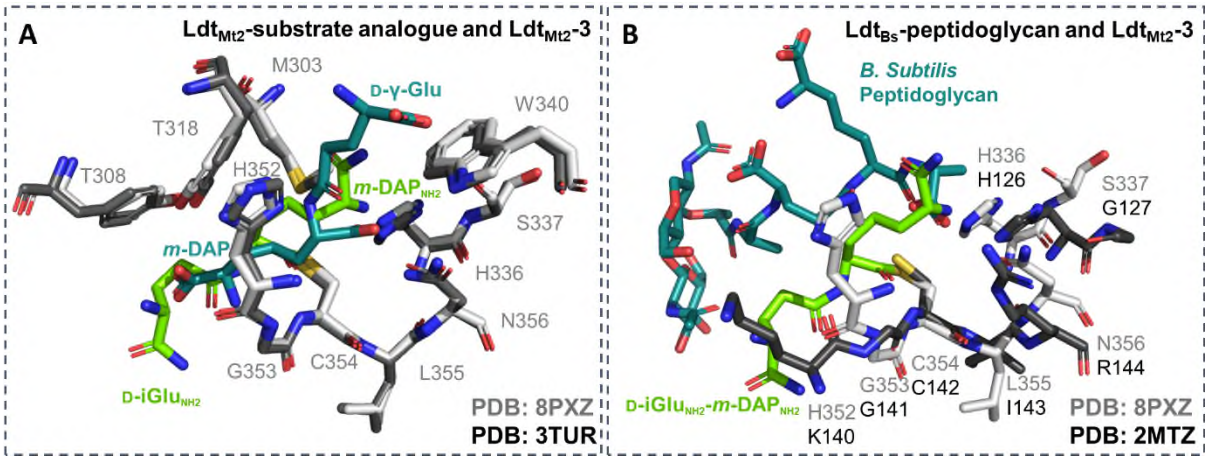

Figure S3.21. Comparison of the active site of Ldt$_{Mt2}$ in complex with 3 with related structures. A. View of the active site of Ldt$_{Mt2}$ in complex with substrate analogue D-γ-Glu-*m*-DAP (**13**, dark grey and teal; PDB 3TUR)[13] and Ldt$_{Mt2}$ in complex with **3** (light grey and green; PDB 8PXZ). **B.** View of the active site of the *B. subtilis* Ldt$_{Bs}$ (dark grey) in complex with intact peptidoglycan (shown here is a monomer in teal; PDB: 2MTZ)[14] and Ldt$_{Mt2}$ in complex with **3** (light grey and green; PDB 8PXZ). The structures of **3** is given in Figure 5.2.

Table S3.4. Data collection and refinement statistics for the crystal structure of Ldt_{Mt2}^{C354S} in complex with 1 and Ldt_{Mt2} in complex with 3.

Datasets	**Ldt_{Mt2}^{C354S} – 1 (PDB: 8PXY)**	**Ldt_{Mt2} – 3 (PDB: 8PXZ)**
Data Collection		
Beamline (Wavelength, Å)	DLS I03 (0.9763)	DLS I03 (0.9763)
Detector	Eiger2 XE 16M	Eiger2 XE 16M
Data Processing	Xia2 dials	Xia2 3dii
Space group	*P* 2_1 2_1 2	*P* 2_1 2_1 2
Cell dimensions		
a,b,c (Å)	76.61, 94.62, 58.79	77.12, 95.83, 59.23
α, β, γ (°)	90.00, 90.00, 90.00	90.00, 90.00, 90.00
No. of molecules/ASU	1	1
No. reflections	23889 (2322)*	31078 (2883)*
Resolution (Å)	58.79-2.15 (2.23-2.15)*	42.18-1.98 (2.05-1.98)*
R_{merge} (I)	0.138 (0.987)*	0.135 (1.997)*
I/σI	10.8 (1.1)*	12.3 (1.4)*
CC-1/2	0.99 (0.8)*	1.00 (0.5)*
Completeness (%)	100.0 (97.0)*	99.6 (94.2)*
Multiplicity	13.2 (13.5)*	13.2 (11.1)*
Wilson B value ($Å^2$)	30.14	35.63
Refinement	PHENIX	PHENIX
R_{work}/R_{free}	0.2032/0.2451	0.1848/0.2259
No. atoms	3073	3069
- Enzyme	2655	2664
- Ligand	81	53
- Water	337	352
Average B-factors	39.90	41.17
- Enzyme	39.40	40.14
- Ligand	52.91	68.86
- Water	40.73	44.86
RMS[$] deviations		
- Bond lengths (Å)	0.003	0.010
- Bond angles (°)	0.55	0.86

[#] ASU = asymmetric unit.

[$] RMS = root mean square.

*Highest resolution shell in parentheses.

A

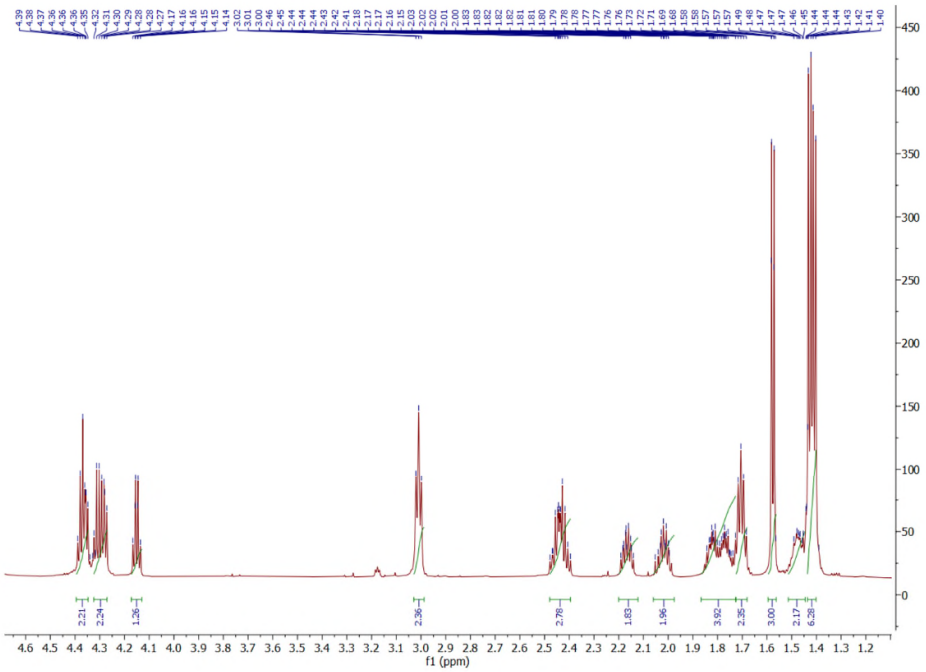

B

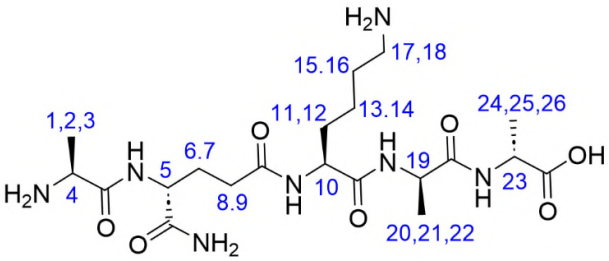

Chemical shift (ppm)	Multiplicity	Integration	Assignment
4.39 – 4.34	m	2H	4,5
4.32 – 4.27	m	2H	10,19
4.17 – 4.13	m	1H	23
3.00	t (*J* = 7.7 Hz)	2H	17,18
2.47 – 2.39	m	2H	Impurity
2.19 – 2.14	m	2H	6,7
2.06 – 1.99	m	2H	8,9
1.85 – 1.73	m	4H	11,12,15,16
1.70	q (*J* = 7.7 Hz)	2H	Impurity
1.58	d (*J* = 7.1 Hz)	3H	1,2,3
1.51 – 1.44	m	2H	13,14
1.42	dd (*J* = 13.6, 7.2 Hz)	6H	20,21,22,24,25,26

Figure S3.22. Characterisation of peptidoglycan analogue 9 by ^{1}H (700 MHz) NMR in D_2O. A. ^{1}H spectrum of **9**. Note that **9** was prepared by solid-phase peptide synthesis, where D-alanine-Wang resin was coupled with Fmoc protected amino acids, followed by cleavage and deprotection using CF_3CO_2H/CH_2Cl_2 (2:1). **B.** Structure of **9** labelled with assignments. See Methods for experimental details.

A

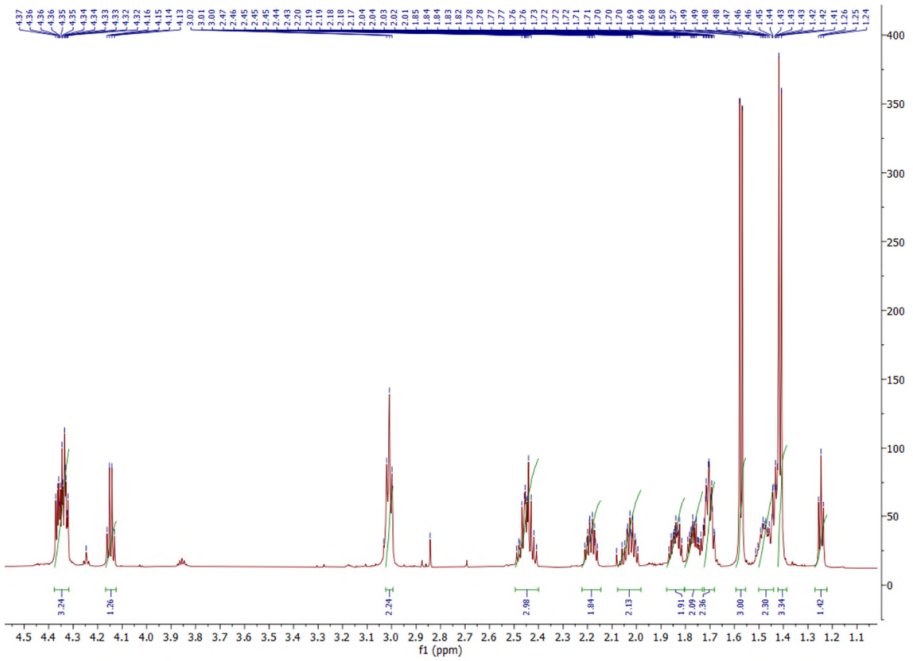

B

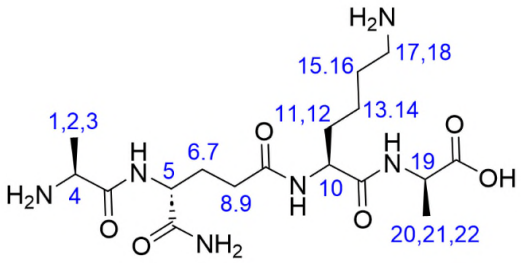

Chemical shift (ppm)	Multiplicity	Integration	Assignment
4.35-4.32	m	3H	4, 5,10
4.15	q (*J* = 7.1 Hz)	1H	19
3.00	t (*J* = 7.7 Hz)	2H	17,18
2.49-2.41	m	3H	Impurity
2.21-2.15	m	2H	6,7
2.08-1.99	m	2H	8,9
1.87-1.81	m	2H	11,12
1.79-1.74	m	2H	15,16
1.73-1.68	m	2H	Impurity
1.57	d (*J* = 7.1 Hz)	3H	1,2,3
1.50-1.44	m	2H	13,14
1.41	d (*J* = 7.3 Hz)	3H	20,21,22
1.25	t (*J* = 6.8 Hz)	1H	Impurity

Figure S3.23. Characterisation of peptidoglycan analogue 11 by ^{1}H (700 MHz) NMR in D_2O. A. ^{1}H spectrum of **11**. Note that **11** was prepared by solid-phase peptide synthesis, where D-alanine-Wang resin was coupled with Fmoc protected amino acids, followed by cleavage and deprotection using CF_3CO_2H/CH_2Cl_2 (2:1). **B.** Structure of **11** labelled with assignments. See Methods for experimental details.

References

1 Sauvage, E., Duez, C., Herman, R., Kerff, F., Petrella, S., Anderson, J. W., Adediran, S. A., Pratt, R. F., Frère, J.-M. & Charlier, P. Crystal Structure of the *Bacillus subtilis* Penicillin-binding Protein 4a, and its Complex with a Peptidoglycan Mimetic Peptide. *J. Mol. Biol.* **371**, 528-539 (2007).

2 Sauvage, E., Kerff, F., Terrak, M., Ayala, J. A. & Charlier, P. The penicillin-binding proteins: structure and role in peptidoglycan biosynthesis. *FEMS Microbiol. Rev.* **32**, 234-258 (2008).

3 de Munnik, M., Lohans, C. T., Lang, P. A., Langley, G. W., Malla, T. R., Tumber, A., Schofield, C. J. & Brem, J. Targeting the *Mycobacterium tuberculosis* transpeptidase Ldt_{Mt2} with cysteine-reactive inhibitors including ebselen. *Chem. Commun.* **55**, 10214-10217 (2019).

4 Huynh, K. & Partch, C. L. Analysis of Protein Stability and Ligand Interactions by Thermal Shift Assay. *Curr. Protoc. Protein Sci.* **79**, 14-21 (2015).

5 de Munnik, M., Lohans, C. T., Langley, G. W., Bon, C., Brem, J. & Schofield, C. J. A Fluorescence-Based Assay for Screening β-Lactams Targeting the *Mycobacterium tuberculosis* Transpeptidase Ldt_{Mt2}. *ChemBioChem* **21**, 368-372 (2020).

6 de Munnik, M., Lang, P. A., De Dios Antos, F., Cacho, M., Bates, R. H., Brem, J., Rodríguez-Miquel, B. & Schofield, C. J. High-Throughput Screen with the L,D-transpeptidase Ldt_{Mt2} of *Mycobacterium tuberculosis* Reveals Novel Classes of Covalently Reacting Inhibitors *Chem. Sci.* **14**, 7262-7278 (2023).

7 de Munnik, M., Lithgow, J., Brewitz, L., Christensen, K. E., Bates, R. H., Rodriguez-Miquel, B. & Schofield, C. J. αβ,α'β'-Diepoxyketones are mechanism-based inhibitors of nucleophilic cysteine enzymes. *Chem. Commun. (Camb)* **59**, 12859-12862 (2023).

8 Lee, J., Worrall, L. J., Vuckovic, M., Rosell, F. I., Gentile, F., Ton, A.-T., Caveney, N. A., Ban, F., Cherkasov, A., Paetzel, M. & Strynadka, N. C. J. Crystallographic structure of wild-type SARS-CoV-2 main protease acyl-enzyme intermediate with physiological C-terminal autoprocessing site. *Nat. Commun.* **11** (2020).

9 Lecoq, L., Dubée, V., Triboulet, S., Bougault, C., Hugonnet, J.-E., Arthur, M. & Simorre, J.-P. Structure of *Enterococcus faecium* L,D-Transpeptidase Acylated by Ertapenem Provides Insight into the Inactivation Mechanism. *ACS Chem. Biol.* **8**, 1140-1146 (2013).

10 Kim, H. S., Kim, J., Im, H. N., Yoon, J. Y., An, D. R., Yoon, H. J., Kim, J. Y., Min, H. K., Kim, S.-J. & Lee, J. Y. Structural basis for the inhibition of *Mycobacterium tuberculosis* L,D-transpeptidase by meropenem, a drug effective against extensively drug-resistant strains. *Acta Crystallogr. D* **69**, 420-431 (2013).

11 Bianchet, M. A., Pan, Y. H., Basta, L. A. B., Saavedra, H., Lloyd, E. P., Kumar, P., Mattoo, R., Townsend, C. A. & Lamichhane, G. Structural insight into the inactivation of *Mycobacterium tuberculosis* non-classical transpeptidase Ldt_{Mt2} by biapenem and tebipenem. *BMC Biochem.* **18** (2017).

12 Laskowski, R. A. & Swindells, M. B. LigPlot+: Multiple Ligand–Protein Interaction Diagrams for Drug Discovery. *J. Chem. Inf. Model.* **51**, 2778-2786 (2011).

13 Liebschner, D., Afonine, P. V., Moriarty, N. W., Poon, B. K., Sobolev, O. V., Terwilliger, T. C. & Adams, P. D. Polder maps: improving OMIT maps by excluding bulk solvent. *Acta Crystallogr. D* **73**, 148-157 (2017).

14 Erdemli, S. B., Gupta, R., Bishai, W. R., Lamichhane, G., Amzel, L. M. & Bianchet, M. A. Targeting the cell wall of *Mycobacterium tuberculosis*: structure and mechanism of L,D-transpeptidase 2. *Structure* **20**, 2103-2115 (2012).

15 Schanda, P., Triboulet, S., Laguri, C., Bougault, C. M., Ayala, I., Callon, M., Arthur, M. & Simorre, J.-P. Atomic Model of a Cell-Wall Cross-Linking Enzyme in Complex with an Intact Bacterial Peptidoglycan. *J. Am. Chem. Soc.* **136**, 17852-17860 (2014).

16 Ahmad, N., Dugad, S., Chauhan, V., Ahmed, S., Sharma, K., Kachhap, S., Zaidi, R., Bishai, W. R., Lamichhane, G. & Kumar, P. Allosteric cooperation in β-lactam binding to a non-classical transpeptidase. *eLife* **11**, e73055 (2022).

Appendix IV. Supplementary information for Chapter 6.

How inhibition of L,D-transpeptidases and penicillin binding proteins leads to inhibition of mycobacteria

Manuscript IV

Unpublished manuscript.

Table S4.1. Activity of Ldt_{Mt2} inhibitors against *Mycobacterium smegmatis*. The *Msm* MIC values were determined in three independent repeats. For reference, previously determined MIC_{50} values against *Mtb* are provided.[1] Note that the *Mtb* MIC_{50} values represent the concentration of inhibitor that inhibited intracellular macrophage *Mtb* growth by 50%, as obtained by extrapolation of the dose-response curve.[1] MIC values represent the lowest concentration in which no bacterial growth is observed, as determined by OD_{600} measurement and resazurin staining. Errors represent standard deviation.

Compound	Structure	*Msm* MIC (µg/mL)	*Mtb* MIC_{50} (µM) in macrophages	*Mtb* MIC_{50} (µM) in media
1	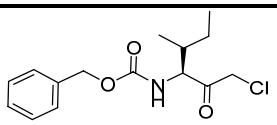	>128	35.5 ± 4.9	>50
2	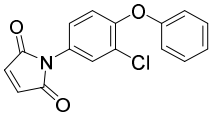	64	25.7 ± 0.30	>50
3	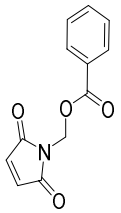	64	39.8 ± 0.0	>50
4	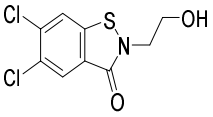	32	7.08 ± 0.16	>50
5	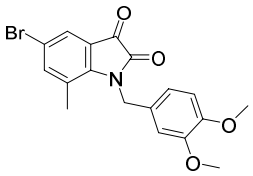	>128	15.1 ± 0.70	>50
6	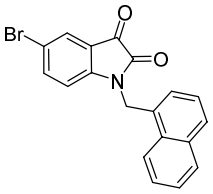	>128	35.5 ± 5.4	>50
7	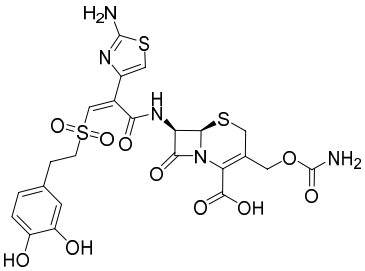	64	38.9 ± 1.8	>50
8	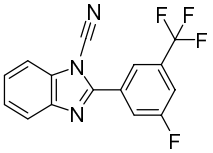	48	12.0 ± 1.5	N.D.
9	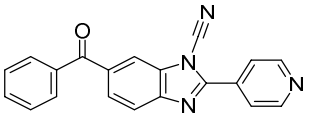	16	29.5 ± 0.0	>50

Compound	Structure	*Msm* MIC (μg/mL)	*Mtb* MIC_{50} (μM) in macrophages	*Mtb* MIC_{50} (μM) in media
10	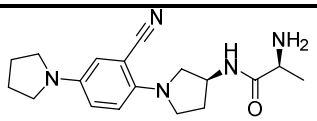	64	28.8 ± 0.0	>50
11	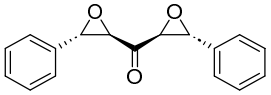	>128	>100	>50
12	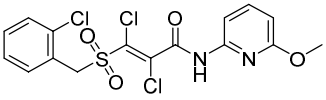	>128	>100	>50
13	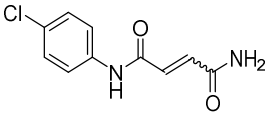	>128	>100	>50
14	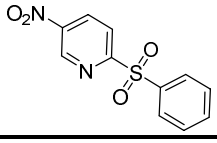	8	>100	11.0

Table S4.2. Activity of control compounds ethambutol, isoniazid, and rifampicin against *Mycobacterium smegmatis.* MIC experiments were performed in triplicate. For reference, reported MICs for ethambutol, isoniazid, and rifampicin activity against *Msm* are provided.[2,3]

Compound	MIC (μg/mL)	Reported MIC (μg/mL)
Ethambutol	0.25	0.25 – 5
Isoniazid	4 – 8	0.2 – 10
Rifampicin	2 – 4	0.8 – 1.6

Table S4.3. Activity of β-lactams again *Mycobacterium smegmatis*. MIC values were determined in three independent repeats.

Compound	Structure	MIC (µg/mL)	MIC (µg/mL) + CLAV (100 µg/mL)
Faropenem	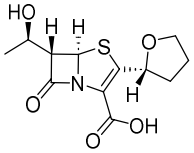	16	N.D.
Meropenem	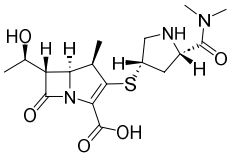	2	N.D.
Imipenem	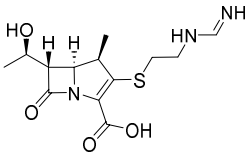	0.125	N.D.
Ceftazidime	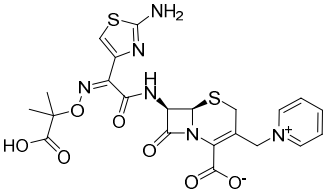	>128	128
Ceftriaxone	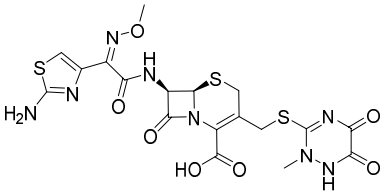	>128	128
Ampicillin	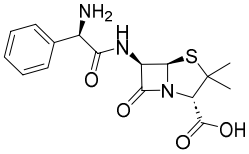	>128	2
Amoxicillin	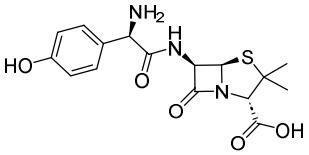	>128	1
Aztreonam	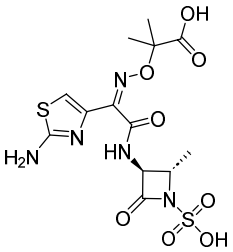	>128	N.D.
Clavulanic acid	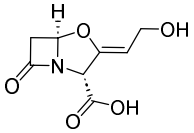	128	N.D.

Table S4.4. MIC studies of *Mycobacterium smegmatis* with dual treatment of Ldt_{Mt2} inhibitors and faropenem or meropenem. MIC values were determined in three independent repeats. Values in blue represent inhibitor combinations that indicate an improved activity compared to single dosing. Hyphens indicate concentration combinations that are above the MIC of the Ldt_{Mt2} inhibitor alone (Table S4.1). Structures of the Ldt_{Mt2} inhibitors can be found in Table S4.1. FAR = faropenem, MER = meropenem.

Ldt_{Mt2} inhibitor	MIC (µg/mL)					
	FAR + 64 µg/mL Ldt_{Mt2} inhibitor	FAR + 16 µg/mL Ldt_{Mt2} inhibitor]	FAR + 4 µg/mL Ldt_{Mt2} inhibitor	MER + 64 µg/mL Ldt_{Mt2} inhibitor	MER + 16 µg/mL Ldt_{Mt2} inhibitor]	MER + 4 µg/mL Ldt_{Mt2} inhibitor
2	-	16	16	-	2	2
4	-	<0.25	8	-	<0.25	2
7	-	16	16	-	2	2
8	-	1	4	-	1	2
9	-	-	8	-	-	2
12	16	16	16	2	2	2
13	16	16	16	2	2	2
14	-	-	<0.25	-	-	<0.25

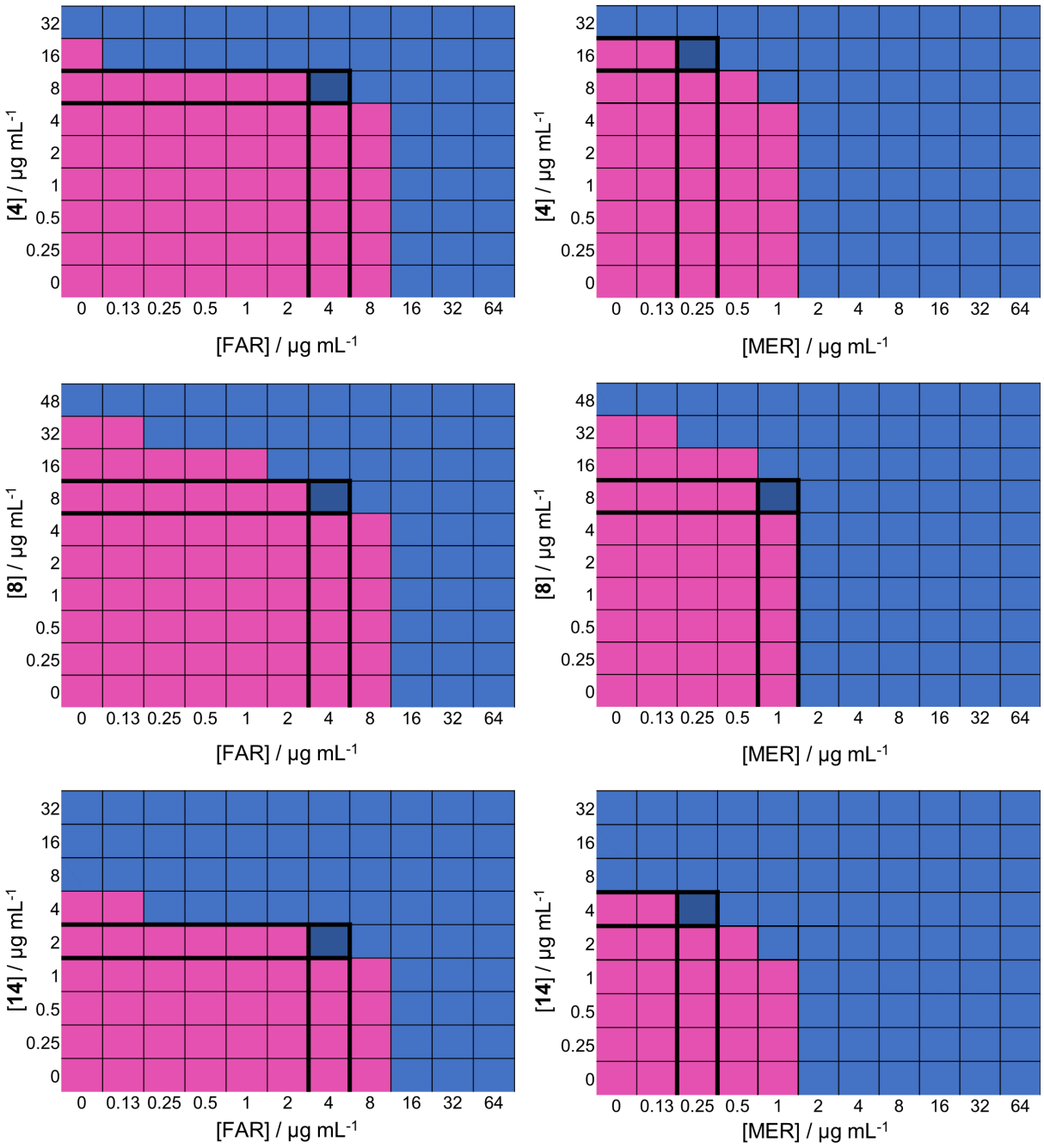

Figure S4.1. Activity of 4, 8, or 14, in combination with faropenem or meropenem against *Mycobacterium smegmatis*. Inhibitor concentrations that result in bacterial growth are in pink. Inhibitor concentrations that result in inhibition of bacterial growth are in blue. Inhibitor concentrations leading to optimal synergistic and/or additive effects are in a darker shade of blue, and bordered by black lines. Experiments were performed in triplicate. FAR = faropenem, MER = meropenem.

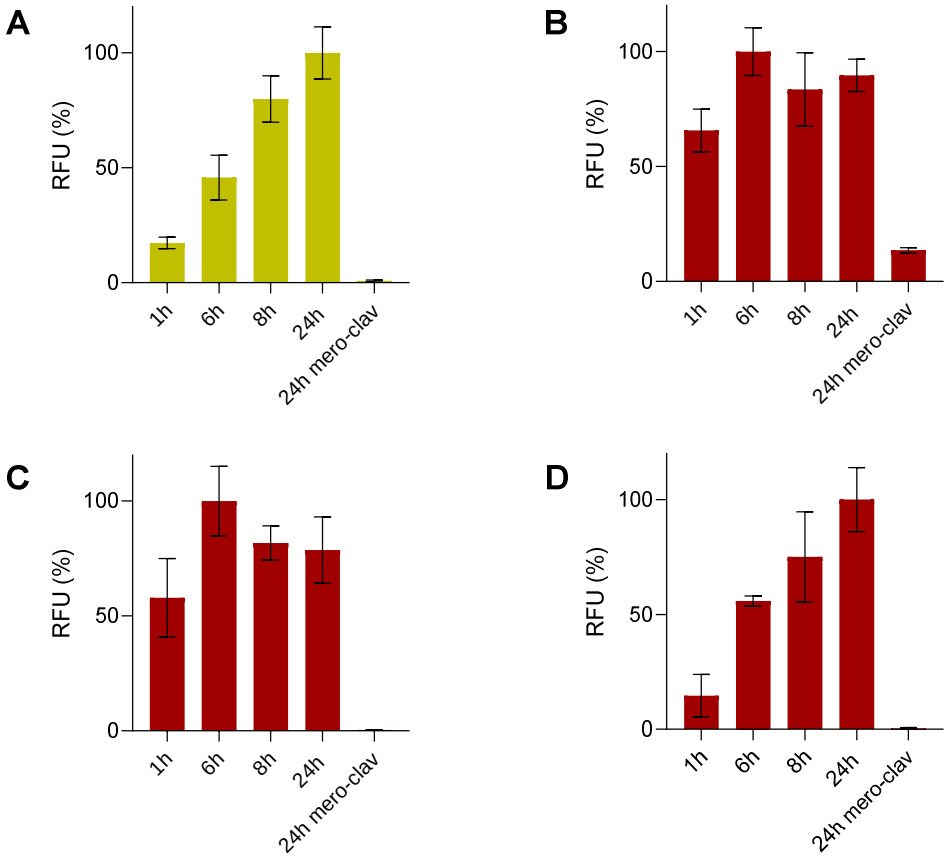

Figure S4.2. Time dependent incorporation of PentaFl (A) or TetraRh (B-D) into *Mycobacterium smegmatis*. A culture of *Msm* (OD_{600} 0.8) was incubated with 50 µM PentaFl (**A**), or 50 µM (**B**), 5 µM (**C**), or 0.5 µM (**D**) TetraRh.[4] At various timepoints, cells were fixated and analysed via flow cytometry. Negative controls consisted of *Msm* treated with meropenem-clavulanic acid (100 µg/mL). Error bars represent standard deviation (n=3).

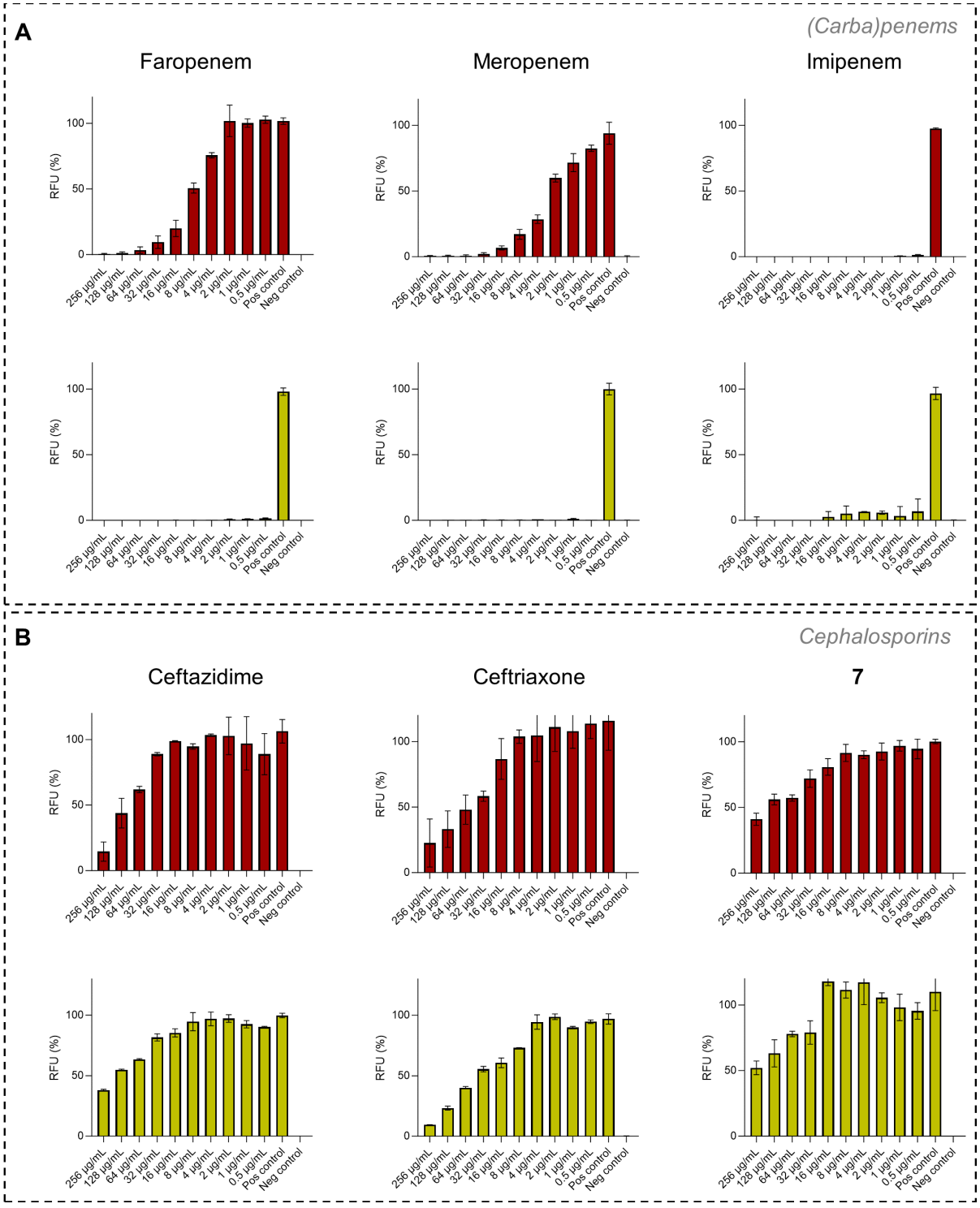

Figure S4.3. Inhibition of penicillin binding proteins and L,D-transpeptidases of Mycobacterium smegmatis. [continues]

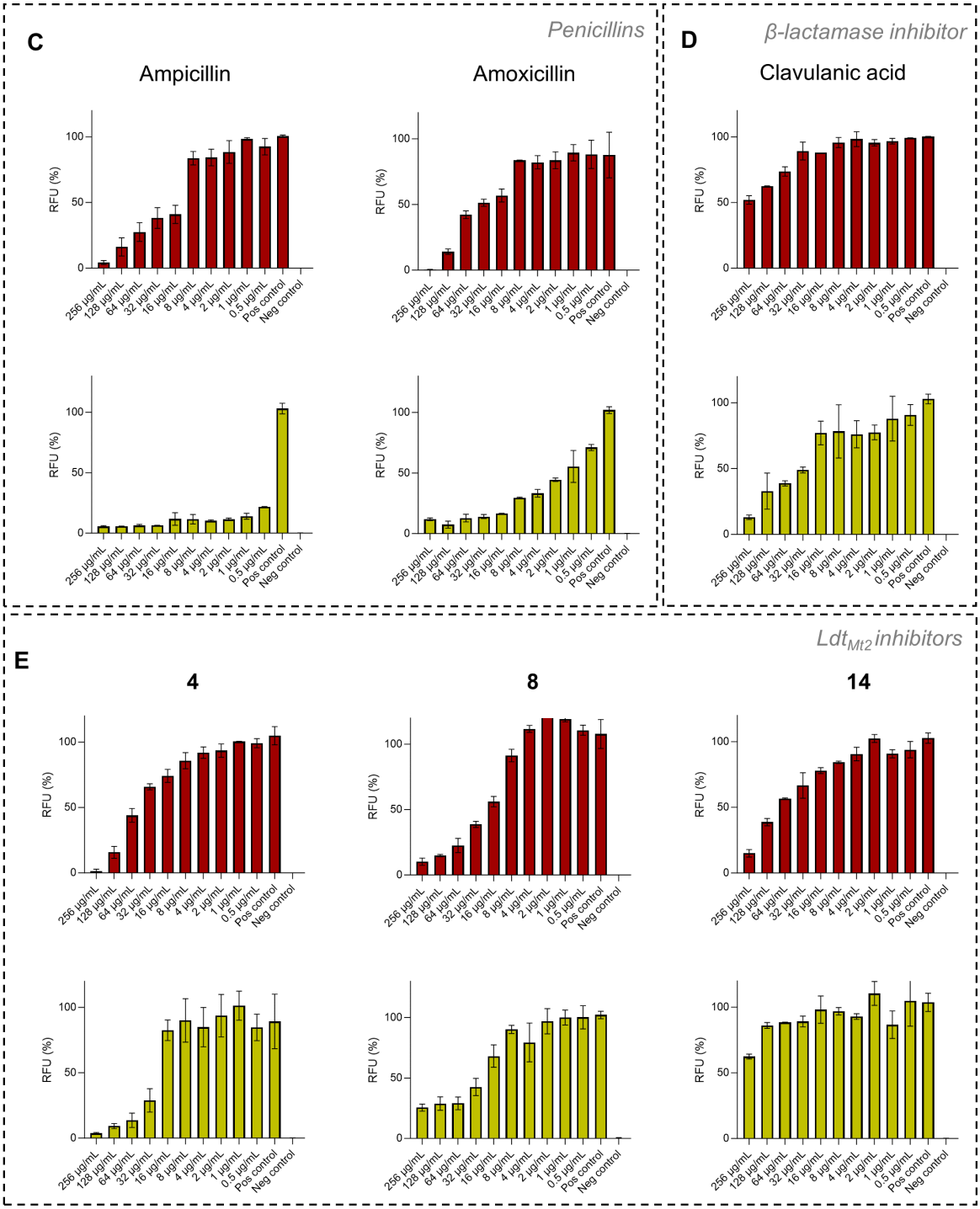

Figure S4.3. Inhibition of penicillin binding proteins and L,D-transpeptidases of Mycobacterium smegmatis. A culture of *Msm* (OD_{600} 0.8) was incubated with 50 µM PentaFl, or 0.5 µM TetraRh in the presence of various concentrations of (carba)penems (**A**), cephalosporins (**B**), penicillins (**C**), a β-lactamase inhibitor (**D**), or Ldt_{Mt2} inhibitors (**E**), and incubated for 24 hours at 37 °C, prior to fixation and analysis by flow cytometry. Red bars represent fluorescence caused by incorporation of TetraRh, a substrate mimic of the Ldts.[4] Green bars represent fluorescence caused by incorporation of PentaFl, a substrate mimic of the PBPs.[4] In the case of **A** and **E**, assays were performed without clavulanic acid, assays in **B** and **C** were performed in the presence of 100 µg/mL clavulanic acid. Error bars represent standard deviation (n=2).

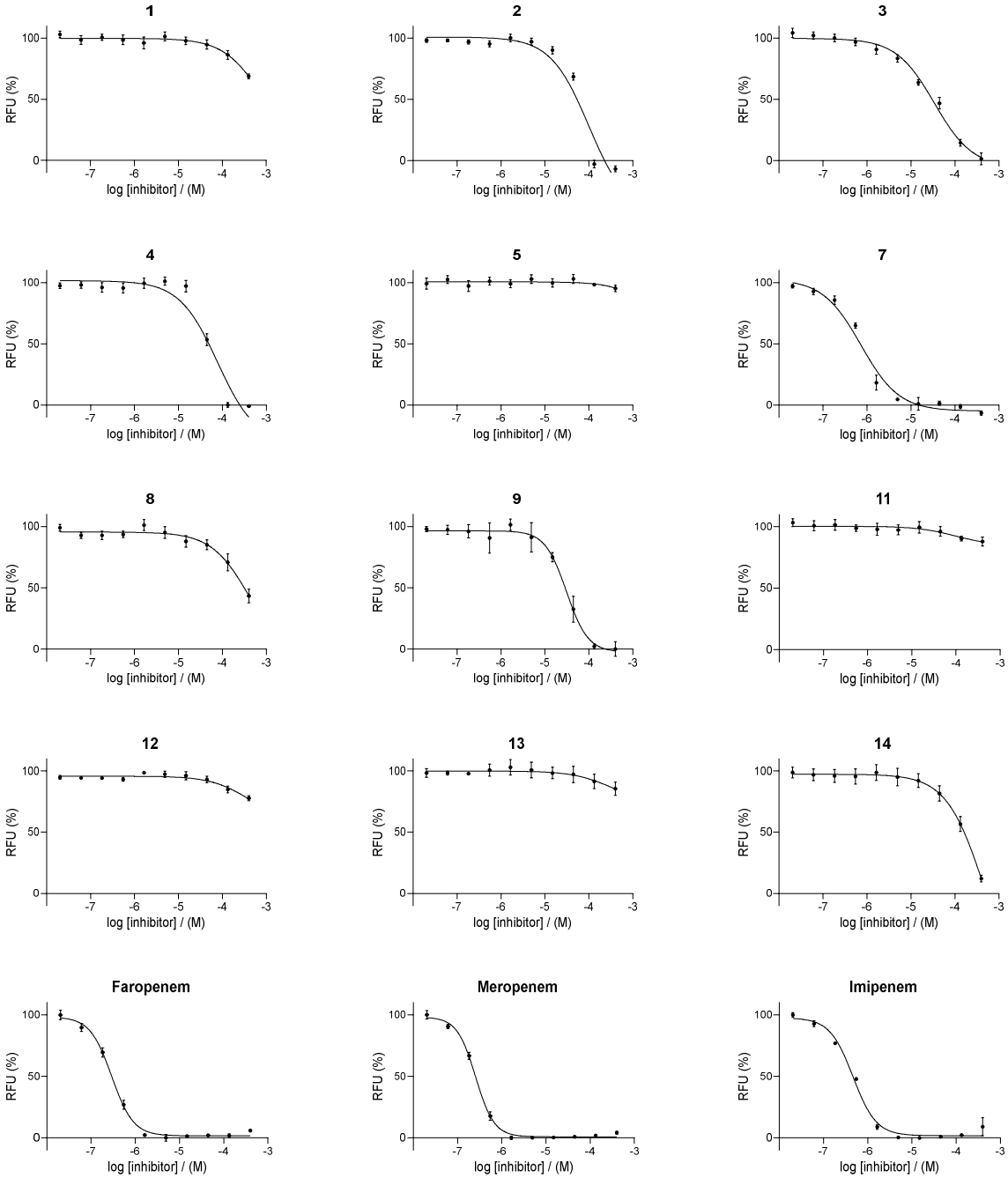

Figure S4.4. Inhibition of PBP3 of *Mycobacterium tuberculosis*. [Continues]

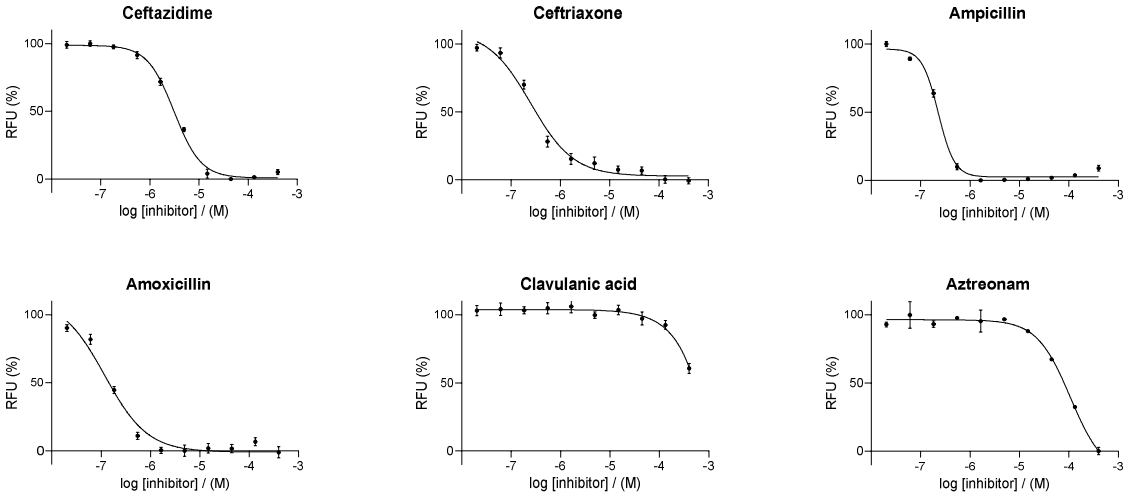

Figure S4.4. Inhibition of PBP3 of *Mycobacterium tuberculosis*. PBP3 (300 nM) was incubated with the specified inhibitor for 10 minutes at room temperature. Activity was assessed with S2d (1.5 mM), monobromobimane (mBBr; 0.05 mM), and D-Ala (1 mM) in 50 mM HEPES pH 7.4, 100 mM NaCl, 0.01% (*v*/*v*) Triton X-100. Error bars represent standard deviation (n=4). The pIC_{50} values and compound structures are provided in Table S4.5.

Table S4.5. Inhibition of PBP3 by Ldt_{Mt2} inhibitors and β-lactams. Assays were performed in quadruplicate; errors represent standard deviation. See methods for experimental details. For reference, reported inhibition data for Ldt_{Mt2} is shown.[1,5]

Compound	Structure	pIC_{50} PBP3 (mean ± SD)	pIC_{50} Ldt_{Mt2} (mean ± SD)
1	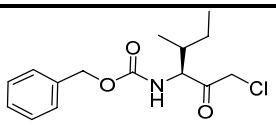	<3.4	7.1 ± 0.045
2	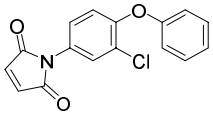	4.0 ± 0.15	7.4 ± 0.010
3	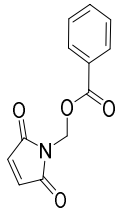	4.5 ± 0.20	7.0 ± 0.00
4	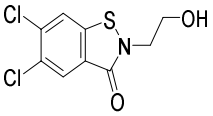	4.1 ± 0.15	8.0 ± 0.040
5	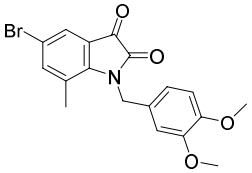	<3.4	6.2 ± 0.14
6	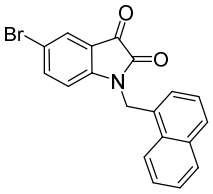	N.D.	6.5 ± 0.005
7	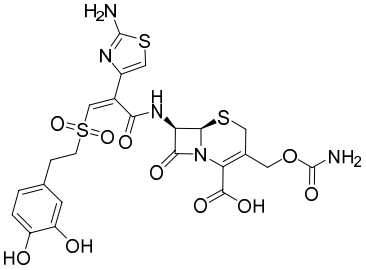	6.1 ± 0.089	5.6 ± 0.045
8	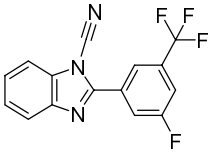	<3.4	7.3 ± 0.065
9	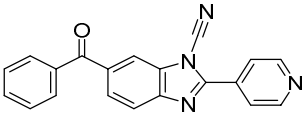	4.5 ± 0.085	7.1 ± 0.050
10	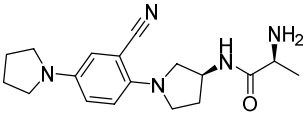	N.D.	6.3 ± 0.065

Compound	Structure	pIC_{50} PBP3 (mean ± SD)	pIC_{50} Ldt_{Mt2} (mean ± SD)
11	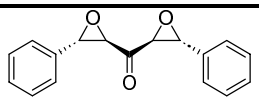	<3.4	7.2 ± 0.012
12	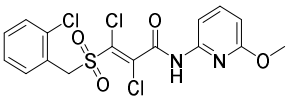	<3.4	7.2 ± 0.035
13	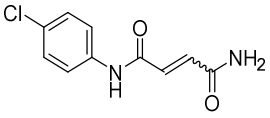	<3.4	6.4 ± 0.080
14	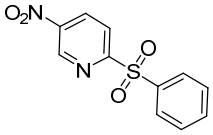	<3.4	5.3 ± 0.1
Faropenem	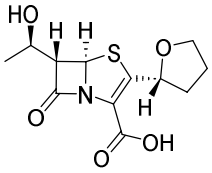	6.5 ± 0.042	6.5 ± 0.042
Meropenem	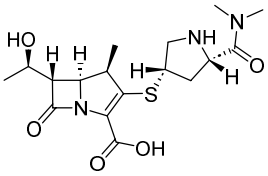	6.6 ± 0.029	5.0 ± 0.1
Imipenem	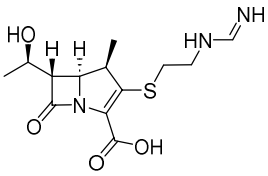	6.3 ± 0.069	6.1 ± 0.1
Ceftazidime	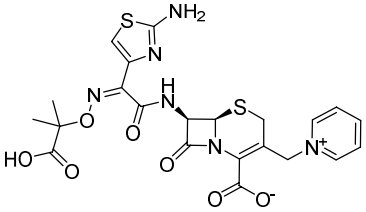	5.5 ± 0.040	<3.4
Ceftriaxone	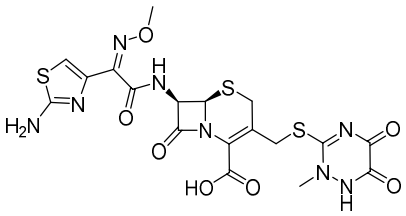	6.6 ± 0.22	<3.4
Ampicillin	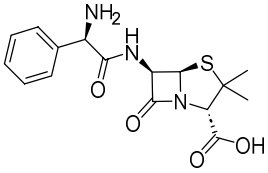	6.6 ± 0.031	<3.4
Amoxicillin	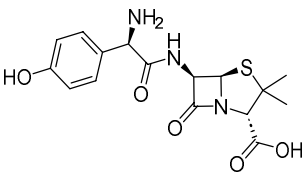	6.9 ± 0.27	<3.4

Compound	Structure	pIC_{50} PBP3 (mean ± SD)	pIC_{50} Ldt_{Mt2} (mean ± SD)
Aztreonam	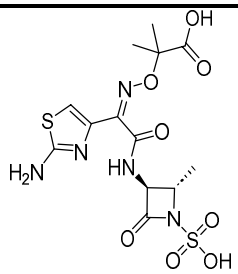	3.8 ± 0.16	<3.4
Clavulanic acid	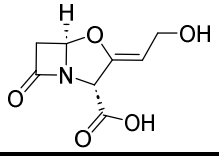	<3.4	3.7 ± 0.1

Table S4.6. Structure-activity relationship studies of sulfonyl pyridines for inhibition of *Mycobacterium smegmatis* and reactivity with Ldt_{Mt2} and glutathione. The calculated modified Ldt_{Mt2} mass corresponds to the mass resulting from an aromatic nucleophilic substitution (S_NAr) reaction (+0 Da = unmodified Ldt_{Mt2}). MIC experiments were performed in triplicate, assays with Ldt_{Mt2} and GSH were performed in quadruplicate. Errors represent standard deviation. See Methods for experimental details.

Compound	Structure	*Msm* MIC (μg/mL)	pIC_{50} Ldt_{Mt2}	k_{inact}/K_I Ldt_{Mt2} (M^{-1} s^{-1})	k_{chem} (M^{-1} s^{-1})	Ldt_{Mt2} calculated mass (Da)	Ldt_{Mt2} observed mass (Da)
14	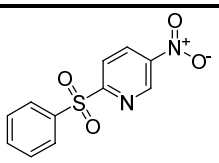	8	5.3 ± 0.12	52.6 ± 0.62	59.7 ± 2.6	38101 (+123)	38101 (+123)
15	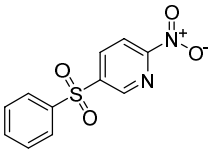	4	4.6 ± 0.34	<10.0	<0.83	38101 (+123)	38196 (+218)
16	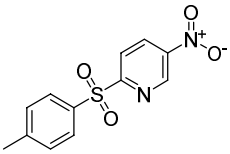	8	5.8 ± 0.15	51.9 ± 2.5	95.8 ± 1.0	38101 (+123)	38101 (+123)
17	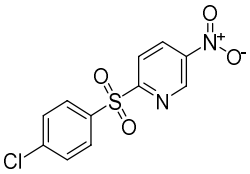	4	5.6 ± 0.15	86.9 ± 1.7	85.9 ± 7.2	38101 (+123)	38101 (+123)
18	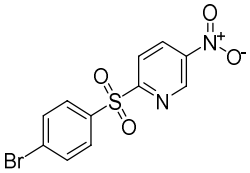	8	6.1 ± 0.12	272 ± 1.7	96.6 ± 1.5	38101 (+123)	38101 (+123)
19	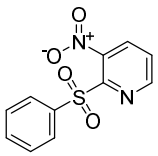	16	4.6 ± 0.26	<10.0	22.6 ± 3.6	38101 (+123)	38101 (+123)
20	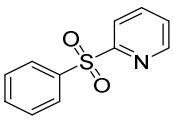	>128	<4.4	<10.0	<0.83	38056 (+78)	37978 (+0)
21	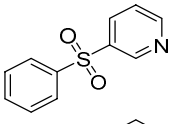	>128	<4.4	<10.0	<0.83	38056 (+78)	37978 (+0)
22	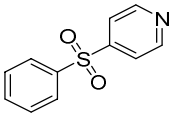	>128	<4.4	<10.0	<0.83	38056 (+78)	37978 (+0)
23	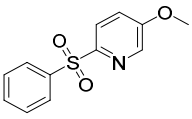	>128	<4.4	<10.0	<0.83	38086 (+108)	37978 (+0)

Compound	Structure	*Msm* MIC (µg/mL)	pIC_{50} Ldt_{Mt2}	k_{inact}/K_I Ldt_{Mt2} (M^{-1} s^{-1})	k_{chem} (M^{-1} s^{-1})	Ldt_{Mt2} calculated mass (Da)	Ldt_{Mt2} observed mass (Da)
24	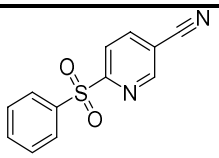	>128	4.6 ± 0.36	<10.0	3.2 ± 0.73	38081 (+103)	38081 (+103)
25	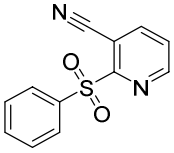	>128	<4.4	<10.0	<0.83	38081 (+103)	38101 (+123), 38222 (+244), 38345 (+367)
26	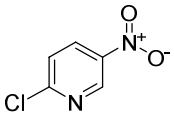	32	<4.4	<10.0	<0.83	38101 (+123)	37978 (+0)
27		>128	<4.4	<10.0	<0.83	38056 (+78)	37978 (+0)
28	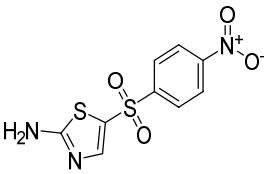	>128	N.D.	N.D.	N.D.	38100 (+122)	38132 (+154)
29	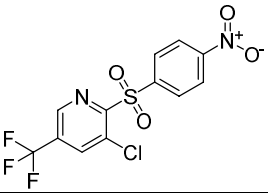	>128	<4.4	<10.0	<0.83	38158 (+180)	38158 (+180)

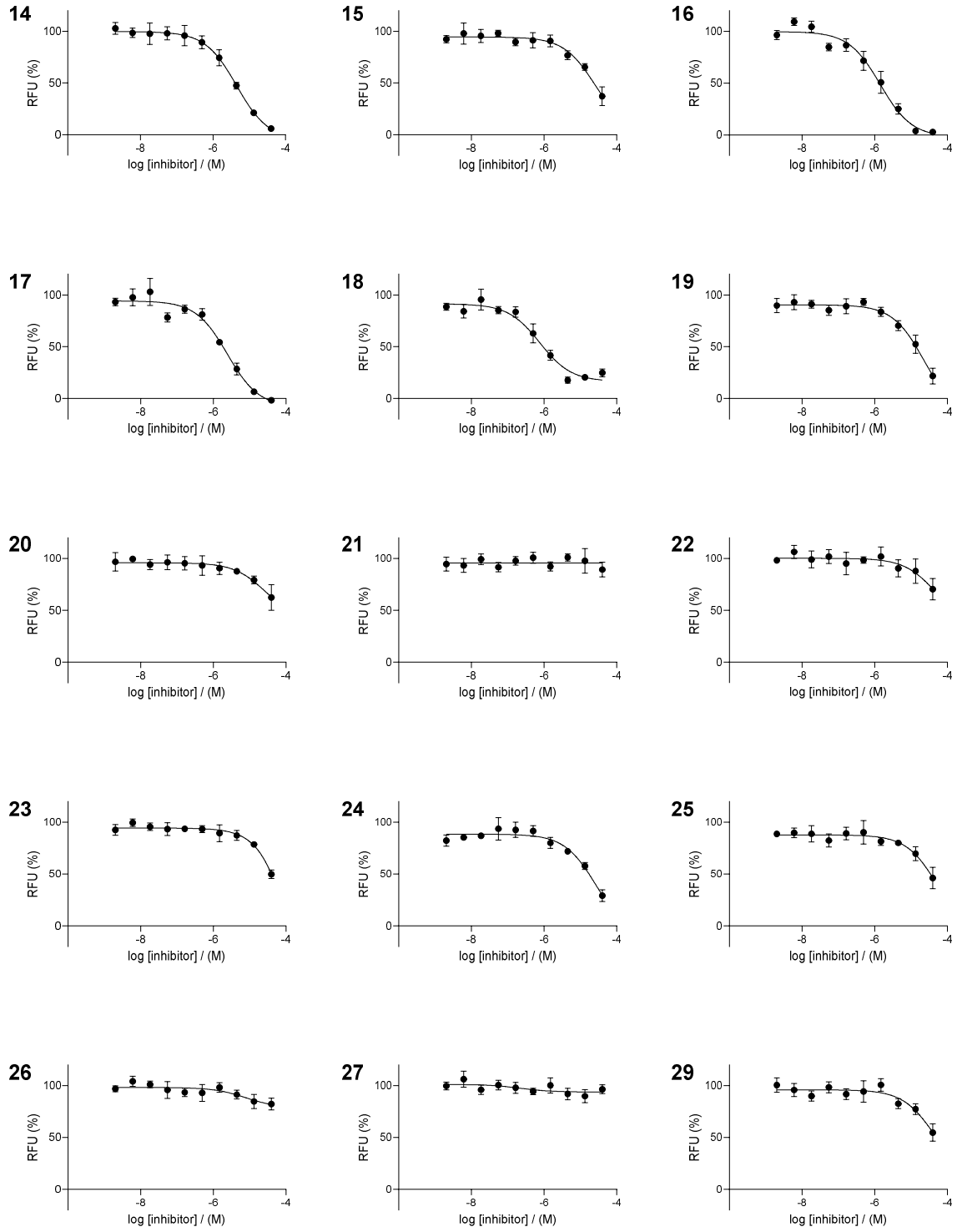

Figure S4.5. Dose-response curves for sulfonyl pyridines 14-29 with Ldt_{Mt2}. Inhibition assays were carried out using 100 nM Ldt_{Mt2} and 25 µM Probe **1** with 10 min pre-incubation at room temperature in 50 mM HEPES, pH 7.2 with 0.01% (*v/v*) Triton X-100. Error bars represent standard deviation (n=4). Average pIC_{50} values and compound structures are given in Table S4.6.

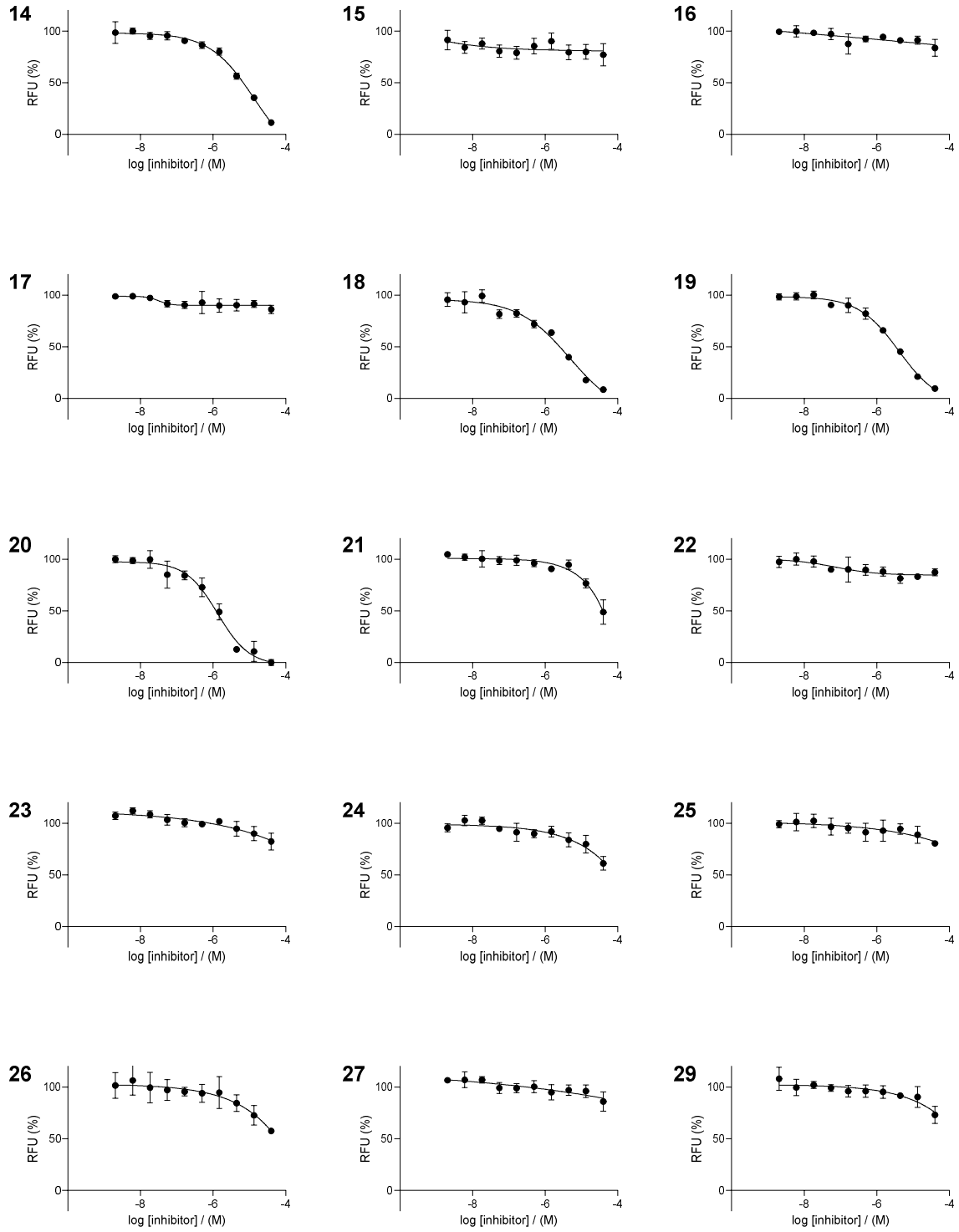

Figure S4.6. Determination of the second-order rate constant for irreversible inhibition (k_{inact}/K_I) of Ldt_{Mt2} by sulfonyl pyridines 14-29. Inhibition assays were carried out using 100 nM Ldt_{Mt2} and 10 µM Probe **1**,[5] with 3 h incubation at rt in 50 mM HEPES, pH 7.2 with 0.01% (*v/v*) Triton X-100. Error bars represent the standard deviation (n=4). Average $(k_{inact}/K_I)_{inhibitor}$ values and compound structures are given in Table S4.6.

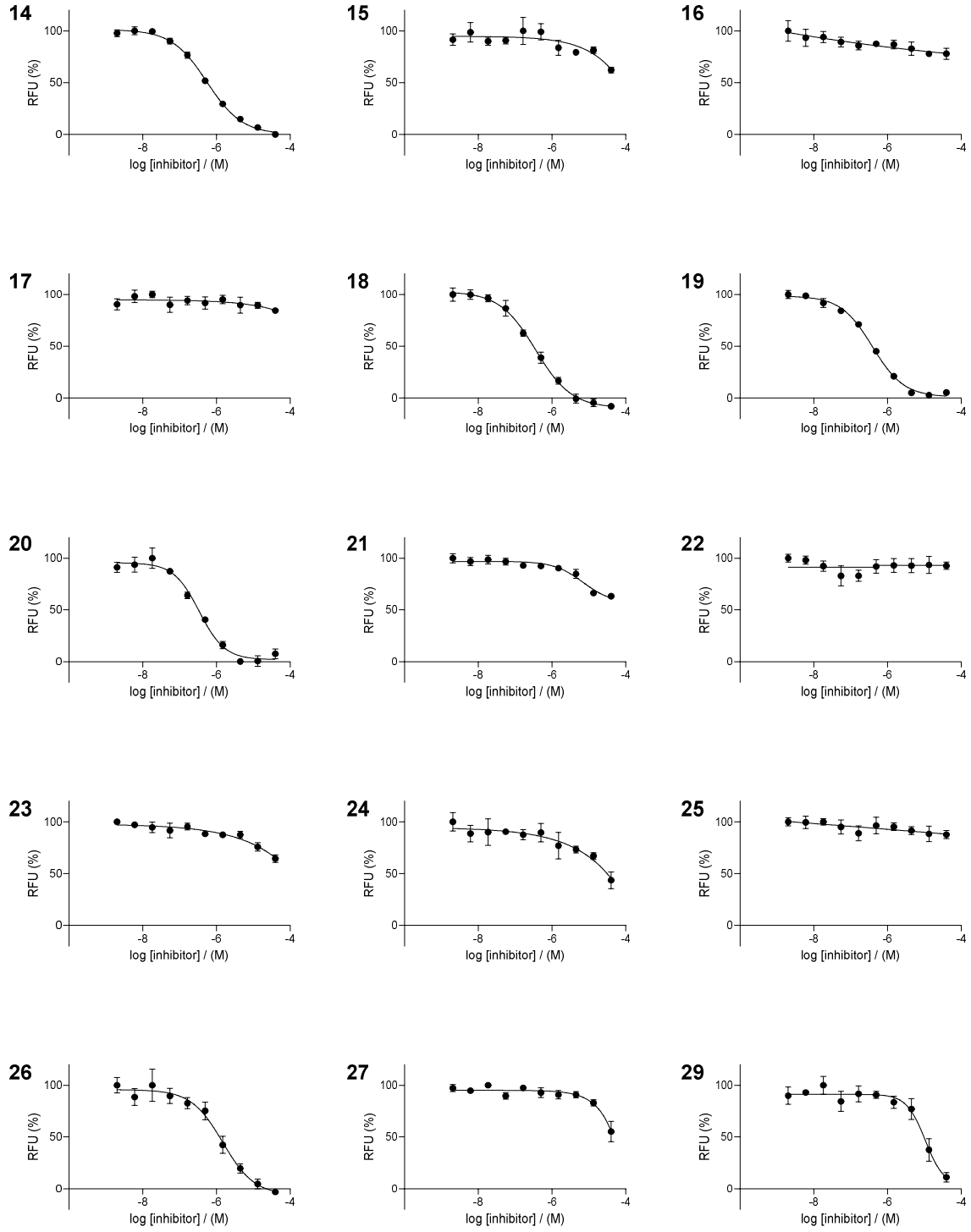

Figure S4.7. Determination of the intrinsic thiol reactivity rate constant (k_{chem}) for sulfonyl pyridines 14-29. Assays were carried out using 500 nM L-glutathione and 10 µM Probe **1** with 16 h incubation at room temperature in 50 mM HEPES, pH 7.2 with 0.01% (*v/v*) Triton X-100. Error bars represent the standard deviation (n=4). Average k_{chem} values and compound structures are given in Table S4.6.

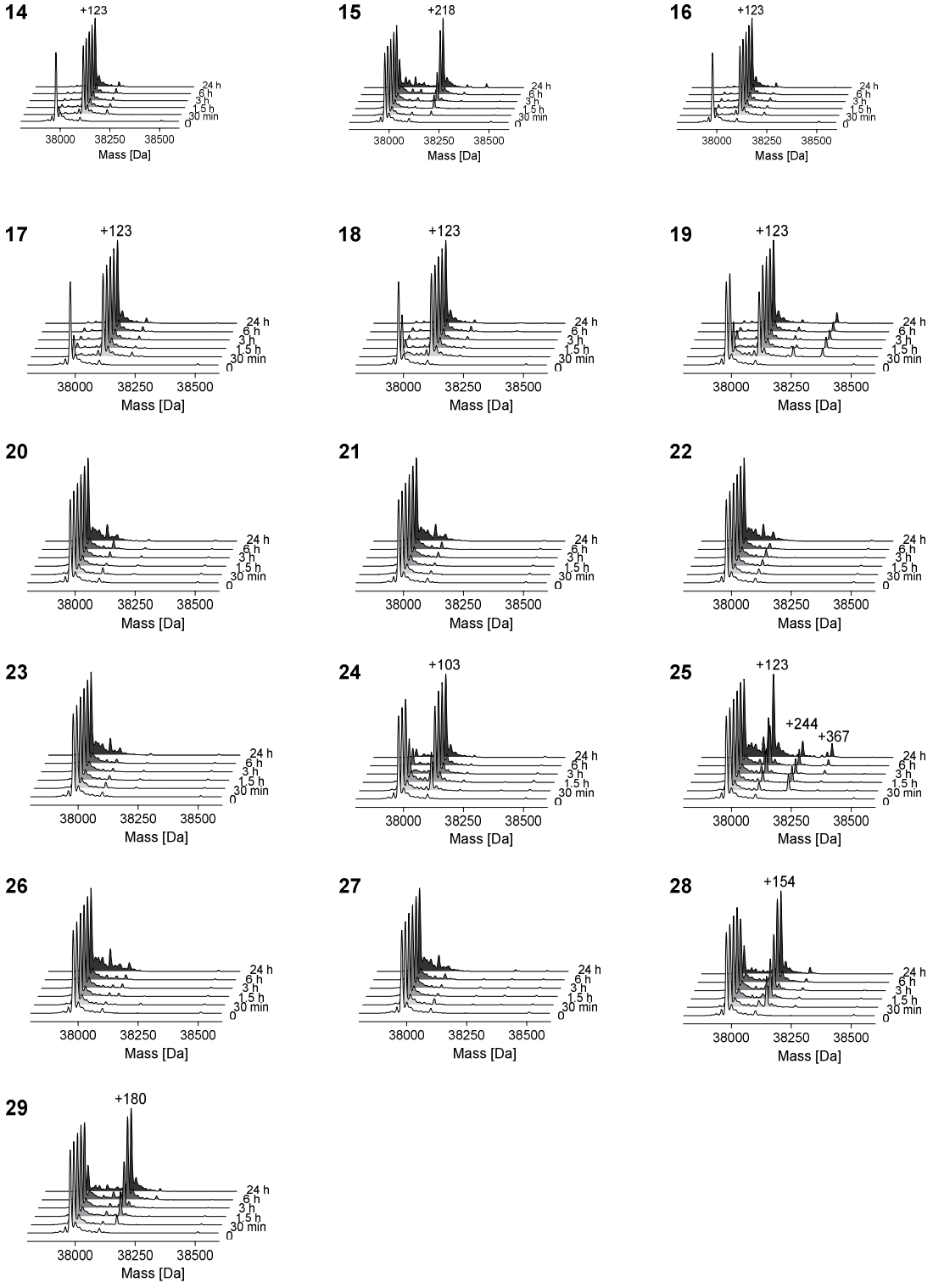

Figure S4.8. Protein observed SPE-MS analysis for the reaction of sulfonyl pyridines 14-29 with Ldt_{Mt2}. Ldt_{Mt2} (1 µM) was incubated with the specified inhibitor (100 µM) at rt in 50 mM Tris, pH 7.5. Samples were analysed after the indicated times. Deconvoluted spectra, obtained using the maximum entropy algorithm in the MassHunter Workstation Qualitative Analysis B.07.00 program (Agilent), are shown. Mass shifts and assignments are given in Table S4.6.

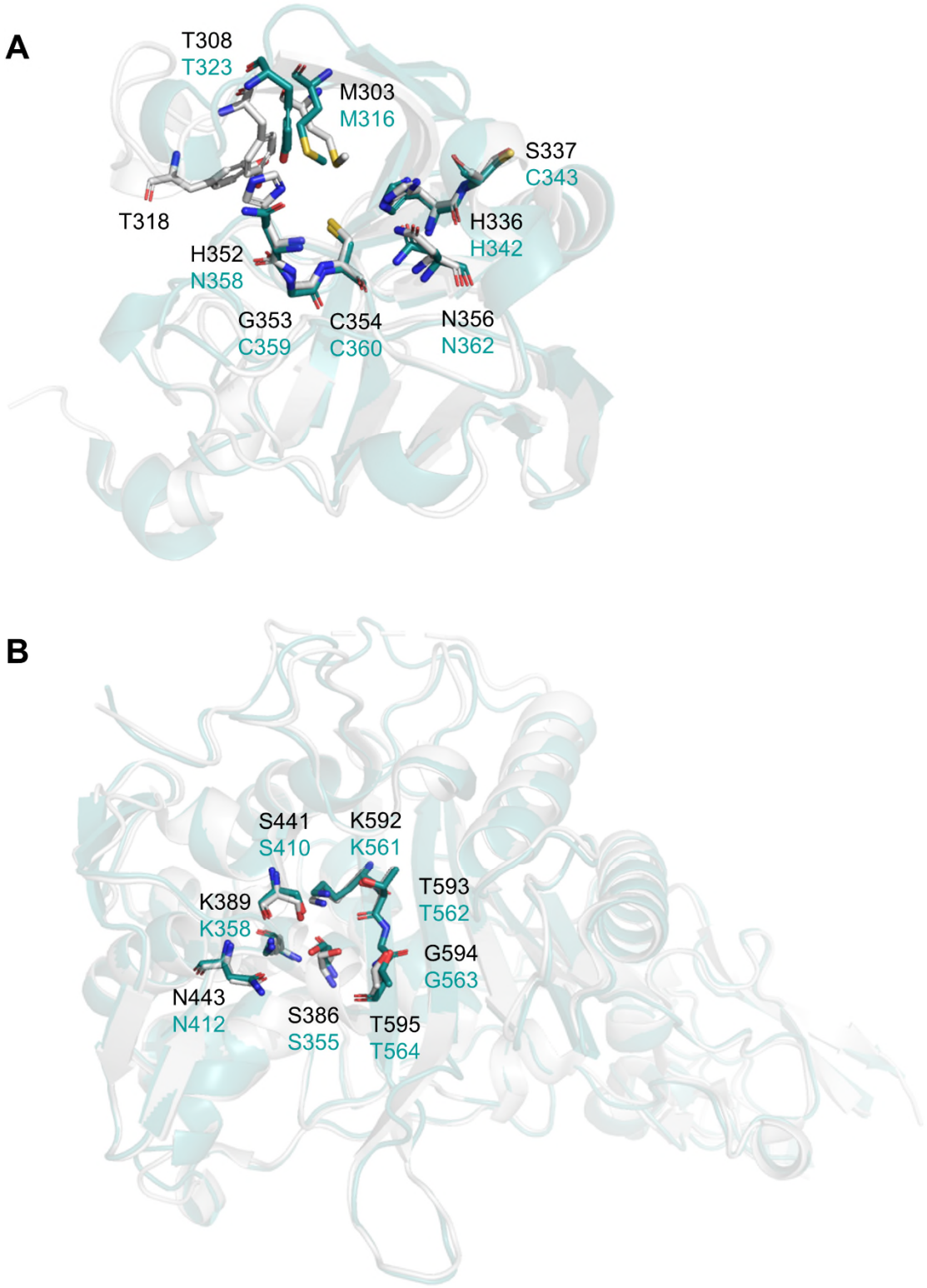

Figure S4.9. Structural comparison between the essential Ldt and PBP from *Mycobacterium tuberculosis* and *Mycobacterium smegmatis*. A. Comparison of the catalytic domain of Ldt_{Mt2} of *Mtb* (PDB 6RLG; grey)[6] and the catalytic domain of LdtC of *Msm* (as predicted with AlphaFold; teal)[7]. **B.** Comparison of the catalytic domain of PBP3 of *Mtb* (PDB 6KGH)[8] and of *Msm* (as predicted with AlphaFold; teal)[7].

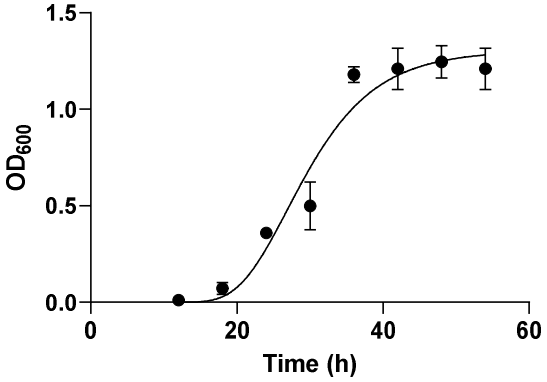

Figure S4.10. Growth curve of *Mycobacterium smegmatis*. A culture if *Msm* was grown in Middlebrook 7H9 broth supplemented with 0.1% (*v*/*v*) Tween-80, 0.5 % (*w*/*v*) bovine albumin fraction V, 0.2% (*w*/*v*) dextrose, and 0.3 % (*v*/*v*) catalase (beef) in 37 °C with aeration following inoculation (0.1%). Growth was assessed with via measurement of OD_{600}. After a lag phase of ~12 h, the *Msm* culture was observed to reach the exponential growth phase with a generation time of 3.6 h, following which time the stationary phase was reached at ~42 h.

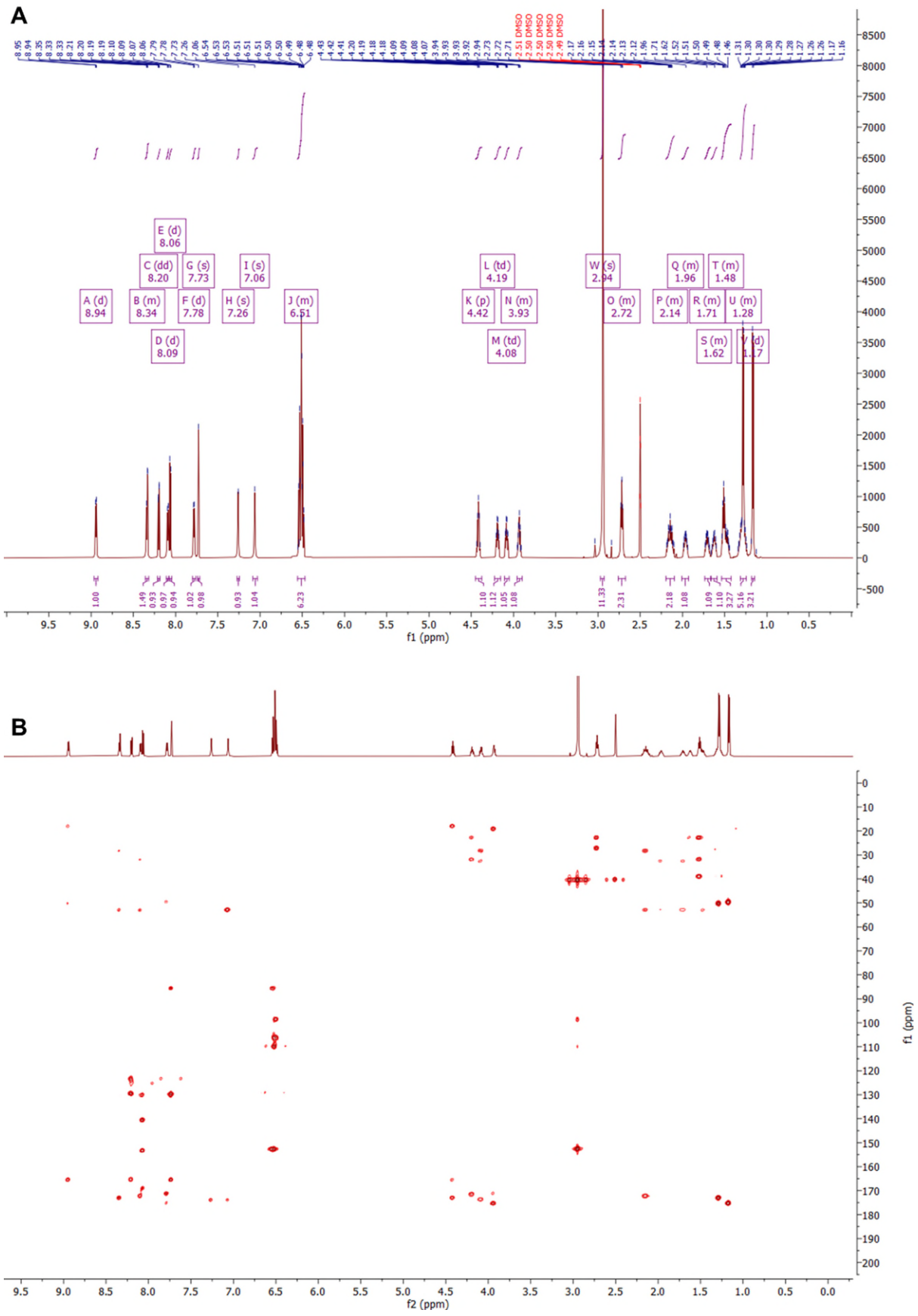

Figure S4.11. Characterisation of TetraRh by ^{1}H (700 MHz) and ^{13}C NMR (700 MHz). [continues]

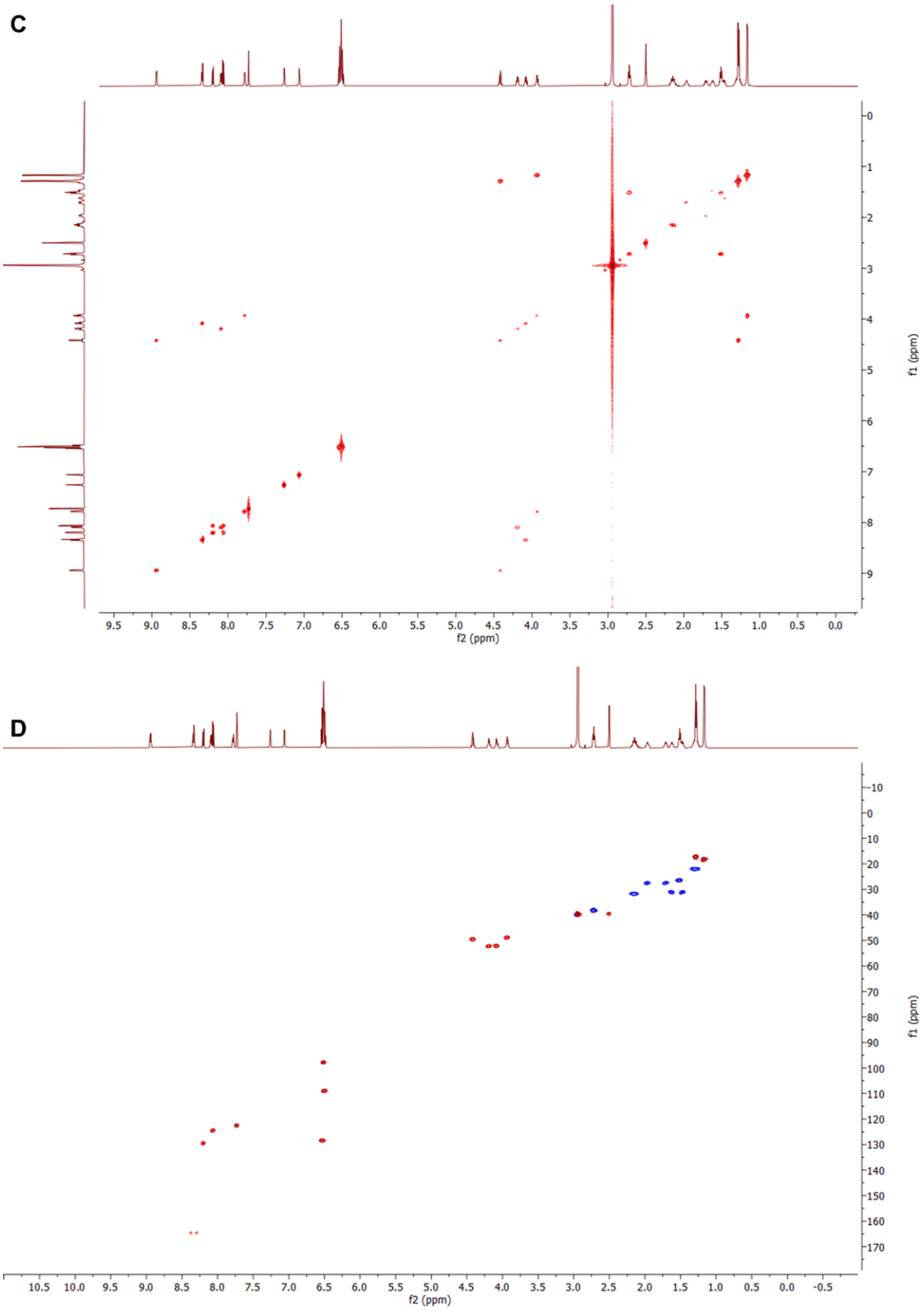

Figure S4.11. Characterisation of TetraRh by ^{1}H (700 MHz) and ^{13}C NMR (700 MHz). NMR analysis of TetraRh comprised of ^{1}H (**A**), HMBC (**B**), COSY (**C**), and HSQC (**D**). Assignment of the ^{1}H chemical shifts can be found in Table S4.7.

Table S4.7. Assignment of ^{1}H-NMR chemical shifts (ppm) for TetraRh. Assignments were based on the spectra shown in Figure S4.11.

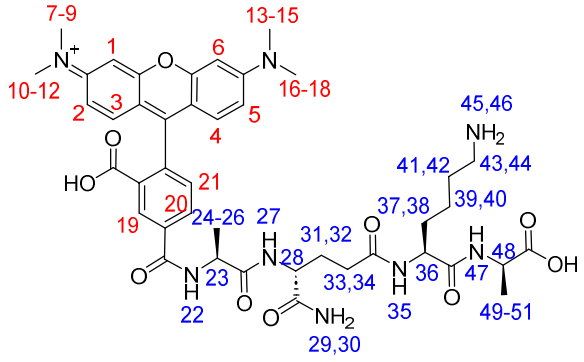

TetraRh

Chemical shift (ppm)	Multiplicity	Integration	Assignment
8.94	d, *J* = 6.5 Hz	1 H	47
8.36 – 8.32	m	1 H	27
8.2	dd, *J* = 8.1, 1.4 Hz	1 H	20
8.09	d, *J* = 8.2 Hz	1 H	35
8.06	d, *J* = 8.1 Hz	1 H	21
7.78	d, *J* = 6.9 Hz	1 H	22
7.73	s	1 H	19
7.26	s	1 H	29
7.06	s	1 H	30
6.56 – 6.47	m	6 H	1-6
4.42	p, *J* = 7.0 Hz	1 H	48
4.19	td, *J* = 8.4, 5.2 Hz	1 H	36
4.08	td, *J* = 8.6, 4.9 Hz	1 H	28
3.96 – 3.90	m	1 H	23
3.94	s	12 H	7-18
2.76 – 2.68	m	2 H	43, 44
2.19 – 2.10	m	2 H	33, 34
2.01 – 1.93	m	1 H	31
1.74 – 1.67	m	2 H	37, 32
1.54 – 1.43	m	3 H	38, 39, 40
1.32 – 1.25	m	5 H	49-51, 41, 42
1.17	d, *J* = 7.1 Hz	3 H	24-26

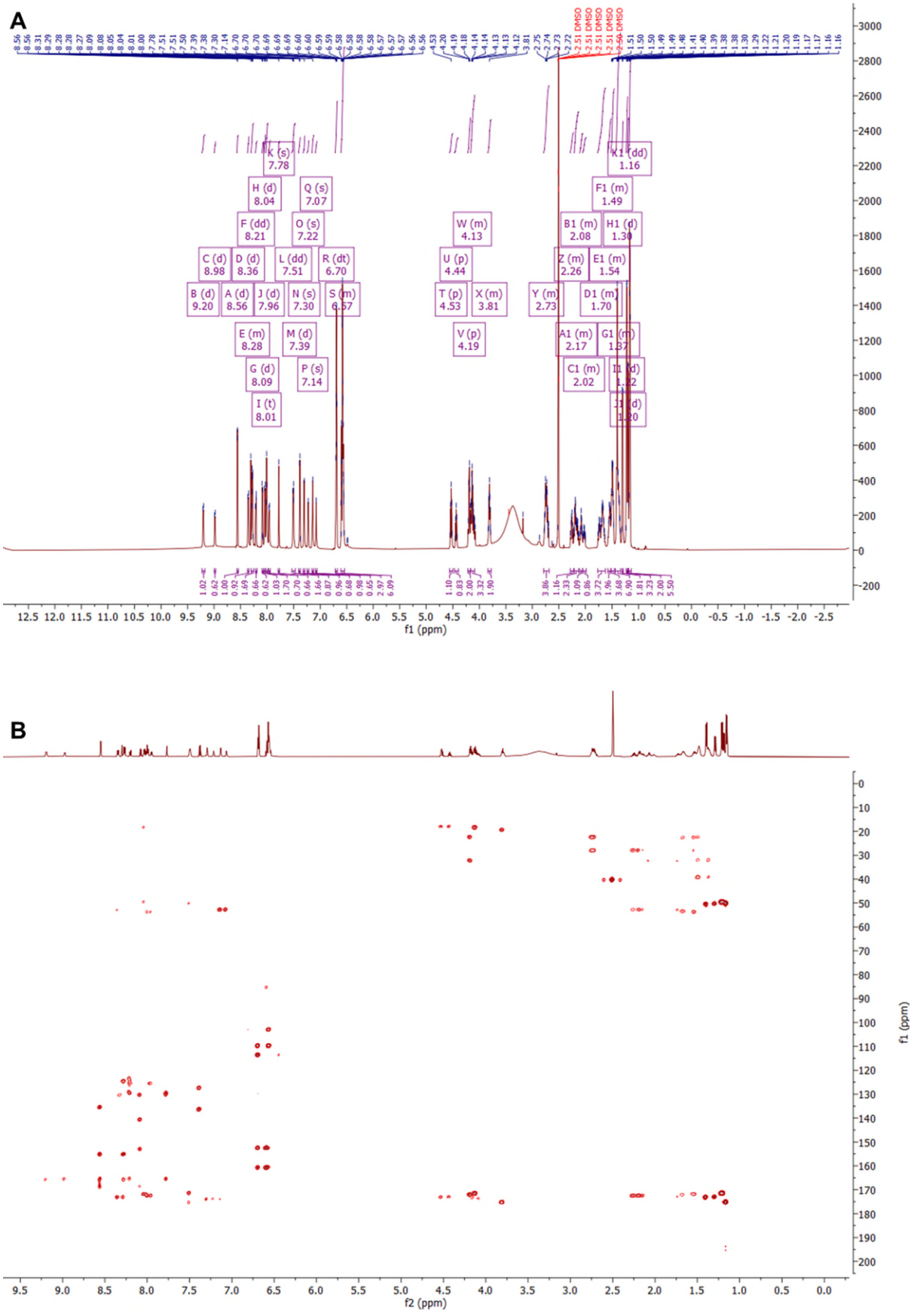

Figure S4.12. Characterisation of PentaFI by ^{1}H (700 MHz) and ^{13}C NMR (700 MHz). [continues]

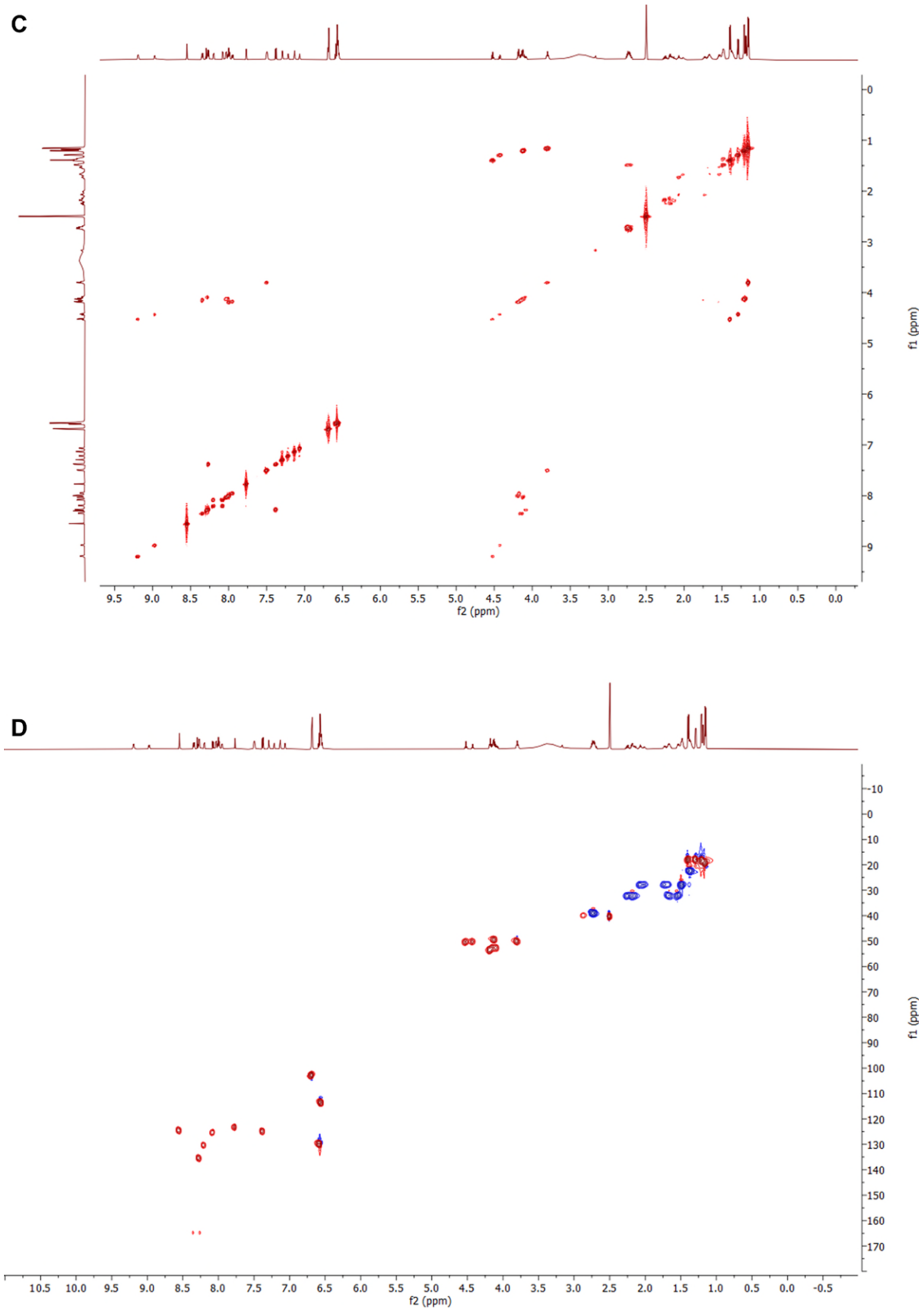

Figure S4.12. Characterisation of PentaFI by ^{1}H (700 MHz) and ^{13}C NMR (700 MHz). NMR analysis of PentaFI comprised of ^{1}H (**A**), HMBC (**B**), COSY (**C**), and HSQC (**D**). Assignment of the ^{1}H chemical shifts can be found in Table S4.8. Note that PentaFI exists as two isomers (ratio 1:0.7).

Table S4.8. Assignment of ^{1}H-NMR chemical shifts (ppm) for PentaFI. Assignments were based on the spectra shown in Figure S4.12. Note that PentaFI exists as two isomers (ratio 1:0.7).

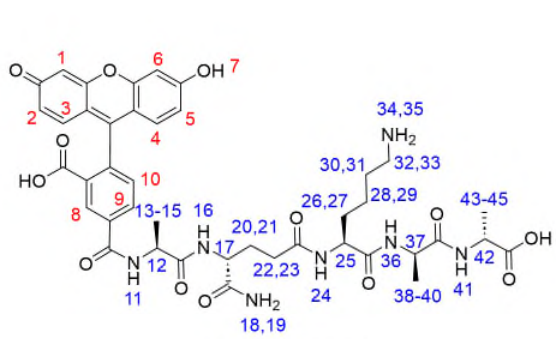

PentaFI, isomer 1

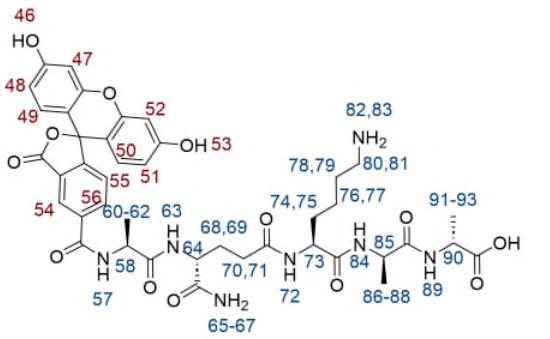

PentaFI, isomer 2

Chemical shift (ppm)	Multiplicity	Integration	Assignment
9.20	d, *J* = 6.7 Hz	1 H	9
8.98	d, *J* = 6.6 Hz	0.7 H	1-6, 47-51
8.56	s	1 H	8
8.36	d, *J* = 8.1 Hz	1 H	7
8.30 – 8.26	m	1.7 H	10, 53, 46
8.21	dd, *J* = 8.0, 1.4 Hz	0.7 H	56
8.09	d, *J* = 8.1 Hz	0.7 H	55
8.04	d, *J* = 7.6 Hz	1 H	NH
8.01	t, *J* = 7.8 Hz	1.7 H	NH
7.96	d, *J* = 7.7 Hz	0.7 H	NH
7.77	s	0.7 H	54
7.51	dd, *J* = 6.5, 3.0 Hz	1.7 H	1-6, 47-51
7.39	d, *J* = 8.0 Hz	1 H	1-6, 47-51
7.30	s	1 H	NH
7.22	s	0.7 H	NH
7.14	s	1 H	NH
7.07	s	0.7 H	NH
6.70	dt, *J* = 6.8, 2.4 Hz	3 H	1-6, 47-51
6.61 – 6.54	m	6 H	1-6, 47-51
4.53	p, *J* = 7.1 Hz	1 H	42
4.44	p, *J* = 7.0 Hz	0.7 H	90
4.19	p, *J* = 6.6 Hz	2 H	64, 73
4.17 – 4.07	m	3 H	37, 17, 85
3.83 – 3.78	m	2 H	12, 58
2.79 – 2.69	m	3.7 H	32, 33, 80, 81
2.29 – 2.22	m	1.2 H	70, 71
2.21 – 2.13	m	2 H	22, 23
2.11 – 2.05	m	1 H	21
2.05 – 1.99	m	0.7 H	69
1.78 – 1.62	m	3.7 H	26, 27, 74, 75
1.58 – 1.52	m	2 H	20, 68
1.52 – 1.46	m	3.7 H	30, 31, 78, 79
1.44 – 1.34	m	7 H	43-45, 28, 29, 76, 77
1.30	d, *J* = 7.1 Hz	2 H	91-93
1.22	d, *J* = 7.3 Hz	3 H	38-40
1.20	d, *J* = 7.3 Hz	2 H	86-88
1.16	dd, *J* = 7.0, 2.0 Hz	5 H	13-15, 60-62

References

1 de Munnik, M., Lang, P. A., De Dios Antos, F., Cacho, M., Bates, R. H., Brem, J., Rodríguez-Miquel, B. & Schofield, C. J. High-Throughput Screen with the L,D-transpeptidase Ldt_{Mt2} of *Mycobacterium tuberculosis* Reveals Novel Classes of Covalently Reacting Inhibitors *Chem. Sci.* **14**, 7262-7278 (2023).

2 Lelovic, N., Mitachi, K., Yang, J., Lemieux, M. R., Ji, Y. & Kurosu, M. Application of Mycobacterium smegmatis as a surrogate to evaluate drug leads against Mycobacterium tuberculosis. *J. Antibiot.* **73**, 780-789 (2020).

3 Agrawal, P., Miryala, S. & Varshney, U. Use of Mycobacterium smegmatis Deficient in ADP-Ribosyltransferase as Surrogate for Mycobacterium tuberculosis in Drug Testing and Mutation Analysis. *PloS one* **10**, e0122076 (2015).

4 Pidgeon, S. E., Apostolos, A. J., Nelson, J. M., Shaku, M., Rimal, B., Islam, M. N., Crick, D. C., Kim, S. J., Pavelka, M. S., Kana, B. D. & Pires, M. M. L,D-Transpeptidase Specific Probe Reveals Spatial Activity of Peptidoglycan Cross-Linking. *ACS Chem. Biol.* **14**, 2185–2196 (2019).

5 de Munnik, M., Lohans, C. T., Langley, G. W., Bon, C., Brem, J. & Schofield, C. J. A Fluorescence-Based Assay for Screening β-Lactams Targeting the *Mycobacterium tuberculosis* Transpeptidase Ldt_{Mt2}. *ChemBioChem* **21**, 368-372 (2020).

6 de Munnik, M., Lohans, C. T., Lang, P. A., Langley, G. W., Malla, T. R., Tumber, A., Schofield, C. J. & Brem, J. Targeting the *Mycobacterium tuberculosis* transpeptidase Ldt_{Mt2} with cysteine-reactive inhibitors including ebselen. *Chem. Commun.* **55**, 10214-10217 (2019).

7 Jumper, J., Evans, R., Pritzel, A., Green, T., Figurnov, M., Ronneberger, O., Tunyasuvunakool, K., Bates, R., Žídek, A., Potapenko, A., Bridgland, A., Meyer, C., Kohl, S. A. A., Ballard, A. J., Cowie, A., Romera-Paredes, B., Nikolov, S., Jain, R., Adler, J., Back, T., Petersen, S., Reiman, D., Clancy, E., Zielinski, M., Steinegger, M., Pacholska, M., Berghammer, T., Bodenstein, S., Silver, D., Vinyals, O., Senior, A. W., Kavukcuoglu, K., Kohli, P. & Hassabis, D. Highly accurate protein structure prediction with AlphaFold. *Nature* **596**, 583-589 (2021).

8 Lu, Z., Wang, H., Zhang, A., Liu, X., Zhou, W., Yang, C., Guddat, L., Yang, H., Schofield, C. J. & Rao, Z. Structures of *Mycobacterium tuberculosis* Penicillin-Binding Protein 3 in Complex with Five β-Lactam Antibiotics Reveal Mechanism of Inactivation. *Mol. Pharmacol.* **97**, 287-294 (2020).

Appendix V. Protein purification.

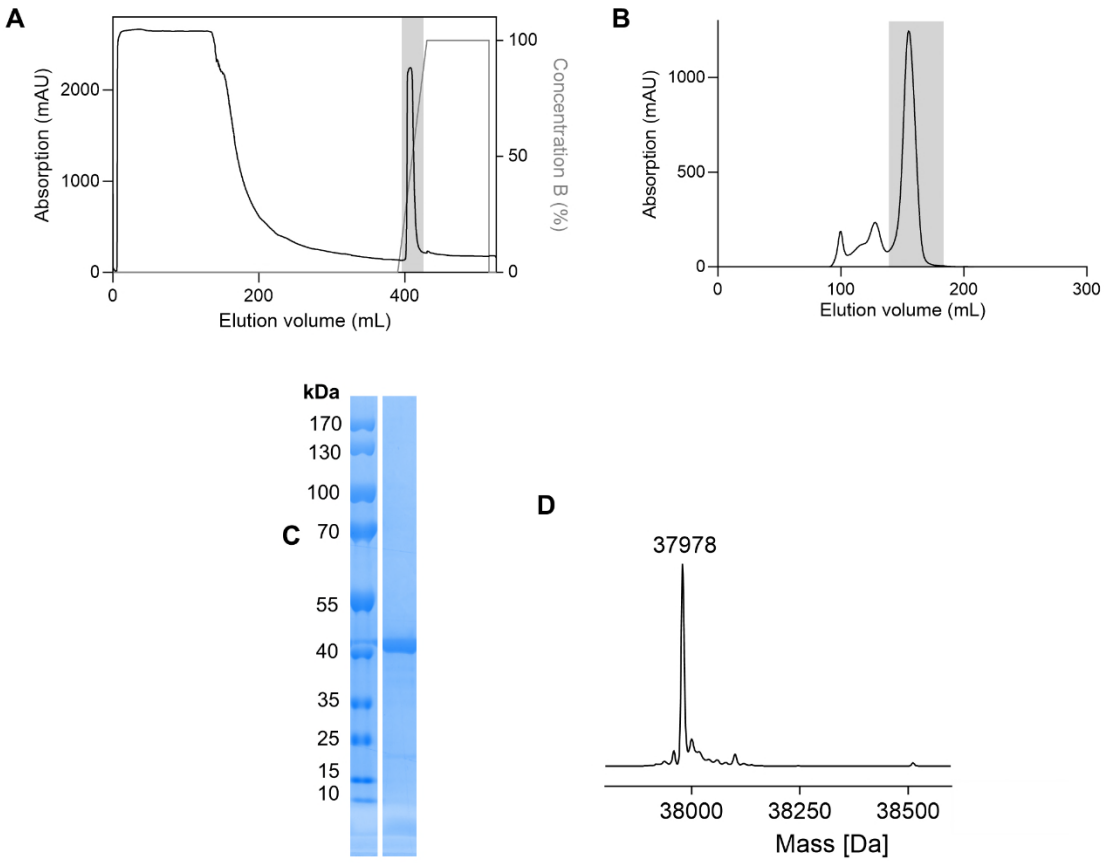

Figure S5.1. Purification of recombinant Ldt_{Mt2} of *Mycobacterium tuberculosis*. A. HisTag affinity chromatography purification of Ldt_{Mt2}. The area in grey represents Ldt_{Mt2} containing fractions. **B.** Size-exclusion chromatography of Ldt_{Mt2}, with the HisTag cleaved. The area in grey represents Ldt_{Mt2} containing fractions. **C.** SDS-PAGE analysis of purified Ldt_{Mt2}. **D.** MS analysis of purified Ldt_{Mt2}. The deconvoluted spectrum is shown.

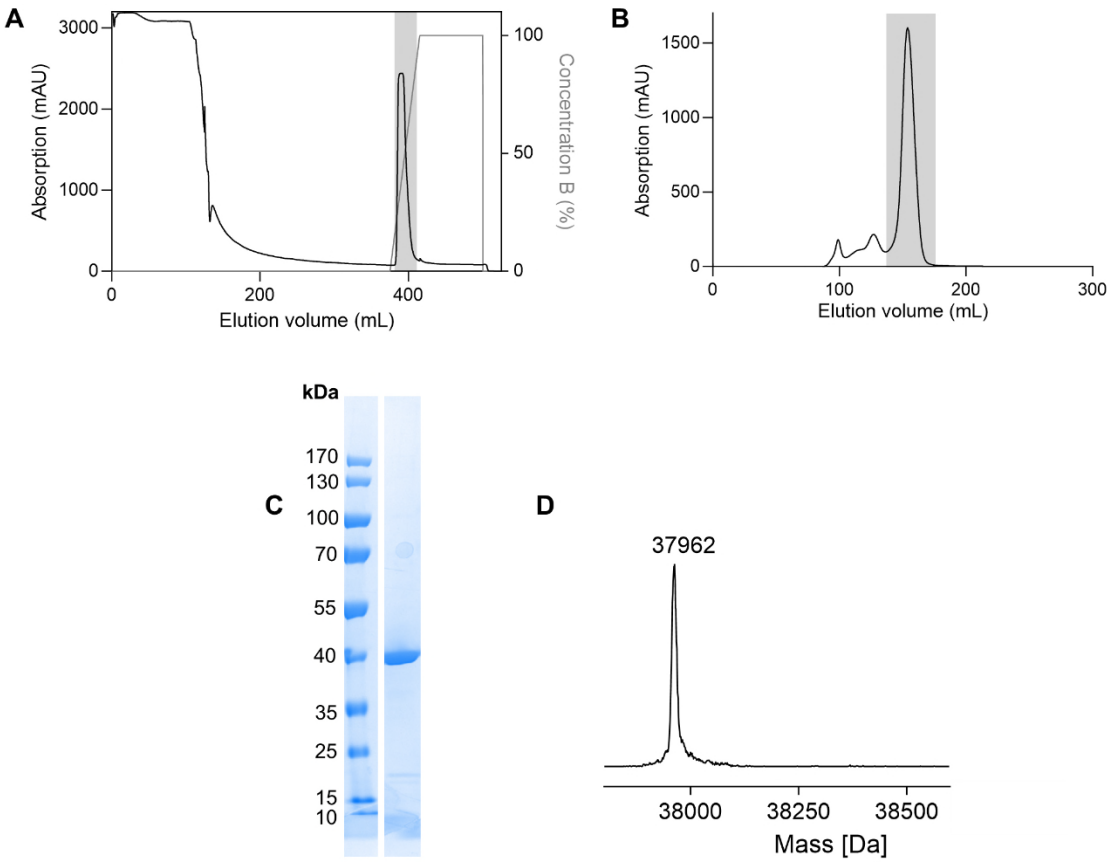

Figure S5.2. Purification of recombinant Ldt_{Mt2}^{C354S} of *Mycobacterium tuberculosis*. A. HisTag affinity chromatography purification of Ldt_{Mt2}^{C354S}. The area in grey represents Ldt_{Mt2}^{C354S} containing fractions. **B.** Size-exclusion chromatography of Ldt_{Mt2}^{C354S}, with the HisTag cleaved. The area in grey represents Ldt_{Mt2}^{C354S} containing fractions. **C.** SDS-PAGE analysis of purified Ldt_{Mt2}^{C354S}. **D.** MS analysis of purified Ldt_{Mt2}^{C354S}. The deconvoluted spectrum is shown.

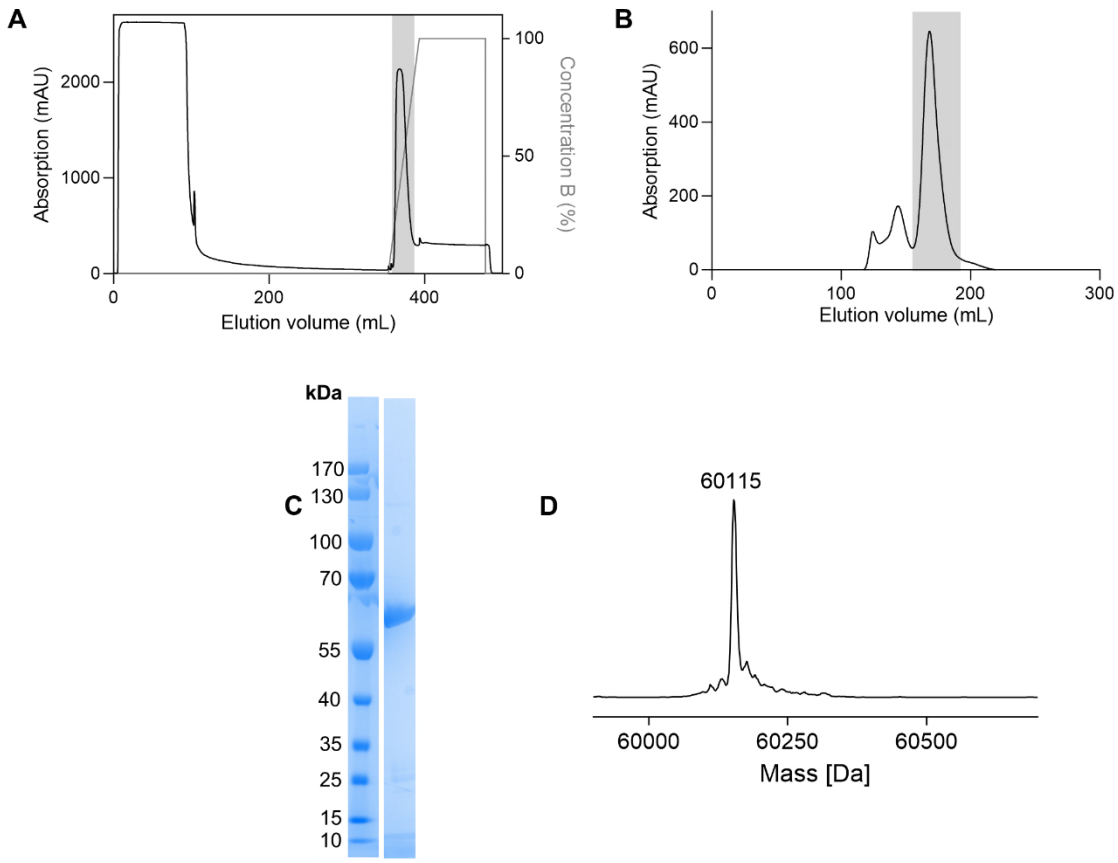

Figure S5.3. Purification of recombinant PBP3 of *Mycobacterium tuberculosis*. A. HisTag affinity chromatography purification of PBP3. The area in grey represents PBP3 containing fractions. **B.** Size-exclusion chromatography of PBP3, with the HisTag cleaved. The area in grey represents PBP3 containing fractions. **C.** SDS-PAGE analysis of purified PBP3. **D.** MS analysis of purified PBP3. The deconvoluted spectrum is shown.

Appendix VI. Sequences of protein constructs

Ldt_{Mt2} (Δ1-55; MW = 37975.34 Da, ε = 71390 M^{-1} cm^{-1})

QSDLLVPKLTASVTDGAVGVTVDAPVSVTAADGVLAAVTMVNDNGRPVAGRLSPDGLRWSTTEQLGY
NRRYTLNATALGLGGAATRQLTFQTSSPAHLTMPYVMPGDGEVVGVGEPVAIRFDENIADRGAAEKAI
KITTNPPVEGAFYWLNNREVRWRPEHFWKPGTAVDVAVNTYGVDLGEGMFGEDNVQTHFTIGDEVIA
TADDNTKILTVRVNGEVVKSMPTSMGKDSTPTANGIYIVGSRYKHIIMDSSTYGVPVNSPNGYRTDVD
WATQISYSGVFVHSAPWSVGAQGHTNTSHGCLNVSPSNAQWFYDHVKRGDIVEVVNTVGGTLPGID
GLGDWNIPWDQWRAGNAKA

Ldt_{Mt2}^{C354S} (Δ1-55; MW = 37959.28 Da, ε = 71390 M^{-1} cm^{-1})

QSDLLVPKLTASVTDGAVGVTVDAPVSVTAADGVLAAVTMVNDNGRPVAGRLSPDGLRWSTTEQLGY
NRRYTLNATALGLGGAATRQLTFQTSSPAHLTMPYVMPGDGEVVGVGEPVAIRFDENIADRGAAEKAI
KITTNPPVEGAFYWLNNREVRWRPEHFWKPGTAVDVAVNTYGVDLGEGMFGEDNVQTHFTIGDEVIA
TADDNTKILTVRVNGEVVKSMPTSMGKDSTPTANGIYIVGSRYKHIIMDSSTYGVPVNSPNGYRTDVD
WATQISYSGVFVHSAPWSVGAQGHTNTSHGSLNVSPSNAQWFYDHVKRGDIVEVVNTVGGTLPGID
GLGDWNIPWDQWRAGNAKA

PBP3 (Δ1-122; MW = 60112.76 Da, ε = 49850 M^{-1} cm^{-1})

GPVDGADLGGQLKVTDVQPAARGSIVDRNNDRLAFTIEARALTFQPKRIRRQLEEARKKTSAAPDPQ
QRLRDIAQEVAGKLNNKPDAAAVLKKLQSDETFVYLARAVDPAVASAICAKYPEVGAERQDLRQYPGG
SLAANVVGGIDWDGHGLLGLEDSLDAVLAGTDGSVTYDRGSDGVVIPGSYRNRHKAVHGSTVVLTLD
NDIQFYVQQQVQQAKNLSGAHNVSAVVLDAKTGEVLAMANDNTFDPSQDIGRQGDKQLGNPAVSSP
FEPGSVNKIVAASAVIEHGLSSPDEVLQVPGSIQMGGVTVHDAWEHGVMPYTTTGVFGKSSNVGTLM
LSQRVGPERYYDMLRKFGLGQRTGVGLPGESAGLVPPIDQWSGSTFANLPIGQGLSMTLLQMTGMY
QAIANDGVRVPPRIIKATVAPDGSRTEEPRPDDIRVVSAQTAQTVRQMLRAVVQRDPMGYQQGTGPT
AGVPGYQMAGKTGTAQQINPGCGCYFDDVYWITFAGIATADNPRYVIGIMLDNPARNSDGAPGHSAA
PLFHNIAGWLMQRENVPLSPDPGPPLVLQAT

BlaC (Δ1-40; MW = 28740.31 Da, ε = 30035 M^{-1} cm^{-1})

GPVDGADLADRFAELERRYDARLGVYVPATGTTAAIEYRADERFAFCSTFKAPLVAAVLHQNPLTHLD
KLITYTSDDIRSISPVAQQHVQTGMTIGQLCDAAIRYSDGTAANLLLADLGGPGGGTAAFTGYLRSLGD
TVSRLDAEEPELNRDPPGDERDTTTPHAIALVLQQLVLGNALPPDKRALLTDWMARNTTGAKRIRAGF
PADWKVIDKTGTGDYGRANDIAVVWSPTGVPYVVAVMSDRAGGGYDAEPREALLAEAATCVAGVLA